TRANSPORT ACROSS THE BOUNDARIES OF THE MAGNETOSPHERE

Cover figure from Gosling, J.T., Thomsen, M.F., Bame, S.J., Onsager, T.G., and Russell, C.T.: 1990, 'The Electron Edge of the Low Latitude Boundary Layer during Accelerated Flow Events', *Geophysical Research Letters* **17**, 1833–1836.

Space Science Series of ISSI

Volume 2

The titles published in this series are listed at the end of this volume.

TRANSPORT ACROSS THE BOUNDARIES OF THE MAGNETOSPHERE

Proceedings of an ISSI Workshop
October 1–5, 1996, Bern, Switzerland

Edited by

BENGT HULTQVIST and MARIT ØIEROSET
International Space Science Institute, Bern, Switzerland

Reprinted from Space Science Reviews, Vol. 80, Nos. 1–2, 1997

KLUWER ACADEMIC PUBLISHERS
DORDRECHT / BOSTON / LONDON

A C.I.P. Catalogue record for this book is available from the Library of Congress.

ISBN-13: 978-94-010-6509-2 e-ISBN-13: 978-94-009-0045-5
DOI: 10.1007/978-94-009-0045-5

Published by Kluwer Academic Publishers,
P.O. Box 17, 3300 AA Dordrecht, The Netherlands

Sold and distributed in the U.S.A. and Canada
by Kluwer Academic Publishers,
101 Philip Drive, Norwell, MA 02061, U.S.A.

In all other countries, sold and distributed
by Kluwer Academic Publishers,
P.O. Box 322, 3300 AH Dordrecht, The Netherlands

Printed on acid-free paper

TABLE OF CONTENTS

ISSI Workshop
Transport Across the Boundaries of the Magnetosphere
October 1-5, 1996, Bern, Switzerland
Group Photograph

1.	D. Taylor	16.	K. Maezawa	31.	W. Lennartsson
2.	T. Terasawa	17.	T. Phan	32.	G. Paschmann
3.	G. Nusser Jiang	18.	M. Andrè	33.	D. Williams
4.	M. Hoshino	19.	R. Walker	34.	R. Thorne
5.	S. Ganguli	20.	M. Blanc	35.	D. Sibeck
6.	E. Shelley	21.	S. Orsini	36.	M. Øieroset
7.	A. Yau	22.	N. Sckopke	37.	T. Moore
8.	S. Fuselier	23.	M. Roth	38.	M. Moldwin
9.	T. Onsager	24.	R. von Steiger	39.	B. Blake
10.	K. Ogilvie	25.	M. Fujimoto	40.	H. Koskinen
11.	J. Geiss	26.	L. Lyons	41.	K. Stasiewicz
12.	M. Temerin	27.	J. Scudder	42.	J. Horwitz
13.	L. Zelenyi	28.	D. Southwood	43.	J. Lemaire
14.	S. Watanabe	29.	S. Christon	44.	R. Lundin
15.	M. Hirahara	30.	D. Alcayde	45.	B. Hultqvist

Not in picture: I. Daglis, A. Egeland, R. Wolf, M. Hapgood, J. Sauvaud, M. Scholer.
For a complete list of participants with addresses, see end of the proceedings.

Foreword

The present volume is the second one in the Space Sciences Series of ISSI (International Space Science Institute) and the October 1997 issue of Space Science Reviews. It contains the proceedings of the first workshop in the ISSI study project on "Source and Loss Processes of Magnetospheric Plasma", which was held at ISSI in Bern on October 1-5, 1996. The participants in the project, the project team, numbered at that time 51, of whom 45 participated in the workshop. The main tasks of the first workshop were to provide a basis for the further work by means of presentation and discussion of those 16 review papers which are published in this volume and to prepare plans for the work of six working groups in the year up to the second workshop in October 1997.

The ISSI study project on "Source and Loss Processes of Magnetospheric Plasma" was selected by ISSI in December 1995 as the first in the solar-terrestrial physics field after consulting a number of groups of senior scientists representing the international space physics community at large. The undersigned, Bengt Hultqvist, is the project leader. A Core Group, consisting of two co-chairs for each of six working groups and four ex-officio members from the Space Science Committee of ISSI (H. Balsiger, A. Galeev, G. Haerendel, and D. Southwood), convened at ISSI in March 1996. At that meeting the plans for the first workshop and the membership of the initial six working groups were established. Invitations to the October 1996 workshop were distributed in April 1996.

The members of the Core Group, who co-chair the working groups, are: R. Lundin and T.E. Moore (WG1), H. Koskinen and L. Lyons (WG2), M. Blanc and J.L. Horwitz (WG3), G. Paschmann and D.G. Sibeck (WG4), W. Lennartsson and N. Sckopke (WG5), and T. Terasawa and D.J. Williams (WG6). All members of the project team participate in the work of the initial six working groups. The topics of the working groups are as follows: WG1, Source processes in the high-latitude ionosphere; WG2, Processes causing losses of magnetospheric plasma into the high-latitude atmosphere; WG3, Source and loss processes at the plasmapause; WG4, Source and loss processes on the dayside magnetopause; WG5, Source and loss processes along the flanks and near-tail magnetopause; WG6, Source and loss processes for magnetospheric plasma in the distant tail.

At the second workshop in October 1997 the working groups will present, for discussion in plenum, drafts of the first six chapters of the Final Report of the study project. After that workshop, summarizing and synthesizing chapters will be written and the Final Report is planned for publication as the January 1, 1999, issue of Space Science Review and as no. 5 in the Space Sciences Series of ISSI.

ISSI wants to express its sincere thanks to the authors of the papers in this volume, as well as to the referees, for good work done. A lot of work remains before the study project is completed and the Final Report is published. That work is shared by all working group members, but the Core Group will carry a large part of it, as it has carried a large part up till now. We, therefore, extend our special thanks to the members of the Core Group for agreeing to join the group and for the valuable assistance they are providing both to the study project and to ISSI.

The ISSI staff, V. Manno, G. Nusser Jiang, M. Preen, and D. Taylor, have carried most of the local organizational work for the workshop. We thank them for their contributions.

Bern, June 1997 B. Hultqvist, M. Øieroset

SOURCES OF ION OUTFLOW IN THE HIGH LATITUDE IONOSPHERE

A. W. YAU
Institute for Space Research, Department of Physics and Astronomy, University of Calgary, Calgary, Alberta, Canada

M. ANDRÉ
Swedish Institute of Space Physics, Umeå Division, Umeå University, Umeå, Sweden.

Received January 20, 1997; Accepted in final form February 21, 1997

Abstract. Ion composition observations from polar-orbiting satellites in the past three decades have revealed and confirmed the occurrence of a variety of ion outflow processes in the high-latitude ionosphere. These processes constitute a dominant source of ionospheric plasma to the Earth's magnetosphere. We review the current state of our observational knowledge on their occurrence, energy, composition, variability, interrelationships, and quantitative contributions to the overall mass input to the magnetosphere. In addition, we identify the prevalent sources and the gaps of our current understanding of these sources.

1. Introduction

In this paper, we review the current state of our observational knowledge on ion outflow processes from the high latitude ionosphere. We discuss the source locations, occurrence distributions, energy, mass composition and other morphological characteristics, variability, and relative importance of the various processes. Our objective is to determine the prevalent sources, i.e., to address the questions of "where" and "how much", and to identify the gaps of our current understanding of these sources. In the companion paper (André and Yau, 1997, this issue), we discuss the theories and observations of the underlying ion energization processes, and address the questions of "why" and "how" for the outflowing populations.

The first evidence of ionospheric ions being a significant source of magnetospheric plasma was inferred from storm-time energetic ion composition observations by Shelley *et al.* (1972) in which the precipitating flux of keV O^+ ions exceeded that of H^+. This was later confirmed by the discovery of energetic (>0.5 keV) upflowing ionospheric H^+ and O^+ ions (UFI) above 5000 km on the polar-orbiting S3-3 satellite. Two types of UFI were observed: in the first type, the velocity distribution was peaked along the upward magnetic field direction (Shelley *et al.*, 1976); in the second, the distribution was peaked at an angle to the magnetic field (Sharp *et al.*, 1977). The two types of UFI were subsequently referred to as "ion beams" and "ion conics", respectively.

A variety of ion outflow processes in the high-latitude ionosphere have been observed from satellites, sounding rockets, and ground-based instruments in the past three decades. These processes may be grouped into two catagories: bulk ion

Space Science Reviews **80**: 1–25, 1997.

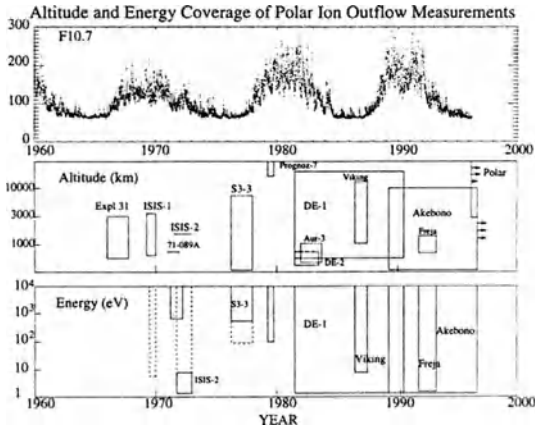

Figure 1. Schematic summary of measurements of ion outflow processes from polar-orbiting satellites. (a) Solar radio flux index, $F_{10.7}$ (top panel). (b) Altitude and epoch ranges of measurements (middle panel). (c) Ion energy ranges of measurements (bottom panel).

flows with energies up to a few eV in which all the ions acquire a bulk flow velocity, and ion energization processes to much higher energies where in general only a fraction of the ions are energized. The former catagory includes the polar wind and thermal O^+ upflow from the topside auroral ionosphere. The latter catagory includes transversely accelerated ions (TAI), upwelling ions (UWI), ion conics, and ion beams. Figure 1 summarizes measurements of ion outflow processes from polar-orbiting satellites over the past three solar cycles (Solar Cycle 20, 21, and 22). Figure 1a shows the daily solar radio flux index, $F_{10.7}$, which is used as a proxy indicator of the solar EUV flux. Near solar maximum, the level of solar EUV flux is highly variable within a 27-day solar rotation. any ion outflow characteristics depend on specific ionospheric conditions which are modulated by the solar EUV flux, and may therefore exhibit significant variability on the time scale of days during these times. Figure 1b depicts the altitude and epoch coverages of the measurements from the different satellites. Data coverage is often concentrated near the apogee in satellites in highly elliptic orbits, because of spacecraft operational reasons. Likewise, coverage is typically more extensive early in a long mission than late in the mission because of gradual degradation of spacecraft operational resources or instrument performance. Figure 1c depicts the ion energy and epoch coverages on the different satellites. The solid rectangles denote ion composition measurements; the dashed rectangles denote energy-per-charge, non-mass-resolved measurements.

The measurements from the different satellites were acquired in different time periods of the 11-year solar cycles. Significant long term variations in ion flow characteristics exist and hence the level of solar activity at the time of measure-

ments is often an important factor. For intercomparison between different measurements, it is important to take into account their energy coverages and their relative phases (epochs) in the solar cycle. The early ion composition measurements of UFI on S3-3, which pointed to the region near 1 R_E altitude as the primary ion acceleration region, were limited to higher ion energies. As ion composition measurements were extended to lower energies on DE-1 and Akebono, the importance of lower-energy ion acceleration processes at lower altitudes gradually became apparent. Indeed, in the topside ionosphere (~500-2000 km), a number of important acceleration processes are now known to occur. The S3-3 data were acquired in 1976-1977, near the solar minimum and the early ascending phase of Cycle 21. On the other hand, the bulk of DE-1 and Akebono data analyzed to date were acquired near the solar maximum in Cycle 21 and 22, respectively.

2. Ion Sources

2.1. Bulk Ion Flows

2.1.1. *The Polar Wind*

The term "polar wind" was coined by Axford (1968) in analogy to the solar wind, and is used here to refer to the ambipolar outflow of thermal ions on or near open magnetic field lines in the polar ionosphere, as a result of acceleration of the ambient ions by ambipolar electric field and other forces. The concept of light ion escape by plasma diffusion as a result of plasma pressure gradient was first proposed in the pioneering work of Nishida (1966) on the formation of the plasmapause. The existence of H^+ and He^+ polar wind was first confirmed by thermal ion measurements on ISIS-2 (Hoffman and Dobson, 1980), and the existence of heavy O^+ polar wind was recently revealed on Akebono (Abe *et al.*, 1993a). The role of photoelectrons in the dynamics of the polar wind was first discussed in Lemaire (1972), and was recently demonstrated in terms of the electron heat flux and the amplitude of the ambipolar electric field in the sunlit polar wind in Tam *et al.* (1995) and Yau *et al.* (1995). Numerous theoretical models of the polar wind exist; see the excellent reviews by Raitt and Schunk (1983) and by Ganguli (1996) for the earlier and more recent models, respectively.

Figure 2 shows the altitude distributions of the averaged polar wind H^+, He^+, and O^+ ion velocities on Akebono (Abe *et al.*, 1993a). The data were acquired near solar maximum in 1990-1991 when $F_{10.7}$ varied between 120 and 270. At a given altitude, the O^+ velocity was smaller than the He^+ velocity, which was in turn smaller than the H^+ velocity. Both on the dayside and on the nightside, the observed velocity generally increased with altitude, and exhibited large variations from a smooth monotonic trend at times, presumably due to latitudinal or local time variations of ionospheric conditions in localized regions of the polar cap. For the three species, the velocity typically reached 1 km/s near 2000, 3000, and 6000

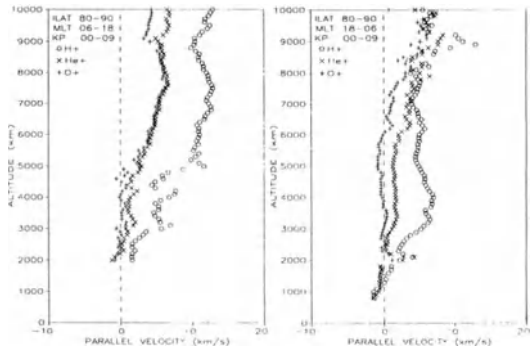

Figure 2. Averaged polar wind ion velocity observed on Akebono above 80° invariant in 1990-1991 near solar maximum, on (a) the dayside (left panel) and (b) the nightside (right panel) as a function of altitude: o = H^+, x = He^+, and + = O^+ (from Abe *et al.*, 1993a).

km, respectively. The rate of velocity increase was largest between 2000 and 4000 km for H^+, and at higher altitudes for He^+ and O^+. Above 5000 km, the observed O^+ polar wind ion velocity increased with altitude, and was ~4 km/s near the Akebono apogee (~10,000 km). The large O^+ velocity near Akebono apogee is in direct contrast with polar wind models which assumed or predicted the O^+ ions to be stationary at all altitudes under typical ionospheric conditions (e.g. Schunk and Watkins, 1981). Horwitz *et al.* (1994) recently reported larger O^+ velocities at higher altitudes (3 R_E geocentric) on DE-1, which they interpreted as centrifugally accelerated polar wind ions. Chandler *et al.* (1991) reported H^+ and He^+ polar wind ion velocities on DE-1 below 4000 km, during periods of high $F_{10.7}$ (>190) in 1981-1983. The DE-1 velocities are in reasonable accord with both the dayside velocities on Akebono and the ISIS-2 measurements at 1400 km (Hoffman and Dobson, 1980), given that they were averaged over both the dayside and the nightside polar ionosphere down to 70° invariant, and may have included contributions from the more energetic ions (<50 eV) and the ion convection velocity component at auroral latitudes.

At a given altitude, the averaged velocity of the polar wind on Akebono was essentially independent of the magnetic activity level; however, its variability was as large as 50% of the mean velocity at active times (Kp > 4) and smaller at quiet times (Abe *et al.*, 1993b). Abe *et al.* (1993b) found that the ion velocity at a given altitude was correlated with the ambient electron temperature. The correlation was believed to reflect the acceleration of the polar wind ions by the ambipolar electric field along the field line, and the dependence of the field amplitude on the electron temperature. The relative increase in ion velocity with electron temperature was largest and the correlation was also strongest at high altitude. This is believed to reflect the cumulative effect of polar wind ion acceleration by the ambipolar electric field along the field line, and provides a direct experimental confirmation

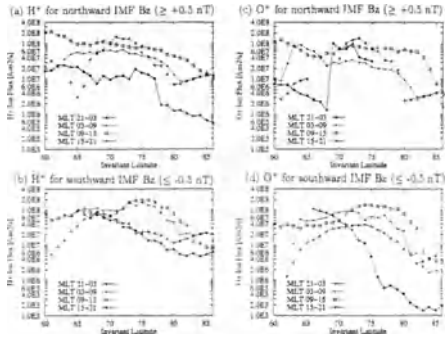

Figure 3. Averaged upward thermal H^+ and O^+ ion flux observed on Akebono at 6000-9000 km in 1990-1991 near solar maximum, and normalized to a reference altitude of 2000 km, as a function of invariant latitude under northward and southward IMF conditions (from Abe *et al.*, 1996).

of the relationship between the magnitude of the ion acceleration and that of the ambipolar electric field at a given altitude.

Figure 3 shows the invariant latitude distributions of the averaged net upward ion flux of observed thermal H^+ and O^+ ions on Akebono in the four MLT sectors, for northward ($B_z > 0.5$ nT) and southward ($B_z < -0.5$ nT) interplanetary magnetic field (IMF), respectively. The measurements were made from early 1990 to late 1991, near the solar maximum, in the 6000-9000 km altitude region, and the measured flux was normalized to a reference altitude of 2000 km. As noted in Abe *et al.* (1996), the polar wind is characterized by thermal energy less than a few eV at Akebono altitudes. In comparison, the "cleft ion fountain" (Lockwood *et al.*, 1985a; see below) has energies in the 2 to 20 eV range, and may co-exist with the polar wind in the polar ionosphere. The observed thermal-energy ions in the polar cap correspond mainly to a polar wind source, but those near the cusp were attributed at least in part to the cleft ion fountain. Figure 3 shows that above 75°, the flux was largest in the noon sector and smallest in the midnight sector; the flux in the noon sector was in the range of 0.1-2 $\times 10^{12} m^{-2} s^{-1}$ for H^+ and slightly smaller for O^+. In the polar cap (>80°), where the flux was due almost exclusively to the polar wind, it was larger on the dayside than on the nightside. The broad latitudinal distributions for both ion species in the dusk sector are in contrast to the corresponding distributions in the midnight sector. This is consistent with the larger ambipolar electric field in the sunlit polar wind in the dusk sector, which is attributed to escaping atmospheric photoelectrons (Yau *et al.*, 1995). In the midnight sector, the ion flux increased with decreasing invariant latitude down to at least 65° for southward IMF, and were peaked near 70°; the observed flux at auroral latitudes is believed to originate from the nightside auroral ionosphere or ions convected from the dayside along the auroral oval.

2.1.2. *Auroral Bulk Upflow*

The existence of bulk thermal O^+ ion upflow in the topside auroral ionosphere (~500 km) was first identified from the scale height analysis of Alouette I sounder data (Lockwood and Titheridge, 1981). Ion upflows in the topside ionosphere (below 1000 km) at velocities exceeding 1 km/s have been observed in the nightside auroral zone and the dayside cleft, both on DE-2 (Heelis *et al.*, 1984) and from ground radars (Wahlund *et al.*, 1992). The observed ion upflow is highly variable in time and location, and generally confined to latitudinally narrow regions. Large upward ion flows generally occurred in regions of large ion convection velocities, and are believed to be dominated by O^+ and at times enhanced in molecular NO^+.

Figure 4 shows the occurrence probability distributions of ion upflows and downflows on the dayside (08-12 MLT) at 600-1000 km on DE-2 (Loranc *et al.*, 1991). The occurrence probability of upflow was generally larger than that of downflow in the auroral zone but smaller in the polar cap on both the dayside and the nightside. Also, its peak spanned the convection reversal on the dayside, and was at a lower latitude and more latitudinally extended on the nightside. The separation between the upflow and downflow regions in this altitude region was more distinct than at lower altitudes, and points to an association of the upflow with the auroral zone, and to the downflow being the return flows of the former on both the dayside and the nightside. Loranc *et al.* (1991) found that the occurrence probability of upflows was several times larger during northward IMF ($B_z > 2$ nT) than during southward IMF ($B_z < -1$ nT; $B_x^2 + B_y^2 < (1\text{ nT})^2$) in the polar cap (above 78° invariant). It was generally greater in the prenoon sector than in the premidnight sector. Also, it is greater in the dawn sector than in the dusk sector during magnetically active periods. The peak occurrence probability for flows exceeding 100 m/s increased and moved equatorward with increasing Kp, from about 0.25 near 78° invariant at Kp $\leq 3-$ to about 0.35 near 70° at Kp ≥ 6 on the dayside; the region of peak flows also broadened. From their dawn-dusk asymmetry and association with large perpendicular ion temperature, Loranc *et al.* (1991) attributed the observed bulk ion upflows to upward ion expansion resulting from frictional heating and perpendicular ion temperature enhancement in regions of intensified $\mathbf{E} \times \mathbf{B}$ drifts, and the subsequent transient change in plasma scale height. However, Liu *et al.* (1995) recently presented examples in which soft (<50 eV) precipitating electrons appear to be the dominant driver of the upflow.

Figure 5 shows the distributions of upward O^+ flux in the noon (1000-1400 LT) and midnight (2200-0200 LT) sectors during equinox, for magnetically quiet (Kp < 2) and active (Kp ≥ 2) conditions respectively (Lockwood and Titheridge, 1981), inferred from observed deviations of plasma scale height from their diffusive equilibrium profiles between 400 and 1000 km on Alouette 1 in 1972-1978 near the solar minimum. Near the F_2 peak, frictional drag between O^+ ions and O atoms dominates the ion motion. For a given neutral temperature, plasma temperature, and plasma temperature gradient, the deviation of the ionospheric scale height

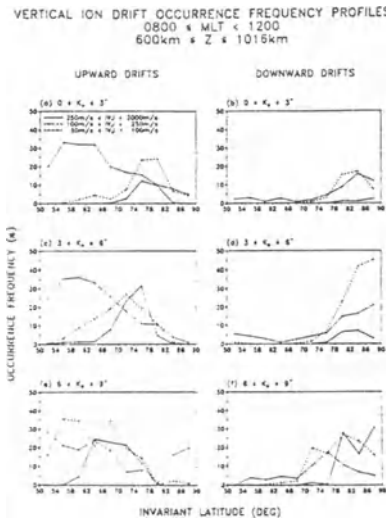

Figure 4. Occurrence probability of bulk thermal O^+ upflows and downflows observed on DE-2 at 600-1000 km and 08-12 MLT, in 1981-1982 near solar maximum, as a function of invariant latitude (from Lorane *et al.*, 1991).

from its diffusive equilibrium value is a function of the upward O^+ ion flux ϕ as a fraction of the limiting flux ϕ_L; ϕ_L is governed by ion-neutral frictional drag.

In Figure 5, the normalized mean dayside flux was $\sim 1 \times 10^{12} m^{-2} s^{-1}$ for Kp < 2 and higher at active times. In the nightside, the flux was upward and peaked at the poleward edge of the statistical auroral oval ($3.5 \times 10^{12} m^{-2} s^{-1}$ for Kp < 2 and $7 \times 10^{12} m^{-2} s^{-1}$ for Kp ≥ 2). During quiet times, ϕ exhibited little variations about its mean value. During active times, it exhibited much larger variations, as reflected by the large statistical deviations in the figure. A number of large flux events were observed in which the inferred ϕ values exceeded $7 \times 10^{12} m^{-2} s^{-1}$, and were associated with the auroral oval. Their occurrence probability was as large as 0.5 between 70° and 80° geomagnetic on the nightside in the winter. They were relatively rare and appeared to cluster around the dayside cleft in the summer. In the largest flux events, ϕ exceeded $2 \times 10^{13} m^{-2} s^{-1}$. Such large fluxes require field-aligned ion velocities of O^+ up to 1 km/s relative to the neutral O, since $\phi \simeq \Delta v_{||} n_i$ where $\Delta v_{||}$ is the field-aligned velocity and n_i is the ion density.

2.2. Ion Energization Processes

A variety of ion energization processes contribute to the formation of suprathermal and energetic upflowing ions from the auroral and polar cap ionosphere. These include ion beams, ion conics, transversely accelerated ions (TAI, a special case of ion conics), and upwelling ions (UWI). In contrast to bulk ion outflow processes

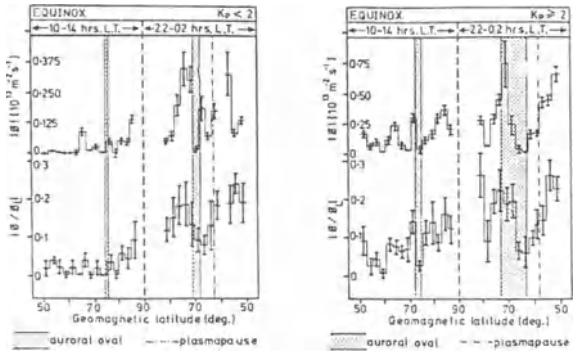

Figure 5. Upward O^+ ion flux distribution at 400-600 km inferred from plasma density altitude profiles on Alouette 1 in 1962-1968 near solar minimum, $| \phi |$, as a function of geomagnetic latitude, for noon and midnight during equinox. ϕ_L is the limiting flux (from Lockwood and Titheridge, 1981).

where the bulk ion distribution participates in the plasma transport, in general only a fraction of the upflowing ions is energized to suprathermal or higher energies in such processes.

2.2.1. *Ion Beams and Conics*

As noted in the introduction, ion beams are upflowing ions which have a peak flux along the upward magnetic field direction, and are generally observed above 5000 km altitude. Note that the ion velocity distribution function of an ion beam, F_i, may have a positive slope, $dF_i/dv_{||} > 0$ where $v_{||}$ is the velocity parallel to the magnetic field, but this feature is usually not apparent or considered in statistical studies. In contrast, ion conics have a peak flux at an angle to the upward magnetic field direction. They have been observed at altitudes down to about 1000 km on sounding rockets and on ISIS-2 (Klumpar, 1979; Yau *et al.*, 1983), and up to several earth radii and beyond on PROGNOZ-7 and ISEE-3 (Hultqvist, 1983; Cattell *et al.*, 1993). Transversely accelerated ions (TAI) have peak pitch angles at or close to 90°, and may be regarded as a special case of ion conics. On the dayside, they are regularly present down to about 3000 km on Akebono (Whalen *et al.*, 1991). On the nightside, they were observed at 1400 km on ISIS-2 (Klumpar, 1979) and ~1700 km on Freja (André et al., 1994) frequently, and down to ~400 km on sounding rockets (Yau *et al.*, 1983; Arnoldy *et al.*, 1992) during active aurora. Ion conics are sometimes interpreted as TAIs from a lower altitude which spiral up the field line as a result of the magnetic mirror force. However, as discussed below, the motion of an ion conic is typically non-adiabatic as it evolves along the field line, and hence it is in general not possible to infer the original source altitude of an observed ion conic by mapping it down the field line assuming adiabatic invariance.

Observed ion beams, ion conics and TAIs typically have energies from 10 eV to a few keV. Lower-energy TAIs do exist and have been reported from sounding

rocket flights (Garbe et al., 1992; Yau et al., 1983), but observationally they are often difficult to investigate in detail from satellite measurements due to limited detector energy resolution, spacecraft velocity, and spacecraft charging.

The occurrence and morphological characteristics of UFIs were the subject of several statistical studies using data from ISIS-1 and -2 (Klumpar, 1979), S3-3 (Ghielmetti *et al.*, 1978; Gorney *et al.*, 1981), DE-1 (Yau *et al.*, 1984, 1985a,b; Kondo *et al.,* 1990; Collin *et al.,*, 1988; Peterson *et al.*, 1992), ISEE-1 (Cattell *et al.*, 1993), Viking (Thelin *et al.*, 1990), Akebono (Miyake *et al.,* 1993, 1996), and Freja (Andre *et al.*, 1997), as well as the topic of overviews by Chappell (1988), Burch (1988), and Shelley and Collin (1991). In the interpretation of statistical UFI distributions, it is important to keep in mind limitations associated with observations of ion beams and TAIs. The limited pitch-angle resolution of ion detectors precludes the distinction of small-angle conics (those within $\sim 10^\circ$ of the magnetic field direction) from ion beams, and of large-angle conics (those within $\sim 10^\circ$ of the perpendicular direction) from TAIs. Also, the energy of a UFI distribution may increase with altitude. For example, conics may be gradually heated as they move upward, and ions may be accelerated by a parallel electric field confined to a rather narrow altitude region. Also, low energy upflowing ion distributions may be energized and appear as beams or conics at higher altitudes. The invariant latitude and MLT of an UFI may also change considerably due to ionospheric convection as it moves upward.

Figure 6 shows the occurrence probability distributions of ion beams and conics, from DE-1 energetic ion composition spectrometer (EICS) data at 8000 to 24000 km altitude for Kp $\leq$ 6+ (Kondo *et al.*, 1990). The UFI distributions were observed both in the statistical auroral oval and in the polar cap (Shelley *et al.*, 1982). Both beams and conics were a common phenomenon, with occurrence frequencies sometimes higher than 50%. The observed H^+ and O^+ UFIs had energies from 10 eV (lower limit of this study) to a few keV, although higher energies occasionally occurred. These findings agree with those from S3-3, ISIS-1 and -2 down to 1000 km altitude (Klumpar, 1979, Ghielmetti *et al.*, 1978, Gorney *et al.*, 1981).

Figure 7 shows the occurrence probability distributions of ion beams and conics at energies between 90 eV and 3.9 keV, as a function of altitude between 1000 and 8000 km from S3-3 (Gorney *et al.*, 1981). These distributions were derived from electrostatic analyzer data and therefore include all ion species. During low magnetic activity, conics were observed uniformly in altitude above 2000 km. At high magnetic activity the occurrence probability increased with altitude; the local minimum at 3000 km is believed to be not statistically significant. The occurrence of ion beams was drastically different, and was generally confined to altitudes above 5000 km. The altitude distributions of beams and conics between 8000 and 24000 km were investigated using DE-1 EICS data (Yau *et al.*, 1984). It was found that the occurrence probability of low energy (<1 keV) ion beams gradually increased with altitude. Above about 15000 km, the occurrence probability of low-energy conics decreased with increasing altitude.

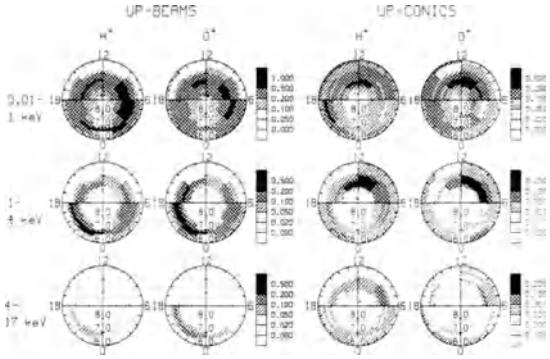

Figure 6. Occurrence probability of H^+ and O^+ ion beams and conics observed on DE-1 at 8000-24000 km in 1981-1986 in the declining phase of the solar cycle, as a function of invariant latitude and MLT. Kp $\leq$ 6+ (from Kondo et al., 1990).

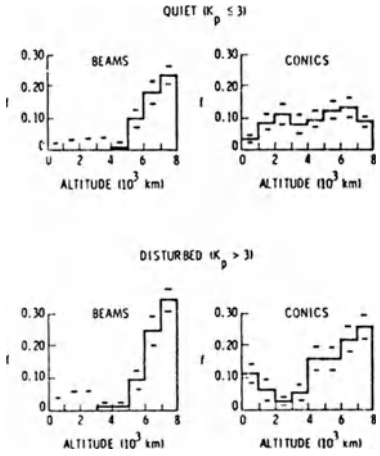

Figure 7. Occurrence probability of ion beams and conics at 0.09-3.9 keV observed on S3-3 in 1976 near solar minimum, from electrostatic analyzer data and integrated over all local times above 54° invariant, as a function of altitude for low and high magnetic activity (from Gorney *et al.*, 1981).

Distributions of UFI may evolve in different ways as they move upward. The occurrence of conics with energies of tens of eV peak at 1 R_E. In comparison, beams of similar energies occur mainly at higher altitudes, indicating an evolution of the UFI distributions as they move upward (Giles *et al.*, 1994). It is clear that ion conics often do not start as TAI distributions heated within a narrow altitude range and then move adiabatically up the geomagnetic field. Statistical studies of the evolution of ion conics along the field line using DE-1 (Peterson *et al.*, 1992) and Akebono data (Miyake *et al.*, 1993, 1996) show that the energy of the ion conics increases with altitude, while their apex angle (angle from the upward magnetic

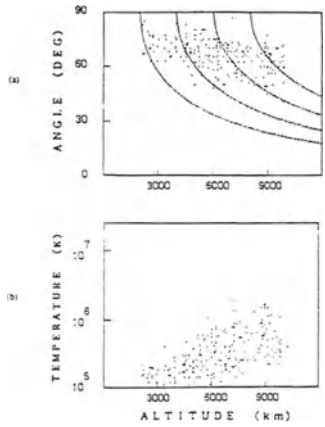

Figure 8. Scatter plot of (a) apex angle and (b) temperature of restricted ion conics in the dayside auroral zone observed on Akebono as a function of altitude. The curves in (a) represent the altitude variation expected from adiabatic invariance along the geomagnetic field (from Miyake *et al.*, 1993).

field direction) decreases with altitude much more slowly than expected from adiabatic motion. In the so-called "restricted" ion conics, the ion distribution has a well defined conical (apex) angle. On the other hand, in the so-called "extended" or "bimodal" conics (Klumpar *et al.*, 1984), the apex angle increases with energy, and the lower energy ions have a significant flux along the field line.

Figure 8 is a scatter plot of the temperature (averaged energy) and apex angle (angle from the magnetic field) of restricted ion conics observed on Akebono in the dayside auroral zone (Miyake *et al.*, 1993). The four curves in Figure 8a represent the expected decrease in the apex angle with altitude assuming adiabatic invariance along the geomagnetic field. The observed decrease was much slower. The temperature of the conics, which was derived from the measured ion velocity distribution in the 0.03-10 keV energy range, increased from $\sim$10 eV near 2000 km to $\leq$ 100 eV near 9000 km. Both these findings are consistent with gradual heating of the conical distributions as they move upward.

The heating of conics depends on some "external" energy source, while heating of beams may depend on "internal" energy exchange between beams of different ion species. Beams of ions with different masses that are associated with a parallel potential drop below the spacecraft should, as a first approximation, all have the same energy, but this is not always the case observationally. Collin *et al.* (1987) compared this simple prediction with the observed O^+ to H^+ ion beam energy ratio using data from both S3-3 and DE-1. Figure 9 is a scatter plot of the observed O^+ to H^+ ion beam energy ratio versus the corresponding ion flux ratio on DE-1. The observations spanned the solar maximum and the declining phase of the solar cycle. The O^+ and H^+ beam energies were comparable in cases where their fluxes were also comparable, but the O^+ beams had higher energies than the H^+ beams in cases

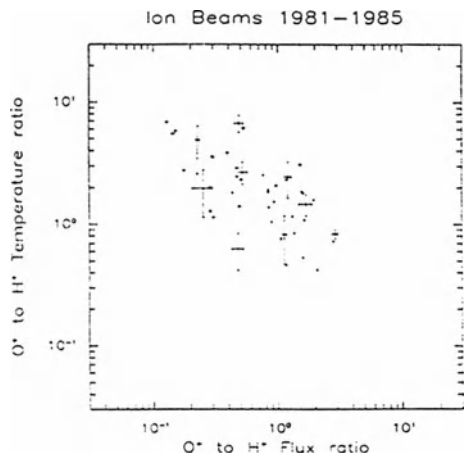

Figure 9. Scatter plot of O^+/H^+ mean energy ratio versus flux ratio in observed ion beams on DE-1, showing a strong tendency for decrease in the energy ratio as the composition of the ion beam becomes dominated by O^+. Dots: data from 1981-1982; crosses: data from 1984-1985 (from Collin *et al.*, 1987).

where the O^+/H^+ flux ratio was smaller than unity, as was observed on S3-3 near solar minimum. As will be shown in Figure 10 and 11 below, the O^+ dominates the beam composition near solar maximum but is a minor component near solar minimum. A reasonable explanation of the varying beam energy ratio is that the O^+ and H^+ beams are initially accelerated by parallel electric field to the same energy and that the difference in their initial velocity triggers a wave instability which accelerates the O^+ ions at the expense of the energy from the H^+ ions only when O^+ is a minor component, as suggested by the simulations of Bergmann and Lotko (1986).

On DE-1, Yau *et al.* (1985a) observed significant seasonal and long-term variations in the O^+ UFI distributions, which were attributed to changes in the incident solar EUV flux on the atmosphere in different seasons of the year and at different phases of the 11-year solar cycle. The corresponding variations in the H^+ UFI distributions were much smaller. Figure 10 shows the averaged active-time ($3- \leq Kp \leq 5+$) H^+ and O^+ UFI occurrence frequencies at DE-1 altitudes between September 1981 and May 1984 (top and middle panels), when the monthly mean solar radio flux index $F_{10.7}$ decreased from about 250 to 100 (bottom panel). In the top two panels, the solid, open, and semi-open circles denote winter, summer, and equinox data, respectively. The upper histogram shows the occurrence probability for all UFI events; the lower one is the frequency for intense events exceeding $10^{11} m^{-2} s^{-1}$ in flux. The occurrence probability of the O^+ UFI decreased by about a factor of 2 from near solar maximum in 1981 to the declining phase in 1984. The decrease in frequency of the intense events was even larger, and about a factor

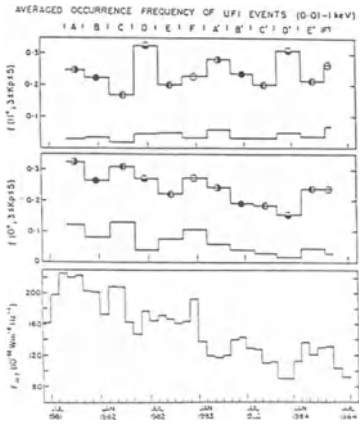

Figure 10. H^+ and O^+ UFI occurrence frequencies observed on DE-1 at 8000–24000 km and monthly mean solar radio flux at 10.7 cm between 1981 and 1984, showing the solar cycle and seasonal dependences of O^+ UFI occurrence. Solid circles: winter data; open circles: summer data; vertically semi-open circles: equinox data; see text (from Yau *et al.*,, 1985a).

of 3-4. There was no discernible change in the H^+ occurrence probability during the same period. Throughout the period, the occurrence probability of O^+ UFI was significantly higher in the summer periods than in the winter periods, the frequency of intense events being about a factor of 2 larger. The altitude range of perpendicular heating also appears to depend on the season. On ISIS-2 at 1400 km, Klumpar (1979) found that the occurrence probability of TAI at 1400 km peaked at the winter midnight sector. Yet, on ISIS-1 near 3000 km, most TAI events were observed in the dayside near summer solstice.

The DE-1 observations indicate an upward shift in the region of perpendicular O^+ energization during periods of increased solar radiation. The occurrence probability of O^+ TAI between 8000 and 14000 km increased by a factor of 3 near solar maximum; the O^+ conic abundance (conic to beam ratio) in the 8000 to 24000 km range also increased (Yau *et al.*, 1985a). The increase in occurrence probability, intensity, and conic abundance of O^+ UFI in periods of increased solar activity resulted in large increases in the corresponding flux and ion outflow rate.

Figure 11 shows the upward fluxes of low-energy (0.01-1 keV) H^+ and O^+ UFIs observed by DE-1, as a function of invariant latitude in each of the 4 MLT sectors during active times ($3 \leq Kp \leq 5$; Yau *et al.*, 1985b). The invariant latitude distributions for both H^+ and O^+ were similar, and peaked near 78° invariant in the noon sector. In the midnight sector the fluxes peaked at lower invariant latitudes (near 70°), and were smaller by a factor of 2 (a factor of 3-5 at quiet times). Data are shown for two periods of different solar activity. The H^+ fluxes in the two periods were similar, while the O^+ flux increased with solar activity. As shown in Yau *et*

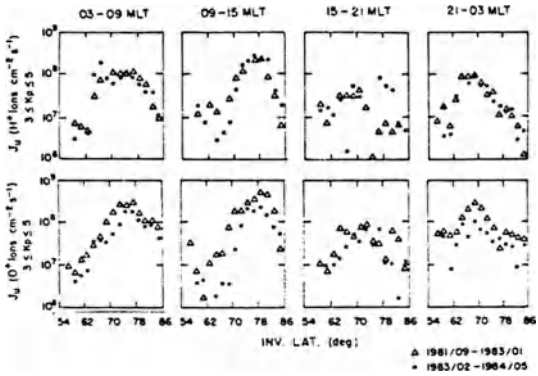

Figure 11. Upward fluxes of H^+ and O^+ UFI below 1 keV observed on DE-1 at 8000-24000 km and normalized to a reference altitude of 1000 km, as a function of the magnetic Kp index. Triangles: data from September 1981 to January 1983, near solar maximum; dots: data from February 1983 to May 1984, in the declining phase of Solar Cycle 21 (from Yau *et al.*, 1985b).

al. (1985b), the observed upward flux was much larger than the downward flux, the upward to downward flux ratio being ~3-5 for H^+ and ~10-20 for O^+.

The influence of solar EUV radiation on O^+ outflow and the energization altitude can be understood in terms of ionospheric and atmospheric scale heights. An enhanced solar EUV flux will heat both the atmosphere and the ionsophere, and increase the scale heights of their respective constituents. This is important for ion outflow since for ion heating mechanisms to be efficient, ions must be present at a sufficiently high altitude where the density is sufficiently low and the effect of collisions and charge-exchange is negligible. Higher solar EUV flux in the summer and near solar maximum increases the scale heights of both O^+ and O. This results in a larger increase in density at high altitude for O and O^+ than for H and H^+. Consequently, more O^+ ions occur at high altitudes where they can be heated and escape. The effect on H^+ ion acceleration is much smaller, because of the smaller increase in H^+ density and the increased effect of resonant charge exchange between H^+ and O.

Ion heating often occurs preferentially in regions of low plasma density. This is evident from studies of individual events (see André and Yau, 1997, this issue). Such a preference is perhaps not surprising since in a lower density plasma, more energy is available to heat an individual ion for a given incident energy flux and local instabilities are more easily triggered for a given current density.

Increased geomagnetic activity has somewhat similar influence on O^+ UFI as increased solar radiation, as it may increase the ionospheric scale height and O^+ density at high altitude through increased auroral ionization and Joule heating; it also makes more energy available for ion energization. This results in a large increase in O^+ UFI flux. The corresponding increase in H^+ UFI flux is smaller.

2.2.2. *Upwelling Ions*

In the superthermal energy range (10-100 eV), differences exist in the energization characteristics between the dayside and the nightside auroral upflowing ions. In the nightside, the observed energization is in the perpendicular direction. The transverse heating affects the bulk of the ion distribution, and perpendicular temperatures of the order of 10 eV are produced. Often, the rate of "folding" of the evolving conical distribution decreases with increasing mass per unit charge, reflecting the larger gravitational effects on the heavier ions in counteracting the magnetic mirror force. In contrast, the dayside events display the effects of both parallel and perpendicular energization from one to tens of eV, resulting in an asymmetry in the ion distribution toward the upward magnetic field direction. At 2000-5000 km on DE-1, the core O^+ distribution was observed to exhibit transverse heating to $\sim$10 eV and carry significant upward number flux ($>10^{12}m^{-2}s^{-1}$) and heat flux ($>3\times10^{-7}$J $m^{-2}s^{-1}$). All observed species (H^+, He^+, O^+, O^{++} and N^+) were heated, and they were termed "upwelling ions" (UWI, Lockwood *et al.*, 1985b). The distinction between upwelling ions in the dayside and transversely accelerated low energy ion conics is not sharp.

Upwelling ions are the most persistent suprathermal ion outflow feature in the cleft region. Craven *et al.* (1985) have shown that even molecular ions (N_2^+, O_2^+, and NO^+) can be injected into the magnetosphere in the upwelling ion region. Pollock *et al.* (1990) presented a detailed study of an upwelling ion event in which the equatorward edge was closely associated with that of a convection velocity shear region and the observed plasma was dominated by large upward O^+ ion flux ($\sim10^{13}m^{-2}s^{-1}$).

On DE-1, the upwelling O^+ ions were observed exclusively in the morning sector of the auroral oval and the lower latitudes of the polar cap. Integrated over the altitude range below $3R_E$ geocentric, the occurrence probability of upwelling ions was up to 0.6 between 75° and 80° invariant (Lockwood *et al.*, 1985b). The integrated probability over invariant latitudes in the morning sector was very close to unity, i.e., upwelling ions were almost always present but their location varied. The region of upwelling ions shifted slightly to higher invariant latitude and the observed ion flow gradually became more field aligned with increasing altitude. The occurrence probability of the field-aligned flow was small (<0.1) in the morning sector, but increased to 0.3 in the afternoon sector. Lockwood *et al.* (1985a) concluded that the ions in the field-aligned flows should be spatially dispersed across the polar cap according to their time of flight, and termed the flow "cleft ion fountain" in analogy to a fountain in the wind.

Pollock *et al.* (1990) analyzed the plasma parameters of 39 upwelling ion events on DE-1, and found O^+ to be the dominant ion species in all cases. Figure 12 is a scatter plot of the measured upward ion flux versus ion density at the low-latitude edge of UWIs for several ion species. The scatter plot shows that at 1.3-2.1 R_E geocentric, the O^+ density was $\sim10^9$ m^{-3} and its upward velocity was about 1-3 km/s. The H^+ density was $\sim10^8$ m^{-3} and its upward velocity was about

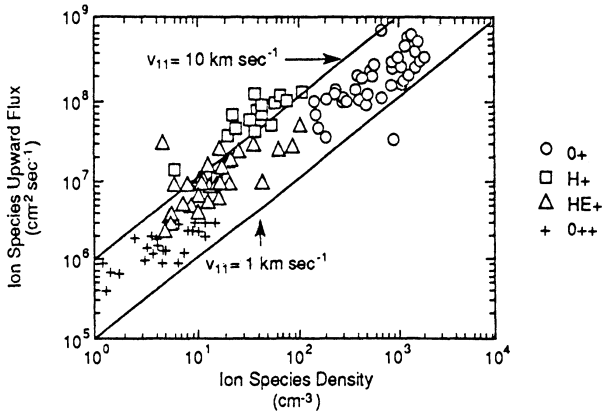

Figure 12. Scatter plot of upward ion flux versus ion density for several upwelling ion species observed on DE-1 at 1.3 to 2.1 R_E geocentric (from Pollock *et al.*, 1990).

10 km/s. The large O^+ density is indicative of increased ionospheric scale height and associated bulk ionospheric ion heating at lower altitudes. The O^+ flux was typically 10^{13} ions $m^{-2}s^{-1}$, far in excess of the polar wind O^+ flux (Abe *et al.*, 1993a), and was generally independent of the orientation of the IMF (B_z) and the location (MLT) of the upwelling ions. Pollock *et al.* (1990) found the UWI O^+ flux and its occurrence probability to be not dependent on the value of B_z in the preceding hours, even though its invariant latitude location correlates strongly with the latter. The observed upwelling O^+ fluxes on DE-1 imply that upward field-aligned ion fluxes on the order of $10^{13}m^{-2}s^{-1}$ should be observed in the ionosphere below the events. Indeed, Lockwood *et al.* (1985c) reported upward field-aligned ion flows of 500 m/s velocity at 900 km on DE-2, on dayside cusp field lines below a region of upwelling ions at 22,000 km observed on DE-1.

Most observations of ion outflows were focussed predominantly on H^+ and O^+ ions, which are typically the two major ion species. However, the composition of both thermal and energetic upflowing ions is highly variable, not only in the O^+/H^+ ratio but also in the relative abundance of ion species which are usually considered minor species. On DE-1, Nagai *et al.* (1984) reported a variable He^+/H^+ polar wind ratio between 0.01 and unity in an orbit pass near 3 R_E geocentric, and Collin *et al.* (1988) observed energetic upflowing He^+ ions about half as often as either H^+ or O^+. On Akebono, Yau *et al.* (1991) found thermal ion flux ratio of 0.1-0.3 for He^+/H^+, 0.1-1.0 for N^+/O^+, and 0.1-0.5 for O^{++}/O^+. The enhancement of N^+ relative to O^+ was largest during disturbed times, particularly in the presence of molecular upflowing ions (Yau *et al.*, 1993). Figure 13 shows a mass spectrum of the observed upflowing ions in the dayside auroral zone near Akebono apogee (76°Λ, ~10 MLT, 9000 km altitude) during the main phase of a large magnetic storm. Intense and comparable fluxes of low-energy, upward, field-aligned H^+, N^+ and O^+ ions were present, as were smaller fluxes of N_2^+, and NO^+, He^+ and O^{++}.

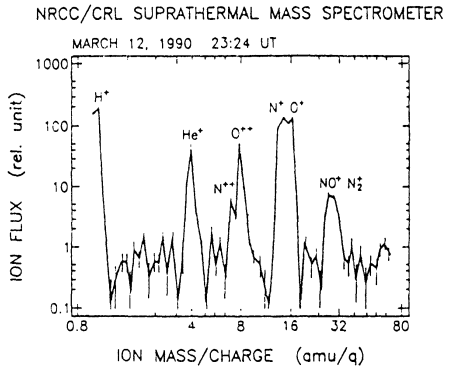

Figure 13. Observed upflowing ion mass spectrum on Akebono in the dayside auroral zone at 9000 km altitude during a magnetic storm, showing the presence of comparable fluxes of H^+, N^+, and O^+ ions and smaller fluxes of He^+, O^{++}, and molecular NO^+ and N_2^+ ions.

Peterson *et al.* (1994) showed that the observed molecular ions must have acquired an energy of the order of 10 eV at ionospheric (F-region) altitudes, in a time short compared with the local dissociative recombination time of the ions, which is of the order of minutes. This points to the likely existence of an as yet unidentified, fast ion energization process at the F-region or topside ionosphere. The large variability in the upflowing ion composition is attributed to variations in both the ambient ion composition at ionospheric altitudes and the height of ion extraction (acceleration), in response to variations in the solar and magnetospheric energy input. The incident solar EUV flux affects the atmospheric and ionospheric scale heights. The precipitating magnetospheric electron energy distribution determines the height of auroral ionization. The nature of incident wave or particle energy input governs the altitude and mode of ion energization.

3. Total Ion Outflow

The ion outflow rate from a bulk ion outflow or ion energization process may be estimated by normalizing the measured ion flux distributions at different altitudes to a reference altitude, to take into account the variation of the (divergent) magnetic flux tube area with altitude, and by integrating the normalized net upward ion flux distribution over all MLT and invariant latitudes in the polar ionosphere. At a given altitude, an energetic ion distribution may be considered to consist of three distinct populations: newly outflowing terrestrial ions, upward and downward mirroring ions, and downward precipitating "magnetospheric" ions. It is not possible to simply equate the upward flux in the upward loss cone with the net terrestrial ion flux, since ion beams may undergo pitch angle diffusion or experience additional transverse heating, giving rise to pitch angle widths wider than the loss cone.

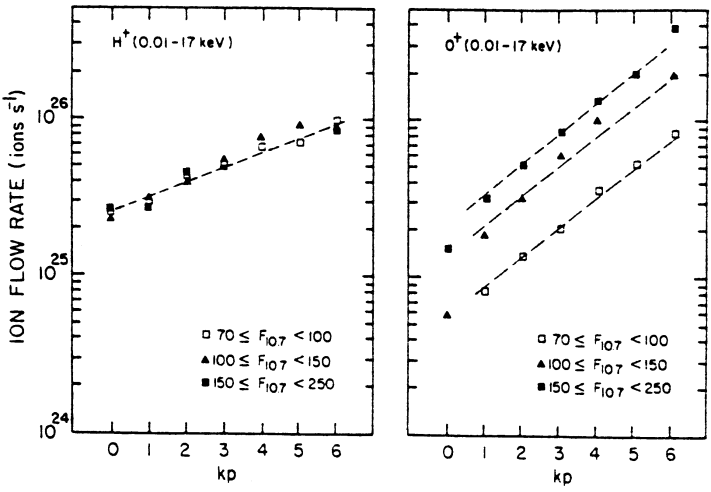

Figure 14. Outflow rates of H^+ and O^+ upflowing ions at 0.01-17 keV observed on DE-1, integrated over all MLT and invariant latitudes above 56° in both hemispheres, as a function of the magnetic Kp index, for different ranges of $F_{10.7}$ (from Yau *et al.*, 1988).

Instead, one must integrate the measured ion flux distribution over the full 180° pitch angle range.

Figure 14 shows the ion outflow rates of H^+ and O^+ ions at 0.01-17 keV observed on DE-1, integrated over all MLT and invariant latitude above 56° in both hemispheres, as a function of the magnetic Kp index, for three $F_{10.7}$ ranges (Yau *et al.*, 1988). The O^+ rate increased exponentially with Kp, by a factor of 20 from Kp = 0 to 6, and exceeded 3×10^{26} ions s^{-1} at times of high solar and magnetic activity. The rate at low solar activity was about a factor of 4 smaller than that at high activity. In contrast, the H^+ rate in the three $F_{10.7}$ ranges was very similar. For all three $F_{10.7}$ ranges, the dependence of the O^+ rate on Kp was similar. In comparison, the H^+ rate increased with Kp more moderately, by a factor of 4 from Kp = 0 to 6. Since the Kp index is a quasi-logarithmic measure of magnetic disturbance, the exponential increase of the ion outflow rates suggests a quasi-linear dependence of UFI outflow with magnetic activity. Yau *et al.* (1988) found a similar exponential dependence of the outflow rates on the Dst index, and power law dependence on the AE index. They also discussed the relative merits and limitations of parametrizing the ion outflow rates using the different indices.

Using the occurrence probability data of Lockwood *et al.* (1985b) on DE-1 for upwelling ions, Pollock *et al.* (1990) estimated the outflow rate of upwelling ions from the two hemispheres at 2×10^{25} O^+, 0.5×10^{25} H^+, and $\sim 0.1 \times 10^{25}$ He^+ ions s^{-1}, for northern hemispheric spring equinox conditions in 1982 near solar

maximum. This compares with a total net auroral zone outflow rate of 2-4 $\times 10^{25}$ H^+ and 1-20 $\times 10^{25}$ O^+ ions at 0.01-17 keV at higher altitudes (Yau *et al.*, 1988).

Abe *et al.* (1996) integrated the observed upward thermal ion flux distributions on Akebono (c.f. Figure 3 above), to estimate outflow rates of thermal-energy H^+ and O^+ in the polar cap and the auroral zone. Their rates are believed to be lower estimates, since they have not been corrected for perpendicular (convection) drifts and for effects of spacecraft potential. In the polar cap (above 75°), where the observed ions were believed to be composed primarily of the polar wind, the H^+ and O^+ outflow rates were essentially independent of Kp, and were on the order of 8×10^{24} s^{-1} and 6×10^{24} s^{-1}, respectively. In contrast, at auroral latitudes (below 75°), the O^+ rate increased exponentially with Kp, by a factor of about 5 from Kp = 0 to 7. The corresponding increase in the H^+ rate was less than a factor of 2.

4. Summary and Discussions

Satellite observations in the past three decades have revealed and confirmed the occurrence of a variety of bulk ion outflows and ion energization processes in the polar ionosphere. These processes constitute a dominant source of ionospheric plasma to the magnetosphere. They include the polar wind, auroral bulk ion flows, and perpendicular and parallel ion energization mechanisms that produce ion beams, ion conics including transversely accelerated ions, and upwelling ions. In principle, each type of distribution may be identified by the ion energy and angular distribution and spatial location. In practice, however, the observed ion distribution at a given altitude often consists of ions from more than one source. Due to ion convection and gradual heating as the different sources of ions move upward, it is not always possible to delineate the contributions from the respective sources in an observed distribution.

Our current knowledge of the occurrence, characteristics, variability and interrelationships of the various ion outflow processes is summarized as follows:

1. The polar wind occurs essentially at all times and at all latitudes poleward of the plasmasphere, being driven by ambipolar electric field and other forces along or near open magnetic field lines. It is characterized by energy less than a few eV and temperature of a fraction of eV, is composed of significant components of H^+, He^+, and O^+, is supersonic above 1500-2000 km, and has larger velocity on the dayside than on the nightside. Its ion outflow rate is ~0.5-1.0 $\times 10^{25}$ H^+ and O^+ ions s^{-1} in the polar cap (>75° invariant) near solar maximum.
2. Bulk ion flow occurs at auroral latitudes, from ~400 km to 1500 km altitude or higher, at velocities up to ~1 km/s and upward fluxes up to $10^{13} m^{-2} s^{-1}$. It is possibly driven by frictional heating of O^+ ions at lower altitudes or increased electron temperature in auroral electron precipitation region. It is normally dominated by O^+ ions, and occasionally has a significant component of NO^+

ions. The bulk of ions in the flow do not reach escape velocity, but do have sufficient energy to reach ion energization regions at higher altitudes.

3. The process of transverse ion acceleration energizes ions predominantly in the perpendicular direction to energies up to hundreds of eV (sometimes keV), via a number of energization mechanisms (see the companion paper, André and Yau, 1997). It occurs both on the dayside and on the nightside, and in general acts on all ion species. The altitude region of ion acceleration is dependent on the season and the solar activity level, and extends down to ~400 km on the nightside in the winter during active aurora. The acceleration often occurs over an extended altitude region. This results in the ions being energized gradually as they evolve along the field line, and appear as ion conics of increasing energy and slowly decreasing conic (apex) angle.
4. Upwelling ions on the dayside are typically less energetic but have higher fluxes than transversely accelerated ions on the nightside. They have characteristic temperatures of a few eV and a parallel energy component, resulting in upward ion fluxes exceeding $10^{12}\mathrm{m}^{-2}\mathrm{s}^{-1}$ in the 2000-5000 km altitude region.
5. Parallel ion acceleration occurs primarily above 5000 km, and leads to the occurrence of field-aligned ion beams up to the few keV range. It is more common in the dusk sector, resulting in a dawn-dusk asymmetry in the occurrence probability distribution of ion beams in favor of the dusk sector.
6. The combination of parallel and perpendicular ion energization processes result in the frequent occurrence of upflowing ion beams and conics which are dominated by H^+ and O^+ ions below 1 keV at high ($<4R_E$) altitude. The characteristics of these upflowing ions are highly dependent on geomagnetic and solar activity conditions.
   a) Near solar maximum, the O^+ flux is significantly larger and the H^+ flux is moderately smaller relative to solar minimum, resulting in a factor of up to 10 variation in the O^+/H^+ ratio.
   b) Near solar maximum, conics are more abundant. Also, energetic (keV) ion beams are less frequent (or shifted to higher altitudes), and the O^+ and H^+ ion beams are comparable in energy and flux. In contrast, the O^+/H^+ flux ratio is smaller than unity and the O^+ beam has higher energy than the H^+ beam near solar minimum, possibly due to a microinstability that may not occur when the O^+ and H^+ densities are similar.
   c) The O^+ flux is strongly dependent on geomagnetic activity. It increases exponentially with the magnetic Kp index, by a factor of 20 from Kp = 0 to 6. The corresponding increase in the H^+ flux is a factor of 4.
   d) The mass composition of upflowing ions is highly variable. It is dominated by H^+ and O^+ at quiet times. However, the flux of the minor ion species, notably He^+, N^+, O^{++}, NO^+, and N_2^+, often exceeds 0.1 and sometimes approaches 0.5-1.0 of the H^+ or O^+ flux.

Table I summarizes the current estimates of outflow rates of the polar wind, upwelling ions, and energetic upflowing ions including ion beams, ion conics,

and TAIs. It updates a similar table in Chappell (1988) using data that have since become available. The rates in the table include the contributions from both hemispheres. Only solar maximum data are available for both the polar wind and the upwelling ions. The polar wind outflow rates are derived from the thermal ion outflow data on Akebono (Abe *et al.*, 1996). As discussed above, these data are believed to be lower estimates, and were divided into the auroral and the polar cap components at 75° invariant. The auroral component is believed to contain a significant component of upwelling ions (or the cleft ion fountain). The H^+ rate in Table I is a factor of 3-4 smaller than the estimate in Chappell (1988), which was derived by assuming uniform polar wind ion flux down to 51° invariant. The upwelling ion data are from Pollock *et al.* (1990). As noted above, these estimates were derived from occurrence probability and typical flux data, and are approximate averages over all magnetic activity conditions. The energetic upflowing ion data are derived from DE-1 measurements (Yau *et al.*, 1985b, 1988), and include both solar maximum and solar minimum data. These data assumed 80° and 76° invariant for the quiet-time and active-time boundary, respectively, between the auroral zone and the polar cap. Note that the observed upflowing ions extended down to 10 eV, and therefore overlapped with the high-energy (>10 eV) upwelling ions; the upwelling ions also overlap with the polar wind ions in the eV energy range. The overlap in ion energy ranges and the difference in assumed polar cap boundary complicate the quantitative comparison. Nevertheless, the table shows that in both the auroral zone and the polar cap, the observed "polar wind" thermal H^+ ion outflow rate is comparable to that of the energetic (>10 eV) upflowing H^+ ions at higher altitudes at both quiet and active times; the same is also true for O^+ at quiet times. This suggests that the thermal polar wind plasma at Akebono altitude (<10000 km), including the contribution from the cleft ion fountain, is a sufficient source (and is likely the primary source) of cold plasma for the energetic upflowing ions at higher altitudes both in the auroral zone and the polar cap. Furthermore, it suggests that a significant fraction of the thermal plasma is energized and becomes energetic upflowing ions above escape energy below 4 R_E altitude. This is significant as it implies that ions from the ionosphere that ultimately escape do not necessarily have to reach escape velocity at ionospheric altitudes. The table also shows that at active times near solar maximum, the thermal O^+ ion outflow rate is small compared with the corresponding UFI outflowing rate. This suggests that a significant fraction of energetic O^+ UFI may be energized to beyond ~60 eV (the upper energy limit of the Akebono polar wind measurements) at Akebono altitudes (<10000 km).

In conclusion, several important questions and gaps in our knowledge remain:

1. What fraction of the observed "polar wind" thermal plasma at Akebono altitude do the upwelling ions constitute? Detailed 3-dimensional analyses of the observed ions in different regions of the polar cap and in a variety of ion convection patterns are needed to address this question.
2. How is the thermal plasma transported from the dayside to the nightside as it flows upward? Specifically, does it convect across the polar cap in a predom-

Table I
Ion Outflow Rates (10^{25} ions s^{-1}; see text).

	Quiet	(Kp=0-2)	Active	(Kp=3-5)
	H^+	O^+	H^+	O^+
Polar Wind (solar max)				
Polar cap	0.9-1.1	0.5-0.7	0.6-0.8	0.6-0.7
Auroral	1.8-2.6	0.8-1.2	3.5-4.0	1.5-2.2
Upwelling ions (solar max)				
Cleft	~0.5	~2.0	~0.5	~2.0
Upflowing ions (solar max)				
Polar cap	0.3-0.5	0.3-1.0	1.2-1.8	3.0-6.0
Auroral	2.0-3.1	1.2-4.1	3.9-6.2	7.0-14.0
Upflowing ions (solar min)				
Polar cap	0.5-0.8	0.1-0.3	1.6-2.6	0.7-2.7
Auroral	1.8-2.8	0.4-0.9	3.4-5.5	1.3-3.6

inantly anti-sunward direction or along L-shells? This has implications on the feeding of cold plasma to the so-called "parallel" auroral acceleration region on the nightside.

3. Is the overall ion outflow dependent on the interplanetary magnetic field (IMF) and the dynamic pressure of the solar wind? The orientation of the IMF affects the ionospheric convection pattern in the polar ionosphere, and is expected to have a direct influence on the transport of the outflowing ions. The dynamic pressure of the solar wind is believed to affect the magnetospheric energy and momentum input to the polar ionosphere. The ionospheric oxygen ion density in the plasma sheet was found to be correlated with the solar wind energy flux (Lennartsson *et al.*, 1995), while its possible B_z dependence was less evident. We have no observational knowledge on the IMF dependence of energetic upflowing ions at low altitude, and little knowledge on that of the polar wind and upwelling ions. Statistical analyses of existing data using recently available IMF data may well provide important clues to this question.
4. How dependent are the polar wind and upwelling ions on solar activity level?
5. How often do some of the minor upflowing ion species become comparable to the major ion species, and when?
6. What fraction if any of the thermal plasma remains un-energized up to very high altitudes, and therefore may have evaded detection so far?

The answers to these questions may well be found in existing data which remain to be analyzed.

Acknowledgements

This work was supported in part by Natural Science and Engineering Research Council (NSERC) Research Grant OGP0183733.

References

Abe, T., Whalen, B. A., Yau, A. W., Horita, R. E., Watanabe, S., and Sagawa, E.: 1993a, 'EXOS-D (Akebono) SMS Observations of the Polar Wind', *J. Geophys. Res.* **98**, 11,191.

Abe, T., Whalen, B. A., Yau, A. W., Watanabe, S, Sagawa, E, and Oyama, K. I.: 1993b, 'Altitude Profile of the Polar Wind Velocity and its Relationship to Ionospheric Conditions', *Geophys. Res. Lett.* **20**, 2825.

Abe, T., Watanabe, S., Whalen, B. A., Yau, A. W., and Sagawa, E.: 1996, 'Observations of Polar Wind and Thermal Ion Outflow by Akebono/SMS', *J. Geomag. Geoelectr.* **48**, 319.

André, M. and Yau, A. W.: 1997, 'Theories and Observations of Ion Energization and Outflow in the High Latitude Magnetosphere', *Space Sci. Rev.*, this issue.

André, M., Norqvist, P., Vaivads, A., Eliasson, L., Norberg, O., Eriksson, A. I., and Holback, B.: 1994, 'Transverse Ion Energization and Wave Emissions Observed by the Freja Satellite', *Geophys. Res. Lett.* **21**, 1915.

André, M., Norqvist, P., Andersen, L., Eliasson, L., Eriksson, A. I., Blomberg, L., Erlandson, R. E., and Waldemark, J.: 1997, 'Ion Energization Mechanisms at 1700 kilometer in the Auroral Region', *J. Geophys. Res.*, submitted.

Arnoldy, R. L., Lynch, K. A., Kintner, P. M., Vago, J., Chesney, S., Moore, T. E., and Pollock, C. J.: 1992, 'Bursts of Transverse Ion Acceleration at Rocket Altitudes', *Geophys. Res. Lett.* **19**, 413.

Axford, W. I.: 1968, 'The Polar Wind and the Terrestrial Helium Budget', *J. Geophys. Res.* **73**, 6855.

Bergmann, R. and Lotko, W.: 1986, 'Transition to Unstable Flow in Parallel Electric Fields', *J. Geophys. Res.* **91**, 7033.

Burch, J. L.: 1988, 'Energetic Particles and Currents: Results from Dynamics Explorer', *Rev. Geophys.* **26**, 215.

Cattell, C. A., Nguyen, T., Temerin, M., Lennartsson, W., and Peterson, W. K.: 1993, 'Effects of Solar Cycle on Auroral Particle Acceleration', *Geophys. Monogr. Ser.* **80**, 219.

Chandler, M. O., Waite Jr., J. H., and Moore, T. E.: 1991, 'Observations of Polar Ion Outflows', *J. Geophys. Res.* **96**, 1421.

Chappell, C. R.: 1988, 'The Terrestrial Plasma Source: A New Perspective in Solar-Terrestrial Processes from Dynamics Explorer', *Rev. Geophys.* **26**, 229.

Collin, H. L., Peterson, W. K., and Shelley, E. G.: 1987, 'Solar Cycle Variation of Some Mass Dependent Characteristics of Upflowing Beams of Terrestrial Ions', *J. Geophys. Res.* **92**, 4757.

Collin, H. L., Peterson, W. K., Drake, J. F., and Yau, A. W.: 1988, 'The Helium Components of Energetic Terrestrial Ion Upflows: Their Occurrence, Morphology, and Intensity', *J. Geophys. Res.* **93**, 7558.

Craven, P. D., Olsen, R. C., Chappell, C. R., and Kakani, L.: 1985, 'Observations of Molecular Ions in the Earth's Magnetosphere', *J. Geophys. Res.* **90**, 7599.

Ganguli, S. B.: 1996, 'The Polar Wind', *Rev. Geophys.* **34**, 311.

Garbe, G. P., Arnoldy, R. L., Moore, T. E., Kintner, P. M., and Vago, J. L.: 1992, 'Observations of Transverse Ion Acceleration in the Topside Auroral Ionosphere', *J. Geophys. Res.* **97**, 1257.

Ghielmetti, A. G., Johnson, R. G., Sharp, R. D., and Shelley, E. G.: 1978, 'The Latitudinal, Diurnal, and Altitudinal Distributions of Upward Flowing Energetic Ions of Ionospheric Origin', *Geophys. Res. Lett.* **5**, 59.

Giles, B. L., Chappell, C. R., Moore, T. E., Comfort, R. H., and Waite Jr., J. H.: 1994, 'Statistical Survey of Pitch Angle Distributions in Core (0-50 eV) Ions from Dynamics Explorer 1: Outflow in the Auroral Zone, Polar Cap, and Cusp', *J. Geophys. Res.* **99**, 17,483.

Gorney, D. J., Clarke, A., Croley, D., Fennell, J. F., Luhmann, J., and Mizera, P.: 1981, 'The Distribution of Ion Beams and Conics below 8000 km', *J. Geophys. Res.* **86**, 83.

Heelis, R. A., Winningham, J. D., Suguira, M., and Maynard, N. C.: 1984, 'Particle Acceleration Parallel and Perpendicular to the Magnetic Field Observed by DE–2', *J. Geophys. Res.* **89**, 3893.

Hoffman, J. H. and Dobson, W. H.: 1980, 'Light Ion Concentrations and Fluxes in the Polar Regions during Magnetically Quiet Times', *J. Geophys. Res.* **85**, 626.

Horwitz, J. L., Ho, C. W., Scarbo, H. D., Wilson, G. R., and Moore, T. E.: 1994, 'Centrifugal Acceleration of the Polar Wind', *J. Geophys. Res.* **99**, 15,051.

Hultqvist, B.: 1983, 'On the Origin of the Hot Ions in the Disturbed Dayside Magnetosphere', *Planet. Space Sci.* **31**, 173.

Klumpar, D. M.: 1979, 'Transversely Accelerated Ions: An Ionospheric Source of Hot Magnetospheric Ions', *J. Geophys. Res.* **84**, 4229.

Klumpar, D. M., Peterson, W. K., and Shelley, E. G.: 1984, 'Direct Evidence for Two-Stage (Bimodal) Acceleration of Ionospheric Ions', *J. Geophys. Res.* **89**, 10,779.

Kondo, T., Whalen, B. A., Yau, A. W., and Peterson, W. K.: 1990, 'Statistical Analysis of Upflowing Ion Beam and Conic Distributions at DE-1 Altitudes', *J. Geophys. Res.* **95**, 12,091.

Lemaire, J.: 1972, 'Effect of Escaping Photoelectrons in a Polar Exospheric Model', *Space Research* **XII**, 1413.

Lennartsson, O. W.: 1995, 'Statistical Investigation of IMF B_z Effects on Energetic (0.1- to 16-keV) Magnetospheric O^+ Ions', *J. Geophys. Res.* **100**, 23,261.

Liu, C., Horwitz, J. L., and Richards, P. G.: 1995, 'Effects of Frictional Ion Heating and Soft-Electron Precipitation on High-Latitude F-region Upflows', *Geophys. Res. Lett.* **22**, 2713.

Lockwood, M. and Titheridge, J. E.: 1981, 'Ionospheric Origin of Magnetospheric O^+ Ions', *Geophys. Res. Lett.* **8**, 381.

Lockwood, M., Chandler, M. O., Horwitz, J. L., Waite Jr., J. H., Moore, T. E., and Chappell, C. R.: 1985a, 'The Cleft Ion Fountain', *J. Geophys. Res.* **90**, 9736.

Lockwood, M., Waite Jr., J. H., Moore, T. E., Johnson, J. F. E., and Chappell, C. R.: 1985b, 'A New Source of Suprathermal O^+ Ions Near the Dayside Polar Cap Boundary', *J. Geophys. Res.* **90**, 4099.

Lockwood, M., Moore, T. E., Waite Jr., J. H., Chappell, C. R., Horwitz, J. L., and Heelis, R. A.: 1985c, 'The Geomagnetic Mass Spectrometer – Mass and Energy Dispersions of Ionospheric Ion Flows into the Magnetosphere', *Nature* **316**, 612.

Loranc, M., Hanson, W. B., Heelis, R. A., and St.-Maurice, J.-P.: 1991, 'A Morphological Study of Vertical Ionospheric Flows in the High-Latitude F Region', *J. Geophys. Res.* **96**, 3627.

Miyake, W., Mukai, T., and Kaya, N.: 1993, 'On the Evolution of Ion Conics along the Field Line from EXOS-D Observations', *J. Geophys. Res.* **98**, 11,127.

Miyake, W., Mukai, T., and Kaya, N.: 1996, 'On the Origins of the Upward Shift of Elevated (Bi-Modal) Ion Conics in Velocity Space', *J. Geophys. Res.* **101**, 26,961.

Nagai, T., Waite, J. H., Green, J. L., Chappell, C. R., Olsen, R. C., and Comfort, R. H.: 1984, 'First Measurements of Supersonic Polar Wind in the Polar Magnetosphere', *Geophys. Res. Lett.* **11**, 669.

Nishida, A.: 1966, 'Formation of Plasmapause, or the Magnetospheric Plasma Knee, by the Combined Action of Magnetospheric Convection and Plasma Escape from the Tail', *J. Geophys. Res.* **71**, 5669.

Peterson, W. K., Collin, H. L., Doherty, M. F., and Bjorklund, C. M.: 1992, 'O^+ and H^+ Restricted and Extended (Bi-Modal) Ion Conics Distributions', *Geophys. Res. Lett.* **14**, 1439.

Peterson, W. K. et al.: 1994, 'On the Sources of Energization of Molecular Ions at Ionospheric Altitudes', *J. Geophys. Res.* **99**, 23, 257.

Pollock, C. J., Chandler, M. O., Moore, T. E., Waite Jr., J. H., Chappell, C. R., and Gurnett, D. A.: 1990, 'A Survey of Upwelling Ion Event Characteristics', *J. Geophys. Res.* **95**, 18,969.

Raitt, W. J. and Schunk, R. W.: 1983, in R. G. Johnson (ed.), 'Composition and Characteristics of the Polar Wind', *Energetic Ion Composition in the Earth's Magnetosphere,* Terra Scientific Publishing, Tokyo, pp. 99–141.

Schunk, R. W. and Watkins, D. S.: 1981, 'Electron Temperature Anisotropy in the Polar Wind', *J. Geophys. Res.* **86**, 91.

Sharp, R. D., Johnson, R. G., and Shelley, E. G.: 1977, 'Observations of an Ionospheric Acceleration Mechanism Producing Energetic (keV) Ions Primarily Normal to the Geomagnetic Field Direction', *J. Geophys. Res.* **82**, 3324.

Shelley, E. G., Johnson, R. G., and Sharp, R. D.: 1972, 'Satellite Observations of Energetic Heavy Ions during a Geomagnetic Storm', *J. Geophys. Res.* **77**, 6104.

Shelley, E. G., Sharp, R. D., and Johnson, R. G.: 1976, 'Satellite Observations of an Ionospheric Acceleration Mechanism', *Geophys. Res. Lett.* **3**, 654.

Shelley, E. G., Peterson, W. K., Ghielmetti, A. G., and Geiss, J.: 1982, 'The Polar Ionosphere as a Source of Energetic Magnetospheric Plasma', *Geophys. Res. Lett.* **9**, 941.

Shelley, E. G. and Collin, H. L.: 1991, in C. I. Meng, M. J. Rycroft, and L. A. Frank (eds.), 'Auroral Ion Acceleration and its Relationship to Ion Composition', *Auroral Physics*, Cambridge University Press, pp. 129-142.

Tam, S. W. Y., Yasseen, F., Chang, T., and Ganguli, S. B.: 1995, 'Self-Consistent Kinetic Photoelectron Effects on the Polar Wind', *Geophys. Res. Lett.* **22**, 2107.

Thelin, B., Aparicio, B., and Lundin, R.: 1990, 'Observations of Upflowing Ionospheric Ions in the Mid-Altitude Cusp/Cleft Region with the Viking Satellite', *J. Geophys. Res.* **95**, 5931.

Wahlund, J.-E., Opgenoorth, H. J., Haggstrom, I., Winser, K. J., and Jones, G. O. L.: 1992, 'EISCAT Observations of Topside Ionospheric Ion Outflows during Auroral Activity: Revisited', *J. Geophys. Res.* **97**, 3019.

Whalen, B. A., Watanabe, S., and Yau, A. W.: 1991, 'Thermal and Suprathermal Ion Observations in the Low Altitude Transverse Ion Energization Region', *Geophys. Res. Lett.* **18**, 725.

Yau, A. W., Whalen, B. A., McNamara, A. G., Kellogg, P. J., and Bernstein, W.: 1983, 'Particle and Wave Observations of Low-Altitude Ionospheric Ion Acceleration Events', *J. Geophys. Res.* **88**, 341.

Yau, A. W., Whalen, B. A., Peterson, W. K., and Shelley, E. G.: 1984, 'Distribution of Upflowing Ionospheric Ions in the High-Altitude Polar Cap and Auroral Ionosphere', *J. Geophys. Res.* **89**, 5507.

Yau, A. W., Beckwith, P. H., Peterson, W. K., and Shelley, E. G.: 1985a, 'Long-Term (Solar-Cycle) and Seasonal Variations of Upflowing Ionospheric Ion Events at DE-1 Altitudes', *J. Geophys. Res.* **90**, 6395.

Yau, A. W., Shelley, E. G., Peterson, W. K., and Lenchyshyn, L.: 1985b, 'Energetic Auroral and Polar Ion Outflow at DE-1 Altitudes: Magnitude, Composition, Magnetic Activity Dependence and Long-Term Variations', *J. Geophys. Res.* **90**, 8417.

Yau, A. W., Peterson, W. K., and Shelley, E. G.: 1988, 'Quantitative Parametrization of Energetic Ionospheric Ion Outflow', *Geophys. Monogr. Series* **44**, 211.

Yau, A. W., Whalen, B. A., and Sagawa, E.: 1991, 'Minor Ion Composition in the Polar Ionosphere', *Geophys. Res. Lett.* **18**, 345.

Yau, A. W., Whalen, B. A., Goodenough, C., Sagawa, E., and Mukai, T.: 1993, 'EXOSD (Akebono) Observations of Molecular NO^+ and N_2^+ Upflowing Ions in the High-Altitude Auroral Ionosphere', *J. Geophys. Res.* **98**, 11,205.

Yau, A. W., Whalen, B. A., Abe, T., Mukai, T., Oyama, K. I., and Chang, T.: 1995, 'Akebono Observations of Electron Temperature Anisotropy in the Polar Wind', *J. Geophys. Res.* **100**, 17,451.

Address for correspondence: A. W. Yau, Institute for Space Research, Department of Physics and Astronomy, University of Calgary, Calgary, Alberta, Canada T2N 1N4.

THEORIES AND OBSERVATIONS OF ION ENERGIZATION AND OUTFLOW IN THE HIGH LATITUDE MAGNETOSPHERE

MATS ANDRÉ
Swedish Institute of Space Physics, Umeå University, Umeå, Sweden

ANDREW YAU
Institute for Space Research, Department of Physics and Astronomy, University of Calgary, Calgary, Alberta, Canada

Received January 17, 1997; Accepted in final form April 1, 1997

Abstract. A review is given of several mechanisms causing outflow at high latitudes of ionospheric ions to the terrestrial magnetosphere. The upward ion motion along the geomagnetic field can be divided into several categories, including polar wind, bulk ion outflow in the auroral region, upwelling ions and ion conics and beams. More than one ion energization mechanism can be operating within each category, and a combination of categories is important for the total ion outflow.

1. Introduction

Many of the ions in the terrestrial magnetosphere originate from the ionosphere. However, for several years it was believed that the solar wind was the major source of magnetospheric plasma, and that essentially all ionospheric plasma was gravitationally bound to low altitudes. In contrast, the first polar orbiting satellites carrying energetic ion mass spectrometers (1971-89A and S3-3) detected significant amounts of O^+ ions that had to be of ionospheric origin (Shelley et al., 1972; 1976a; Sharp et al., 1977). It is now clear that the high latitude ionosphere is an important source of H^+, O^+ and other ions in the magnetospheric plasma (Chappell, 1988; Shelley, 1988).

In this review we summarize and discuss some of the mechanisms transforming and concentrating energy of solar wind origin to cause the outflow of ionospheric ions at high latitudes (invariant latitude above 50°–60°). An overview of the statistical properties of the high latitude ion outflow as observed by several spacecraft and radars is given in a companion paper (Yau and André, this issue). The outflowing ions can be divided into categories such as polar wind, auroral bulk ion upflow, upwelling ions, ion beams and ion conics. The average energies of about 0.1 eV in the collisional lower ionosphere must be increased to about 1 to 10 eV (for H^+ and O^+, respectively), possibly by gradual energization as the ions move upward, for the ions to reach escape velocity. Average energies of up to several keV directly associated with outflow are observed at altitudes of several thousand kilometers. The ions may be energized either directly in the upward direction parallel to the geomagnetic field, or in the perpendicular direction. In the latter case, motion in the divergent magnetic field subsequently gives a parallel velocity component. There is not one single mechanism that can explain all ion outflow. In the

Space Science Reviews **80**: 27–48, 1997.

following we discuss several mechanisms believed to be important for the ionospheric ion outflow. We concentrate on perpendicular ion energization, and on bulk ion outflows caused by other mechanisms than a parallel auroral electric field. The auroral potential drop usually occuring at altitudes between 2000 and 15000 km (Reiff et al., 1988) is of course an important source of upgoing ion beams with energies between hundreds of eV and tens of keV, but the various mechanisms possibly causing this acceleration region are not reviewed here (see e.g., Borovsky, 1993 and André, 1997). We note that these regions of upward acceleration may be supplied with ions from below by some of the mechanisms discussed in the following. Several ion energization mechanisms may presently be studied in detail only in space plasmas near Earth, but may well operate also in the magnetospheres of other astrophysical objects.

2. Bulk Ion Outflows

2.1. The Polar Wind

The term polar wind refers to the ambipolar outflow of thermal ions in the polar ionosphere. The polar wind flow is the result of acceleration of the ambient ions by an ambipolar electric field and other forces. This bulk outflow (all particles in the population have the same drift velocity in addition to their thermal velocity) occurs on or near open magnetic field lines, e.g., over the polar cap. The polar wind outflow results from ion acceleration by an ambipolar electric field, caused by a slight charge separation, in order to achieve quasi-neutrality with the lighter and faster upflowing electrons. Other accelerating forces include plasma pressure gradients, magnetic mirror forces, and $\mathbf{E} \times \mathbf{B}$ convection in a region of magnetic field curvature; decelerating forces include gravitation and ion-neutral collisions.

The polar wind plasma consists primarily of electrons, and H^+, He^+, and O^+ ions. The source of plasma is the F-region of the polar ionosphere, which is dominated by oxygen ions (O^+). The hydrogen ions in the polar wind result from the resonant charge exchange reaction between oxygen ions and atmospheric hydrogen in the topside ionosphere. The helium ions are produced by the photoionization of atmospheric helium. The polar wind undergoes four major transitions as it flows up the field line: from chemical to diffusion dominance at 500-800 km, from subsonic to supersonic flow at 1000-2000 km, from the collision-dominated to the collisionless altitude regime at 1500-2500 km, and from heavy to light ion composition at about 5000-10000 km.

The term "polar wind" was coined by Axford (1968) to describe the supersonic ion flow at collisionless altitudes, in analogy to the hydrodynamic plasma expansion in the solar wind. The majority of the early models of the polar wind were steady state and one-dimensional. These models are discussed in excellent review papers by Raitt and Schunk (1983) and Schunk (1988). More recent models, some

of which are time-dependent and three-dimensional, are discussed in the recent comprehensive review by Ganguli (1996).

The early "classical" polar wind models emphasized the plasma pressure gradient along the field line, and were based on steady state hydrodynamic continuity and momentum equations or collisionless kinetic equations. These models predicted the supersonic flow of H^+ and He^+ ions at limiting fluxes above the subsonic-to-supersonic transition altitude (about 1500 km for H^+ and 2500 km for He^+) while the O^+ ions were assumed to be stationary. More advanced models are based on generalized transport equations, and emphasize the ion and electron temperature anisotropies in the polar wind (e.g. Gombossi and Rasmussen, 1991, Blelly and Schunk, 1993). Some of these models include the possibility of O^+ flows at high altitudes in the case of highly elevated electron temperature (Barakat and Schunk, 1983) or transient ion heating (Gombosi et al., 1985). However, the models often depend strongly on the assumed ionospheric boundary conditions (Demars and Schunk, 1987; 1989; Yasseen and Retterer, 1991). Also, most of these models assume a downward electron heat flux, which is inconsistent with recent observations in the sunlit polar wind on the Akebono satellite (Yau et al., 1995), in which the observed heat flux was upward and dominated by the escaping photoelectrons (with energies above 10 eV) and the anisotropic temperature distribution by the thermal-energy (below 5 eV) electrons.

The effects of escaping photoelectrons on the polar wind were studied by Lemaire (1972) using collisionless kinetic equations, and more recently by Yasseen et al. (1989) and Tam et al. (1995) using collisional kinetic equations. These latter studies included the effects of Coulomb collisions, parallel electric fields, and the magnetic mirror force, and showed that the presence of photoelectrons can increase the ambipolar electric field in the sunlit polar wind to a magnitude that is comparable to that inferred from DE-2 electron flux measurements (Winningham and Gurgiolo, 1982). The study of Tam et al. (1995) represents an important advance in polar wind modeling in two respects: it used a hybrid approach in which the thermal component of the polar wind plasma was described by transport equations and the suprathermal photoelectrons by kinetic equations, and it calculated in a self-consistent manner the electric field required to maintain quasi-neutrality along the field line in the presence of the photoelectrons.

Because of the magnetic field curvature in the polar cap, the convection electric field is a possible source of energization for the polar wind plasma. Cladis (1986) pointed out that in the presence of large convection electric field, significant energization of O^+ ions is possible in the high altitude polar cap. Here the curvature of the geomagnetic field in effect produces a centrifugal acceleration to the convecting plasma (in its frame of reference). However, the importance of centrifugal acceleration of various polar wind ion species is not yet clear (Swift, 1990; Horwitz, 1994).

Observationally, ion composition observations on the ISIS-2, DE-1, and Akebono satellites have confirmed the existence of polar wind ion flows in the 1000-

10000 km altitude region whose velocity and flux characteristics are basically consistent with those predicted by the classical polar wind models. However, the Akebono observations revealed that above 3500 km altitude, O^+ ions are often an important constituent of the polar wind, and the observed O^+ velocity at high altitude is much larger than the values expected from most models.

On Akebono, Abe et al. (1993a) measured the averaged altitude profiles of the polar wind velocities for the three major ion species (H^+, He^+, and O^+). For all three species, the ion velocity increased with altitude, and was larger on the dayside than on the nightside. At a given altitude, the velocity was smallest for the heavy O^+ ions and largest for the H^+ ions, and was more variable during active times than at quiet times. The velocity of the three species reached 1 km/s near 2000, 3000, and 6000 km, respectively. The ion velocity at a given altitude was found to correlate with the ambient electron temperature (Abe et al., 1993b), Figure 1a. Here the correlations are attributed to the cumulative effect of ion acceleration due to the ambipolar electric field along the field line, and the direct relationship between the local magnitude of the ion acceleration and that of the ambipolar electric field responsible for the acceleration. In a related Akebono study, Yau et al. (1995) found electron velocity distributions with higher temperatures in the upward direction along the geomagnetic field than in the perpendicular and downward directions, Fig 1b. The higher electron temperature in the upward direction resulted in an estimated upward heat flux of approximately 1.0×10^{-5}W m^{-2} at an altitude of about 2500 km. Yau et al. (1995) noted that the heat flux carried by the observed suprathermal atmospheric photoelectrons and thermal-energy electrons was 1 to 2 orders of magnitude larger than the downward heat flux predicted or assumed in many polar wind models (e.g., Schunk and Watkins, 1981). The observed electron temperature is anisotropic because of the large ambipolar electric field that is required to maintain quasi-neutrality along the field line in the presence of escaping atmospheric photoelectrons, and because of the Coulomb collisions between the low-energy ambient electrons and the more energetic photoelectrons. The larger ambipolar electric field in the sunlit polar wind is consistent with the day-to-night asymmetry of the observed polar wind ion velocity.

In summary, the Akebono observations have confirmed the significant effect of ambipolar electric fields arising from escaping atmospheric photoelectrons, as well as the significant effect of plasma pressure gradients, on the polar wind acceleration. However, the relative importance between the two effects remains to be quantified, due in part to the lack of quantitative plasma pressure measurements at high altitudes. Also, theoretical results indicate that the effects are intimately coupled (Tam et al., 1995).

2.2. Auroral Bulk Upflow

Some of the bulk ion upflow closely related to auroral latitudes at all local times does not seem to be caused by an auroral potential drop. This upflow consists main-

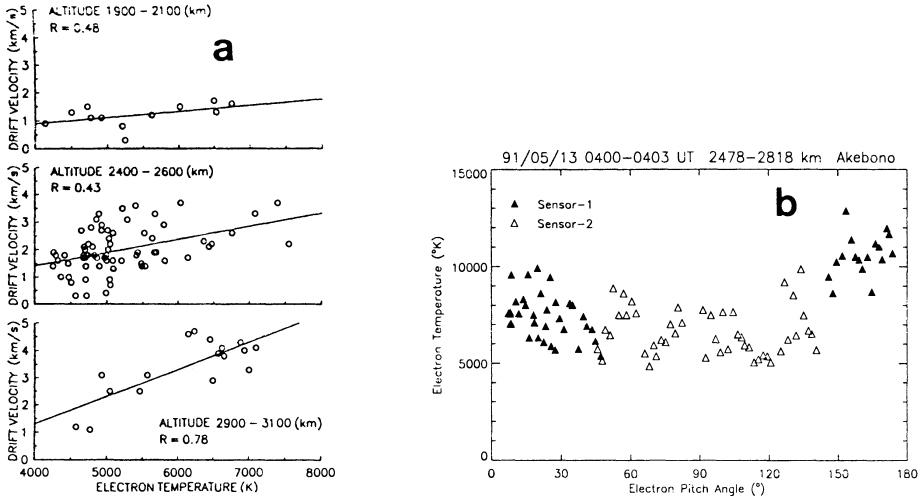

Figure 1. a) Scatter plots of H^+ polar wind ion velocity versus electron temperature observed on the Akebono satellite in three different altitude regions. The correlation is strongest at the highest altitude, and reflects the direct relationship between the magnitude of the ion acceleration and the ambipolar electric field at a given altitude. (From Abe et al., 1993b). b) Polar wind electron temperature observed by two sensors on Akebono at 2500–2800 km in the dayside polar cap displayed as a function of pitch angle. The measured temperature was largest near the upward magnetic field direction (>150° electron pitch angle) (From Yau et al., 1995).

ly of O^+, sometimes with a significant NO^+ component. The ions are observed by satellites and radars from altitudes of about 400 km up to at least 1500 km. The upward velocity and number flux can be up to about 1 km/s and at least 10^{13} O^+ ions/m^2s, respectively (Loranc et al., 1991; Wahlund et al., 1992, and references therein). Most ions do not reach escape velocity unless they are further energized by additional mechanisms. (This is in contrast to the polar wind bulk outflow which starts at about 1000 km for protons, consists of H^+, He^+, and O^+ at higher altitudes, and where the ions can escape).

One important mechanism causing this auroral upflow is probably frictional heating of O^+ ions at altitudes below a few hundred kilometers where collisions are very important. Perpendicular electric fields exceeding a hundred mV/m correspond to $\mathbf{E} \times \mathbf{B}$ drifts of a few km/s, which via collisions give enhanced (several thousand K) perpendicular ion temperatures, and subsequently (again via collisions) increased parallel ion temperatures (e.g. Heelis et al., 1993; Wilson, 1994). The enhanced temperature at low altitudes increases the preexisting parallel pressure gradient, and the ions respond by flowing to higher altitudes to attain a new equilibrium scale height distribution. Although the increase of the scale height is a transient feature, the upflow can remain since new plasma is horizontally convected into the heating region. Many ions do not reach escape velocity and may fall down when convected out of the heating flux tube (e.g. Loranc et al., 1991).

At least sometimes strong perpendicular electric fields are observed adjacent to auroral arcs and the frictional ion heating mechanism may be important for ion upflow, while in regions of auroral precipitation only weak electric fields, but significant ion upflows, are found (Wahlund et al., 1992). Alternative mechanisms are needed to explain these upflows directly associated with electron precipitation, and one possibility is increased electron temperatures causing an ambipolar electric field (Barakat and Schunk, 1983; Liu et al., 1995). It has also been suggested that anomalous resistivity due to ion acoustic fluctuations, caused by either a strong current carried by electrons or by a relative drift of O^+ and H^+ ions, and an associated parallel electric field cause the ion upflow (Collis et al., 1991; Wahlund et al., 1992). Furthermore, ion upflows can often be related to shear in the convective velocity, which in a two-step process can seed plasma waves important for ion energization (Ganguli et al., 1994). Other mechanisms have also been considered as discussed by, for example, Wilson (1994) and references therein. The ions in the bulk upflow at auroral latitudes are an important source for other auroral energization mechanisms, as discussed below.

3. Energetic Auroral Ions–Conics and Beams

3.1. Transverse Ion Energization–Ion Conics

Much of the ionospheric ion outflow is directly associated with the auroral oval, and is caused by energization of all major ion species perpendicularly to the geomagnetic field. These energized ions can then move up the field lines of the divergent terrestrial magnetic field and form so-called conics in velocity space. These distributions are observed by rockets at altitudes of a few hundred kilometers (e.g. Whalen et al., 1978; Kintner et al., 1986; 1992; 1996) and by satellites up to several Earth radii (e.g. Sharp et al., 1977; 1981; Klumpar, 1986; Burch, 1988; André et al., 1990; 1997; Lundin and Eliasson, 1991; André and Chang 1993; Miyake et al., 1996). Typical mean ion energies range from a few eV up to at least about 1 keV, see Figure 2.

The energization is caused by the essentially perpendicular component of electric fields oscillating within some frequency range. Several wave modes can, in principle, cause perpendicular ion energization; see reviews by Klumpar (1986), Lysak (1986), André and Chang, (1993) and André (1997). These waves range from static structures and waves much below the ion gyrofrequencies (Borovsky, 1984; Hultqvist, 1991), via waves at and just above the ion gyrofrequencies (Ashour-Abdalla and Okuda, 1984; Chang et al., 1986), to waves above the lower hybrid frequency (Chang and Coppi, 1981). Several of the proposed mechanisms may not be of any practical importance, at least not in the terrestrial auroral zone. In the following we briefly discuss some mechanisms that seem to be of major importance in the terrestrial ionosphere and magnetosphere.

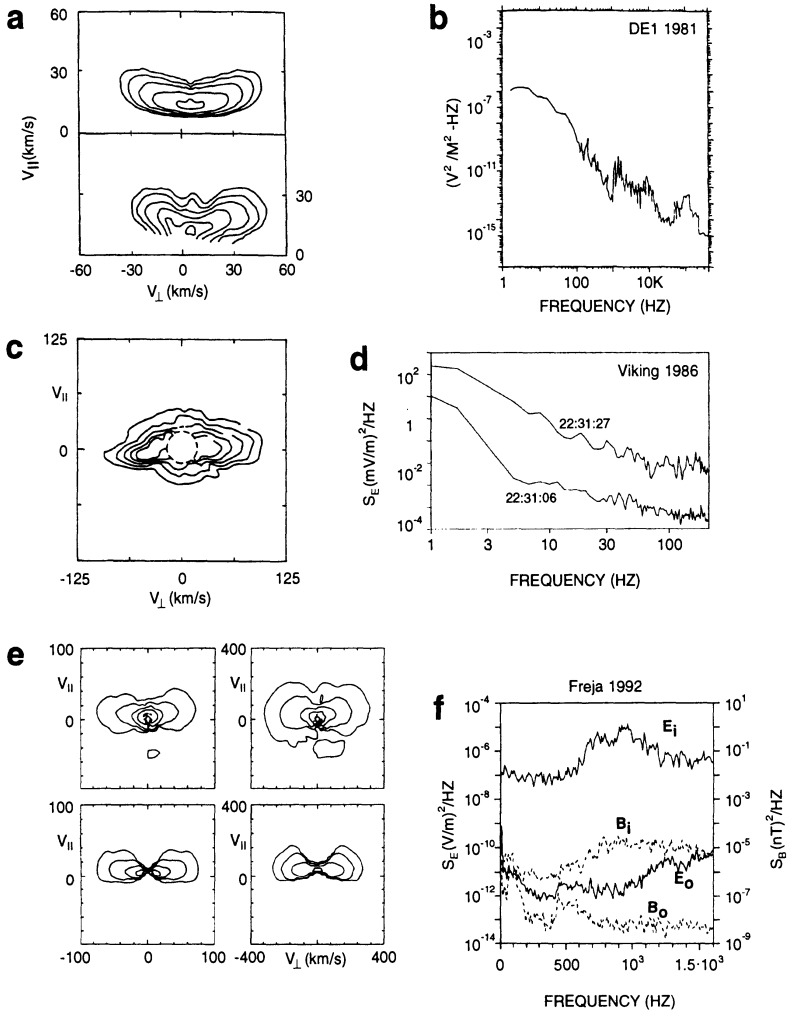

Figure 2. a) Lower panel: O^+ distribution function (ion conic) with mean energy of 70 eV, displayed with contours of constant phase space density, observed by the DE 1 satellite; and upper panel: corresponding O^+ distribution obtained with a Monte Carlo simulation using observed wave fields as input. Only upflowing ions are shown. From Chang et al. (1986) and Retterer et al. (1987). b) Electric field spectral density observed simultaneously with the O^+ distribution in panel a (f_{O^+} = 6 Hz). From Chang et al. (1986). c) Ion distribution function (TAI) with mean energy of 100 eV (assumed to be O^+) observed by the Viking satellite and d) the corresponding electric field spectral density in the ion heating region (22:31:27 UT) and just outside (f_{O^+} = 2 Hz). (Both from André et al. (1988)). e) Upper left (right): O^+ (H^+) distribution functions with mean energies of 31 and 67 eV observed by the Freja satellite, and lower left (right): corresponding O^+ (H^+) distributions obtained with Monte Carlo simulations using observed wave fields as input and f) the corresponding electric and magnetic field spectral densities in the ion heating region (E_i and B_i), and just outside (E_o and B_o), (f_{O^+} = 25 Hz, $f_{LH} \approx$ 600 Hz) (Both from André et al., 1994).

One common type of ion heating is associated with broadband low-frequency electric wave fields (Figure 2a-d). These waves cover frequencies from less than one Hz up to several hundred Hz, thus including the gyrofrequencies of the major ion species at least for altitudes from about 1000 km up to a few earth radii. Such broadband waves near the ion gyrofrequency can efficiently heat ions. A maximum heating rate corresponding to such waves can be obtained by assuming that the perpendicular wavevector is much smaller than the inverse of the ion gyroradius (as would be the case for some Alfvén waves), and that the left-hand polarized fraction of the waves is heating the ions. The ion cyclotron heating rate (Chang et al., 1986) is then given by

$$\frac{dW}{dt} = S_L q^2 (2m)^{-1} \tag{1}$$

where q and m are the charge and the mass of the ion, and S_L is the electric field spectral density at the ion gyrofrequency due to left-hand polarized waves. Relation (1) is convenient to use when estimating the ion heating rate from the observed spectral densities. An exact calculation of the ion energies that can be caused by the observed waves requires detailed information concerning the waves, such as distribution in wavevector space, which usually is not available. The successful use of relation (1) in several studies is not necessarily an indication that the long wavelength Alfvén wave is the dominant wave mode in the observed broadband low-frequency spectra. For example, recent studies indicate that a significant fraction of these emissions sometimes may be ion acoustic waves (Wahlund et al., 1996) or electrostatic ion cyclotron waves (Bonnell et al., 1996). The simple cyclotron heating mechanism can nevertheless be useful when estimating the effects of observed waves on the ions. Assuming that some fraction, which must be less than 100%, of the observed electric field spectral density near the ion gyrofrequency is due to left-hand Alfvén waves is, as a first approximation, the same as assuming that the same fraction of the waves is in resonance with the ions, regardless of wave mode. Studies of events in various regions of the magnetosphere show that fractions from less than one percent, up to tens of percent, of the observed waves need to be in resonance to explain the observed ion conical distributions (Chang et al., 1986; Retterer et al., 1987; André et al., 1988; 1990; 1997; Norqvist et al., 1996).

In Transversely Accelerated Ion (TAI) distributions the ions have pitch-angles close to 90°. These distributions can be regarded as a special case of ion conics, where the magnetic mirror force has not yet changed the parallel velocity component. (In some other reports the term TAI is used to denote the mechanism of transverse acceleration. These accelerated ions are not necessarily observed at 90°, and ion conics may then be regarded as a special case of TAIs.) Figures 2c-d show a TAI distribution observed in the dayside cusp/cleft region by the Viking satellite, and the simultaneously observed broadband waves. At this altitude of about 13500 km it might at first seem surprising that, within observational limits of a few degrees, the ions have not traveled far enough in altitude to give the distribution an

obvious conical shape. The reason seems to be that cool ions from the equatorward edge of the cusp/cleft are drifting poleward into a region filled with broadband low-frequency waves, which then can heat the ions (André et al., 1988; 1990; Norqvist et al, 1996; Knudsen et al., 1997). Thus ions at altitudes of several thousand kilometers can be heated over an altitude range over only a few hundred kilometers, and may appear as TAI distributions.

Observations by the SCIFER sounding rocket at 1400 km near 10:00 Magnetic Local Time (MLT) in the cleft again show ion energization clearly associated with broadband low-frequency waves (Kintner et al., 1996; Moore et al., 1996; Arnoldy et al., 1996). The energization is associated with clear density depletions with sharp boundaries, Figure 3. These density depletions are tens of kilometers in the perpendicular direction. The depletions are consistent with even larger regions of low plasma density, broadband low-frequency waves and ion heating observed by the Viking (Hultqvist, 1991) and Freja satellites (Lundin et al., 1994; André et al., 1997) at altitudes up to 13500 km (Viking apogee). These ion heating events occur at various local times, and similar ion energization in a sharply confined spatial region poleward of a nightside auroral arc has recently been observed by the AMICIST sounding rocket at 900 km, near 23:00 MLT (Lynch et al., 1996). This nightside rocket observation is typical in that the broadband low-frequency waves are loosely associated with keV auroral electrons (accelerated by a quasi-static potential drop). However, the waves and the ion energization do not occur on exactly the same field lines as the auroral electrons. Another example of this (small-scale) anti-correlation between auroral electrons and ion heating to energies above 5–10 eV is shown in the Freja morningside event in Figure 4. Here the heated O^+ ions observed by the spinning satellite can be seen as vertical stripes in panel 1, the anti-correlated keV electrons in panel 4, and the broadband low-frequency waves are found in panel 5. In summary we find that ion heating at all local times often is associated with broadband low-frequency waves that can resonantly heat the ions.

There are waves also above the lower hybrid frequency, f_{LH}, at about 1 kHz in Figure 4. These emissions are not well correlated with the ion energization, are weaker than the waves near the oxygen gyrofrequency, f_{O^+}, and are not important for the ion energization. During other events, waves near f_{LH} are the major heating mechanism. Figure 2e-f shows an afternoon event where waves above f_{LH} are more intense than waves at f_{O^+} and f_{H^+}. Here "pre-heating" by waves near the ion gyrofrequencies can be important for the ions to get high enough velocities to be in resonance with the waves above the lower hybrid frequency, but most of the heating is then caused by waves above f_{LH} (André et al., 1994). While these Freja observations from about 1700 km show waves in widespread regions (hundreds of kilometers), observations by sounding rockets at altitudes up to about 1000 km show good correlation between waves above f_{LH} occuring in thin filamentary density cavities ("lower hybrid cavities", LHCs) and transverse ion energization to characteristic energies of up to about 10 eV (Kintner et al., 1992; Vago et al., 1992;

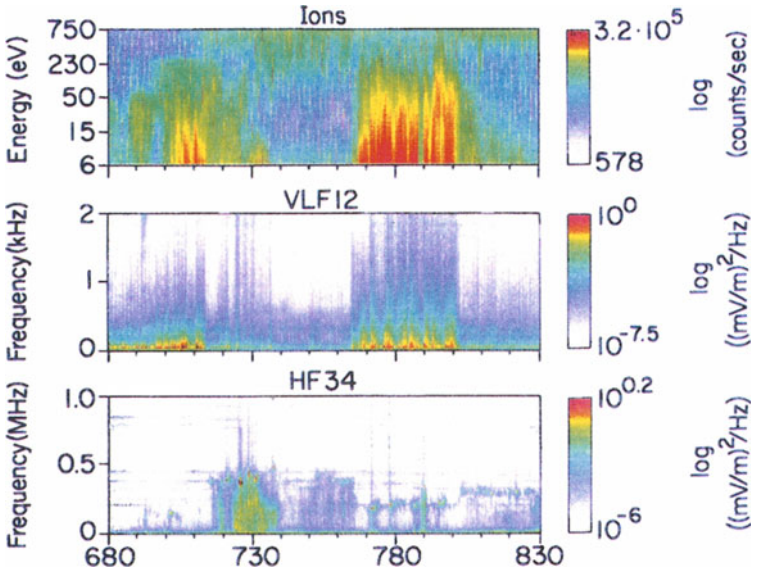

Figure 3. Overview from 680 s to 830 s flight time of the SCIFER sounding rocket showing ion energies (top panel), and electric fields to 2 kHz and 1 MHz (middle and lower panels). Transversely accelerated ions occur together with broadband low-frequency waves and decreased Langmuir wave frequency (decreased density) between 765 and 800 s (from Kintner et al., 1996).

Chang, 1993; Singh, 1994; Ergun et al., 1995; Lynch et al., 1996). The cavities are about 50–100 meters wide in the direction perpendicular to the geomagnetic field, and probably much longer in the parallel direction. A possible scenario is that downgoing keV electrons from a quasi-static auroral potential drop generate lower hybrid waves which in some places collapse to form LHCs.

Auroral electrons may also generate waves below an ion gyrofrequency (Temerin and Lysak, 1984; Gustafsson et al., 1990). These electromagnetic ion cyclotron (EMIC) waves can, in principle, heat ions at the higher ion gyrofrequency by the less efficient so-called "double cyclotron resonance" mechanism (Temerin and Roth, 1986; Ball, 1989) but this mechanism might not often be important in practice (Ball and André, 1991a). However, the EMIC emissions below one ion gyrofrequency can occur above the gyrofrequency of some heavier ions, e.g., the waves may be at frequencies between f_{H^+} and f_{O^+}. The EMIC waves above f_{O^+} may heat O^+ ions in a way similar to waves above f_{LH} (Ashour-Abdalla et al., 1988) and Freja observations indicate that this mechanism sometimes is important (Erlandson et al., 1994; André et al., 1997).

An additional heating mechanism, giving ion energies of probably only a few eV, is mode conversion and resonant absorption of downgoing electromagnetic waves (auroral hiss) near f_{H^+} in an oxygen dominated plasma (Le Quéau et al.,

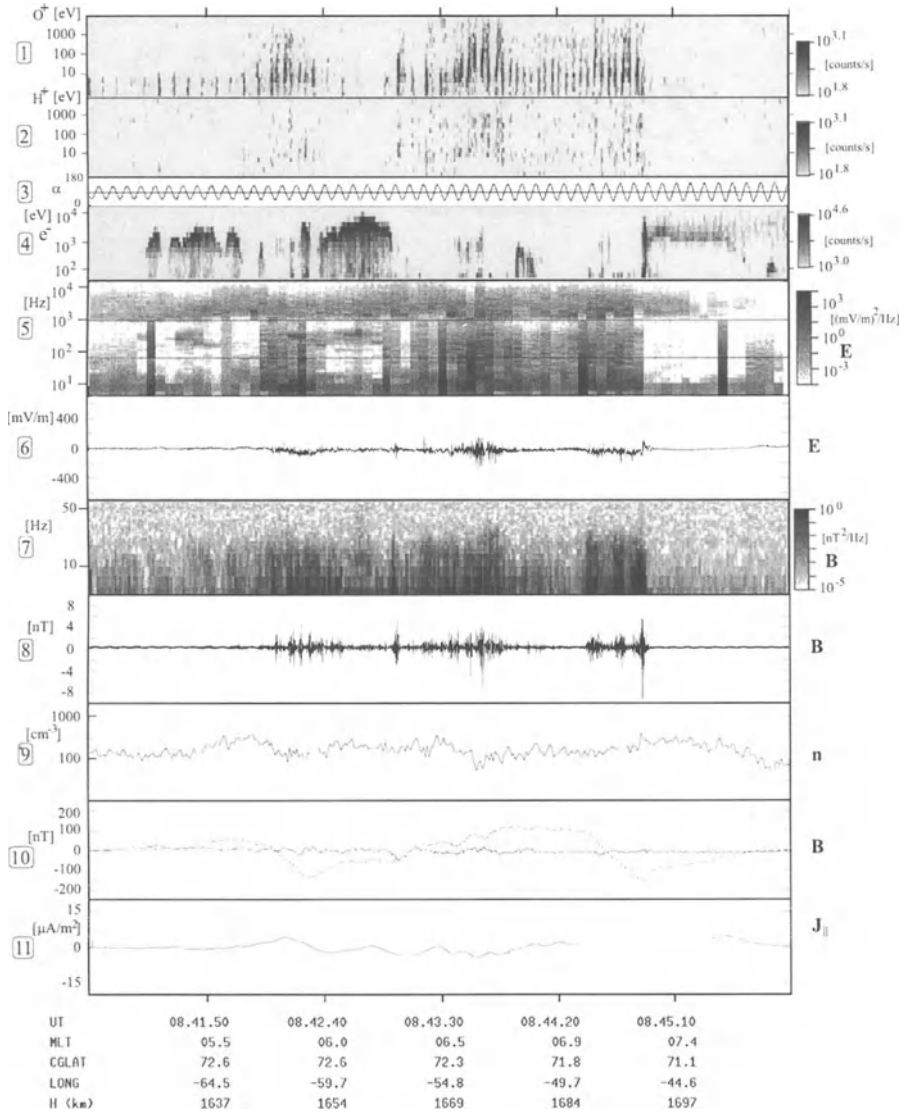

Figure 4. Data from a morningside ion heating region observed by the Freja satellite; panels 1 and 2 show O^+ and H^+ ions; panel 3 the corresponding pitch-angle; panel 4 downgoing electrons; panels 5 and 6 electric fields to 10 kHz and a time series of the nearly static electric field; panels 7 and 8 the magnetic field between 1.5 and 60 Hz and the corresponding time series; panel 9 the density; and panels 10 and 11 the perturbations of the geomagnetic field and the field-aligned current estimated from these perturbations. Perpendicular O^+ energization (panel 1) is associated with broadband low-frequency waves (5), but not with auroral electrons (4). From André et al. (1997).

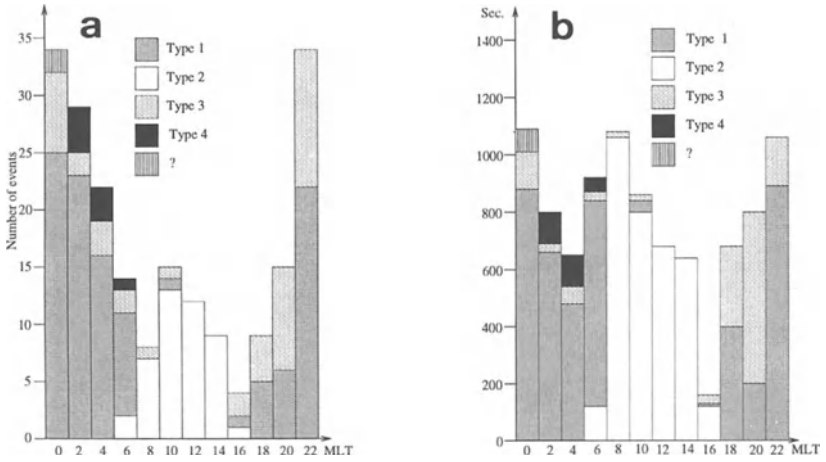

Figure 5. Different types of ion heating events observed by the Freja satellite near 1700 km during about 1300 passes. a) number of events and b) number of seconds spent in each type of event. Type 1 and 2 are both associated with broadband low-frequency waves, Type 3 is connected with auroral electrons and waves near $1/2 f_{H^+}$ or waves around f_{LH}, while Type 4 is associated with precipitating H^+ or O^+ and, again, waves around f_{LH}. From André et al. (1997).

1993; Rauch et al., 1993; Johnson et al., 1995). Yet another mechanism to be considered is non-resonant "sloshing" by waves much below the ion gyrofrequency (Hultqvist, 1991; 1996; Ball and André, 1991b). At these low frequencies the ions will respond to the electric field essentially by a changing $\mathbf{E} \times \mathbf{B}$ drift. This often gives energies up to some eV at low altitudes (a few thousand kilometers), but may give much higher energies to heavy ions at higher altitudes (weaker geomagnetic field).

Recent satellite and rocket observations indicate that broadband low-frequency emissions is the most important wave signature associated with perpendicular ion energization, probably followed by waves around f_{LH}. In a preliminary statistical study of Freja data obtained near 1700 km (André et al., 1997), perpendicular O^+ ion heating to mean energies above 5–10 eV were classified as belonging to one of four types, Figure 5a-b. Type 1 and 2 are both associated with broadband low-frequency waves, Type 3 is connected with auroral electrons and waves near $1/2 f_{H^+}$ or waves around f_{LH}, while Type 4 is associated with precipitating H^+ or O^+ and, again, waves around f_{LH}. From Figure 5a-b it is clear that broadband low-frequency waves is the most common wave signature in this study. Also, these events are associated with the highest O^+ mean energies at 1700 km (hundreds of eV on the night and morningside) and the highest outflow (10^{13} O^+ ions/m^2s on the dayside), while intense eveningside events associated with waves near f_{LH} usually have ion energies and fluxes an order of magnitude lower.

3.2. Parallel Ion Energization

Some ion conics do not have flux maxima only at a nearly constant pitch-angle, but over an extended range of angles. These distributions include a significant flux of low energy ions aligned with the geomagnetic field, and can be said to be "lifted" in velocity in the parallel direction (see e.g. Figure 2a). Statistical studies of DE 1 and Akebono data (Peterson et al., 1992, Miyake et al., 1996) indicate that many high energy conics are lifted as a result of ion heating over an extended altitude range in a diverging magnetic field (Temerin, 1986), while some conics on the eveningside have been accelerated upward by a parallel electric field (Klumpar et al., 1984), but that the in principle possible velocity filtering effect (Horwitz, 1986) appears to be less important. The statistical studies also indicate that the cone angle of many conical distributions stays constant in altitude, rather than decreasing toward the upward direction as expected from adiabatic particle motion. Both the constant cone angle, and the lifting of conics, can be the result of gradual perpendicular resonant ion energization by waves at, e.g., the ion gyrofrequency as the ions move upward. In cases when the perpendicular energization is not intense enough at higher altitudes, the ion motion will become more field aligned, and due to limited detector resolution the distribution may be observed as an ion beam (peak flux along the magnetic field direction). Field-aligned ion energization of several eV may result also from strong (hundreds of mV/m) perpendicular electric fields at much lower (non-resonant) frequencies due to the pondermotive force caused by the gradient of the $\mathbf{E} \times \mathbf{B}$ drift in the diverging geomagnetic field (Li and Temerin, 1993; Witt et al., 1995; Schukla et al., 1996).

4. Upwelling Ions

Many dayside ion outflow events display the effects of both parallel and perpendicular energization to energies from one to tens of eV. The ion distributions appear as a single peak in detector count rate near the satellite ram direction but with a notable asymmetry toward the upward magnetic field. During these "upwelling ion" (UWI) events the ion and satellite velocities are nearly equal (some kilometers per second), complicating studies of the ion distribution. These UWI distributions are important for understanding of the total ion outflow as well as ion energization mechanisms, and they have been extensively studied with the RIMS mass spectrometer on DE 1 (Lockwood et al., 1985a; Moore et al., 1986; Pollock et al., 1990; Giles et al., 1994).

The distinction between upwelling ions in the dayside and transversely accelerated low energy ion conics is not sharp. However, by comparing observations reported as UWI and conical distributions we find that the UWI distributions are more upward moving (higher upward mean velocity) than ion conics with the same perpendicular energy. At higher perpendicular energies (above about 10 eV) perpendicularly heated dayside ion distributions are not reported to have special prop-

erties, but at these higher energies some asymmetries in the parallel direction may observationally be masked by the perpendicular energization.

When observed at 2000–6000 km, the core of UWI O^+ distributions exhibit transverse heating to about 10 eV, and carry significant upward number flux ($>10^{12}m^{-2}s^{-1}$) and heat flux ($>3\times10^{-7}W\ m^{-2}$). All other observed species (H^+, He^+, O^{++} and N^+) are also warmed. A detailed study of an intense upwelling ion event is summarized in Figure 6. The sharp equatorward edge of the upwelling ion event (panels a and e) was closely associated with electric field oscillations (panel b) and with a convection velocity shear region (panel c), where transverse ion heating was observed (panel a, see also Moore et al., 1986). The transverse ion energization at the equatorward edge, associated with electric field emissions, is very similar to other satellite observations (André et al., 1988, 1990; Norqvist et al., 1996; Knudsen et al., 1997), although in many of these cases the heated ion distributions had higher energies and were reported as conics. Detailed studies of some events show that resonant energization by electric fields at frequencies of the order of the ion gyrofrequecny can explain the ion conics in this region (André et al., 1988, 1990; 1997; Norqvist et al., 1996; see also Kintner et al., 1996) and it is likely that UWI distributions are energized in a similar way, but to lower energies. As for ion conics, non-resonant sloshing may be significant at low (a few eV) energies. This scenario does not explain why dayside UWI distributions should be more upwelling than an ion conic with the same energy, and additional understanding of the observed parallel energization is needed.

From the narrow nature of the upwelling ion source region, Lockwood et al. (1985b) concluded that ions should be spatially dispersed across the polar cap according to their time of flight (the "cleft ion fountain"). For a given ion species, lower energy ions will be convected further toward the nightside; as will heavier ions for a given ion energy (Horwitz, 1984; Moore et al., 1985). Similar dispersion may affect ions originating in the auroral bulk outflow (Loranc et al., 1991), and ions in the cusp (Shelley et al., 1976b) and in the plasma mantle (Rosenbauer et al., 1975).

5. Summary and Discussion

Different types of ion distributions, energized by different mechanisms, flow upward along the geomagnetic field lines at high latitudes. A simplified overview of some ion upflows is given in Figure 7. The polar wind is a bulk ion (H^+, He^+ and O^+) outflow which for protons starts at altitudes of about 1000 km, and has a typical velocity of about 1 km/s at an altitude of about 2000 km. This outflow, occuring on or near open field lines, is at least partly caused by plasma pressure gradients and ambipolar electric fields arising from escaping atmospheric photoelectrons, but the relative importance of these coupled mechanisms is not clear. The auroral bulk ion upflow is observed from about 400 km and is composed mainly of O^+. Upward velocities reach about 1 km/s at an altitude of 1000 km, but most ions cannot escape

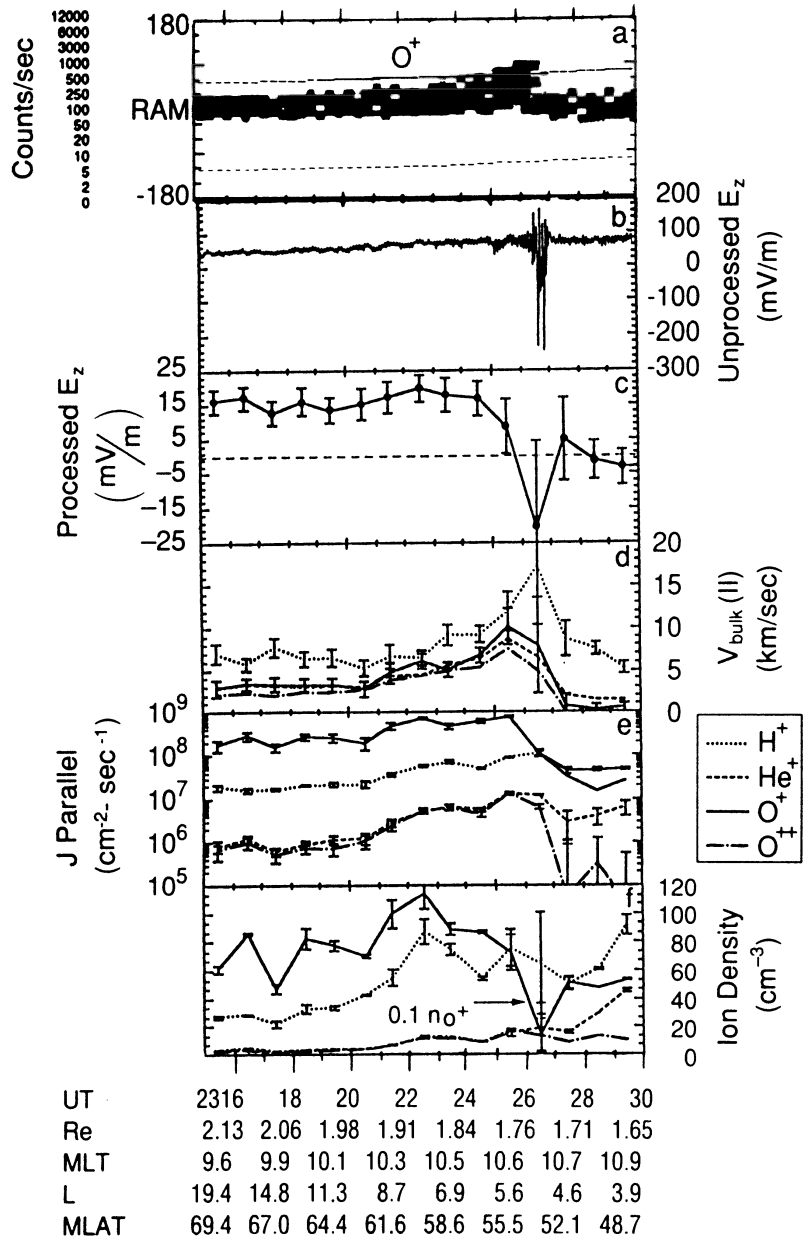

Figure 6. DE 1 observation of an intense upwelling ion event on March 1, 1982; distances are geocentric. a) O^+ spin angle versus time spectrogram from RIMS. The dashed line indicates the upgoing direction. There is transverse energization near 23:27 UT. b) one component of dc electric field data from the PWI instrument; c) processed (averaged) electric field data; d) derived ion flow velocities; e) upward ion fluxes; f) ion densities (the O^+ ion density is divided by 10) (From Pollock et al. 1990).

unless they are further energized. In the auroral zone, strong perpendicular electric fields in the collisional ionosphere can cause heating and transient changes in the parallel pressure gradient, generating ion upflow. Electron precipitation, causing increased electron temperatures and an ambipolar electric field, as well as waves related to shear in the convection velocity and other phenomena, can also contribute to the ion energization and bulk upflow in the auroral region. So-called upwelling ion distributions in the dayside auroral region have energies between one and tens of eV, an upward velocity of 1–10 km/s, and often higher perpendicular than parallel characteristic energy. Upwelling ion distributions are similar to low energy ion conics, but seem for some unknown reason(s) to have higher relative parallel characteristic energies. Ion conical distributions in the auroral region are energized mainly in the perpendicular direction. Motion in the divergent geomagnetic field then gives an upward velocity component and the conical shape in velocity space. Conics have mean energies from a few eV up to at least about 1 keV, with the higher energies typically occuring at higher altitudes. The corresponding parallel velocities range from a few km/s up to a few hundred km/s, with lighter ions having higher velocities. The most common and important energization mechanism seems to be resonant heating by broadband low-frequency waves at frequencies of the order of the ion gyrofrequencies. Resonant heating is also caused by waves near the lower hybrid frequency, sometimes confined in density cavities, and by electromagnetic ion cyclotron waves. Non-resonant heating by electric field oscillations below the ion gyrofrequencies can be important for energization to some eV at low altitudes, and to much higher energies at higher altitudes (weaker geomagnetic field). Ion beams are caused by parallel electric fields, and by magnetic pitch-angle folding of some upward moving conics, and typically have energies from a few eV to tens of keV. Parallel velocities are then between a few km/s and thousands of km/s, again with lighter ions having the higher velocities.

The ion number flux of the various types of upflowing ion distributions varies considerably between different events, and varies also systematically with, e.g., magnetic activity, season, and magnetic local time. As discussed by Yau and André (this issue), the high latitude ion outflow is an important source of magnetospheric plasma. Here we just note that during solar maximum and high magnetic activity the total outflow of H^+ and O^+ is a few times 10^{26} ions/s, often with O^+ as the dominating species during these active conditions.

The ion distributions labeled with different names are not necessarily distinctly different, or caused by distinctly different mechanisms. Both polar wind and auroral ion bulk upflow can be accelerated parallel to the geomagnetic field by pressure gradients and ambipolar electric fields, and the upwelling ions and ion conics can be energized in the perpendicular direction by the same oscillating electric fields. Furthermore, an ion distribution can be gradually heated by different mechanisms as it flows upwards, and will be labeled accordingly when observed at different altitudes. Auroral bulk upflow is, together with some transverse ion heating causing low energy conics, supplying ions to regions above 1000 km where more intense

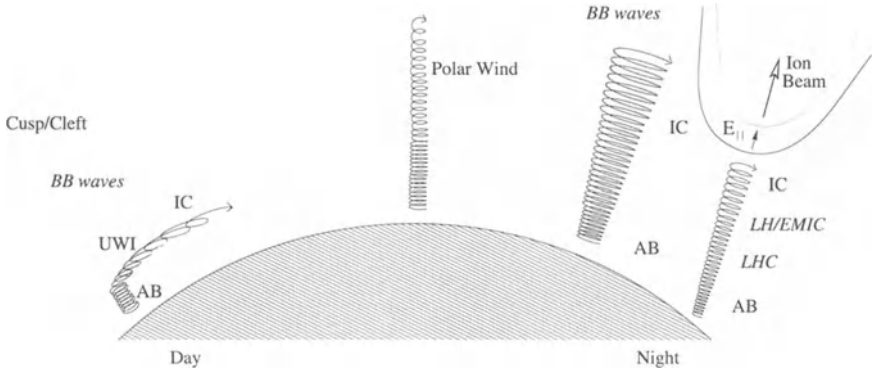

Figure 7. Schematic overview of some categories of high latitude ion upflow: polar wind, auroral bulk outflow (AB), upwelling ions (UWI), ion conics (IC) and ion beams. The parallel quasi-static auroral electric field ($E_{||}$) is indicated together with some wave phenomena causing energization perpendicular to the geomagnetic field: broadband low-frequency waves (*BBwaves*, shaded regions), waves near the lower hybrid frequency (*LH*) and similar waves occuring in density cavities (*LHC*) and electromagnetic ion cyclotron (*EMIC*) waves below the proton gyrofrequency (Figure supplied by Patrik Norqvist).

perpendicular energization can create ion conics. These conical distributions can then be further gradually heated up to altitudes of at least several earth radii (Figure 7, nightside). When the perpendicular heating is not intense enough at higher altitudes, motion in the divergent geomagnetic field will change the ion motion to be more field aligned, and the distributions may be detected as ion beams. Ion beams may also be generated by an acceleration region with a parallel auroral electric field, occuring at altitudes of a few thousand kilometers. These regions may be supplied with ions from below by some of the mechanisms discussed above. Some ion distributions on the dayside may start as auroral bulk outflow, be gradually heated to appear as upflowing ions, and further gradually energized in the perpendicular direction to achieve a distinct conical shape (Figure 7, dayside). These ions may then be $\mathbf{E} \times \mathbf{B}$ convected toward the polar cap, and the lowest energy ions may fall down again unless they have reached escape velocity.

Even during one specific event an upward flowing ion distribution may be affected by more than one major mechanism. The ions are often gradually energized as they move upward, and the distribution may be changing in invariant latitude and magnetic local time due to convection. Thus, investigations of the com-

binations of mechanisms causing gradual ion energization are needed to further improve our understanding of the ion outflow from low altitudes to the outer magnetosphere.

Acknowledgements

This work was supported in part by Natural Science and Engineering Research Council (NSERC) Research Grant OGPIN-017.

References

Abe, T., Whalen, B. A., Yau, A. W., Horita, R. E., Watanabe, S., and Sagawa, E.: 1993a, 'EXOS D (Akebono) Suprathermal Mass Spectrometer Observations of the Polar Wind', *J. Geophys. Res.* **98**, 11,191.

Abe, T., Whalen, B. A., Yau, A. W., Watanabe, S., Sagawa, E., and Oyama, K. I.: 1993b, 'Altitude Profile of the Polar Wind Velocity and its Relationship to Ionospheric Conditions', *Geophys. Res. Lett.* **20**, 2825.

André, M., Koskinen, H., Matson, L., and Erlandson, R.: 1988, 'Local Transverse Ion Energization In and Near the Polar Cusp', *Geophys. Res. Lett.* **15**, 107.

André, M., Crew, G. B., Peterson, W. K., Persoon, A. M., Pollock, C. J., and Engebretson, M. J.: 1990, 'Ion Heating by Broadband Low-Frequency Waves in the Cusp/Cleft', *J. Geophys. Res.* **95**, 20,809.

André, M. and Chang, T.: 1993, 'Ion Heating Perpendicular to the Magnetic Field', *Physics of Space Plasmas (1992)* **12**, Scientific Publishers, Cambridge, MA, 35.

André, M., Norqvist, P., Vaivads, A., Eliasson, L., Norberg, O., Eriksson, A. I., and Holback, B.: 1994, 'Transverse Ion Energization and Wave Emissions Observed by the Freja Satellite,' *Geophys. Res. Lett.* **21**, 1915.

André, M.: 1997, 'Waves and Wave-Particle Interactions in the Auroral Region', *J. Atmos. Terr. Phys.*, in press.

André, M., Norqvist, P., Andersson, L., Eliasson, L., Erikson, A. I., Blomberg, L., Erlandson, R. E., and Waldemark, J.: 1997, 'Ion Energization Mechanisms at 1700 km in the Auroral Region', *J. Geophys. Res.*, in press.

Arnoldy, R. L., Lynch, K. A., Kintner, P. M., Bonnell, J., Moore, T. E., and Pollock, C. J.: 1996, 'SCIFER–Structure of the Cleft Ion Fountain at 1400 km Altitude', *Geophys. Res. Lett.* **23**, 1869.

Ashour-Abdalla, M. and Okuda, H.: 1984, 'Turbulent Heating of Heavy Ions on Auroral Field Lines', *J. Geophys. Res.* **89**, 2235.

Ashour-Abdalla, M., Schriver, D., and Okuda, H.: 1988, 'Transverse Ion Heating in Multicomponent Plasmas Along Auroral Zone Field Lines', *J. Geophys. Res.* **93**, 12,826.

Axford, W. I.: 1968, 'The Polar Wind and the Terrestrial Helium Budget', *J. Geophys. Res.* **73**, 6855.

Ball, L.: 1989, 'Can Ion Acceleration by Double-Cyclotron Absorption Produce O^+ Ion Conics?', *J. Geophys. Res.* **94**, 15,257.

Ball, L. and André, M.: 1991a, 'Heating of O^+ Ions in the Cusp/Cleft: Double-Cyclotron Absorbtion Versus Cyclotron Resonance', *J. Geophys. Res.* **96**, 1429.

Ball, L. and André, M.: 1991b, 'What Parts of Broadband Spectra are Responsible for Ion Conic Production?' *Geophys. Res. Lett.* **18**, 1683.

Barakat, A. R. and Schunk, R. W.: 1983, 'O^+ Ions in the Polar Wind', *J. Geophys. Res.* **88**, 7887.

Blelly, P. L. and Schunk, R. W.: 1993, 'A Comparative Study of the Time-Dependent Standard 8-, 13-, and 16-Moment Transport Formulations of the Polar Wind', *Annales Geophys.* **11**, 443.

Bonnell, J., Kintner, P., Wahlund, J.-E., Lynch, K., and Arnoldy R.: 1996, 'Interferometric Determination of Broadband ELF Wave Phase Velocity Within a Region of Transverse Auroral Ion Acceleration', *Geophys. Res. Lett.* **23**, 3297.

Borovsky, J. E.: 1984, 'The Production of Ion Conics by Oblique Double Layers', *J. Geophys. Res.* **89**, 2251.

Borovsky, J. E.: 1993, 'Auroral Arc Thickness as Predicted by Various Theories', *J. Geophys. Res.* **98**, 6101.

Burch, J. L.: 1988, 'Energetic Particles and Currents: Results From Dynamics Explorer', *Rev. Geophys.* **26**, 215.

Chang, T. and Coppi, B.: 1981, 'Lower Hybrid Acceleration and Ion Evolution in the Supraauroral Region', *Geophys. Res. Lett.* **8**, 1253.

Chang, T., Crew, G. B., Hershkowitz, N., Jasperse, J. R., Retterer, J. M., and Winningham, J. D.: 1986, 'Transverse Acceleration of Oxygen Ions by Electromagnetic Ion Cyclotron Resonance with Broadband Left-Hand-Polarized Waves', *Geophys. Res. Lett.* **13**, 636.

Chang, T.: 1993, 'Lower-Hybrid Collapse, Caviton Turbulence, and Charged Particle Energization in the Topside Auroral Ionosphere and Magnetosphere', *Phys. Fluids B* **5**, 2646.

Chappell, C. R.: 1988, 'The Terrestrial Plasma Source: A New Perspective in Solar-Terrestrial Processes From Dynamics Explorer', *Rev. Geophys.* **26**, 229.

Cladis, J. B.: 1986, 'Parallel Acceleration and Transport of Ions From Polar Ionosphere to Plasma Sheet', *Geophys. Res. Lett.* **13**, 893.

Collis, P., Häggström, I., Kaila, K., and Rietveld, M. T.: 1991, 'EISCAT Radar Observations of Enhanced Incoherent Scatter Spectra; Their Relation to Red Aurora and Field-Aligned Currents', *Geophys. Res. Lett.* **18**, 1031.

Demars, H. G. and Schunk, R. W.: 1987, 'Temperature Anisotropies in the Terrestrial Ionosphere and Plasmasphere', *Rev. Geophys.* **25**, 1659.

Demars, H. G. and Schunk, R. W.: 1989, 'Solutions to Bi-Maxwellian Transport Equations for the Polar Wind', *Planet. Space Sci.* **37**, 85.

Ergun, R. E., Klementis, E., Delory, G. T., McFadden, J. P., and Carlsson, C. W.: 1995, 'VLF Wave Localization in the Low-Altitude Auroral Oval', *Geophys. Res. Lett.* **22**, 2099.

Erlandson, R. E., Zanetti, L. J., Acũna, M. H., Eriksson, A. I., Eliasson, L., Boehm, M. H., and Blomberg, L. G.: 1994, 'Freja Observations of Electromagnetic Ion Cyclotron ELF Waves and Transverse Ion Acceleration on Auroral Field Lines', *Geophys. Res. Lett.* **21**, 1855.

Ganguli, S. B.: 1996, 'The Polar Wind', *Rev. Geophys.* **34**, 311.

Ganguli, G., Keskinen, M. J., Romero, H., Heelis, R., Moore, T., and Pollock, C. J.: 1994, 'Coupling of Microprocesses and Macroprocesses due to Velocity Shear: An Application to the Low-Altitude Ionosphere', *J. Geophys. Res.* **99**, 8873.

Gombosi, T. I., Cravens, T. E., and Nagy, A. F.: 1985, 'A Time Dependent Theoretical Model of the Polar Wind: Preliminary Results', *Geophys. Res. Lett.* **12**, 167.

Gombosi, T. I. and Rasmussen, C. E.: 1991, 'Transport of Gyration-Dominated Space Plasmas of Thermal Origin, 1, Generalized Transport Equations', *J. Geophys. Res.* **96**, 7759.

Gustafsson, G., André, M., Matson, L., and Koskinen, H.: 1990, 'On Waves Below the Local Proton Gyrofrequency in Auroral Acceleration Regions', *J. Geophys. Res.* **95**, 5889.

Giles, B. L., Chappell, C. R., Moore, T. E., Comfort, R. H., and Waite Jr., J. H.: 1994, 'Statistical Survey of Pitch Angle Distributions in Core (0–50 eV) Ions from Dynamics Explorer 1: Outflow in the Auroral Zone, Polar Cap, and Cusp', *J. Geophys. Res.* **99**, 17,483.

Heelis, R. A., Bailey, G. B., Sellek, R., Moffett, R. J., and Jenkins, B.: 1993, 'Field-Aligned Drifts of Subauroral Ion Drift Events', *J. Geophys. Res.* **98**, 21,493.

Horwitz, J. L.: 1984, 'Features of Ion Trajectories in the Polar Magnetosphere', *Geophys. Res. Lett.* **11**, 1111.

Horwitz, J. L.: 1986, 'Velocity Filter Mechanism for Ion Bowl Distributions (Bimodal Conics)', *J. Geophys. Res.* **91**, 4513.

Horwitz, J. L., Ho, C. W., Scarbo, H. D., Wilson, G. R., and Moore, T. E.: 1994, 'Centrifugal Acceleration of the Polar Wind', *J. Geophys. Res.*, **99**, 15,051.

Hultqvist, B.: 1991, 'Review Paper: Extraction of Ionospheric Plasma by Magnetospheric Processes', *J. Atmos. Terr. Phys.* **53**, 3.

Hultqvist, B.: 1996, 'On the Acceleration of Positive Ions by High-Latitude, Large-Amplitude Electric Field Fluctuations', *J. Geophys. Res.* **101**, 27111.

Johnson, J. R., Chang, T., and Crew, G. B.: 1995, 'A Study of Mode Conversion in an Oxygen-Hydrogen Plasma', *Phys. Plasmas* **2**, 1274.

Kintner, P. M., LaBelle, J., Scales, W., Yau, A. W., and Whalen, B. A.: 1986, 'Observations of Plasma Waves Within Regions of Perpendicular Ion Acceleration', *Geophys. Res. Lett.* **13**, 1113.

Kintner, P. M., Vago, J., Chesney, S., Arnoldy, R. L., Lynch, K. A., Pollock, C. J., and Moore, T. E.: 1992, 'Localized Lower Hybrid Acceleration of Ionospheric Plasma', *Phys. Rev. Lett.* **68**, 2448.

Kintner, P. M., Bonnell, J., Arnoldy, R., Lynch, K., Pollock, C., and Moore, T.: 1996, 'SCIFER-Transverse Ion Acceleration and Plasma Waves', *Geophys. Res. Lett.* **23**, 1873.

Klumpar, D. M., Peterson, W. K., and Shelley, E. G.: 1984, 'Direct Evidence for Two-Stage (Bimodal) Acceleration of Ionospheric Ions', *J. Geophys. Res.* **95**, 10,779.

Klumpar, D. M.: 1986, 'A Digest and Comprehensive Bibliography on Transverse Auroral Ion Acceleration', *Ion Acceleration in the Magnetosphere and Ionosphere*, American Geophysical Union, Washington D. C., 389.

Knudsen, D. J., Clemmons, J. H., and Wahlund, J.-E.: 1997, 'Correlation Between Core Ion Energization, Suprathermal Electron Bursts, and Broad-Band ELF Plasma Waves', *J. Geophys. Res.*, in press.

Lemaire, J.: 1972, 'Effect of Escaping Photoelectrons in a Polar Exospheric Model', *Space Res.* **12**, 1413.

Le Quéau, D., Roux, A., Rauch, J. L., Lefeuvre, F., and Bosqued, J. M.: 1993, 'Heating of Protons by Resonant Absorption in a Multicomponent Plasma, 2. Theoretical Model', *J. Geophys. Res.* **98**, 13,363.

Li, X. and Temerin, M.: 1993, 'Ponderomotive Effects on Ion Acceleration in the Auroral Zone', *Geophys. Res. Lett.* **20**, 13.

Liu, C., Horwitz, J. L., and Richards, P. G.: 1995, 'Effects of Frictional Heating and Soft-Electron Precipitation on High-Latitude F-Region Upflows', *Geophys. Res. Lett.* **22**, 2713.

Lockwood, M., Waite Jr. J. H., Moore, T., Johnson, J. F. E., and Chappell, C. R.: 1985a, 'A New Source of Suprathermal O^+ Ions Near the Dayside Polar Cap Boundary', *J. Geophys. Res.* **90**, 4099.

Lockwood, M., Chandler, M. O., Horwitz, J. L., Waite Jr., J. H., Moore, T. E., and Chappell, C. R.: 1985b, 'The Cleft Ion Fountain', *J. Geophys. Res.* **90**, 9736.

Loranc, M., Hanson, W. B., Heelis, R. A., and St.-Maurice, J. P.: 1991, 'A Morphological Study of Vertical Ionospheric Flows in the High-Latitude F Region', *J. Geophys. Res.* **96**, 3627.

Lundin, R. and Eliasson, L.: 1991, 'Auroral Energization Processes', *Annales Geophys.* **9**, 202.

Lundin, R., Haerendel, G., Boehm, M., and Holback, B.: 1994, 'Large-Scale Auroral Plasma Density Cavities Observed by Freja', *Geophys. Res. Lett.* **21**, 1903.

Lynch, K. A., Arnoldy, R. L., Kintner, P. M., and Bonnell, J.: 1996, 'The AMICIST Auroral Sounding Rocket: A Comparison of Transverse Ion Acceleration Mechanisms', *Geophys. Res. Lett.* **23**, 3293.

Lysak, R. L.: 1986, 'Ion Acceleration by Wave-Particle Interaction', *Ion Acceleration in the Magnetosphere and Ionosphere*, American Geophysical Union, Washington D. C., 261.

Miyake, W., Mukai, T., and Kaya, N.: 1996, 'On the Origins of the Upward Shift of Elevated (Bimodal) Ion Conics in Velocity Space', *J. Geophys. Res.* **101**, 26,961.

Moore, T. E., Chappell, C. R., Lockwood, M., and Waite Jr., J. H.: 1985, 'Superthermal Ion Signatures of Auroral Acceleration Processes', *J. Geophys. Res.* **90**, 1611.

Moore, T. E., Lockwood, M., Chandler, M. O., Waite Jr., J. H., Chappell, C. R., Persoon, A., and Sugiura, M.: 1986, 'Upwelling O^+ Ion Source Characteristics', *J. Geophys. Res.* **91**, 7019.

Moore, T. E., Pollock, C. J., Adrian, M. L., Kintner, P. M., Arnoldy, R. L., Lynch, K. A., and Holtet, J. A.: 1996, 'The Cleft Ion Plasma at Low Solar Activity', *Geophys. Res. Lett.* **23**, 1877.

Norqvist, P., André, M., Eliasson, L., Erikson, A. I., Blomberg, L., Lühr, H., and Clemmons, J. H.: 1996, 'Ion Cyclotron Heating in the Dayside Magnetosphere', *J. Geophys. Res.* **101**, 13,179.

Peterson, W. K., Collin, H. L., Doherty, M. F., and Bjorklund, C. M.: 1992, 'O^+ and He^+ Restricted and Extended (Bi-Modal) Ion Conic Distributions', *Geophys. Res. Lett.* **19**, 1439.

Pollock, C. J., Chandler, M. O., Moore, T. E., Waite Jr., J. H., Chappel, C. R., and Gurnett, D. A.: 1990, 'A Survey of Upwelling Ion Event Characteristics' *J. Geophys. Res.* **95**, 18,969.

Raitt, W. J. and Schunk, R. W.: 1983, *Energetic Ion Composition in the Earth's Magnetosphere*, Terra Scientific Publishing, Tokyo, 99.

Rauch, J. L., Lefeuvre, F., Le Quéau, D., Roux, A., Bosqued, J. M., and Berthelier, J. J.: 1993, 'Heating of Proton Conics by Resonant Absorption in a Multicomponent Plasma 1. Experi- mental Evidence', *J. Geophys. Res.* **98**, 13,347.

Reiff, P. H., Collin, H. L., Craven, J. D., Burch, J. L., Winningham, J. D., Shelley, E. G. Frank, L. A., and Friedman, M. A.: 1988, 'Determination of Auroral Electrostatic Potentials Using High and Low-Altitude Particle Distributions', *J. Geophys. Res.* **93**, 7441.

Retterer, J. M., Chang, T., Crew, G. B., Jasperse, J. R., and Winningham, J. D.: 1987, 'Monte Carlo Modeling of Ionospheric Oxygen Acceleration by Cyclotron Resonance with Broadband Electromagnetic Turbulence', *Phys. Rev. Lett.* **59**, 148.

Rosenbauer, H., Grünwaldt, H., Montgomery, M. D., Paschmann, G., and Sckopke, N.: 1975, 'Heos 2 Plasma Observations in the Distant Polar Magnetosphere: The Plasma Mantle', *J. Geophys. Res.* **80**, 2723.

Sharp, R. D., Johnson, R. G., and Shelley, E. G.: 1977, 'Observations of an Ionospheric Acceleration Mechanism Producing Energetic (keV) Ions Primarily Normal to the Geomagnetic Field Direction', *J. Geophys. Res.* **82**, 3324.

Sharp, R. D., Carr, D. L., Peterson, W. K., and Shelley, E. G.: 1981, 'Ion Streams in the Magnetotail', *J. Geophys. Res.* **86**, 4639.

Shelley, E. G., Johnson, R. G., and Sharp, R. D.: 1972, 'Satellite Observations of Energetic Heavy Ions During a Geomagnetic Storm', *J. Geophys. Res.* **77**, 6104.

Shelley, E. G., Sharp, R. D., and Johnson, R. G.: 1976a, 'Satellite Observations of an Ionospheric Acceleration Mechanism', *Geophys. Res. Lett.* **3**, 654.

Shelley, E. G., Sharp, R. D., and Johnson, R. G.: 1976b, 'He^{++} and H^{+} Flux Measurements in the Day Side Cusp: Estimates of Convection Electric Field', *J. Geophys. Res.* **81**, 2363.

Shelley, E. G.: 1988, *Adv. Space Res.* **6-3**, 121.

Shukla, P. K., Stenflo, L., Bingham, R., and Dendy, R. O.: 1996, 'Ponderomotive Force Acceleration of Ions in the Auroral Region', *J. Geophys. Res.* **101** 27,449.

Schunk, R. W. and Watkins, D. S.: 1981, 'Electron Temperature Anisotropy in the Polar Wind', *J. Geophys. Res.* **86**, 91.

Schunk, R. W.: 1988, *Modeling Magnetospheric Plasma*, Geophys. Monogr. Ser. **44**, American Geophysical Union, Washington D. C., 219.

Singh, N.: 1994, 'Ponderomotive Versus Mirror Force in the Creation of the Filamentary Cavities in Auroral Plasma', *Geophys. Res. Lett.* **21**, 257.

Swift, D.: 1990, 'Simulation of the Ejection of Plasma from the Polar Ionosphere', *J. Geophys. Res.* **95**, 12103.

Tam S. W. Y., Yasseen, F., Chang, T., Ganguli, S. B., and Retterer, J. M.: 1995, 'Self-Consistent Kinetic Photoelectron Effects on the Polar Wind', *Geophys. Res. Lett.* **22**, 2107.

Temerin, M.: 1986, 'Evidence for a Large Bulk Ion Conic Heating Region', *Geophys. Res. Lett.* **13**, 1059.

Temerin, M. and Lysak, R. L.: 1984, 'Electromagnetic Ion Cyclotron Mode (ELF) Waves Generated by Auroral Electron Precipitation', *J. Geophys. Res.* **89**, 2849.

Temerin, M. and Roth, I.: 1986, 'Ion Heating by Waves with Frequencies Below the Ion Gyrofrequency', *Geophys. Res. Lett.* **13**, 1109.

Vago, J. L., Kintner, P. M., Chesney, S. W., Arnoldy, R. L., Lynch, K. A., Moore, T. E., and Pollock, C. J.: 1992, 'Transverse Ion Acceleration by Localized Lower Hybrid Waves in the Topside Auroral Ionosphere', *J. Geophys. Res.* **97**, 16,935.

Wahlund, J.-E., Opgenoorth, H. J., Häggström, I., Winser, K. J., and Jones, G. O. L.: 1992, 'EISCAT Observations of the Topside Ionospheric Ion Outflows During Auroral Activity: Revisited', *J. Geophys. Res.* **97**, 3019.

Wahlund J.-E., Eriksson, A. I., Holback, B., Boehm, M. H., Bonnell, J., Kintner, P. M., Seyler, C. E., Clemmons, J. H., Eliasson, L., Knudsen, D. J., Norqvist, P., and Zanetti, L. J.: 1996, 'Broadband ELF Plasma Emissions During Auroral Energization, 1, Slow Ion Acoustic Waves', *J. Geophys. Res.*, in press.

Whalen, B. A., Bernstein, W., and Daly, P. W.: 1978, 'Low Altitude Acceleration of Ionospheric Ions', *Geophys. Res. Lett.* **5**, 55.

Wilson, G. R.: 1994, 'Kinetic Modeling of O^+ Upflows Resulting from E×B Convection Heating in the High-Latitude *F* Region Ionosphere', *J. Geophys. Res.* **99**, 17,453.

Winningham, J. D. and Gurgiolo, C.: 1982, 'DE-2 Photoelectron Measurements Consistent With a Large Scale Parallel Electric Field over the Polar Cap', *Geophys. Res. Lett.* **9**, 977.

Witt, E., Hudson, M. K., Li, X., Roth, I., and Temerin, M.: 1995, 'Ponderomotive Effects on Distributions of O^+ Ions in the Auroral Zone', *J. Geophys. Res.* **100**, 12,151.

Yasseen, F., Retterer, J. M., Chang, T., and Winningham, J. D.: 1989, 'Monte-Carlo Modeling of Polar Wind Photoelectron Distributions with Anomalous Heat Flux', *Geophys. Res. Lett.* **16**, 1023.

Yasseen, F. and Retterer, J. M.: 1991, 'Critical Points in the 16-Moment Approximation', *J. Geophys. Res.* **96**, 1827.

Yau, A. W., Whalen, B. A., Abe, T., Mukai, T., Oyama, K. I., and Chang, T.: 1995, 'Akebono Observations of Electron Temperature Anisotropy in the Polar Wind', *J. Geophys. Res.* **100**, 17,451.

Yau, A. W. and André, M.: 1997, 'Sources of Ion Outflow in the High Latitude Ionosphere', *Space Sci. Rev.*, this issue.

Address for correspondence: Mats André, Swedish Institute of Space Physics, Umeå University, S-901 87 Umeå, Sweden

FOUR CONTEMPORARY ISSUES CONCERNING IONOSPHERIC PLASMA FLOW TO THE MAGNETOSPHERE

J. L. HORWITZ
Center for Space Plasma and Aeronomic Research, The University of Alabama in Huntsville, Huntsville, USA

T. E. MOORE
Space Plasma Branch, Space Sciences Laboratory, Marshall Space Flight Center, Alabama, USA

Received February 21, 1997; Accepted in final form March 17, 1997

Abstract. In this review, we examine four specific questions/issues of contemporary interest within the overall topic of ionospheric plasma outflow into the magnetosphere. These four question areas are framed here as: (1) Are high-latitude F-region upflows predominantly driven by soft auroral electron precipitation?; (2) Is the O^+ within the polar cap magnetosphere supplied primarily by the cleft ion fountain or a direct polar cap ionospheric source?; (3) Is centrifugal acceleration an important mechanism in the acceleration of ionospheric plasma outflows?; and (4) Are lobe ionospheric outflows captured by the plasma sheet?

Key words: Magnetosphere, Ionosphere, Plasma, Transport

1. Introduction

Although in the early years of the magnetospheric exploration it was often conjectured that the principal plasma source for the main magnetospheric regions is the solar wind (e.g., Hill, 1974), the consensus view has shifted toward a much greater role for ionospheric supply, with some authors contending that the ionospheric may be the dominant source of the plasma within the plasma sheet and other magnetospheric plasma regions (e.g., Chappell et al., 1987), or at least within the more near-Earth portions of the magnetosphere (e.g., Moore and Delcourt, 1995). Thus, there have been numerous reviews written over the years which have been concerned partially or largely with ionospheric plasma supply to the magnetosphere (e.g., Horwitz, 1982, 1987, 1995; Moore and Delcourt, 1995; Shelley, 1995).

The purpose of this review will not be to cover all aspects of ionospheric supply to the magnetosphere, but we will target four topical question areas around which there has been recent progress and substantial controversy: (1) Are high-latitude F-region upflows predominantly driven by soft auroral electron precipitation?; (2) Is the O^+ within the polar cap magnetosphere supplied primarily by the cleft ion fountain or a direct polar cap ionospheric source?; (3) Is centrifugal acceleration an important mechanism in the acceleration of ionospheric plasma outflows?; and (4) Are lobe ionospheric outflows captured by the plasma sheet?

Space Science Reviews **80**: 49–76, 1997.

2. Are high-latitude F-region upflows predominantly driven by soft auroral electron precipitation?

Spacecraft and radar observations have established that upper F-region/topside ionosphere field-aligned flows arise in response to **ExB**-driven heating and auroral particle precipitation (e.g., Heelis et al., 1984, 1992, Tsunoda et al., 1989, Wahlund et al., 1992), and some observations and theory have suggested that convection shears might also produce low-altitude upflows (Ganguli et al., 1994). Coinciding with this recent progress on upflows, there have also been large-scale radar (e.g., Foster,1993) and model-satellite data comparisons (Sojka et al., 1992, 1994) showing how convection transports enhanced ionization regions horizontally at high latitudes. Statistical global patterns of these field-aligned F-region flows are beginning to emerge (e.g., Loranc et al., 1991; Heelis et al., 1992). These patterns show that upflows tend to be observed in auroral regions and downflows in the polar cap, indicating an overall "breathing" motion of the ionosphere in response to the enhancements and reductions of upflow drivers during the convection cycles.

Very recently there have been case event model-data comparison investigations in which the effects of soft electron (here referring to electrons below 0.5 keV) precipitation on high-latitude F-region/topside ionospheric upflows were more carefully examined. Such electron precipitation may exist over broad zones of the high-latitude ionosphere, particularly during northward IMF conditions (e.g., Makita et al., 1988). In this case, we are primarily focusing ultimately on the F-region/topside ionization and thermal electron heating effects of large fluxes of such precipitating electrons, rather than possible transverse ion heating effects and other derivative consequences of such electrons (e.g., possible associated field-aligned currents) (cf. Eliasson et al., 1994).

Liu et al. (1995) successfully modeled evening auroral zone passes of ionopheric plasma and soft-electron precipitation measurements from both HILAT and DE-2, using an ionospheric fluid plasma transport model with the spacecraft-measured ion convection velocities and soft-electron precipitation characteristics as inputs for frictional ion heating and ionization and thermal electron heating, respectively. An example from Liu et al. (1995) of such a model-data comparison for the high latitude topside ionosphere is displayed in Figure 1. The agreement between measured ionospheric temperatures, densities and bulk vertical flows and the modelled ionosphere using the convection-driven frictional heating and the soft electron precipitation input parameters from the DE-2 data is fairly close. Details of the model and the data are provided in Liu et al. (1995). However, careful examination of the modeling responses to the independent inputs (see Liu et al. (1995)), indicated that the soft-electron precipitation effects were sufficient to explain the peak upflow velocities and fluxes observed as well as the electron temperatures, whereas the convection-driven frictional heating inputs were significant in reproducing the local ion temperatures but were of secondary importance in the driving of these ionospheric upflows.

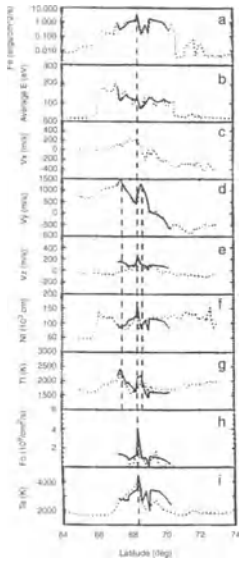

Figure 1. Comparison of measurements (dotted lines) of ionospheric parameters for a DE-2 high-latitude pass (at 700-800 km altitude on November 4, 1981) and ionospheric fluid model results (solid lines). The top four panels show the average energy and energy flux for precipitating soft ($\leq$ 1 keV) electrons (from LAPI), and the convection components along and perpendicular to the satellite track (from IDM/RPA), which are considered the "drivers" for ionospheric dynamics. The remaining panels show what may be regarded as the ionospheric "responses" to such "drivers": the ion (O^+) vertical drift, density, temperature, upflux (from IDM/RPA), and the electron temperature (from LANG). Copyright, American Geophysical Union, 1995.

Further model-data comparisons suggesting the importance of soft electron precipitation in the propulsion of the upward high-latitude ionospheric flows were provided by Caton et al. (1996a), who simulated three snapshot profiles of plasma densities, temperatures, and field-aligned flow velocities for the 200-900 km altitude range as measured by the EISCAT incoherent radar facility, using the same ionospheric plasma transport code that was employed by Liu et al. (1995). Although the model-radar data comparison by Caton et al. (1996a) relied on adjustable inputs for the soft electron precipitation parameters, the close agreement attained for the 200-900 km profiles for the inputs that were used again indicated a dominant role for soft-electron precipitation, as well as downward magnetospheric heat fluxes, in driving these simulated and observed F-region/topside ionospheric upflows.

The most conclusive evidence on the upflow-driving role of the thermal electron temperatures (as heated by soft electron precipitation processes) is contained in the very recent statistical results of Seo et al. (1997). Figures 2a and b show topside field-aligned velocities and fluxes plotted versus local electron temperatures as measured by instruments on Dynamics Explorer-2, for seven auroral region passes in the 850-950 km altitude range. Averages within narrow temperature bins were

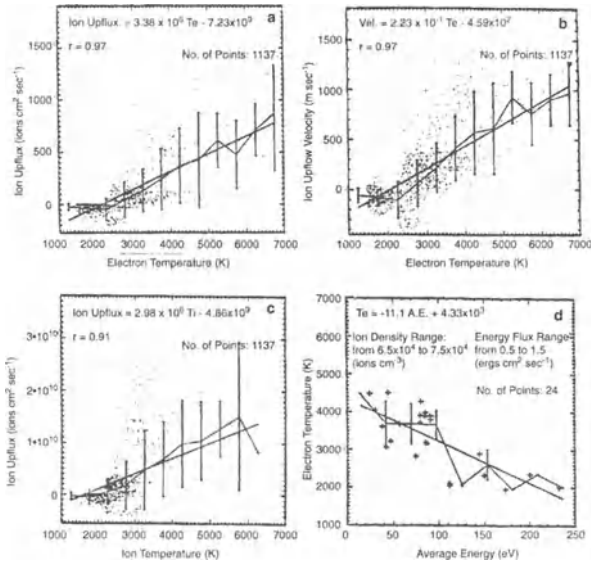

Figure 2. (a) DE-2 measurements of field-aligned topside ionospheric ion velocities versus electron temperatures. (b) Field-aligned topside ionospheric ion velocities versus ion temperatures. (c) Field-aligned topside ion fluxes versus average energies of soft electron precipitation. (d) Electron temperature versus average soft electron precipitation energy for restricted ranges of both local plasma density (6.5-7.5× 10^4 ions/cm^3) and soft electron precipitation energy flux (0.5-1.5 ergs-cm^{-2}-sec^{-1}). From Seo et al. (1997). Copyright, American Geophysical Union, 1997.

calculated together with the indicated standard deviations, and a linear least square straight line fit for each point set was also computed and supplied. As may be seen, the linear correlation of the fluxes with the electron temperatures is very high, with a correlation coefficitent of r=0.97. The correlation of the flow velocities is also high at r=0.97. The Seo et al. (1997) correlations of field-aligned velocities and fluxes with the ion temperatures were slightly lower, at r=0.91 and 0.94, respectively. This suggests that the ambipolar electric field, which is directly proportional to the electron temperature, may be more influential in driving these upflows than the ion pressure gradient. A similar closer correspondence with electron than ion temperatures of upflows and fluxes was observed in EISCAT radar observations of upflows at lower altitudes by Keating et al. (1990) and more recently by Sandridge et al. (1996b).

Figures 2c and 2d, also from Seo et al. (1997), further show the relationship of the field-aligned flows to direct properties of soft auroral electron precipitation. Figure 2c displays the ion fluxes versus the average energies of the corresponding soft electron precipitation spectrum, which were obtained by integrating over the measured spectrum for electrons below 1 keV (and above the 5 eV threshold of the instrument). As can be seen, the only instances in which very large flux-

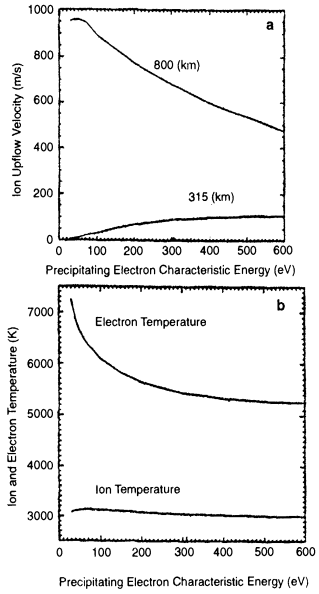

Figure 3. (a) Modeling results for the ionospheric field-aligned ion velocity at 315 and 800 km altitude versus the characteristic electron precipitation energy, for a fixed precipitation energy flux of 1.75 ergs-cm^{-2} sec^{-1}. (b) Ion and electron temperatures at 800 km altitude versus precipitation average energy. From Caton et al. (1996b).

es ($\geq 5 \times 10^9 ions - cm^{-2} - sec^{-1}$) were observed were during periods when the average soft-electron precipitation energies were below 80-90 eV. Figure 2d indicates a further interesting relationship between the electron temperature and the soft electron precipitation average energy. These data were highly filtered for narrow ranges in ambient density and soft electron precipitation energy flux, as indicated, to largely remove expected variations with these parameters. The resulting samples showed an inverse relationship of the local electron temperature with the precipitation average energy, with a linear fit correlation coefficient of -.90. Seo et al. (1997) also demonstrated a strong correlation between upflows and the energy fluxes of the soft electron precipitation.

These various pieces of evidence lead to the tentative conclusion that soft auroral electron precipitation is the primary driver for F-region/topside upflows. It would appear that the direct connection between the soft electron precipitation and the upflows is through precipitation-induced enhancements of the ionospheric electron temperature, with ionization gradients produced by the precipitation as well.

The above observations and model-data comparisons prompted Caton et al. (1996b) to perform a systematic modeling study of the effects of soft electron precipitation events on ionospheric field-aligned flows. Figure 3a displays the relationship of the asymptotically-attained field-aligned flow velocity at 800 km and 315 km altitude for sustained precipitation with an energy flux of 1.75 ergs-cm^{-2}-

sec^{-1}, distilled from several runs, again using the ionopheric transport model as employed by Liu et al. (1995) and Caton et al. (1996a). As can be seen, for this constant energy flux, the modeled steady upflow velocities decline with the average energy of the precipitation at 800 km, while they increase the average energy at 315 km. Qualitatively, at least, the trends at 800 km are consistent with the statistical observations for fluxes and velocities as presented for the topside altitude range by Seo et al. (1997). Figure 3b further shows that the model produces electron temperatures in the topside which also decline with soft electron precipitation energy, as did the observed electron temperatures. In the model these electron temperature increases are produced by Coulomb collisions between the soft electron precipitation and the thermal electron plasma. As the characteristic energy declines, for constant energy flux, the number flux of incident auroral electrons increases and the collision cross section for interaction and energy transfer to the thermal electrons increases as well. The overall level of the electron temperatures is higher in the model, which may be a result of use of a different characteristic atmosphere than was actually present during the DE-2 observations; however, the qualitative trends in both the electron and ion temperatures versus soft electron precipitation characteristic energy are consistent with those of the DE-2 observations.

There may be additional processes involved in the energy transfer from the soft electron precipitation and in the driving of the upflowing topside ionosphere, particularly for the largest fluxes (e.g., $\geq 5\times10^9$ ions-cm^{-2}-sec^{-1}) which are observed only when the average soft electron precipitation energy lies below 80 eV. These additional processes may be non-collisional in nature. However, we believe, as discussed here, that there is mounting evidence in support of the idea that soft electron precipitation being the primary driver of high-latitude F-region and topside upflows.

3. Is the O^+ within the polar cap magnetosphere supplied primarily by the cleft ion fountain or a direct polar cap ionospheric source?

Substantial outflowing streams of low-energy O^+ were discovered during the mid-1980's in the mid-altitude polar cap magnetosphere (e.g., Waite et al., 1985) and in the tail lobes (e.g., Candidi et al., 1988). Around the same time, measurements by Dynamics Explorer-1 revealed a large source of upflowing or "upwelling" ionospheric ions, particularly O^+, associated with the pre-noon cleft topside ionosphere (e.g, Lockwood et al., 1985a). This restricted source of ionospheric ions and the consequentflow outward into the mid-altitude polar cap magnetosphere soon after was termed the "cleft ion fountain" (Lockwood et al., 1985b; Horwitz and Lockwood, 1985).

Given that substantial O^+ is present in the mid-altitude polar cap magnetosphere, as well as the tail lobes, we may pose the central question as stated in the title of this section: Is this ion population primarily supplied by the cleft ion

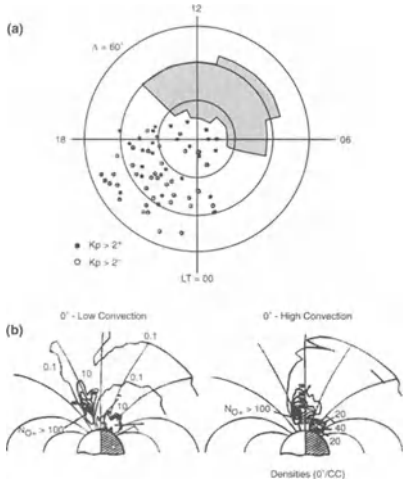

Figure 4. (a) Ends of DE-1 polar cap orbital segments on which low-energy O^+ counts were observed for high and low Kp. Also shown is the region of lower altitude upwelling events detected by Lockwood et al. (1985a). From Lockwood et al. (1985b). Copyright, American Geophysical Union, 1985. (b) O^+ density contours within the polar magnetosphere for high and low convection levels computed with a two-dimensional kinetic model (Horwitz and Lockwood, 1985b). Copyright, American Geophysical Union, 1985.

fountain, or does the central polar cap contribute an important portion of this polar cap magnetospheric O^+ population?

In the mid-1980's the Dynamics Explorer-1 low-energy ion measurements and concurrent kinetic modelling seemed to point toward the cleft ion fountain as the primary source of the O^+. For example, Waite et al. (1985) utilized measured field-aligned bulk streaming velocities of O^+ and used low-altitude measurements of the ionospheric anti-sunward convection to estimate the mapped-back source location of these O^+ streams, finding that they mapped to the ionospheric cleft region. The concept of the cleft ion fountain supply to the polar cap magnetosphere is supported and illustrated, respectively, by Figures 4a and b. Figure 4a, from Lockwood et al. (1985b), displays nightward extension ends of DE-1 orbital segments on which O^+ counts were "significant" (very roughly, corresponding to 1 O^+/cm^3) for traversals of the 3-5 R_E polar cap magnetosphere for low and high Kp. Also shown as the shaded region is the lower altitude "upwelling event" concentration , from Lockwood et al. (1985a). It can be seen that the "O^+-observed" segment ends for the high Kp cases extend significantly further in the antisunward direction over the polar cap than do those for the low Kp cases. The differences for high and low Kp could include several factors, but one is likely to be that the anti-sunward convection level over the polar cap is higher during enhanced Kp, which would tend to blow the cleft-origin upwelling O^+ further over the polar cap during these periods. This phenomenon is illustrated in Figure 4b, which shows contours of O^+ densi-

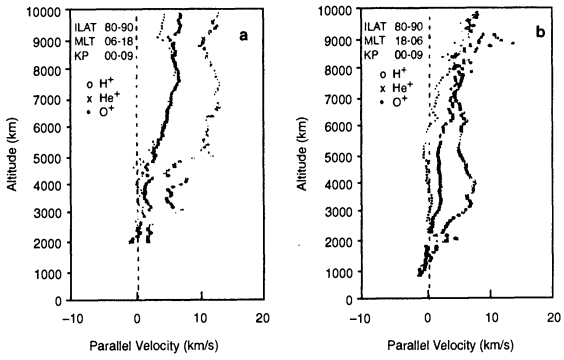

Figure 5. (a) Average ion bulk outflowing velocities for the dayside polar magnetosphere at very high latitudes as detected by Akebono. (b) Average ion velocities for the nightside. From Abe et al. (1993a) Copyright, American Geophysical Union, 1993.

ty for low and high convection levels computed with a two-dimensional kinetic model (Horwitz and Lockwood, 1985). For the same upwelling region "source" levels, the O^+ densities within the polar cap up to at least 2-3 R_E are indicated to be significantly higher, at 1-10 O^+ ions/cm^3, in the central and nightside polar cap magnetosphere during high Kp than during low Kp.

More recent Akebono observations of outflowing O^+ at very high latitudes above 5000-6000 km have prompted consideration of a steady outflowing O^+ component to the polar wind perhaps across the broad polar cap region. Figures 5a and b display, for the dayside and nightside, respectively, averaged ion bulk streaming velocities measured by Abe et al. (1993) versus altitude for invariant latitudes greater than 80°. It is evident that especially on the dayside, the O^+ is measured to be flowing outward at streaming velocities of greater than 0.5 km/s at least above 2500 km altitude.

If there is a significant O^+ component to the steady polar wind out of the polar cap proper (i.e., in the absence of auroral processes), there are a number of mechanisms that have been proposed for producing this. Barakat and Schunk (1983) essentially suggested that high electron temperatures, perhaps associated with the polar rain effects, could lead to large ambipolar electric fields which would accelerate the O^+ component. Horwitz et al. (1994a) showed that convection-driven centrifugal acceleration (see next section) may propel the outward flows observed by Akebono. Very recently, Tam et al. (1995) have performed calculations which suggest that significant electrostatic potential drops associated with photo-electron fluxes would exist at relatively low altitudes (below 700 km altitude), and that these would accelerate to supersonic speeds both the H^+ and O^+ ion populations. Tam et al. (1995) suggested that this photo-electron-driven polar wind mechanism could explain the H^+ and O^+ field-aligned velocity profiles observed by Akebono,

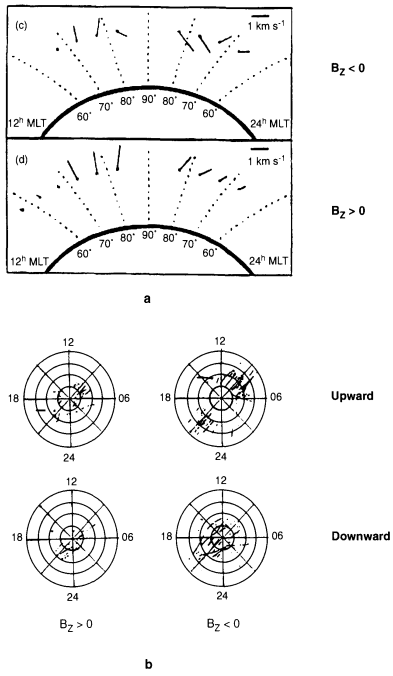

Figure 6. (a) Average two-dimensional O^+ bulk velocities for 4000 km altitude as projected into the noon-midnight meridian, for southward (upper panel) and northward (lower panel) IMF conditions. From Chandler (1995). Copyright, American Geophysical Union, 1995. (b) DE-2 orbital segments (300-1000 km altitude range) containing downward or upward vertical flows for northward and southward IMF conditions as indicated. From Loranc et al. (1991). Copyright, American Geophysical Union, 1991.

including the dayside asymmetry observed at very high latitudes (e.g., Figures 5a and 5b).

We believe that important clues to the origin of the high-altitude O^+ in the polar cap magnetosphere may be found in the nature of the field-aligned flows at comparatively low altitudes, say below 4000 km. Figures 6a and b, from DE-1 and -2 ion observations, indicate where and under what conditions O^+ was observed to be flowing upward or downward at high-latitudes. Figure 6a shows averaged two-dimensional O^+ bulk velocity vectors averaged from the range 2000-4000 km altitude from DE-1 0-50 eV ion measurements (Chandler, 1995). The two panels are for southward (upper panel) and northward (lower) interplanetary magnetic field conditions. It may be seen that the field-aligned component of the O^+ flow is generally downward within the polar cap for southward IMF conditions, and upward for northward IMF conditions.

Further evidence supporting this trend is seen in Figure 6b, which displays lower altitude DE-2 (300-1000 km) orbital segments on a polar grid for high latitudes for which vertical flows were either upward or downward (Loranc et al., 1991). It is

readily seen from Figure 6b that upward flows are seen in the central polar cap region only for northward IMF. During intervals of southward IMF, vertical flows at these altitudes are only downward at the most poleward latitudes, while upward flows are seen in locations which would generally coincide with the auroral oval distribution.

The above data suggest that plasma field-aligned flow directions at altitudes below approximately 4000 km are downward during in the nominal polar cap region during southward IMF conditions, and generally upward (though not always) during northward IMF conditions. Our preliminary interpretation is that during southward IMF, the upward flows of O^+ that are seen *above* 5000-6000 km altitude or so in Akebono and DE-1 data originate in the cleft ion fountain, or at least the dayside auroral oval. The downward flows at lower altitudes in the polar cap thus are simply the gravitationally-bound portion of the cleft ion fountain. The upward flows at low altitudes observed within the "nominal polar cap" during *northward* IMF can reasonably be associated with auroral processes. These would include theta arcs (Frank et al., 1986) or, more generally, polar aurora which thread the very high latitude regions only during northward IMF conditions. In this sense, we are arguing that there is no evidence for an O^+ component to the polar wind coming from the "polar cap proper", i.e., ionospheric regions free of auroral precipitation and associated processes. As indicated by the picture summarized by Newell et al. (Newell et al., 1997), such a polar cap proper regin might even essentially vanish under conditions of strongly northward IMF sustained over several hours.

These comments, of course, do not apply to the H^+ streams over the polar cap, which most likely do originate frequently from the polar cap ionosphere proper. Even if these arguments are largely correct on the basis of the data analyzed to date, however, there may still be a solar illumination dependence that factors into possible O^+ up/outflow from the polar cap ionosphere proper. In other words, it could be that an O^+ component to the polar wind, for example, be supplied from a strongly sunlit polar cap ionosphere but not a weakly sunlit polar cap ionosphere. This indeed would be consistent with the photo-electron driven H^+/O^+ polar wind interpretation of the Akebono data suggested, for example, by Tam et al. (1995). However, for the time being, we believe that outward flows of low-energy plasma seen above 6000 km at very high-latitudes should be mainly attributed to the cleft ion fountain during southward IMF conditions, and theta auroral processes for northward IMF conditions.

4. Is centrifugal acceleration an important mechanism in the acceleration of ionospheric plasma outflows?

Cladis (1986) was probably the first to suggest the importance of convection-driven parallel acceleration of ions, particularly O^+, as a possibly important energization mechanism for plasma sheet ions. Figure 7a shows ion energies as functions of time

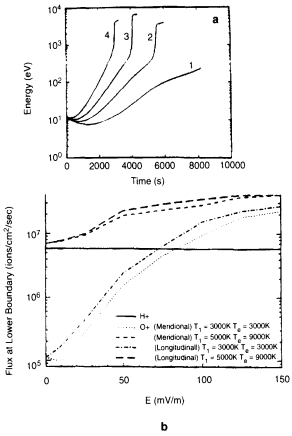

Figure 7. (a) O^+ energies versus time for cleft ion fountain ions launched under the influence of four different polar ionospheric convection electric fields. From Cladis (1986). Copyright, American Geophysical Union, 1986. (b) Steady-state escaping fluxes of O^+ from the polar ionosphere versus the ionospheric convection electric field level for warm and cool topside ionospheric source distributions, and longitudinal and meridional high-latitude convection. From Horwitz et al. (1994a). Copyright, American Geophysical Union, 1994.

for initially low-energy O^+ ions launched from the cleft ion fountain and convected antisunward into the polar cap magnetosphere and the plasma sheet region, for four different polar cap ionospheric electric fields, from ion trajectory calculations performed by Cladis (1986). As can be seen, the O^+ ion energies, starting from about 10 eV characteristic cleft ión fountain energies, for the larger convection fields are calculated to attain more than 1 keV in their trajectories , which include passage through the neutral sheet region (the neutral sheet region energy gain is seen in the steep sloped portion of curves 2-4). Horwitz (1987) coined the term "centrifugal" to refer to an important term in this convection-driven parallel acceleration. This is because of the close mechanical analogy between the parallel acceleration of particles convecting through rotating magnetic field lines and the outward "centrifugal" flinging of a bead on a rotating rod. In the reminder of this section, we shall use this term to refer to the principal parallel acceleration effects experienced by polar plasma outflows convecting through "rotating" magnetic field directions. A somewhat related mechanism for possibly driving ionospheric outflows which will not be be discussed further is the so-called ponderomotive force which originates with low-frequency electromagnetic wave modes (e.g., Li and Temerin, 1993; Witt et al., 1995).

Swift (1990) developed a sophisticated fluid simulation in curvilinear coordinates to study self-consistent polar plasma outflow with particular attention to the effects of this "centrifugal acceleration". Swift (1990) concluded that O^+ outflow is effectively smothered by H^+ unless additional heating processes are present. However, it may be that additional "fine tuning" of the ionospheric processes involved

will be required for incorporation into Swift's calculations before this conclusion can be fully interpreted.

Horwitz et al. (1994a) used a time-dependent semikinetic model to systematically explore the effects of centrifugal acceleration on the polar wind outflow. Horwitz et al. (1994a) derived a simple expression for the centrifugal acceleration along exactly polar field lines, which may be considered an approximation for outflow along general high-latitude field lines, as:

$$a = 1.5 \frac{E_i^2}{B_i^2} \frac{1}{r_i^3} r^2$$

where E_i, B_i and r_i are the ionospheric-level convection electric field, magnetic field and geocentric distance, respectively, and r is the geocentric distance where the parallel acceleration is to be evaluated. The expression above elucidates how the centrifugal acceleration increases dramatically approximately as the square of the geocentric distance.

Figure 7b shows the effect that the centrifugal acceleration can have on the net outflow of ions from the polar ionosphere. Under steady convection and ionospheric source conditions, the net escape flux of O^+ is predicted to increase by a factor of about 100 from ionospheric convection electric field of zero to a convection electric field of 100 mV/m, if the topside ionosphere at 2000 km is fairly cool (both ions and electrons at 3000 K). The increase in O^+ escape flux is predicted to be a much less dramatic factor of about 4 or so over the same convection electric field range when the topside temperature is already relatively warm, at T_i=5000 K and T_e=9000 K. The H^+ escape flux level is completely unaffected by the centrifugal acceleration. The source temperature differences in the computed O^+ escape flux result from the fact that in the warm source case, more of the source O^+ is already able, even in the absence of centrifugal acceleration, to escape at the higher temperatures, due directly to a greater proportion of the source distribution's tail having escape energies with the elevated ion temperatures as well as an enhanced ambipolar electric field. In the case of H^+, at the source altitudes the H^+ is already a fully outflowing polar wind and so the acceleration has no effect on the net outflux, though the H^+ bulk velocity is accelerated to high speeds (cf. Horwitz et al., 1994a).

Figure 8a shows the statistical average high-latitude O^+ field-aligned velocity profile obtained from Akebono core ion measurements by Abe et al. (1993), as compared with O^+ velocity profiles computed for the centrifugally-accelerated polar wind, from Horwitz et al. (1994a). These velocity profiles were computed under steady-state conditions at ionospheric convection electric field levels of 50 and 100 mV/m, and for an expansion under 50 mV/m conditions at 1500 seconds after initiation of the expansion. Since the steady-state case involving a 100 mV/m ionospheric convection field is probably not realistic for the typical polar ionosphere (unless the convection increases faster with altitude than simply according to the mapping along equipotential field lines). It would appear from this comparison that the case with the combination of the expansion process and the 50 mV/m

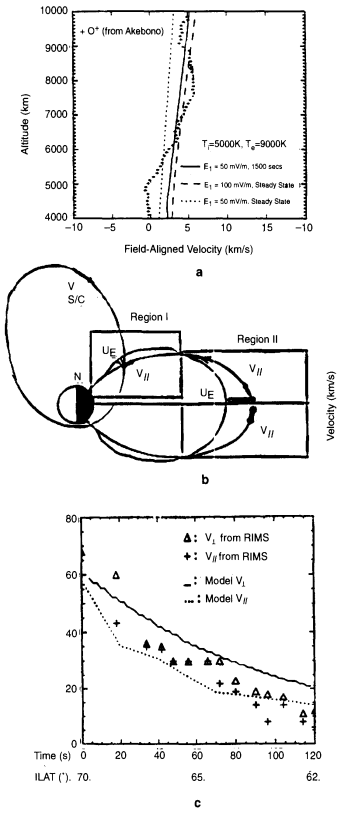

Figure 8. (a) Average O^+ bulk outward flow velocity profile at high latitudes measured with Akebono, together with velocity profile computed for steady-state conditions at ionospheric convection levels of 50 and 100 mV/m as well as 1500 seconds into a polar wind expansion at a convection electric field level of 50 mV/m. From Horwitz et al. (1994a). Copyright, American Geophysical Union, 1994. (b) Schematic illustration of a substorm dipolarization event showing reconfiguring magnetic field lines and the DE-1 orbit sampling parallel and perpendicular ion velocities at mid-altitudes along middle magnetospheric field lines. From Liu et al. (1994b). Copyright, American Geophysical Union, 1994. (c) Bulk ion parallel and perpendicular velocities detected during a two-minute segment of a substorm dipolarization event as compared with modeled velocity components for the spacecraft position as computed using a time-dependent semikinetic simulation model of the ionospheric ion outflow. From Horwitz and Liu, 1995b.

convection field level is both most realistic and most closely duplicative of the Akebono velocity profile. From this comparison, Horwitz et al. (1994a) suggested that centrifugal acceleration would be a viable contributing mechanism for explaining even the Akebono velocity profiles for O^+.

A very intriguing set of Dynamics Explorer-1 measurements that appears to conclusively demonstrate centrifugal acceleration was reported by Liu et al. (1994), who obtained ion distribution functions for core H^+, He^+ and O^+ measured at 2-3 R_E geocentric distance along middle magnetospheric field lines during a sub-

storm "dipolarization event". Figure 8b shows a schematic illustration of the DE-1 orbit and the magnetic field line re-configuration evolution envisioned by Liu et al. (1994). In this schematic, the dipolarizing middle magnetosphere field lines move poleward between ionospheric and mid-latitudes, and this fast poleward convection drives the outward centrifugal acceleration of the ionospheric ions. Figure 8c shows a comparison between some of the ion parallel and perpendicular velocity data points during a substorm dipolarization event and corresponding semikinetic modeling of this event (Horwitz and Liu, 1995). The modeling involved tracking the evolution of injected ionospheric ion distribution functions along various middle-magnetosphere field lines which were modeled as undergoing dipolarizing reconfigurations during the substorm onset. The modeled bulk velocities displayed versus time in Figure 8c were then taken for the spacecraft position as different field lines passed through that position during the 2-minute substorm onset interval shown. The invariant latitudes of the footpoints of these field lines are shown along with the time in this plot. As can be seen, both the modeled and measured perpendicular and parallel velocity data points exhibited a decline from about 60 km/s to 20 km/s over this interval, and the trends in the data are quite well-replicated by the model.

In the model traces, the parallel velocities computed result entirely from outward centrifugal acceleration driven by the poleward convection associated with the moving dipolarizing field lines (Figure 8b). The fact that they agree with the data suggests that this centrifugal acceleration mechanism is likely to be the driving force for these outward flows. The most telling signature in Figure 8c is that the measured parallel and perpendicular ion bulk velocity data points (plusses and triangles, respectively) are essentially equal throughout. Horwitz et al. (1994a) demonstrated that when convection-driven centrifugal acceleration dominates, the parallel and convection velocities asymptotically approach equality; i.e., the flow streaming angle approaches 45° to the magnetic field direction.

Our conclusion from the available evidence is that centrifugal acceleration has been clearly established (Liu et al., 1994; Horwitz and Liu, 1995) as a dominant driver for outflows on middle magnetospheric field lines for substorm dipolarization events. Regarding more general polar outflows, at this point, we would suggest that the importance of centrifugal acceleration to high-latitude polar outflows is neither clearly demonstrated as important or unimportant. A key signature that can possibly elucidate the level of importance of centrifugal acceleration in outflows may come from relatively high-altitude three-dimensional bulk ion velocity vector measurements which are currently being made by the POLAR spacecraft, in particular the Thermal Ion Dynamics Experiment (Moore et al., 1995). As the data analysis techniques are finalized, it will soon be possible to accurately measure in particular the streaming angle of the high-latitude outflows in the geocentric distance range 2-9 R_E. These measurements should begin to establish the role of centrifugal acceleration in more general high-latitude outflows.

5. Are lobe ionospheric outflows captured by the plasma sheet?

Driven by the effects described above, and others, the ionosphere is now understood to circulate in radius as well as local time and latitude, in a generalized form of the refilling and corotation flows that form the plasmaspause region, but with much greater extent throughout the magnetosphere. This wide-ranging ionospheric circulation gives rise to the possibility that the ionospheric plasma contributes significantly to the formation and dynamics of the plasma sheet, which clearly lies in the circulation path from the polar cap to subauroral latitudes, where the plasma flow subsequently returns to the dayside.

The total electron density is much lower outside the plasmasphere than inside it, at a given altitude, reflecting substantial differences in the prevailing conditions experienced during the circulation history of plasma flux tubes. Relatively dense but still only partially-full flux tubes convect into the polar cap from the subauroral return flow. As they pass through the dayside auroral oval, they are simultaneously stretched at a very large rate, increasing their volume and reducing the plasma pressure within them, and subjected to low altitude heating in various forms. Both effects contribute to the rate of outflow attempting to fill the flux tube. As flux tubes convect antisunward through the lobes into the tail, the convection and field-aligned expansion of the plasma compete within a continuum of possibilities expressed as a ratio of convection to parallel flow speeds:

a) Convection of flux tubes is slow relative to the expansion velocity along the flux tubes, such that the outflow keeps pace with the stretching, outflows from the two hemispheres significantly interpenetrate, and the flux tube remains near the L=4 equilibrium density profile. Flux tubes return to the near-Earth region with their plasma significantly redistributed to higher altitudes.

b) Convection and expansion proceed at comparable rates, plasma streams from the two hemispheres barely interpenetrate at maximum downtail extent, and plasma density remains well below the equilibrium limit. Nevertheless, flux tubes return to the near-Earth region with appreciable redistriution of plasma content to high altitudes.

c) Convection of the flux tubes is fast relative to the expansion velocity along the flux tubes, such that the extended parts of the tubes remain essentially empty of low-energy ionospheric plasma throughout their period of extreme stretching in the magnetotail. Flux tubes return to the near-Earth region with little if any change in their plasma distribution.

An ionospheric plasma flux tube can exhibit different behaviors on this spectrum of possibilities in each of the major ion species present in the plasma, owing to their mass or energy and therefore thermal speed differences, as well as different degrees of adiabaticity. Clearly, the heavy species such as O^+ tend toward the c) end of the scale while the H^+ tends toward the a) end, though that extreme would only be realized for very slow convection and midrange behavior is more typical. O^+ begins to behave like H^+ when its thermal speed is raised to values comparable

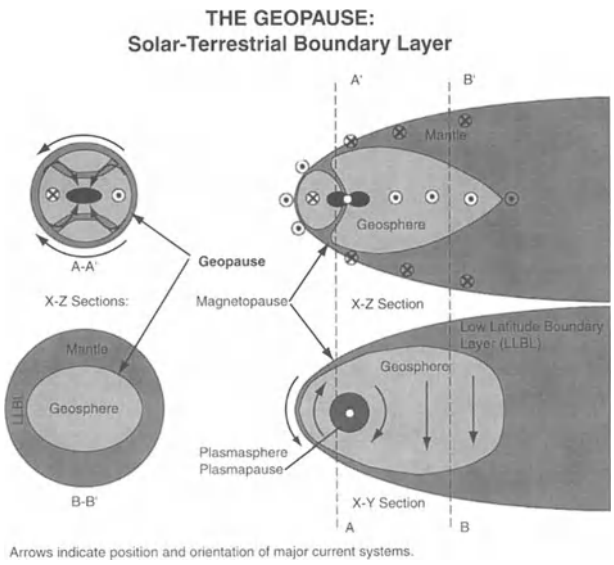

Figure 9. The geopause of Moore and Delcourt (1995). Copyright, American Geophysical Union, 1995.

with those typical of H^+. Highly energized outflows that occur in the auroral zone clearly tend toward the a. end of the scale, but consist of nonthermal populations that may not significantly redistribute the bulk of the plasma.

Since H^+ is redistributed to high altitude under typical magnetospheric conditions, the main question, addressed herein, is the degree to which ionospheric H^+ is captured in the energetic phenomena of the plasma sheet.

Several lines of argument (Moore, 1991; Moore and Delcourt, 1995) suggest that magnetospheric circulation remains somewhat segregated by source region, with primarily ionospheric plasma circulating within the inner magnetosphere and central polar cap, while primarily solar wind plasma circulates in the boundary layers, including the auroral oval, and of course the distant parts of the tail. Since there cannot be a truly sharp boundary between the two, Moore and Delcourt suggested that the surface in which the two sources make equal contributions to the plasma could serve as a useful demarcation, which they termed as the "geopause" (Figure 9). In this section we'll look at the evidence and arguments for ionospheric dominance of the central streamlines of magnetospheric circulation, extending through the plasma sheet.

5.1. CENTRIFUGALLY-ACCLERATED CLEFT OUTFLOWS

As first pointed out by Cladis (1986), ions originating in the dayside cusp region, at a few tens of eV, experience centrifugal acceleration to an important degree

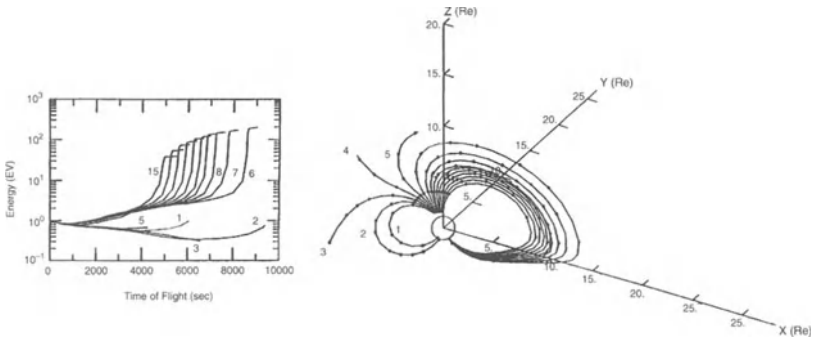

Figure 10. Centrifugal acceleration found by Cladis (1986) to accelerate low energy ions emitted from the ionosphere near the dayside cusp. Copyright, American Geophysical Union, 1986.

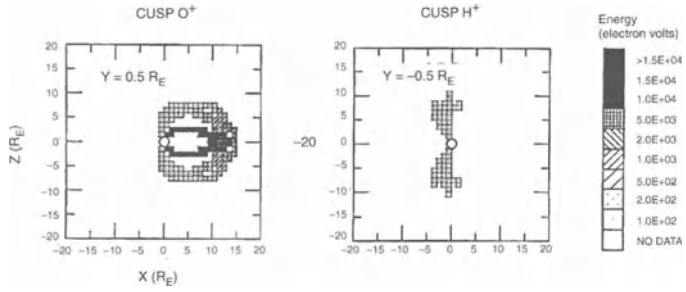

Figure 11. Formation of an ionospheric O^+ plasma sheet in the 3D model of Delcourt et al. (1989). Copyright, American Geophysical Union, 1989.

over the polar cap, but maximally after transport to the nightside neutral sheet (Figure 10). In a simple adiabatic approach, ions acquire primarily parallel energy as they convect across the polar cap and whip through the neutral sheet, forming an Earthward streaming boundary layer on the opposite side of the sheet. This is highly reminiscent of the plasma sheet boundary layer, where cold tailward streams coexist with accelerated Earthward streams. The quantitative location where they reach the neutral sheet, and the resultant degree of acceleration, clearly depend on the initial conditions of the ion, the strength of high latitude convection, and the thickness of the neutral sheet as a function of downtail distance.

5.2. THREE-DIMENSIONAL MODEL OF IONOSPHERIC OUTFLOWS

Delcourt et al. (1989) constructed a trajectory-based 3D model of the inner magnetosphere that results from ionospheric outflows of all sorts, including energetic auroral zone outflows. The most prominent features include a simple inner plasma sheet containing substantial densities of O^+ with Earthward-streaming boundary

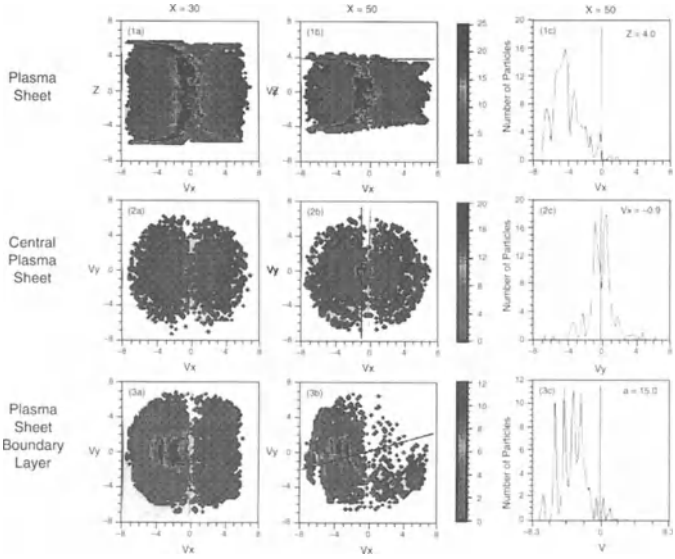

Figure 12. Formation of an isotropic central plasma sheet from incident streams of protons in the midrange plasma sheet, after Abdalla et al. (1991). Copyright, American Geophysical Union, 1991.

layers, but not much of a central plasma sheet (Figure 11). In this model, most of the H^+ was lost through the outer boundaries of the model system owing to the limited range of the magnetic field model used (geocentric distance less than 17 R_E).

5.3. NONADIABATIC PLASMA SHEET MODEL

Abdalla et al. (1991) showed that nonadiabatic motions of ions falling into the neutral sheet would preserve the Earthward streaming boundary layers, but would also generate an isotropic low Mach number, Earthward-convecting plasma sheet qualitatively like that actually observed (Figure 12). These calculations were done for H^+ ions characteristic of the mantle, but are equally valid for low energy ionospheric protons entering the neutral sheet (a much more credible source in central plasma sheet). It is easily shown that particles backtracked from the starting position used in this study are actually originating from the polar ionosphere (Moore and Delcourt, 1995). It became clear with this work that the scattering mechanism required to create the central plasma sheet is intrinsic in the sharp curvature of neutral sheet field lines, even in an empirical field model that is perhaps not as sharply curved as the real plasma sheet.

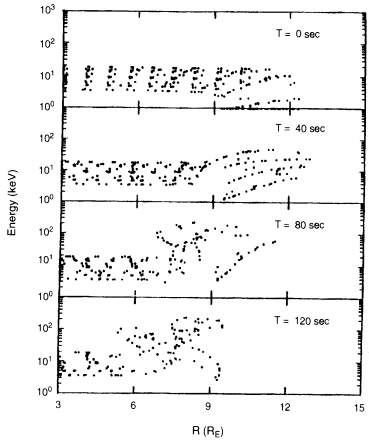

Figure 13. Simulation of dipolarization effects on O^+ in the plasma sheet, according to Delcourt et al. (1991). Copyright, American Geophysical Union, 1991.

5.4. Cleft Ion Fountain Contribution to Plasma Sheet

O^+ transported to the plasma sheet by whatever route is subject to temporal as well as spatial nonadiabaticity, owing to dipolarization events. While the steady state population of O^+ is limited to the keV range of energies when accelerated Earthward of 15 R_E, dipolarization events are found to raise the energies of these O^+ ions substantially, to as high as 200 keV in the simulation example shown (Figure 13), from Delcourt et al. (1991).

5.5. Mantle and Low Latitude Boundary Layer as a Source of the Plasma Sheet

In the Abdalla et al. works (Abdalla et al., 1991, 1993), the source plasma was taken to be mantle-like. Yet it was also taken to be introduced essentially at the plasma sheet boundary layer, well within the lobe regions. While the mantle cannot typically cross the lobes this close to Earth, Lennartsson (1992) has pointed out that low latitude boundary layer (LLBL) plasma tubes are transported along streamlines that "corkscrew" away from the LLBL along the plasma sheet boundary layer toward the center of the tail as they extend downtail (Figure 14). Depending on the "pitch angle" of these streamlines, the plasma tubes may reach the neutral sheet in time to be part of the inner magnetospheric circulation back toward Earth from the plasma sheet. Such plasma tubes re-enter the LLBL at the dayside with significant ionospheric content resulting from their passage through the inner magnetosphere. To the degree that the plasma tubes also acquire additional magnetosheath plasma during their passage antisunward along the LLBL, this plasma would enjoy direct entry to at least the flanks of the plasma sheet.

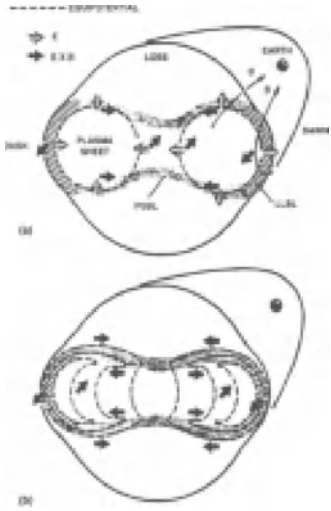

Figure 14. Low latitude boundary layer flows having a corkscrew shape, as proposed by Lennartsson (1992) to transport solar wind plasma into the central plasma sheet. Copyright, American Geophysical Union, 1992.

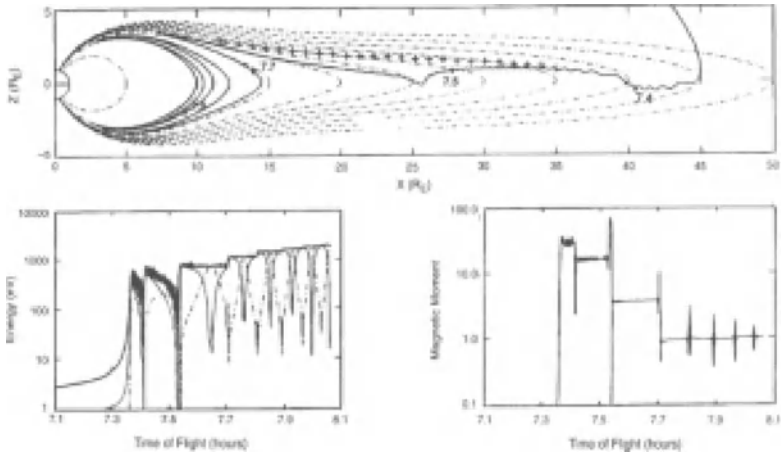

Figure 15. Illustration of the centrifugal trapping of low energy incident ions in the plasma sheet, after neutral sheet acceleration, after Delcourt et al. (1993). Copyright, American Geophysical Union, 1993.

5.6. POLAR WIND CONTRIBUTION TO THE PLASMA SHEET

Delcourt et al. (1993, 1994) switched to a more comprehensive magnetic field model to examine the motion of polar wind protons originating from the polar cap and traveling down the tail to $> 40\ R_E$. In addition to finding that the polar wind H^+ flows are captured and return toward the Earth in the plasma sheet, they found that

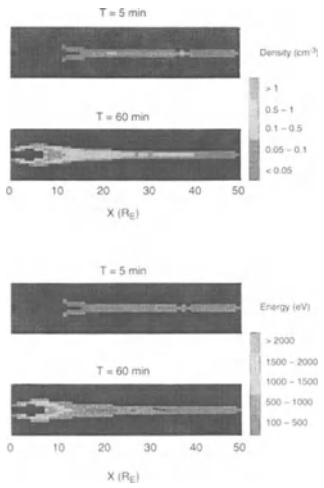

Figure 16. Cold polar wind outflow population of the plasma sheet for quiet (upper panel) and active (lower panel) convection conditions, after Delcourt et al. (1993). Copyright, American Geophysical Union, 1993.

a new form of centrifugal trapping occurs for such low energy ions, producing a thinner plasma sheet than would otherwise exist (Figure 15) for higher energy proton inputs to the plasma sheet. However, it was also found that the polar wind is more successful in populating the plasma sheet during quiet times than in active times, because it is so slow that for fast convection speeds, it is recirculated into the inner magnetosphere before it can reach the more stretched parts of the neutral sheet (Figure 16). Of course, the cold polar wind is not the only source of protons in this region, the hot cleft ion fountain providing significantly faster protons that would not be as readily recirculated into the inner magnetosphere.

Recently reported results of global MHD modeling suggest that a self-consistent view of this situation may be essential, however (Goodrich et al., 1996). In this model, a strong plasma density/pressure minimum appears in the magnetospheric lobes, as is observed. More importantly, however, the lobe density minimum connects along plasma flow streamlines directly to the merging neutral line in the magnetotail (Figure 17). This association is physically appealing when it is appreciated that the neutral line represents a maximum rate of plasma inflow to the neutral sheet, which may reasonably be associated with a relative "vacuum" region in the flow. As an intense neutral line flow moves to the inner plasma sheet during a substorm simulation, the lobe vacuum region follows it, suggesting a self-consistent causative relationship. The implications are that a) the neutral line region is a demarcation boundary between slower-moving terrestrial plasma and rapidly-moving magnetosheath plasma, and b) the regions near or earthward of the neutral

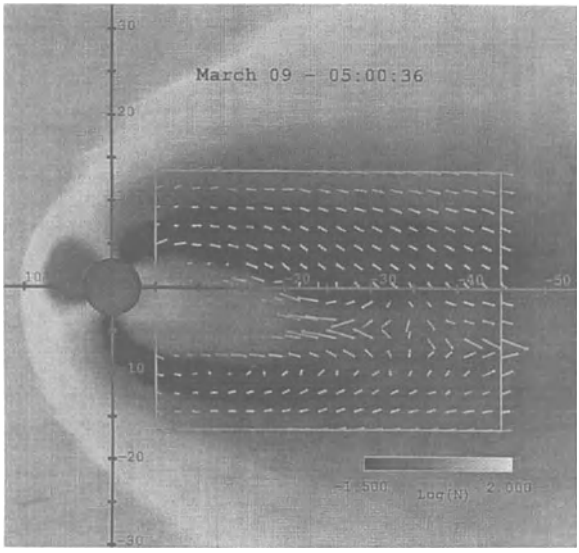

Figure 17. Illustration of the vacuum pulled on the polar caps in a global MHD model of the magnetosphere during a substorm episode, from Goodrich et al. (1996). Note that the low pressure region connects directly with the neutral line flow region. This was a simulation for the March 9, 1996 substorm, with the snapshot shown being for close to the onset time.

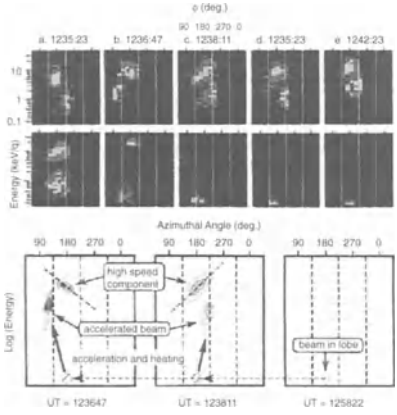

Figure 18. Illustration of adjacent regions of cold tailward streams and accelerated plasma at the plasma sheet boundary layer, after Hirahara et al. (1994). Copyright, American Geophysical Union, 1994.

line are supplied by plasma tubes from the magnetospheric lobes or inner magnetosphere.

5.7. GEOTAIL PLASMA SHEET OBSERVATIONS

Recent observations from the Geotail spacecraft (Mukai et al., 1994; Hirahara et al., 1994, Hirahara et al., 1996) (Figure 18), show that the midrange plasma sheet boundary layer is often a boundary between a) relatively cold tailward plasma streams that may contain O^+ as well as H^+, on one hand, and b) much more energetic populations of ions streaming Earthward. The lobe streams appear to be of clear ionospheric origin, while the nearby energetic plasmas appear to have been generated by acceleration of the cold streams inside the plasma sheet. Though it cannot be totally precluded that plasma entering from the mantle or LLBL has also contributed by Earthward convection from a more distant entry location, it is clear from these observations that ionospheric H^+ (and at times O^+) of polar cap lobe origin, are contributing directly to the plasma sheet.

5.8. SPECIES DEPENDENCES

It is fairly clear from the observations and theory summarized above, that ionospheric outflows do indeed become captured by and contribute to the plasma sheet. There are, however, significant differences in the behavior of ionospheric ion species, owing to the wide range of mass per charge represented. These effects lead to large differences in the mass composition of the ionospheric contribution to high altitude plasmas. Such variations, in the absence of a clear differentiation of ionospheric and solar H^+, give the false appearance of large changes in ionospheric content in the plasma.

The large mass range of ionospheric ion species results in significant species differences in behavior at low altitudes. H^+ routinely expands throughout the magnetosphere relatively unheeded by gravity, whereas O^+ outflows are gravitationally limited and respond strongly to low altitude energy inputs. The bulk of the O^+ outflows are more slowly moving than the H^+ polar wind (Lockwood, 1985a; Abe et al., 1993), and at low altitudes in the polar cap O^+ is ballistic and non-escaping (Horwitz, 1984; Chandler, 1995). Through some combination of velocity filtering and stream interactions, O^+ arrives at the plasma sheet with nearly the same speed as the H^+ of ionospheric origin. Nevertheless, the gravitational stratification of H^+ and O^+ must be preserved in the plasma sheet, with a ratio of ionospheric O^+/H^+ that decreases with downtail distance and increases at all distances with increasing low altitude heating and acceleration of the O^+. Thus, the O^+ content of the magnetospheric plasma is an ambiguous indicator of the ionospheric plasma content.

Other species differences result from differing degrees of adiabaticity of the ion species and therefore behavior within the plasma sheet (Delcourt et al., 1991). For example, as noted above, inner plasma sheet variations are known to occur on the time scale of the O^+ cyclotron period. In the more distant neutral sheet, H^+ is also subject to temporal nonadiabaticity effects. There the field is weaker and dynamics occurs on scales closer to the H^+ cyclotron period, though clearly this is to some

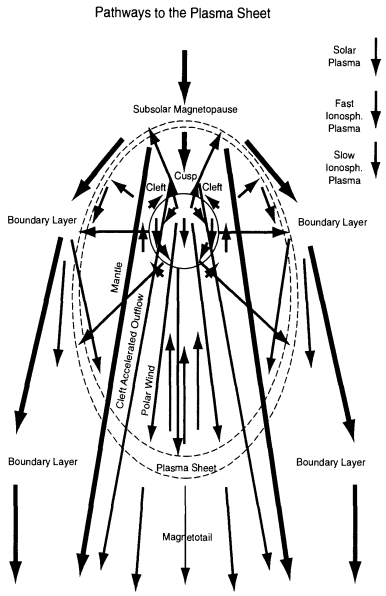

Figure 19. Illustration of possible flow paths or pathways to and from the plasma sheet.

degree dependent upon the detailed nature of the dynamic effects, such as bursty bulk flows. Thus, nonadiabatic effects should appear at greater distances in the magnetotail for lower mass per charge species. In practice, substorm energization effects may be largely limited to heavier ion species within the inner magnetotail.

6. Conclusions

In this review we have focused on four topics of contemporary interest in the context of ionospheric outflows toward the magnetosphere. Our first topic considered very recent observational and corroborating modeling evidence that the effects of soft electron precipitation are perhaps the dominant driver for the original upflows in the F-region and topside ionosphere at high-latitudes. The indications are that such large fluxes of soft electrons (below 1 keV, and indeed, usually below 100 eV) lead to thermal electron heating, and that the enhanced ambipolar electric fields associated with the large ionospheric electron temperatures drive the upflows.

We next examined the origin of the O^+ component often found within the mid-altitude polar cap magnetosphere as well as the magnetotail lobes. We concluded that during southward IMF periods, when the polar cap ionosphere is largely free of auroral processes, this O^+ is likely to have originated in the cleft ion fountain or elsewhere in the dayside auroral ionosphere, and not the polar cap ionosphere itself. During northward IMF, the O^+ at very high latitudes in the polar magnetosphere is more likely to have arisen from very high latitude ionospheric regions owing to the

presence of auroral processes and generally the presence of ionizing and heating energetic particles at these latitudes.

We then examined an issue that has become at times rather heated at recent meetings, the importance of convection-driven 'centrifugal' acceleration in the supply and acceleration of high-latitude ionospheric outflows. We believe that the existence of strong centrifugal acceleration has been demonstrated beyond any doubt in the observations during substorm dipolarizations (e.g., Liu et al., 1994a). At present, however, there is no clear observational evidence of centrifugal acceleration playing a critical role in the ejection of ionospheric ions into the polar cap. Further opportunities to examinine this issue may come from the new high-altitude measurements by the POLAR mission.

Concerning our fourth topic, it is abundantly clear that the bulk of ionospheric outflows are indeed captured in the plasma sheet earthward of the typical neutral line location. However, beyond the typical neutral line location, energetic ionospheric outflows from the dayside auroral oval region are subject to loss from the system down the tail, owing to their large parallel velocities. The structure of the magnetosphere, combined with the distribution of incident plasma from the solar wind and ionosphere, preserves a rough stratification between the two plasmas, with the mean demarcation surface (the geopause) corresponding to the plasma flow streamline from the high latitude cusp entry layer to the magnetic neutral line nearest to Earth at any given time.

7. Acknowledgements

This work was supported in part by NSF grant ATM-9402310 to The University of Alabama in Huntsville.

References

Abe, T., Whalen, B. A., Yau, A. W., Horita, R. E., Watanabe, S., and Sagawa, E.: 1993, 'EXOS D (Akebono) suprathermal mass spectrometer observations of the polar wind', *J. Geophys. Res.* **98**, 11,191.

Ashour-Abdalla, M., Berchem, J., Buchner, J., and Zelenyi, L. M.: 1991, 'Large and small scale stuctures in the plasma sheet: A signature of chaotic motion and resonance effects', *Geophys. Res. Lett.* **18**, 1603.

Ashour-Abdalla, M., Berchem, J., Buchner, J., and Zelenyi, L. M.: 1993, 'Shaping of the magnetotail from the mantle: Global and local structuring', *J. Geophys. Res.* **98**, 5651.

Barakat, A. R., and Schunk, R. W.: 1983, 'O^+ ions in the polar wind', *J. Geophys. Res.* **88**, 7887.

Candidi, M., Orsini, S., and Horwitz, J. L.: 1988, 'The tail lobe ion spectrometer: Theory and observations', *J. Geophys. Res.* **93**, 14,401.

Caton, R., Horwitz, J. L., Richards, P. G., and Liu, C.: 1996a, 'Modeling of F-region ionospheric upflows observed by EISCAT', *Geophys. Res. Lett.* **23**, 1537.

Caton, R., Horwitz, J. L., and Richards, P. G.: 1996b, 'Systematic modeling study of the response of F-region ionospheric upflows to soft electron precipitation', *J. Geophys. Res.* **101**, submitted.

Chandler, M. O.: 1995, 'Observations of downward moving O^+ in the polar topside ionosphere', *J. Geophys. Res.* **100**, 5795.

Chappell, C. R., Moore, T. E., and Waite, Jr., J. H.: 1987, 'The ionosphere as a fully adequate source of plasma for the Earth's magnetosphere', *J. Geophys. Res.*,**92**, 5896.

Cladis, J. B.: 1986, 'Parallel acceleration and transport of ions from polar ionosphere to plasma sheet', *Geophys. Res. Lett.* **13**, 893.

Delcourt, D. C., Chappell, C. R., Moore, T. E., and J. H. Waite, Jr.: 1989, 'A three-dimensional numerical model of ionospheric plasma in the magnetosphere', *J. Geophys. Res.* **94**, 11893.

Delcourt, D. C., Moore, T. E., and Sauvaud, J. A.: 1991, 'Gyro-phase effects near the storm-time boundary of energetic plasma', *Geophys. Res. Lett.* **18**, 1485.

Delcourt, D. C., Sauvaud, J. A., and Moore, T. E.: 1993, 'Polar wind ion dynamics in the magneto-tail', *J. Geophys. Res.* **98**, 9155.

Delcourt, D. C., Moore, T. E., and Chappell, C. R.: 1994, 'Contribution of low-energy ionospheric protons to the plasma sheet', *J. Geophys. Res.* **99**, 5681.

Foster, J. C.: 1993, 'Storm time plasma transport at middle and high latitudes', *J. Geophys. Res.* **98**, 1675.

Frank, L. A., Craven, J. D., Gurnett, D. A., Shawhan, S. D., Weimer, D. R., Burch, J. L., Winningham, J. D., Chappell, C. R., Waite, J. H., Heelis, R. A., Maynard, N. C., Sugiura, M., Peterson, W. K., and Shelley, E. G.: 1986, 'The theta aurora', *J. Geophys. Res.* **91**, 3177.

Ganguli, G., Keskinen, M. J., Romero, H., Heelis, R., Moore, T. E., and Pollock, C. J.: 1994, 'Coupling of microprocesses and macroprocesses due to velocity shear: An application to the low-altitude ionosphere', *J. Geophys. Res.* **99**, 8873.

Goodrich, C., Lopez, R. E., Wiltberger, M., and and, J. G. Lyon: 1996, 'The March 9 1995 substorm: Overview and comparison to spacecraft', *Trans. Am. Geophys. Un.* **77**, F594.

Heelis, R. A., Winningham, J. D., Sugiura, M., and Maynard, N. C.: 1984, 'Particle acceleration parallel and perpendicular to the magnetic field observed by DE 2', *J. Geophys. Res.* **89**, 3893.

Heelis, R. A., Coley, W. R., Loranc, M., and Hairston, M. R.: 1992, 'Three-dimensional ionospheric plasma circulation', *J. Geophys. Res.* **97**, 13,903.

Hill, T. W.: 1974, 'Origin of the plasma sheet', *Rev. Geophys.* **12**, 379.

Hirahara, M., Nakamura, M., Terasawa, T., Mukai, T., Saito, Y., Yamamoto, T., Nishida, A., Machida, S., and Kokubun, S.: 1994, 'Acceleration and heating of cold ion beams in the plasma sheet boundary layer observed with geotail', *Geophys. Res. Lett.* **21**, 3003.

Hirahara, M., Horwitz, J. L., Germany, G., Moore, T. E., Spann, J. F., Chandler, M. O., and Giles, B. L.: 'Properties of upflowing ion conics and magnetosheath proton precipitation at 5000 km altitude over cusp/cleft auroral forms: Initial observations from the TIDE and UVI instruments on POLAR', 1996: Presented to the Huntsville96 Workshop on Encounters Between Global Models and Observations in the ISTP Era, Guntersville, Alabama, September.

Horwitz, J. L.: 1982, 'The ionosphere as a source for magnetospheric ions', *Rev. Geophys. Spc. Phys.* **20**, 929.

Horwitz, J. L.,: 1984, 'Features of ion trajectories in the polar magnetosphere', *Geophys. Res. Lett.* **11**, 1111.

Horwitz, J. L.: 1987, 'Core plasma in the magnetosphere', *Rev. Geophys. Spc. Phys.* **25**, 579.

Horwitz, J. L.,: 1995, 'The ionosphere's wild ride in outer space', *Rev. Geophys.* **33**, 703.

Horwitz, J. L. and Liu, C.: 1995, 'Simulation of dipolarization-driven ionospheric outflows', *Trans. Am. Geophys. Un.* **76**, F505.

Horwitz, J. L., and Lockwood, M.: 1985, 'The cleft ion fountain: A two-dimensional kinetic model', *J. Geophys. Res.* **90**, 9749.

Horwitz, J. L., Wilson, G. R., and Singh, N.: 'Core plasma behavior on L=4-7 flux tubes: A starting point for understanding magnetosphere-ionosphere coupling': In T. Chang and Jasperse, J. R. (eds.), *Physics of Space Plasmas (1992)*, volume 12, pp 403–426. Scientific Publishers, Inc., Cambridge, Mass., 1994a.

Keating, J. G., Mulligan, J., Doyle, D. B., Winser, K. J., and Lockwood, M.: 1990, 'A statistical study of large field-aligned flows of thermal ions at high-latitudes', *Planet. Space Sci.* **38**, 1187.

Lennartsson, O. W.: 1992, 'A scenario for solar wind penetration of the Earth's magnetic tail based on ion composition data from the ISEE-1 spacecraft', *J. Geophys. Res.* **97**, 19,221.

Li, X. and Temerin, M.: 1993, 'Ponderomotive effects on ion acceleration in the auroral zone', *Geophys. Res. Lett.* **20**, 13.

Liu, C., Perez, J. D., Moore, T. E., and Chappell, C. R.: 1994, 'Low-energy particle signature of substorm dipolarization', *Geophys. Res. Lett.* **21**, 229.

Liu, C., Horwitz, J. L., and Richards, P. G.: 1995, 'Effects of convection ion heating and soft-electron precipitation on high-latitude F-region upflows', *Geophys. Res. Lett.* **22**, 2713.

Lockwood, M., J. H. Waite, Jr., Moore, T. E., Johnson, J. F. E., and Chappell, C. R.: 1985a, 'A new source of suprathermal O^+ ions near the dayside polar cap boundary', *J. Geophys. Res.* **90**, 4099.

Lockwood, M., Chandler, M. O., Horwitz, J. L., J. H. Waite, Jr., Moore, T. E., and Chappell, C. R.: 1985b, 'The cleft ion fountain', *J. Geophys. Res.* **90**, 9736.

Loranc, M., Hanson, W. B., Heelis, R. A., and St.-Maurice, J.-P.: 1991, 'A morphological study of vertical ionospheric flows in the high-latitude F-region', *J. Geophys. Res.* **21**, 3627.

Makita, K., Meng, C.-I., and Akasofu, S.-I.: 1988, 'Latitudinal electron precipitation patterns during large and small IMF magnitudes for northward IMF conditions', *J. Geophys. Res.* **93**, 97.

Moore, T. E.: 1991, 'Origins of magnetospheric plasma', *Rev. Geophys.* **29**, 1039.

Moore, T. E. and Delcourt, D. C.: 1995, 'The Geopause', *Rev. Geophys.* **33**, 175.

Moore, T. E., Chappell, C. R., Chandler, M. O., Fields, S. A., Pollock, C. J., Reasoner, D. L., Young, D. T., Burch, J. L., Eaker, N., J. H. Waite, Jr., McComas, D. J., Nordholdt, J. E., Thomsen, M. F., Berthelier, J. J., and Robson, R.: 1995, 'The Thermal Ion Dynamics Experiment and Plasma Source Instrument', *Space Sci. Rev.* **71**, 409.

Mukai, T., Hirahara, M., Machida, S., Saito, Y., Terasawa, T., Kaya, N., and Nishida, A.: 1994, 'Geotail observations of cold ion streams in the medium distance magnetotail lobe in the course of a substorm', *Geophys. Res. Lett.* **21**, 1023.

Newell, P.T., Xu, D., Meng, C.-I., and Kivelson, M. G.: 1997, 'Dynamical polar cap: A unified approach', *J. Geophys. Res.* **102**, 127.

Sandridge, N., Horwitz, J. L., and Caton, R.: 1996b, 'Statistical properties of high-latitude F-region/topside upflows from EISCAT radar observations', *J. Geophys. Res.* **101**, submitted.

Seo, Y., Caton, R., and Horwitz, J. L.: 1997, 'Statistical relationships between high-latitude ionospheric F-region/topside upflows and their drivers: DE-2 observations', *J. Geophys. Res.* **102**, 7493.

Shelley, E. G.: 1995, 'The auroral acceleration region: The world of beams, conics, cavitons and other plasma exotica', *Rev. Geophys.* **33**, 709.

Sojka, J. J., Bowline, M., Schunk, R. W., Craven, J. D., Frank, L. A., Sharber, J. R., Winningham, J. D., and Brace, L. H.: 1992, 'Ionospheric simulation compared with Dynamics Explorer observations for November 22, 1981', *J. Geophys. Res.* **97**, 1245.

Sojka, J. J., Schunk, R. W., and Denig, W. F.: 1994, 'Ionospheric response to the sustained high geomagnetic activity during the March 89 great storm', *J. Geophys. Res.* **99**, 21,341.

Swift, D. W.: 1990, 'Simulation of the ejection of plasma from the polar ionosphere', *J. Geophys. Res.* **95**, 12,103.

Tam, S., Yasseen, F., Chang, T., and Ganguli, S. B.: 1995, 'Self-consistent kinetic photoelectron effects on the polar wind', *Geophys. Res. Lett.* **22**, 2107.

Tsunoda, R. T., Livingston, R. C., Vickrey, J. F., Heelis, R. A., Hanson, W. B., Rich, F. J., and Bythrow, P.: 1989, 'Dayside observations of thermal-ion upwellings at 800-km altitude: An ionospheric signature of cleft ion fountain', *J. Geophys. Res.* **94**, 15,277.

Wahlund, J.-E., Opgenoorth, H. J., Haggstrom, I., Winser, K. J., and Jones, G. O. L.: 1992, 'EISCAT observations of topside ionospheric ion outflows during auroral activity: Revisited', *J. Geophys. Res.* **97**, 3019.

Waite, J. H., Jr., Nagai, T., Johnson, J. F. E., Chappell, C. R., Burch, J. L., Killeen, T. L., Hays, P. B., Carignan, G. R., Peterson, W. K., and Shelley, E. G.: 1985, 'Escape of suprathermal O^+ ions in the polar cap', *J. Geophys. Res.* **90**, 1619.

Witt, E., Hudson, M. K., Li, X., Roth, I., and Temerin, M.: 1995, 'Ponderomotive effects on distributions of O^+ ions in the auroral zone', *J. Geophys. Res.* **100**, 12,151.

Address for correspondence: J. L. Horwitz, Center for Space Plasma and Aeronomic Research, The University of Alabama in Huntsville, Huntsville, AL 35899, USA

HIGH-LATITUDE PARTICLE PRECIPITATION AND ITS RELATIONSHIP TO MAGNETOSPHERIC SOURCE REGIONS

T. G. ONSAGER
NOAA Space Environment Center
Boulder, Colorado, USA

M. LOCKWOOD
Rutherford Appleton Laboratory
Chilton, Didcot, Oxon, England

Received February 25, 1997; Accepted in final form May 23, 1997

Abstract. Two central issues in magnetospheric research are understanding the mapping of the low-altitude ionosphere to the distant regions of the magnetsphere, and understanding the relationship between the small-scale features detected in the various regions of the ionosphere and the global properties of the magnetosphere. The high-latitude ionosphere, through its magnetic connection to the outer magnetosphere, provides an important view of magnetospheric boundaries and the physical processes occurring there. All physical manifestations of this magnetic connectivity (waves, particle precipitation, etc.), however, have non-zero propagation times during which they are convected by the large-scale magnetospheric electric field, with phenomena undergoing different convection distances depending on their propagation times. Identification of the ionospheric signatures of magnetospheric regions and phenomena, therefore, can be difficult. Considerable progress has recently been made in identifying these convection signatures in data from low- and high-altitude satellites. This work has allowed us to learn much about issues such as: the rates of magnetic reconnection, both at the dayside magnetopause and in the magnetotail; particle transport across the open magnetopause; and particle acceleration at the magnetopause and the magnetotail current sheets.

Key words: Magnetosphere, Ionosphere, Low Latitude Boundary Layer, Cusp, Mantle, Polar Rain, Plasma Sheet, Plasma Sheet Boundary Layer, Particle Precipitation

1. Introduction

The high-latitude ionospheric regions are typically described in terms of the measured particle populations that, due to particles moving freely along the magnetic field in a collisionless plasma, give an indication of the properties of the distant magnetospheric regions. The magnetospheric regions are discussed primarily from the viewpoint of low-altitude particle measurements. The regions are: the low latitude boundary layer (LLBL), the cusp, the mantle, the polar rain, the plasma sheet boundary layer (PSBL), and the plasma sheet, including the dayside and nightside boundary plasma sheet (BPS) and the central plasma sheet (CPS). Progress in these and other related research areas has recently been reviewed (Lyons, 1995; Newell, 1995; Galperin and Feldstein, 1996; Smith and Lockwood, 1996).

An important advantage of the low-altitude measurements over those made in the magnetospheric source regions, either near the magnetopause or in the magnetotail, is that in a relatively short time (seconds to minutes) a low-altitude satellite

Space Science Reviews **80**: 77–107, 1997.

can cross magnetic field lines that extend over broad areas in the magnetosphere. The spacecraft then can obtain snapshots of the large-scale magnetospheric regions and the boundaries separating them. This contrasts with high-altitude spacecraft that can take considerably longer (hours to days) to traverse these same regions and boundaries. By investigating the particle properties in the low-altitude regions and comparing the measured velocity-space distributions with those expected under either steady or temporally varying conditions, it is possible to differentiate between the different regions and to study remotely the processes occurring in the distant magnetosphere.

A key point to be addressed relates to the identification of the various low-altitude precipitation regions. Vasyliunas (1979) considered the ionospheric precipitation regions to be the field-aligned projections of magnetospheric source regions, and they are usually given the same names as a result. Furthermore, the classification scheme for the different regions is largely based upon this philosophy, because in its derivation, particle energy spectra at low altitudes were compared to those at high altitudes. Thus, for example, Newell and Meng (1992) regarded their map of the ionospheric regions as a map of the magnetosphere.

This philosophy, however, neglects magnetospheric convection and particle motion in the crossed electric and magnetic fields that, in many cases have a dominant effect on the observed plasma properties (e.g., Rosenbauer et al., 1975; Hill and Reiff, 1977; Onsager et al., 1993; Lockwood and Smith, 1993). Using a frozen-in-flux, ideal-MHD formulation, the existence of a convection electric field means that although particles move along magnetic field lines, the particles also convect perpendicular to the magnetic field. Thus the trajectories are not field-aligned but rather depend on the energy and pitch angle of the particle. Indeed, this is the very basis of the observed velocity filter effects described below. Thus not only does a spectrum of different-energy particles (at one pitch angle) from one point in the magnetosphere map to a spread of locations in the ionosphere, but also a spread of energies seen at any one point in the ionosphere maps to a spread of source locations in the magnetosphere. Similarly, a spread of pitch angles at one energy also reveals an extended source region.

This effect is highly significant for low-energy magnetosheath ions, and velocity filter effects associated with electron flight times have also been detected. It is also significant for the magnetosheath electrons, since, although high-energy electrons do have much smaller flight times and thus much more field-aligned trajectories, the fluxes of electrons are modified by those of the ions in order to maintain quasi-neutrality (Burch, 1985). This means that any classification scheme that depends on either the fluxes of ions or electrons, or both, is subject to strong influence by this effect. As described below, all these cusp effects also have a corresponding analogue on the nightside of the Earth at the boundary between the polar cap and the plasma sheet.

In this review, the low-altitude dayside and nightside ionospheric precipitation regions are discussed in terms of the magnetospheric regions they map to magnet-

ically, and in terms of the evolution of the plasma in the convection electric field. Recent advances in describing the low-altitude precipitation in terms of the distant source regions are also discussed, and progress in using the low-altitude measurements to sense remotely the properties of the distant magnetosphere are examined. Considerable advances have been made in utilizing dayside low-altitude measurements to estimate quantitatively key properties of the reconnection process under southward Interplanetary Magnetic Field (IMF) conditions, for which the cusp signatures are well understood (e.g., Lockwood and Smith, 1992; Lockwood et al., 1994; Newell and Meng, 1995a). Progress has also been made in characterizing and understanding some of the more complex cusp signatures (e.g., Yamauchi and Lundin, 1994), cusp signatures under northward IMF conditions (e.g., Woch and Lundin, 1992a; Matsuoka et al., 1996), and the high-latitude precipitation regions near dawn and dusk (e.g., Woch and Lundin, 1992b; Nishida et al., 1993; Lyons et al., 1996).

A primary emphasis here is on the identification of magnetic separatrices, and on a description of the plasma regions in terms of their evolution following magnetic reconnection, either on the dayside magnetopause or in the distant magnetotail. Of course, not all observations of low-altitude particle precipitation can be described by this scenario, but it does provide a useful framework that accounts for the commonly observed features, and it can serve as a point of reference to compare with observations that appear to require additional physical mechanisms. It has also been demonstrated that when interpreted in this way, the observations often allow quantitative estimates to be made of the reconnection process, including its rate and location, and the plasma properties in the vicinity of the reconnection site.

2. Dayside Precipitation Regions

The dayside particle precipitation regions can be understood most simply by considering the evolution of magnetospheric plasma following magnetic reconnection on the dayside magnetopause and the subsequent evolution of the open flux it produces. For southward IMF, the open flux moves tailward into the lobe under the action of the magnetosheath flow and the magnetic tension force; for northward IMF, the tension force can act in the opposite direction to the magnetosheath flow. In general, the reconnected field lines evolve in a complex manner, depending on the balance between these two influences (e.g., Cowley and Owen, 1989). The dayside precipitation regions that will be discussed in this way are the Central Plasma Sheet (CPS), the Boundary Plasma Sheet (BPS), the Low Latitude Boundary Layer (LLBL), the cusp, the mantle, and the polar rain. These regions are illustrated in Figure 1, from Newell and Meng (1992). The CPS precipitation consists of magnetospheric plasma on closed field lines; and the cusp, mantle, and polar rain precipitation are generally considered to occur on open field lines. As described

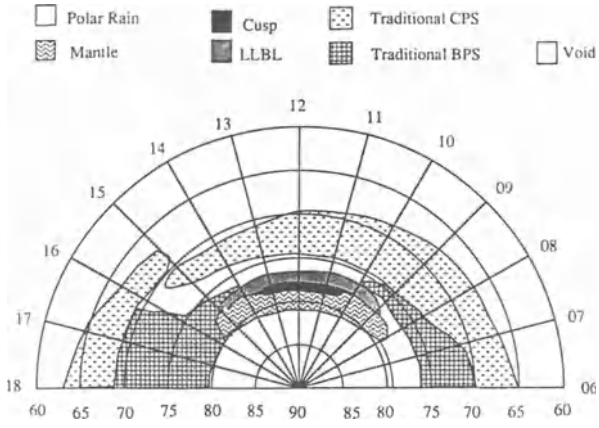

Figure 1. An illustration of the regions of low-altitude dayside particle precipitation, from Newell and Meng (1992).

in more detail below, there is still an active debate on the association of BPS and LLBL plasma with open or closed field lines.

2.1. Cusp - Mantle - Polar Rain

If one considers, for example, a reconnection X-line extending across the dayside magnetopause in the equatorial plane (for a purely southward orientation of the IMF), the low-altitude footprint of the X-line in the ionosphere will, broadly speaking, be the boundary between plasma precipitation characteristic of the closed magnetosphere (the CPS) and the plasma characteristic of the magnetosheath/solar wind (the cusp, the mantle, and the polar rain). When the magnetosheath magnetic field interconnects with the magnetospheric field, particles will cross the magnetopause by flowing along the magnetic field that interconnects across the magnetopause. The previously trapped CPS plasma will escape out across the open magnetopause, and the magnetosheath plasma will flow into the magnetosphere. As the particle velocities parallel to the magnetic field allow the plasmas to intermix freely across the magnetopause, the magnetosheath flow and the tension force give a boundary-tangential electric field that convects the open flux tube along the magnetopause toward the magnetotail. The combination of the parallel velocities of the particles and the perpendicular convection will result in the trajectories sketched in Figure 2, from Gosling et al. (1990a). Note that for both entering and escaping particles, not all are transmitted through the boundary, but some are scattered by the current sheet and reflect back into the magnetosheath or magnetosphere.

Near the subsolar magnetopause, the magnetosheath typically has its highest density and temperature and its lowest bulk velocity (e.g., Spreiter and Stahara, 1985). The magnetosheath density and temperature decrease and the boundary-

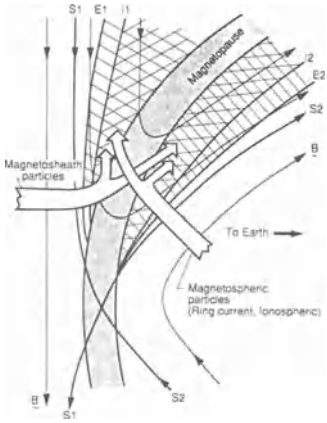

Figure 2. An illustration of the particle layers that form inside and outside the magnetopause on recently-reconnected field lines, from Gosling et al. (1990a).

tangential velocity increases with distance away from the subsolar point. Therefore when open field lines thread the magnetopause near the subsolar region, the highest fluxes of magnetosheath plasma will be injected into the magnetosphere by flowing across the magnetopause. This region of high-density magnetosheath plasma inside the magnetosphere and in the ionosphere is identified as the cusp (e.g., Newell and Meng, 1992). As the magnetopause crossing point of the flux tube convects away from the subsolar point, the magnetosheath plasma outside the magnetopause will decrease in density and temperature and increase in downtail velocity. These changes in the magnetosheath source population will result in reduced particle fluxes and energies in the ionosphere and magnetosphere, and the fluxes will decay to levels that are identified as mantle, and then to lower levels identified as polar rain (e.g., Winningham and Heikkila, 1974; Fairfield and Scudder, 1985; Wing et al., 1996).

The cusp, whose defined location is based on particle flux and average energy levels, will then be spatially localized and confined to the magnetic field lines that map to the most dense portion of the dayside magnetosheath. Moving in local time or in latitude away from connection to the subsolar magnetosheath will result in reduced fluxes and average energies, eventually reaching levels below the threshold for identification as cusp. This spatial localization will occur even if the entire magnetopause is open to magnetosheath entry; no localization of particle entry is required to account for the commonly observed cusp features.

The flux levels of precipitating magnetosheath plasma are also affected by particle acceleration as the magnetosheath plasma crosses the magnetopause current layer (Hill and Reiff, 1977; Cowley, 1982). The theory of particle distributions resulting from current sheet acceleration Cowley (1982) has been highly successful in predicting the ion distribution functions seen at the dayside magnetopause

(Smith and Rodgers, 1991; Fuselier et al., 1991; Gosling et al., 1990a) and in predicting the cusp and mantle precipitation of magnetosheath-like plasma resulting from magnetopause reconnection (Onsager et al., 1993; Lockwood and Davis, 1996a). As discussed earlier, the result of the velocity filter effect is that the spectrum of energies seen in the magnetosphere and ionosphere at a single location arises from a spread of magnetopause injection locations. The spectrum seen at any one point and time is then a convolution of many effects; the spatial distribution of the source magnetosheath plasma, the magnetopause acceleration, and the time-of-flight velocity filter. The above calculations of particle precipitation allow for these factors, as has recently been discussed in detail by Lockwood (1995).

An important application of our understanding of the particle signatures that result from the reconnection process has been the quantification of the reconnection rate. Observations in the ionosphere have a great advantage since they can exploit the fact that the ionosphere is "incompressible" - the magnetic field is dominated by currents in the Earth's interior and remains at roughly $5x10^4$ nT, independent of the magnitude of the currents that flow as part of solar-terrestrial interactions. This means that the transfer of magnetic flux from one region to another in the magnetosphere must correspond to the changing of the area of the regions in the ionosphere. This is the basis of a method that allows cusp and mantle dispersion signatures to be used to calculate the recent history of the magnetopause reconnection rate (Lockwood and Smith, 1992).

This theory has also been used to compute the ion precipitation characteristics seen for a variety of reconnection rate behaviors from mid- and low-altitude spacecraft moving either latitudinally or longitudinally (Lockwood and Smith, 1994; Lockwood and Davis, 1996a). The modeled signatures agree well with many of the observed signatures, and they depend critically on the speed of the satellite motion normal to the open-closed field line boundary, as a ratio of convection speed in the same direction. The synthesized precipitating ion spectra have been used to test the accuracy of the method for computing the reconnection rate from experimental data (Lockwood and Davis, 1996a).

The low-altitude particle data have been used to reconstruct the source distribution in the vicinity of the reconnection site also, and to infer numerous properties of the reconnection process (Lockwood et al., 1994). By combining the low-altitude measurements with solar wind data, it was possible to estimate: the density, flow, magnetic field, and Alfven speed of the magnetosheath; the magnetic shear across the X-line; the magnetospheric field; and the transmission factor for the magnetosheath ions across the open magnetopause. The ion heating at the magnetopause and the reconnection rate were also estimated.

Based on these same velocity filter effect concepts, the measured particle spectra have also been used to estimate the length of time that reconnection may cease at the dayside magnetopause (Newell and Meng, 1995b). The results suggested that reconnection is nearly always occurring. An upper limit of about 1 min was put on the duration that reconnection could cease and still be consistent with the

observed particle precipitation. However, one of their examples was also studied by Lockwood and Davis (1996b) who computed the reconnection rate directly with calculated uncertainties. These authors found a much longer interval (about 5 min) during which the reconnection rate was less than the detectable threshold.

These quantitative estimates of the reconnection process described above have been made under conditions when the cusp/mantle ion distributions are well described by the velocity filter effect following reconnection on the dayside magnetopause with a dawn-to-dusk directed magnetospheric electric field. It is also the case, however, that many satellite passes through the cusp indicate a much more complex ion precipitation or, as in cases when the IMF is directed northward, a velocity filter dispersion with the ion energy/latitude progression consistent with high-latitude reconnection and a dusk-to-dawn directed electric field. A recent study of cusp signatures under both northward and southward IMF conditions has found evidence for current sheet acceleration on the most recently reconnected field lines in both cases (Woch and Lundin, 1992a). The acceleration was observed at the low-latitude edge of the cusp when the IMF was southward and at the high-latitude edge of the cusp when the IMF was northward, consistent with the expected sense of dispersion for these two cases.

Reconnection configurations that give rise to the observed particle acceleration and velocity dispersion are illustrated schematically in Figure 3, which contrasts the situation of subsolar reconnection during southward IMF (3a) with two of several possibilities during northward IMF (3b and 3c). In each case the left-hand diagram shows a view of the magnetosphere from the dusk flank, and the right-hand diagram shows the corresponding convection flow streamlines in the northern polar ionosphere. In all cases the numbers relate to the locations of newly opened field lines (o) as they evolve after reconnection.

The evolution of the field lines causes evolution of the particle precipitation along the flow streamlines. In (3a), the tailward progression of open flux gives rise to an antisunward dispersion signature in the precipitating particles. Namely, the highest acceleration due to particle motion across the current-sheet will be observed near the low-latitude edge of the cusp on the most recently reconnected field lines, and the particle precipitation will have progressively lower energies with anti-sunward distance along the flow streamlines.

In (3b), field lines that had been opened during a prior period of southward IMF are reconfigured through high-latitude reconnection causing a "stirring" circulation of open flux and a precipitation dispersion signature that is opposite to that observed under southward IMF conditions. The reconnection in the northern hemisphere lobe generates "overdraped lobe" field lines (Crooker, 1992) that drape over the dayside magnetosphere. In this case, a large acceleration on the most recently reconnected field lines will be observed on the high-latitude edge of the cusp, with the lower-energy precipitation observed sunward along the flow streamlines. In (3c), the overdraped lobe field lines (ol) generated through reconnection in the northern hemisphere are later re-closed by reconnection in the southern lobe. The

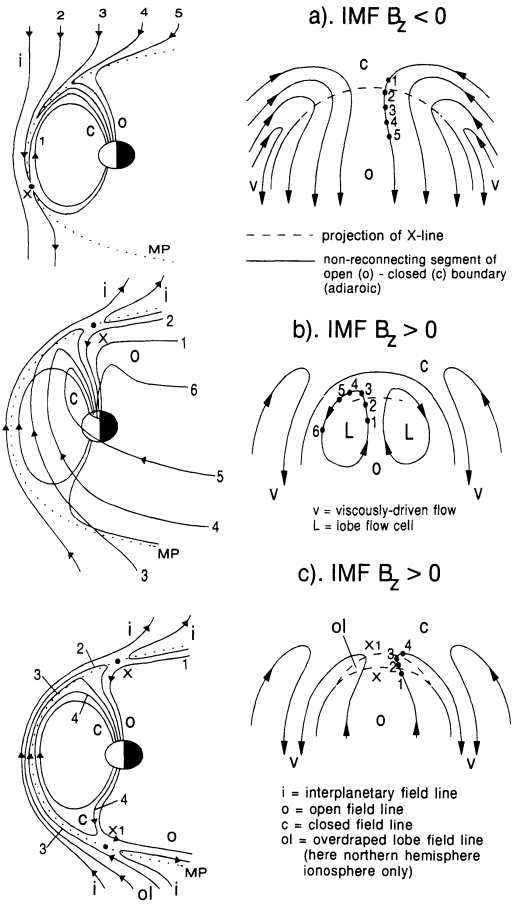

Figure 3. An illustration of field-line evolution along the magnetopause (left) and flow stream-lines in the ionosphere (right). Reconnection occurring near the subsolar magnetopause under southward IMF conditions (3a) is contrasted with reconnection occurring at high latitudes under northward IMF conditions (3b and 3c).

occurrence of reconnection at high-latitudes in both hemispheres has been suggested as a source of high-altitude LLBL plasma on closed field lines (Song and Russell, 1992). Signatures of the overdraped lobe topology have been reported at the dayside magnetopause (Fuselier et al., 1997).

An extensive survey of ion precipitation in the polar cap under northward IMF conditions has also found that the ion energy dispersion in regions of sunward ionospheric flow is consistent with high-latitude reconnection and the velocity filter effect (Matsuoka et al., 1996). Because of the high latitudes where these events were observed, the magnetosheath flow velocity at the estimated reconnection locations was estimated to be super-Alfvenic. In order to explain the sunward ionospheric convection, a mechanism was postulated where feedback from the iono-

sphere results in a slowing of the magnetosheath flow on the recently reconnected field lines to sub-Alfvenic, allowing the tension force to overcome the magnetosheath flow.

An important variation to the straighforward cusp/mantle dispersion described above is the observation of multiple, overlapping ion injections in the cusp (e.g., Yamauchi et al., 1995; Norberg et al., 1994). The various dispersion signatures have recently been catagorized in detail, including both the large-scale energy/latitude dispersion and the smaller scale structure seen within the large-scale patterns (Yamauchi and Lundin, 1994). Some of this more complex cusp structure may be the result of changing IMF conditions and a reconfiguration of the cusp during the satellite pass through it (Yamauchi et al., 1995). These signatures could also arise from pulsed reconnection with violation of frozen-in-flux by curvature and gradient-B drifts giving regions of overlapping precipitation (Lockwood and Smith, 1994). Other explanations have been proposed (e.g., Yamauchi and Lundin, 1994) which do not fit easily into the basic scenario outlined above for the simple, single cusp dispersion signatures. Thus, it is still unclear if the overlapping signatures are a complication of the open magnetosphere model or represent an entirely different mechanism.

2.2. Low Latitude Boundary Layer - Boundary Plasma Sheet

As described above, the combination of current sheet acceleration and the velocity filter effect provides a quantitative explanation for much of the commonly observed cusp and mantle precipitation. The plasma in these regions consists of the directly-entering magnetosheath particles. The region identified as LLBL at low altitudes has a lower density and a somewhat higher temperature than the cusp, and is found just equatorward of the cusp (Newell et al., 1991a). The low-altitude LLBL, therefore, is thought to correspond to the high-altitude LLBL, located just inside the magnetopause, that is observed to have a mixture of magnetosheath and magnetospheric plasma. In the classification of low-altitude precipitation regions by Newell et al. (1991a), the BPS region is not uniquely defined, consisting of plasma populations that did not fit well into the other defined catagories. This region typically has ions with energies higher than found in the cusp, often resembling the nightside plasma sheet.

An interesting aspect of the LLBL/BPS ions is that in many cases these ions are seen to exhibit a continuous velocity dispersion ramp with the cusp ions, suggesting that the generation and transport of both the dayside BPS and the LLBL ions are at times intimately linked with that of the cusp ions. However, the current sheet acceleration described above that provides some energization to the entering magnetosheath ions that form the cusp typically is not adequate to explain the high fluxes of the most energetic LLBL/BPS ions. For example, the open magnetosphere models of the cusp by Onsager et al. (1993), Lockwood and Smith (1994), and Lockwood and Davis (1996a) all give a plateau of peak ion energies

(with detectable fluxes) of only 7 to 10 keV. In many of the cases presented (e.g., Pinnock et al., 1993; Newell and Meng, 1994), a region equatorward of the cusp classed as either LLBL or dayside BPS contains ions with energies elevated well above those of the shocked solar wind plasma in the magnetosheath, up to well over the 30 keV limit of the ion instrument.

Several ideas have been proposed to explain the energetic LLBL/BPS ions. Newell and Meng (1992) regard the dayside BPS as an extension of the nightside BPS, implying that the ions are accelerated on newly-closed field lines in the tail, as initially implied by Vasyliunas (1979). Alem and Delcourt (1995) suggested an explanation in terms of chaotic orbits in a closed field-line magnetic cusp topology, and Curran and Goertz (1989) also considered chaotic ion orbits within an open LLBL as a mechanism to accelerate the magnetosheath protons. None of these mechanisms, though, would produce ions with an energy dispersion that is continuous with that of the ions in the cusp region, which is clearly the case for several observed examples (Newell et al., 1991b; Pinnock et al., 1993; Newell and Meng, 1994). The closed magnetic cusp topology invoked by Alem and Delcourt is also not consistent with the cusp precipitation seen poleward of the BPS on open field lines.

Using a generalization of the theory of magnetopause particle distributions by Cowley (1982), a different description has recently been supplied to explain both the BPS and LLBL ions in terms of the open magnetospheric model (Lockwood et al., 1996). This explanation invokes acceleration by reflection of magnetospheric ions off of two Alfven waves at the magnetopause. The resulting reconnection layer has a form shown schematically in Figure 4, where "S" refers to the magnetic separatrices, "E" refers to the exterior Alfven wave, and "I" is the interior Alfven wave. The interior Alfven wave is launched by the reconnection site into the inflow region where magnetospheric plasma flows towards the reconnecting magnetopause. An exterior Alfven wave is also launched into the magnetosheath side of the boundary and stands in the magnetosheath inflow. The majority of the field rotation takes place at the exterior wave, which can then be identified as the main magnetopause current sheet.

The interior wave forms the inner edge of the reconnection layer (also called the open LLBL), and its existence can be inferred from the fact that the field in the LLBL has a slightly different orientation to that of closed field lines in the magnetosphere proper (Cowley et al., 1983; Hapgood and Bryant, 1992). It has been shown that the effect of the waves is to produce accelerated ions that precipitate into the low-altitude LLBL and BPS regions and that are continuous in their dispersion with the magnetosheath ions injected along the open field lines and seen in the cusp precipitation region at low altitudes (Lockwood et al., 1996). By reflection off the magnetopause (exterior) wave, magnetospheric ions can achieve energies of about 15 keV with fluxes detectable by current instruments; energies slightly above the 7 - 10 keV plateau predicted for injected sheath ions can then be generated. Because of the lower plasma density on the magnetospheric side of the boundary, however,

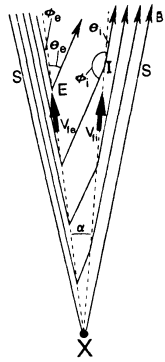

Figure 4. Illustration of a reconnection layer formed by two Alfven waves (dashed lines), from Lockwood et al. (1996). The interior Alfven wave (I) travels at a higher speed than the exterior Alfven wave (E), and, therefore, particles that reflect off the interior wave will undergo a larger acceleration than those that reflect off the interior wave.

the interior wave has a much higher speed and can generate detectable fluxes up to the order of 30 keV. By invoking partial reflection of the magnetospheric plasma at each of the Alfven waves, it was possible to quantitatively reproduce the LLBL/cusp transition for the satellite observations originally presented by Newell et al. (1991b) (which has been the subject of a great many of the other studies mentioned above; specifically, Onsager et al. (1993), Lockwood et al. (1994), and Alem and Delcourt (1995) all discussed this one example). Lockwood and Moen (1996) have applied the theory of Lockwood et al. (1996) to explain another example of BPS and LLBL ions, as reported by Moen et al. (1996).

2.3. Are LLBL Field Lines Open or Closed?

The open magnetosphere model predicts that the precipitation at low altitudes evolves from cusp to mantle and then to polar rain as the field line evolves over the magnetopause away from the reconnection site and into the tail lobe (Cowley et al., 1991b; Lockwood and Smith, 1993, 1994; Onsager et al., 1993; Lockwood, 1995). This evolution is seen in full along the flow streamlines in the steady-state case and so may sometimes be seen if the satellite follows the flow streamline quite closely. Recently, several authors have suggested the low-altitude LLBL precipitation is also on open field lines (e.g. Lockwood and Smith, 1993; Lyons et al., 1994; Lockwood et al., 1996; Moen et al., 1996). It has been argued that the velocity filter effect makes it impossible to place the open-closed field line boundary between the adjacent cusp and LLBL precipitations, at least near noon where convection is poleward into the polar cap (Lockwood and Smith, 1993).

At the magnetopause current sheet (which is associated with the exterior Alfven wave), application of tangential stress-balance tests to particle and field data [e.g., Paschmann et al., 1986, Sonnerup et al., 1986) reveals that there is an open LLBL,

i.e., a layer of accelerated magnetosheath plasma mixed with magnetospheric plasma which is formed by the two populations flowing along newly-opened field lines at the local Alfven speed in the rest frame of the field lines (i.e., the Whalen relation is found to apply). Other observations, like the directions of the accelerated flows (Gosling et al., 1990b), the form of their ion distribution functions (Smith and Rodgers, 1991; Fuselier et al., 1991) and electron and ion edges due to time-of-flight dispersion effects (Gosling et al., 1990a) leave little doubt that at least part, and at time perhaps all, of the LLBL is on newly-opened field lines.

Other magnetopause observations have shown a mixture of magnetosheath-like and magnetosphere-like plasmas on northward-pointing field lines and have been interpreted as an LLBL on closed field lines (Eastman and Hones, 1979; Eastman et al., 1976; Mitchell et al., 1987, Traver et al., 1991; Lotko and Sonnerup, 1995). That these field lines are genuinely closed is not certain because the use of particle distributions to infer the magnetic topology is notoriously difficult. This is because of the effects of particle flight times and of magnetic mirrors on open field lines (Scholer et al., 1982; Daly and Fritz, 1982; Cowley and Lewis, 1990).

In addition, unlike the open LLBL, the mechanisms responsible for introducing magnetosheath plasma into a closed LLBL are not clear. It has been pointed out that the observed wave amplitudes are not adequate to drive the cross-field diffusion required to populate closed field lines with sufficient fluxes of magnetosheath plasma to explain the LLBL (Sonnerup, 1980). This finding has been confirmed by later studies (Owen and Slavin, 1992; Winske et al., 1995; Treumann et al., 1995].

Other mechanisms proposed for populating a closed LLBL involve the opening and re-closing of magnetic flux at the magnetopause. Nishida (1989) proposed a mechanism where reconnection may be responsible for plasma populations on a closed LLBL when the IMF points northward. He invoked highly patchy reconnection, where field lines that opened at one reconnection site were re-closed at a later time elsewhere. During the time that the field line was open, magnetosheath plasma was free to flow in and magnetosphere plasma to flow out, giving the observed plasma mixture. Recently Song and Russell (1992) and Song et al. (1990) proposed a similar mechanism, but involving only two large-scale reconnection sites, poleward of the cusps. Numerical simulations by Richard et al. (1994) indicate that magnetosheath plasma could indeed get onto closed field lines in this way.

It is important here to draw a distinction between the high-altitude and the low-altitude LLBL populations; namely, that the low-altitude LLBL precipitation consists of particles largely within the loss cone. Thus for the low-altitude LLBL to persist, there must be a continuous source of particles to refill the loss cone. After the reclosure of open flux, as suggested by Nishida (1989) and Song and Russell (1992), the LLBL will only persist for a time scale on the order of the ion bounce time. Whereas the high-altitude LLBL ions may be observable on both open and closed field lines, the low-altitude LLBL will only be observable on open field lines, and then for a brief period after field-line closure.

The low-altitude ionospheric precipitation classed as LLBL shows many features that are consistent with an open LLBL at the magnetopause. For example, Hill and Reiff (1977) and Woch and Lundin (1992a) have shown that the cusp ion energies increase in the low-altitude velocity-filter dispersion ramp to energies above those in the magnetosheath, providing evidence that the highest energy ions of the accelerated ion flows at the magnetopause do indeed appear in the ionosphere close to the magnetic separatrix, the boundary between open and closed field lines. However, the direct association between the plasma measurements made in the high-altitude LLBL near the magnetopause and in the low-altitude LLBL can also be complicated by the velocity filter effect. The models of Onsager et al. (1993), Lockwood and Smith (1994), and Lockwood (1995) stress the role of the velocity filter effect and show that the precipitation at any one point in the ionosphere arise from a spread of locations on the magnetopause. Lockwood and Smith (1993) used realistic field line velocities over the magnetopause to show that the spread of magnetopause source locations supplying ions to one point in the ionosphere was very large, being of order 10-20 Earth radii (R_E). The expected low-altitude signatures resulting from an open and a closed LLBL will be contrasted in the following section.

The above studies on low-altitude LLBL precipitation have concentrated mainly on observations within a few hours of local time on either side of noon. Recent results have also provided interesting new insights on the precipitation of magnetosheath plasma in the dawn and dusk regions that could map to the high-altitude LLBL on the flanks of the magnetosphere. A region of high-latitude ion precipitation has been identified and referred to as circumpolar ion precipitation (CPIP) (Nishida et al. 1993; Nishida and Mukai, 1994). Some of the interesting characteristics of this regions are: the presence of energetic ion precipitation, electron precipitation that suggests open field lines, and sunward convection. A potentially related region has also been identified in the morning and afternoon high-latitude ionosphere and referred to as the soft electron zone (SEZ) (Lyons et al., 1996). This region contains magnetosheath-like electron and ion precipitation and is suggested to be largely on open field lines. The SEZ region is likely, therefore, to correspond to the low-altitude signature of the open LLBL. A strong dawn-dusk asymmetry of the SEZ region is observed and has been correlated with the IMF B_y component. In addition, the identification of LLBL plasma has been further extended along the flanks to within 3 to 4 hours from midnight (Woch and Lundin, 1993). These observations by the Viking spacecraft identify a magnetosheath-like ion component having a density correlated with the solar wind density extending from near noon well into the night sector.

2.4. Comparisons of Different Separatrix Locations

The debate about the magnetic topology within the LLBL at the magnetopause certainly has implications for the precipitation classed as LLBL at low altitudes,

even though the relationship between the two is not always clear. Figure 5, from Lockwood (1997), contrasts two possible relationships of the dayside precipitation regions (shaded according to code bar) to the ionospheric convection streamlines (thin lines with arrows) and to the open-closed boundary (thick line). The key difference between the two plots in Figure 5 is the location of the open-closed field line boundary and, in particular, the consequent topology of field lines within the ionospheric LLBL and BPS regions. In Figure 5a, the LLBL and BPS precipitations are on closed field lines, whereas in Figure 5b they are on open field lines. The open/closed boundary is dashed where magnetic flux is transferred across it (i.e. at the "merging" gap which maps to the magnetopause reconnection X-line) and solid where it is not (i.e. an adiaroic segment, meaning "not flowing across" (Siscoe and Huang, 1985)). In Figure 5a, the open-closed boundary is at the boundary between cusp and LLBL, whereas in Figure 5b it is further equatorward than this and lies near the poleward edge of the CPS. Both cases are drawn for the steady-state limit, with strongly southward interplanetary magnetic field ($B_z < 0$) which has no major dawn-dusk component ($B_y \approx 0$). The figures could readily be adapted to non-steady situations, for example during the growth phases of a substorm when the polar cap is expanding and the adiaroic segments of the boundary migrate equatorward (Siscoe and Huang, 1985; Cowley and Lockwood, 1992) and/or for large IMF $|B_y|$ (Cowley et al., 1991a, b).

The regions of precipitation shown in Figure 5 are broadly as sketched by Newell and Meng (1992; 1994) (see Figure 1). However, the region near noon between the CPS and the LLBL that previously has been characterised as "void" (Newell and Meng, 1992) has not been included in Figure 5. This has been done because void can occur when and where the flux falls below the one-count level, which depends on the instrument geometric factor (and thus its sensitivity threshold) as much as on the geophysical conditions. From the occurrence frequency of the void classification it is clear that it usually arises because either the BPS and/or CPS fluxes are below the one-count level. In addition, Newell and Meng (1994) are careful to note that the void region between the CPS and LLBL is often not devoid of precipitation, but that the precipitation present cannot be easily identified with any of the other classifications. The occurrence frequency plots by Newell and Meng (1992; 1994) show that the minimum occurrence probability of BPS is around noon but is still of order 25%. Indeed, the examples given by Pinnock et al. (1993), de la Beaujardiere et al. (1993) and Ohtani et al. (1995) all show precipitation classed as BPS close to noon. Consequently, we here re-classify the void region near noon (between CPS and LLBL) as being part of the dayside BPS which therefore extends across all MLT around noon.

There are a number of difference in these two schematics of boundary locations that have implications for the interpretation of the observed precipitation characteristics, such as: the local time extent of the different regions, the convection pattern in the cusp, and the location of the open-closed field line boundary relative to the observed particle signatures. For example, the statistical results of Newell

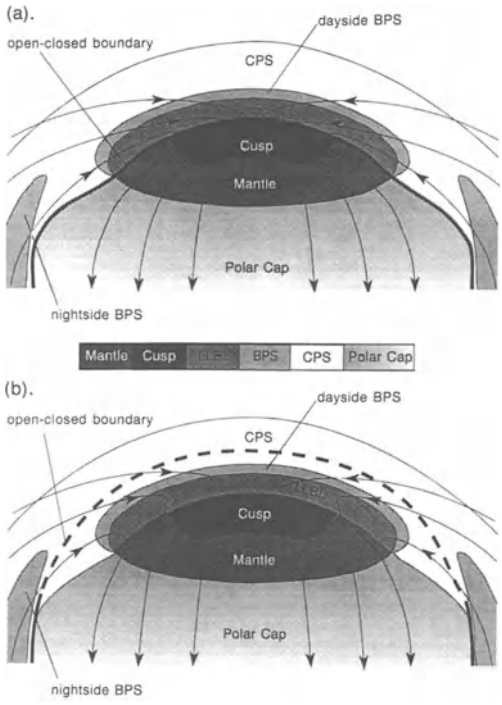

Figure 5. Comparison of ionospheric flow and precipitation regions for two open-closed field line boundary locations, from Lockwood (1997). The upper panel illustrates the ionospheric regions under the assumption that the LLBL, BPS, and CPS occupy closed field lines, with the longitudinal width of the cusp corresponding to the width of the separatrix. In the lower panel, the separatrix is taken to lie within the CPS, at its poleward edge. Under these conditions, the longitudinal width of the cusp is determined from the magnetosheath properties.

and Meng (1992; 1994) show the cusp precipitation occurrence to cover a relatively small range of MLT (about 3 hours), compared to the mantle and LLBL which both cover about 7 hours. This has been reflected in Figure 5. In Figure 5a the narrow cusp extent is set by the length of the merging gap. The LLBL, being on closed field lines and populated by a different mechanism, does not share this extent. However, the results of Newell and Meng indicate that the LLBL has roughly the same length in MLT as the mantle on open field lines. This has to be attributed to coincidence in Figure 5a. On the other hand, in Figure 5b the widths of the LLBL and the mantle both reflect the MLT extent of the merging gap. As described earlier, the smaller longitudinal extent of the cusp is due to the limited region in the dayside magnetosheath where the plasma densities and temperatures are high enough to produce low-altitude flux levels above the criteria for identification as cusp.

Another difference between Figures 5a and 5b relates to the poleward flow speeds in the cusp and the reconnection voltage. The observed transpolar volt-

age, and its dependence on the orientation of the IMF, show that magnetopause reconnection produces a voltage of order 110 kV when the IMF points strongly southward (e.g., Cowley, 1984). If the cusp represents the location of newly-opened field lines and if the LLBL is closed, then all the flow streamlines in the polar cap must first channel though a narrow constriction, often referred to as the "throat" (Heelis et al., 1976.), as in Figure 5a. This requires a voltage of order 110 kV across the cusp and, for the longitudinal width of 1000 km suggested by the statistics of Newell and Meng (1992; 1994), a poleward flow speed through the cusp of order 2 km/s. Such a speed is somewhat higher than is typically observed for this component of the flow and the throat flow pattern is not often seen. Rather, the flow pattern tends to show a broad convection reversal throughout the dayside as reported by Jorgensen et al. (1984) and reproduced in statistical models of the convection pattern (e.g. Heppner and Maynard, 1987; Shue and Weimer, 1994; see also discussion by Lockwood (1991)). As shown in Figure 5b, the broader region of flow reversal into the polar cap is consistent with the idea that the LLBL is not closed but rather that it is on the most recently opened field lines. The extent of the LLBL of order 2000 km implied by the statistics of Newell and Meng gives a more reasonable poleward plasma speed of 1 km/s for the transpolar voltage of 110 kV.

Many definitions of precipitation regions use the electron characteristics as well as those of the ions. When we allow for the velocity filter effect, this causes some conceptual difficulties because the electrons generally have much smaller flight times and so are swept a smaller distance downtail than are ions of comparable energy. Thus for adiabatic scatter-free motion of both ions and electrons, the two populations seen by a satellite at any one point and time would not share a common source. However, the situation is more complex than this because quasi-neutrality is maintained at all points along the field lines, and therefore the ions do exert an influence on the electrons. It is not fully understood how this balance is achieved, requiring that caution be exercised when using electron characteristics as identifiers of precipitation regions.

The location of the electron edge of the LLBL observed at low latitudes also has implications for the low-altitude LLBL identification. This electron edge (Gosling et al., 1991a) would be seen just poleward of the LLBL-cusp boundary in Figure 5a, whereas in Figure 5b it would be near the CPS-BPS border. At the electron edge, a satellite flying from closed to open field lines notes a loss of high-energy field-aligned magnetospheric (CPS) electrons for the first time: these are lost by flowing out along the newly-opened field lines through the magnetopause. Very shortly thereafter, lower-energy magnetosheath-like electrons, flowing in the opposite direction, are seen for the first time. However, fluxes of the incoming sheath electrons are restricted by the slower ions so that charge neutrality is maintained (Burch, 1985). Low-altitude observations often reveal the energetic CPS electrons very clearly and, when they are seen, their loss is evident and is equatorward of the LLBL and near the CPS-BPS border, as discussed by Lockwood et al. (1996). This

can also be seen, for example, in Figure 2 of Watermann et al. (1993), Plates 1 and 3 of Newell et al. (1991a), Plates 1a-1c of de la Beaujardiere et al. (1993), and Plates 1, 3 and 4 of Ohtani et al., (1995). This feature is sometimes referred to as the trapping boundary (e.g. Nishida et al., 1993) and is never, by definition of the LLBL, poleward of the LLBL. Thus if we associate this observed feature (on the dayside) with the electron edge discussed by Gosling et al. (1990a), its ionospheric location calls for the situation in Figure 5b, and Figure 5a cannot apply.

In Figure 5b, some magnetospheric-like electrons must persist poleward of the electron edge, particularly at large pitch angles, giving a double loss cone type distribution on open field lines. This has frequently been used to argue that the BPS and the LLBL are closed. The extension of some of the CPS electron population onto the most recently opened field lines could have a number of causes, including: electron scattering at the magnetopause current sheet; magnetic mirroring due to the field strength being larger near the magnetopause crossing point of the field line than closer to Earth in the cusp; gradient and curvature drifting of electrons from closed field lines onto open ones; and electrostatic potential differences associated with the maintenance of quasi-neutrality. Such effects would mean that electron fluxes (at low energies and large pitch angles) would decay away over an extended region poleward of the initial loss of high energy, low pitch angle electrons at the electron edge (CPS-BPS boundary). Using the definition of Newell et al. (1991), the decay of this remnant CPS population would cause the BPS classification to evolve into LLBL. Thus, if the above processes can be shown to be sufficient, the electron characteristics would also be consistent with Figure 5b.

3. Nightside Precipitation Regions

The nightside precipitation regions exhibit many of the same velocity-filter effect signatures that are observed throughout the dayside regions, and have provided important clues as to the dynamics of the magnetotail. While the dayside features often reflect the evolution in plasma following the opening of magnetic flux on the dayside magnetopause, the nightside features can often be associated with the closing of magnetic flux at a distant magnetotail reconnection site and its subsequent evolution. Among the issues that can be addressed from the low- and mid-altitude particle measurements are: the location of the open/closed field line boundary, the location of the distant reconnection site, the rate of reconnection in the magnetotail, and the downtail source regions of auroral arcs.

3.1. Low-Altitude Polar Cap - PSBL - Plasma Sheet Transition

As with the above description of the dayside precipitation regions, the discussion here will concentrate on conditions when the IMF is directed southward. Under these conditions, the polar cap electron fluxes are either below the detection thresh-

old of typical spacecraft instruments, or the fluxes are at a low and spatially unstructured level that is referred to as polar rain (e.g., Winningham and Heikkila, 1974; Fairfield and Scudder, 1985; Wing et al., 1996). On the other hand, under northward IMF conditions the polar cap tends to fill with intense, spatially localized fluxes of low-energy electrons (e.g., Winningham and Heikkila, 1974; Hardy et al., 1984). The average energy of the precipitating electrons is found to be on the order of 100 eV, suggesting a magnetosheath source (Obara et al., 1996). In addition, at these times the plasma sheet tends to cool and become quite structured, with a characteristic energy that can decrease to 100 eV or below (Sandahl and Lindqvist, 1990). Under these conditions, the distinction between the open polar cap and the closed plasma sheet becomes difficult to determine from the precipitation measurements.

When the spatially-uniform polar rain electrons are present, or when the polar cap is void of electron precipitation, low-altitude spacecraft typically detect an abrupt transition between the open field lines in the polar cap and the closed plasma sheet or plasma sheet boundary layer (e.g., Zelenyi et al., 1990; Fukunishi et al., 1993; Bosqued et al., 1993a; Onsager and Mukai, 1995). This transition is thus an indicator of the open-closed field line boundary that maps to the distant reconnection site, provided reconnection is occurring in the tail at the relevant local time. The low-altitude footprint of the separatrix is thus often clearly identifiable from the observed particle precipitation, although allowance must be made for the fact that even highly energetic electrons will be displaced equatorward by the dawn-dusk electric field. The properties of the precipitating electrons and ions and their variation with latitude provide clues as to the downtail properties of the distant plasma sheet and the variation of the plasma sheet with distance earthward from the X-line.

An illustration of the typical electron and ion precipitation observed in the nightside auroral zone is shown in Figure 6, from Fukunishi et al. (1993). For the discussion given in this paper, we have concentrated on the high-latitude regions, corresponding to the regions in Figure 6 labeled Polar Cap, PSBL, and Outer CPS, and we refer to the Outer CPS as simply the plasma sheet. As a spacecraft moves from the high-latitude polar cap toward lower latitudes, the first indication that the separatrix has been crossed is seen as a decrease in the polar rain electron flux (when the polar rain is present). The flux decrease is first seen at the highest energies, followed by a decrease at progressively lower energies. Slightly equatorward of the initial decrease in polar rain flux, the higher-energy (> 1 keV) electrons of plasma sheet origin are first detected. This plasma population is reasonably continuous down to lower latitudes where the field lines map to the earthward edge of the plasma sheet. The electron flux levels are consistent with the expected plasma sheet electron densities and temperatures. The gradual increase in flux levels with decreasing latitude reflects a gradual increase in the plasma sheet density and temperature with earthward location in the neutral sheet (Onsager and Mukai, 1995).

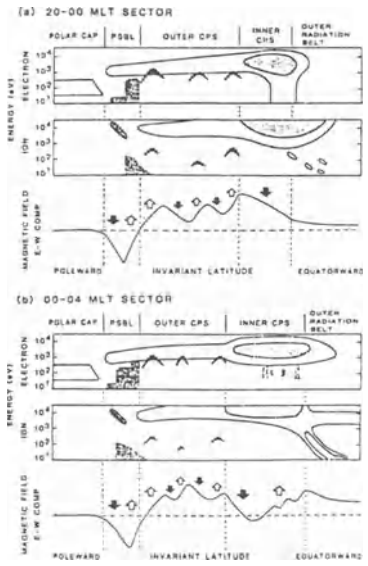

Figure 6. Diagram of the high-latitude electron and ion precipitation regions in the nightside auroral region, from Fukunishi et al. (1993). The spatial relationship between the polar cap electron precipitation, the PSBL ion beams, and the CPS precipitation are illustrated.

Equatorward of the high-latitude edge of the plasma sheet electrons is the region of velocity-dispersed ion precipitation, referred to as the Velocity Dispersed Ion Signature (VDIS) (Zelenyi et al., 1990; Saito et al., 1992; Bosqued et al., 1993a). The VDIS are produced by the velocity filter effect due to the equatorward ExB drift of plasma sheet boundary layer ions as they travel earthward along the magnetic field from the distant neutral sheet. It is interesting to note that the velocity versus latitude curve that one obtains from the VDIS smoothly matches the velocity versus latitude curve seen in the decrease of polar rain electron flux at slightly higher latitudes (Maezawa, private communication, 1995). An example of this can be seen in Plate 3d of Fukunishi et al. (1993). This observation strengthens the above mentioned association of the decline in polar rain flux with the separatrix location.

Further equatorward of the VDIS there is typically a region with a minimum in ion precipitation, referred to as the gap (Bosqued et al., 1993a), followed by ion precipitation that can be identified with the plasma sheet. Calculations of the expected low-altitude precipitation equatorward of the gap based on a model of plasma sheet sources and transport (Spence and Kivelson, 1993) have been shown to agree well with observations and have illustrated the local time dependence of the low-altitude precipitation (Hirsch et al., 1996).

The observations summarized above indicate the following evolution of magnetic topology and low-altitude particle precipitation. In the open polar cap, only

polar rain electron precipitation is observed, consisting of the high energy tail of the solar wind electron distributions. When reconnection occurs at the distant X-line, the open lobe field lines become closed plasma sheet field lines. The solar wind electron source is thereby disconnected; and any lobe, mantle, or ionospheric plasma contained on the newly closed flux tube will, in its field-aligned bounce motion, have the opportunity to encounter the distant neutral sheet where particle energization may occur. The decrease in polar rain flux and the arrival of the plasma sheet electron and ion flux will then be observed with the characteristic velocity filter signature as the flux tube evolves equatorward at low altitudes and earthward in the distant neutral sheet, as expected with a cross-tail electric field directed dawn to dusk.

The latitudinal variation in the nightside precipitation has a number of features similar to those seen in the dayside precipitation. In both cases, the distinctive particle signatures can be described well in terms of the evolution of plasma following reconnection. There are, however, many low-altitude satellite passes where these particle signatures are not detected. For example, it has been estimated that the probability of observing the VDIS on an individual nightside satellite pass is about 15%, based on AUREOL-3 data (Bosqued et al., 1993b) and about 45%, based on Akebono data (Saito et al., 1992). These can be considered lower limits to the occurrence probability of active reconnection in the distant tail, since there will be times when the velocity-dispersed particle fluxes will be below the instrument detection threshold. While the observations are able in many cases to provide the location of the separatrix at a given local time, the longitudinal extent of the separatrix at low altitudes corresponding to the cross-tail extent of the distant reconnection line cannot be inferred from these measurements. Combined use of ground-based instruments, low-altitude satellites, and polar images are likely to lead in the future to more comprehensive estimates of the global magnetic flux transport in the magnetotail.

3.2. Downtail Lobe - PSBL - Plasma Sheet Transition

The characteristic features of the electron and the ion distributions in the magnetotail (roughly 10 - 20 R_E downtail from Earth) show a strong correspondence to particle features seen at low altitudes. A similar spatial ordering of the plasma is also present at these downtail distances in the transition from the lobe, to the PSBL, and to the plasma sheet as observed, for example, by ISEE 1 and 2 (e.g., Forbes et al., 1981; Takahashi and Hones, 1988; Onsager et al., 1991) and by AMPTE-IRM (Nakamura et al., 1992). These observations are summarized by the illustration shown in Figure 7, after Takahashi and Hones (1988). Figure 7 illustrates schematically the earthward and the tailward field-aligned electron and ion fluxes encountered as a spacecraft traverses from the lobe (top), across the separatrix, through the PSBL, and into the plasma sheet (bottom).

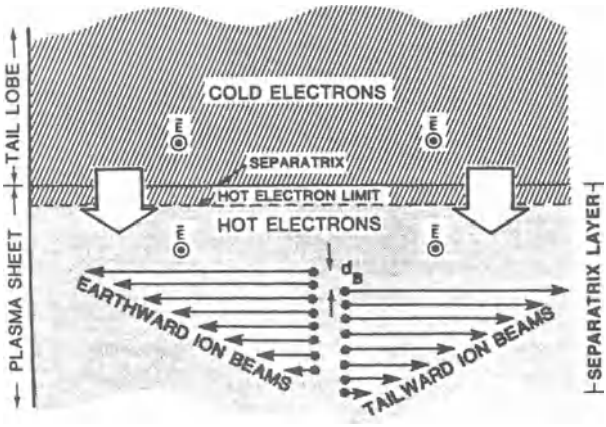

Figure 7. Diagram of the electron and ion regions at the downtail interface between the lobe and the plasma sheet, from Takahashi and Hones (1988). The high-latitude edge of the separatrix layer (PSBL) is identified by the hot plasma sheet electrons. Further equatorward, ion beams corresponding to the low-altitude VDIS are observed.

The first indication that the separatrix has been crossed is seen in the electron distributions, corresponding to the high-latitude edge of the > 1 keV PSBL electrons shown in Figure 6. These are electrons that presumably are streaming earthward from near the distant reconnection site on the most recently reconnected field lines. More equatorward of the separatrix, the velocity-dispersed ion beams are observed. The ion beams are observed equatorward of the electrons due to their slower field-aligned speeds and due to the fact they have undergone a larger ExB drift in traveling from the distant neutral sheet to the location where they are detected. The ions are first detected flowing earthward from the downtail acceleration region, and then flowing tailward after mirroring in the strong magnetic field near Earth. The velocity dispersed ion beams correspond to the VDIS observed at low altitudes. Recent calculations have demonstrated that a specified downtail plasma sheet profile in the equatorial plane can account for both the low-altitude and the downtail PSBL electron and ion measurements described above (Onsager and Mukai, 1996).

The close correspondence between the low-altitude and the downtail PSBL measurements clearly demonstrates the global nature of these features. And in addition to the large-scale spatial structure seen throughout the magnetotail, the detailed velocity-space features at low altitudes and downtail show similar distinctive features. The velocity-space features have been used to provide quantitative estimates of the plasma properties in the distant neutral sheet and estimates of the location of the distant reconnection site. From the VDIS observed at low altitudes, the downtail reconnection site source was estimated in one case to be located about 70 R_E downtail (Saito et al., 1992). The distribution function reconstructed from the

latitudinally dispersed ions had a temperature and a bulk energy of approximately 460 eV and 6.7 keV, respectively, consistent with the PSBL measurements downtail (Takahashi and Hones, 1988) and with previous theoretical calculations based on current sheet acceleration (Lyons and Speiser, 1982). In addition, the measured distribution functions in the downtail PSBL have been used to infer the plasma properties in the distant neutral sheet and to estimate the temporal variability in the reconnection site location (Elphic et al., 1995).

3.3. Downtail Plasma Sheet

Large advances have been made recently in understanding the average plasma convection in the equatorial plasma sheet and the average locations of the distant and the near-Earth neutral lines (Nishida et al. 1996a,b). These statistical results from the Geotail mission have provided a large-scale view of the net transport of northward and southward magnetic flux over downtail distances ranging from 36 R_E to 169 R_E during geomagnetically active times. A clear transition in the transport of magnetic flux is observed at about 140 R_E downtail. Earthward of this location, a net earthward transport of northward magnetic flux is observed, while tailward of this location a net tailward transport of southward flux is observed. The interpretation is that during active times, the distant X-line on average resides in the vicinity of 140 R_E downtail of Earth. The net earthward transport of northward magnetic flux is consistent with the dawn-dusk electric field required to account for the ion energization and the velocity filtering observed at low altitudes and in the mid-tail.

Results from recent statistical studies of energetic particle distributions in the magnetotail are consistent with the above estimates of the reconnection site location. Energetic ion measurements by Geotail have shown that earthward of 70 - 100 R_E downtail, flux levels are roughly comparable for both earthward- and tailward-directed fluxes (Christon et al., 1996). However, tailward of 100 R_E, the tailward fluxes dominate. The tailward fluxes do not decrease with further downtail distance (observed to 208 R_E) whereas the earthward fluxes continue to decrease with downtail distance. The dominance of tailward-directed energetic ion flux downtail of roughly 100 R_E is consistent with the statistical location of the distant reconnection site of about 140 R_E mentioned above (Nishida et al., 1996a).

3.4. Estimates of the Magnetotail Reconnection Rate

The high-latitude particle precipitation, and in particular the sharp discontinuity between the polar rain and the plasma sheet precipitation, has allowed the separatrix location and the reconnection electric field to be estimated from ground observations (de la Beaujardiere et al., 1994; Blanchard et al., 1996). In one technique, the separatrix was identified from the gradient in the ionospheric E region density, using incoherent scatter radar (de la Beaujardiere et al., 1994). The radar

also measures the ExB drift of the plasma, yielding the rate of flux transport across the separatrix, or the reconnection electric field.

In a more extensive analysis, the separatrix location was inferred from 630 nm optical emissions produced by the precipitating plasma sheet electrons (Blanchard et al., 1996). The ionospheric flow velocities were determined from incoherent scatter radar measurements. Estimates of the reconnection rate were obtained at all nightside magnetic local times and over varying solar wind conditions. Averaged over all levels of geomagnetic activity, reconnection electric fields were measured at all nightside local times and were found to peak over a 4-hour local-time sector centered on 2330 MLT. A weak correlation was found between the magnitude of the reconnection electric field and the southward component of the interplanetary magnetic field. The maximum correlation occurred with a 70 min lag, corresponding roughly to the time for open flux in the ionosphere to convect from the dayside reconnection site across the polar cap. The ratio of the estimated reconnection electric field to the solar wind electric field was found to be about 0.1, similar to estimates of the efficiency of dayside reconnection.

3.5. Source Regions for Auroral Activity

As illustrated schematically by the inverted V's in Figure 6, localized electron acceleration can be detected throughout the low-altitude extension of the plasma sheet. There is often evidence, however, that auroral activity is concentrated at the high-latitude and at the low-latitude edges of the plasma sheet. Two distinct locations of auroral luminosity have been described as the double auroral oval (Elphinstone et al., 1995a). From images taken by the Viking spacecraft, the presence of a nightside band of auroral luminosity near the open-closed field line boundary and a second band at lower latitudes has been described. This double oval is commonly observed during the late expansion and the recovery phases of substorms. The high-latitude auroral luminosity is likely to correspond to the electron acceleration that was shown to be colocated with the VDIS and with a region at the low-latitude boundary of the VDIS characterized by a void in ion precipitation, i.e., the gap (Bosqued et al., 1993a).

Two interpretations for the ion precipitation gap have been presented, with implications for the magnetotail processes responsible for the electron acceleration observed at high latitudes near the transition between the VDIS and the main plasma sheet. In one interpretation, the gap is due to strong non-adibatic motion in the neutral sheet (Bosqued et al., 1993b; Ashour-Abdalla et al., 1992). The magnetic field configuration expected to cause the non-adiabatic particle trajectories typically exist roughly 10-15 R_E downtail from Earth. This interpretation would place the high-latitude portion of the double oval, and therefore also the separatrix, at roughly this downtail location. However, recent calculations of ion motion in the plasma sheet have contradicted this interpretation of the gap (Delcourt et al., 1996). In this study, it is argued that the near-Earth plasma sheet (roughly 10-15 R_E

downtail) should be the site of sufficient pitch angle scattering to maintain the ion precipitation, and therefore would not be the location of a gap in ion precipitation. It is suggested that the ion dynamics that could create a minimum in ion flux are likely to occur in the more downtail plasma sheet.

Another interpretation of the ion precipitation gap is that it maps to the transition from fast, earthward, post-reconnection flows in the distant plasma sheet to the more slowly convecting plasma sheet nearer Earth (Onsager and Mukai, 1995; 1996). The lack of ion precipitation is due simply to the low density and low temperature in the distant plasma sheet. The auroral arcs that were found to be co-located with the gap (Bosqued et al., 1993a) would then map to the location in the plasma sheet where there is a sharp gradient in the earthward convection speed in the neutral sheet. This high-latitude arc system mapping to just earthward of the distant reconnection site would be well separated from the low-latitude arc system, which presumably maps to the near-Earth edge of the plasma sheet, thus accounting for the observed double oval.

In the region equatorward of the open-closed field line boundary, interesting features are often observed in the form of equatorward-drifting auroral arcs (Persson et al., 1994a, b; Gazey et al., 1995). These are seen in the late growth phase and early expansion phase of substorm activity; however, their importance in the overall sequence of substorm events is not yet clear. What is known is that the poleward expansion of the substorm aurora does not alter their equatorward drift nor their luminosity, implying that they are formed in a region which is quite distinct from the substorm onset region where the cross-tail current is initially disrupted.

The formation of these arcs has been monitored by de la Beaujardiere et al. (1994) who associated them with weak bursts of reconnection at the distant reconnection site in quite times. The arcs do indeed appear to be on closed field lines. The electrons that cause these arcs are seen poleward of the persistent aurora that intensifies at onset (Elphinstone et al., 1995b) but equatorward of the field-aligned currents on the open-closed field line boundary (Fukunishi et al., 1993).

4. Summary

This article has described some of the recent advances in understanding the high-latitude, low-altitude particle precipitation in terms of the large-scale processes occurring in the magnetosphere. The discussion has concentrated primarily on our understanding of the low-altitude particle signatures in terms of the evolution of plasma following the occurrence of magnetic reconnection, either at the dayside magnetopause or in the magnetotail. Although it is certainly the case that not all observations can be understood by this simple paradigm, the commonly observed precipitation regions are typically well described in this way. Furthermore, the identification of the particle signatures as being the result of plasma evolution fol-

lowing reconnection has led to a number of important advances in our ability to identify separatrices locations and to quantify the rate and effects of reconnection.

In the dayside ionosphere, the cusp, mantle, and polar rain have all been shown conclusively to lie on open field lines. The particle flux levels and their spatial and temporal variability have been described quantitatively in terms of magnetosheath transport across open magnetic field lines. The specific features of the velocity-space distribution functions have provided important clues on the details of the reconnection process and on plasma transport across the magnetopause.

A debate still exists, however, on the location of the dayside separatrix relative to the low latitude boundary layer. There is considerable observational evidence near the low-latitude magnetopause to support both the open and the closed interpretation of the LLBL. The ambiguities near the magnetopause are further complicated at low altitudes by the convection of the magnetospheric and ionospheric plasma that spread the plasma originating from a given location in the distant magnetosphere over a broad region in the ionosphere.

In this paper, two possible separatrix locations in the ionosphere relative to the particle precipitation regions have been contrasted. In one case, the low-altitude CPS, BPS, and LLBL regions have been assumed to be on closed field lines, which is the more conventional interpretation. In the other case, the separatrix has been assumed to be within the CPS region, just equatorward of its polarward boundary. The local-time extent of the various regions, the ionospheric convection, and the precipitation features throughout the dayside ionosphere have been discussed for these two separatrix locations. It is argued here that the separatrix location within the CPS provides a more consistent description of the high-latitude ionospheric regions.

The discussion of the nightside precipitation regions has emphasized the clear transition from the open polar cap to the closed plasma sheet that is expected when reconnection is active in the magnetotail. The distinctive low-altitude plasma signatures have been compared with the commonly observed features in the downtail PSBL and with observations in the distant neutral sheet. From the observations in these different regions it is possible to demonstrate the global coherence over large distances of the processes occurring in the magnetotail.

From the identification of the low-altitude separatrix and the distinctive velocity space features measured in the particle precipitation, it has been possible to estimate remotely the properties of the distant tail reconnection. The rate of reconnection, the location of the reconnection site, and the properties of the plasma in the distant neutral sheet have all been obtained from the low-altitude measurements.

In addition, the location of the nightside particle precipitation regions relative to auroral luminosity have provided clues as to the regions in the magnetosphere where the auroral arcs map. The existence of the double auroral oval and the association of auroral arcs with the VDIS and the ion precipitation gap at its equatorward boundary indicate that this high-latitude arc system maps to the distant magnetotail, just earthward of the distant reconnection site. The low-latitude portion of the

double oval maps presumably to the near-Earth plasma sheet and is the region of auroral luminosity where substorm onset is seen.

Acknowledgements

The authors would like to sincerely acknowledge the support for this research provided by the International Space Science Institute. The collaborative workshops held at the Institute allowed for a critical exchange of ideas that contributed greatly to this manuscript. We would also like to thank the reviewers for their helpful comments and suggestions.

References

Alem, F. and Delcourt, D.C.: 1995, 'Nonadiabatic Precipitation of Ions at the Cusp Equatorward Edge', *J. Geophys. Res.* **100**, 19,321.

Ashour-Abdalla, M., Zelenyi, L.M., Bosqued, J.M., Peroomian, V., Whang, Z., Schriver, D., Richard, R.L.: 1992, 'The formation of the wall region: Consequences in the near Earth magnetotail', *Geophys. Res. Lett.* **19**, 1739.

Blanchard, G.T., Lyons, L.R., de la Beaujardiere, O., Doe, R.A., and Mendillo, M.: 1996, 'Measurement of the magnetotail reconnection rate', *J. Geophys. Res.* **101**, 15,265.

Bosqued, J. M., Ashour-Abdalla, M., El Alaoui; M., Zelenyi, L.M., and Berthelier, A.: 1993a, 'AUREOL-3 observations of new boundaries in the auroral ion precipitation', *Geophys. Res. Lett.* **20**, 1203.

Bosqued, J. M., Ashour-Abdalla, M., El Alaoui, M., Peroomian, V., Zelenyi, L. M., and Escoubet, C. P.: 1993b, 'Dispersed ion structures at the poleward edge of the auroral oval: Low-altitude observations and numerical modeling', *J. Geophys. Res.*, **98** 19,181.

Burch, J. L.: 1985, 'Quasi-neutrality in the polar cusp', *Geophys. Res. Lett.* **12**, 469.

Christon, S. P., Gloeckler, G., Williams, D. J., McEntire, R. W., and Lui, A. T. Y.: 1996, 'The downtail distance variation of energetic ions in Earth's magnetotail region: Geotail measurements at X > -208 R_E', *J. Geomag. Geoelectr.* **48**, 615.

Cowley, S.W.H.:1982, 'The causes of convection in the Earth's magnetosphere: A review of developments during IMS', *Rev. Geophys.* **20**, 531.

Cowley, S.W.H.:1984, 'Solar wind control of magnetospheric convection, in Achievements of the international magnetospheric study', IMS, 483-494, ESA SP-217, ESTEC, Noordwijk, The Netherlands.

Cowley, S.W.H., and Owen, C. J.,: 1989, 'A simple illustrative model of open flux tube motion over the dayside magnetopause', *Planet. Space Sci.* **37**, 1461.

Cowley, S.W.H. and Lewis, Z.V.: 1990, 'Magnetic trapping of energetic particles on open dayside boundary layer flux tubes', *Planet. Space Sci.* **38**, 1343.

Cowley, S.W.H., and Lockwood, M.: 1992, 'Excitation and decay of solar wind-driven flows in the magnetosphere-ionosphere system', *Ann. Geophys.* **10**, 103.

Cowley, S.W.H., Southwood, D. J., and Saunders, M. A.: 1983, 'Interpretation of magnetic field perturbations in the Earth's magnetopause boundary', *Planet. Space Sci.* **31**, 1237.

Cowley, S.W.H., Morelli, J. P., and Lockwood, M.: 1991a, 'Dependence of convective flows and particle precipitation in the high-latitude dayside ionosphere on the X and Y components of the interplanetary magnetic field', *J. Geophys. Res.* **96**, 5557.

Cowley, S.W.H., Freeman, M. P., Lockwood, M., and Smith, M. F.: 1991b, 'The ionospheric signature of flux transfer events', in *CLUSTER - dayside polar cusp*, ed. C.I Barron, ESA SP-330, 105-112, European Space Agency Publications, Nordvijk, The Netherlands.

Crooker, N. U.: 1992, 'Reverse Convection', *J. Geophys. Res.* **97**, 19,363.

Curran, D.B., and Goertz, C. K.: 1989, 'Particle distributions in a two- dimensional reconnection field geometry', it J. Geophys. Res. **94**, 272.

Daly, P.W. and Fritz, T. A.: 1982, 'Trapped electron distributions on open field lines', *J. Geophys. Res.* **87**, 6081.

de la Beaujardiere, O., Newell, P., and Rich, R.: 1993, 'Relationship between Birkeland current regions, particle participation, and electric fields', *J. Geophys. Res.* **98**, 7711.

de la Beaujardiere, O., Lyons, L. R., Ruohonieme, J. M., Friis- Christensen, E., Danielsen, C., Rich, F. J., and Newell, P. T.: 1994, 'Quiet-time intensifications along the poleward auroral boundary near midnight', *J. Geophys. Res.* **99**, 287.

Delcourt, D. C., Sauvaud, J.-A., Martin Jr., R. F., and Moore, T. E.: 1996, 'On the nonadiabatic precipitation of ions from the near-Earth plasma sheet', *J. Geophys. Res.* **101**, 17,409.

Eastman, T.E. and Hones, Jr., E. W.: 1979, 'Characteristics of the magnetospheric boundary layer as observed by IMP-6', *J. Geophys. Res.* **84**, 2109.

Eastman, T.E., Hones, Jr., E. W., Bame, S. J., and Ashbridge, J. R.: 1976, 'The magnetospheric boundary layer: site of plasma, momentum and energy transfer from the magnetosheath to the magnetosphere', *Geophys. Res. Lett.* **3**, 685.

Elphic, R. C., Onsager, T. G., Thomsen, M. F., and Gosling, J. T.: 1995, 'Nature and location of the source of plasma sheet boundary layer ion beams', *J. Geophys. Res.* **100**, 1857.

Elphinstone, R. D., Murphree, J. S., Hearn, D. J., Cogger, L. L., Sandahl, I., Newell, P. T., Klumpar, D. M., Ohtani, S., Sauvaud, J. A., Potemra, T. A., Mursula, K., Wright, A., and Shapshak, M.: 1995a, 'The double oval UV auroral distribution, 1, Implications for the mapping of auroral arcs', *J. Geophys. Res.* **100**, 12,075.

Elphinstone, R. D., Hearn, D. J., Cogger, L. L., Murphree, J. S., Singer, H., Sergeev, V., Mursula, K., Klumpar, D. M., Reeves, G. D., Johnson, M., Ohtani, S., Potemra, T. A., Sandahl, I., Nielsen, E., Persson, M., Opgenoorth, H., Newell, P. T., and Feldstein, Y. I.: 1995b 'Observations in the vicinity of substorm onset: Implications for the substorm process', *J. Geophys. Res.* bf 100, 7937.

Fairfield, D. H., and Scudder, J. D.: 1985, 'Polar rain: Solar coronal electrons in the Earth's magnetosphere', *J. Geophys. Res.* **90**, 4055.

Forbes, T. G., Hones Jr., E. W., Bame, S. J., Asbridge, J. R., Paschmann, G., Sckopke, N., and Russell, C. T.: 1981, 'Evidence for the tailward retreat of a magnetic neutral line in the magnetotail during substorm recovery', *Geophys. Res. Lett.* **8**, 261.

Fukunishi, H., Takahashi, Y., Nagatsuma, T., Mukai, T., and Machida, S.: 1993, 'Latitudinal structures of nightside field-aligned currents and their relationships to the plasma sheet regions', *J. Geophys. Res.* **98**, 11,235.

Fuselier, S.A., Klumpar, D. M., and Shelley, E. G.: 1991, 'Ion reflection and transmission during reconnection at the Earth's subsolar magnetopause', *Geophys. Res. Lett.* **18**, 139.

Fuselier, S.A., Anderson, B.J., and Onsager, T.G.: 1997, 'Electron and ion signatures of field line topology at the low-shear magnetopause', *J. Geophys. Res.* **102**, 4847.

Galperin, Y. I., and Feldstein, Y. I.: 1996, 'Mapping of the precipitation regions to the plasma sheet', *J. Geomag. Geoelectr.* **48**, 857.

Gazey, N.G.J., Lockwood, M., Smith, P.N., Coles, S., Bunting, R.J., Lester, M., Aylward, A.D., Yeoman, T.Y., and Luhr, H.: 1995, 'The development of substorm cross-tail current disruption as seen from the ground', *J. Geophys. Res.* **100,** 9633.

Gosling, J.T., Thomsen, M. F., Bame, S. J., Onsager, T. G., and Russell, C. T.: 1990a, 'The electron edge of the low-latitude boundary layer during accelerated flow events', *Geophys. Res. Lett.* **17**, 1833.

Gosling, J.T., Thomsen, M. F., Bame, S. J., Elphic R. C., and Russell, C. T.: 1990b, 'Plasma flow reversals at the dayside magnetopause and the origin of asymmetric polar cap convection', *J. Geophys. Res.* **95**, 8073.

Hapgood, M.A., and Bryant, D. A.: 1992, 'Exploring the magnetospheric boundary layer', *Planet. Space Sci.* **40**, 1431.

Hardy, D. A.: 1984, 'Intense fluxes of low-energy electrons at geomagnetic latitudes above 85 degrees', *J. Geophys. Res.* **89**, 3833.

Heelis, R.A., Hanson, W. B., and Burch, J. L.: 1976, 'Ion convection reversals in the dayside cleft', *J. Geophys Res.* **81**, 3803.

Heppner, J. P. and Maynard, N. C.: 1987, 'Empirical high-latitude electric field models', *J. Geophys. Res.* **92**, 4467.

Hill, T.W. and Reiff, P. H.: 1977, 'Evidence of magnetospheric cusp proton acceleration by magnetic merging at the dayside magnetopause', *J. Geophys. Res.* **23**, 3623.

Hirsch, K. L., Spence, H. E., Onsager, T. G.: 1996, 'Low altitude signatures of the plasma sheet: Model predictions of local time dependence', *J. Geomag. Geoelectr.* **48**, 887.

Jorgensen, T. S., Friis-Christiansen, E., Wickwar, V. B., Kelly, J. D., Clauer, C. R., and Banks, P. M.: 1984, 'On the reversal from "sunward" to "antisunward" plasma convection in the dayside high latitude ionosphere', *Geophys. Res. Lett.* **1**, 887.

Lockwood, M.: 1991, 'On flow reversal boundaries and cross-cap potential in average models of high latitude convection', *Planet. Space Sci.* **39**, 397.

Lockwood, M.: 1995, 'The location and characteristics of the reconnection X-line deduced from low-altitude satellite and ground-based observations: 1. Theory', *J. Geophys. Res.* **100**, 21,791.

Lockwood, M.: 1997, 'The relationship of dayside auroral precipitations, the open-closed field line boundary and the convection reversal boundary', *J. Geophys. Res.* in press.

Lockwood, M. and Davis, C. J.: 1996a, 'On the longitudinal extent of magnetopause reconnection bursts', *Annales Geophys.* **14**, 865.

Lockwood, M. and Davis, C. J.: 1996b, 'An analysis of the accuracy of magnetopause reconnection rate variations deduced from cusp ion dispersion characteristics', *Annales Geophys.* **14**, 149.

Lockwood, M. and Moen, J.: 1996, 'Ion populations on open field lines within the low-latitude boundary layer: theory and observations during a dayside transient event', *Geophys. Res Lett.* **23**, 2895.

Lockwood, M. and Smith, M. F.: 1992, 'The variation of reconnection rate at the dayside magnetopause and cusp ion precipitation', *J. Geophys. Res.* **97**, 14,841.

Lockwood, M. and Smith, M. F.: 1993, 'Comment on "Mapping the dayside ionosphere to the magnetosphere according to particle precipitation characteristics" by Newell and Meng', *Geophys. Res. Lett.* **20**, 1739.

Lockwood, M. and Smith, M. F.: 1994, 'Low- and mid-altitude cusp particle signatures for general magnetopause reconnection rate variations: I - Theory', *J. Geophys. Res.* **99**, 8531.

Lockwood, M., Onsager, T. G., Davis, C. J., Smith, M. F., and Denig, W. F.: 1994, 'The characteristics of the magnetopause reconnection X-line deduced from low-altitude satellite observations of cusp ions', it Geophys. Res. Lett. **21**, 2757.

Lockwood, M., Cowley S. W. H., and Onsager, T. G.:1996, 'Ion acceleration at both the interior and exterior Alfven waves associated with the magnetopause reconnection site: signatures in cusp precipitation', *J. Geophys. Res.* **101**, 21,501.

Lotko, W., and Sonnerup, B. U. O.: 1995, 'The low-latitude boundary layer on closed field lines, in Physics of the magnetopause', *Geophys. Mono.* **90**, ed. P. Song, B.U.O. Sonnerup and M. Thompsen, pp 371-383.

Lyons, L. R.: 1995, 'The ionosphere as a screen for magnetospheric processes', U.S. National Report to the IUGG, 1991-1994, *Rev. Geophys.*, supplement, 715.

Lyons, L. R., and Speiser, T. W.: 1982, 'Evidence for current sheet acceleration in the geomagnetic tail', *J. Geophys. Res.* **87**, 2276.

Lyons, L. R., Schulz, M., Pridmore-Brown D. C., and Roeder, J. L.: 1994, 'Low-latitude boundary layer near noon: An open field line', *J. Geophys. Res.* **99**, 2227.

Lyons, L. R., Lu, G., de la Beaujardiere, O., and Rich, F. J.: 1996, 'Synoptic maps of polar caps for stable interplanetary magnetic field intervals during January 1992 geospace environment modeling campaign', *J. Geophys. Res.* **101**, 27,283.

Matsuoka, A., Tsuruda, K., Hayakawa, H., Mukai, T., and Nishida, A.: 1996, 'Electric field structure and ion precipitation in the polar region associated with northward interplanetary magnetic field', *J. Geophys. Res.* **101**, 10,711.

Mitchell, D.G., Kutchko, F., Williams, D. J., Eastman, T. E., Frank, L. A., and Russell, C. T.: 1987, 'An extended study of the low-latitude boundary layer on the dawn and the dusk flanks on the magnetosphere', *J. Geophys. Res.* **92**, 7394.

Moen, J., Evans, D., Carlson, H. C., and Lockwood, M.: 1996, 'Dayside moving auroral transients related to LLBL dynamics', *Geophys. Res. Lett.* **23**, 3247.

Nakamura, M., Paschmann, G., Baumjohann, W., and Sckopke, N.: 1992, 'Ion distributions and flows near the neutral sheet', *J. Geophys. Res.* **96**, 5631.

Newell, P. T.: 1995, 'Do the dayside cusps blink?, U.S. National Report to the IUGG, 1991-1994', *Rev. Geophys., supplement.*

Newell, P.T. and Meng, C.-I.: 1992, 'Mapping the dayside ionosphere to the magnetosphere according to particle precipitation characteristics', *Geophys. Res. Lett.* **19**, 609.

Newell, P.T. and Meng, C.-I.: 1994, 'Ionospheric projections of magnetospheric regions under low and high solar wind pressure conditions', *J. Geophys. Res.* **99**, 273.

Newell, P.T. and Meng, C.-I.: 1995a, in P. Song, B.U.O. Sonnerup, and M. Thomsen (ed.), 'Magnetopause dynamics as inferred from plasma observations on low-altitude satellites', *Physics of the Magnetopause*, Geophys. Monogr. Ser. **90**, p. 407, AGU, Washington, D.C.

Newell, P. T., and Meng, C.-I.: 1995b, 'Cusp low-energy ion cutoffs: A survey and implications for merging', *J. Geophys. Res.* **100**, 21,943.

Newell, P.T. Burke, W. J., Sanchez, E. R., Meng, C.-I., Greenspan, M. E., and Clauer, C. R.: 1991a, 'The low-latitude boundary and the boundary plasma sheet at low altitude: prenoon precipitation regions and convection reversal boundaries', *J. Geophys. Res.* **96**, 21,013.

Newell, P.T., Burke, W. J., Meng, C.-I., Sanchez, E. R., and Greenspan, M. E.: 1991b, 'Identification an observation of the plasma mantle at low altitude', *J. Geophys. Res.* **96**, 35.

Nishida, A.: 1989, 'Can random reconnection on the magnetopause produce the low-latitude boundary layer?', *Geophys. Res. Lett.* **16**, 227.

Nishida, A., and Mukai, T.: 1994, 'Reply to comment on "Unexpected features of the ion precipitation in the so-called cleft/low latitude boundary layer region: association with sunward convection and occurrence on open field lines', *J. Geophys. Res.* **99**, 23,367.

Nishida, A., Mukai, T. Hayakawa, H., Matsuoka, A., and Tsuruda, K.: 1993, 'Unexpected features of the ion precipitation in the so-called cleft/low-latitude boundary layer region: association with sunward convection and occurrence on open field lines', *J. Geophys. Res.* **98**, 11,161.

Nishida A., Mukai, T., Yamamoto, T., Saito, Y., and Kokubun, S.: 1996a, 'Magnetotail convection in geomagnetically active times, 1, Distance to the neutral lines', *J. Geomag. Geoelectr.* **48**, 489.

Nishida A., Mukai, T., Yamamoto, T., Saito, Y., and Kokubun, S,: 1996b, 'Magnetotail convection in geomagnetically active times, 2, Dawn- dusk motion in the plasma sheet', *Geomag. Geoelectr.* **48**, 503.

Norberg, O., Yamauchi, M., Eliasson, L., and Lundin, R.: 1994, 'Freja observations of multiple injection events in the cups', *Geophys. Res. Lett.* **21**, 1919.

Obara, T., Mukai, T., Hayakawa, H., Tsuruda, K., Matsuoka, A., and Nishida, A.: 1996, 'Signature of electric field associated with localized electron precipitation in the polar cap region - Akebono (EXOS-D) results', *J. Geomag. Geoelectr.* **48**, 327.

Ohtani, S.-I., Potemra, T. A., Newell, P. T., Zanetti, L. J., Iijima, T., Wantanabe, M., Yamauchi, Y., Elphinstone, R. D., de la Beaujardiere, O., and Blomberg, L. G.: 1995,, 'Simultaneous prenoon and postnoon observations of three field-aligned current systems from Viking and DMSP-F7', *J. Geophys. Res.* **100**, 119.

Onsager, T.G. and Mukai, T.: 1995, 'Low altitude signature of the plasma sheet boundary layer: Observations and model', *Geophys. Res. Lett.* **22**, 855.

Onsager, T. G., and Mukai, T.: 1996, 'The structure of the plasma sheet and its boundary layers', *J. Geomag. Geoelectr.* **48**, 687

Onsager, T. G., Thomsen, M. F., Elphic, R. C., and Gosling, J. T.: 1991, 'Model of electron and ion distributions in the plasma sheet boundary layer', *J. Geophys. Res.* **96**, 20,999.

Onsager, T. G., Kletzing, C. A., Austin, J. B., and MacKiernan, H.: 1993, 'Model of magnetosheath plasma in the magnetosphere: Cusp and mantle precipitations at low altitudes', *Geophys. Res. Lett.* **20**, 479.

Owen, C.J. and Slavin, J. A.: 1992, 'Viscously driven plasma flows in the deep geomagnetic tail', *Geophys. Res. Lett.* **19**, 1443.

Paschmann, G., Papamastorakis, I., Baumjohann, W., Sckopke, N., Carlson, C. W., Sonnerup, B. U. O., and Luhr, H.: 1986, 'The magnetopause for large magnetic shear: AMPTE/IRM observations', *J. Geophys. Res.* **91**, 11,099.

Persson, M.A.L, Aikio, A.T., and Opgenoorth, H.J.: 1994a, Late growth and early expansion phase of a substorm', in *Substorms 2, Proc. 2nd. Intl. Conf. on Substorms*, pp. 421-428, Geophysical Institute, Fairbanks, Alaska.

Persson, M.A.L., Opgenoorth, H.J., Pulkkinen, T.I., Eriksson, A.I, Dovner, P.O., Reeves, G.D., Belian, R.D., Andre, M., Blomberg, L.G., Erlandson, R.E., Boehm, M.H., Aikio, A.T., and Haggstrom, I.: 1994b, 'Near-earth substorm onset: A coordinated study', *Geophys. Res. Lett.* **21**, 1875.

Pinnock M., Rodger, A. S., Dudeney, J. R., Baker, K. B., Newell, P. T., Greenwald, R. A., and Greenspan, M. E.: 1993, 'Observations of an enhanced convection channel in the cusp ionosphere', *J. Geophys. Res.* **98**, 3767.

Richard, R.L., Walker, R. J., and Ashour-Abdalla, M.: 1994, 'The population of the magnetosphere by solar wind ions when the interplanetary magnetic field is northward', *Geophys. Res. Lett.* **21**, 2455.

Rosenbauer, H., Gruenwaldt, H., Montgomery, M. D., Paschmann, G.,and Sckopke, N.: 1975, 'HEOS 2 plasma observations in the distant polar magnetosphere: the plasma mantle', *J. Geophys. Res.* **80**, 2723.

Saito, Y., Mukai, T., Hirahara, M., Machida, S., and Kaya, N.: 1992, 'Distribution function of precipitating ion beams with velocity dispersion observed near the poleward edge of the nightside auroral oval', *Geophys. Res. Lett.* **19**, 2155.

Sandahl, I., and Lindqvist, P.-A.: 1990, 'Electron populations above the nightside auroral oval during magnetic quiet times', *Planet. Space Sci.* **38**, 1031.

Scholer, M., Daly, P. W., Paschmann, G., and Fritz,, T. A.: 1982, 'Field line topology determined by energetic particles during a possible magnetopause reconnection event', *J. Geophys. Res.* **87**, 6073.

Shue, J.-H. and Weimer, D. R.: 1994, 'The relationship between ionospheric convection and magnetic activity', *J. Geophys. Res.* **99**, 401.

Siscoe, G. L. and Huang, T. S.: 1985, 'Polar cap inflation and deflation', *J. Geophys. Res.* **90**, 543.

Smith, M.F. and Rodgers, D.J.: 1991, 'Ion distributions at the dayside magnetopause', *J. Geophys. Res.* **95**, 11,617.

Smith, M. F., and Lockwood, M.: 1996, 'Earth's magnetospheric cusps', *Rev. of Geophys.* **34**, 233.

Song, P., and Russell, C. T.: 1992, 'Model of the formation of the low- latitude boundary layer for strongly northward interplanetary magnetic field', *J. Geophys. Res.* **97**, 1411.

Song, P., Elphic, R. C., Russell, C. T., Gosling, J. T., and Cattell, C. A.: 1990, 'Structure and properties of the subsolar magnetopause for northward IMF: ISEE observations', *J. Geophys. Res.* **95**, 6375.

Sonnerup, B.U.O.: 1980, 'Theory of the low-latitude boundary layer', *J. Geophys. Res.* **85**, 2017.

Sonnerup, B.U.O., Papamastorakis, I., Paschmann, G., and Luhr, H.: 1986, 'The magnetopause for large magnetic shear: analysis of convection electric fields from AMPTE/IRM', *J. Geophys. Res.* **95**, 10,541.

Spence, H. E., and Kivelson, M. G.: 1993, 'Contributions of the low- latitude boundary layer to the finite width magnetotail convection model', *J. Geophys. Res.* **98**, 15,487.

Spreiter, J. R., and Stahara, S. S.: 1985, in B. T. Tsurutani and R. G. Stone (ed.), 'Magnetohydrodynamic and gasdynamic theories for planetary bow waves', *Collisionless Shocks in the Heliosphere: Reviews of Current Research*, Geophys. Monogr. Ser., **35**, pp. 85-107, AGU, Washington, D.C.

Takahashi, K., and Hones, Jr., E. W.: 1988, 'ISEE 1 and 2 observations of ion distributions at the plasma sheet-tail lobe boundary', *J. Geophys. Res.* **93**, 8558.

Traver, D.P., Mitchell, D. G., Williams, D. J., Frank, L. A., and Huang, C. Y.: 1991, 'Two encounters with the flank low-latitude boundary layer: further evidence for closed field line topology and investigation of internal structure', *J. Geophys. Res.* **96**, 21,025.

Treumann, R.A., LaBelle, J., and Bauer, T. M.: 1995, in P. Song, B.U.O. Sonnerup, and M. Thomsen (ed.), 'Diffusion processes: An observational perspective', *Physics of the magnetopause*, Geophys. Monogr. Ser. **90**, pp. 331-341, AGU, Washington, D.C.

Vasyliunas, V.M.: 1979, 'Interaction between the magnetospheric boundary layers and the ionosphere', in *Proceedings of the Magnetospheric Boundary Layers Conference*, Alpbach, pp. 387-394, ESA SP-148, ESA, Paris.

Watermann, J., de la Beujardiere, O., and Spence, H. E.: 1993, 'Space-time structure of the morning aurora inferred from coincident DMSP-F6,-F8, and Sondrestrom incoherent scatter radar observations', *J. Atmos. Terr. Phys.* **55**, 1728.

Wing, S., Newell, P. T., and Onsager, T. G.: 1996, 'Modeling the entry of magnetosheath electrons into the dayside ionosphere., it J. Geophys. Res. **101**, 13,155.

Winningham, J. D., and Heikkila, W. J.: 1974, 'Polar cap auroral electron fluxes observed with Isis 1., *J. Geophys. Res.* **79**, 949.

Winske, D., Thomas, V. A., and Omidi, N.: 1995, in P. Song, B.U.O. Sonnerup, and M. Thomsen (ed.), 'Diffusion at the magnetopause: A theoretical perspective', *Physics of the magnetopause*, Geophys. Monogr. Ser. **90**, pp. 321-330, AGU, Washington, D.C.

Woch, J., and Lundin, R: 1992a, 'Magnetosheath plasma precipitation in the polar cusp and its control by the interplanetary magnetic field', *J. Geophys. Res.* **97**, 1421.

Woch, J., and Lundin, R.: 1992b. 'Signature of transient boundary layer processes observed with Viking', *J. Geophys. Res.* **97**, 1431.

Woch, J. and Lundin, R.: 1993, 'The low-latitude boundary layer at mid- altitudes: Identification based on Viking hot plasma data', *Geophys. Res. Lett.* **20**, 979.

Yamauchi, M., and Lundin, R.: 1994, in J. A. Holtet and A. Egeland (eds.), 'Classification of large-scale and meso-scale ion dispersion patterns observed by Viking over the cusp-mantle region', *Physical Signatures of Magnetospheric Boundary Layer Processes*, Klewar Academic Publishers, p. 99.

Yamauchi, M., Lundin, R., and Potemra, T.A.: 1995, 'Dynamic response of the cusp morphology to the interplanetary magnetic field changes: An example observed by Viking', *J. Geophys. Res.* **100**, 7661.

Zelenyi, L. M., Kovrazkhin, R. A., and Bosqued, J. M.: 1990, 'Velocity- dispersed ion beams in the nightside auroral zone: AUREOL 3 observations', *J. Geophys. Res.* **95**, 12,119.

Address for correspondence: T. G. Onsager, NOAA Space Environment Center, 325 Broadway, Boulder, CO 80303, USA

MAGNETOSPHERIC PROCESSES LEADING TO PRECIPITATION

L. R. LYONS
Department of Atmospheric Sciences, University of California, Los Angeles, California, USA

and

Space and Environment Technology Center, The Aerospace Corporation, Los Angeles, California, USA

Received January 17, 1997; Accepted in final form April 1, 1997

Abstract. Important causes of the precipitation of magnetospheric particles into the ionosphere are reviewed, and critical areas where further study is needed are identified. This review begins with a description of the precipitation that occurs within the region of open, polar-cap magnetic field lines. Precipitation of polar rain, cusp/mantle, and energetic solar particles is described as a result of the direct entry into the magnetosphere of particles that cross the magnetopause along open field lines. An extended region of soft electron precipitation is also often observed poleward of the plasma sheet; however the extent to which this region is within the region of open polar-cap field lines has not yet been definitively ascertained. Next the precipitation of plasma sheet particles by current sheet scattering is considered. It is shown that current sheet scattering can account for the ion precipitation that occurs throughout most of the plasma sheet along field lines that cross the equatorial plane on the nightside. Such scattering also accounts for electron precipitation that occurs in a narrow region adjacent to the poleward boundary of the plasma sheet. However, electron precipitation, as well as ion precipitation, occurs throughout most of the plasma sheet. The electron precipitation away from the poleward boundary of the plasma sheet appears to be predominantly the result of scattering by wave-particle interactions; however the responsible distribution of waves has yet to be identified. Finally, the precipitation of energetic radiation belt electrons and ions by Coulomb collisions, charge exchange, and wave particle interactions is briefly addressed.

1. Introduction

Precipitation of magnetospheric particles to the upper atmosphere occurs in a variety of regions and via a variety of processes. Magnetosheath particles have access to the magnetosphere by flowing along magnetic field lines that cross the magnetopause, and those within the loss cone precipitate in the polar-cap region of open magnetic field lines. Particles trapped on closed field lines precipitate via processes that cause violation of the first adiabatic invariant and move particles into the loss cone. The primary causes of such scattering are non-guiding center motion in weak magnetic-field regions, scattering by plasma waves, and field-aligned acceleration by parallel (to the magnetic field) electric fields. Each of the above processes is included in this review.

Space Science Reviews **80**: 109–132, 1997.

Discussion starts with precipitation that occurs within the polar caps. Plasma sheet particles (~100 eV to ~30 keV) are treated next. These particles are predominantly on drift trajectories that move inward on the night side, divert around the Earth, and then cross the dayside magnetopause. Finally the loss of more energetic ($\gtrsim$ 30 keV) radiation belt particles is addressed. Such particles have a much higher magnetic drift speed than do the lower energy plasma sheet particles and are thus predominantly confined to the magnetosphere along drift trajectories that encircle the Earth without crossing the magnetopause.

2. Polar-Cap Precipitation

Particle data from the polar-orbiting DMSP spacecraft are shown in Figure 1 and are used to illustrate precipitation phenomena that are common over the polar cap. Figure 1 shows black and white versions of particle spectrograms for three DMSP traversals of one of the polar caps; original color spectrograms for these and other orbits can be found in Lyons et al. (1996). For each orbit, precipitating electron (top panels) and ion (bottom panels) fluxes are shown versus particle energy (50 eV - 20 keV) and UT.

The high-energy tail of the solar wind electron distribution has access to the entire region of open polar-cap field lines, as can be seen in the top example of Figure 1. In this example, the polar-cap is the region between ~10600 s and 11160 s UT that has a relatively uniform flux of precipitating electrons at energies below a few hundred eV and no detectable ion fluxes. The regions equatorward of the polar caps consist of precipitation of plasma sheet particles. The plasma sheet particles have broad energy spectra with measurable fluxes extending up to several keV for electrons and to the upper limit (20 keV) of the ion detector. The plasma sheet cuts off quite sharply at its boundary with polar rain. This boundary is generally accepted to be very close to the magnetic separatrix (the boundary between open and closed magnetic field lines).

Uniform electron precipitation is nearly always observed within the polar caps when not obscured by other precipitation, and is known as polar rain (Winningham and Heikkila, 1974; Fennell et al., 1975). Because more interplanetary electrons flow along field lines in the direction away from the sun than in the direction towards the sun, polar rain is more intense over the polar cap that connects to interplanetary field lines that come from the solar direction than over the polar cap that connects to field lines that come from the anti-solar direction. During the time of the examples in Figure 1 the interplanetary magnetic field (IMF) had a positive x-component, so that the polar rain was more intense in the southern hemisphere than the northern hemisphere.

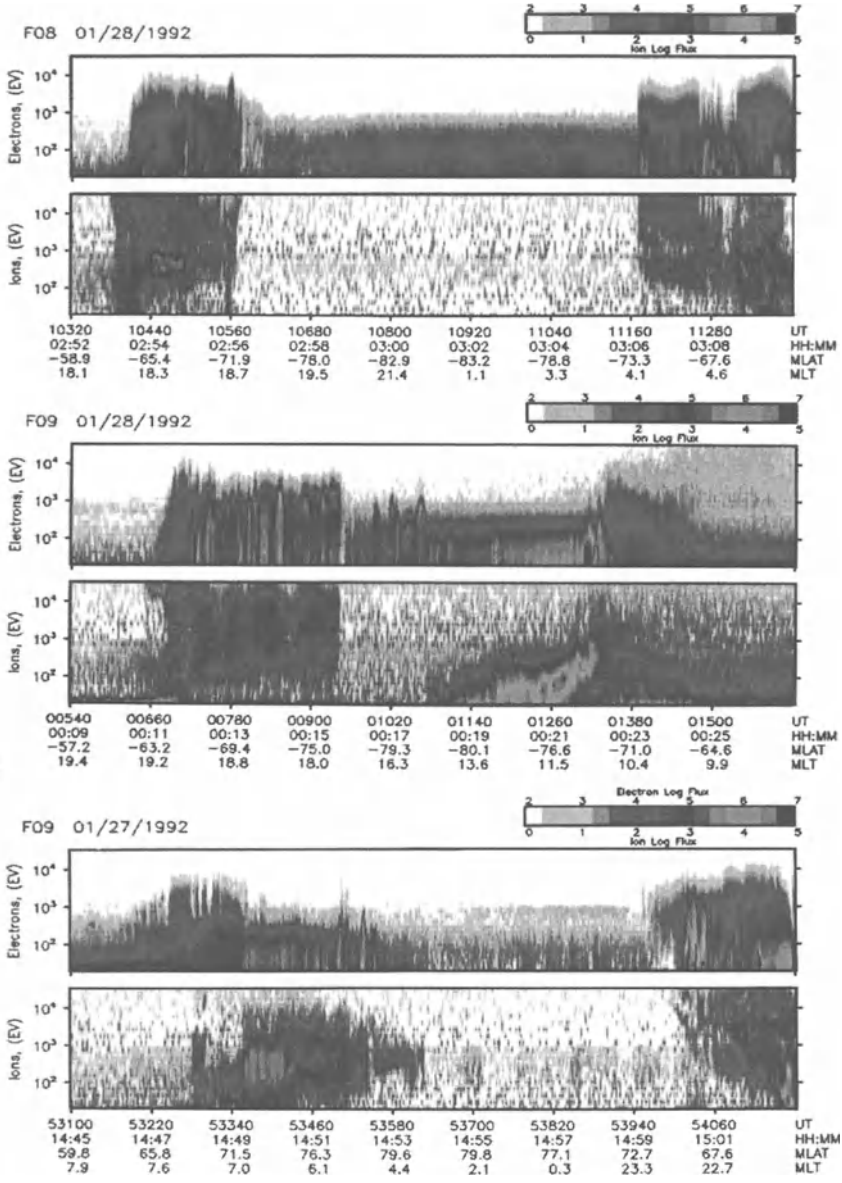

Figure 1. Precipitating particle fluxes versus energy and UT from three polar-cap traversal of the low-altitude, polar-orbiting DMSP spacecraft. These are black and white versions of color spectrograms that can be found in Lyons et al. (1996).

Energetic interplanetary particles generally have fluxes that are too low to be detected with most satellite instrumentation. However solar activity can lead to vastly increased fluxes of > 100 keV particles (during what are called "solar particle events") that can be detected over the polar caps (see, for example: Reid and Leinbach, 1959; Hultqvist, 1979; Reid and Sauer, 1967; West and Vampola, 1971; Van Allen et al., 1971), detectable solar proton events being much more common than detectable solar electron events.

Solar wind plasma is strongly heated when it crosses the portion of the bow shock in front of the magnetosphere. This leads to heated magnetosheath plasma which has access to the polar caps in the vicinity of 1200 MLT. This heated plasma can be seen in the middle example of Figure 1. In this example, the polar cap extends from ~0940 s to ~1320 s UT. Within the dayside portion of the polar cap, enhanced fluxes of electrons and ions from the magnetosheath can be seen. The enhanced electron fluxes occur at energies below ~100 eV. The enhanced ion fluxes extend to above 1 keV near the separatrix, and they show an energy dispersion with increasing magnetic latitude that is characteristic of this region (Reiff et al., 1977).

The energy dispersion is a time-of-flight effect resulting from electric field drift, which is generally in the anti-sunward direction near noon. At an ionospheric distance $R_E \Delta\Lambda$ away from the separatrix, particles can only precipitate if they have a parallel (to the magnetic field) velocity $v_{||}$ greater than a minimum value $v_{||,min}$ given by

$$v_{||,\,min} = \left(\frac{h}{R_E \Delta\Lambda}\right) V_E$$

Here R_E is an Earth radius, $\Delta\Lambda$ is the difference in magnetic latitude between a point in the ionosphere and the separatrix, and V_E is the component of the ionospheric electric-field-drift speed in the direction normal to the separatrix. This gives a minimum energy for ions that can reach the ionosphere that is proportional to $(\Delta\Lambda)^{-2}$ and accounts for the lower energy cutoff to the ion precipitation. The equatorward portion of this region of dispersed ion precipitation is referred to as the cusp, since most of the observed ions come from the vicinity of one of the dayside minima in magnetospheric magnetic field known as the cusps. The poleward portion of the region is referred to as the mantle, since most of the observed ions come from magnetosheath particles that form a magnetospheric mantle poleward of the cusps. However, the two regions are in actuality one continuous region. The decrease in magnetosheath particle energy with distance away from the nose of the magnetosphere leads to the decrease in the upper limit of observable cusp/mantle ion fluxes with increasing magnetic latitude.

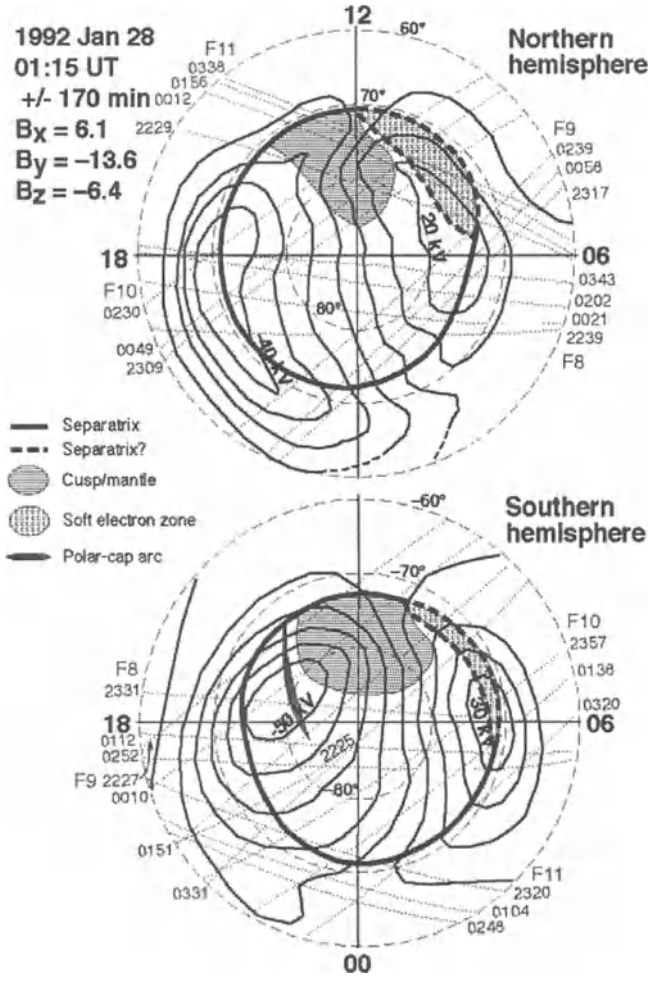

Figure 2. Polar maps of magnetic local time versus magnetic latitude for the northern and southern hemispheres for the time interval 01:15 UT +/- 170 min on 28 January. Light dashed lines give the trajectories of all the DMSP passes within the interval, each trajectory identified by the DMSP satellite number and the UT at which it moved poleward across 60° latitude. DMSP F10 was within the southern polar cap at the beginning of this time interval (2225 UT), so that its location at 2225 UT is indicated. Particle precipitation regions and the magnetic separatrix, based on the DMSP particle data , are identified in the figure. Solid curves give equipotential contours at 10 kV intervals obtained from the procedure of Richmond et al. (1992) for this interval. B_X, B_Y, and B_Z are the IMF components at the center of the time interval.

Figure 2 shows maps of both polar caps during an approximately 6 hr period of relatively stable IMF (from Lyons et al., 1996), and the spatial extent of the region near noon where cusp/mantle ions were detected is indicated. These maps were obtained during a unique period when four DMSP spacecraft were

operating, and particle data was used from each satellite pass (indicated by light-dashed lines) over each polar cap during the stable IMF interval. The top and middle examples in Figure 1 are two of these passes. The heavy solid curve in Figure 2 gives the location of the separatrix determined from the observed boundaries between the plasma sheet and either polar rain or the cusp. For this case the open field line region was approximately circular and centered near the magnetic pole. Ionospheric electric equipotentials are also shown in Figure 2. These have been obtained by a fitting procedure (Richmond, 1992) that uses the electric fields observed on the DMSP spacecraft and by ground-based radars and those inferred from ground-based magnetometers.

Two additional precipitation features are identified within the polar caps in Figure 2, a region of polar-cap arcs in the southern hemisphere and regions in the pre-noon sector identified as "soft-electron zone" (SEZ). Auroral arcs are relatively narrow precipitation features consisting of electrons that are accelerated towards the ionosphere by upward-directed, magnetic field-aligned electric fields lying above the ionosphere. The region of narrow arcs identified within the southern hemisphere polar cap in Figure 2 can be seen in the middle example of Figure 1 near 1020s UT, observable electron precipitation extending up to ~1 keV. Auroral arcs occur where ionospheric electric fields cause a convergence of horizontal ionospheric currents that is too large to be carried out of the ionosphere by upward going ionospheric ions and magnetospheric electrons within the loss cone. The parallel electric field increases the flux of magnetospheric electrons within the loss cone, thereby increasing the outward current carried by the electrons as they precipitate into the atmosphere. A review of this process for the formation of stable auroral arcs is given by Lyons (1992).

The SEZ precipitation (Burch, 1968; Eather, 1969; Eather and Mende, 1972; Hardy et al., 1982; Feldstein and Galperin, 1985; Galperin and Feldstein, 1991) lies between the plasma sheet and the region of polar rain, and is seen in the bottom example of Figure 1 from ~53345s to ~53585s UT. It is readily identifiable by a discontinuous decrease in $\gtrsim 1$ keV plasma sheet electrons that is essentially the same as that observed at the equatorward boundary of the cusp. As described by Burch (1968, p.3585), the soft zone lies poleward of the main auroral zone, and "is nearly always evidenced by sudden spectral softening and the onset of pronounced spatial or temporal" structure. The relation between the SEZ and Newell and Meng's (1992, and references therein) well-accepted nomenclature for the identification of precipitation regions is addressed by Newell et al. (1991) and Newell and Meng (1994). There it is stated that the SEZ maps into the cusp, mantle, the low-latitude boundary layer (LLBL), and the dayside BPS. The SEZ identified here excludes the cusp and mantle, which we identify separately, but includes the LLBL and dayside BPS. The observations used to construct Figure 2 suggest that, with the cusp and mantle excluded, the SEZ is a continuous region lying between the plasma

sheet and the polar rain (Lyons et al., 1996). Thus, it appears to not be appropriate to separate the SEZ into LLBL and BPS portions. The SEZ can appear at both afternoon and morning local times and can extend onto the nightside (Nishida et al., 1993; Nishida and Mukai, 1994; Lyons et al., 1996).

Rich et al. (1990) analyzed distributions of precipitating ions within the SEZ during a period of positive IMF B_Z. They found the ion fluxes to be highly peaked as a function of energy and to be well represented by flowing (~200-600 km/s) Maxwellians with thermal energies of ~30-400 eV. (A high energy tail was also observed at energies well above that of the peak). Such energy spectra are very much like those observed in the magnetosheath (e.g., Rosenbauer et al., 1975), though the magnetosheath ion densities are much higher. This is consistent with a magnetosheath origin for the ions but inconsistent with a plasma sheet origin (Rich et al., 1990). These relatively cool, magnetosheath-like ion spectra, having fluxes peaked at a several hundred eV can be seen throughout the SEZ in the bottom example of Figure 1. It is clear that these SEZ ion distributions are very much different from the plasma sheet ion distributions in the examples of Figure 1, the plasma sheet particles having a much broader energy spectrum. This suggests that magnetosheath ions, and not plasma sheet ions, reach the ionosphere along SEZ magnetic field lines, which may be possible if the field lines are open. At this time, it has not been definitively determined whether or not the SEZ is entirely on open field lines, so that the separatrix is shown as possibly lying on either side of the SEZ in Figure 2. The identification of the SEZ as a continuous region as suggested here, a determination of the spatial extent of the SEZ versus the IMF and geomagnetic activity, and a determination of the extent to which the SEZ is located on open or closed magnetic field lines are important problems that require further study.

3. Plasma-Sheet Precipitation

Particles may enter the plasma sheet from the mantle, the low-latitude boundary layer, and the ionosphere. As of the present time, the relative combination of these different plasma sheet sources has not been adequately determined. All particles which enter the distant tail plasma sheet from any of these sources will interact with the tail current sheet as illustrated by the calculated magnetotail particle trajectories shown in Figure 3 (from Ashour-Abdalla et al., 1993). Figure 3 shows trajectories of sample particles from the mantle as they move along field lines and electric field drift toward the distant current sheet. The particles follow guiding center trajectories until they reach the current sheet. Within the current sheet, their motion violates the guiding center approximation leading to particle scattering in pitch angle and/or particle

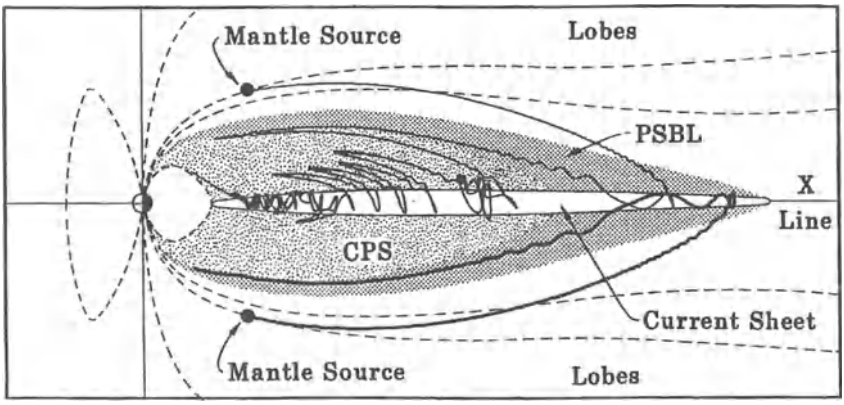

Figure 3. Calculated trajectories of sample mantle particles showing their interactions with the tail current sheet and their earthward drift (from Ashour-Abdalla et al., 1993).

energization. After leaving the current sheet, particles again follow guiding center trajectories until they return to the current sheet after mirroring. Electric field drift causes each successive encounter with the current sheet to be closer to the Earth than the previous encounter.

The magnetic field **B** in the lobes of the distant tail is primarily tangential to the current sheet. There is also a weak normal component of magnetic field B_n that crosses the current sheet and gives the closed topology of the magnetic field. The motion of particles in such a current sheet with a weak normal component of **B** was first evaluated by Speiser (1965). This motion is illustrated in Figure 4 (from Lyons, 1984), and is often referred to as "Speiser motion". The direction of particle motion along the trajectory in Figure 4 is appropriate for electrons; the direction is reversed for ions. Once particles enter the current sheet, their motion can be divided into two components: an oscillation about the plane of the current sheet with frequency ω that is due to the reversal of B_x across the current sheet, and a gyration about $\mathbf{B}_n$ with frequency Ω. Particles are ejected from the current sheet after executing onehalf a gyro-orbit about $\mathbf{B}_n$. Thus particles undergoing Speiser motion in a current sheet move one gyro-diameter in the direction of the current, which leads to particle energization within the current sheet if there is an electric field parallel to the current.

The character of the particle motion within the current sheet depends upon the ratio of the two oscillation frequencies (Lyons, 1984), or equivalently the ratio κ^2 (Sergeev et al., 1983) of the minimum radius of curvature of field lines to the maximum particle gyroradius. The ratio is given by (Büchner and Zelenyi, 1989)

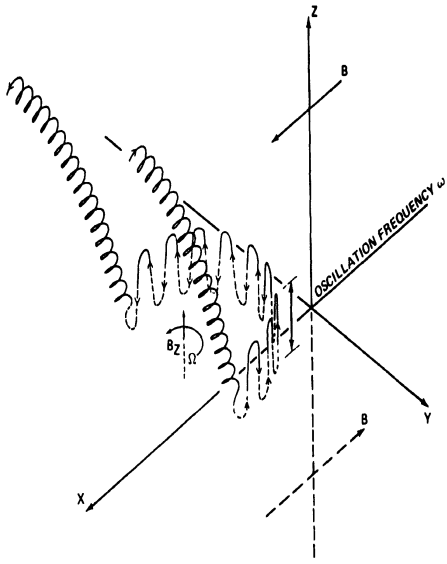

Figure 4. Illustration of Speiser motion in a current sheet with a weak normal magnetic field B_Z across the sheet and no electric fields. Directions are appropriate for negatively charged particles (from Lyons, 1984)

$$\kappa^2 = \frac{qLB_n^2}{mvB_{lobe}} = \left(\frac{\Omega}{\omega}\right)^2 \tag{1}$$

where q is the magnitude of the particle charge, v is particle velocity, B_{lobe} is the magnetic field strength in the lobes above and below the current sheet, and L is the scale length for changes in the tangential component of **B** as it reverses in direction across the current sheet. Particle motion for $\kappa^2 \gg 1$ satisfies the guiding center approximation within a current sheet, whereas particles having $\kappa^2 \ll 1$ undergo Speiser motion. Pitch-angle scattering does not occur for either of these cases. Particles with intermediary κ^2 values undergo motion that is far more chaotic, and such particles undergo significant pitch-angle scattering during their interaction with current sheet. From (1), the value of κ^2 for electrons and protons in the tail can be written as

$$\kappa^2 = \left(\frac{K_o}{K}\right)^{1/2}\left(\frac{B_n}{1nT}\right)^2\left(\frac{L}{1000\,km}\right)\left(\frac{20nT}{B_{lobe}}\right) \tag{2}$$

Table I
Range of energies for which strong pitch-angle scattering is expected for different regions of the nightside magnetosphere.

Region	Electrons	Protons
Distant tail (B_n ~ 1 nT, B_{lobe} ~ 10 nT, L ~ 10^3 km)	.014 - 90 keV	.008 eV - 50 eV
Mid-tail (B_n ~ 5 nT, B_{lobe} ~ 20 nT, L ~ 5 x 10^3 km)	.054 - 350 MeV	.030 - 190 keV
Near-tail (B_n ~ 30 nT, B_{lobe} ~ 60 nT, L ~ 10^4 km)	31 - 2 x 10^5 MeV	.017 - 110 MeV
Synchronous orbit (quiet times) (based on Sergeev et al. 1983)		~.15 - 960 MeV

where K is particle energy, K_0 is 0.12 eV for protons and 220 eV for electrons and B_n, B_{lobe}, and L have been normalized to nominal tail values.

Strong pitch-angle scattering, which fills the loss cones, has been found to occur for κ^2 values between ~0.1 (Lyons, 1984) and 8 (Sergeev et al., 1983). Since $K \propto \kappa^{-4}$, strong pitch angle diffusion for each particle species occurs over nearly a four order-of-magnitude range of energies at any given location within a current sheet. The range of particle energies for which strong pitch-angle scattering would be expected for various regions of the nighttime magnetosphere is given in Table I. Parameters that have been used to obtain these estimates are given in the table for each of the regions.

Electrons entering the distant tail plasma sheet from the mantle or low-latitude boundary layer typically have energies of the order of 100 eV and an observable high-energy tail that extends up to ~100 keV. From Table 1, it can be seen that these electrons would be expected to undergo strong pitch angle scattering within the tail current sheet, and to thus precipitate with isotropic pitch-angle distributions. This accounts for (West et al., 1978; Lyons, 1984) the isotropic precipitation of electrons observed (O'Brien, 1964; Fritz, 1968, 1970; Lyons and Evans, 1984) at the high-altitude boundary of the plasma sheet.

Ions entering the distant tail have a mean energy of several hundred eV, and thus undergo Speiser motion in the current sheet. These ions are significantly energized in the tail current sheet, leading to beams of energized ions that form a layer along the outer boundary of the plasma sheet (Lyons and Speiser, 1982). The energization is proportional to B_n^{-1}, and particles ejected from the current

sheet are energized primarily in the direction parallel to **B** (Speiser, 1965; Cowley, 1980). This leads to the isotropic precipitation of energized ions along the outer boundary of the plasma sheet (Lyons and Evans, 1984). Because of the decrease of B_n with increasing radial distance in the distant tail and the velocity dispersion that results from equatorward electric field drift, the isotropic precipitation of protons at the outer boundary of the plasma sheet shows a well-defined energy dispersion (Zelenyi et al., 1990). In Figure 1, this proton precipitation can be seen in narrow regions at the outer edge of the duskside plasma sheet in the upper example (at ~02:56 UT) and at the outer edge of the near-midnight plasma sheet in the lower example (at ~15:00 UT). The energy of the precipitating protons is ~10-20 keV at its poleward-most boundary and the energy of peak precipitating fluxes decreases to ~1 keV within ~1° of latitude. Electric field drift displaces ~10-20 keV ions up to ~1-2° equatorward of the poleward boundary of plasma sheet electron precipitation (Sergeev and Bösinger, 1993), and the poleward boundary of the energy-dispersed plasma-sheet ions in Figure 1 can be seen to be displaced ~1° equatorward of the poleward boundary of observable plasma sheet electron precipitation. In the ~1° wide region poleward of the observable ion precipitation, fluxes of precipitating plasma-sheet electrons are reduced from that seen at lower latitudes by a downward directed ambipolar electric field that acts to maintain charge neutrality along the outer boundary of the plasma sheet.

The particle energy corresponding to a given value of κ varies as $B_n^{-4} \cdot B_n$ increases with decreasing radial distance in the tail, so that the range of energies subject to strong scattering within the current sheet increases strongly with decreasing radial distance in the tail. The increase is far larger than the increase in particle energy associated with inward convection. Thus, except at the outer boundary of the plasma sheet, electrons undergo guiding center motion throughout the plasma sheet, and no precipitation is expected from interactions with the current sheet. Plasma sheet protons, on the other hand, are subject to strong pitch-angle scattering throughout almost all of the tail plasma sheet. As indicated in Table 1, the strong scattering cuts off somewhat beyond synchronous orbit during quiet times; however it may extend inward to the vicinity of synchronous orbit during the periods of enhanced convection that bring plasma sheet plasma to the vicinity of synchronous orbit. Thus isotropic proton precipitation is expected from throughout almost the entire nightside plasma sheet.

The difference in the latitude extent of strong proton and electron scattering shows clearly in observations of energetic particle precipitation on low-altitude satellites. Figure 5 shows a typical example of such observations (Lyons and Evans, 1984) from the NOAA-6 satellite. The observations of energetic ions (middle panel) and energetic electrons (bottom panel) are from detectors measuring precipitating particles (0°) and detectors measuring trapped particles (90°). Pitch-angle isotropy gives equal counts in the two electron detectors,

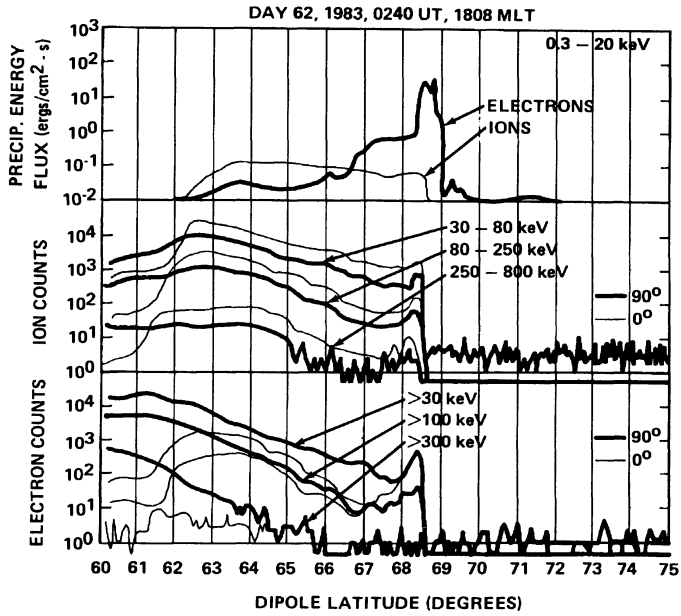

Figure 5. Example of NOAA 6 particle observations over the auroral zone at 850 km. Each panel shows smooth curves drawn through the data points space ~0.1° apart. Upper panels show the total precipitating electron energy fluxes from 0.3 to 20 keV. Middle and lower panels show energetic electron and ion count rates at 0° and 90° to the vertical. Pitch-angle isotropy gives equal energetic electron counts in the two directions, whereas energetic proton isotropy gives about a factor of two higher counts at 0° than at 90° (from Lyons and Evans, 1984).

whereas proton isotropy gives counts in the 0° that are about a factor of two higher than in the 90° detector. Isotropy of the energetic ions is clearly indicated by the extended regions where counts in the two detectors maintain a constant ratio. In Figure 5 energetic electron isotropy can be seen in a narrow region at the poleward boundary of observable fluxes. Energetic ion isotropy, on the other hand, extends over a much broader region. Additionally, isotropy can be seen to extend to lower latitudes with increasing particle energy for both electrons and ions. This is just what is expected from scattering in the tail current sheet, since the lowest energy subject to scattering increases with decreasing radial distance as a result of the equatorial variation in B_n.

At times, highly structured bursts of isotropic energetic (>0.15 - 1 MeV) electron precipitation can extend a significant distance equatorward of the isotropic electron precipitation region that lies at the poleward boundary of observable fluxes (Blake et al., 1996). It is interesting to consider the possibility that these bursts may be due to current sheet scattering. Because the particle energy for a given value of κ varies as B_n^{-1}, the minimum particle energy for significant pitch angle scattering in a current sheet varies as B_n^{-1}. Thus factor of ~2-3 variations in B_n will give factors of 10-100 variation in the

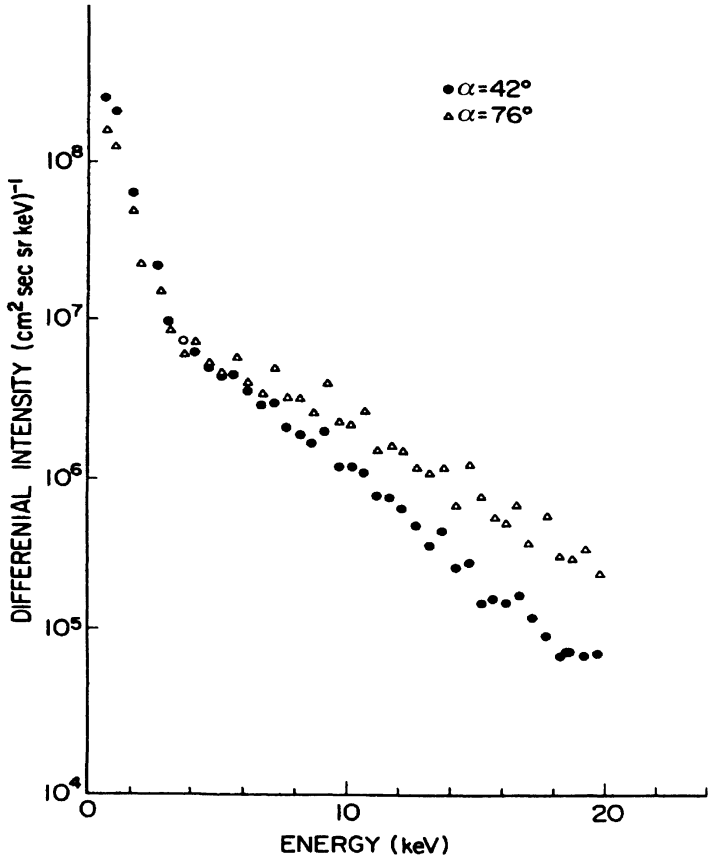

Figure 6. Electron differential flux versus energy measured at two pitch angles a within diffuse aurora (from Whalen and McDiarmid, 1973).

minimum particle energy for pitch angle scattering. Based on the nominal values in Table 1, such variation in B_n could easily cause the minimum energy for strong scattering in the mid-to-far tail to vary from being within the ~0.1 - 1 MeV range to being well above that energy range. Thus it is plausible the bursts of energetic electron precipitation are caused by current-sheet scattering. Such an explanation would require, however, that B_n in the tail have considerable short-time-scale variations. Since the bursts can have time scales <1 s, it would be necessary for B_n to occasionally vary with time scales < 1 s.

Total energy fluxes of precipitating electrons and ions over the energy range 0.3-20 keV, which covers the bulk of the plasma sheet particle distributions, are shown in the top panel of Figure 5. Enhanced precipitating ion energy fluxes extend over a broad latitude range, but cut off further poleward than do the fluxes of precipitating energetic ions. This is as expected from scattering in the tail current sheet. However, enhanced electron precipitation is also observed in the 0.3-20 keV energy range. The precipitation is observed over nearly the

same latitude range as for the ions and extends well equatorward of the region of energetic electron precipitation. Except in its poleward portion, this electron precipitation is at energies far too low for scattering in the current sheet.

The portion of the electron precipitation region with high ($\gtrsim 1$ erg/cm^2-s) precipitating energy fluxes is due to auroral arcs. Auroral arc precipitation is generally quite structured, and arcs are far more common within the plasma sheet than within the polar caps. Narrow arcs can be seen within the plasma sheet regions of Figure 1. As within the polar caps, the arcs are associated with upward-directed, magnetic field-aligned electric fields that accelerate electrons so as to maintain current continuity in the ionosphere.

The remainder of the 0.3-20 keV electron precipitation in Figure 5 leads to what is referred to as the "diffuse aurora". Diffuse auroral electron precipitation generally is isotropic at lower energies. At higher energies, the precipitation becomes anisotropic, the anisotropy increasing with increasing electron energy. An example of the energy spectra of precipitating electrons observed at two pitch angles within the loss cone on a rocket within diffuse aurora is shown in Figure 6. In this example, the transition to anisotropic distributions is at ~ 5 keV, which is typical transition energy for the diffuse aurora. This type of variation of pitch-angle distribution with energy is characteristic of pitch angle scattering by wave-particle interactions, so that the diffuse aurora has generally been attributed to such pitch-angle scattering.

Kennel et al. (1970) proposed that electrostatic waves observed on auroral field lines at ~3/2 the electron gyrofrequency (referred to as "electrostatic 3/2" waves) could resonate with plasma sheet electrons and be responsible for diffuse auroral electron precipitation. Lyons (1974) evaluated the pitch-angle scattering rates for the electrons as a function of electron energy using wave amplitudes observed (Kennel et al., 1970; Scarf et al., 1973) on the OGO 5 satellite. These calculations showed that the pitch angle-energy dependence of diffuse auroral electron precipitation could be quantitatively explained by resonant interactions with these waves, and it became generally accepted that the waves are indeed responsible for the diffuse aurora.

However ensuing observations with more sophisticated instrumentation (Belmont et al., 1983; Roeder and Koons, 1989) showed wave amplitudes to be very much less than those reported from OGO 5 and far too low to account for the diffuse aurora. This implied that the OGO 5 instrumentation had lead to a significant over-estimate of electrostatic 3/2 wave amplitudes, and that the cause of the electron scattering responsible for the diffuse aurora had yet to be determined. The cause of this scattering has still not been determined, leaving the cause of the diffuse aurora as a major unsolved problem in magnetospheric physics.

Another unanswered question concerns the cause of auroral ion precipitation on magnetic field lines that cross the equator on the dayside. Ion precipitation from the plasma sheet occurs on the dayside, and can be seen to extend ~10° in

latitude equatorward of the cusp/mantle precipitation in the middle example of Figure 1. Field lines on the dayside are not distorted as they are on the nightside by the cross-tail current, so that current-sheet scattering cannot account for dayside ion precipitation. Some of this precipitation can be explained by violation of the guiding center approximation near the high-latitude minima in B associated with the magnetospheric cusps (Lyons et al., 1994), but this can only account for a small portion of the precipitation near the equatorward edge of the cusp particle precipitation. The cause of the majority of the dayside ion precipitation is yet to be determined.

In addition, the temporal and spatial dependencies of dayside ion precipitation apparently have not been determined. Thus the morphology of the dayside ion precipitation warrants further study. At times, ion precipitation is not seen on the dayside. For example, no ion (or electron) precipitation is observed in the region equatorward of the cusp in Plates 1 and 5 of Newell and Meng (1988). Hultqvist et al. (1981) noted decreases in ion fluxes on the day side during the early stages of geomagnetic disturbances, and they suggested that the decrease may result from convection away from that region by enhanced convection electric fields. It would be interesting to determine when and where there is no observable precipitation.

4. Energetic Radiation Belt Particles

The isotropic precipitation of energetic particles from the outer portions of the radiation belts via pitch-angle scattering in weak magnetic field regions was included in the previous section. This section briefly summarizes what is known about the anisotropic precipitation due to weak pitch-angle scattering throughout the region of closed particle drift trajectories within, and in the vicinity of, the plasmapause. Additional details can be found in Chapter 5 of Lyons and Williams (1984) and references therein and in references below.

During quiet times, energetic electrons maintain a stable two zone structure. The solid lines in Figure 7 show equatorial electron fluxes at four energies measured from L = 1.6 to L = 5.2 during an extended quiet period with stable fluxes. At the higher energies, a deep flux minimum separates the inner and outer zones of electrons. This minimum, which decreases in relative depth with decreasing electron energy, is referred to as the electron slot. The stability of quiet-time radiation belt fluxes implies that a balance is maintained between electron sources and losses during quiet times.

Lyons and Thorne (1973) showed that the stable structure of radiation belt electrons during quiet times could be explained by a balance between known source and loss processes. Throughout the slot region and outer zones, losses were attributed to resonant interaction with a band of whistler-mode waves, known as plasmaspheric hiss, that is observed throughout the plasmasphere

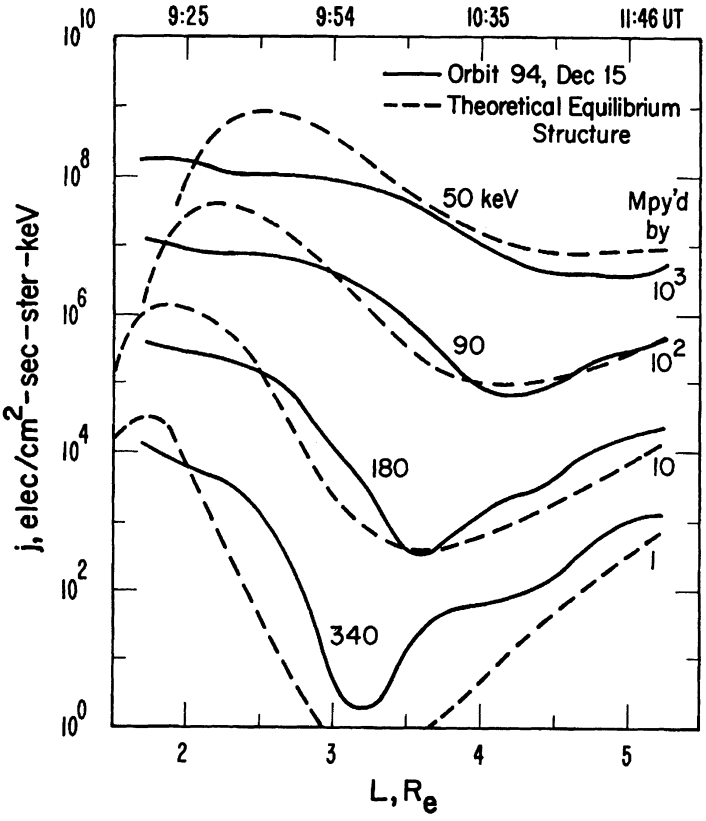

Figure 7. Comparison between quiet time radial profiles of radiation belt electrons observed very near the equator in the direction normal to the geomagnetic field by the Explorer 45 satellite on December 15, 1971 (solid lines) and the theoretical equilibrium profiles(dashed lines) of Lyons and Thorne (1973). The theoretical profiles are for the energies indicated in the figure, which are the geometric mean energies of the four Explorer 45 energy channels. The 180-, 90-, and 50-keV fluxes have been multiplied by 10^1, 10^2, and 10^3, respectively (from Lyons and Williams, 1975a).

(e.g., Thorne et al., 1973). The minimum electron energy for resonant interaction with the hiss increases with decreasing L, so that such interactions do not occur within the inner zone. Within the inner zone, losses occur via the generally much slower process of Coulomb collisions. Resonant interactions extend to decreasing L with increasing electron energy, so that the outward extension of the inner zone decreases with increasing electron energy.

Since radiation belt electrons are on closed drift trajectories during quiet times, direct injection from high L to the region of the radiation belts shown in Figure 7 does not occur during quiet times. However, fluctuations of the convection electric field cause drifting electrons to be slowly scattered in drift shell leading to an inward diffusion of particles from the outer zone. This

process is known as radial diffusion (see Schulz and Lanzerotti, 1974). If it is assumed that outer zone fluxes (beyond the plasmapause) are maintained by convection at relatively steady, time-averaged values, then it is possible to balance the radial diffusion source with losses from Coulomb collisions and resonant interaction with plasmaspheric hiss. The balance was calculated as a function of electron energy and L by Lyons and Thorne (1973), leading to a quantitative explanation of the two-zone structure. The results of their calculation are shown by the dashed line in Figure 7, which can be seen to reproduce the overall observed two-zone structure of radiation belt electrons. Such a balance between source and losses implies that there is a steady precipitation of electrons from the $L \lesssim 5.2$ region of the radiation belt during quiet times. Given the equatorial electron fluxes as a function of L and energy, electron precipitation fluxes can be calculated using the electron lifetimes of Lyons and Thorne.

During geomagnetic storms, enhanced fluxes of electrons result from a direct injection of electrons deep into the radiation belts. Observations of such an injection are shown in Figure 8. In this figure, the solid line gives observed fluxes of equatorially mirroring energetic electrons versus L following a storm injection. The upper left panel gives the fluxes observed less than one day after the storm injection. The large change in fluxes due to the storm can be seen by comparing the stormtime fluxes with the quiet-time fluxes in Figure 7, which are shown by the dashed lines in Figure 8. Subsequent panels give the fluxes observed approximately once every other day until eleven days after the storm. These profiles show that radiation belt electron fluxes gradually recovered to their pre-storm equilibrium structure over a period of about 10 days. Assuming electron lifetimes during the recovery period following storms are similar to their quiet-time values, precipitation fluxes following a storm should be enhanced by approximately the ratio of the fluxes at any particular time to those during quiet times. This should give significant enhancements in precipitation fluxes at L-values and energies of large stormtime flux enhancements. Such post-storm loss of energetic electrons can affect the mid-latitude ionosphere and is believed to be an important mid-latitude source of D-region ionization (Spjeldvik and Thorne, 1975).

Radiation belt ions also achieve a balance between sources and losses during quiet periods and have significant injections during geomagnetic storms. Weak precipitation occurs during quiet times, and this precipitation is enhanced following stormtime injections. Injection of particles in the ~20-200 keV energy range constitutes the geomagnetic storm ring current. The magnetic effects of this ring current, as measured on the ground at mid-latitudes, is used to identify storms.

Evaluating the equilibrium structure of ions is far more complex than for electrons for several reasons. First, collisions between energetic ions and cold neutral hydrogen of the geocorona lead to a charge exchange interaction.

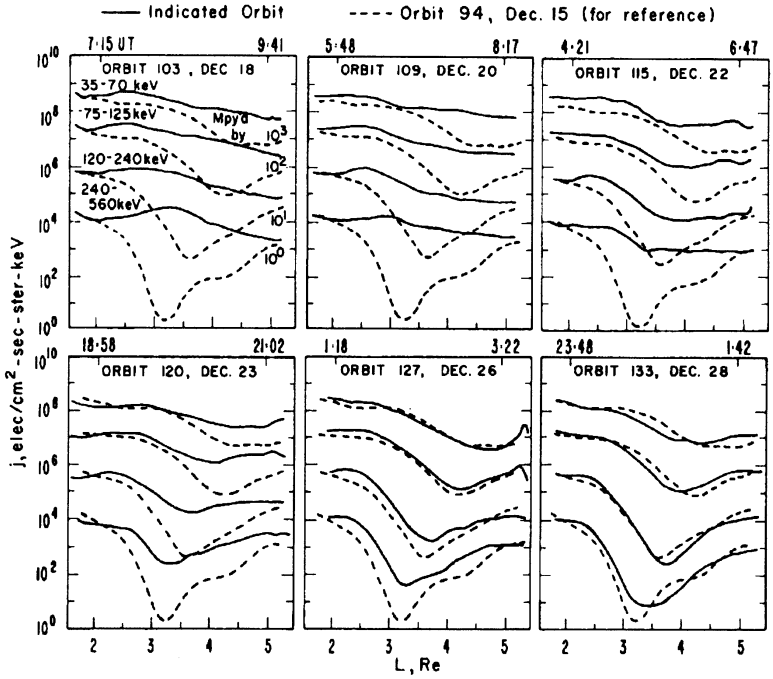

Figure 8. Observed radial profiles of the flux of equatorially mirroring electrons observed on Explorer 45 for the period following a moderate geomagnetic storm on December, 17, 1971. Solid curves give the profiles approximately every other day from the outbound portion of the orbit indicated in each panel, and the dashed curves give the prestorm, quiet-time profiles from Figure 7 (from Lyons and Williams, 1975b).

For singly charged ions, the charge exchange leads to an energetic neutral and a cold proton. The addition of cold protons in this way is of little consequence to the cold plasma population. However, the energetic neutrals are no longer confined by the geomagnetic field and rapidly leave the radiation belt. A significant number of these neutrals strike the atmosphere at low- and mid-latitudes (Levasseur and Blamont, 1973). This is an important source of low-altitude E-region ionization (Lyons and Richmond, 1978). Also re-ionization of the energetic neutrals as they approach the atmosphere causes a significant population of energetic ions (~10 keV to 1.5 MeV) at low altitudes (~400 km) near the equator (Moritz, 1972; Hovestadt et al., 1972; Mizera and Blake, 1973). In addition to ion loss, charge exchange causes a mixing of ions of different charge states, which is important for Helium and Oxygen ions in the radiation belts.

The second complexity for ion losses is that energy losses from Coulomb collisions cannot be ignored. For electrons, it is sufficient to treat Coulomb collisions as solely a loss process. However, for ions energy losses dominate pitch angle scattering leading to a mixing of particles of different energies (Nakada and Mead, 1965; Cornwall, 1972). A final complication is the effects

of wave-particle interactions. It has been known for a long time (e.g., Cornwall et al., 1970) that resonant interactions with ion-cyclotron waves can be an important loss process for radiation belt ions. However, verifiable estimates of ion loss rates due to these interactions have been difficult to obtain. This is in part due to the difficulty in measuring ion cyclotron waves and to the complexities inherent in a plasma with several important ion species. Progress is now being made on obtaining such loss rates (e.g., Jordanova et al., 1996), so that it may not be long before the effects of wave driven losses can be evaluated for ions as they have been for electrons.

Despite the above complexities, progress has been made on understanding the losses of radiation belt ions by just including charge exchange and Coulomb collisions. This has lead to reasonable understanding of the quiet time distributions of energetic radiation belt protons (Spjeldvik, 1977), helium ions (Spjeldvik and Fritz, 1978a), and oxygen ions (Spjeldvik and Fritz, 1978b). Calculations of the equilibrium structure of protons has also been extended to the lower energies representative of the ring current (Chen et al., 1994). In addition, considerable progress has been made in understanding the contributions of charge exchange and Coulomb collisions to the decay of the stormtime ring current (e.g., Fok et al., 1991, 1993, and references therein).

5. Summary

A fairly complete understanding of a number of important processes responsible for the precipitation of magnetospheric particles has now been obtained. However, a number of important questions remain. Over the polar caps, precipitation occurs directly from particles flowing into the magnetosphere from the magnetosheath. Polar rain, energetic particles during solar particle events, and cusp/mantle precipitation are clearly the result of such direct entry to the magnetosphere. Auroral arcs within the polar caps are formed by the additional electron energization that results from the parallel electric fields that are necessary to maintain current continuity in the ionosphere. The major unanswered question concerning large-scale precipitation processes with the polar caps regards the SEZ. In order to fully understand the SEZ precipitation, it will be necessary to ascertain the extent to which the SEZ is located on open or closed magnetic field lines.

Precipitation from the plasma sheet occurs via a combination of current-sheet scattering and wave-particle interactions, in addition to the electron acceleration by parallel electric fields that causes auroral arcs. Current sheet scattering appears to be the dominant cause of ion precipitation throughout the plasma sheet. For electrons, on the other hand, current sheet scattering is generally effective only within a relatively narrow region adjacent to the poleward boundary of the plasma sheet. Highly structured bursts of

precipitation of energetic electrons occur equatorward of this narrow region which may also be the result of current sheet scattering. For this explanation of the precipitation bursts to be correct, it is necessary that there be considerable short-time-scale structure in the component of magnetic field that crosses the tail current sheet.

Diffuse auroral electron precipitation at energies $\lesssim 30$ keV cannot occur as a result of current sheet scattering. The variation of pitch angle distribution with energy for this precipitation suggests that the precipitation is due to wave-particle interactions. However, a distribution of waves with sufficient power to cause the diffuse auroral electron precipitation has yet to be identified. Other unanswered questions concern the cause of plasma sheet ion precipitation along magnetic field lines that cross the equatorial plane on the dayside. Most of this precipitation cannot be explained by current sheet scattering. As of the present time, both the causes and the morphology of dayside ion precipitation needs to be determined.

The large-scale weak precipitation of radiation belt electrons from within the plasmasphere has been quantitatively explained as a result of resonant interactions with plasmaspheric hiss and Coulomb collisions. On the other hand, further study is needed to understand the dominant causes of radiation belt ion precipitation. The effects of charge exchange and Coulomb collision losses are reasonably well understood. However, the effects of ion cyclotron waves, which may well be an additional important cause of ion precipitation, have not yet been quantitatively evaluated.

Acknowledgements

I thank Bengt Hultqvist for his encouragement and hospitality during the workshops at the International Space Science Institute. This work was supported by NSF grant ATM-9401317 and NASA grant NAGW-3968 to The Aerospace Corporation, and the Aerospace Sponsored Research Program.

References

Ashour-Abdalla, M., Berchem, J. P., Büchner, J., and Zelenyi, L. M.: 1993, 'Shaping of the magnetotail from the mantle: Global and local structuring,' *J. Geophys. Res.* **98**, 5651.

Belmont, G., Fontaine, D., and Canu, P.: 1983, 'Are equatorial electron cyclotron waves responsible for diffuse auroral electron precipitation?', *J. Geophys. Res.* **88**, 9163.

Blake, J. B., Looper, M. P., Baker, D. N., Nakanura, R., Klecker, B., and Hovestadt, D.: 1996, 'New high temporal and spatial resolution measurements of the precipitation of relativistic electrons,' *Adv. Space. Res.* **18,** (8) 171.

Büchner, J. and Zelenyi, L. M.: 1989, 'Regular and chaotic charged particle motion in magnetotail-like field reversals 1. Basic theory of trapped motion,' *J. Geophys. Res.* **94**, 11,821.

Burch , J. L.: 1968, 'Low-energy electron fluxes above the auroral zone,' *J. Geophys. Res.*, **73**, 3585.

Chen, M. W., Lyons, L. R., and Schulz, M.: 1994, 'Simulation of phase space distributions of storm time proton ring current,' *J. Geophys. Res.* **99**, 5745.

Cornwall, J. M.: 1972, 'Radial diffusion of ionized helium and protons: A probe for magnetospheric dynamics,' *J. Geophys. Res.* **77**, 1756.

Cornwall, J. M., Coroniti, F. V., and Thorne, R. M.: 1970, 'Turbulent loss of ring current protons,' *J. Geophys. Res.* **75**, 4699.

Cowley, S. W. H.: 1980, 'Plasma populations in a simple open model magnetosphere,' *Space Science Reviews* **26**, 217.

Eather, R. H.: 1969, 'Latitudinal distribution of auroral and airglow emissions: The 'soft' zone,' *J. Geophys. Res.* **74**, 153.

Eather, R. H. and Mende, S. B.: 1972, in K. Folkestad, (ed.), 'High latitude particle precipitation and source regions in the magnetosphere,' *Magnetosphere-Ionosphere Interactions*, Universitetsforlaget, Oslo, pp. 139.

Feldstein, Y. I., and Galperin, Y. I.: 1985, 'The auroral luminosity structure in the high-latitude upper atmosphere: Its dynamics and relationship to the large-scale structure of the Earth's magnetosphere,' *Rev. Geophys.* **23**, 217.

Fennell, J. F., Mizera, P. F., and Croley, D. R.: 1975, 'Low energy polar cap electrons during quiet times,' *Proc. Int. Conf. Cosmic Rays* **14**, MG8-3, 1267.

Fok, M.-C., Kozyra, J. U., Nagy, A. F., and Cravens, T. E.: 1991, 'Lifetime of ring current particles due to Coulomb collisions in the plasmasphere,' *J. Geophys. Res.* **96**, 7861.

Fok, M.-C., Kozyra, J. U., Nagy, A. F., Rasmussen, C. E., and Khavanov, G. C.: 1993, 'Decay of equatorial ring current ions and associated aeronomical consequences,' *J. Geophys. Res.* **98**, 19,381.

Fritz, T. A.: 1968, 'High-latitude outer-zone boundary region for > 40-keV electrons during geomagnetically quiet periods,' *J. Geophys. Res.* **73**, 7245.

Fritz, T. A.: 1970, 'Study of the high-latitude, outer-zone boundary region for > 40-keV electrons with satellite Injun 3,' *J. Geophys. Res.* **75**, 5387.

Galperin, Y. I., and Feldstein, Y. I.: 1991, in C.-I. Meng, M. J. Rycroft, and L. A. Frank, (eds.), 'Auroral luminosity and its relationship to magnetospheric plasma domains,' *Auroral Physics*, Cambridge University Press, Cambridge, pp. 207-222.

Hardy, D. A., Burke, W. J., and Gussenhoven, M. S.: 1982, 'DMSP optical and electron measurements in the vicinity of polar cap arcs,' *J. Geophys. Res.* **87**, 2413.

Hovestadt, D., Häusler, B., and Scholer, M.: 1972, 'Observations of energetic particles at very low altitude near the geomagnetic equator,' *Phys. Rev. Lett.* **28**, 134.

Hultqvist, B.: 1959, 'On the interpretation of ionization in the lower ionosphere occurring on both day and nightside of the earth within a few hours after some solar flares,' *Tellus* **11**, 332.

Hultqvist, B., Aparicio, B., Borg, H., Arnoldy, R., and Moore, T. E.: 1981, 'Decrease of keV electron and ion fluxes in the dayside magnetosphere during the early phase of magnetospheric disturbances,' *Planet. Space Sci.* **29**, 107.

Jordanova, V. K., Kozyra, J. U., and Nagy, A. F.: 1996, 'Effects of heavy ions on the quasi-linear diffusion coefficients from resonant interactions with electromagnetic ion cyclotron waves,' *J. Geophys. Res.* **101**, 19,771.

Kennel, C. F., Scarf, F. L., Fredricks, R. W., McGehee, J. H., and Coroniti, F. V.: 1970, 'VLF electric field observations in the magnetosphere,' *J. Geophys. Res.* **75**, 6136.

Levasseur, A. C. and Blamont, J. E.: 1973, 'Satellite observations of strong Balmer alpha atmospheric emissions around the magnetic equator,' *J. Geophys. Res.* **78**, 3881.

Lyons, L. R.: 1974, 'Electron diffusion driven by magnetospheric electrostatic waves,' *J. Geophys. Res.* **79**, 575.

Lyons, L. R.: 1984, 'Electron energization in the geomagnetic tail current sheet,' *J. Geophys. Res.* **89**, 5479.

Lyons, L. R.: 1992, 'Formation of auroral arcs via magnetosphere-ionosphere coupling,' *Rev. Geophys.* **30**, 93.

Lyons, L. R. and Evans, D. S.: 1984, 'An association between discrete aurora and energetic particle boundaries,' *J. Geophys. Res.* **89**, 2395.

Lyons, L. R. and Richmond, A. D.: 1978, 'Low-latitude E region ionization by energetic ring current particles,' *J. Geophys. Res.* **83**, 2201.

Lyons, L. R. and Thorne, R. M.: 1973, 'Equilibrium structure of radiation belt electrons,' *J. Geophys. Res.* **78**, 2142.

Lyons, L. R. and Speiser, T. W.: 1982, 'Evidence for current-sheet acceleration in the geomagnetic tail,' *J. Geophys. Res.* **87**, 2276.

Lyons, L. R. and Williams, D. J.: 1975a, 'The quiet time structure of energetic (35-560 keV) radiation belt electrons,' *J. Geophys. Res.* **80**, 943.

Lyons, L. R. and Williams, D. J.: 1975b, 'The storm and post-storm evolution of energetic (35-560 keV) radiation belt electrons,' *J. Geophys. Res.* **80**, 3985.

Lyons, L. R. and Williams, D. J.: 1984, *Quantitative Aspects of Magnetospheric Physics*, D. Reidel Publ. Co., Dordrecht-Holland.

Lyons, L. R., Schulz, M., Pridmore-Brown, D. C., and Roeder, J. L.: 1994, 'The low-latitude boundary layer near noon: An open-field line model,' *J. Geophys. Res.* **99**, 17,367.

Lyons, L. R., Lu, G., de la Beaujardière, O., and Rich, F. J.: 1996, 'Synoptic Maps of Polar Caps for Stable IMF Intervals during January 1992 GEM Campaign,' *J. Geophys. Res.* (in press).

Mizera, P. F. and Blake, J. B.: 1973, 'Observations of ring current protons at low altitudes,' *J. Geophys. Res.* **78**, 1058.

Moritz, J.: 1972, 'Energetic protons at low equatorial altitudes: A newly discovered radiation belt phenomena and its explanation,' *J. Geophys.* **38**, 701.

Nakada, N. P. and Mead, G. D.: 1965, 'Diffusion of protons on the outer radiation belt,' *J. Geophys. Res.* **70**, 4777.

Newell, P. T. and Meng, C.-I.: 1988, 'The cusp and the cleft/boundary layer: low-altitude identification and statistical local time variation,' *J. Geophys. Res.* **93**, 14,549.

Newell, P. T. and Meng, C.-I.: 1992, 'Mapping the dayside ionosphere to the magnetosphere according to particle precipitation characteristics,' *Geophys. Res. Lett.* **19**, 609.

Newell, P. T. and Meng, C.-I.: 1994, 'Comment on "Unexpected features of the ion precipitation in the so-called cleft/low-latitude boundary layer region: Association with sunward convection and occurrence on open field lines" by A. Nishida, T. Mukai, H. Hayakawa, A. Matsuoka, K. Tsuruda, N. Kaya, and H. Fukunishi,' *J. Geophys. Res.* **99**, 19,609.

Newell, P. T., Burke, W. J., Sanchez, E. R., Meng, C.-I., Greenspan, M. E., and Clauer, C. R.: 1991, 'The low-latitude boundary layer and the boundary plasma sheet at low-altitude: Prenoon precipitation regions and convection reversal boundaries,' *J. Geophys. Res.* **96**, 21,013.

Nishida, A. and Mukai, T.: 1994, 'Reply to Comment on "Unexpected features of the ion precipitation in the so-called cleft/low-latitude boundary layer region: Association with sunward convection and occurrence on open field lines" by A. Nishida et al.,' *J. Geophys. Res.* **99**, 23,367.

Nishida, A., Mukai, T., Hayakawa, H., Matsuoka, A., Tsuruda, K., Kaya, N., and Fukunishi, H.: 1993, 'Unexpected features of the ion precipitation in the so-called cleft/low-latitude boundary layer region: Association with sunward convection and occurrence on open field lines,' *J. Geophys. Res.* **98**, 11,161.

O'Brien, B. J.: 1964, 'High-latitude geophysical studies with Injun 3, 3, Precipitation of electrons into the atmosphere,' *J. Geophys. Res.* **69**, 13.

Reid, G. C. and Leinbach, H.: 1959, 'Low-energy cosmic-ray events associated with solar flares,' *J. Geophys. Res.* **64**, 1801.

Reid, G. C. and Sauer, H.: 1967, 'Evidence for non-uniformity of solar proton precipitation over the polar caps,' *J. Geophys. Res.* **72**, 4383.

Reiff, P. H., Hill, T. W., and Burch, J. L.: 1977, 'Solar wind plasma injection at the dayside magnetospheric cusp,' *J. Geophys. Res.* **82**, 479.

Rich, F. J., Hardy, D. A., Redus, R. H., and Gussenhoven, M. S.: 1990, 'Northward IMF and patterns of high-latitude precipitation and field-aligned currents: The February 1986 storm,' *J. Geophys. Res.* **95**, 7893.

Richmond, A. D.: 1992, 'Assimilative mapping of ionospheric electrodynamics,' *Adv. Space Res.* **6**, 59.

Roeder, J. L. and Koons, H. C.: 1989, 'A survey of electron cyclotron waves in the magnetosphere and the diffuse auroral electron precipitation,' *J. Geophys. Res.* **94**, 2529.

Rosenbauer, H., Grünwaldt, H., Montgomery, M. D., Paschmann, G., and Sckopke, N.: 1975, 'Heos 2 plasma observations in the distant polar magnetosphere: The plasma mantle,' *J. Geophys. Res.* **80**, 2723.

Scarf, F. L., Fredricks, R. W., Kennel, C. F., and Coroniti, F. V.: 1973, 'Satellite studies of magnetospheric substorms on August 15, 1968: OGO 5 plasma wave observations,' *J. Geophys. Res.* **78**, 3119.

Schulz, M. and Lanzerotti, L. J.: 1974, *Particle Diffusion in the Radiation Belts*, Springer-Verlag, New York.

Sergeev, V. A. and Bösinger, T.: 1993, 'Particle dispersion at the nightside boundary of the polar cap,' *J. Geophys. Res.* **98**, 233.

Sergeev, V. A., Sazhina, E. M., Tsyganenko, N. A., Lundblad, J. A., and Soraas, F.: 1983, 'Pitch-angle scattering of energetic protons in the magnetotail current sheet as the dominant source of their isotropic precipitation into the nightside ionosphere,' *Planet. Space Sci.* **31**, 1147.

Speiser, T. W.: 1965, 'Particle trajectories in model current sheets, 1, Analytical solutions,' *J. Geophys. Res.* **70**, 4219.

Spjeldvik, W. N.: 1977, 'Equilibrium structure of equatorially mirroring radiation belt protons,' *J. Geophys. Res.* **82**, 2801.

Spjeldvik, W. N. and Fritz, T. A.: 1978a, 'Energetic ionized helium in the quiet time radiation belts: Theory and comparison with observations,' *J. Geophys. Res.* **83**, 654.

Spjeldvik, W. N. and Fritz, T. A.: 1978b, 'Theory for charge states of energetic oxygen ions in the earth's radiation belts,' *J. Geophys. Res.* **83**, 1583.

Spjeldvik, W. N. and Thorne, R. M.: 1975, 'The cause of storm aftereffects in the middle latitude D-region,' *J. Atmos. Terr. Phys.* **37**, 777.

Thorne, R. M., Smith, E. J., Burton, R. K., and Holzer, R. E.: 1973, 'Plasmaspheric hiss,' *J. Geophys. Res.* **78**, 1581.

West, H. I., Jr., Buck, R, M,, and Kivelson, M. G.: 1978, 'On the configuration of the magnetotail near midnight during quiet and weakly disturbed periods: State of the magnetosphere,' *J. Geophys. Res.* **83**, 3805.

Van Allen, J. A., Fennell, J. F., and Ness, N. F.: 1971, 'Asymmetric access of energetic solar protons to the earth's north and south polar caps,' *J. Geophys. Res.* **76**, 4262.

West, H. I., Jr. and Vampola, A. L.: 1971, 'Simultaneous observations of solar-flare electron spectra in interplanetary space and within Earth's magnetosphere,' *Phys. Rev. Lett.* **26**, 458.

West, H. I., Jr., Buck, R. M., and Kivelson, M. G.: 1978, 'On the configuration of the magnetotail near midnight during quiet and weakly disturbed periods: State of the magnetosphere,' *J. Geophys. Res.* **83**, 3805.

Whalen, B. A. and McDiarmid, I. B.: 1973, 'Pitch angle diffusion of low-energy auroral electrons,' *J. Geophys. Res.* **78**, 1608.

Winningham, J. D. and Heikkila, W. J.: 1974, 'Polar cap electron fluxes observed with Isis 1,' *J. Geophys. Res.* **79**, 949.

Zelenyi, L. M., Kozrazhkin, R. A., and Bosqued, J. M.: 1990, 'Velocity-dispersed ion beams in the nightside auroral zone: AUREOL 3 observation,' *J. Geophys. Res.* **95**, 12,119.

Address for correspondence: L. R. Lyons, Department of Atmospheric Sciences, University of California, Los Angeles, Box 951565, Los Angeles, CA 90095-1565, USA.

OBSERVATIONS OF MAGNETOSPHERIC WAVES AND THEIR RELATION TO PRECIPITATION

H. E. J. KOSKINEN
Finnish Meteorological Institute, Helsinki, Finland.

Received January 17, 1997; Accepted in final form February 17, 1997

Abstract. Magnetospheric wave observations are discussed from the viewpoint of their potential importance for precipitation of charged particles into the auroral zones. While wave processes are a fundamental part of magnetospheric plasma physics, occurring most of the time in most of the magnetospheric regions, their direct role in and relative importance for auroral precipitation are not easy to assess. The role of the waves varies from one spatial region to another and is very different for electrons and ions. Furthermore, the distinction between wave processes and other precipitation mechanisms is not at all straightforward. This review focuses on four main topics: The problem of diffuse electron precipitation, the recent surprise on the detailed structure of broad-banded electrostatic noise in the plasma sheet boundary layer, ion precipitation through electromagnetic ion cyclotron waves, and the role of low-altitude waves in precipitation. It is concluded that, while the observational status of high-altitude ion cyclotron waves is reasonably good, in most areas more thorough studies of existing data as well as refined observations are very much needed. Successful observational studies are to be carried out jointly with theoretical work as well as with studies on the large-scale context of the often localized wave processes. This is especially important when interests are moving toward more nonlinear phenomena, such as shocks, double layers, or strong quasi-static gradients, where a strict adherence to classical wave concepts is becoming more and more diffuse and less motivated.

1. Introduction

Wave phenomena are a central factor in magnetospheric plasma physics. When plasma is perturbed, its natural reaction is to set up oscillations. These may be rapidly damped or growing, or they may propagate long distances without considerable attenuation. The excited waves transfer energy and momentum between different particle populations, modify these populations, and transfer energy and information from one location to another. The fundamental role of wave phenomena is illustrated by the fact that much of basic plasma physics is formulated in terms of response functions in the frequency-wave number space. Because the magnetosphere is a vast region of magnetized plasma, where the plasma parameters vary in a very wide range, the number of possible wave modes to be excited and to propagate is large and their detailed properties, such as frequency, wave length, phase or group velocity, and polarization, can be very different. This makes the physics of magnetospheric waves a difficult discipline, both empirically and theoretically.

Actually, a strict separation between observations and theory is not a useful approach to wave problematics. Without a solid theoretical foundation it is hopeless to try to interpret the observed signals from wave sensors in a physically meaningful way. And on the other hand, due to the practically infinite number of pos-

Space Science Reviews **80**: 133–152, 1997.

sible wave solutions, pure theory only seldom leads to a realistic description. In this review we approach the magnetospheric waves from the observational direction, acknowledging the value of the underlying theoretical understanding that has been gained from the early days of modern plasma physics, such as Alfvén's revelation of magnetohydrodynamic waves (Alfvén, 1942) or Landau's solution to the Vlasov equation (Landau, 1946). These are two well-known examples of fundamental building blocks of modern magnetospheric physics. Alfvén waves form the most important class of large-scale wave phenomena and Landau damping the key microscopic process of wave-particle interactions.

The amount of observational and theoretical literature on magnetospheric waves accumulated since the early 1960's is huge, and the time is ripe for an extensive general review of the topic. However, that clearly is beyond the scope of this review, which originated as a talk on "The observational status of magnetospheric waves that are important for precipitation" at the International Space Science Institute (ISSI) workshop on Source and Loss Processes of Magnetospheric Plasma. During preparation of the talk, it soon became clear that the proposed title was a bit too optimistic. While it is possible to give a status report of wave observations to any depth desired, it is still very unclear whether these waves are really important for precipitation, and, if important, in what sense. Thus this review is redefined as a discussion of waves that may be important for the precipitation of charged particles into the auroral ionosphere. Although this is certainly an obvious topic for wave studies, it is remarkable that it has been discussed only occasionally in literature during the last several years. The foci of modern magnetospheric plasma wave studies have been in identification of observed wave modes, in discussion of their excitation mechanisms and free-energy sources, and in determination of the propagation characteristics. These are, of course, important research topics and necessary to understand the role of the waves in the precipitation processes as well.

The question of potential importance of waves for precipitation is a complex issue. The most direct effect of waves is to pitch-angle scatter particles in the velocity space to the atmospheric loss cone or to accelerate them in the direction of the magnetic field and in that way to reduce the pitch-angles toward the loss cone (Figure 1). Instead of introducing the basic concepts of wave-particle interactions here, we refer to Chapter 5 of the monograph by Lyons and Williams (1984), which in addition to introducing the theoretical background discusses some examples that are relevant for our present purposes. However, the indirect effects of waves may finally be more important than the direct scattering processes. Waves are an essential part of magnetospheric plasma circulation. A particle precipitating into the atmosphere has most likely encountered a variety of wave fields during its recent history in the magnetosphere, being accelerated, decelerated, and pitch-angle scattered by these. Another indirect effect of waves is in large-scale reconfiguration processes of the magnetosphere, such as dayside reconnection or substorm development. Not only the wave-related microprocesses are of interest but also various

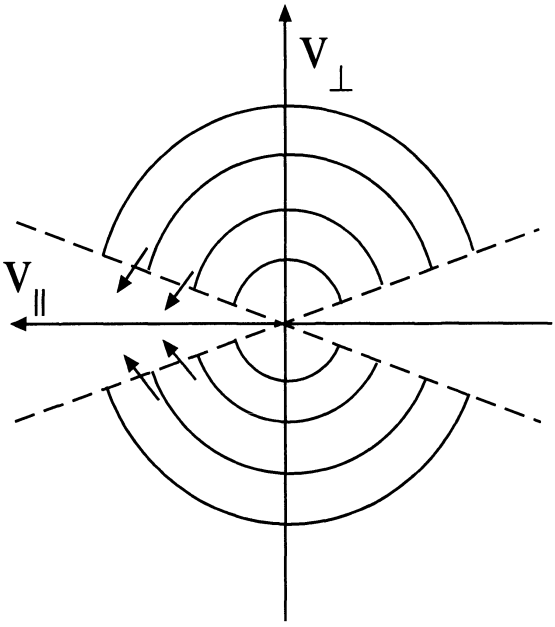

Figure 1. Schematic illustration of pitch-angle scattering in the velocity space. The loss cone is indicated by dashed lines. The small arrows illustrate the particles moving toward the loss cone. The actual position and direction of the arrows depend on the resonant energy and wave vector direction and are thus different for different scattering mechanisms.

large-scale wave effects, like launching of Alfvén wave pulses, creation of standing shocks around an X-line, etc.

As already noted, the literature on magnetospheric waves is huge. We have decided to refer only to a few classic studies in the older literature and give a preference to the most recent publications in order to illustrate that wave studies are an important part of modern magnetospheric research. Unfortunately, it is not easy to find a good comprehensive review to the history of wave observations. A recommendable starting point to the "menagerie" of plasma waves is Shawhan (1979). It contains the history of early observations up to the preliminary reports on ISEE-1 and -2 measurements. By that time most of the major magnetospheric wave modes had been found, although it was not possible to determine all their characteristics and their role in magnetospheric physics to the extent we know them today.

At high altitudes much of the pioneering observations were made by means of the OGO-5 and IMP-6 spacecraft. Several wave modes were identified and foundations were laid for later observations. From the second half of 1970's to about 1990 the observational basis of magnetospheric plasma waves rapidly expanded. Important contributions were obtained through ISEE-1 and -2, GEOS-1 and -2, ATS-6, SCATHA, and the three AMPTE spacecraft, some examples of whose observations are discussed in the following sections.

Of lower altitude observations several instructive summaries are available (e.g., Gurnett, 1983; 1991). One of the most important early satellites was Injun 5, which characterized most of the auroral plasma waves and their association to particle populations. These wave modes were later studied in much more detail using observations from the polar-orbiting satellites S3-3, DE-1, Viking, and Akebono, which, in addition to contributing to the detailed information to the previously observed wave emissions, made it possible to study the microstructure of one of the most intriguing magnetospheric regimes, the auroral acceleration region about 5000–15000 km above the discrete auroras.

During the last few years we have witnessed wave observations from CRRES, GEOTAIL, and most recently, POLAR. More than being a comprehensive review of wave observations, this review describes the status of the author's present understanding of waves in the precipitation process. It was written at the time when much of the early wave observations until ISEE-1 and -2, AMPTE, DE-1 and -2, and Viking had been relatively thoroughly analyzed, some important results from CRRES were still quite fresh, and most of the available GEOTAIL material had yet to be considered as preliminary. No material from POLAR was used because POLAR observations were not yet published.

Figure 2 illustrates the main magnetospheric regions covered by the present review. In Section 2 we discuss the history of the so-called $n + 1/2$ harmonic electrostatic waves and diffuse electron precipitation. Section 3 discusses one of the main surprises from the GEOTAIL wave instrument, the waveform observations of the broad-banded electrostatic noise. Section 4 deals with the ULF frequency range and ion precipitation, and Section 5 with low- and mid-altitude observations. In Section 6 we briefly discuss the large-scale nonlinear aspects. Section 7 contains conclusions on the present status of the wave observations from the precipitation viewpoint and tries to look toward future needs in this field.

2. What causes diffuse electron precipitation?

Diffuse electron precipitation to the auroral zone is one of the most persistent processes in auroral physics. The precipitation covers most of the auroral region for most of the time. Its equatorward border maps to the plasmapause (e.g., Gussenhoven *et al.*, 1983; Hardy *et al.*, 1985). Diffuse precipitation can be divided into two zones. The equatorward zone, whose field-aligned mapping in the nightside equatorial region extends from the plasmapause to distances of 8–12R_E, depending on magnetospheric activity, is characterized by harder precipitation in the energy range 1–20 keV, whereas the energies in the poleward zone are below 1 keV. On the other hand, the poleward region is where discrete arcs mostly occur. These two precipitation zones are often called CPS (for central plasma sheet) and BPS (for boundary plasma sheet), although this terminology is somewhat unlucky because of the risk of confusing BPS with the plasma sheet boundary layer (PSBL), which

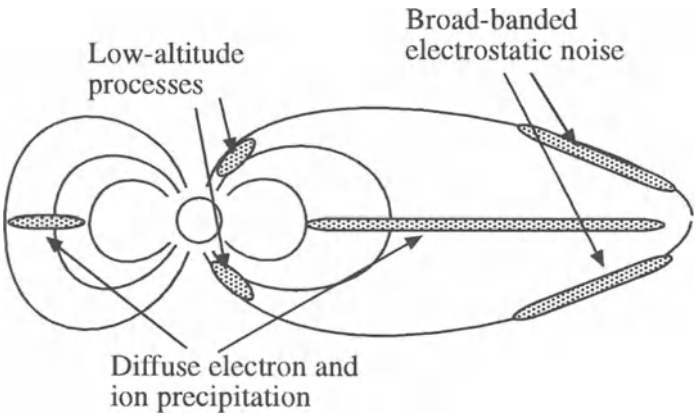

Figure 2. The magnetospheric regions where most of wave phenomena discussed in this review occur. The equatorial plasma sheet is the origin of diffuse electron and ion precipitation. The detailed structure of the broad-banded electrostatic noise in the plasma sheet boundary layer belongs to the most surprising new observational results. The low- and mid-altitude part of auroral field lines is a complicated region where wave processes contribute to the final processes leading to auroral arcs.

maps to a very thin poleward strip of the auroral oval. For a thorough discussion of this problem we refer to Galperin and Feldstein (1991). For our present purposes, it is sufficient to keep in mind that the boundary between the hard equatorward diffuse precipitation and the softer poleward precipitation coincides approximately with the trapping boundary of 30 keV electrons. This means that at this boundary electrons of energies below 30 keV cross the magnetic equator on adiabatic orbits. Closer to the earth the trapping energy becomes higher because the equatorial curvature radius of the magnetic field increases, whereas farther out the curvature radius becomes smaller and electrons of smaller energies become nonadiabatic. It is important to understand that the trapping energy is much higher than the typical energy of diffuse precipitation in both zones.

Although diffuse electron precipitation is such a common feature, it is extremely difficult to explain theoretically. Of course, some amount of precipitation results from the particles' adiabatic curvature and gradient drifts across electric equipotentials in the magnetosphere. However, that produces only weak precipitation with large pitch-angles in the ionosphere, not the almost-filled loss cone observed. Thus the fundamental question is how to break the first adiabatic invariant of the electrons to move them into the atmospheric loss cone efficiently enough in the appropriate energy ranges of 1–20 keV, in the inner region, and below 1 keV, in the outer region, over a sufficiently broad region of the magnetosphere to cover the entire diffuse oval. As discussed in the accompanying paper by Lyons (this issue), it is possible to scatter particles in the tail current sheet if the curvature radius of the magnetic field is comparable to the gyro radius of the particles or smaller. In such a case the particle orbit through the current sheet becomes nonadiabatic (chaotic)

and particles may fill the loss cone, especially in the tail where the loss cone is narrow. However, as noted above, the curvature radius of the field at radial distances, where the diffuse oval maps to, is so large that the energies of electrons becoming chaotic are much larger than the energies of electrons producing the diffuse auroral light.

Another possible scattering mechanism is wave-induced diffusion, which could explain the diffusion if appropriate wave fields were present. A plausible scenario would be a loss cone instability emitting electrostatic cyclotron waves at the expense of perpendicular energy of electrons close to the loss cone in velocity space. In 1970 it was widely believed that such a precipitation mechanism in the equatorial magnetotail was found when Kennel *et al.* (1970) published observations from the OGO-5 satellite. The observations indicated strong electrostatic waves in frequency bands centered close to odd-half multiples of the electron gyro frequency, $(n + 1/2)f_{ce}$. Consequently, these emissions are often called electron cyclotron harmonic (ECH), or $n+1/2$ harmonic, waves. The electron gyro frequency is given by the formula f_{ce}(Hz) = $28B$(nT), and has values 0.5–6 kHz in the regions where the diffuse precipitation is expected to originate. Kennel *et al.* (1970) estimated the ECH wave amplitudes to be in the range 1–10 mV/m. Similar amplitudes were later observed by IMP 6 in the altitude range from the plasmapause up to $10R_E$ (Shaw and Gurnett, 1975).

These amplitudes were large enough to suggest that the diffuse electron precipitation is due to wave-induced pitch-angle diffusion (Kennel *et al.*, 1970; Lyons, 1974). This remained the status quo for several years as is documented, e.g., in the monograph by Lyons and Williams (1984). However, together with the appearance of modern wave instruments, estimates for typical amplitudes started to decrease. The initial results from ISEE-1 and -2 indicated amplitudes from a few μV/m to 1 mV/m (Gurnett *et al.*, 1979). After carefully analyzing GEOS-1 and -2 data Belmont *et al.* (1983) noted that the typical amplitudes were actually well below 0.1 mV/m. Higher amplitudes were not uncommon, but they were limited to a small region close to the magnetic equator. Belmont *et al.* (1983) found amplitudes exceeding 1 mV/m only in 2% of cases, when GEOS-2 was within 3° of the magnetic equator and in 15% of cases very close to it. This led them to question the pitch-angle diffusion by the ECH waves as an explanation for diffuse electron precipitation. The fact that the most intense waves were observed close to the magnetic equator was already noted by Fredricks and Scarf (1973) but had not been taken fully into account in theoretical calculations. The electrons having pitch-angles close to the loss cone near the equator, which is about 4° near the plasmapause and about 2° outside the geostationary orbit, spend too little time under wave fields strong enough to scatter them in sufficient amount to fill the loss cone.

There was still the possibility that most of the diffusion would take place further down the tail where the wave amplitudes would, perhaps, be stronger. This possibility was examined by Roeder and Koons (1989) who analyzed data from SCATHA and AMPTE/IRM, covering radial distances 4–20R_E. Their results were consis-

tent with those by Belmont *et al.* (1983) and no sufficient wave fields were found in this region. Beyond $L = 8$ the ECH wave amplitudes exceeded 12 μV/m only in 26% of cases and were limited to within $\pm 10^\circ$ of the magnetic equator. Note that, further out from the geostationary orbit, the magnetic equator can be increasingly far from the tail current sheet, which increases the spread in observed locations of the waves. After these results, remarkably little attention has been paid to the problem in the literature. One may wonder how widely this problem is known at all!

A natural alternative wave mode that would come into question is the whistler mode at frequencies below the local electron gyro frequency. The idea was already introduced before space observations by Dungey (1963), who suggested that lightning-induced whistlers would precipitate radiation belt electrons. Kennel *et al.* (1970) argued that the whistler mode would interact efficiently enough only with electrons of too high energy, and favored the recently found half-harmonic emissions discussed above. Cornilleau-Wehrlin *et al.* (1985) investigated the whistler-induced diffusion using GEOS-1 and -2 observations and concluded that pitch-angle scattering by whistler waves was efficient for electron energies above 15 keV, which was the low-energy limit of their instrument. Recently, Johnstone *et al.* (1993) re-activated whistler mode explanation, arguing that there is no low-energy limit for efficient electron interaction with the whistler mode. They substantiated their claim with details of CRRES electron observations that are consistent with theoretical characteristics of diffusion by the whistler mode.

The whistler mode interaction was studied theoretically by Villalón and Burke (1995). They pointed out that the earlier studies were made for frequencies much below f_{ce} which, indeed, interact with electrons of energies above 10 keV. Villalón and Burke studied frequencies closer to f_{ce} and found that at the limit $f \to f_{ce}$ the resonance energy is less than 1 keV. Furthermore, they found that wave amplitudes of 1 μV/m would be sufficient to scatter electron pitch-angles more than 1° near the edge of the loss cone. Whether this is enough is not quite clear, but the CRRES observations published by Burke *et al.* (1995) indicate even higher amplitudes in the whistler mode band, at least occasionally. The spectrogram in their Plate 2 suggests that the spectral density of the whistler mode exceeded 1 $\mu\mathrm{mVm}^{-1}\mathrm{Hz}^{-1/2}$ which, considering the bandwidth of about 500 Hz, yields wave amplitudes of more than 20 μV/m. These observations were made when the spacecraft was in the plasmasheet beyond the plasmapause on L-shells between 6 and 7. It is interesting to note that spectra of about the same amplitudes in the whistler mode frequency range were published by Roeder and Koons (1989; Plate 2 and Fig. 4, which we have reproduced as Figure 3). These waves were observed by AMPTE/IRM at radial distances 7.5–9R_E. However, in both of these examples, i.e., Burke *et al.* (1995) and Roeder and Koons (1989), the peak of the whistler mode emission was centered near the frequency of about $f_{ce}/3$, which may interact with electrons of too high energies. This observation is consistent with the theoretical investigation by Thorne and Horne (1996), who found that for frequencies above $f_{ce}/3$ the whistler

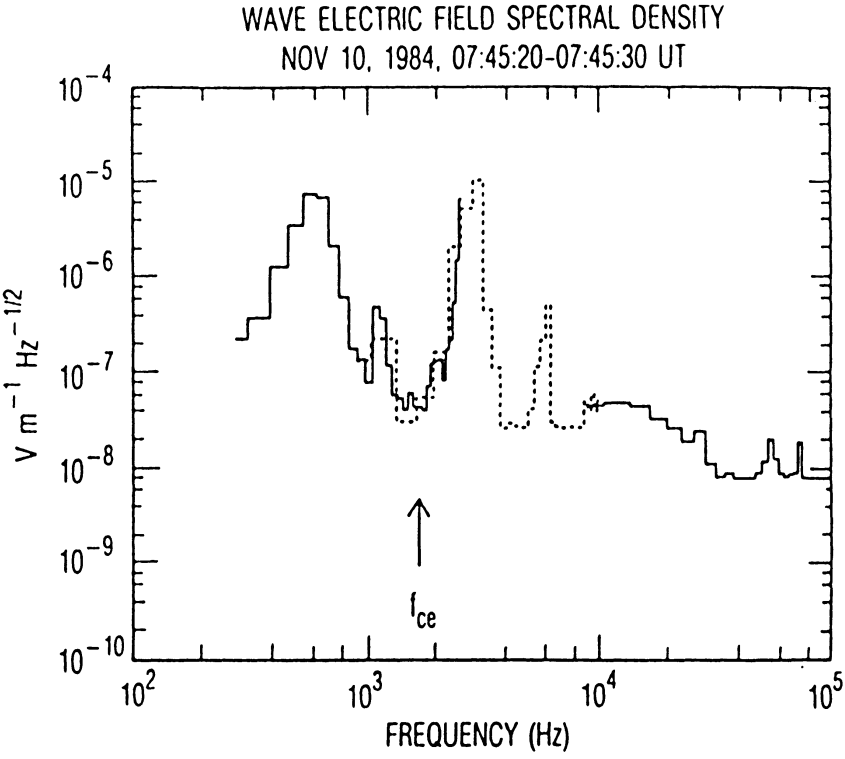

Figure 3. Observed wave electric field spectral density from AMPTE/IRM at a distance of about $8.5R_E$ in the morning sector. The total electric field in the first ECH band (around 1.75 f_{ce}) was 0.25 mV/m (from Roeder and Koons, 1989). Note that the spectral density in the whistler mode band is of the same order of magnitude but, due to the smaller width in frequency, the total electric field is about 10–20 μV/m.

mode would be strongly damped by electron heating perpendicular to the magnetic field, an effect moving electrons away from the loss cone. Thus the conclusion by Roeder and Koons (1989) that "there exist no known waves in the equatorial magnetosphere of the required intensity which occur in semicontinuous basis" may still be valid. However, because the required amplitude for whistler mode interaction appears to be smaller than for the ECH waves, this conclusion should be carefully re-examined. High enough whistler wave amplitudes seem to be possible to find but whether they occur often enough, within large enough region, and at sufficiently high frequencies to explain the diffuse precipitation seem, for the time being, to be open issue.

We may also speculate that the pitch-angle scattering into the loss cone would take place almost the whole way from the equatorial plane down to the ionosphere. This will to some extent most likely happen, and especially at lower altitudes the auroral region exhibits much wave activity (see Section 5 below). However, the filling of the loss cone is easiest in the region where it is smallest, i.e., in the equa-

torial plane. For example, at altitudes of the auroral acceleration region (2–3R_E geocentric) the loss cone width is 10–20° and wave-particle interaction can fill the loss cone only near its edges

3. Broad-banded electrostatic noise and solitary waves

Broad-banded electrostatic noise (BEN) is a generic name for electrostatic emissions that produce noisy wide-band spectra. BEN emissions, of very variable origins, have been observed in various regions of the magnetosphere. The first report came from the bow shock (Scarf *et al.*, 1974), and soon thereafter Gurnett *et al.* (1976) reported BEN observations by the IMP-8 satellite in the plasma sheet boundary layer (PSBL), which is the relevant region of our present discussion. A brief summary of the observational and theoretical status of BEN before the GEOTAIL mission can be found in Onsager *et al.* (1993).

In the PSBL BEN has been observed in the frequency range from the local lower hybrid frequency up to the electron plasma frequency, i.e., in the range 10 Hz–10 kHz, depending on local plasma parameters. Since the first observations (Gurnett *et al.*, 1976) the emissions were associated with ion beams. This led to extensive investigations of ion-beam-driven processes to produce the waves. While this approach was successful in explaining the low-frequency part of the BEN, it was much harder to understand the frequencies up to the electron plasma frequency. Thus it was natural to start looking for a possible relationship with electrons.

Parks *et al.* (1984) examined the high-resolution particle data from ISEE-1 and -2 and showed that large-amplitude BEN occurred in the thin outermost layer of the PSBL that contained electron beams moving in both directions along the ambient magnetic field, earthward streaming ion beams, and a considerable density gradient. The positive slope in the electron distribution function observed suggested that the waves might be generated by electron instabilities.

Most probably BEN is a mixture of waves arising from different instabilities. The lowest frequencies may well be associated with ion modes, whereas the higher frequencies, most likely, are related to electrons. BEN is also a sobering example of how different theoretical approaches are able to produce solutions resembling observations, but how only detailed observations can tell when theories are proceeding in the right direction. After all these theoretical studies Onsager *et al.* (1993) selected examples of ISEE-1 and -2 crossings from the lobe to the PSBL that lasted long enough to resolve the internal structure of the boundary layer. Their conclusion was that the most intense high-frequency BEN emissions could be excited by electron distributions in the outermost layer of the PSBL. They also concluded that the observed high-speed tails of the electron distribution function would be the cause, instead of the consequence, of the waves. Thus the electrons should gain their energy either in the plasma sheet or in the downtail reconnection site.

However, a big surprise was to come with the GEOTAIL mission. Before GEOTAIL all observations were performed in the frequency domain, for example, by means of swept frequency analyzers or filterbanks. GEOTAIL was the first spacecraft in the outer magnetosphere with a device for waveform capture to high enough frequencies to cover the BEN. According to Matsumoto *et al.* (1994) and Kojima *et al.* (1994), most of the BEN in the PSBL appears to consist of strongly nonlinear electrostatic solitary wave (ESW) pulses. Translated to the frequency domain these pulses give an appearance of broad-banded signals. However, it is not correct to interpret the frequency spectra as unstructured noise or "turbulence" in the time domain (Figure 4).

Various scenarios to generate the ESWs were studied by Omura *et al.* (1996). They concluded that the most likely mechanism was a bump-on-tail instability of the electron population. This conclusion is consistent with the results of Onsager *et al.* (1993) concerning the high-frequency part of the BEN spectra, although Onsager *et al.* did not yet know about the detailed waveforms of the emissions. This result of GEOTAIL is a severe warning for applying time series analysis uncritically to non-periodic signals. After the actual observations of the solitary waveforms one could speculate that the often observed bursty and intermittent behavior of the BEN should have already indicated that the underlying turbulence might be something else than just broad-banded noise. It is rather remarkable that this was never brought up, especially after the fact that solitary waves of similar shape but, evidently, of very different physical origin had been observed at lower altitudes in the auroral acceleration region by S3-3 (Temerin *et al.*, 1982) and Viking (Boström *et al.*, 1988).

It is not only the interpretation of frequency spectra but also of other properties of the waves that may be misled by the use of frequency domain data alone. Gurnett *et al.* (1976) concluded that the low-frequency part of the BEN has the wave electric field perpendicular to the ambient magnetic field, whereas Onsager *et al.* (1993) found that the high-frequency part was polarized parallel to the magnetic field. Kojima *et al.* (1994) pointed out that these results should also be considered carefully, since the lack of resolution may lead to erroneous determination of the wave normal directions.

From the point of view of this review, we must also ask the question of what role these waves play in auroral precipitation. The data are too inconclusive to give a definite answer. The earthward-streaming ions in the PSBL are often interpreted as originating from the distant neutral line, and the most field-aligned of them are expected to be the source of velocity-dispersed ion structures (VDIS) at the poleward edge of the auroral oval (Bosqued *et al.*, 1993). Of course, the loss cone at these distances is very small ($\lesssim 2°$) and it would be advantageous for the ion precipitation to get extra kicks toward the loss cone during the way down in order to avoid mirroring before the ionosphere. The low-frequency part of BEN might do this but that is rather speculative. Concerning BEN's role in electron precipitation Onsager *et al.* (1993) concludes that the high-energy electrons are more likely the

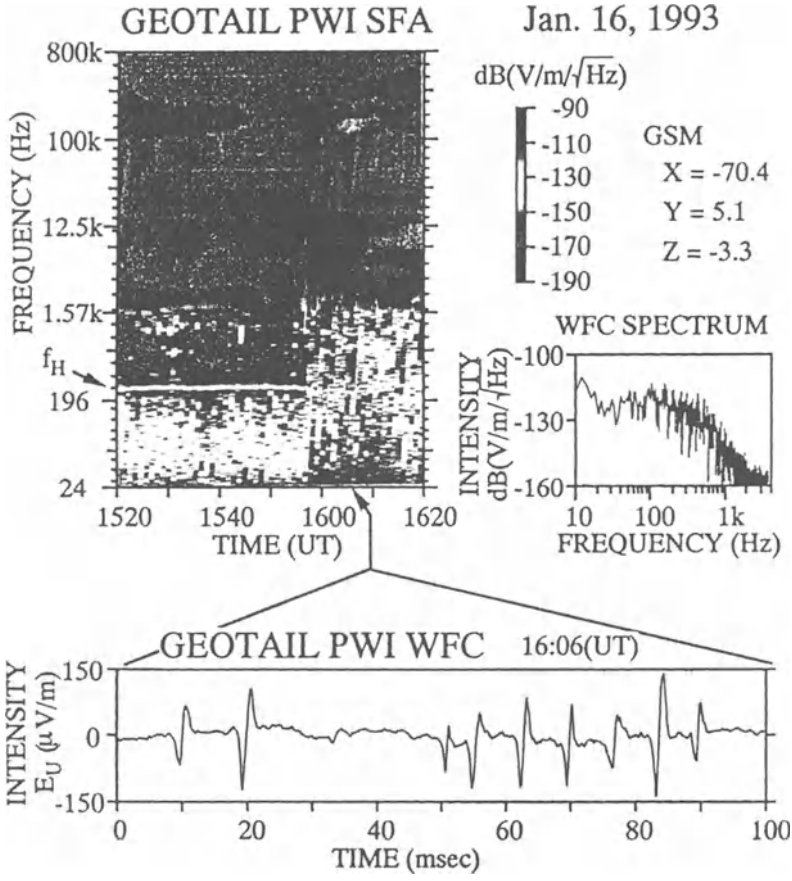

Figure 4. An example of GEOTAIL observations of BEN in the PSBL. The waveform consists of solitary wave pulses in the time domain that produce a broadbanded spectrum in the frequency domain (from Matsumoto *et al.*, 1994).

cause than the consequence of BEN. The simulation results by Omura *et al.* (1996) point into the same direction. They find the bumb-on-tail instability as the most likely process to drive the ESWs. This implies that while the electron beam gets heated, its thermal width increases mostly on the side of lower velocity. Thus both of these studies suggest that BEN would more likely reduce than enhance electron precipitation.

4. ULF waves and ion precipitation

Although the number flux of ions precipitating to the whole auroral oval is only 2.4% (for Kp $\geq$ 6−) to 1.5% (for Kp = 0) of the number flux of electrons and ion energy flux is also a factor of 6-9 smaller than the electron energy flux (Hardy et al, 1989), ion precipitation is an important loss process of magnetospheric plasma, including the decay of ring current after geomagnetic storms.

Waves that can result in pitch-angle scattering of protons in the equatorial region at auroral L-shells must have frequencies of the order of 0.1–1 Hz, which is the local proton gyro frequency in the equatorial region. These frequencies are covered by the ULF waves, the so-called Pc 1–2 pulsations (0.1–5 Hz), which have been thoroughly studied. Observations of Pc 1 pulsations on the ground were first reported well before the space age by Harang (1936) and Sucksdorff (1936). The great advantage of these waves is that they can be observationally studied at all altitudes, from the ground to the equatorial plane. Examples of recent studies from low-altitude spacecraft are Mursula *et al.* (1994), and Erlandson and Anderson (1996), using Freja and DE-2 data, respectively, and from mid-altitude spacecraft, Erlandson *et al.* (1990), using Viking. From high altitudes, including the geostationary orbit, some of the most important studies have been based on data from OGO-5 (e.g., Kaye and Kivelson, 1979), GEOS-1 and -2 (e.g., Roux *et al.* 1982), ATS-6 (e.g., Fraser and McPherron, 1982), AMPTE-CCE (e.g., Anderson *et al.*, 1992a,b), and CRRES (e.g., Fraser *et al.*, 1996).

Another important reason that electromagnetic waves in the Pc 1–2 range belong to the best known of all magnetospheric waves is that in this frequency range it is possible to sample simultaneously several components of the electric and magnetic field waveforms, and more importantly, that these waveforms can be transmitted to the earth. This has made it possible to experimentally determine the polarization properties (e.g., Anderson *et al.*, 1996) and the Poynting flux (e.g., Fraser *et al.*, 1996) of the waves. Furthermore, modern particle instruments are able to sample particle distribution functions in comparable time scales, i.e., 1–10 s. Thus we can be rather confident that the characterization of the waves as electromagnetic ion cyclotron (EMIC) waves in their generation region close to the equator is correct. The EMIC instability in the equatorial plane is explained as being driven by temperature anisotropy $T_\perp \gg T_\parallel$ of energetic ions in the energy range 10–100 keV (Cornwall, 1965; see also Lyons and Williams, 1984). This reduces the perpendicular energy of the ions, of which a few are scattered into the loss cone, resulting in ion precipitation.

But are EMIC waves important for ion precipitation? We refer again to the accompanying paper by Lyons (this issue) and note that it is much easier to understand ion precipitation than electron precipitation in terms of pitch-angle scattering due to non-adiabatic motion through the equatorial region of the magnetosphere. This is simply because the gyro radius scales as $\sqrt{m}$. However, from the plasmapause up to geostationary orbit the ions still are stably trapped during quiet times up

to energies of more than 100 keV, and the wave-particle interaction becomes a useful mechanism to scatter the ions into the loss cone, especially in the dayside where the curvature radius of the magnetic field is larger than in the nightside. According to Anderson *et al.* (1992a) the normalized occurrence rate of EMIC waves in AMPTE/CCE data was highest in the dayside for all L shells beyond 4. The wave-particle interaction is also important for the loss of ring current ions after geomagnetic storms, although its relative importance compared to charge-exchange and Coulomb collisions still remains unclear. Note also that the EMIC waves, driven by the anisotropy of the energetic ions, are able to heat the low-energy plasma (10–50 eV) during the plasma circulation around the earth, as recently studied by Fuselier and Anderson (1996).

5. Low- and mid-altitude waves

It is likely that some amount of pitch-angle scattering close to the edges of the loss cone takes place everywhere along the magnetic field line from the equatorial plane down to the ionosphere. The importance of this is difficult to estimate quantitatively and depends on various factors such as the intensity of the scattering waves. The auroral field lines closer to the earth are well known to be rich in wave phenomena (e.g., Gurnett, 1991). Figure 5 is a summary spectrogram of the major wave modes encountered by a polar-orbiting satellite passing above the evening sector auroral oval. The main reason for this richness in wave phenomena is that in this region tenuous, hot plasma from the magnetosphere interacts with cold, denser plasma originating from the ionosphere. In particular, physical processes in the so-called auroral acceleration region at altitudes of 5000–15000 km are important for precipitation. It is likely that much of the final formation of discrete auroral arcs takes place due to the parallel electric potential difference between the ionosphere and the magnetosphere in the region of upward field-aligned currents.

Although there is a wealth of observational evidence of net electron acceleration down to the ionosphere and ion acceleration upward (see the accompanying papers by André and Yau, and Yau and André, in this issue) in the auroral acceleration region, its detailed physical spatio-temporal structure remains unknown. A clear distinction of what is caused by waves and what by something else is not possible. For example, a physical process, which may look quasi-static ("quasi-DC" electric field) in the temporal scale of electron interaction, may look like a wave phenomenon for ions. This has been suggested as an explanation for simultaneous acceleration of electrons and ions in the same direction (Hultqvist *et al.*, 1988).

An extreme view has been advocated by Bryant *et al.* (1991), who claim that the acceleration of the primary electrons would not be by the large-scale electric field but by waves, in this case the lower-hybrid waves (Bingham *et al.*, 1984), perhaps driven by ion beams in the PSBL field-lines. While a lower-hybrid mode with right phase speed along the magnetic field lines undoubtedly could accelerate the elec-

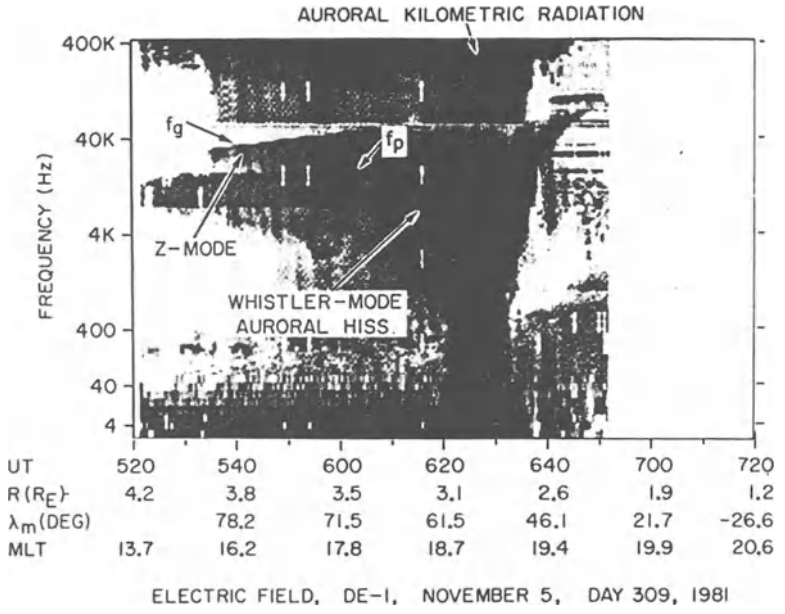

Figure 5. Summary spectrogram illustrating the wave environment above the evening sector auroral zone observed by DE-1 (from Gurnett, 1983). Characteristics of the wave data allow for determination of the electron gyro frequency (f_g) and electron plasma frequency (f_p) from which we can derive the local magnetic field and plasma density. Auroral kilometric radiation and auroral hiss are discussed further in the text.

tron beam, there is so far no positive observational evidence that such waves exist in the right place. Furthermore, this mechanism leaves open the observational fact that ionospheric ions experience parallel acceleration upward in the same region (e.g., Reiff *et al.*, 1988). It is true that there is an important wave emission covering the lower-hybrid frequency range associated with down-flowing electrons, the so-called auroral hiss (see Figure 5). However, this mode is most likely driven at the expense of the parallel energy of the downward accelerated "inverted-V" electrons (Gurnett and Frank, 1972). Thus it weakly reduces, not enhances, the precipitation.

The physical structure of the parallel acceleration region may well be somehow determined by wave phenomena. Various wave-related mechanisms to sustain the parallel electric field have been proposed, e.g., anomalous resistivity through electrostatic waves, turbulence, or double layers (c.f. Fälthammar, 1983). While quasi-linear processes involving electrostatic waves do not seem to provide enough resistivity to support the parallel electric field, more strongly nonlinear processes may be important. The most thoroughly investigated phenomenon is the formation of ion-scale weak double layers (WDL) observed by S3-3 (Temerin *et al.*, 1982) and Viking (Boström *et al.*, 1988). Detailed study of the plasma environment of WDLs

(Koskinen *et al.*, 1990) showed that they are intimately associated with the structure of the auroral acceleration region. However, the statistical analysis by Mälkki *et al.* (1993) left some doubt about how much total parallel potential difference really can be attributed to WDLs. Clearly, more observations and fresh theoretical ideas are needed to understand the physics of the auroral acceleration region.

Perhaps the most intensively studied wave mode originating from the auroral region is auroral kilometric radiation (AKR). This emission can be studied only in space because electromagnetic radiation at frequencies of a few hundred kilohertz (300 kHz corresponds to the wavelength of 1 km) cannot penetrate the ionosphere. The most widely studied, though not the only, excitation mechanism for AKR is cyclotron maser interaction inside the plasma cavity, probably produced by the large-scale parallel electric field. This was already indicated by early observations (see Gurnett, 1983) and got strong support from the in-situ observations in its generation region by Viking (Roux *et al.*, 1993). The excitation mechanism moves electrons into the loss cone, although this probably is not a very significant precipitation process. While perhaps a secondary process for auroral precipitation, AKR is the most important radio emission from the earth. Understanding of AKR is of fundamental importance for understanding other radio sources throughout the universe.

Low- and mid-altitude ion waves may also contribute to ion precipitation. Observations of electrostatic ion cyclotron harmonic (ICH) waves by Viking were discussed by Koskinen *et al.* (1987). The ICH waves are ordered by the ion gyro frequency in much the same way as the ECH waves, discussed in Section 2, are ordered by the electron gyro frequency. Viking observations took place near the equatorward boundary of the auroral oval, and Koskinen *et al.* (1987) identified the ion loss cone near 1 keV energies, observed simultaneously with the waves, as the most probable free-energy source. The instability moves ions to the loss cone, which contributes to ion precipitation. In the whole precipitation process this may be of minor importance, but it illustrates that some amount of scattering into the loss cone really can take place over a long distance when ions are moving toward the earth.

6. Beyond quasi-linear processes

In the previous four sections we have focused on waves that can and do induce particle precipitation through wave-particle interaction, which in most cases can be categorized as quasi-linear diffusion. The exceptions were the nonlinear solitary waves in the plasma sheet boundary layer and in the auroral acceleration region. There are, however, other important nonlinear phenomena, such as magnetohydrodynamic (MHD) shocks or discontinuities, current sheet disruptions, etc., in the magnetosphere that print their signatures in the auroral precipitation. Much of the dayside precipitation, whether it comes through the cusp or from the low-latitude

boundary layer, originates from processes that can be described in terms of nonlinear wave phenomena. Discussion of these would take us too far from the main topic of this review but we would like to end with some remarks on MHD shock waves.

The slow mode shock predicted by the Petschek (1964) reconnection model is a particularly important phenomenon that has gained new attention with recent observations and data analysis. Positive identification of slow shocks associated with the distant neutral line from ISEE-3 data took some time (Ho *et al.*, 1994, 1996), and now the more complete instrumentation of GEOTAIL appears to have proven their existence (Seon *et al.*, 1995, Saito *et al.*, 1995). The slow mode shock accelerates particles into the PSBL and may be the major source of the streaming populations associated with the BEN observations discussed in Section 3. Of course, we have even less unambiguous observational information from the distant magnetotail than we have from the regions closer to the earth. Considering all difficulties we have in understanding the precipitation from these closer regions, we should remain cautious about the details of processes that evidently take place much further down the tail. Furthermore, when it comes to the details of particle energization, the MHD picture may not be fully satisfactory, and other approaches such as large-scale kinetic theory (Ashour-Abdalla *et al.*, 1995) require further studies.

7. Conclusions

Our conclusions on the importance of various wave modes in the precipitation process necessarily remain rather weak. The case for wave-induced ion precipitation from the plasmapause to geostationary orbit appears to be the strongest, and it is quite likely that the electromagnetic ion cyclotron waves play an important role at low L-shells. While the waves would be much more desired as an explanation for the main diffuse electron precipitation, the negative results reached by Belmont *et al.* (1983) and Roeder and Koons (1989) left the field in confusion. The recent revival of the idea that whistler mode waves would provide the required diffusion should be investigated very carefully. We claim that the failure to understand diffuse electron precipitation must be considered one of the major unsolved problems in magnetospheric physics.

Although wave emissions above the auroral zone closer to the earth have been rather extensively registered by several polar-orbiting satellites, many of the details on how these waves contribute to the final formation of auroral arcs remain unclear. This is intimately coupled to our insufficient understanding of the formation of the auroral acceleration region. Finally, the observations of nonlinear solitary waves, both in the auroral acceleration region and in the plasma sheet boundary layer, express an important warning that the detailed physics may sometimes be much

more complicated than we would expect from pictures drawn according to old observations and simplified theories.

Does the weakness of our conclusions mean that the observational status is still too weak or that our fundamental and theoretical understanding are too poor? It is clear that the observations in many cases are insufficient and will certainly remain so. The magnetosphere is a vast region and in-situ observations will always be more sparse than we would like. A serious experimental problem is that it is not possible to store and transmit waveform data of several electric and magnetic field components in the frequency range up to several kilohertz, which is the frequency range of electron interaction. However, the GEOTAIL experience clearly suggests that future wave instruments should be designed to do so, at least intermittently. At the same time we must not forget that, during the last three decades, an enormous amount of useful data has been collected and much unknown information is just waiting to be revealed after thorough analysis. Thus the observational status of waves may be much better than we actually know. Actually, throughout the history of magnetospheric physics it has been easier to put resources into new, exciting observational missions and publication of "initial results" from these than into long-term analysis of old data.

To proceed from the present status of understanding the relationship between magnetospheric waves and auroral precipitation we need, in addition to more refined observations and more thorough data analysis, more interaction between scientists specializing in different aspects of this problem area. The same message applies equally well to those working with the distant magnetosphere or with the auroral zone, with observations or with theory.

Acknowledgements

I am indebted to a large number of colleagues for numerous enlightening discussions on magnetospheric waves and on auroral precipitation. I especially wish to mention the international science team of the Swedish Viking satellite. Most of what I know of wave observations and wave-particle interactions I learned during those years of enthusiasm and devotion. I also wish to thank Bengt Hultqvist for persuading me to undertake this task at the very late stage of the planning of the ISSI workshop. The fact that I have not been directly involved in magnetospheric wave observations during the last few years made the task more demanding, but also more rewarding, than I had thought. On the other hand, the aurora-related work at the Finnish Meteorological Institute was of great help in tying the wave and precipitation aspects together. I wish there were much more cross-talk between the magnetospheric wave community and those studying precipitation into the ionosphere.

References

Alfvén, H.: 1942, 'Existence of Electromagnetic-Hydrodynamic Waves', *Nature* **150**, 405.

Anderson, B. J., Erlandson, R. E., and Zanetti, L. J.: 1992a, 'A Statistical Study of Pc 1-2 Magnetic Pulsation in the Equatorial Magnetosphere 1. Equatorial Occurrence Distributions', *J. Geophys. Res.* **97**, 3075.

Anderson, B. J., Erlandson, R. E., and Zanetti, L. J.: 1992b, 'A Statistical Study of Pc 1-2 Magnetic Pulsation in the Equatorial Magnetosphere 2. Wave Properties', *J. Geophys. Res.* **97**, 3089.

Anderson, B. J., Denton, R. E., and Fuselier, S. A.: 1996. 'On Determining Polarization Characteristics of Ion Cyclotron Wave Magnetic Field Fluctuations', *J. Geophys. Res.* **101**, 13,195.

Ashour-Abdalla, M., Zelenyi, L. M., Peroomian, V., Richard, R. L., and Bosqued, J. M.: 1995, 'The Mosaic Structure of Plasma Bulk Flows in the Earth's Magnetotail', *J. Geophys. Res.* **100**, 19191.

Belmont, G., Fontaine, D., and Canu, P.: 1983: 'Are Equatorial Electron Cyclotron Waves Responsible for Diffuse Auroral Precipitation?', *J. Geophys. Res.* **89**, 9163.

Bingham, R., Bryant, D. A., and Hall, D. S.: 1984, 'A Wave Model for the Aurora', *Geophys. Res. Lett.* **11**, 327.

Bosqued, J. M., Ashour-Abdalla, M., El Alaoui, M., Peroomian, V., Zelenyi, L. M., and Escoubet, C. P.: 1993, 'Dispersed Ion Structures at the Poleward Edge of the Auroral Oval: Low-Altitude Observations and Numerical Modelling', *J. Geophys. Res.* **98**, 19,181.

Boström, R., Gustafsson, G., Holback, B., Holmgren, G., Koskinen, H., and Kintner, P.: 1988, 'Characteristics of Solitary Waves and Weak Double Layers in the Magnetospheric Plasma', *Phys. Rev. Lett.* **61**, 82.

Bryant, D. A., Cook, A. C., Wang, Z.-S., de Angelis, U., and Perry, C. H.: 1991, 'Turbulent Acceleration of Auroral Electrons', *J. Geophys. Res.* **96**, 13,829.

Burke, W. J., Rubin, A. G., Hardy, D., and Holeman, E. G.: 1995, 'Banded Electron Structures in the Plasmasphere', *J. Geophys. Res.* **100**, 7759.

Cornilleau-Wehrlin, N., Solomon, J., Korth, A., and Kremser, G.: 1985, 'Experimental Study of the Relationship Between Energetic Electrons and ELF Waves Observed on Board GEOS: A Support to Quasi-Linear Theory', *J. Geophys. Res.* **90**, 4141.

Cornwall, J. M.: 1965, 'Cyclotron Instabilities and Electromagnetic Emission in the Ultra Low Frequency and Very Low Frequency Ranges', *J. Geophys. Res.* **70**, 61.

Dungey, J. W.: 1963, 'The Loss of Van Allen Electrons Due to Whistlers', *Planet. Space Sci.* **11**, 591.

Erlandson, R. E., and Anderson, B.: 1996, 'Pc 1 Waves in the Ionosphere: A Statistical Study', *J. Geophys. Res.* **101**, 7843.

Erlandson, R. E., Zanetti, L. J., Potemra, T. A., Block, L. P., and Holmgren, G.: 1990, 'Viking Magnetic and Electric Field Observations of Pc 1 Waves at High Latitudes', *J. Geophys. Res.* **95**, 5941.

Fälthammar, C.-G.: 1983, 'Magnetic Field-Aligned Electric Fields', *ESA Journal* **7**, 385.

Fraser, B. J., and McPherron, R. L.: 1982, 'Pc 1–2 Magnetic Pulsation Spectra and Heavy Ion Effects at Synchronous Orbit: ATS-6 Results', *J. Geophys. Res.* **87**, 4560.

Fraser, B. J., Singer, H. J., Hughes, W. J., Wygant, J. R., Anderson, R. R., and Hu, Y. D.: 1996, 'CRRES Poynting Vector Observations of Electromagnetic Ion Cyclotron Waves Near the Plasmapause', *J. Geophys. Res.* **101**, 15,331.

Fredricks, R. W., and Scarf, F. L.: 1973, 'Recent Studies of Magnetospheric Electric Field Emissions Above the Electron Gyrofrequency', *J. Geophys. Res.* **78**, 310.

Fuselier, S. A., and Anderson, B. J.: 1996, 'Low-Energy He^+ and H^+ Distributions and Proton Cyclotron Waves in the Afternoon Equatorial Magnetosphere, *J. Geophys. Res.* **101**, 13,255.

Galperin, Yu. I., and Feldstein, Ya. I.: 1991, in C.-I. Meng, M. J. Rycroft, and L. A. Frank (eds.), 'Auroral Luminosity and Its Relationship to Magnetospheric Plasma Domains', *Auroral Physics*, Cambridge University Press, Cambridge, pp. 207–222.

Gurnett, D. A.: 1983, in B. Hultqvist and T. Hagfors (eds.), 'High Latitude Electromagnetic Plasma Wave Emissions', *High-Latitude Space Plasma Physics*, Plenum Press, New York, pp. 355–375.

Gurnett, D. A.: 1991, in C.-I. Meng, M. J. Rycroft, and L. A. Frank (eds.), 'Auroral Plasma Waves', *Auroral Physics*, Cambridge University Press, Cambridge, pp. 241–254.

Gurnett, D. A., and Frank, L. A.: 1972, 'VLF Hiss and Related Plasma Observations in the Polar Magnetosphere', *J. Geophys. Res.* **77**, 172.

Gurnett, D. A., Frank, L. A., and Lepping, R. P.: 1976, 'Plasma Waves in the Distant Magnetotail', *J. Geophys. Res.* **81**, 6059.

Gurnett, D. A., Anderson, R. R., Scarf, F. L., Fredricks, R. W., and Smith, E. J.: 1979, 'Initial Results from the ISEE-1 and -2 Plasma Wave Investigation', *Space Sci. Rev.* **23**, 103.

Gussenhoven, M. S., Hardy, D. A., and Heinemann, N.: 1983, 'Systematics of the Equatorward Diffuse Auroral Boundary', *J. Geophys. Res.* **88**, 5692.

Harang, L.: 1936, 'Oscillations and Vibrations in Magnetic Records at High-Latitude Stations', *Terr. Magn. and Atm. Electr.* **41**, 329.

Hardy, D. A., Gussenhoven, M. S., and Holeman, E.: 1985, 'A Statistical Model of Auroral Electron Precipitation', *J. Geophys. Res.* **90**, 4229.

Hardy, D. A., Gussenhoven, M. S., and Brautigam, D.: 1989, 'A Statistical Model of Auroral Ion Precipitation', *J. Geophys. Res.* **94**, 370.

Ho, C. M., Tsurutani, B. T., Smith, E. J., and Feldman, W. C.: 1994, 'A Detailed Examination of a X-line Region in the Distant Tail: ISEE-3 Observations of Jet Flow and Bz Reversals and a Pair of Slow Shocks', *Geophys. Res. Lett.* **21**, 3031.

Ho, C. M., Tsurutani, B. T., Smith, E. J., and Feldman, W. C.: 1996, 'Properties of Slow-Mode Shocks in the Distant (¿200 RE) Geomagnetic Tail', *J. Geophys. Res.* **101**, 15,277.

Hultqvist, B., Lundin, R., Stasiewicz, K., Block, L., Lindqvist, P.-A., Gustafsson, G., Koskinen, H., Bahnsen, A., Potemra, T. A., and Zanetti L. J.: 1988, 'Simultaneous Observation of Upward Moving Field-Aligned Energetic Electrons and Ions on Auroral Zone Field Lines', *J. Geophys. Res.* **93**, 9765.

Johnstone, A. D., Walton, D. M., Liu, R., and Hardy, D. A.: 1993, 'Pitch Angle Diffusion of Low-Energy Electrons by Whistler Mode Waves', *J. Geophys. Res.* **98**, 5959.

Kaye, S. M., and Kivelson, M. G.: 1979, 'Observations of Pc12 Waves in Outer Magnetosphere', *J. Geophys. Res.* **84**, 4267.

Kennel, C. F., Scarf, F. L., Fredricks, R. W., McGehee, J. H., and Coroniti, F. V.: 1970, 'VLF Electric Field Observations in the Magnetosphere', *J. Geophys. Res.* **75**, 6136.

Kojima, H., Matsumoto, H., Miyatake, T., Nagano, I., Fujita, A., Frank, L. A., Mukai, T., Paterson, W. R., Saito, Y., Machida, S., and Anderson, R. R.: 1994, 'Relation Between Electrostatic Solitary Waves and Hot Plasma Flow in the Plasma Sheet Boundary Layer: GEOTAIL Observations', *Geophys. Res. Lett.* **21**, 2919.

Koskinen, H. E. J., Kintner, P. M., Holmgren, G., Holback, B., Gustafsson, G., André, M., and Lundin, R.: 1987, 'Observations of Ion Cyclotron Harmonic Waves by the Viking Satellite', *Geophys. Res. Lett.* **14**, 459.

Koskinen, H. E. J., Lundin, R., and Holback, B.: 1990, 'On the Plasma Environment of Solitary Waves and Weak Double Layers', *J. Geophys. Res.* **95**, 5921.

Landau, L. D.: 1946, 'On the Vibrations of the Electronic Plasma', J. Phys. U.S.S.R. 10, 25.

Lyons, L. R.: 1974, 'Electron Diffusion Driven by Magnetospheric Electrostatic Waves', *J. Geophys. Res.* **79**, 575.

Lyons, L. R., and Williams, D. J.: 1984, *Quantitative Aspects of Magnetospheric Physics*, Reidel, Dordrecht.

Mälkki, A., Eriksson, A. I., Dovner, P.-O., Boström, R., Holback, B., Holmgren, G., and Koskinen, H. E. J.: 1993, 'A Statistical Survey of Auroral Solitary Waves and Weak Double Layers 1. Occurrence and Net Voltage', *J. Geophys. Res.* **98**, 15,521.

Matsumoto, H., Kojima, H., Miyatake, T., Omura, Y., Okada, M., Nagano, I., and Tsutsui, M.: 1994, 'Electrostatic Solitary Waves (ESW) in the Magnetotail: BEN Wave Forms Observed by GEOTAIL', *Geophys. Res. Lett.* **21**, 2915.

Mursula, K., Blomberg, L. G., Lindqvist, P. A., Marklund, G. T., Bräysy, T., Rasinkangas, R., and Tanskanen, P.: 1994, 'Dispersive Pc 1 Bursts Observed by Freja', *Geophys. Res. Lett.* **21**, 1851.

Omura, Y., Matsumoto, H., Miyake, T., and Kojima, H.: 1996, 'Electron Beam Instabilities as Generation Mechanism of Electrostatic Solitary Waves in the Magnetotail', *J. Geophys. Res.* **101**, 2685.

Onsager, T. G., Thomsen, M. F., Elphic, R. C., Gosling, J. T., Anderson, R. R., and Kettmann, G.: 1993, 'Electron Generation of Electrostatic Waves in the Plasma Sheet Boundary Layer', *J. Geophys. Res.* **98**, 15,509.

Parks, G. K., McCarthy, M., Fitzenreiter, R. J., Etcheto, J., Anderson, K. A., Anderson, R. R., Eastman, T. E., Frank, L. A., Gurnett, D. A., Huang, C., Lin, R. P., Lui, A. T., Ogilvie, K. W., Pedersen, A., Reme, H., and Williams, D. J.: 1984, 'Particle and Field Characteristics of the High-Latitude Plasma Sheet Boundary Layer', *J. Geophys. Res.* **89**, 8885.

Petschek, H. E.: 1964, in W. N. Hess (ed.), 'Magnetic Field Annihilation', *AAS-NASA Symposium on the Physics of Solar Flares*, NASA Publ. SP-50, NASA, Washington, D. C., pp. 425–439.

Reiff, P. H., Collin, H. L., Craven, J. D., Burch, J. L., Winningham, J. D., Shelley, E. G., Frank, L. A., and Friedman, M. A.: 1988, 'Determination of Auroral Electrostatic Potentials Using High- and Low-Altitude Particle Distributions', *J. Geophys. Res.* **93**, 7441.

Roeder, J. L., and Koons, H. C.: 1989, 'A Survey of Electron Cyclotron Waves in the Magnetosphere and the Diffuse Auroral Electron Precipitation', *J. Geophys. Res.* **94**, 2529.

Roux, A., Perraut, S., Rauch, J. L., de Villedary, C., Kremser, G., Korth, A., and Young, D. T.: 1982, 'Wave-Particle Interactions Near WHe+ Observed on Board GEOS 1 and 2, 2, Generation of Ion Cyclotron Waves and Heating of He+ Ions', *J. Geophys. Res.* **87**, 8174.

Roux, A., Hilgers, A., de Feraudy, H., le Queau, D., Louarn, P., Perraut, S., Bahnsen, A., Jespersen, M., Ungstrup, E., and André, M.: 1993, 'Auroral Kilometric Radiation Sources: In Situ and Remote Observations From Viking', *J. Geophys. Res.* **98**, 11,657.

Saito, Y., Mukai, T., Terasawa, T., Nishida, A., Machida, S., Hirahara, M., Maezawa, K., Kokubun, S., and Yamamoto, T.: 1995, 'Slow-Mode Shocks in the Magnetotail', *J. Geophys. Res.* **100**, 23,567.

Scarf, F., Frank, L. A., Ackerson, K., and Lepping, R.: 1974, 'Plasma Wave Turbulence at Distant Crossings of the Plasma Sheet Boundaries and Neutral Sheet', *Geophys. Res. Lett.* **1**, 189.

Seon, J., Frank, L. A., Paterson, W. R., Scudder, J. D., Coroniti, F. V., Kokubun, S., and Yamamoto, T.: 1995, 'Observations of a Slow-Mode Shock at the Lobe-Plasma Sheet Boundary in Earth's Distant Magnetotail', *Geophys. Res. Lett.* **22**, 2981.

Shaw, R. R., and Gurnett, D. A.: 1975, 'Electrostatic Noise Bands Associated with the Electron Gyro Frequency and Plasma Frequency in the Outer Magnetosphere', *J. Geophys. Res.* **80**, 4259.

Shawhan, S. D.: 1979, in Lanzerotti, L. J., Kennel, C. F., and Parker, E. H. (eds.), 'Magnetospheric Plasma Waves', *Solar System Plasma Physics*, Vol. III, North Holland, pp. 211–269.

Sucksdorff, E.: 1936, 'Occurrence of Rapid Micropulsations at Sodankylä During 1932–1935', *Terr. Magn. and Atm. Electr.* **41**, 337.

Temerin, M., Cerny, K., Lotko, W., and Mozer, F. S.: 1982, 'Observations of Double Layers and Solitary Waves in the Auroral Plasma', *Phys. Rev. Lett.* **48**, 1175.

Thorne, R. M., and Horne, R. B.: 1996, 'Whistler Absorption and Electron Heating near the Plasmapause', *J. Geophys. Res.* **101**, 4917.

Villalón, E., and Burke, W. J.: 1995, 'Pitch Angle Scattering of Diffuse Auroral Electrons by Whistler Mode Waves', *J. Geophys. Res.* **100**, 19,361.

Address for correspondence: H. E. J. Koskinen, Finnish Meteorological Institute, Geophysical Research, P.O.Box 503, FIN 00101 Helsinki, Finland

EROSION AND RECOVERY OF THE PLASMASPHERE IN THE PLASMAPAUSE REGION

D. L. CARPENTER
Space, Telecommunications and Radioscience Laboratory, Stanford University, Stanford, California, USA

J. LEMAIRE
Institute d'Aéronomie Spatiale de Belgique, Brussels, Belgium

Received February 3, 1997; Accepted in final form April 15, 1997

Abstract. Understanding the basic plasmasphere erosion/recovery cycle remains a major, as yet largely unmet, challenge to the space science community. We do not yet have a description of the formation of a new plasmapause boundary, nor have we been able to map the evidently complex electric fields that develop at subauroral latitudes during the process of plasmasphere erosion. Density structure regularly observed in the plasmapause region suggests that instabilities play an as yet unassessed role in the erosion/recovery cycle. Electron density interior to a newly formed plasmapause boundary tends to be reduced by factors of up to 3 in association with the erosion process, so that refilling during recovery occurs there as well as in the more deeply depleted plasmatrough region beyond. The number of electrons lost from this interior region, apparently through interchange with the ionosphere, can be of order 50% of the number lost from beyond the new boundary through flow perpendicular to **B.** Evidence has been found that of order 20% of the plasma removed from the main plasmasphere during an erosion event remains in the outer afternoon-dusk magnetosphere for extended periods. It is not yet known whether eroded plasmas entering the Earth's boundary layers make a geophysically important contribution to the plasma sheet. New insights into these and other important questions await both future photon and radio imaging of the plasmasphere from high altitude as well as continued work with certain excellent, as yet only partially exploited, satellite data sets.

1. Introduction

This paper concerns sources and losses of plasma in the Earth's plasmapause region. For decades, conventional wisdom on this subject has been that plasma exterior to a newly established plasmapause is lost from a larger plasmasphere by magnetospheric convection (e.g., Nishida, 1966; Brice, 1967); global-scale flow perpendicular to **B** carries the "removed" plasma generally sunward into the magnetospheric boundary layers. Density recovery in a region thus eroded occurs through refilling from the underlying ionosphere, or flow parallel to **B**.

A familiar form of evidence of loss and recovery is shown in Figure 1, which contains four electron density profiles obtained in 1983 using the sweep frequency receiver (SFR) technique on ISEE (Gurnett and Shaw, 1973). These were near-equatorial passes in the period August 3-12; a typical case spanned

Space Science Reviews **80**: 153–179, 1997.

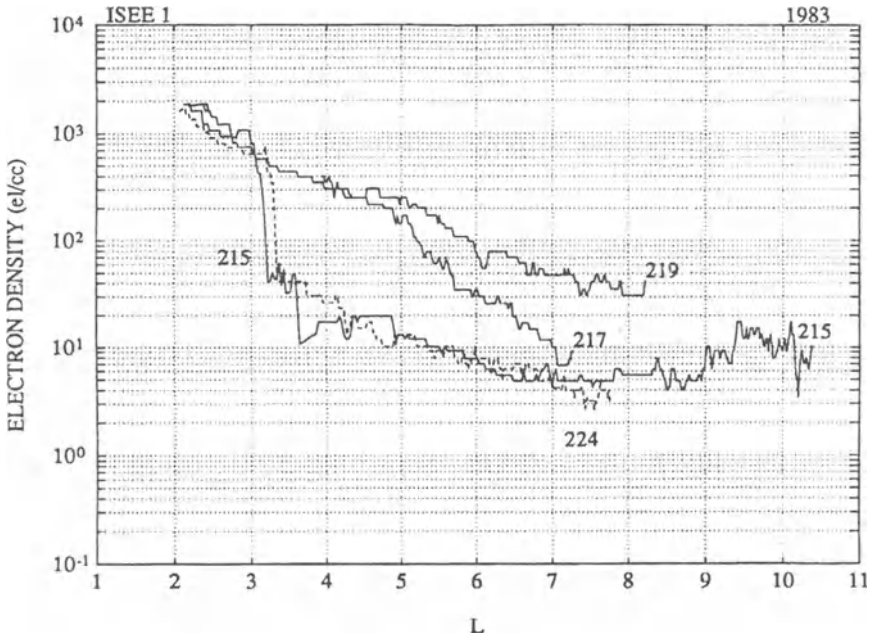

Figure 1. Post-noon electron density profiles obtained from ISEE 1 in 1983 illustrating the effects of plasmapause formation near L=3 (data from days 215 and 224) as well as states of recovery (data from intermediate days). Adapted from Carpenter and Anderson (1992).

several hours from post dawn to post noon. On day 215 a well defined plasmapause was crossed at L~3.2, and the density beyond that point was at typical dayside plasmatrough levels to at least L=8. On the next orbit, ~2 1/2 days later (day 217) the density had reached plasmasphere levels out to at least L=5, and on the following orbit (day 219) the plasmasphere appeared to extend to at least L=8. That such recovery is attributable primarily to refilling from the ionosphere is indicated by Figure 2, which shows profiles of flux tube electron content N_T and equatorial electron density vs L on successive nights in June, 1965. These are smoothed curves based on whistler measurements during an exceptionally long 8-day recovery period following a major magnetic storm on June 15-17 (Park, 1974).

The "conventional wisdom" noted above is at best only a starting point for study of plasma source and loss processes near the plasmapause. In order to understand plasmasphere erosion, we need to know what actually happens in subauroral regions, that is, in the immediate vicinity of the outer plasmasphere, during periods of enhanced convection activity. Our limited experimental evidence indicates that convection activity there is not describable by simple

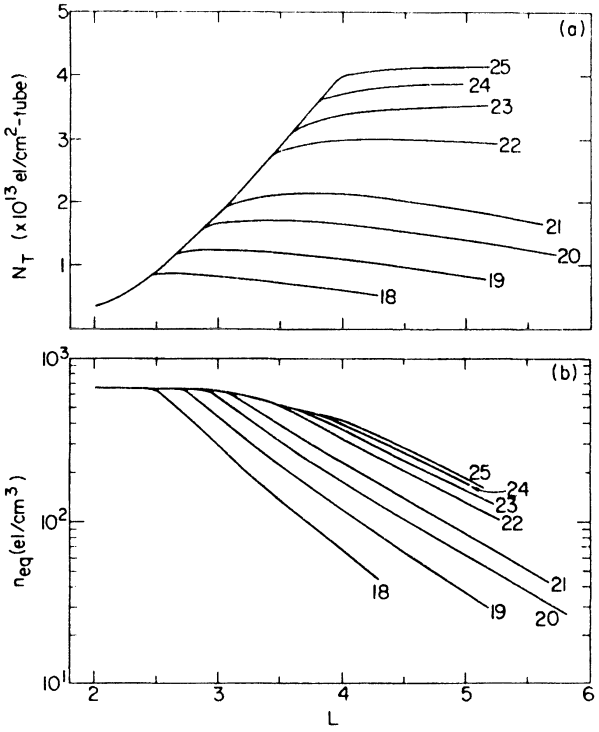

Figure 2. (a) Flux tube electron content profiles illustrating day-to-day refilling of the plasmasphere during an extended quiet period following a magnetic storm. The profiles were obtained by drawing smooth curves through data points from whistlers. The numbers indicate Universal Time days in June, 1965. (b) Equatorial electron concentration profiles corresponding to the tube content data. After Park (1974).

global-scale convection models. Furthermore, the plasmapause region is characterized by the development of irregular density structure, which points to the existence of both MHD turbulence and instabilities (e.g., Lemaire, 1974; Richmond, 1973; Roth, 1975; Huang et al., 1990, LeDocq et al., 1994; Moldwin et al., 1995). There is evidence of significant plasma loss through flow from the plasmasphere into the underlying ionosphere during substorm activity. To further complicate matters, there is evidence that the process of cold plasma transport into the boundary layers is inefficient, and that significant amounts of plasma eroded from the main plasmasphere remain "trapped" for extended periods in the outer afternoon-dusk magnetosphere (Carpenter et al., 1993).

We will now discuss processes involved in plasmasphere erosion/recovery cycles. Emphasis will be upon the erosion phase, rather than the recovery/refilling process.

2. Evidence for Processes Involved in Plasmasphere Erosion

2.1. GLOBAL SCALE CONVECTION

The evidence suggests that while global-scale convection originating in the solar wind dynamo acts as the driver of the loss process in the plasmasphere erosion phase, the pattern of erosion activity that actually results depends upon the cooperation of several processes that are active in the subauroral region.

The evidence for global scale convection includes: 1) data showing an inverse relation between plasmapause radius and measures of magneto-spheric disturbance (e.g., Carpenter, 1967; Chappell et al., 1970a; Carpenter and Anderson, 1992), 2) evidence of an outer region (density trough) in which density levels are substantially below expectations based upon outward density extrapolations from inner regions (Gringauz et al., 1960; Gringauz, 1963; Carpenter, 1963; Angerami and Carpenter, 1966; Carpenter and Anderson, 1992), 3) near-equatorial satellite detection of disturbance-associated sunward plasma flows (e.g., Lennartsson and Reasoner, 1978), including the almost immediate appearance of plasmasphere ions at synchronous orbit (and in earlier than usual local time sectors) following certain SSCs (Elphic et al., 1997; Weiss et al., 1997), 4) appearance of cold He^+, presumably of plasmaspheric origin, within the LLBL or adjacent dayside magnetosphere (Peterson et al., 1982; Fuselier, 1989).

The evidence of global scale convection also includes indications of interplay between the electric field associated with the Earth's rotation and solar-wind induced sunward convection, such as 1) observations of a duskside bulge of the plasmasphere that tends to be detected at earlier local times during periods of increased disturbance and at later times (or not at all) during quieting periods (Carpenter, 1966, 1970; Ho and Carpenter, 1976; Higel and Wu, 1984; Moldwin et al., 1994), and 2) observations suggesting transport by quiet-time corotation into the premidnight sector of narrow plasmasphere extensions or "plumes" created during earlier convection episodes (Ho and Carpenter, 1976; Ober et al., 1997a).

Additional evidence for a combination of sunward and corotational flow is a "day-night" boundary in the plasma trough region (exterior to the plasmasphere) in the dusk sector. At this boundary, reported from GEOS 2 synchronous orbit data by Carpenter et al. (1993), the electron density drops from ~ 10 to ~ 1 electron per cm^3. This change was interpreted as evidence of a separatrix in the combined flow: plasma elements on the westward side of the separatrix had recently been exposed to prolonged dayside upflows, while elements on the eastward side had experienced only nightside conditions of nearly zero or negative upflow. Figure 3 shows an example of GEOS 2

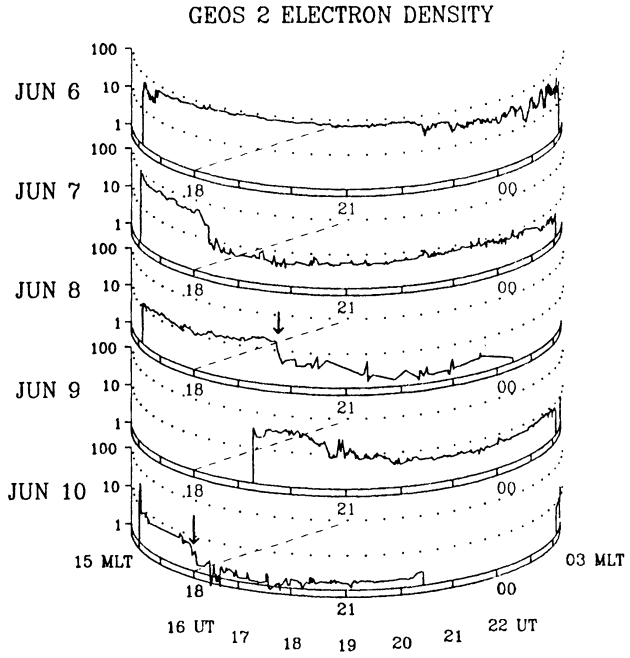

Figure 3. GEOS 2 electron density data for June 6-10, 1982, acquired by radio sounding at synchronous orbit. Log n_e is plotted versus MLT and UT for the ~1600-0200 MLT period. The dotted curves on the stacked perspective plots indicate, respectively, the typical late-dayside plasmatrough electron density level of ~8 per cm^3 and the corresponding saturated or quiet-time plasmasphere level of ~70 electrons per cm^3 at synchronous orbit. From Carpenter et al. (1993).

electron density data near dusk on six successive days in June, 1982. Density levels characteristic of the plasmasphere and of the afternoon plasmatrough are shown dotted. Transitions from daytrough to nighttrough conditions occurred on June 8 and 10, as indicated by arrows. A familiar type of density transition, from plasmasphere bulge region to dayside trough, occurred on June 7 and 9.

The importance of corotation in the combined flow is suggested by two phenomena: 1) delays in the detection of plasmasphere erosion effects on the dayside with respect to their observation on the nightside (Chappell et al., 1971; Décréau et al., 1982) and 2) the tendency of the "main plasmasphere", or innermost observed plasmapause radius at a given longitude, to be nearly circular, with only a slight bulge at dusk (Carpenter et al., 1993). The idea here is that from an observational standpoint there is a main plasmasphere that evolves toward a roughly circular form as nightside erosion effects are transmitted through corotation to the dayside. Meanwhile, the bulge region exists as one or more outlying features either connected to or effectively

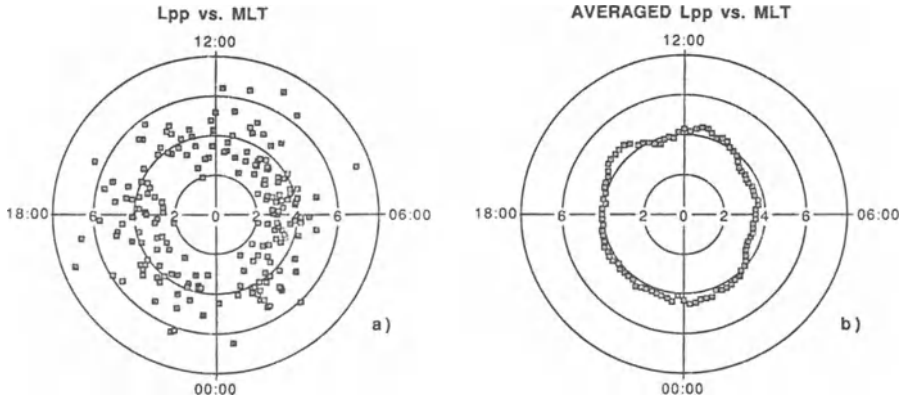

Figure 4. Plots of plasmapause L value versus MLT, illustrating the tendency of the main plasmasphere to become roughly circular in the aftermath of plasmasphere erosion events. (a) Scatter plot of 208 plasmapause crossings identified in ISEE 1 SFR data. (b) Two-hour running average of the data of (a). After Carpenter and Anderson (1992).

detached from the main plasmasphere. Figure 4a shows innermost plasmapause crossing locations vs magnetic local time from approximately two years of ISEE sweep frequency receiver (SFR) data taken along either inbound or outbound near-equatorial passes (Carpenter and Anderson, 1992). These data were limited to cases in which there was a density jump by a factor of 5 or more within $0.5R_E$; hence they tended to represent periods either concurrent with or within tens of hours following multihour episodes of enhanced magnetospheric convection. In Figure 4b, a two hour running mean of the data shows a difference of only about $0.5R_E$ in the dawn and dusk plasmasphere radii.

Figure 5a shows an example of an ISEE profile in the afternoon/dusk sector in which evidence of both the main plasmasphere and the bulge appears (Carpenter et al., 1993). A projection of the orbit is shown by the inset in coordinates of geocentric distance versus MLT. An inner plasmapause appeared at L~3. From L~2.9 to 3.5 there was a trough, at dayside density levels, while an outlying plasmasphere-level feature with plasmapause-like boundaries appeared between L~3.5 and L~4.2. Beyond L=4.2 the density was at nightside trough levels. In this case the authors interpreted the main plasmasphere as being limited to within L=2.9 and suggested that the dense outlying feature was part of the bulge region. That feature may have been connected to the main body of the plasmasphere, but the morphology of the connection was not known.

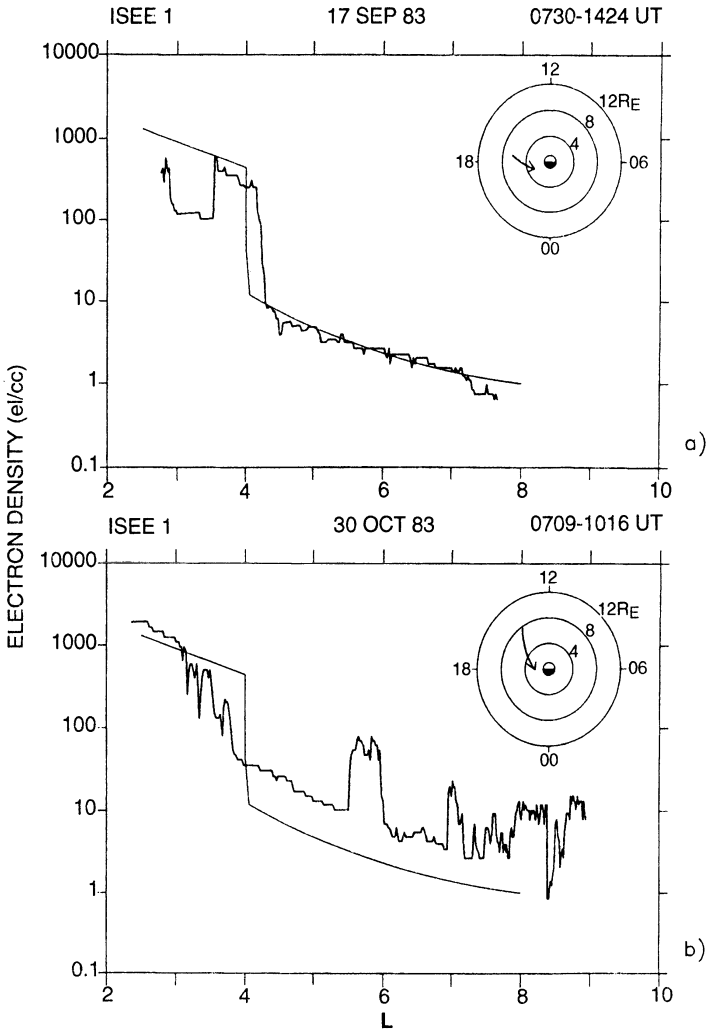

Figure 5. ISEE near-equatorial electron density profiles acquired along orbits in the afternoon-dusk sector. Insets show the geocentric distance of the satellite versus MLT. The accompanying curves are reference profiles from the empirical modeling work of Carpenter and Anderson (1992). The trough levels they show represent nighttime conditions in the aftermath of disturbance. (a) Profile showing evidence of an inner plasmapause, an inner trough inside a high-density feature, and an outer, lower-density trough. (b) Profile showing density structure in the plasmapause region near dusk and in the middle and outer afternoon magnetosphere. From Carpenter et al. (1993).

We now consider processes that appear to act in response to the imposition of high latitude convection electric fields.

2.2. SHIELDING OF THE INNER PLASMASPHERE BY THE ALFVEN LAYER

Shielding of the inner plasmasphere from a global scale dawn-dusk electric field is proposed to occur because of a charge separation electric field that develops at the inner edge of the plasma sheet or Alfven layer as the latter is displaced Earthward (e.g., Block, 1966; Karlson, 1971; Jaggi and Wolf, 1973; Wolf, 1983). For many years shielding has been included in an *ad hoc* manner in global scale electric field models used to study the evolving plasmasphere shape (e.g., Volland, 1973; Stern, 1974). It has appeared in calculations of the response of the coupled magnetosphere-ionosphere system to the imposition of a high latitude electric potential distribution (e.g., Spiro et al., 1981) and in cases in which statistical data on the location of the Alfven layer are employed along with assumptions about the role of that layer in the shielding process (Galperin et al., 1997).

There is evidence for shielding effects; low altitude polar orbiting satellite drift meter and E field measurements suggest that the transition from a low/middle latitude region of corotation to a high latitude convection regime is often relatively abrupt (e.g., Cauffman and Gurnett, 1972; Heppner and Maynard, 1987). Two case studies from the Millstone Hill incoherent scatter radar during disturbed periods showed fast westward flows in the premidnight sector with relatively sharp low latitude limits (Yeh et al., 1991). Similar findings were obtained from AKEBONO at ~10,000 km altitude along subauroral field lines by Okada et al. (1993). However, the connections between shielding and the erosion process are not clear. Prior to midnight, erosion would appear to occur (leaving aside questions of local processes, instabilities, etc.) through predominantly westward flow that erodes the plasmasphere as the Earthward "edge" of the flow, presumably the Alfven layer, is displaced progressively inward to some stormtime limiting configuration, meanwhile leaving the plasmaspheric region interior to the flow essentially free of cross-L inward drifts (e.g., Park, 1978). The apparent ionospheric effects of such a process, albeit observed in the predawn sector, were reported from COSMOS 900, in polar orbit at 480 km, by Afonin et al. (1997), who tracked the stormtime equatorward displacements of a sharp latitudinal front between a subauroral electron temperature enhancement, assumed to mark the ionospheric projection of the plasmapause, and enhanced auroral ionization.

In the postmidnight sector, shielding action appears to be less effective; whistler studies have shown evidence that although high latitude east-west electric fields do not penetrate the plasmasphere efficiently prior to the expansion phase of subsorms, cross-L inward drifts of whistler paths in the

outer postmidnight plasmasphere become sharply enhanced as the expansion phase of a substorm begins (Carpenter et al., 1972: Carpenter and Akasofu, 1972).

2.3. DEVELOPMENT OF NONGLOBAL (MESOSCALE) STRUCTURE IN SUBAURORAL CONVECTION

2.3.1. *The Subauroral Ion Drift (SAID) Phenomenon*

A remarkable feature of plasma flow in the premidnight sector during substorms is the subauroral ion drift, or SAID. At ionospheric heights, SAIDs are observed as fast westward plasma flows at speeds of ~1-4 km-s^{-1}, which usually develop within a narrow, ~1° latitude range near 60° invariant (e.g. Galperin et al., 1974; Smiddy et al., 1977; Anderson et al., 1991, 1993). It has been suggested that these fast drifts are a consequence of field aligned currents established at the inner edge of the intruding plasmasheet (e.g., Anderson et al., 1993). The associated large electric fields develop because of the low Pedersen conductivity in the subauroral region just equatorward of the belt of auroral electron precipitation.

The SAID phenomenon, as well as latitudinally somewhat broader westward surges observed near dusk (e.g., Freeman et al., 1992), occur in the invariant latitude range where new plasmapause boundaries are most frequently created, i.e., L~3.5-4 (Carpenter and Park, 1973). A related phenomenon has been observed near 50° invariant during a great magnetic storm (Yeh et al., 1991) forming a peak at the equatorward edge of a latitudinally broad (~15°) region of westward flow observed over a ~6 h period near dusk by the Millstone Hill radar. It seems clear that such flow effects must be included in dynamic models if we are to understand the plasmasphere erosion process. The flow speed observations imply that a plasma element could be displaced by ~2000 km within a period of 20 min, or several hours in local time. Velocity shear effects could become important; dense regions poleward of the SAID channel might be effectively "detached" from the main plasmasphere. "Biteouts," variously narrow density depressions, have been observed interior to the plasmasphere during recovery periods (Ho and Carpenter, 1976; Horwitz et al., 1990). Recent modeling work by Ober et al. (1997b) suggests that some of these effects may be the result of SAID activity.

2.3.2. *Mesoscale Variations in Plasmasphere Radius*

Although the details of erosion patterns on the nightside are not known, it appears that their effects are detected at other local times through rotation of the distorted plasmasphere with the Earth. Studies from a single station (Angerami and Carpenter, 1966) and longitudinally spaced stations (Smith et al., 1981) have shown evidence of variations in plasmasphere radius of a few

tenths of an Earth radius with spatial scales of ~15-30° longitude. It was suggested that these longitudinal ripples were imposed on the nightside by temporally and spatially structured convection activity and then appeared with rotational delays at the local times of observation.

2.3.3. *Differing Effects of Temporally Isolated and Prolonged Disturbances*
Whistler studies have shown that during temporally isolated substorms, the plasmasphere undergoes distortion by penetrating electric fields but not a significant change in global average radius (Carpenter et al., 1972, 1979). Evidence for the distortion effect comes from observations of compensating outward cross-L drifts immediately following the cross-L inward drifts observed in the postmidnight sector during temporally isolated substorms (Carpenter et al., 1972, 1979; Carpenter and Akasofu, 1972). In contrast, when substorm activity is prolonged, a significant reduction in global average plasmasphere radius occurs. At such times postmidnight cross-L inward drifts observed from whistlers are not followed by compensating outward flows (Carpenter et al., 1972, 1979). The outward flow effect remains to be explained.

2.4. INSTABILITIES AND TURBULENCE

The plasmapause appears to be a "source" region for density structure (e.g., Carpenter et al., 1993). Structure is reported to occur in conjunction with increases in magnetic disturbance activity (Moldwin et al., 1995), and the spatially structured and time varying nightside electric field during substorms may be imagined to support a number of processes, including the development of turbulence in dense plasma regions subject to enhanced flow speeds, shear flow instability in regions of subauroral ion drifts (SAID), gradient drift instability in the region of steep plasmapause density gradients, and gravitational interchange instability in regions where fast eastward drifts occur (Lemaire, 1974, 1975; Lemaire and Gringauz, 1997). However, the role of density irregularities in the loss process is not clear. The presence of irregularities with large peak to valley density ratios interior to, within, and just beyond the region of steep density gradients (e.g., Park and Carpenter, 1970; Oya and Ono, 1987; Koons, 1989; Horwitz et al., 1990; Carpenter et al., 1993; LeDocq and Gurnett, 1994) suggests that dense plasma elements can be detached from or shed by the plasmasphere, perhaps by analogy to the manner in which icebergs are "calved" from a glacier.

Substantial sources of data on irregular structure are now available. Electron density profiles taken along CRRES near-equatorial orbits using the sweep frequency receiver (SFR) radio technique provide a unique source of data on irregularities. LeDocq and Gurnett (1994) found indications of MHD

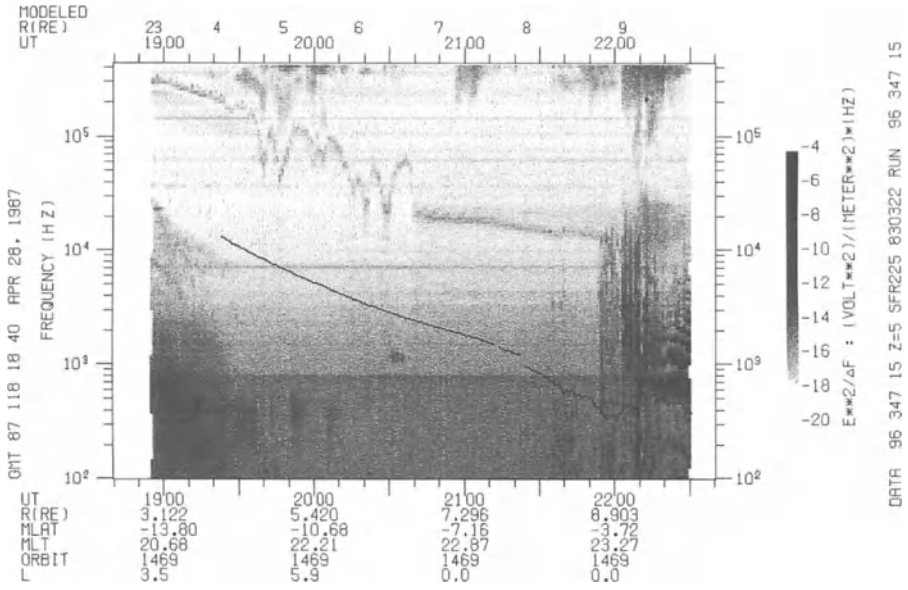

Figure 6. Sweep Frequency Record from ISEE illustrating irregular density structure in the nightside outer plasmasphere and in the plasmapause region. The density structure is revealed in the upper hybrid resonance (UHR) trace which falls at first smoothly from the upper left and then exhibits density variations with peak to valley ratios of ~4 in frequency and hence ~16 in total electron density. The thin dark curve below represents the total magnetic field (electron gyrofrequency) determined from the onboard magnetometer. Courtesy of R. R. Anderson.

turbulence near the plasmapause through Fourier analysis of CRRES time series of electron density data. They also reported evidence of spatially quasiperiodic structures near the plasmapause. From whistlers and ISEE records, Carpenter et al. (1993) reported irregularities inside the recovering, post-erosion-phase plasmasphere within a belt extending inward from the plasmapause. At a given longitude this belt was found to be of order ΔL=1 in width. On occasion it exhibited an abrupt inner limit inside which the profile remained relatively smooth, a limit that may be a measure of the limits of penetration of the stronger components of the nightside subauroral electric field. The major irregular features were often a few tenths of an Earth radius along an ISEE orbit.

The SFR record of Figure 6 shows an example of outer plasmasphere structure observed along an ISEE pass near 23 MLT (courtesy of R. R. Anderson). The density structure is revealed by the upper hybrid resonance (UHR) trace, which falls, at first smoothly, from the upper left and then exhibits variations with peak to valley ratios of ~4 in frequency and hence ~16 in total plasma density. The data were acquired during a very quiet period following a day of mild substorm activity. A single plasmapause location is not defined, but a nightside trough region is clearly present beyond ~6 R_E, as revealed by the dark trace (the plasma frequency) just below a band of diffuse continuum radiation. The thin dark curve superimposed on the lower part of the record represents the total magnetic field (electron gyrofrequency) determined from the onboard magnetometer.

Carpenter et al. (1993) found that in the aftermath of weak magnetic storms, irregular structure appeared in the premidnight sector just beyond and within the region of steep density gradients. A possibly related phenomenon, the occurrence of irregularities in auroral activity at the low-latitude edge of the diffuse aurora, has been discussed by Kelley (1986) as evidence of a shear flow instabilitiy associated with SAIDs.

Instabilities along field lines in the outer afternoon magnetosphere may cause a disconnection between the convection activity at ionospheric heights and that at greater altitudes. Dense plasmas, apparently of plasmaspheric origin, have been observed beyond synchronous orbit, mostly in the afternoon-dusk sector (Chappell et al., 1970b, 1971; Chappell, 1974). Carpenter et al. (1993) found examples whose extent and regularity of occurrence suggested that in the aftermath of a period of enhanced convection they formed a belt of dense plasma several Earth radii across interior to the magnetopause in the afternoon-dusk region. An example of such a case, from ISEE on July 9, 1982, is shown in Figure 5b. It thus appeared that erosion of the plasmasphere is not an efficient process, insofar as the expulsion of eroded plasma from the dayside outer magnetosphere is concerned.

2.5. PLASMA FLOW INTO THE IONOSPHERE

2.5.1. *Dumping of Plasma during Periods of Enhanced Convection*

Whistler data have shown that in addition to reductions in main plasmasphere size during periods of disturbance, there are reductions in electron density by factors ranging from ~1.2 to 3 in the outer part of the newly eroded plasmasphere (e.g., Park and Carpenter, 1970; Carpenter et al., 1993). These reductions tend to occur within a belt that often has a well defined inner limit, coincident with the belt of irregularities noted above. The density decreases in the outer plasmasphere, while not uniform in longitude, appear to involve

amounts of plasma comparable to the amounts eroded from the plasmasphere through transport perpendicular to **B**.

The mechanism of this plasma loss was discussed by Park (1973) in terms of the combined action of a downward component of cross-L flow (inward component of flow at the equator) and draining of plasma along **B**. Park proposed that the downward component of cross-L drift reduces the O^+ concentration at a given altitude. In the altitude range below the critical level, where H^+ is in chemical equilibrium with O^+, this reduction in O^+ must be accompanied by a corresponding reduction in H^+. The H^+ reduction induces the draining along **B** of H^+ from the protonosphere.

A downward component of cross-L drifts may explain some fraction of the loss of plasma beyond a new plasmapause, since inward motions may occur on the nightside both for flux tubes that later remain within the eroded plasmasphere and for some that remain outside the main plasmasphere.

2.5.2. *Dumping of Plasma within and beyond the Plasmapause Region*

Limited evidence points to the possibility that new plasmapause formation is in part a local process involving dumping of plasma into the ionosphere. In their study of well defined plasmapause density profiles, Carpenter and Anderson (1992) found that the scale width of the boundary, or equatorial distance within which the density changed by an order of magnitude, was not a strong function of L value. The scale width would be expected to decrease with decreasing L if the plasmapause were formed strictly as the result of the inward entrainment and consequent steepening of a preexisting boundary region.

There are indications that flux tube electron content may not be preserved during inward convection from the tail region on the nightside, at least in the premidnight sector. Density data reported from GEOS 2 at synchronous orbit by Higel and Wu (1984) indicated that the lowest densities observed, in the ~0.1-1 electrons per cm^3 range, were in the premidnight sector, often following passage through an outlying bulge feature near dusk. Even at ~1 electron per cm^3, such densities would be difficult to explain as the result of electron-content preserving convection of plasma from greater nightside distances. Total densities in the near tail region are probably not below 0.1-1 electrons per cm^3. Assuming inward displacement at the equator from 12 to $6R_E$, we would expect a density increase by roughly the fourth power of tube radius, or a factor of 16, putting the trough level at L~6 above 1 electron per cm^3 and thus above the range in which it is believed to be near the time of plasmapause formation. A possible explanation of the situation is that during inward drift some type of dumping process occurred (in addition to the loss associated with an increase in size of the loss cone as a field tube convects inward). The quantity of electrons dumped would not have to be large, since the inward convecting flux tubes involved are already low in tube electron content.

3. Evidence for Processes Involved in Plasmasphere Recovery

3.1. PLASMASPHERE REFILLING THROUGH INTERCHANGE FLUXES FROM THE IONOSPHERE

Statistical as well as case study data on plasmasphere refilling provide clear evidence of post-disturbance recovery through refilling from the ionosphere. As suggested by Figure 2, this process is distinguished by its slowness, requiring of order days, and by its roughly uniform distribution throughout regions of depleted density, indicated by the changes in the tube content curves of Figure 2a.

Data on changes in plasma density in the trough region provide strong evidence of refilling flows from the ionosphere (e.g., Song et al., 1988). In the immediate aftermath of erosion events a given upward flux can produce very large relative changes in concentration (e.g., Angerami and Carpenter, 1966; Higel and Wu, 1984; Carpenter and Anderson, 1992). From a study of GEOS relaxation sounder data, Song et al. (1988) found that at synchronous orbit the refilling rate varies inversely with the absolute value of the *Dst* index. This dependence was interpreted as being due to changes in the ion composition in the topside ionosphere during disturbed conditions.

There exist a number of in situ measurements of refilling fluxes as well as modeling studies of the effects of "polar wind" flows into closed field line regions of the magnetosphere. These are beyond the scope of the present report.

3.2. CROSS-*L* DIFFUSION

Statistical data suggest that the mean density gradient in the plasmapause region is on average steeper on the nightside than on the dayside (e.g., Chappell, 1972; Nagai et al., 1985; Oya and Ono, 1987; Carpenter and Anderson, 1992). Cross-*L* diffusion, perhaps in association with instabilities, is probably responsible for this difference, in combination with the effects of rotation of plasma regions with the Earth away from nightside locations of plasmapause formation. Horwitz (1983) suggested that cross-*L* diffusion should not be important for "large scale considerations of the plasmasphere density profile." This may partially account for the fact that even during the most extended periods of quiet, the radial plasma density profile at the equator does not approach a hydrostatic equilibrium distribution, but instead appears dominated by boundary conditions at the ionospheric endpoints of flux tubes and by plasma interchange along **B.**

3.3. GLOBAL SCALE CONVECTION DURING RECOVERY

Some accretion of plasma may occur during periods of quieting when plasma in the bulge region begins to rotate with the Earth. In cases of tail-like features, simulations predict an inward spiralling effect, such that the plasma involved "wraps around" the main plasmasphere (e.g., Chen and Wolf, 1972; Kurita and Hayakawa, 1985). Evidence of the tendency of tail-like bulge features to rotate with the Earth has been found from whistlers (Carpenter, 1970; Ho and Carpenter, 1976) and in the results from syn-chronous orbit reported by Higel and Wu (1984) and Moldwin et al. (1994).

4. Numerical Estimates of Losses and Recovery Rates

4.1. LOSSES FROM OUTSIDE A NEW PLASMAPAUSE

The number of electrons lost from outside a newly established plasmapause boundary is of order $1x10^{31}$. This estimate is based upon removal of essentially all plasma in a belt extending globally from L=3.5 to L=5 and upon the assumption that inside L=5 the pre-disturbance plasmasphere flux tube electron content between 1000 km altitude and the equator is ~$5x10^{13}$ electrons in a field tube of 1 cm^2 cross section at 1000 km (e.g. Park, 1974). Elphic et al. (1997) have obtained a similar estimate based upon encounters with dense plasma at synchronous orbit during periods of enhanced convection activity.

It seems likely that most of this loss occurs through transport perpendicular to **B** by convection (however structured that convection may be). Some of the strongest evidence for this comes from observations, noted above, of sunward and outward displacements of dense plasma. The loss through transport perpendicular to **B** may be enhanced by instabilities to an extent that is not yet known. As noted above, a fraction of the overall loss beyond a newly formed plasmapause may be due to the downward flow of plasma into the ionosphere under conditions of inward cross-L motion.

To a limited extent, the losses from beyond a new plasmapause involve a redistribution within the magnetosphere. Based upon ISEE data, Carpenter et al. (1993) estimated that roughly 20% of the plasma convected away from the main plasmasphere during a weak magnetic storm remained trapped within the outer afternoon-dusk magnetosphere. Elphic et al. (1997) suggest that such long residence times might be explained by an outer afternoon region of relatively low electric potential gradient.

4.2. LOSSES FROM INSIDE A NEW PLASMAPAUSE

The number of electrons lost from within a newly eroded plasmasphere is substantial, in the neighborhood of 50% of the amount lost from outside. Some loss tends to occur at all longitudes, but the amounts of loss are not uniform. In some regions there may be a reduction by only of order 30%, while in others the density may be reduced from quiet time levels by a factor of 2 or in the most severe cases, 3.

These losses from within an eroded plasmasphere are believed to involve transport downward into the ionosphere. In one documented case, noted earlier, the inferred downward electron flux was ~$1x10^9$ per cm^2 per second during a several hour period (Park, 1973). This was believed to occur, as noted above, by a combination of flow transverse and parallel to **B**.

4.3. GAINS DUE TO REFILLING FROM THE IONOSPHERE

Here we emphasize day-to-day changes in total density or tube electron content in the magnetosphere. A pioneering whistler case study by Park (1974), summarized in Figure 2, shows how the plasmatrough region recovered from the magnetic storm of June 15-17, 1965 over a multiday interval of quieting. Details near the plasmapause, which was originally near L=2.5, are not shown, nor are what were probably the earliest stages of recovery. The data of Figure 2a represent total electron content between ~1000 km and the equator in a flux tube with ~1 cm^2 cross section at 1000 km . They show a net daily gain of $5x10^{12}$ electrons until the plasmasphere appeared to reach equilibrium with the underlying ionosphere. From earlier work on this case, Park (1970) had inferred daytime upward electron fluxes of ~$3x10^8$ per cm^2 per second and nighttime downward fluxes of ~$1.5x10^8$ in the refilling region. As illustrated in Figure 2a, the recovery time varied with L value, ranging from ~1 day at L=2.5 to ~8 days at L=4. Thus there tended to be two distinct regions, with a time variable boundary between an inner "saturated" plasmasphere and an outer "unsaturated" one.

Day to day changes in equatorial density have been measured that are consistent with these numbers. Carpenter et al. (1993), from a combination of satellite and ground whistler data, observed average increases of ~80 electrons per cm^3 per day at L~4.5 near the equator during a several day recovery period following a weak magnetic storm.

Song et al. (1988), as noted above, found evidence that at synchronous orbit the refilling rate varies inversely with the absolute value of the *Dst* index. Electron density was found to increase within the range ~10 to 25 per cm^3 per day. The corresponding refilling time constant (to a saturation electron density

level of 70.5 per cm^3) ranged from ~3 days to more than 7 days, depending on the *Dst* index.

The depleted outer plasmasphere has been found to recover at rates that are roughly comparable to those in the refilling plasmatrough region (e.g., Tarcsai, 1985; Saxton and Smith, 1989). The reported persistence of such flows well into quiet periods, coupled with evidence that the quiet time equatorial radial profile falls off more steeply than would a hydrostatic distribution, led to a suggestion by Lemaire and Schunk (1992, 1994) that there is a slow plasmaspheric wind transporting plasma by interchange motion from the inner toward the outer plasmasphere.

4.4. GAINS DUE TO CROSS-*L* OUTWARD MOTIONS

In the early stages of a convection episode, cross-*L* outward moving plasma on the dayside should move some ionospheric plasma upward, effectively increasing the plasmasphere electron content. The magnitude of this effect is not known.

5. Balance Between Source and Loss Processes

It seems clear that in terms of erosion/recovery cycles, losses predominate during the erosion phase, which is of order a few hours to tens of hours in duration. Replenishment processes dominate during the middle and later parts of the recovery phase, which is typically several days in duration. To go beyond this simple picture, with questions pertinent to the comparative effects of specific loss and replenishment processes, requires a level of understanding that has yet to be reached. For example, what is the interplay between processes of loss and recovery during a "noisy" recovery cycle, when significant erosion effects have already occurred but substorm activity continues at reduced levels, often for days? This is a highly probable state of the magnetosphere, but we know little of such interplay observationally or from theory.

6. Gaps in Knowledge and Understanding

6.1. BACKGROUND

Gaps in knowledge about the plasmapause/plasmasphere are in part a consequence of rapid progress in that subject area in the 1960 discovery era. By 1967, a year when the plasmasphere had only begun to be explored by spacecraft, understanding of the processes giving rise to the plasmapause

phenomenon appeared to be substantially complete. Some 30 years later, in 1997, many in the community remain with that impression and are largely unaware of the accumulated evidence and arguments to the contrary that have been offered over the years (e.g., Dungey, 1967; Carpenter, 1970; Chen and Wolf, 1972; Lemaire, 1975, 1985; Morfill, 1978; Carpenter et al., 1993; Moldwin et al., 1994; Carpenter, 1995).

Gaps are also attributable to limitations in the number and nature of pertinent investigations in the years since the discovery phase. Observational work has not been matched to the huge size and dynamic nature of the plasmasphere. The available measurements permit us a number of inferences about plasmapause/plasmasphere dynamics but are largely anecdotal, non-uniformly distributed in local time, and unrepresentative of conditions during erosion activity. Thus they have not provided direct information about the process of plasmasphere erosion and new plasmapause formation. Since the outer plasmasphere is located at subauroral latitudes, its modification must occur near the inner limits of penetration of hot plasma sheet plasmas. Changes in the plasmasphere by processes associated with the hot/cold plasma interface probably take place on substorm time scales and for this reason alone would be expected to be observationally elusive.

6.2. PLASMASPHERE EROSION AND PLASMAPAUSE FORMATION

6.2.1. *Plasmapause Formation*

Lacking direct observations of the plasmapause formation process, we do not know how that process is distributed in space or over what time scales a new profile develops. We wish to know how the density profile evolves with time during plasmapause formation, and whether the process includes local dumping of plasma into the ionosphere as well as motion perpendicular to **B**. We wish to know what aspects of the hot/cold plasma interface may be involved and how formation may depend upon the properties of the underlying ionosphere. We do not know to what extent the physics of the process depend upon the intensity of the high latitude convection field. Is plasmapause formation always underway at some location? How do its physics depend upon the starting conditions on the density profile? In particular, what happens to the process during periods of quieting? We need to place plasmapause formation within the context of substorm activity and hence within the full range of high-to-middle latitude disturbance phenomena of which it is a part.

6.2.2. *Plasmasphere Erosion*

As in the case of plasmapause formation, we see various effects of plasmasphere erosion through anecdotal data, without having direct global scale or mesoscale observations of the erosion process itself. Thus we often see

the density profile of an eroded plasmasphere as well as outlying dense features in data taken along individual satellite orbits, but do not know how some original plasmasphere configuration evolved so as to appear this way. We do not know in what geophysically important ways the ionosphere and overlying regions may be coupled during the erosion process. Thermal coupling appears to be particularly important, as emphasized by Afonin et al. (1997), who showed how the subauroral ionospheric electron temperature enhancement, traditionally associated with the plasmapause (e.g., Brace and Theis, 1974), can exhibit a surprisingy steep falloff (~0.1°) on its poleward side and be displaced progressively equatorward during a magnetically disturbed period.

What kind of temporal and spatial structure develops in the subauroral electric field during periods of enhanced high latitude convection? How does a process of plasmapause formation interplay with corotation or instabilities to produce a plasmasphere boundary on a global scale? What aspects of the formation process explain longitudinal variations in plasmasphere radius? In what sense is the process of plasmasphere erosion different from that of plasmapause formation?

Numerical modeling of plasmasphere dynamics using global scale electric field models has been successful in simulating certain statistical aspects of plasmasphere observations (e.g., Gallagher et al., 1995). Recently, stormtime changes in dense plasma encounters at synchronous orbit by multiple satellites have been successfully simulated using models that increasingly employ observed or derived geophysical quantities as inputs (e.g., Weiss et al., 1997). Furthermore, Ober et al. (1997b) have shown how density troughs in the duskside bulge region can develop as a consequence of SAID-like flows. Serious efforts to understand plasmasphere erosion are clearly being made, although we are still in the early stages of this effort.

6.2.3. *Instabilities and Turbulence*

Available data on instabilities show us various types of plasma structure but do not tell us much about the conditions under which the structure develops. We don't know when, where, and under what geophysical conditions instabilities occur and what role they may play in the shedding of plasma by the plasmasphere. Where and when does MHD turbulence develop? We wish to know the extent of the affected regions in longitude. We need to know how instabilities may be driven, whether by velocity shear flow or by other gradients in the plasma parameters. How does the structure that appears in the outer plasmasphere differ in origin from the structure that is seen in the region of steep density gradients? We wish to know how the development of irregular structure in the outer plasmasphere interplays with processes involved in plasma dumping into the ionosphere and with the penetration of the

plasmasphere by perturbing convection electric fields. What accounts for the sharp inner limit on irregular structure observed in the outer plasmasphere?

6.2.4. *Density Loss through Plasma Flow into the Ionosphere*
We do not know where and when plasma is dumped into the ionosphere during periods of erosion activity. What are the geophysical consequences for the ionosphere of any such dumping? To what extent are changes in ionospheric boundary conditions involved, as well as electric fields parallel to **B** and increases in the size of the loss cone during cross-L inward drifts? How extensive in longitude are the affected regions? Is the loss process ongoing during the early stages of recovery, or is it primarily a phenomenon of the principal erosion phase?

6.2.5. *Fate of Entrained Dense Plasmas*
What happens to plasmasphere plasma carried sunward and outward from the main plasmasphere? Under what conditions are such plasmas detached from or continuous with the main plasmasphere? What fraction of the plasma eroded from the main plasmasphere enters the magnetosphere boundary layers? It was proposed as early as 1962 (Carpenter, 1962), and later in more detail (Nishida, 1966; Brice, 1967) that plasma in the region beyond the plasmapause circulates along non dipole-enclosing paths (e.g., Axford and Hines, 1961) that extend into the geotail region or into regions of tailward flow near the magnetopause. The idea that recently eroded plasmasphere plasma could circulate into the geotail region has been discussed by Freeman et al. (1977), and recently Elphic et al. (1997) and Ober et al. (1997c) have suggested that such plasma, following entry into the LLBL and energization to ~1-2 keV, may contribute substantially to the population of the stormtime plasma sheet. Further study of this issue is clearly needed, as is study of the heating to suprathermal (~5-50 eV) energies of plasma in the vicinity of the plasmapause (e.g., Gurnett, 1976; Horwitz et al., 1981; Olsen et al., 1987).

What is the geophysical significance of regions of dense plasma that remain near the outer dayside magnetopause in the aftermath of erosion activity? What effects, if any, do they have on particle scattering and precipitation due to resonant wave-particle interactions? Is there a disconnection at high invariant latitudes on the dayside between the low altitude convection system and plasma flow at high altitudes? Or can such long residence times be well explained in terms of regions of small total electric field, as suggested by Elphic et al. (1997)?

6.2.6. *Plasmasphere Refilling*
What are the starting conditions for upflows of plasma from the ionosphere into the trough region beyond a newly formed plasmasphere? What processes

govern the interchange flows of plasma throughout the period from plasmapause formation into extended quiet? To what extent is the refilling rate dependent upon the disturbance level? What are the principal factors governing the observed quiet time equatorial density profile and its failure to approach a hydrostatic distribution? What role does dayside refilling play in the distribution and density profiles of outlying dense plasmas in the afternoon-dusk sector?

7. Ways to Fill Gaps in Knowledge and Understanding

7.1. GLOBAL AND MESOSCALE PROBLEMS

Only with global scale imaging on multihour time scales will we be able to address major questions posed above about the conditions of plasmapause formation and the evolving structure of the main plasmasphere during the erosion process. Photon imaging (e.g., Frank et al., 1994) from the outer magnetosphere would be particularly helpful in obtaining global views of the evolving plasmasphere shape and in placing changes in plasmasphere morphology within the context of auroral activity and hot plasma dynamics. Photon imaging may also supply at least coarse infomation on the spatial and temporal conditions of plasmapause formation.

Radio sounding (e.g., Calvert et al., 1995) from high altitude would permit remote studies of plasmapause formation and plasmasphere evolution within the changing radio view of the sounder, and also supplement them with detailed measurements along the satellite orbit as the sounder penetrates the boundaries it has recently sounded or will subsequently probe. Radio sounding offers the possibility of comparing plasmapause dynamics with information on magnetopause location and structure.

Radio tomography, using multiple satellites, is attractive as a way of studying the development of irregular plasma structure and obtaining information on mesoscale features such as regions of dense plasma trapped in the outer dayside magnetosphere.

Modelers can contribute toward understanding of the physics of the erosion process by continuing to develop and apply more realistic models of the subauroral electric field.

7.2. MICROSCALE PROCESSES

For study of the physics of plasmapause formation and associated plasmasphere erosion effects, multiinstrument methods such as those currently employed for study of the auroral region need to be exploited. By use of such

methods with existing or future data sets, it should be possible to investigate small scale relationships among hot plasmas, electric fields, field aligned currents, local plasma density, and plasma bulk flows, and to make rendezvous comparisons between satellites at different altitudes. Those cases representative of the elusive plasmapause formation process may be few in number and should be patiently sought. Multiinstrument data from satellites should be used to study the physical processes at the hot/cold plasma interface. The knowledge thus gained can be used to interpret data on erosion activity and plasmapause formation obtained by the global and mesoscale imaging techniques. Much variability in erosion phenomena may be expected; the complexity in this area should reflect that already found from imaging of substorm activity.

Instruments designed to study the auroral regions often are not sensitive to or designed for conditions in the subauroral region in the immediate vicinity of the plasmapause. Future satellite missions should be designed with attention to this problem.

Incoherent scatter measurements from the ground near L=3 as well as bottomside sounding experiments in the L=3-4 range should be conducted with a view to describing low altitude changes that occur during plasmapause formation.

8. Differences in Views

Major differences in perspective on plasma sources and losses in the plasmapause region exist between those who actively study the properties of the region and those who do not. The latter are inclined to dismiss the region and its dynamics as being relatively well understood or perhaps of minor geophysical importance. Meanwhile the former find themselves in what might still be considered a discovery phase, constantly challenged by new findings that reveal how little is in fact known, particularly about the erosion of the plasmasphere and the fate of eroded plasmas.

As future satellite photon and radio imaging missions are developed, one of their principal targets will be the plasmasphere. In this new era we may expect discussion and interpretation of the region to become more widespread and to be based upon increased community awareness of the region's observed properties. Until that time much can be done to reduce the present differences in perspective through study and interpretation of existing data.

References

Afonin, V. V., Bassolo, V. S., Smibauer, Y. and Lemaire, J.: 1997, 'Motion and erosion of the nightside plasmapause region and of the associated subauroral electron temperature enhancement: COSMOS-900 observations',*J. Geophys. Res.* **102**, 2093.

Anderson, P. C., Heelis, R. A. and Hanson, W. B.: 1991, 'The ionospheric signatures of rapid subauroral ion drifts', *J. Geophys. Res.* **96**, 5785.

Anderson, P. C., Hanson, W. B., Heelis, R. A., Craven, J. D., Baker, D. N. and Frank, L. A.: 1993, 'A proposed production model of rapid subauroral ion drifts and their relationship to substorm evolution', *J. Geophys. Res.* **98**, 6069.

Angerami, J. J. and Carpenter, D. L.: 1966, 'Whistler studies of the plasmapause in the magnetosphere, 2, Equatorial density and total tube electron content near the knee in magnetospheric ionization', *J. Geophys. Res.* **71**, 711.

Axford, W. I. and Hines, C. O.: 1961, 'A unifying theory of high-latitude geophysical phenomena and geomagnetic storms', *Canad. J. Phys.* **39**, 1433.

Block, L. P.: 1966, 'On the distribution of electric fields in the magnetosphere', *J. Geophys. Res.* **71**, 855.

Brace, L. H. and Theis, R. F.: 1974, 'The behavior of the plasmapause at midlatitudes: ISIS 1 Langmuir probe measurements', *J. Geophys. Res.* **79**, 1871.

Brice, N. M.: 1967, 'Bulk motion of the magnetosphere', *J. Geophys. Res.* **72**, 5193.

Calvert, W. et al.: 1995, 'The feasibility of radio sounding in the magnetosphere', *Radiosci.* **30**, 1577.

Carpenter, D. L.: 1962, 'The magnetosphere during magnetic storms; a whistler analysis', Ph.D. thesis, Stanford University.

Carpenter, D. L.: 1963, 'Whistler evidence of a 'knee' in the magnetospheric ionization density profile', *J. Geophys. Res.* **68**, 1675.

Carpenter, D. L.: 1966, 'Whistler studies of the plasmapause in the magnetosphere, 1, Temporal variations in the position of the knee and some evidence on plasma motions near the knee', *J. Geophys. Res.* **71**, 693.

Carpenter, D. L.: 1967, 'Relations between the dawn minimum in the equatorial radius of the plasmapause and Dst, Kp and the local K at Byrd Station', *J. Geophys. Res.* **72**, 2969.

Carpenter, D. L.: 1970, 'Whistler evidence of the dynamic behavior of the duskside bulge in the plasmasphere', *J. Geophys. Res.* **75**, 3837.

Carpenter, D. L.: 1995, 'Earth's plasmasphere awaits rediscovery', *Eos, trans. AGU,* **76**, 89.

Carpenter, D. L. and Akasofu, S.-I.: 1972, 'Two substorm studies of relations between westward electric fields in the outer plasmasphere, auroral activity, and geomagnetic perturbations', *J. Geophys. Res.* **77**, 6854.

Carpenter, D. L. and Anderson, R. R.: 1992, 'An ISEE/whistler model of equatorial electron density in the magnetosphere', *J. Geophys. Res.* **97**, 1097.

Carpenter, D. L. and Park, C. G.: 1973, 'On what ionosphere workers should know about the plasmapause-plasmasphere', *Rev. Geophys. Space Phys.* **11**, 133.

Carpenter, D. L., Stone, K., Siren, J. C. and Crystal, T. L.: 1972, 'Magnetospheric electric fields deduced from drifting whistler paths', *J. Geophys. Res.* **77**, 2819.

Carpenter, D. L., Park, C. G. and Miller, T. W.: 1979, 'A model of substorm electric fields deduced from drifting whistler paths', *J. Geophys. Res.* **84**, 6559.

Carpenter, D. L., Giles, B. L., Chappell, C. R., Décréau, P. M. E., Anderson, R. R., Persoon, A. M., Smith, A. J., Corcuff, Y. and Canu, P.: 1993, 'Plasmasphere dynamics in the dusk-side bulge region: a new look at an old topic', *J. Geophys. Res.* **98**, 19,243.

Cauffman, D. P. and Gurnett, D. A.: 1972, 'Satellite measusrements of high latitude convection electric fields', *Space Sci. Rev.* **13**, 369.

Chappell, C. R.: 1972, 'Recent satellite measuremenets of the morphology and dynamics of the plasmasphere', *Rev. Geophys. Space Phys.* **10**, 951.

Chappell, C. R.: 1974, 'Detached plasma regions in the magnetosphere', *J. Geophys. Res.* **79**, 1861.

Chappell, C. R., Harris, K. K. and Sharp, G. W.: 1970a, 'A study of the influence of magnetic activity on the location of the plasmapause as measured by OGO 5', *J. Geophys. Res.* **75**, 50.

Chappell, C. R., Harris, K. K. and Sharp, G. W.: 1970b, 'The morphology of the bulge region of the plasmasphere', *J. Geophys. Res.* **75**, 3848.

Chappell, C. R., Harris, K. K. and Sharp, G. W.: 1971, 'The dayside of the plasmasphere', *J. Geophys. Res.* **76**, 7632.

Chen, A. J. and Wolf, R. A.: 1972, 'Effects on the plasmasphere of time-varying convection electric fields', *Plan. Space Sci.* **20**, 483.

Décréau, P. M. E., Beghin, C. and Parrot, M.: 1982, 'Global characteristics of the cold plasma in the equatorial plasmapause region as deduced from the GEOS 1 mutual impedance probe', *J. Geophys. Res.* **87**, 695.

Dungey, J. W.: 'The theory of the quiet magneto-sphere', in J. King and W. Newman (eds.), *Proceedings of the 1966 Symposium on Solar-Terrestrial Physics, Belgrade,* Academic Press, Inc., London and New York, pp. 91-106.

Elphic, R. C., Weiss, L. A., Thomsen, M. F. and McComas, D. J.: 1996 "Evolution of plasmaspheric ions at geosynchronous orbit during times of high geomagnetic activity', *Geophys. Res. Lett.* **23**, 2189.

Elphic, R. C., Thomsen, M. F. and Borovsky, J. E.: 1997, 'The fate of the outer plasmasphere', *Geophys. Res. Lett.* **24**, 365.

Frank, L. A. et al.: 1994, 'Imagers for the magnetosphere, aurora, and plasmasphere', *Optical Eng.,* **33(2)**, 391.

Freeman, J. W., Hills, H. K., Hill, T. W. and Reiff, P. H.: 1977, 'Heavy ion circulation in the earth's magnetosphere', *Geophys. Res. Lett.* **4**, 195.

Freeman, M. P., Southwood, D. J., Lester, M., Yeoman, T. K. and Reeves, G. D.: 1992, 'Substorm-associated radar auroral surges', *J. Geophys. Res.* **97**, 12,173.

Fuselier, S. A., Peterson, W. K., Klumpar, D. M. and Shelley, E. G.: 1989, 'Entry and acceleration of He^+ in the low latitude boundary layer, *Geophys. Res. Lett.* **16**, 751.

Gallagher, D. L., Craven, P. D.., Comfort, R. H. and Moore, T. E.: 1995, 'On the azimuthal variation of core plasma in the equatorial magnetosphere', *J. Geophys. Res.* **100**, 23,597.

Galperin, Y. I., Khalipov, V. L. and Zosimova, A. G.: 1974, 'Plasma convection in the polar ionosphere', *Ann Geophys.* **30**, 1.

Galperin, Y. I., Soloviev, V. S., Torkar, K., Foster, J. C. and Veselov, M. V.: 1997, 'Predicting plasmaspheric radial density profiles', *J. Geophys. Res.* **102**, 2079.

Gurnett, D. A.: 1976, 'Plasma wave interactions with energetic ions near the magnetic equator', *J. Geophys. Res.* **81**, 2765.

Gurnett, D. A. and Shaw, R. R.: 1973, 'Electromagnetic radiation trapped in the magneto-sphere above the plasma frequency', *J. Geophys. Res.* **78**, 8136.

Gringauz, K. I.: 1963, 'The structure of the ionized gas envelope of earth from direct measurements in the USSR of local charged particle concentrations', *Planet. Space Sci.* **11**, 281.

Gringauz, K. I., Kurt, V. G., Moroz, V. I. and Shklovsky, I. S.: 1960, 'Results of observations of charged particles up to R=100000 km with the aid of charged particle traps on Soviet cosmic rockets', *Astron. Zhurnal* **4**, 716.

Heppner, J. P. and Maynard, N. C.: 1987, 'Empirical high latitude electric field models', *J. Geophys. Res.* **92**, 4467.

Higel, B. and Wu, L.: 1984, 'Electron density and plasmapause characteristics at 6.6 R_E: A statistical study of the GEOS 2 relaxation sounder data',*J. Geophys. Res.* **89**, 1583.

Ho, D. and Carpenter, D. L.: 1976, 'Outlying plasmasphere structure detected by whistlers', *Planet. Space Sci.* **24**, 987.

Horwitz, J. L.: 1983, 'Plasmapause diffusion',*J. Geophys. Res.* **88**, 4950.

Horwitz, J. L., Baugher, C. R., Chappell, C. R., Shelley, E. G. and Young, D. T.: 1981, 'Pancake pitch angle distributions in warm ions observed with ISEE 1',*J. Geophys. Res.* **86**, 3311.

Horwitz, J. L., Comfort, R. H. and Chappell, C. R.: 1990, 'A statistical characterization of plasmasphere density structure and boundary locations',*J. Geophys. Res.* **95**, 7937.

Huang, T. S., Wolf, R. A. and Hill, T. W.: 1990, 'Interchange instability of the Earth's plasmapause',*J. Geophys. Res.* **95**, 17,187.

Jaggi, R. K. and Wolf, R. A.: 1973, 'Self-consistent calculation of the motion of a sheet of ions in the magnetosphere',*J. Geophys. Res.* **78**, 2852.

Karlson, E. T..: 1971, 'Plasma flow in the magnetosphere. I. A two-dimensional model of stationary flow',*Cosmic Electrodynamics* **1**, 474.

Kelley, M. C.: 1986, 'Intense sheared flow as the origin of large-scale undulations of the edge of the diffuse aurora',*J. Geophys. Res.* **91**, 3225.

Koons, H. C.: 1989, 'Observations of large-amplitude, whistler mode wave ducts in the outer plasmasphere',*J. Geophys. Res.* **94**, 15,393.

Kurita, K. and Hayakawa, M.: 1985, 'Evaluation of the effectiveness of theoretical model calculation in determining the plasmapause structure',*J. Geophys.* **57**, 130.

LeDocq, M. J., Gurnett, D. A. and Anderson, R. R.: 1994, 'Electron number density fluctua-tions near the plasmapause observed by the CRRES spacecraft',*J. Geophys. Res.* **99**, 23,661.

Lemaire, J.: 1974, 'The "Roche-limit" of ionospheric plasma and formation of the plasma-pause', *Planet. Space Sci.* **22**, 757.

Lemaire, J.: 1975, 'The mechanisms of formation of the plasmapause',*Ann. Géophys.* **31**,175.

Lemaire, J.: 1985, 'Frontiers of the plasmasphere', Thèse d'agrégation de l'enseignement supérieur, Editions Cabay, Louvain-la-Neuve, Belgium.

Lemaire, J. and Gringauz, K. I.: 1997, *The Earth's Plasmasphere,* Cambridge University Press (in press).

Lemaire, J. and Schunk, R. W.: 1992, 'Plasmaspheric wind',*J. Atmos. Terr. Phys.* **54**, 467.

Lemaire, J. and Schunk, R. W.: 1994, 'Plasmasphere convection with non-closed streamlines', *J. Atmos. Terr. Phys.* **56**, 1629.

Lennartsson, W. and Reasoner, D. L.: 1978, 'Low-energy plasma observations at synchronous orbit', *J. Geophys. Res.* **83**, 2145.

Moldwin, M. B., Thomsen, M. G., Bame, S. J., McComas, D. J. and Moore, K. R.: 1994, 'An examination of the structure and dynamics of the outer plasmasphere using multiple geosynchronous satellites', *J. Geophys. Res.* **99**, 11,475.

Moldwin, M. B. Thomsen, M. F., Bame, S J., McComas, D. J. and Reeves, G. D.: 1995, 'The fine scale structure of the outer plasmasphere', *J. Geophys. Res.* **100**, 8021.

Morfill, G. E.: 1978, 'A review of selected topics in magnetospheric physics,' *Rep. Prog. Phys.* **41**, 303.

Nagai, T., Horwitz, J. L., Anderson, R. R. and Chappell, C. R.: 1985, 'Structure of the plasmapause from ISEE 1 low energy ion and plasma wave observations', *J. Geophys. Res.* **90**, 6622.

Nishida, A.: 1966, 'Formation of plasmapause, or magnetospheric plasma knee, by the combined action of magnetospheric convection and plasma escape from the tail', *J. Geophys. Res.* **71**, 5669.

Ober, D. M., Horwitz, J. L., Thomsen, M. F., Elphic, R. C., McComas, D. J., Belian, R. D. and Moldwin, M. B.: 1997a, 'Premidnight plasmaspheric "plumes"', *J. Geophys. Res.* **102**, in press.

Ober, D. M., Horwitz, J. L. and Gallagher, D. L.: 1997b, 'Formation of density troughs embedded in the outer plasmasphere by subauroral ion drifts (SAID)', *J. Geophys. Res.* **102**, in press.

Ober, D. M., Horwitz, J. L. and Gallagher, D. L.: 1997c, 'Convection of plasmaspheric plasma into the outer magnetosphere and boundary layer region: Initial results', submitted to *Encounters between global observations and models in the ISTP era,* American Geophysical Union, Washington, D. C.

Okada, T., Hayakawa, H., Tsuruda, K., Nishida, A. and Matsuoka, A.: 1993, 'EXOS D observations of enhanced electric fields during the giant magnetic storm in March 1989', *J. Geophys. Res.* **98**, 15,417.

Olsen, R. C., Shawhan, S. D., Gallagher, D. L., Green, J. L., Chappell, C. R. and Anderson, R. R.: 1987, 'Plasma observations at the magnetic equator', *J. Geophys. Res.* **92**, 2385.

Oya, H. and Ono, T.: 1987, 'Stimulation of plasma waves in the magnetosphere using satellite JIKIKEN (EXOS-B) Part II: Plasma density across the plasmapause', *J. Geomag & Geoel.* **39**, 591.

Park, C. G.: 1970, 'Whistler observations of the interchange of ionization between the ionosphere and the protonosphere', *J. Geophys. Res.* **75**, 4249.

Park, C. G.: 1973, 'Whistler observations of the depletion of the plasmasphere during a magnetospheric substorm', *J. Geophys. Res.* **78**, 672.

Park, C. G.: 1974, 'Some features of plasma distribution in the plasmasphere deduced from Antarctic whistlers', *J. Geophys. Res.* **79**, 169.

Park, C. G.: 1978, 'Whistler observations of substorm electric fields in the nightside plasmasphere', *J. Geophys. Res.* **83**, 5773.

Park, C. G. and Carpenter, D. L.: 1970, 'Whistler evidence of large-scale electron density irregularities in the plasmasphere', *J. Geophys. Res.* **75**, 3825.

Peterson, W. K., Shelley, E. G., Haerendel, G. and Paschmann, G.: 1982, 'Energetic ion composition in the subsolar magnetopause and boundary layer', *J. Geophys. Res.* **87**, 2139.

Richmond, A. D.: 1973, 'Self-induced motions of thermal plasma in the magnetosphere and the stability of the plasmapause', *Radio Sci.* **8**, 1019.

Roth, M.: 1975, 'The plasmapause as a plasma sheath: a minimum thickness', *J. Atmos. Terr. Phys.* **38**, 1065.

Saxton, J. M. and Smith, A. J.: 1989, 'Quiet time plasmaspheric electric fields and plasmasphere-ionosphere coupling flluxes at L=2.5', *Planet. Space Sci.* **37**, 283.

Smiddy, M., Kelley, M. C., Burke, W., Rich, F., Sagalyn, R., Shuman, B., Hays, R. and Lai, S.: 1977, 'Intense poleward-directed electric fields near the ionospheric projection of the plasmapause', *Geophys. Res. Lett.* **4**, 543.

Smith, A. J., Carpenter, D. L. and Lester, M.: 1981, 'Longitudinal variations in plasmapause radius and the propagation of VLF noise within small (ÆL~0.5) extensions of the plasmapause', *Geophys. Res. Lett.* **8**, 5819.

Song, X-T., Gendrin, R. and Caudal, G.: 1988, 'Refilling process in the plasmasphere and its relation to magnetic activity', *J. Atmos. Terr. Phys.* **50**, 185.

Spiro, R. W., Harel, M., Wolf, R. A. and Reiff, P. H.: 1981, 'Quantitative simulation of a magnetospheric substorm. 3. Plasmaspheric electric fields and evolution of the plasmapause', *J. Geophys. Res.* **86**, 2261.

Stern, D. P.: 1974, 'Models of the Earth's electric field', *NASA/GSFC X Doc. 602-74-159.*

Tarcsai, Gy.: 1985, 'Ionosphere-plasmasphere electron fluxes at middle latitudes obtained from whistlers',*Adv. Space Res.* **5(4)**, 155.

Volland, H.: 1973, 'A semiempirical model of large-scale magnetospheric electric fields', *J. Geophys. Res.* **78**, 171.

Weiss, L. A., Lambour, R. L., Elphic, R. C. and Thomsen, M. F.: 1997, 'Study of plasmaspheric evolution using geosynchronous observations and global modeling',*Geophys. Res. Lett.* **24**, 599.

Wolf, R. A.: 1983, 'The quai-static (slow-flow) region of the magnetosphere', in R. L. Carovillano and J. M. Forbes, (eds.), *Solar-Terrestrial Physics, Principles and Theoretical Foundations,* D. Reidel, Dordrecht, pp. 303--329.

Yeh, H.-C., Foster, J. C., Rich, F. J. and Swider, W.: 1991, 'Storm time electric field pene-tration observed at mid-latitude, *J. Geophys. Res.* **96**, 5707.

Address for correspondence: D. L. Carpenter, Space, Telecommunications and Radioscience Laboratory, Stanford University, Stanford, CA 94305, USA

OUTER PLASMASPHERIC PLASMA PROPERTIES: WHAT WE KNOW FROM SATELLITE DATA

MARK B. MOLDWIN
Department of Physics and Space Sciences
Florida Institute of Technology, Melbourne Florida, USA

Received March 3, 1997; Accepted in final form April 4, 1997

Abstract. Our understanding of the composition, density, and temperature structure of the outer plasmasphere has undergone several major revisions since the discovery of the plasmasphere over 35 years ago. Each new era of understanding was brought about by the launching of satellites carrying suites of plasma diagnostic experiments each more sophisticated than its predecessor. Instead of each new generation of missions providing incremental advancement in our knowledge of the plasmasphere's plasma properties, they most often than not, initiated a complete re-thinking of our understanding. There are still a number of observational "puzzles" and large gaps in our knowledge of how plasmaspheric structure and plasma properties change with geomagnetic storm and substorm activity. As we develop new missions to attempt to globally image the outer plasmasphere in order to put simultaneous multi-spacecraft observations into context, we undoubtedly will uncover new tantalizing observations that will cause us to re-think our mental picture of the plasmasphere. What we have learned from satellite data about the chemical composition, density, temperature and pitch-angle distribution properties and their variability is outlined in this review paper.

1. Introduction

The plasmapause defines a transition region between plasmas whose dynamics are predominately determined by the Earth's corotation electric field and those particles whose dynamics are determined by highly variable geomagnetic electric fields. The region near the plasmapause (including both sides of the boundary) is often called the outer plasmasphere. Due to the rapid time and the large amplitude variability of convective and inductive electric fields during storms and substorms the outer plasmasphere is virtually always in a state of flux. Therefore the location of the plasmapause, which is determined by the interplay between dayside "refilling" from the underlying ionosphere and flux tube "emptying" by changing geomagnetic electric fields, is highly variable. The plasmapause has been observed at geocentric distances of $< 3\ R_E$ out to distances beyond geosynchronous orbit. Occasionally no well defined plasmapause region is observed at all out to the magnetopause (e.g., Carpenter and Anderson, 1992).

Several plasma regimes have been defined in the inner magnetosphere. Each regime is characterized by different plasma densities, temperatures, chemical

Space Science Reviews **80**: 181–198, 1997.

compositions, and pitch angle distributions. Each plasma regime also has different source regions and different loss mechanisms. In addition, their boundary locations are determined by the energy state of the magnetosphere. Of course even within a particular regime the plasma properties can change as a function of geomagnetic activity, local time, and geomagnetic latitude. The outer plasmasphere overlaps or borders virtually all of the inner magnetospheric plasma regimes including the ionosphere, the ring current, the plasmasheet, the trough, and occasionally the lobe, and magnetosheath (e.g., McComas et al., 1993) (Figure 1).

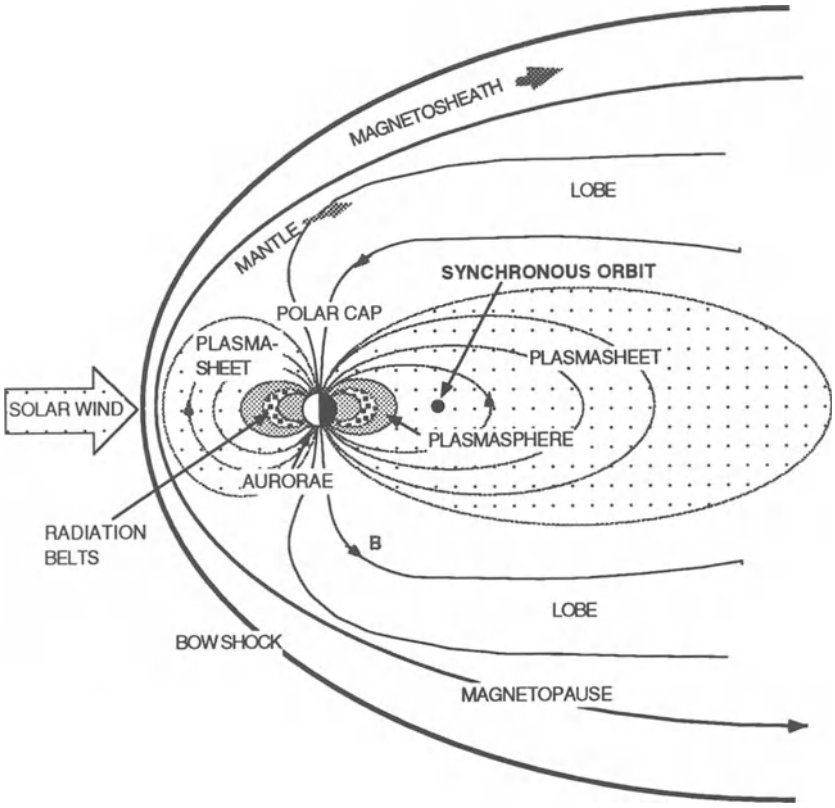

Figure 1. A meridional view of the inner magnetosphere. Note the plasmasphere borders or overlaps all of the inner magnetosphere plasma regimes.

This brief review paper will look at the properties of the thermal plasma observed in the outer plasmasphere. Though the heating, loss, pitch angle scattering, and dynamics of the thermal plasma are integrally related by interactions with the other plasma regimes as well as the rich set of waves that exist in the inner magnetosphere, this paper will concentrate solely on the

observed thermal plasma properties. The review paper by Carpenter and Lemaire (this issue) describes the important processes responsible for the dynamics observed in the outer plasmasphere region. This paper starts with a brief review of the structure and dynamics of the plasmasphere to emphasize the extreme variability in the location of the plasmapause. Then a description of the satellite observations made to date which describe the thermal plasma density, temperature, chemical composition, and pitch angle distribution and their dynamics with respect to geomagnetic activity. The paper concentrates on recent in situ observations of the plasma properties but digresses briefly to outline the progression of our understanding of the plasmaspheric properties since the discovery of the plasmasphere. The paper concludes with a set of open questions that still remain despite the nearly 40 years of plasmaspheric research. Readers are referred to review papers by Chappell (1972) and Rycroft (1975) for a perspective of the earliest observations, and a paper by Farrugia et al., (1989) which examines the composition, temperature and density structure of the plasmasphere observed by GEOS 1. Table 1 shows a list of some of the spacecraft missions that have contributed to our present understanding of the plasmaspheric plasma properties.

Table I.
Selected missions that have contributed to understanding the plasma properties of the plasmasphere.

Prognoz	Bezrukikh and Gringauz, 1976
IMP 2	Serbu and Maier, 1966
OGO 3 and 5	Taylor et al., 1970; Chappell, 1972
GEOS-1 and 2	Higel and Wu, 1984; Farrugia, 1989
DE-1	Horwitz et al., 1984
ISEE 1	Carpenter and Anderson, 1992
LANL Geosynchronous	Moldwin et al., 1994; 1995
SCATHA	Olsen, 1981
ATS 6	Comfort and Horwitz, 1981

2. Plasmaspheric Structure and Dynamics

The plasmasphere is a toroidal region surrounding the Earth characterized by high plasma densities (thousands to tens of particles cm^{-3}), and low plasma temperatures (a few eV or less). It is formed by the outflow of ionospheric plasma along closed geomagnetic flux tubes. There is often a sharp density gradient between the plasmasphere and the inner magnetospheric trough region. This boundary is called the plasmapause. It is often characterized by an order of

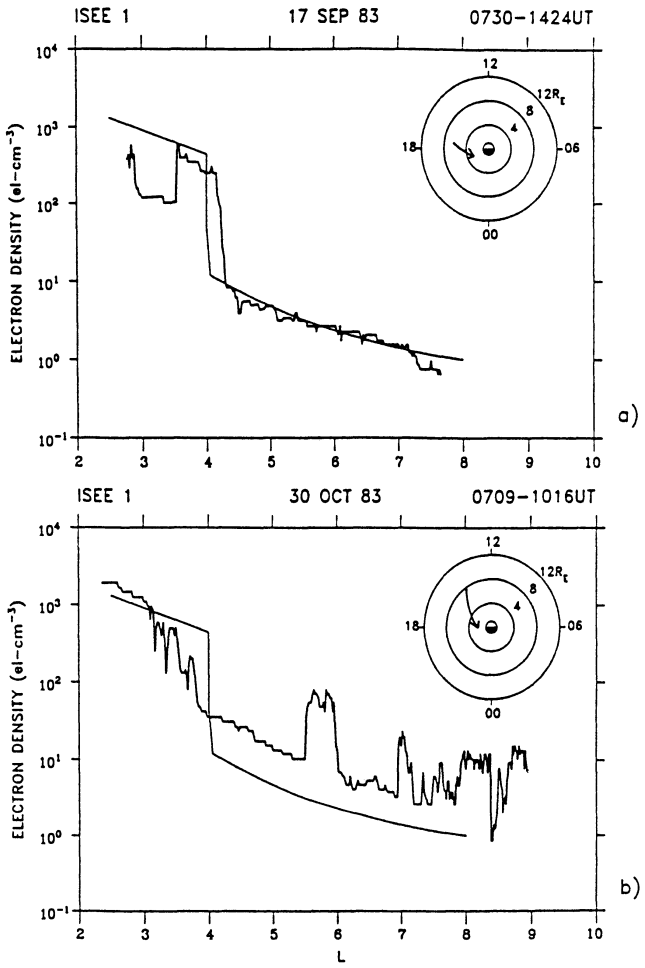

Figure 2. Two ISEE profiles of electron number density with L-shell. Note that there is density structure outside the innermost plasmapause which is defined by the about order of magnitude density decrease within a fraction of an L-shell.

magnitude density gradient within a fraction of an Earth radii (note the inner most rapid density gradient at L of about 3 in Figures 2). It was discovered in the early 1960's from both ground based whistler observations (Carpenter, 1963) and from in situ plasma measurements (Gringauz, 1963). The location of the plasmapause is determined by the interplay between the Earth's corotation electric field and magnetospheric electric fields. As geomagnetic activity increases the plasmapause is observed to move closer to the Earth and move outward for low geomagnetic activity conditions. There is also a dawn-dusk (Carpenter, 1966) and noon-midnight radial asymmetry (Gringauz and Bezrukikh, 1976). The dawn-dusk asymmetry has received significantly more

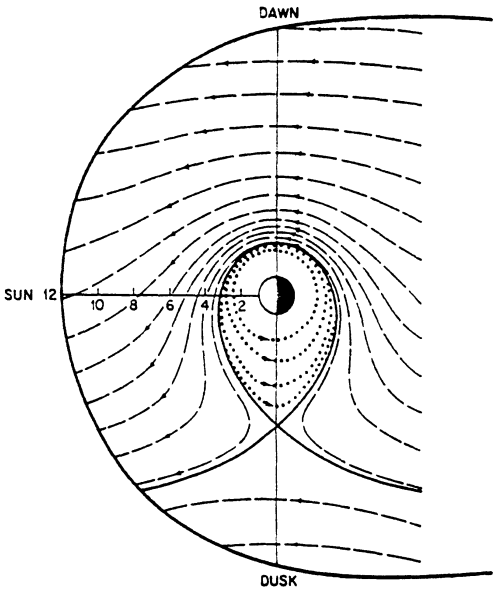

Figure 3. Equatorial flow lines of flux tubes within the magnetosphere. Dashed lines show flux tubes whose motion is dominated by convection, while the dotted lines show flux tubes dominated by corotation (from Chappell et al., 1970).

attention even though the magnitude of the two asymmetries are often comparable (e.g., Gringauz, 1985). The dusk (and noon) side location of the plasmapause is usually at a farther distance from the Earth than the dawn (and night) side plasmapause for similar geomagnetic activity levels. The interplay between the corotation and geomagnetic electric fields was first modeled for DC electric fields and a dipole magnetic field in the mid-1960's (Nishida, 1966, Brice, 1967, and Dungey, 1967). Figure 3 shows the equipotential contours of these superimposed electric fields. In this model the convection electric field is assumed to be directed from dawn to dusk and is uniform throughout the magnetosphere. The last closed potential (or streamline for a zero energy particle) was thought to represent the plasmapause. This simple MHD model is able to reproduce the dynamics of the size of the plasmasphere (i.e., for increased values of the convection electric field, the plasmasphere shrank). However, it was not able to explain the local time variability of the bulge region itself. The local time variation was modeled by Grebowsky (1970) by including a time varying convection electric field to the above MHD models. He found that besides the variation in the size of the plasmasphere, the bulge

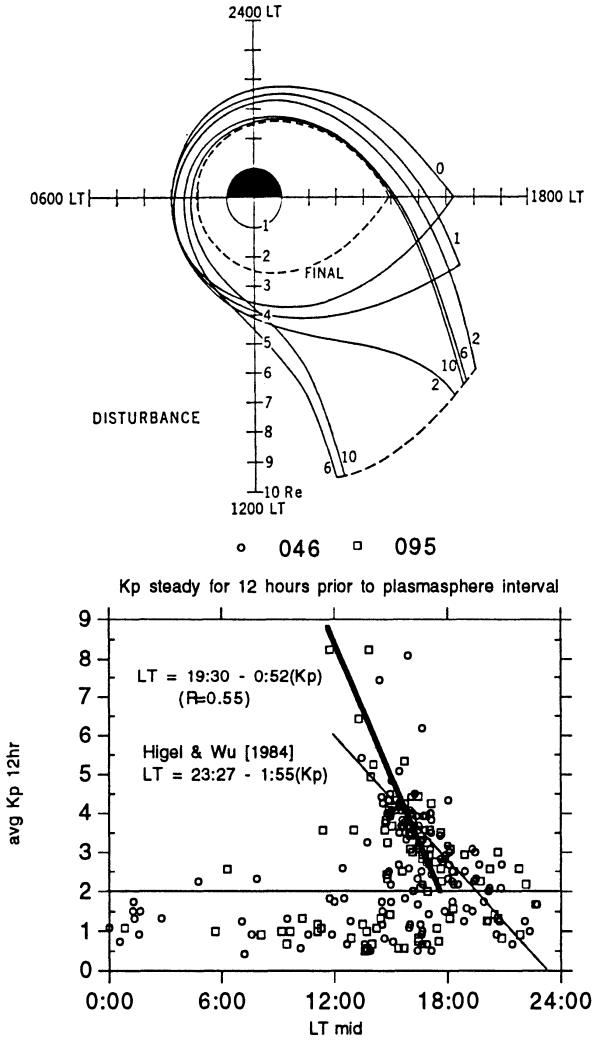

Figure 4. The last closed equipotential line for the superposition of a corotation and time-varying dawn-dusk convection electric field (from Grebowsky, 1970). The mid-point of the plasmaspheric intervals observed at geosynchronous orbit as a function of K_p (from Moldwin et al., 1994).

region moves to earlier local times with increasing convection electric field, in agreement with observations (Figure 4).

Outside the nominal plasmapause there is usually significant structure in the thermal plasma density (see second panel of Figure 2). These plasma regions are either completely disconnected from the main plasmasphere or are plasma plumes or tails extending from the dusk region (e.g., Maynard and Chen, 1975). Recently, sophisticated models such as the Rice Convection Model (Lambour et al., 1997) and the model by Ober et al. (1997) have successfully modeled these detached plasma region's dynamics.

Despite these modeling successes, there is still much to learn about the plasmasphere's structure and dynamics particularly the often complex and fine scale structure and dynamics of the outer plasmasphere region (e.g., Carpenter et al., 1993). The response of the plasmasphere to short-lived substorm convective and inductive electric fields has recently been addressed (Moldwin et al., 1996). Intriguing new relationships between the growth phase of substorms and the appearance of dense plasmaspheric regions in the midnight outer plasmasphere region has led to the suggestion that inductive electric fields may play a role in detaching plasmaspheric regions from the inner plasmasphere. This study has renewed attention to the cause of the noon-midnight asymmetry first observed by Gringauz.

With a single spacecraft it is often difficult if not impossible to place the in situ observations in context with the global plasmasphere and inner magnetospheric structure. Therefore recent studies have emphasized simultaneous multiple spacecraft observations. Complex, rapid variability is often observed even for periods of relatively quiet geomagnetic activity (e.g., Moldwin et al., 1994, 1995). These studies point out the need for further multi-point and sophisticated modeling efforts to try and understand the dynamics of the outer plasmasphere region. In addition to the often puzzling and complex observations of the location of the outer plasmasphere there is extreme variability with regards to the plasma properties observed in the outer plasmasphere. The remaining sections of this paper will outline what we have observed to date with regard to these plasma properties. Of course much of the complexity of the outer plasmasphere is due to the dependence of one parameter upon several other (i.e., the pitch angle distributions observed in the outer plasmasphere are dependent on ion composition, charge state, temperature, and geomagnetic activity and history). Despite these inter-dependencies, I follow an outline attempting to separate the different plasma properties.

3. Plasmaspheric Density and Temperature Behavior

In general, the density of the plasmasphere is about 10^3 cm^{-3} at L=3 with the density relatively smoothly decreasing following an L^{-4} density profile out to

the plasmapause (Figure 2) (e.g., Chappell, 1972, 1974; Farrugia et al., 1989; Carpenter and Anderson, 1992). This is due to the same dependence of flux

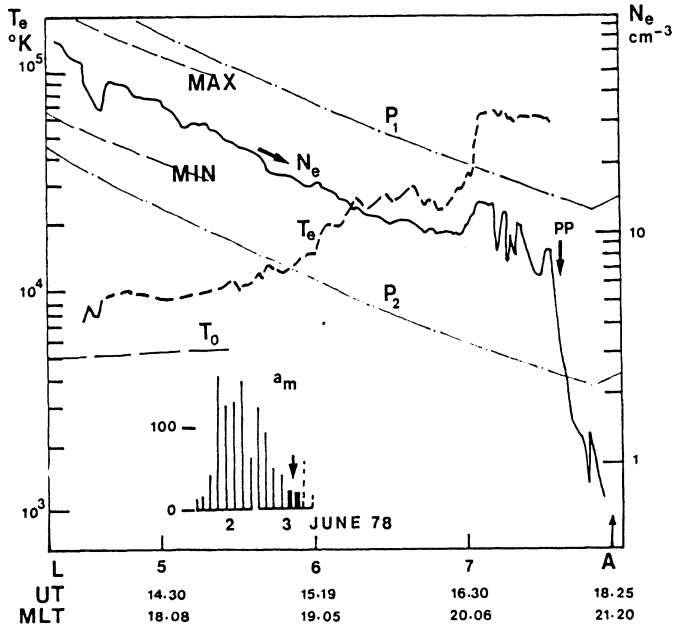

Figure 5. Example of electron density and temperature profile from GEOS-1 (from Decreau et al., 1982). Ne and Te are the electron density and temperature, respectively. PP marks the location of the plasmapause and P1 and P2 are L^{-4} density profiles.

tube volume with radial distance in a dipole magnetic field. The temperature structure is usually anti-correlated with density (Figure 5) with temperatures usually between 1 and a few eV (e.g., Serbu and Maier, 1970; Decreau et al., 1982; Comfort et al., 1985; Moldwin et al., 1995; Comfort, 1996). This relationship, high density regions are cool ($\approx$ 1 eV) and low density regions are warm ($\approx$ several to 10 eV), is followed not only as a function of radial distance but also as a function of time during plasmaspheric refilling. In addition, in the outer plasmasphere this relationship holds in the detached plasma regions

(Figure 6) and even in regions of fine scale structure (e.g., Moldwin et al., 1995). In the outer plasmasphere most often these two populations (dense and cold, and warm and tenuous) do not coexist. However, occasionally one can

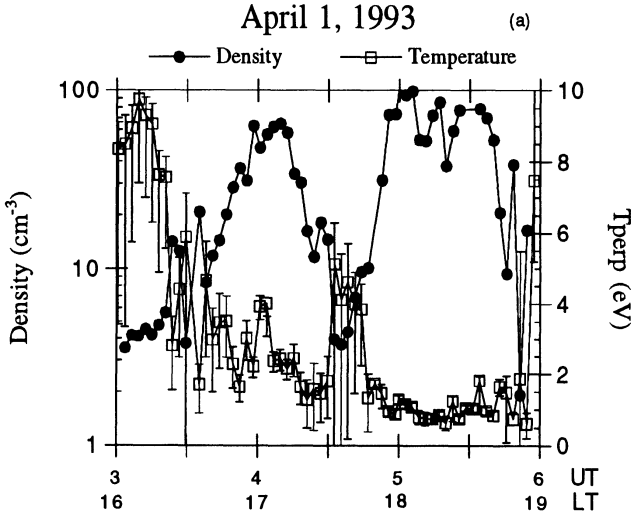

Figure 6. Temperature and density of the outer plasmasphere observed from geosynchronous orbit (from Moldwin et al., 1995).

observe a superposition of these two populations (Figure 7) (Moldwin et al., 1995). While in the inner plasmasphere ($L \approx 4$) these two populations often co-exist (Comfort et al., 1985).

It has been suggested that within the plasmasphere L-shells can be considered quasi-isothermal and that the plasmasphere can be divided into a inner "cold zone" and an outer "hot zone." (Bezrukikh and Gringauz, 1976). The term "warm plasma" was coined by Lennartsson and Reasoner (1978) and Horwitz and Chappell (1979) to distinguish the population of thermal plasma with energies greater than 3eV from the "cold" dense plasmaspheric plasma. "Hot" is now generally reserved for plasma sheet populations with energies greater than about 100 eV. It is now thought that the "cold" zone is the inner plasmasphere proper, while the "warm" zone is just beyond the plasmapause in regions of flux tube refilling (or trough region).

Originally it was thought that the plasmasphere was just an extension of the topside ionosphere and that the plasma distributions would be cold < 1 eV (reflecting their ionospheric source) Maxwellians corotating with Earth (e.g., Banks and Holzer, 1969). With the launch of the GEOS and ISEE spacecraft in the 1970's it was quickly realized that this understanding of the thermal structure of the plasmasphere was oversimplified (e.g., Young et al., 1977; Baugher et al., 1980). Though Maxwellian distributions are observed in the

inner magnetosphere, the outer magnetosphere is characterized by highly variable and non-Maxwellian distributions (e.g., Horwitz and Chappell, 1979) and ion temperatures are usually several to 10 eV. Even in the relatively dense

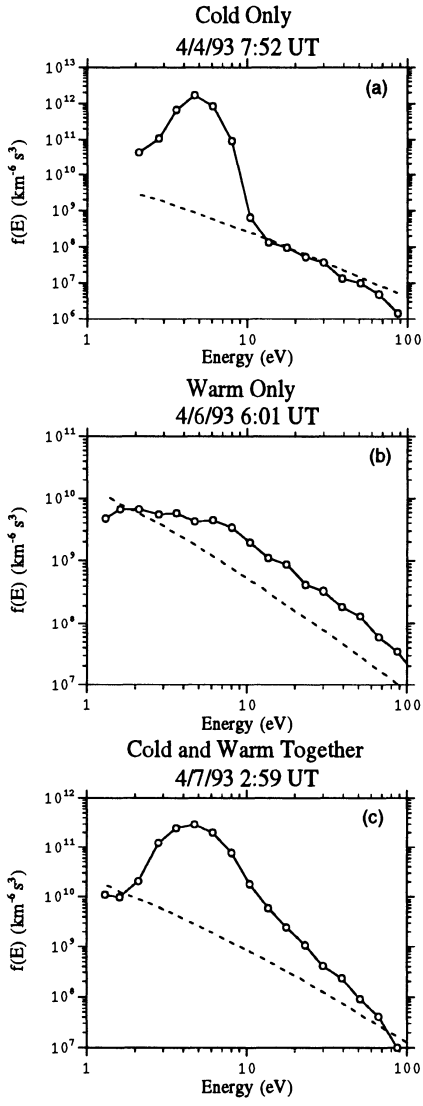

Figure 7. Distribution functions observed in the outer plasmasphere. Usually a "cold" or "warm" distribution are observed separately. On occasion both distributions can be observed together (from Moldwin et al., 1995). The background f(E) level is shown as a dashed line.

outer plasmasphere, the ion temperatures are typically in the few eV range (e.g., Horwitz et al., 1981b; Moldwin et al., 1995).

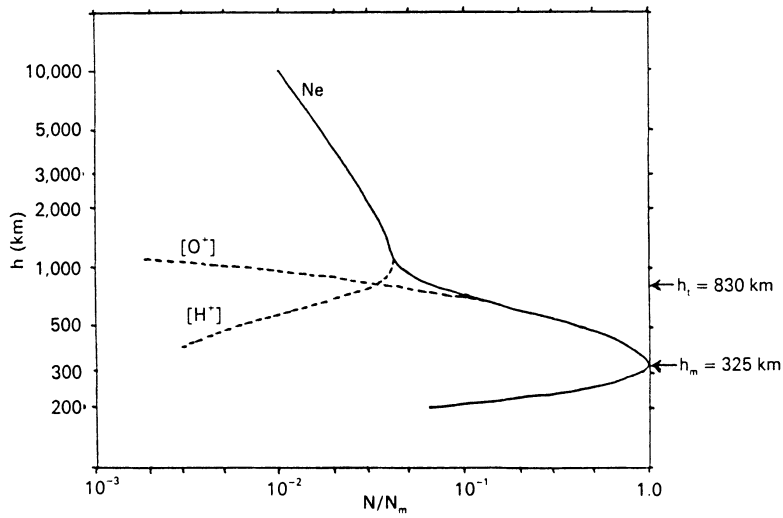

Figure 8. Model ionospheric profile, showing transition between O^+ and H^+, for equatorial night at Boulder, Colorado (from Hargreaves, 1992).

4. Plasmaspheric Chemical Composition

The plasmasphere, originally called the protonosphere and whose base was defined at the altitude at which the dominating ion species switched from O^+ to H^+ (Figure 8), generally consists of mostly hydrogen. The earliest mass spectrometer results suggested that the plasmasphere was 99% hydrogen (see review by Chappell, (1972)). Later results using GEOS 1 and ISEE 1 among others found that the ions He^+ and O^+ are the primary heavy ions present in the plasmasphere and are generally found at levels between 2 to 6% and 1%, respectively. However, concentrations relative to H^+ of He^+ as high as over 100% have been observed (e.g., Young et al., 1977; Geiss et al., 1978, Horwitz et al., 1981b; and Chappell et al., 1982a; Farrugia et al., 1989). Observations from DE-1 have even suggested that O^+ densities can occasionally become comparable to the H^+ densities (Horwitz et al., 1984). In addition, the doubly charged ions O^{++} , He^{++} (Young et al., 1977; Geiss et al., 1978), D^+ (Geiss et al., 1978) and N^+ (Chappell et al., 1982a), have also been observed in the

plasmasphere, with the O^{++} density in the equatorial plasmasphere occasionally equaling the O^{+} density (Figure 9).

Though hydrogen follows an L^{-4} fall off within the plasmasphere, He^{+} falls off quicker and for the dusk sector during quiet times follows an $L^{-4.7}$ slope

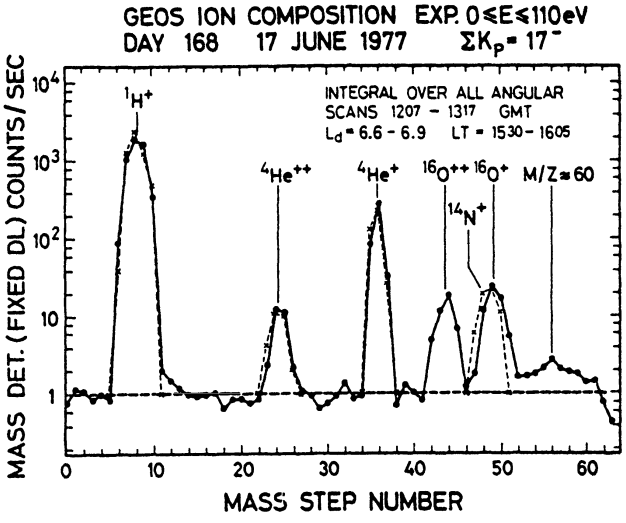

Figure 9. GEOS thermal mode mass spectrum showing presence of doubly ionized heavy ions (from Young et al., 1977). The dashed line is the single count threshold.

(Farrugia et al., 1989). Little information on the radial dependence of the other minor ion species has been reported in the literature. However, Horwitz et al., (1981) find that on several passes of DE-1 from L of about 2.5 to 6, the O^{+} density decreases much slower than the light ion species and suggests that the outer plasmasphere can be somewhat O^{+} enriched relative to the inner region during plasmaspheric replenishment intervals. In addition, they find that there is a sharp peak of O^{+} and O^{++} ions just inside L=4 on a number of passes and suggest that a heavy ion torus or shell is formed in the vicinity of previously formed plasmapause.

5. Plasmaspheric Pitch Angle Distributions

In the vicinity of the plasmapause, there are often complex pitch angle distributions (PADs) observed in the thermal ions (e.g., Horwitz, 1980; Comfort and Horwitz, 1981; Horwitz et al., 1981; Chappell et al., 1982;

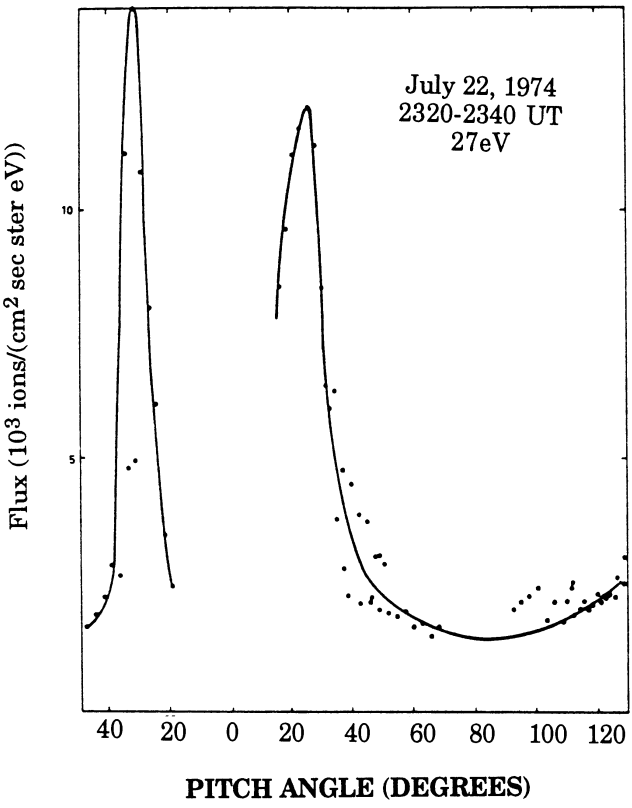

Figure 10. A conical distribution observed at synchronous orbit (from Horwitz, 1980).

Reasoner et al., 1983; Sojka et al., 1984; Decreau et al., 1986; Chandler and Chappell, 1986; Olsen et al., 1987). Much less attention (e.g., Wrenn et al., 1979) has been paid to the thermal electrons because of the difficult nature of the measurements due to spacecraft potential and spacecraft photoelectron emissions. However, Fillingim (1997) have begun examining the PAD behavior of suprathermal electrons using data from the Los Alamos National Laboratory's geosynchronous satellites. Understanding the evolution of the pitch angle distributions of the thermal plasmas is important for understanding the refilling process (see for example the special issue on plasmaspheric refilling in the February, 1992, *Journal of Geophysical Research*). In addition, the evolution of the PADs can give clues to the wave particle interactions that are present (Mauk, 1982), or conversely, the presence of light and heavy ions with different PADs can give clues to the types of waves that are present (e.g., Young et al., 1981).

Just beyond the plasmapause in the region of plasmaspheric refilling is where most of the non-Maxwellian PAD observations are found. However, within the plasmapause sharply peaked trapped (or "pancake") distributions of both H^+ and He^+ (Olsen, 1981; Horwitz et al., 1981; Quinn and Johnson, 1982) are also found near the geomagnetic equator. Simultaneously measured O^+ is usually either undetectable or field-aligned.

Ion conics (Figure 10) are observed just outside the plasmapause and are associated with plasmaspheric refilling processes (Horwitz, 1980). In general at geosynchronous orbit, field-aligned PADs (Figure 10) of "warm" ions, with the characteristic source cone angle ranging from 10 to 20°, are observed at all local times regardless of geomagnetic activity, while the cold pancake distributions are primarily observed in the dusk region. Ion conics, with peaks occurring in the 15-35° pitch angle range, are also observed at all local times.

There is limited observations of the pitch angle distributions in the outer plasmasphere's "detached" plasma structures. However, Chappell et al. (1982b) using DE-1 RIMS mid-latitude data found that the PADs of detached plasma regions appeared to be field-aligned. This is inconsistent with the interpretation of the OGO-5 data. The interpretation of the detached plasma regions observed with OGO 5 was that the plasma was removed from the bulge region due to enhanced convection. Therefore the plasma would be expected to exhibit either a Maxwellian or trapped PAD distribution of the main plasmasphere. A more detailed study of the PADs within "detached" plasma regions needs to be done and could perhaps address the origin and "connectedness" of these regions to the main plasmasphere.

6. Some Open Questions

This brief review of in situ satellite observations of the thermal plasma properties of the outer plasmasphere showed the often complex behavior and strong inter-dependencies that the thermal plasma populations often exhibit. Though considerable effort has been expended in trying to understand this region over the last 35 years there are still open questions which need to be addressed. I suggest a half-dozen questions in light of the future IMAGE mission which will attempt to reconstruct an "image" of the global plasmaspheric structure and dynamics.

1) How do the H^+ and He^+ plasma populations track throughout the plasmasphere as a function of L-shell and geomagnetic activity?

2) How do the light ion plasma populations track throughout the plasmasphere as a function of L-shell and geomagnetic activity with the heavy ion component?

3) What is the latitudinal structure of the outer plasmasphere?

4) What is the PAD distributions of the "detached" plasma regions? Is it consistent with a convective motion out from the duskside bulge region?

5) What is the relationship between the midnight sector outer plasmasphere and the inner edge of the plasma sheet?

6) How does the thermal ion composition of the outer plasmasphere change as a function of geomagnetic and substorm activity?

Acknowledgments

The author thanks D. Carpenter and M. Thomsen for discussions regarding this paper. This work was supported in part by NASA SR&T grant NAGW-5153 and the International Space Science Institute.

References

Banks, P.M. and Holzer, T.E.: 1969, 'High latitude plasma transport: the polar wind', *J. Geophys Res.* **74**, 6317.

Bezrukikh, V.V., and Gringauz, K.I.: 1976, 'The hot zone in the outer plasmasphere of the Earth', *J. Atmos. and Terr. Physics* **38**, 1085.

Brice, N.M.: 1967, Bulk motion of the magnetosphere, *J. Geophys. Res.* **72,** 5193.

Carpenter, D.L.: 1963, 'Whistler evidence of a "knee" in the magnetospheric ionization density profile', *J. Geophys. Res.* **68,** 1675.

Carpenter, D.L.: 1966, 'Whistler studies of the plasmapause in the magnetosphere, 1, Temporal variations in the position of the knee and some evidence on plasma motions near the knee', *J. Geophys. Res.* **71,** 693.

Carpenter, D.L., and Anderson, R. R.: 1992, 'An ISEE/Whistler model of equatorial electron density in the magnetosphere', *J. Geophys. Res.* **97,** 1097.

Carpenter, D.L., Park, C. G., and Miller, T. R.: 1979, 'A model of substorm electric fields in the plasmapause based on whistler data', *J. Geophys. Res.* **84,** 6559.

Carpenter, D.L., Giles, B. L., Chappell, C. R., Décréau, P. M. E., Anderson, R. R., Persoon, A. M., Smith, A. J., Corcuff, Y, and Canu, P.: 1993, 'Plasmasphere dynamics in the duskside bulge region: A new look at an old topic', *J. Geophys. Res.* **98,** 19,243.

Chandler, M.O., Chappell, C. R.: 1986, 'Observations of the flow of H^+ and He^+ along magnetic field lines in the plasmasphere', *J. Geophys. Res.,* **91,** 8847.

Chappell, C. R.: 1971, 'The dayside of the plasmasphere', *J. Geophys. Res.* **76,** 7632.

Chappell, C. R.: 1972, 'Recent satellite measurements of the morphology and dynamics of the plasmasphere', *Rev. Geophys. Space Phys.* **10,** 951.

Chappell, C.R.: 1974, 'Detached plasma regions in the magnetosphere' *J. Geophys. Res.* **79,** 1861.

Chappell, C. R., Olsen, R. C., Green, J. L., Johnson, J. F. E., and Waite, J. H., Jr.: 1982a, 'The discovery of nitrogen ions in the Earth's magnetosphere' *Geophys. Res., Lett.* **9,** 937.

Chappell, C.R., Green, J. L., Johnson, J. F. E., and Waite, J. H., Jr.: 1982b, 'Pitch angle variations in magnetospheric thermal plasma-initial observations from dynamics explorer-1', *Geophys. Res., Lett.* **9,** 933.

Comfort, R.H.: 1996, 'Thermal Structure of the Plasmasphere' *Adv. Space Res.* **17,** (10)175.

Comfort, R.H. and Horwitz, J. L.: 1981, 'Low energy ion pitch angle distributions observed on the dayside at geosynchronous altitudes', *J. Geophys. Res.* **86,** 1621.

Comfort, R.H., Waite, J. H., Jr., and Chappell, C. R.: 1985, 'Thermal ion temperatures from the retarding ion mass spectrometer on DE 1', *J. Geophys. Res.* **90,** 3475.

Decreau, P. M. E., Beghin, C., and Parrot, M.: 1982, ' Global characteristics of the cold plasma in the equatorial plasmapause region as deduced from the GEOS 1 mutual impedance probe, *J. Geophys. Res.* **87,** 695.

Decreau, P.M.E., Carpenter, D., Chappell, C. R., Comfort, R. H., Green, J., Olsen, R. C., and Waite, J. H., Jr.: 1986, 'Latitudinal plasma distribution in the dusk plasmaspheric bulge: refilling phase and quasi-equilibrium state', *J. Geophys. Res.* **91,** 6929.

Dungey, J.W.: 1967, 'The theory of the quiet magnetosphere', in *Proceedings of the 1966 Symposium on Solar-Terrestrial Physics, Belgrade,* edited by J.W. King and W.S. Newman, p. 91, Academic Press Inc., London.

Farrugia, C.J., Young, D.T., Geiss, J., and Balsinger, H.: 1989, 'The composition, temperature, and density structure of cold ions in the quiet terrestrial plasmasphere: GEOS 1 Results', *J. Geophys. Res.* **94,** 11,865.

Fillingim, M. O.: 1997, 'Characterization of 15-200 eV electrons observed at geosynchronous orbit, M.S. Thesis, Florida Institute of Technology.

Geiss, J., Balsinger, H., Eberhardt, P.. Walker, H.P., Weber, L., and Young, D.T.: 1978, 'Dynamics of magnetospheric ion composition as observed by the GEOS mass spectrometer', *Space Sci. Rev.* **22,** 537.

Grebowsky, J.M.: 1970, 'Model study of plasmapause motion' *J. Geophys. Res.* **75,** 4329.

Gringauz, K.I.: 1963, 'The structure of the ionized gas envelope of earth from direct measurements in the U.S.S.R. of local charged particle concentrations', *Planet. Space Sci.* **11,** 281.

Gringauz, K.I..: 1985, 'Structure and properties of the Earth's plasmasphere', *Adv. Space Res.* **5,** 391.

Gringauz, K. I., and Bezrukikh, V. V.: 1976, 'Asymmetry of the Earth's plasmasphere in the direction noon-midnight from Prognoz and Prognoz-2 data', *J. Atmos. and Terr. Phys.* **38,** 1071.

Hargreaves, J.K.: 1992, *The Solar-Terrestrial Environment,* Cambridge University Press.

Higel, B., and Wu Lei: 1984, 'Electron density and plasmapause characteristics at 6.6 R_E: A statistical study of the GEOS 2 Relaxation sounder data', *J. Geophys. Res.* **89,** 1583.

Horwitz, J.L.: 1980, 'Conical distributions of low-energy ion fluxes at synchronous orbit', *J. Geophys. Res.* **85,** 2057.

Horwitz, J. L., and Chappell, C. R.: 1979, 'Observations of warm plasma in the dayside plasma trough at geosynchronous orbit, *J. Geophys. Res.* **84,** 7075.

Horwitz, J.L., Baugher, C. R., Chappell, C. R., Shelley, E. G., and Young, D. T.: 1981a, 'Pancake pitch angle distributions in warm ions observed with ISEE 1', *J. Geophys. Res.* **86,** 3311.

Horwitz, J.L., Baugher, C. R., Chappell, C. R., Shelley, E. G., Young, D. T., and Anderson, R. R.: 1981b, 'ISEE 1 observations of thermal plasma in the vicinity of the plasmasphere during periods of quieting magnetic activity',*J. Geophys. Res.* **86,** 9989.

Horwitz, J.L., Comfort, R. H., and Chappell, C. R.: 1984, 'Thermal ion composition measurements of the formation of the new outer plasmasphere and double plasmapause during storm recovery phase',*Geophys. Res. Lett.* **11**, 701.

Lambour, R.L., Weiss, L. A., Elphic, R. C., and Thomsen, M. F.: 1997, 'Global modeling of the plasmasphere following storm sudden commencements', in press,*J. Geophys. Res.*

Lennartsson, W., and Reasoner, D. L.: 1978, 'Low energy plasma observations at synchronous orbit',*J. Geophys. Res.* **83,** 2145.

Mauk, B.: 1982, 'Helium resonance and dispersion effects on geostationary Alfven/ion cyclotron waves, *J. Geophys. Res.* **87,** 9107.

Maynard, N.C., and Chen, A. J.: 1975, 'Isolated cold plasma regions: Observations and their relation to possible production mechanisms',*J. Geophys. Res.* **80,** 1009.

McComas, D.J., S.J. Bame, S. J., Barraclough, B. L., Donart, J. R., Elphic, R. C., Gosiling, J. T., Moldwin, M. B., Moore, K. R., and Thomsen, M. F.: 1993, 'Magnetospheric plasma analyzer (MPA): Initial three-spacecraft observations from geosynchronous orbit', *J. Geophys. Res.* **98,** 13,453.

Moldwin, M.B., Thomsen, M. F., Bame, S. J., McComas, D. J., and Moore, K. R.: 1994, 'The structure and dynamics of the outer plasmasphere: A multiple geosynchronous satellite study', *J. Geophys. Res.* **99,** 11,475.

Moldwin, M.B., Thomsen, M. F., Bame, S. J., McComas, D. J., and Reeves, G. D.: 1995, 'The fine-scale structure of the outer plasmasphere',*J. Geophys. Res.* **100,** 8021.

Moldwin, M.B., Thomsen, M. F., Bame, S. J., McComas, D. J., Weiss, L. A., Reeves, G. D., and Belian, R. D.: 1996, 'The appearance of plasmaspheric plasma in the outer magnetosphere in association with the substorm growth phase',*Geophys. Res. Lett.* **23,** 801.

Nishida, A.: 1966, 'Formation of plasmapause, or magnetospheric plasma knee, by the combined action of magnetospheric convection and plasma escape from the tail', *J. Geophys. Res.* **71,** 5669.

Ober, D. L., Horwitz, J. L., Thomsen, M. F., Elphic, R. C., McComas, D. J., Belian, R. D., Moldwin, M. B.: 1997, 'Premidnight plasmaspheric "plumes", in press,*J. Geophys. Res.*

Olsen, R.C.: 1981, 'Equatorially trapped plasma populations'*J. Geophys. Res.* **86,** 11,235.

Olsen, R.C., Shawhan, S. D., Gallagher, D. L., Green, J. L., Chappell, C. R., and Anderson, R. R.: 1987, 'Plasma Observations at the Earth's Magnetic Equator'*J. Geophys. Res.* **92,** 2385.

Quinn, J.M., and Johnson, R. G.: 1982, 'Composition measurements of warm equatorially trapped ions near geosynchronous orbit',*Geophys. Res. Lett.* **9,** 777.

Reasoner, D.L., Craven, P. D., and Chappell, C. R.: 1983, 'Characteristics of low-energy plasma in the plasmasphere and plasma trough',*J. Geophys. Res.* **88,** 7913.

Rycroft, M. J.: 1975, 'A review of in situ observations of the plasmapause'*Ann. Geophys.* **31,** 1.

Serbu, G.P. and Maier, E. J. R.: 1966, ' Low energy electrons measured on IMP-2',, *J. Geophys. Res.* **71,** 3755.

Serbu, G.P., and Maier, E. J. R.: 1970, 'Observations from Ogo 5 of the thermal ion density and temperature within the magnetosphere',*J. Geophys. Res.* **75,** 6102.

Sojka, J.J., and Wrenn, G. L., and Johnson, J. F. E.: 1984, 'Pitch angle properties of magnetospheric thermal protons and satellite sheath interference in their observations', *J. Geophys. Res.* **89,** 9801.

Taylor, H.A., Brinton, H. C., and Deshmukh, A. R.: 1970, 'Observations of irregular structure in thermal ion distributions in the duskside magnetosphere',*J. Geophys. Res.* **75,** 2481.

Wrenn, G. L., Johnson, J. F. E., and Sojka, J. J.: 1979, 'Stable "pancake" distributions of low energy electrons in the plasma trough, *Nature* **279,** 512.

Young, D. T., Geiss, T. J., Balsiger, J., Eberhardt, P., Ghiedmetti, A., and Rosenbauer, H.: 1977, 'Discovery of He^{2+} and O^{2+} ions of terrestrial origin in the outer magnetosphere', *Geophys. Res. Lett.* **4,** 561.

Young, D. T., Perraut, S., Roux, A., deVilledary, C., Gendrin, R., Korth, A., Kremser, G., and Jones, D.: "Wave-particle interactions near Ω_{He+} observed on GEOS 1 and 2, 1, Propagation of ion cyclotron waves in He^{+} -rich plasma', *J. Geophys. Res.* **86,** 6755.

Address for correspondence: M. B. Moldwin, Florida Institute of Technology, Dept. of Physics and Space Sciences, 150 W. University Blvd., Melbourne, FL 32901-6988, USA

NUMERICAL MODELING OF THE RING CURRENT AND PLASMASPHERE

R. A. WOLF and R. W. SPIRO
Department of Space Physics and Astronomy, Rice University, Houston, Texas, USA

Received January 24, 1997; Accepted in final form May 29, 1997

Abstract. Over the last 25 years, considerable scientific effort has been expended in the development of quantitative models of the dynamics of Earth's inner magnetosphere, particularly on studies of the injection of the storm-time ring current and of dynamic variations in the shape and size of the plasmasphere. Nearly all modeling studies of ring-current injection agree that time-varying magnetospheric convection can produce approximately the ion fluxes that are observed in the storm-time ring current, but the truth of that assumption has never been demonstrated conclusively. It is not clear that the actual variations of convection electric fields are strong enough to explain the observed flux increases in ~100 keV ions at the peak of the storm-time ring current. Observational comparisons are generally far from tight, primarily due to the paucity of ring-current measurements and to basic limitations of single-point observations. Also, most of the theoretical models combine state-of-the-art treatment of some aspects of the problem with highly simplified treatment of other aspects. Even the most sophisticated treatments of the sub-problems include substantial uncertainties, including the following: (*i*) There is still considerable theoretical and observational uncertainty about the dynamics of the large-scale electric fields in the inner magnetosphere; (*ii*) No one has ever calculated a force-balanced, time-dependent magnetic-field model consistent with injection of the storm-time ring current; (*iii*) The most obvious check on the overall realism of a ring-current injection model would be to compare its predicted *Dst* index against observations; however, theoretical calculations of that index usually employ the Dessler-Parker-Sckopke relation, which was derived from the assumption of a dipole magnetic field and cannot be applied reliably to conditions where the plasma pressure significantly distorts the field; (*iv*) Although loss rates by charge exchange and Coulomb scattering can be calculated with reasonable accuracy, it remains unclear whether wave-induced ion precipitation plays an important role in the decay of the ring current. However, considerable progress could be made in the next few years. Spacecraft that can provide images of large regions of the inner magnetosphere should eliminate much of the present ambiguity associated with single-point measurements. On the theoretical side, it will soon be possible to construct models that, for the first time, will solve a complete set of large-scale equations for the entire inner magnetosphere. The biggest uncertainty in the calculation of the size and shape of the plasmasphere lies in the dynamics and structure of the electric field. It is still not clear how important a role interchange instability plays in determining the shape of the plasmapause or in creating density fine structure.

Key words: Ring Current, Plasmasphere, Convection, Magnetic Storm

Abbreviations: IMF – Interplanetary Magnetic Field, MSFM – Magnetospheric Specification and Forecast Model, R_E – Earth radius

1. Introduction

Numerical modeling has largely confirmed a "standard picture" of ring-current and plasmasphere dynamics, but that picture is still a bit fuzzy, and we are not completely sure it is right. Some elements of the standard picture are the following:

1. The ring current consists primarily of H^+ and O^+ ions in the energy range 10-200 keV, located at L-values between 2.5 and 7.
2. The storm-time ring current is injected primarily by surges of enhanced magnetospheric convection, but inductive effects due to substorm magnetic-field collapse and magnetospheric compression and expansion also play a role, as does the direct injection of ions up from the ionosphere. Processes that conserve the first two adiabatic invariants dominate ring-current injection, but nonadiabatic processes also play a role.
3. The loss of ring current ions is primarily by charge exchange, but Coulomb collisions and pitch-angle scattering also play a role.
4. The plasmasphere consists of cold (1 eV or less) particles of ionospheric origin. The plasmapause, the usually-sharp outer boundary of the plasmasphere, divides the region filled with cold particles that have been circulating on closed drift paths about the Earth for days from the region where the cold plasma has recently drifted in from the magnetotail.

We will be confident that we understand the inner magnetosphere when there is accurate and convincing quantitative agreement between comprehensive and rigorous theory and multi-point observations. However, a rigorous, comprehensive theory of the region has yet to be achieved, partly because of computational limitations: we are just now approaching the point where it is feasible to solve the simplest reasonable set of basic differential equations describing the inner magnetosphere. While complete particle observations may be available at the location of a spacecraft, there are never more than a few observing craft in the magnetosphere at any given time. Since the equation of motion of a charged particle in an electromagnetic field is known, along with various useful approximations, we should, in principle, be able to calculate particle fluxes in the inner magnetosphere as a function of time if we know the following:
(*i*) The large-scale inner-magnetospheric magnetic field as a function of space and time (discussed in Section 2).
(*ii*) The large-scale inner magnetospheric electric field as a function of space and time (discussed in Section 3).
(*iii*) Fluxes of ions flowing up from the ionosphere (discussed by Horwitz and Moore (1997), Yau and André (1997), and André and Yau (1997)).
(*iv*) Fluxes of particles flowing down into the ionosphere from the magnetosphere (discussed by Lyons (1997), Onsager and Lockwood (1997), and Koskinen (1997).
(*v*) Loss rates of magnetospheric ions due to charge exchange (which depend on densities in Earth's exosphere) and cross sections for Coulomb collisions (discussed briefly in Section 4).
(*vi*) Inner magnetospheric particle fluxes at some initial time. Different modeling approaches to estimating these fluxes are discussed briefly in Section 5.
(*vii*) Particle fluxes at the outer boundary of the inner magnetosphere. Different modeling approaches to estimating these fluxes are also discussed very briefly in Section 5.

2. Inner-Magnetospheric Magnetic Fields

Although one can do very useful order-of-magnitude modeling of ring-current injection utilizing a dipole or other simple model for the magnetic field, quantitatively accurate modeling requires magnetic-field models that are inflated to be consistent with the model ring current. In a magnetic storm, the energy density of the ring-current plasma is comparable to the energy density in the magnetic field and is thus able to distort the field significantly. The plasma $\beta(= 2\mu_o p/B^2)$ exceeds ~ 0.5 at $L > 7$ even in quiet times, and the region where β exceeds 0.5 extends to $L \sim 3$ in major storms (e.g., Lui et al., 1987). It should also be noted that a large fraction of the total particle energy in the magnetosphere is in the plasma sheet, where the magnetic field is far from dipolar.

Sophisticated empirical models of the magnetospheric magnetic field have been developed. Of these, the ones that are based most solidly on observations characterize the state of magnetospheric activity in terms of a single parameter like *Kp* (e.g., Tsyganenko, 1989, 1995). Some recent models use several parameters to describe magnetospheric activity (e.g., Hilmer and Voigt, 1995). However, no one would claim that any presently available empirical model provides a quantitatively accurate representation of the magnetosphere in the dynamic process of ring-current injection.

The theoretically correct way to model the magnetic field in a dynamic situation is to calculate the inner-magnetospheric magnetic field self-consistently with the plasma distribution. This difficult numerical problem is now surmountable. Cheng (1995) has computed inner-magnetospheric magnetic fields that solve the magnetostatic-equilibrium equations $\nabla p = \mathbf{J} \times \mathbf{B}$ and $\nabla \times \mathbf{B} = \mu_o \mathbf{J}$ for realistic ring-current pressure distributions. Toffoletto et al. (1996) have developed a friction-code solver that solves the equilibrium equations and can be connected to the Rice Convection Model (RCM), which computes the time-evolution of the plasma distribution. The code still needs improvements before it will run easily and reliably, and it will be a few years before fully self-consistent dynamic calculations will be ready for meaningful comparison with observations of a magnetic storm. However, the move toward self-consistent ring-current modeling is inevitable, in the long run.

One problem related to the inner-magnetospheric magnetic field involves use of the *Dst* index, a measurement of the average deviation from the quiet-time horizontal magnetic field observed by low-latitude stations. It has long been used as the conventional measure of the total strength of the ring current, and, as such, it offers the most obvious check on the validity of theoretical models of ring-current injection. Ring-current modelers have typically used the Dessler-Parker-Sckopke relationship (Dessler and Parker, 1959; Sckopke, 1966) to connect model-computed energy in ring-current particles to the magnetic index *Dst*. However, the Dessler-Parker-Sckopke relation was derived for a dipole field and becomes inaccurate when the magnetic field is distorted by the presence of the ring-current plasma.

Campbell (1996) even maintains that *Dst* should be abandoned as a ring-current index. Controversy over the validity of *Dst* as a check on ring-current models will be reduced when models can calculate magnetic-field changes, including *Dst*, self-consistently.

3. Inner-Magnetospheric Electric Fields

The large-scale magnetospheric electric field can conveniently be divided into four parts: (*i*) The convection electric field, which is directed roughly from dawn to dusk, when viewed in the equatorial plane in a reference frame that rotates with the Earth; we will define it by a potential that is constant along magnetic field lines; (*ii*) The induction electric field, which is driven by changes in B; (*iii*) The corotation electric field, which is directed toward lower L-values and must be added to transform from a reference frame that rotates with the Earth to one that does not; (*iv*) Changes in the electric field at low altitudes that result from magnetic-field-aligned potential drops. In this review, we concentrate mainly on (*i*) and (*ii*), since both convection and induction have large and complicated effects on inner-magnetospheric dynamics. The corotation effect (*iii*) can be calculated easily, if the planetary rotation axis is assumed to be parallel to the magnetic dipole (e.g., Wolf, 1995). Field-aligned potential drops (item (*iv*)) play an important role in the dynamics of the auroral ionosphere and the middle and outer magnetosphere, but their role in the ring-current and plasmasphere regions is not clear, and they will not be discussed here.

Magnetic reconnection and other processes act to couple the solar wind to the outermost portion of the magnetosphere, causing flux tubes in those regions to $\mathbf{E} \times \mathbf{B}$ drift antisunward. These flux tubes thread mainly through the ionospheric polar cusp and polar cap, where antisunward plasma flow is typically observed. The total strength of convection can be inferred from estimates of the polar cap potential drop, which is the rate at which polar-cap magnetic flux is transported antisunward. A discussion of statistics-based formulas for estimating the polar-cap potential drop from the IMF and other solar-wind parameters can be found in the paper of Boyle et al. (1997). A strongly northward IMF complicates the flow pattern in the polar cap, and a dawn-dusk component of IMF shifts it from side to side, but these complications have only a minor effect on the inner magnetosphere, which, of course, lies on interior field lines well inside the magnetopause.

The key physical process that complicates inner-magnetospheric electric fields is the tendency (first noted by Schield et al. (1969) and Vasyliunas (1970, 1972)) for the inner edge of the plasma sheet (which is close to the low-latitude edge of the auroral zone) to shield the low-L region of the ionosphere and magnetosphere from the convection electric field. This shielding should not be visualized as being perfect, however. Theory predicts that it should often be ineffective, particularly when convection is changing rapidly. A sharp increase in the strength of magnetospheric

convection is theoretically expected to cause a dawn-to-dusk E-field at low L, as viewed in the equatorial plane. The left side of Figure 1 shows results of a computer simulation that was carried out with the Rice Convection Model to demonstrate this effect: The model was run for several hours, to allow the inner plasma sheet to come to approximate equilibrium with a total cross-tail potential drop of 45 kV. The shielding effect is evident at time T_o: equipotentials are far apart in the inner magnetosphere, indicating a weak electric field. Then just after time T_o, the potential drop was suddenly increased to 90 kV, which produced a strong electric field in the inner magnetosphere, roughly in a dawn-to-dusk direction. The inner edge of the plasma sheet gradually readjusted to shield out the stronger convection. The shielding effect was noticeable after just ten minutes and was nearly complete within two hours. (For a detailed theoretical discussion of shielding, see, e.g., Wolf (1983)).

A sharp decrease in convection causes a "backwards" (or dusk-to-dawn) electric field at low L, as illustrated on the right side of Figure 1. At time T_1, the total cross-tail potential drop was suddenly decreased from 90 kV to 20 kV, causing a strong dusk-to-dawn electric field at low L. This phenomenon is often called "overshielding": at T_1, the inner edge of the plasma sheet is configured to shield out a strong cross-tail electric field; when the cross-tail field is suddenly reduced, the inner magnetosphere is overshielded. However, note that the modeled overshielding effect weakens considerably in ten minutes and nearly disappears after another ten minutes.

Figure 1 displays the typical response of the Rice Convection Model to increases and decreases in convection. However, strong shielding does not always occur when model inputs are held steady for a long time. Theoretical calculations indicate that shielding should be weak when the plasma sheet is unusually hot (Spiro et al., 1988).

It must be emphasized that Figure 1 does not provide a complete picture of inner-magnetospheric and subauroral electric fields, because neutral-atmospheric winds also generate electric fields in that region. The winds are driven in several different ways: solar heating of the day side of the Earth, which drives the large-scale winds that are dominant in times of geomagnetic quiet and cause the Sq (Solar quiet) ionospheric currents; lower-atmospheric weather, which generates tidal winds that propagate upward to ionospheric heights; and dissipation of magnetospheric energy by particle precipitation, Joule heating, and ion drag, which combine to drive gravity waves and disturbance-dynamo winds that propagate to low latitudes. (For a general review of these processes, see, for example, Richmond (1983)). These neutral-atmospheric processes complicate our efforts to understand ring-current injection in two ways:

(*i*) They may directly affect the east-west electric fields near the inner edge of the plasma sheet, the fields that inject the storm-time ring current and move the plasmapause in and out (e.g., Forbes and Harel, 1989). Adequate theoretical treatment of this problem will require development of computer-simulation machinery that

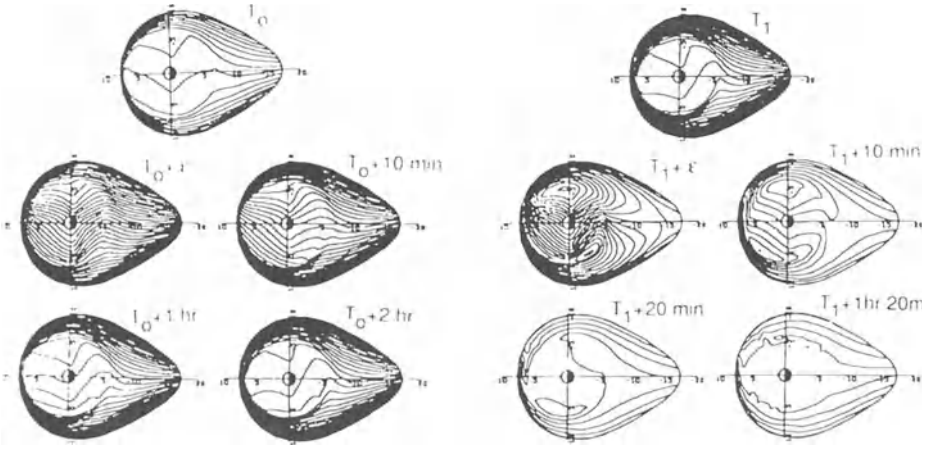

Figure 1. Demonstration of the shielding effect with the Rice Convection Model. The diagrams show equipotentials in the equatorial plane, with the Sun to the left. Only the convection electric field is displayed, although the effect of the Earth's rotation was included in the calculation. The model was run for several hours with steady inputs, including a total potential drop of 45 kV. The potential drop was suddenly increased to 90 kV at time T_0, held at that value for two hours until time T_1, when it was decreased to 20 kV. For this run, the plasma-sheet ion temperature was set equal to 4 keV at x=–13. From Spiro et al. (1988).

can treat the magnetosphere, ionosphere, and thermosphere all self-consistently, including all of the mechanisms for generating low-latitude ionospheric electric fields. Such an effort is technically feasible but would require collaboration among multiple research groups.

(*ii*) They make it difficult to perform clean observational tests of the theory of electrostatic penetration through the shielding layer (e.g., Figure 1), which clearly plays an important role in injecting the ring current. Signatures of direct penetration to low ionospheric latitudes have been observed on many occasions from incoherent-backscatter radars (review by Fejer (1986)), but the observations exhibit substantial inconsistency and unpredictability. For example, a sudden northward turning of the IMF often causes an eastward electric field in the postmidnight sector at the magnetic equator, which was interpreted in terms of the overshielding effect illustrated on the right side of Figure 1 (e.g., Kelley et al., 1979); however, a postmidnight eastward equatorial electric field perturbation does not accompany every sudden northward turning of the IMF. It has been clear for years that part of the unpredictability lies in separating direct-penetration effects in the data from neutral-wind effects.

Recently, however, Fejer and Schlerliess (1995) have found a statistical method of analyzing the observations that elegantly separates different effects, utilizing a very large dataset containing almost twenty years of incoherent-backscatter data. They assume that the disturbance electric field at a given local time is a linear

functional of the Auroral Electrojet (AE) index over the last day and determine the relevant coefficients by best fitting the large dataset. Thus they separate the fast-time-scale low-latitude response to auroral activity from the delayed response. The work of Fejer and Schlerliess (1995), which was based on data from the Jicamarca radar at the magnetic equator, showed that the fast-time-scale response was in good agreement with the theoretical predictions from the simulation shown in Figure 1, while the longer-time-scale response resembled the disturbance-dynamo calculations of Blanc and Richmond (1980).

Induction electric fields that occur in magnetic storms can be as strong as — or stronger than — the potential electric fields associated with strong convection. There are several obvious ways in which the magnetospheric **B** field changes in a magnetic storm, and each corresponds to a characteristic induction electric field:
(*i*) A classic magnetic storm begins with a Storm Sudden Commencement, which is a magnetospheric compression caused by an increase in solar-wind ram pressure. The result is a strengthened inner-magnetospheric **B** field and a westward induction **E** field, both being stronger on the day side than on the night side. Not every magnetic storm begins with a sudden commencement. However, storms frequently involve series of expansions and compressions of the magnetosphere. Occasionally, a magnetic storm includes a sudden, massive compression of the magnetosphere that rearranges the radiation belts as well as the ring current (Li et al.,1993; Hudson et al., 1995).
(*ii*) The magnetic field in the nightside inner plasma sheet stretches during the growth phase of a classic magnetospheric substorm, corresponding to an eastward induction **E**. At the onset of the expansion phase, the midnight region suddenly dipolarizes, corresponding to a strong westward induction **E**.
(*iii*) The buildup of the stormtime ring current inflates and weakens the inner magnetospheric **B**-field, corresponding to an eastward induction E at all local times. Conversely, the **B**-field gradually returns to a more dipolar shape during the recovery phase, accompanied by a westward induction **E**.

All of these induction electric fields are quantitatively important and emphasize the importance of including realistic global magnetic field changes in any adequate computational representation of a magnetic storm, either by using a time-series of quasi-static magnetic field models or by self-consistent calculation with the computed plasma distribution. It must also be mentioned that MHD waves make a major contribution to the electric fields observed in the inner magnetosphere. The electric-field amplitudes of such waves are frequently larger than the convection **E**, and they may play a significant role in radial transport (Li et al., 1991,1993).

4. Ion Loss and Source Processes

Ion source and loss processes must be properly included if the ring current is to be modeled accurately. We summarize briefly present understanding of these processes.

Charge exchange with exospheric hydrogen seems, overall, to be the most important loss process for ring-current ions. It can be calculated with relatively good accuracy from measured atomic cross sections and numerical models of the Earth's exosphere. Such computed lifetimes are shown as dashed curves in Figure 2, taken from Fok et al. (1991). Lifetimes of ring-current ions due to repeated Coulomb collisions with plasmaspheric particles are also shown. Note that charge exchange generally dominates at high energies, while Coulomb decay dominates for the lowest energies. Note also that both lifetimes are long (many days) for protons above about 100 keV. Coulomb decay is very slow outside the plasmasphere. Coulomb scattering of the energetic ring-current ions off cooler plasmasphere ions heats the outer plasmasphere (Jordanova et al., 1996).

Wave-particle interactions scatter pitch angles and can result in precipitation of ring-current ions into the atmosphere, but it is not clear whether this type of plasma process plays a major role in the loss of ring-current particles. Electromagnetic ion cyclotron waves were suggested long ago (Thorne, 1972) as a loss mechanism for ions inside the plasmasphere, and they have recently been studied with a new and sophisticated loss algorithm (Kozyra et al., 1997). Kozyra et al. (1994) have also suggested that ducted plasmaspheric hiss could diffuse pitch angles of $\sim$ 100 keV protons. The ionosphere is a significant source of ions for the magnetosphere, and considerable statistical information has been collected concerning rates of upflow for ions of various kinds. (See reviews by Daglis (1997) and Yau and André (1997)). The strongest and most obvious upward ion flows are on field lines that lie outside the inner magnetosphere, in the cleft ion fountain and in the region of upward region-1 Birkeland currents. Such ions typically enter an inner-magnetosphere model through the high-L boundary condition when they convect earthward from the tail. However, the ring current may also be significantly affected by ions that flow up from the ionosphere directly into the inner magnetosphere. Source/loss information that ring-current modelers still need include: (*i*) An empirical model of upward flux of ions of different energies that is keyed not to general magnetic indices like Kp but to local physical parameters that the models compute, such as density of upward Birkeland current and plasma-sheet number density and pressure. (*ii*)A way of specifying ion precipitation (not easy, since it still isn't clear what causes such precipitation from the inner magnetosphere). See Lyons (1997).

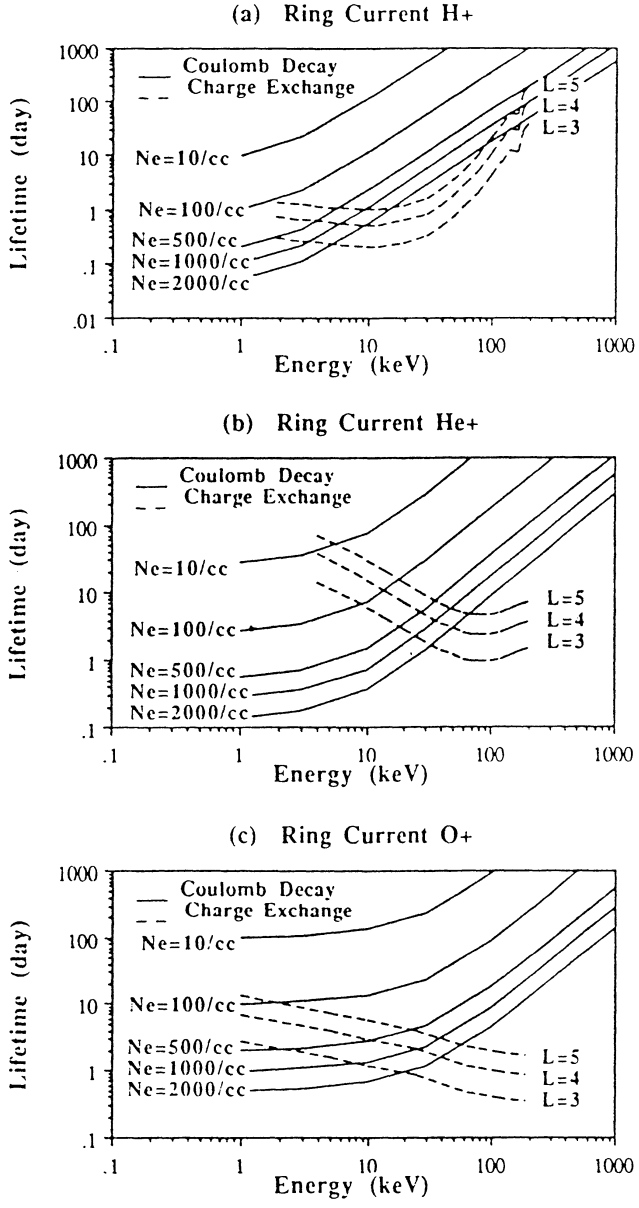

Figure 2. Comparison of Coulomb-decay (solid lines) and charge-exchange (dashed lines) lifetimes of ring-current ions. Coulomb decay lifetimes were calculated for four different electron densities. From Fok et al. (1991).

Table I
Characteristics of some Recent Ring-Current Models

Model	Chen et al. (1994)	Fok et al. (1996)	Wolf et al. (1997)
Population Studied	Equatorially mirroring ring current H^+	Ring current protons in 3D model, conserving μ and J	Ring current H^+, assuming isotropic pitch angles
Electrostatic Potential	$(-AL^2 + BL)sin\phi$ with random sawtooth time dependence in B.	$-AL^2 sin\phi$, where A is estimated from *Kp*.	Polar cap potential drop estimated from DMSP ion-drift-meter data. Penetration field estimated separately from main auroral-zone sunward flow.
Magnetic Field Model	Dipole – 14 nT	Dipole, but uses Tsyganenko (1989) model to inflate and collapse tail in substorm	Hilmer Voigt (1989) model, driven by *Dst*, standoff distance, auroral boundary index, substorm collapse.
Initial Condition	Balance of diffusion and charge exchange gives quiet time distribution, in terms of power laws.	Fit to Sheldon and Hamilton (1993) quiet time distribution	MSFM empirical model.
Boundary Condition	'Neutral line' at 8.549 R_E. Experimented with increase by factors 2-4 in storm.	From AMPTE/CCE at 6.75 R_E.	Huang and Frank (1986) statistical plasma sheet applied at –13 R_E on night side.
Loss	Charge exchange (for equatorially mirroring particles)	Full charge exchange and Coulomb loss	Flux-tube-averaged charge exchange from Bishop (1996)

5. Recent Ring-Current Models

Table I compares the approaches used in recent numerical models of the injection of the storm-time ring current.

The model of Chen et al. (1994) is mathematically the most elegant of the modern ring-current-injection models, and it has been compared extensively with observations (Chen et al., 1997). It concentrates on equatorially mirroring particles, conserving the first adiabatic invariant μ but setting the second invariant $J = 0$. It utilizes a very simple magnetic field model (dipole plus constant southward field). Its model of the potential electric field consists of a time-independent Stern-Volland model (e.g., Volland, 1978) plus a time-dependent, spatially uniform cross-tail electric field. The time dependence consists of a series of substorm dis-

turbances, each consisting of an upward step, followed by an exponential decline. The amplitudes of the substorm electric fields and the time between successive substorms were allowed to vary in a somewhat random pattern. These model calculations have successfully reproduced most of the observed characteristics of ring-current injections. It was necessary to vary the fluxes at the outer boundary of the calculations (at 8.547 R_E) to obtain good agreement with observed fluxes in the storm-time ring current, although the adjustments were in the reasonable range (factors of 2-4). One departure from strict realism is that, in order to get sufficient increases in ion fluxes at $\sim$ 100 keV at $L \sim 3$, Chen et al. (1994) had to assume rather strong substorm electric fields, often with cross-tail potential drops up to 400 kV, i.e., larger drops than have ever been observed across the polar cap.

The results of Chen et al. (1994) thus raise a fundamental question of whether time-varying convection is sufficient to inject enough 100 keV ions to $L \sim 3$ for consistency with observed fluxes. We suspect that the discrepancy results from the assumption that the injecting electric field is uniform across the tail. Note that the more complex patterns from the Rice Convection Model (Figure 1) show the strongest fields near the inner edge of the plasma sheet on the dusk side, which is where fresh ring-current particles are injected. Clean comparisons of the shapes of observed and modeled electric fields are sorely needed, but they are not easy: measurements of magnetospheric **E**-fields are infrequent and difficult, and they are hard to place in a global context; ionospheric measurements suffer from uncertainty in mapping to the magnetosphere.

The model of Fok et al. (1996) conserves both μ and J and considers all possible equatorial pitch angles. Most runs have simply employed a dipole magnetic field. The assumed potential electric field consists of a Stern-Volland potential adjusted according to *Kp*. The outer boundary condition (at 6.75 R_E) was adjusted from observations by AMPTE/CCE spacecraft. The Fok et al. (1996) model employs the most sophisticated loss model, including charge exchange and Coulomb loss computed for the full range of m and J. Figure 3 shows a sample comparison between predicted and observed fluxes, for a specific magnetic storm that occurred in May, 1986.

The Magnetospheric Specification and Forecast Model (MSFM) was developed for the U. S. Air Force primarily for the purpose of operational calculation of kilovolt electron fluxes in the inner and middle magnetosphere (see Wolf et al., 1997 and references therein). However, the MSFM was designed to be able to calculate ion fluxes as well. Although its ability to predict ring-current ions has not been tested comprehensively, initial results suggest that it does a reasonable job. The MSFM employs more elaborate representations of the electric and magnetic field than other inner-magnetospheric models. The total strength of the convection field is normally estimated from measured polar-cap potential drops. Furthermore, the spatial form of the convection potential is designed to imitate typical results obtained with the Rice Convection Model, as described in Section 3. The penetration electric field is adjusted separately from the overall strength of convection

and is designed to give a dawn-dusk penetration field when activity is increasing as well as a dusk-dawn penetration field when activity is decreasing. The magnetic-field model (Hilmer and Voigt, 1995) includes Chapman-Ferraro, ring, and tail currents that are adjusted to maintain consistency with the observed solar-wind ram pressure and *Dst*; the strength of the tail current is adjusted according to the size of the auroral zone, as measured by the Auroral Boundary Index (Gussenhoven et al., 1983), which is the latitude of the equatorward edge of the auroral zone at local midnight, as estimated from the electron detector on DMSP spacecraft. The midnight-region field can be collapsed in the expansion phase of a magnetic storm. The outer boundary condition of the MSFM is placed out in the main part of the plasma sheet. The density and temperature are designed for consistency with the plasma-sheet statistical study of Huang and Frank (1986) at $x = -13$.

Both Fok et al. (1996) and Wolf et al. (1997) have performed computer experiments aimed at determining whether the collapse of the midnight-region magnetic field in the plasma sheet plays a decisive role in the injection of the storm-time ring current. In the simulations of Fok et al. (1996), the net amount of energy in the ring current turned out to be smaller in a case where the midnight-region tail field was expanded and collapsed in imitation of a series of substorms. The collapse increases ring-current energy, but then the subsequent expansion decreases it. In the computer experiments carried out by Wolf et al. (1997), the net effect of tail-field collapse on ring-current injection turned out to be very small. Some recent observational and theoretical research seems consistent with the modeling results: the data-analysis study of Iyemori and Rao (1996) showed that *Dst* tends to increase at substorm onset, and Siscoe and Petschek (1997) have shown that their result can be interpreted naturally in terms of energy theorems.

6. Electric Field Control of Plasmasphere Dynamics

The plasmasphere consists of a region of fairly dense, cold (1 eV or less) plasma surrounding the Earth with a relatively sharp outer boundary (the plasmapause), where the plasma concentration typically decreases by more than order of magnitude. The plasmapause is generally interpreted as separating two distinct plasma regions with different convection histories. The inner region (the plasmasphere) is populated by cold plasma from the ionosphere filling closed flux tubes that have been circulating about Earth for several days, while the region outside the plasmapause is populated by cold plasma on flux tubes that have recently drifted in from the magnetotail. In steady state, the plasmapause thus corresponds to the boundary between drift paths (equipotentials) that circle the Earth and drift paths that connect the tail to the dayside magnetopause. This steady-state picture is rarely applicable to the real magnetosphere: drift around the Earth takes about one day and flux-tube refilling takes several days, but convection never remains constant for such long periods. Thus realistic representation of the plasmasphere requires more detailed

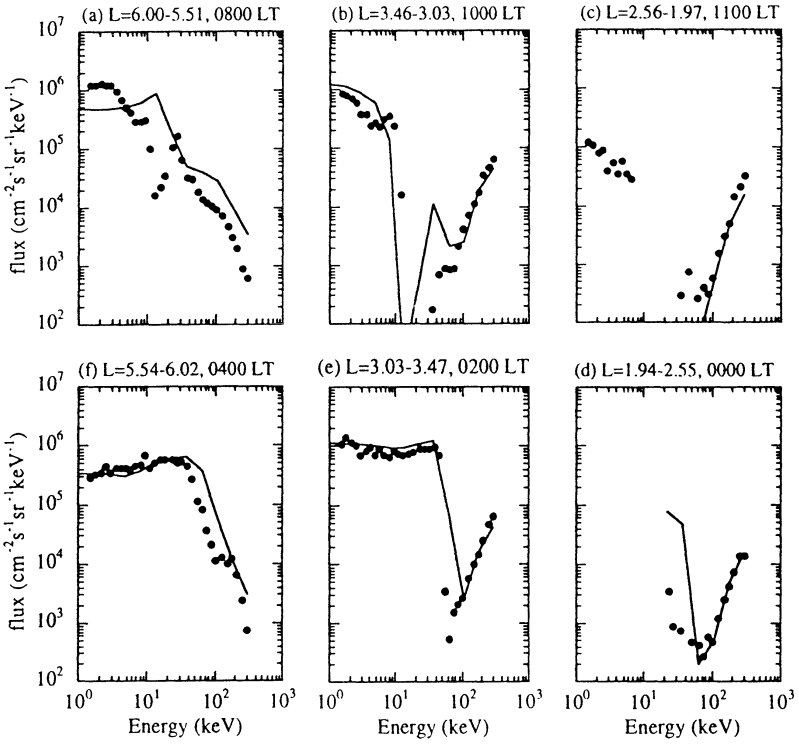

Figure 3. Comparison of modeled and observed ion fluxes in the magnetic storm of May 2, 1986. From Fok et al. (1996).

time-dependent modeling of the transport of plasma through Earth's convection cycle.

Carpenter and Lemaire (1997) describe the development of our present physical picture of the plasmasphere. Here we just briefly describe the status of present modeling efforts.

Hydrodynamic models that solve for plasma density and flow velocity along a given flux tube have been used to calculate the distribution of plasma within the flux tube (e.g., Moffett et al., 1989). Rasmussen and Schunk (1990) used a model of this type to calculate the distribution along flux tubes at different L-values in order to generate a three-dimensional picture of the plasmasphere. Performing such 3D calculations for the entire magnetosphere and for time-varying geomagnetic conditions is an enormous computational task, and, for this reason, they have not been routinely performed to investigate the global scale response of the plasmasphere to changing geomagnetic conditions. To get around these computational limits, Rasmussen et al. (1993) developed a two-dimensional model of the plasmasphere to study the time-dependent evolution of plasma density in the equatorial plane of the magnetosphere. They reduced the 3D problem to 2D by integrating

the continuity equation along a flux tube from ionosphere to conjugate ionosphere. They assume that the plasma density is constant along a field line and follows the equation $DN/Dt = (N_o - N)/\tau$, where N is the number of plasmasphere particles per unit magnetic flux, N_o represents a saturation level of N, τ is a characteristic flux tube refilling time, and DN/Dt is a convective derivative that includes the effects of drift perpendicular to **B**. The model results indicate that, for prolonged quiet conditions, it would take depleted flux tubes approximately three days at L = 3 to refill and up to 100 days at L = 5.

The 2D approach has been extended recently using more elaborate time- dependent electric and magnetic field models to simulate specific well-observed events. Weiss (1997) have used the computational machinery of the MSFM along with the parametric flux tube refilling model of Rasmussen et al. (1993) to explore the evolution of the plasmasphere during and following magnetic storms. As described in Section 5, the MSFM attempts to realistically mimic the penetration of magnetospheric electric field effects into the inner magnetosphere.

Model calculations (e.g., Grebowsky, 1970; Chen and Wolf, 1972; Grebowsky et al., 1974; Weiss, 1997) have long established that a sustained increase in convection strips plasma off the plasmasphere and transports it to the dayside magnetopause. In general, time dependence in the electric field near the plasmapause causes the formation of long, thin strands of plasma that connect the main body of the plasmapause to the magnetopause. Density fine structure is frequently observed between the main plasmapause and the magnetopause, particularly in active times (Moldwin et al., 1995). Model-computed density structures for specific events have agreed well with observed fine structure (Grebowsky et al., 1974 ; Weiss, 1997), lending confidence that we basically understand the origin of the observed plasma structures.

Although much of the observed density fine structure is clearly due to time-varying convection, another process may be involved: the plasmapause, with its sharp inward pressure gradient and outward centrifugal force, tends to be unstable to interchange (Richmond, 1973; Lemaire, 1975). The process is complicated and inhibited by gravity and the presence of ring-current particles, which tend to be interchange-stable (Richmond, 1973; Huang et al., 1990). There are two fundamental unresolved questions related to the effects of interchange instability of the plasmapause. Does it substantially affect the location of the plasmapause, as Lemaire (1975, 1976) suggested? Does it play a major role in the generation of the observed density fine structure at the plasmapause? Answering these questions theoretically will require modeling that combines large-scale convection with fine-scale treatment of the plasmapause region.

7. Summary

Better models and tighter comparisons with observations will be required to finally settle the question of whether time-varying convection is the principal agent responsible for creating the storm-time ring current. All present computational models of the ring current have obvious theoretical defects, though the specific defects vary from model to model. It is now feasible to construct a theoretical model of ring-current injection that calculates pitch-angle distributions in detail, self-consistently including **E**, **B**, charge exchange, and Coulomb scattering. That major step forward in theoretical rigor and completeness should be completed in a few years. Tighter comparisons between modeled and observed electric and magnetic fields are needed.

The outer (high-L) boundary condition represents another major uncertainty for theoretical ring-current models, because data from individual spacecraft have never provided simultaneous flux measurements at many points along the nightside model boundary. However, the planned IMAGE mission may provide such information.

Uncertainty in the electric field remains the primary difficulty with modeling the evolution of the plasmasphere, and the uncertainty is the same as for ring-current modeling. An additional theoretical problem for plasmaspheric physics is adequate treatment of the interchange instability, the importance of which is still unclear.

Acknowledgements

The authors are grateful to L. Lyons for helpful discussions and to F. Toffoletto and A. Chan for technical help with the manuscript. This research was supported by the Atmospheric Sciences Division of the National Science Foundation under grant ATM-9613824 and by the National Aeronautics and Space Administration under grant NAGW-2826.

References

André, M., and Yau, A.: 1997, 'Theory and observations of ion energization and outflow in the high-latitude ionosphere', *Space Sci. Rev. (this volume).*

Bishop, J.: 1996, 'Multiple charge exchange and ionization collisions within the ring current-geocorona-plasmasphere system: Generation of a secondary ring current on inner L shells', *J. Geophys. Res.* **101**, 17,325.

Blanc, M., and Richmond, A.D.: 1980, 'The ionospheric disturbance dynamo', *J. Geophys. Res.* **85**, 1669.

Boyle, C.B., Reiff, P.H., and Hairston, M.R., 'Empirical polar cap potentials', *J. Geophys. Res.* **102**, 111.

Campbell, W.H.: 1996, 'Geomagnetic storms, the Dst ring-current myth and lognormal distributions', *J. Atmos. Terr. Phys.* **58**, 1171.

Carpenter, D.L., and Lemaire, J.: 1997, 'The plasmapause, from discovery to present', *Space Sci. Rev. (this volume).*

Chen, A.J., and Wolf, R.A.: 1972, 'Effects on the plasmasphere of a time-varying convection electric field', *Planet. Space Sci.* **20**, 483.

Chen, M.W., Lyons, L.R., and Schulz, M.: 1994, 'Simulations of phase space distributions of storm time proton ring current', *J. Geophys. Res.* **99**, 5745.

Chen, M.W., Schulz, M., and Lyons, L.R.: 1996, 'Modeling of ring current formation and decay: A review', in B.T. Tsurutani, J.K. Arballo, W.D. Gonzalez, and Y.Kamide (eds.), , Am. Geophys. Un., Washington, D. C., *Magnetic Storms*, Am. Geophys. Un., Washington, D. C., pp. 173–186.

Cheng, C.Z.: 1995, 'Three-dimensional magnetospheric equilibrium with isotropic pressure', *Geophys. Res. Lett.* **22**, 2401.

Daglis, I.: 1997, 'The role of magnetosphere-ionosphere coupling in magnetic storm dynamics', in B.T. Tsurutani, W.D. Gonzalez, Y. Kamide and J.K. Arballa (eds.), *Magnetic Storms*, Am. Geophys. Un., Washington, D. C., pp. 107–116.

Dessler, A.J., and Parker, E.N.: 1959, 'Hydromagnetic theory of geomagnetic storms', *J. Geophys. Res.* **64**, 2239.

Fejer, B.G.: 1986, 'Equatorial ionospheric electric fields associated with magnetospheric disturbances', in Y. Kamide and J.A. Slavin (eds.), *Solar Wind-Magnetosphere Coupling*, Terra Sci. Publ. Co., Tokyo, pp. 519–545.

Fejer, B.G., and Scherliess, L.: 1995, 'Time-dependent response of equatorial ionospheric electric fields to magnetospheric disturbances', *Geophys. Res. Lett.* **22**, 851.

Fok, M.-C., Kozyra, J.U., Nagy, A.F., and Cravens, T.E.: 1991, 'Lifetime of ring current particles due to Coulomb collisions in the plasmasphere', *J. Geophys. Res.* **96**, 7861.

Fok, M.-C., Moore, T.E., and Greenspan, M.E.: 1996, 'Ring current development during storm main phase', *J. Geophys. Res.* **101**, 15,311.

Forbes, J.M., and Harel, M.: 1989, 'Magnetosphere-thermosphere coupling: An experiment in interactive modeling', *J. Geophys. Res.* **94**, 2631.

Grebowsky, J.M.: 1970, 'Model study of plasmapause motion', *J. Geophys. Res.* **75**, 4329.

Grebowsky, J.M., Tulanay, Y.K., and Chen, A.J.: 1974, 'Temporal variations in the dawn and dusk midlatitude trough and plasmapause position', *Planet. Space Sci.* **22**, 1089.

Gussenhoven, M.S., Hardy, D.A., and Heinemann, N.: 1983, 'Systematics of the equatorward diffuse auroral boundary', *J. Geophys. Res.* **88**, 5692.

Hilmer, R.V., and Voigt, G.-H.: 1995, 'A magnetospheric magnetic field model with flexible current systems driven by independent physical parameters', *J. Geophys. Res.* **100**, 5613.

Horwitz, J.L., and Moore, T.E.: 1997, 'Four general questions on the transport of ionospheric plasmas into the magnetosphere', *Space Sci. Rev. (this volume).*

Huang, C.Y., and Frank, L.A.: 1986, 'A statistical study of the central plasma sheet: Implications for substorm models', *Geophys. Res. Lett.* **13**, 652.

Huang, T.S., Wolf, R.A., and Hill, T.W.: 1990, 'Interchange instability of the Earth's plasmapause', *J. Geophys. Res.* **95**, 17,187.

Hudson, M.K., Kotelnikov, A.D., Li, X., Roth, I., Temerin, M., Wygant, J., Blake, J.B., and Gussenhoven, M.S.: 1995, 'Simulation of proton radiation belt formation during the March 24, 1991, SSC', *Geophys. Res. Lett.* **22**, 291.

Iyemori, T., and Rao, D.R.K.: 1996, 'Decay of the Dst field of geomagnetic disturbance after substorm onset and its implication to storm-substorm relation', *Ann. Geophys.* **14**, 608.

Jordanova, V.K., Kistler, L.M., Kozyra, J.U., Khazanov, G.V., and Nagy, A.F.: 1996, 'Collisional losses of ring current ions', *J. Geophys. Res.* **101**, 111.

Kelley, M.C., Fejer, B.G., and Gonzales, C.A.: 1979, 'An explanation for anomalous ionospheric electric fields associated with a northward turning of the interplanetary magnetic field', *Geophys. Res. Lett.* **6**, 301.

Koskinen, H.E.J.: 1997, 'On observations of magnetospheric waves and their relation to precipitation', *Space Sci. Rev. (this volume).*

Kozyra, J.U., Jordanova, V.K., Horne, R.B., and Thorne, R.M.: 1994, 'Interaction of ring current and radiation belt protons with ducted plasmaspheric hiss, 1, Diffusion coefficients and timescales', *J. Geophys. Res.* **99**, 4069.

Kozyra, J.U., Rasmussen, C.E., Miller, R.H., and Lyons, L.R.: 1997, 'Modeling of the contribution of electromagnetic ion cyclotron waves to stormtime ring current erosion', in B.T. Tsurutani, W. D. Gonzales, Y. Kamide and J.K. Arballo, *Magnetic Storms*, Am. Geophys. Un., Washington, D.C., pp. 187–202.

Lambour, R.L.: 1994, *Calibration of the Rice Magnetospheric Specification and Forecast Model for the Inner Magnetosphere*, Ph. D. thesis, Rice University, Houston, Texas.

Lemaire, J.: 1975, 'The mechanisms of formation of the plasmapause', *Ann. Geophys.* **31**, pp. 175.

Lemaire, J.: 1976, 'Steady state plasmapause positions deduced from McIlwain's electric field models', *J. Atm. Terr. Phys.* **38**, pp. 1041.

Li, X., Chan, A., Hudson, M., and Roth, I.: 1991, 'Ring current ion interaction with micropulsations', in J.R. Kan, T.A. Potemra, S. Kokubun, and T. Iijima (eds.), *Magnetospheric Substorms*, Am. Geophys. Un., Washington, D. C., pp. 469–476.

Li, X., Hudson, M., Chan, A., and Roth, I.: 1993, 'Loss of ring current O^+ ions due to interaction with Pc 5 waves', *J. Geophys. Res.* **98**, 215.

Li, X., Roth, I., Temerin, M., Wygant, J.R., Hudson, M.K., and Blake, J.B.: 1993, 'Simulation of the prompt energization and transport of radiation belt particles during the March 24, 1991 SSC', *Geophys. Res. Lett.* **20**, 2423.

Lui, A.T.Y., McEntire, R.W., and Krimigis, S.M.: 1987, 'Evolution of the ring current during two geomagnetic storms', *J. Geophys. Res.* **92**, 7459.

Lyons, L.: 1997, 'Magnetospheric processes leading to precipitation', *Space Sci. Rev. (this volume).*

Moffett, R.J., Bailey, G.J., Quegan, S., Rippeth, Y., Samson, A.M., and Sellek, R.: 1989, 'Modelling the ionospheric and plasmaspheric plasma', *Phil. Trans. R. Soc. Lond.* **A328**, 255.

Moldwin, M.B., Thomsen, M.F., Bame, S.J., McComas, D., and Reeves, G.D.: 1995, 'The fine-scale structure of the outer plasmasphere', *J. Geophys. Res.* **100**, 8021.

Onsager, T.G., and Lockwood, M.: 1997, 'Magnetospheric sources of precipitation regions in the ionosphere', *Space Sci. Rev. (this volume).*

Rasmussen, C.E., and Schunk, R.W.: 1990, 'A three-dimensional time-dependent model of the plasmasphere', *J. Geophys. Res.* **95**, 6133.

Rasmussen, C.E., Guiter, S.M., and Thomas, S.G.: 1993, 'A two-dimensional model of the plasmasphere: refilling time constants', *Planet. Space Sci.* **41**, 35.

Richmond, A.D.: 1973: 'Self-induced motions of thermal plasma in the magnetosphere and stability of the plasmapause', *Rad. Sci.* **8**, 1019.

Richmond, A.D.: 1983, 'Thermospheric dynamics and electrodynamics', in R.L. Carovillano and J.M. Forbes (eds.), *Solar-Terrestrial Physics: Principles and Theoretical Foundations*, D. Reidel, Dordrecht-Holland, pp. 523–607.

Schield, M.A., Freeman, J.W., and Dessler, A.J.: 1969, 'A source for field-aligned currents at auroral latitudes', *J. Geophys. Res.* **74**, 247.

Sckopke, N.: 1966, 'A general relation between the energy of trapped particles and the disturbance field near the Earth', *J. Geophys. Res.* **71**, 3125.

Sheldon, R.B., and Hamilton, D.C.: 1993, 'Ion transport and loss in the Earth's quiet ring current, 1. Data and standard model', *J. Geophys. Res.* **98**, 13,491.

Siscoe, G.L., and Petschek, H.E.: 1996, 'On storm weakening during substorm expansion phase', *Ann. Geophys.* **15**, 211.

Spiro, R.W., Wolf, R.A., and Fejer, B.G.: 1988, 'Penetration of high-latitude-electric-field effects to low latitudes during SUNDIAL 1984', *Ann. Geophys.* **6**, 39.

Thorne, R.M.: 1972, 'Stormtime instabilities of the ring current', in K. Folkestad (ed.), *Magnetosphere Ionosphere Interactions*, University Press, Oslo, pp. 185–202.

Toffoletto, F.R., Spiro, R.W., Wolf, R.A., Hesse, M., and Birn, J.: 1996, 'Self-consistent modeling of inner magnetospheric convection', in E.J. Rolfe and B. Kaldeich (eds.), *Proceedings of the ICS-3 Substorm Meeting, SP-389*, ESA Publications Division, ESTEC, Noordwijk, The Netherlands, pp. 223–230.

Tsyganenko, N.A.: 1989, 'A magnetospheric magnetic field model with a warped tail current sheet', *Planet. Space Sci.* **37**, 5.

Tsyganenko, N.A.: 1995, 'Modeling the Earth's magnetospheric magnetic field confined within a realistic magnetopause', *J. Geophys. Res.* **100**, 5599.

Vasyliunas, V.M.: 1970, 'Mathematical models of magnetospheric convection and its coupling to the ionosphere', in B. M. McCormac (ed.) *Particles and Fields in the Magnetosphere*, D. Reidel, Hingham, MA, pp. 60–71.

Vasyliunas, V.M.: 1972, 'The interrelationship of magnetospheric processes', in B.M. McCormac (ed.), *The Earth's Magnetospheric Processes*, D. Reidel, Dordrecht, Holland, pp. 29-38.

Volland, H.: 1978, 'A model of the magnetospheric electric convection field', *J. Geophys. Res.* **83**, 2695.

Weiss, L.A., Lambour, R.L., Elphic, R.E., and Thomsen, M.F.: 1997, 'Study of plasmaspheric evolution using geosynchronous observations and global modeling', *Geophys. Res. Lett.* **24**, 599.

Wolf, R.A.: 1995, 'Magnetospheric configuration', in M.G. Kivelson and C.T. Russell (eds.), *Introduction to Space Physics*, Cambridge University Press, Cambridge, England, pp. 288–329.

Wolf, R.A.: 1983, 'The quasi-static (slow-flow) region of the magnetosphere', in R.L. Carovillano and J.M. Forbes (eds.), *Solar-Terrestrial Physics: Principles and Theoretical Foundations*, D. Reidel, Hingham, MA, pp. 303-368.

Wolf, R.A., Freeman, J.W., Jr., Hausman, B.A., Spiro, R.W., Hilmer, R.V., and Lambour, R.L.: 1997, 'Modeling convection effects in magnetic storms', in B.T. Tsurutani, J.K. Arballo, W.D. Gonzalez, and Y. Kamide (eds.), *Magnetic Storms*, Am. Geophys. Un., Washington, D. C., pp. 161–172.

Yau, A.W., and André, M.: 1997, 'Sources of ions', *Space Sci. Rev. (this volume).*

Address for correspondence: R. A. Wolf, Space Physics and Astronomy Dept., Rice University MS108, 6100 S. Main St., Houston, TX 77005, USA.

OBSERVATIONAL EVIDENCE FOR TRANSFER OF PLASMA ACROSS THE MAGNETOPAUSE

GÖTZ PASCHMANN
Max-Planck-Institut für extraterrestrische Physik
Garching, Germany

Received January 23, 1997; Accepted in final form March 4, 1997

Abstract. There is a long history of particle measurements that have established that plasma is being transferred across Earth's magnetopause in both directions. The paper reviews the nature of the observational evidence as well as the implications regarding the transfer mechanisms and their efficiencies.

Key words: Magnetopause, Boundary Layer, Magnetic Reconnection, Diffusion, Transport

Abbreviations: FTE – flux transfer event; IMF – interplanetary magnetic field; LLBL – low-latitude boundary layer; MSBL – magnetosheath boundary layer; RD – rotational discontinuity; TD – tangential discontinuity

1. Introduction

The magnetopause is the outer boundary of Earth's magnetosphere. Therefore any plasma transfer across the magnetopause constitutes, by definition, a source or loss of magnetospheric plasma, depending on the direction of transfer. Evidence for magnetopause plasma transfer has been obtained by a variety of methods, most directly by comparisons of particle spectra and ion composition, but also indirectly by, for example, tests of momentum balance that imply such a transfer.

The purpose of the paper is to review the observational results concerning the identification of the transfer processes, the location of the transfer, and the transfer rates.

2. Observational Signatures

We begin by reviewing briefly the methods by which plasma transfer across the magnetopause has been ascertained, with emphasis on in-situ measurements.

2.1. Energy Spectra

Similarities between energy spectra observed at low altitudes and typical energy spectra known from the magnetosheath provided the first observation suggestive of solar wind plasma entry (Frank, 1971; Heikkila and Winningham, 1971). Later on, in-situ measurements of spectra established that a boundary layer of sheath-like

Space Science Reviews **80**: 217–234, 1997.

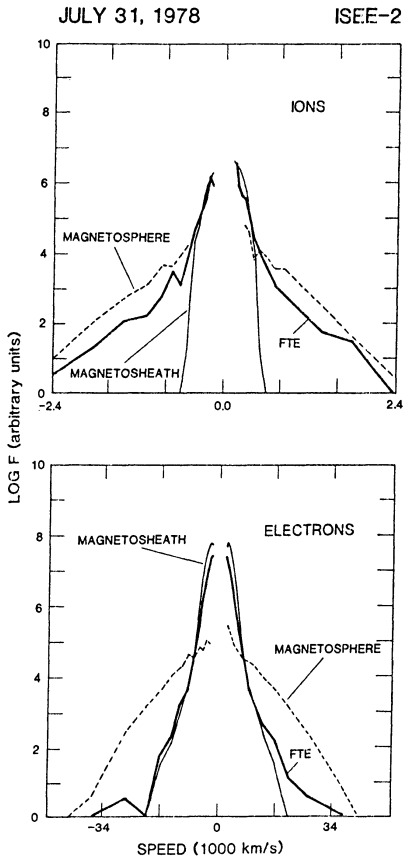

Figure 1. Comparison of ion and electron phase-space distributions measured in the magnetosheath, boundary layer (here labeled FTE), and magnetosphere on the dayside (from Thomsen et al., 1987).

plasma existed Earthward of the magnetopause essentially everywhere one probed the magnetopause. Figure 1 demonstrates the close similarity of ion and electron spectra measured across the magnetopause. Figure 2 demonstrates the gradual transition from the magnetosheath to the magnetosphere spectra, with both populations coexisting in the boundary layer. In support of outward directed plasma transfer, a layer of magnetospheric particles, often termed magnetosheath boundary layer (MSBL), is usually observed outside the magnetopause.

2.2. Ion Composition

Measurements of ion composition have provided conclusive proof that plasma is being transferred across the magnetopause. Figure 3 illustrates how solar wind and magnetospheric ions (of ionospheric origin) both can contribute to the low-latitude boundary layer (LLBL). Figure 4 shows that ions of indisputably solar origin, He^{++}

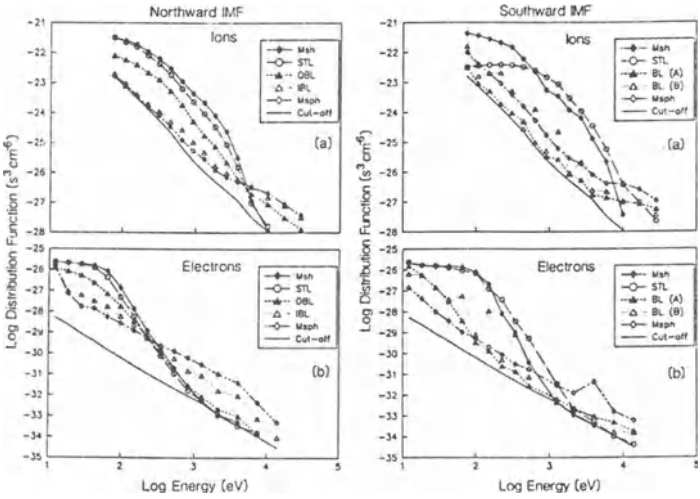

Figure 2. Sequence of measured ion and electron phase-space distributions, from the magnetosheath (Msh) to the magnetosphere (Msph), for the cases of northward and southward IMF (from Song et al., 1989).

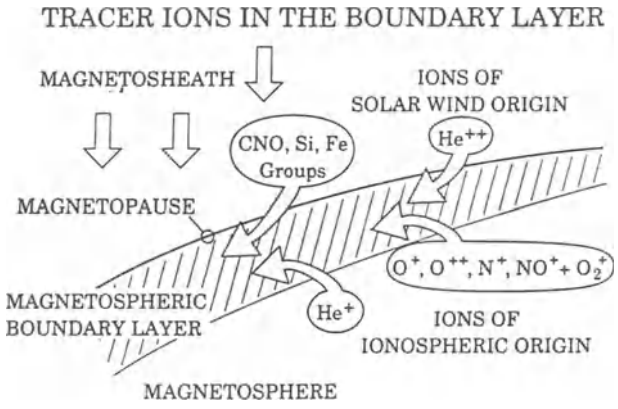

Figure 3. Ions that can be used to distinguish solar wind from ionospheric origin of plasma in the boundary layer (from Eastman and Christon, 1995).

and O^{6+}, are observed well inside the magnetosphere, establishing beyond any doubt that solar wind plasma is transferred across the magnetopause. Similarly, observations outside the magnetopause of singly-ionized O^+ ions that can only originate in Earth's ionosphere have shown that transfer also occurs in the opposite direction, causing a loss of magnetospheric plasma to the magnetosheath (e.g., Peterson et al., 1982; Fuselier et al., 1995).

Ion composition measurements have provided evidence for some mass discrimination in the plasma transfer. Specifically, the He^{++} to H^+ density ratio has been

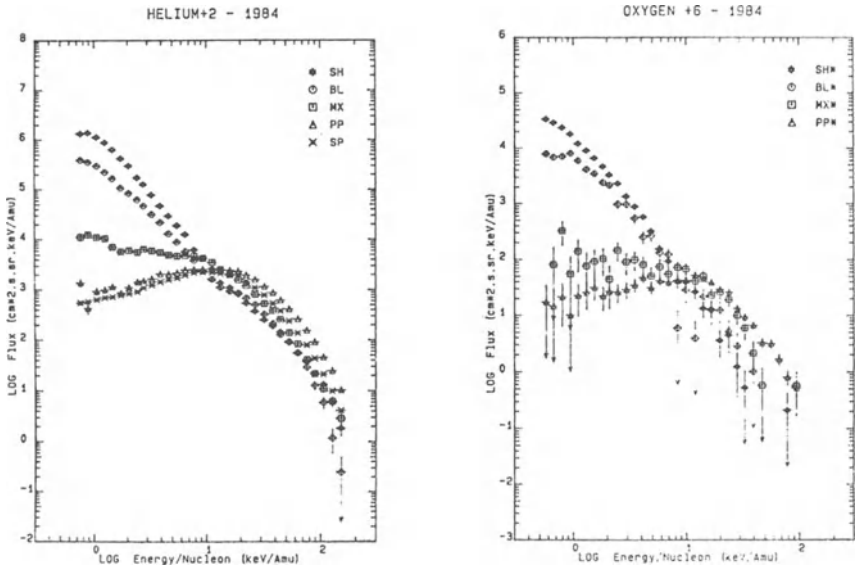

Figure 4. Sequence of energy spectra of ions of solar wind origin, He^{++} and O^{6+}, from the magnetosheath (SH) to the magnetosphere (SP) (from Eastman and Christon, 1995).

reported to decrease significantly (by 40%) between the magnetosheath and the magnetosphere (Fuselier et al., 1997). The reasons for this mass-dependence are not understood at present. In fact, the He^{++} to H^{+} ratio should increase if transfer of particles were facilitated by larger gyro radii, for example.

2.3. FLUID-PARAMETERS

Plasma transfer has been inferred also from similarities of the plasma fluid parameters. Figure 5 shows such parameters for an outbound magnetopause crossing just sunward of the (northern) polar cusp, demonstrating the presence of plasma with the same density and temperature as that in the magnetosheath, but with oppositely directed flow velocity, Earthward of the magnetopause. Since the high density and large width of the layer suggested an efficient entry mechanism, that particular part of the boundary layer is sometimes referred to as the entry layer. Observations of plasma fluid flow across the magnetopause would constitute more direct evidence, but such flows are much more difficult to measure reliably.

3. Transfer Processes

The physical processes that can cause plasma transfer across the magnetopause, and their observable signatures have been thoroughly discussed in a recent mono-

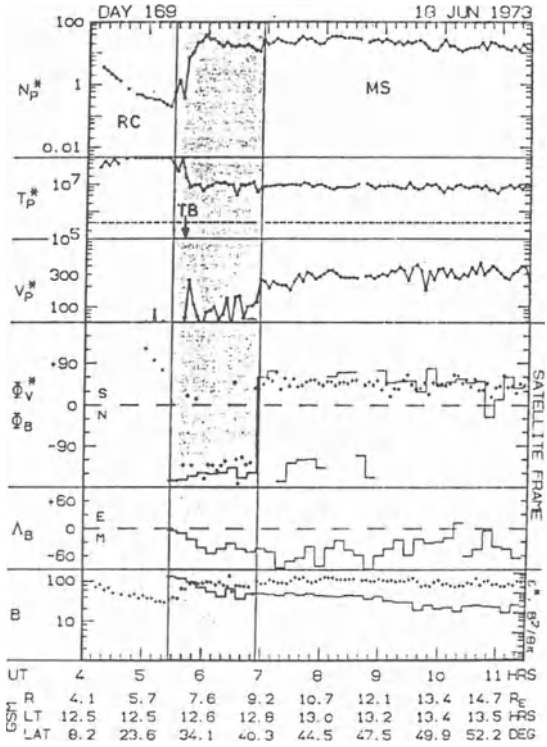

Figure 5. Plasma fluid parameters for an outbound pass from the ring current (RC) through the entry layer (shaded) into the magnetosheath (MS) (from Paschmann et al., 1976).

graph, 'Physics of the Magnetopause' (edited by Song et al., 1995) . Only a brief summary is therefore provided here, and some recent observations are added.

3.1. Magnetic Reconnection

Magnetic reconnection is the transfer process for which observational tests are well-defined, as recently reviewed by Sonnerup et al. (1995). When the interplanetary and terrestrial magnetic fields have become interconnected through this process, the magnetic field attains a finite component B_n normal to the magnetopause surface, and the plasma can flow across the magnetopause with a finite velocity, V_n. These normal components are, however, difficult to measure reliably because, for reasonable reconnection rates, they are small compared with the tangential components and the magnetopause normals are usually not known well enough to allow a precise decomposition of the vectors. In addition, the measured V_n is contaminated by the magnetopause normal motion which is often large compared with the expected cross-magnetopause flow. A similar limitation holds for measurements of

the electric field tangential to the magnetopause, E_t, that is another signature of reconnection. In this case it is the normal component that usually dominates.

In lieu of reliable direct indicators of magnetic reconnection, much of the in-situ evidence for its occurrence has come from observations of accelerated plasma flows along the magnetopause that result from the tension implied by the sharp bend in the interconnected magnetic field lines. The velocity increment imposed by this tension force is equal to the Alfvèn velocity based on the difference in **B** across the magnetopause. When this difference is large, i.e., for large magnetic field shear, and the external flow speed is low, i.e., in the subsolar region, the accelerated flows stand out by their large speeds, up to 500 km/s. This plasma jetting away from the reconnection site was discovered in the flow measurements on ISEE (Paschmann et al., 1979), but has been commonly observed in the subsolar region since. Depending on the directions and magnitudes of the external flow velocity and the field tension, the effect of the acceleration might simply be a rotation of the flow velocity vector, or even a reduction in flow speed.

In the fluid description the magnetopause is a rotational discontinuity (RD) if reconnection is occurring, while without reconnection it remains a tangential discontinuity (TD). For an RD, a strict quantitative relationship (often referred to as the 'Walén relation') exists between the changes in **B** and in **V** on the basis of tangential stress balance, while for a TD the flows on the two sides are unrelated. Figure 6 shows two applications of the Walén test, one where the good agreement indicates that the spacecraft was crossing an RD, and another, where the complete disagreement indicates a crossing of a TD. Note that in these tests the plasma velocity is expressed in the so-called deHoffmann-Teller frame, i.e., the frame that moves along the magnetopause at such a velocity, V_{HT}, that the plasma flow is magnetic field aligned. V_{HT} is identical with the velocity at which reconnected field lines move along the magnetopause. For an RD, the flow velocity V_n across the magnetopause is Alfvènic, i.e., fully determined by B_n and the mass density ρ.

Tangential stress balance can also be expressed as a jump relation across the magnetopause. Based on tests of this jump relation, it has been concluded that the low-latitude dayside magnetopause approximately met the criterion for an RD in 60% of the crossings at times when the magnetic shear angle was larger than 45° (Phan et al., 1996). RD identifications of the magnetopause have also been made at other locations along the magnetopause, notably near the dusk magnetopause (Gosling et al., 1986) and further down the magnetotail (Sanchez et al., 1990).

Evidence for reconnection has also been found in features of plasma velocity distributions, such as 'D'-shaped ion distributions or reflected-accelerated ions. D-shaped distributions (Cowley, 1982) occur because the flux-tube motion along the magnetopause implied by reconnection imposes a velocity threshold below which magnetosheath particles cannot enter the boundary layer. Particles that are reflected at the magnetopause undergo the same kind of acceleration as transmitted particles. This is true regardless of whether these are particles incident on the magnetopause from the inside or from the outside, and both cases have been observed (e.g., Son-

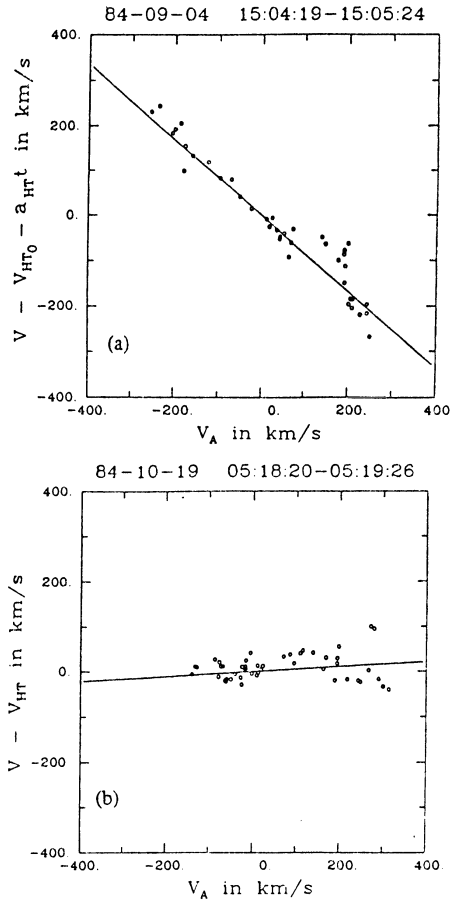

Figure 6. Results of a successful (top) and unsuccessful (bottom) application of the Walén test. Plotted are the measured plasma velocities in the deHoffmann-Teller frame vs. the local Alfvén velocity, modified for the effects of pressure anisotropy. For a successful test the slope of the regression line should be near plus or minus one (from Sonnerup et al., 1990).

nerup et al., 1981; Scholer and Ipavich, 1983; Smith and Rogers, 1991; Fuselier et al., 1991).

Another piece of evidence is based on velocity-filter effects that arise from the superposition of particle and field-line motion (cf. Figure 7). Particles follow different trajectories according to the ratio of the particles' speed along the field line and the speed at which the field line moves along the magnetopause because of its interconnection with the IMF. Particles entering at the X-line with different speeds will become spatially dispersed as a result of the noted effect and form a wedge, with the faster ones at the Earthward edge, and the slowest ones at the inner edge of the wedge. Such spatial profiles, with magnetosheath electrons separated from the much slower sheath ions, have been observed near the low-latitude dayside mag-

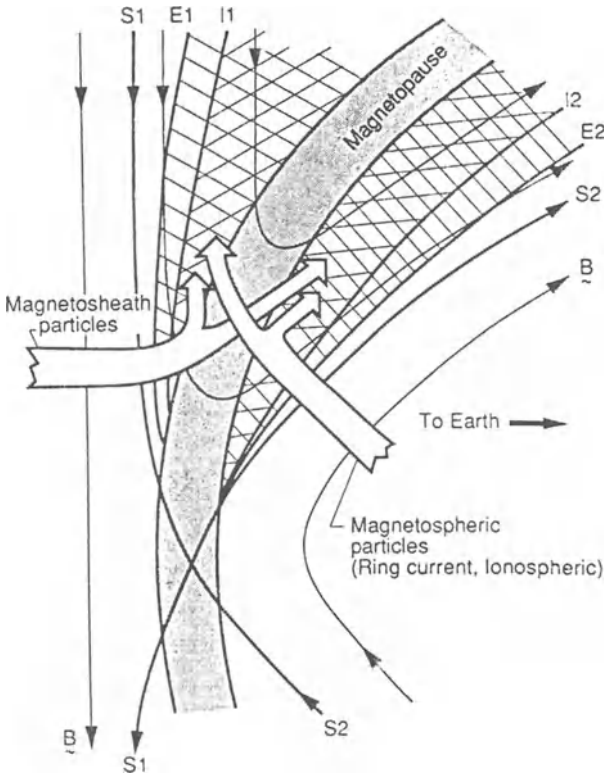

Figure 7. Sketch of the magnetopause near a reconnection site, illustrating the possible fate (reflection and/or transmission) for magnetosheath and magnetosphere particles. The lines labeled E_1 and I_1 denote the limits of electron and ion access in the MSBL resulting from the velocity-filter effects described in the text. Corresponding limits, labeled E_2 and I_2, are shown for the LLBL (from Gosling et al., 1990).

netopause (Gosling et al., 1990). The same kind of velocity-filter effects also occur when particles traverse the magnetopause in the other direction, as demonstrated by Nakamura et al. (1996).

The commonly observed absence of a plasma depletion and magnetic-flux pile-up region outside the magnetopause at times of high magnetic shear have also been interpreted as evidence for magnetic reconnection (Phan et al., 1994). For low-shear crossings, magnetic flux-tubes are expected (and observed) to pile up in front of the magnetospheric obstacle, becoming depleted of plasma in the process. When magnetic shear is high, one expects reconnection to remove the extra flux by transferring it into the geomagnetic tail. This is exactly what is observed in high-shear magnetopause crossings that take place under normal solar wind dynamic pressure conditions (cf. Figure 8).

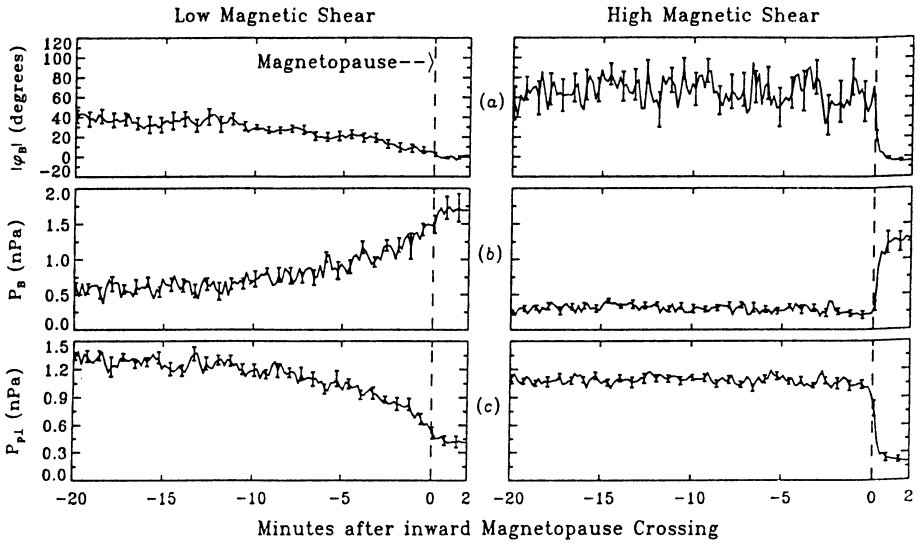

Figure 8. Superposed epoch analyses of the plasma and magnetic pressures for AMPTE/IRM low-shear (on the left) and high-shear crossings (on the right), showing, respectively, the presence and absence of a plasma depletion and magnetic flux pile-up region (after Phan et al., 1994).

It should be noted, however, that for high-shear crossings that occur while the solar wind dynamic pressure is higher than normal, some plasma depletion and magnetic flux pile-up is observed (Andersen et al., 1997). Under such conditions the plasma β (i.e., the ratio between plasma and magnetic field pressures) in the magnetosheath is much higher, and the authors have interpreted their result to imply a reduction in the reconnection rate with increasing β. Direct observations of reconnection flows have earlier suggested that their occurrence rate were reduced at large β (Paschmann et al., 1986).

3.2. DIFFUSION

Reconnection produces a boundary layer that is located entirely on magnetospheric field lines that are open, i.e., cross the magnetopause. The boundary layer does, however, continue to exist when reconnection in the subsolar region should not be effective (i.e., for northward IMF, or low magnetic shear), and is also observed on field lines that appear to be closed. This is usually taken as evidence that other entry mechanisms must be operating; a prime candidate is diffusion. Contrary to the case of reconnection, however, there is no direct confirmation of this hypothesis from particle data. In fact, it has been argued that, during times of northward IMF, attachment of flux tubes to the dayside magnetosphere via reconnection in the polar cusp regions could effectively produce a boundary layer on closed field lines

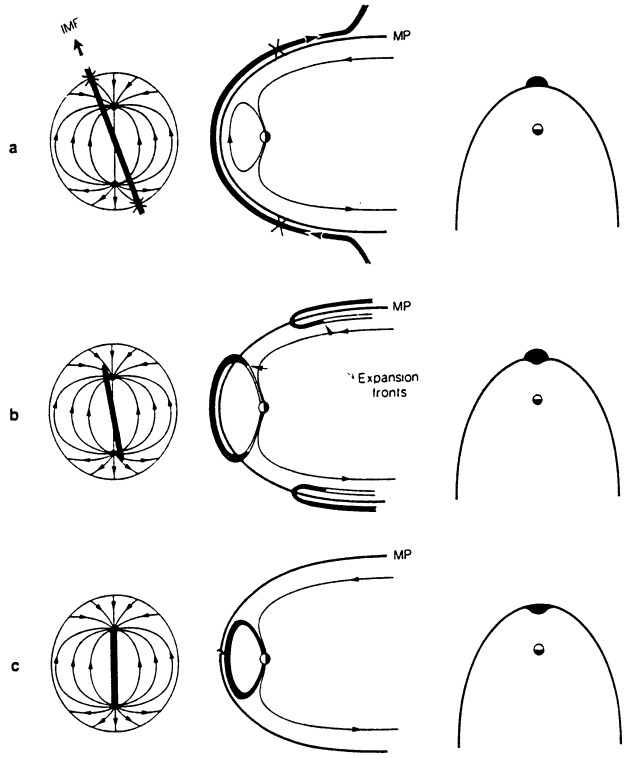

Figure 9. Illustration of how attachment of magnetosheath flux tubes through reconnection at the polar cusps could effectively produce a boundary layer on closed field lines for northward IMF (from Song and Russell, 1992).

without invoking diffusive or other entry mechanisms (cf. Figure 9). The subject of diffusive transport at the magnetopause is reviewed by Scholer and Treumann (1997).

4. Transfer Locations

Reconnection is initiated in a small region around an X- (or reconnection-) line that is located somewhere on the dayside magnetopause for southerly IMF, but moves beyond the polar cusp region for northerly IMF. If reconnection proceeds for sufficiently long times, the subsequent transport by the magnetosheath flow along the magnetopause will generate a swath of interconnected flux that will extend down the entire magnetotail. All along that swath plasma can enter with a flow speed proportional to the local B_n. Thus reconnection, when sustained for sufficiently long times, automatically generates plasma transfer over a substantial portion of the entire magnetopause, extending downstream from the reconnection site. If

reconnection is transient, on the other hand, only a slab of open magnetic flux and plasma transfer is created that is moving tailward.

For a number of reasons, the polar cusp regions are considered key regions for plasma transfer (e.g., Haerendel, 1978). The cusp-like indentation of the magnetopause that has given these regions their name severely perturbs the external magnetosheath flow, setting up fluctuation levels in plasma and field parameters that are hypothesized to cause plasma transfer. The magnetic field lines that are threading the cusps spread in all directions along the magnetopause, providing favorable reconnection sites regardless of the orientation of the IMF. The observation of a particularly thick boundary layer in the cusp region is strong evidence for efficient local plasma transfer. Measurements presently carried out in the cusp regions by the Interball and Polar missions, and future measurements by Cluster-II or Phoenix, will certainly clarify the role of the cusps for plasma transfer, and the nature of the transfer processes.

Regardless of the location of the plasma transfer across the magnetopause, subsequent transport along the magnetopause can mask the actual entry location. For example, it is conceivable that the LLBL is actually fed from the thick boundary layer at high latitudes. Because the properties of the magnetosheath plasma vary strongly with distance from the subsolar point, the plasma properties observed in the boundary layer carry information about the entry location, although velocity-filter effects upon entry and subsequent transport to the location of observation must be taken into account (see the review by Onsager and Lockwood, 1997).

5. Transfer Rates

This section deals with the quantitative assessment of the rates at which plasma is being transferred across the magnetopause.

5.1. Reconnection Rates

If reconnection occurs, plasma transfer is determined by the reconnection rate, a dimensionless number commonly defined as $M_{An} = V_n/V_A = B_n/B$ where V_A is the Alfvén speed in the inflow region. B_n has been reliably determined only in a few cases, with values that imply reconnection rates of order 0.1.

As mentioned earlier, V_n is difficult to measure directly. But some upper limit for the average V_n has been inferred from a statistical study of dayside AMPTE/IRM data by Phan and Paschmann (1996). They found that in most cases the sign of V_n, measured in the spacecraft frame, agrees with the sign implied by the sense of the magnetopause crossing (positive for inbound, negative for outbound crossings). This means that the measured V_n values were dominated by the magnetopause motion which on average was ≈ 23 km/s. Thus the true normal flow speeds across the magnetopause must have been much less than 23 km/s. As the average V_A for

these observations was 205 km/s, the average reconnection rate must have been substantially less than 0.1.

Another measure of the reconnection rate is the tangential electric field E_t measured in the frame moving with the magnetopause. From a statistical study of ISEE data, an average E_t of 0.4 mV/m and an average convection speed of 20 km/s (both measured in the magnetopause rest frame) have been reported (Lindqvist et al.,1990). Taking as typical magnetosheath magnetic fields and densities 30 nT and 30 cm^{-3}, respectively, the authors obtained 120 km/s as the average Alfvén speed. With these separately averaged numbers, one obtains an estimate of the average reconnection rate of $20/120 \approx 0.17$. Noting that E_t is related to B_n via $E_t = V_{HT}B_n$, where V_{HT} is the deHoffmann-Teller velocity, one can also take an alternate route, and convert the average E_t into an average B_n. Taking V_{HT} = 200 km/s as a typical value, the 0.4 mV/m corresponds to B_n = 2 nT. This would imply a reconnection rate that is only $2/30 \approx 0.07$, less than half the previous estimate. But both estimates must be considered rather crude because of the average Alfvén and deHoffmann-Teller speeds that were assumed.

In this context it is important to note that observations of plasma flows that obey the Walén relation, although establishing that reconnection is (or has been) occurring, do not provide a value for the reconnection rate because the force that accelerates the plasma is independent of the reconnection rate (e.g., Sonnerup, 1984).

If the reconnection rate is known, one can compute the total transfer rate (in terms of the number of particles per second entering the magnetosphere) by noting that the flux of solar wind particles impinging on the cross-sectional area of the magnetopause (assumed to be a circle with $40\,R_E$ diameter) is $\approx 10^{29}s^{-1}$. The reconnection rate determines what fraction of this incident flux actually enters the magnetosphere. If the reconnection rate is 0.1, consistent with above crude estimates, and reconnection occurs over the entire dayside magnetopause, then on average $\approx 10^{28}$ particles would enter each second.

Obviously, shorter reconnection lines and/or temporal reductions in the reconnection rate would reduce the total number of particles that enter at any given time, and there is strong evidence that temporal variations in the reconnection rates and/or the spatial extent of the reconnection region indeed occur. The most striking examples are some well-documented magnetopause crossings in which no boundary layer was observed in high time-resolution plasma data (Papamastorakis et al., 1984; Eastman et al., 1996), even though these were high-shear crossings where reconnection was expected to occur. Reconnection either simply did not occur at all in these cases, or the observation sites were located outside the path of interconnected flux created by a spatially limited reconnection line.

A hint as to which of the two possibilities is actually responsible is provided by the studies of the flux pile-up and plasma depletion layer already referred to above. The absence of such a layer for high-shear crossings holds namely also for the subset of the crossings where no reconnection flow signatures were observed. If reconnection were not going on at all, one would have expected flux pile-up

to occur at those times for the same reason as for low-shear crossings. Thus it seems likely that reconnection was occurring in all high-shear crossings, but in such a patchy and/or transient fashion that the local reconnection signatures were often missed, but yet flux pile-up was prevented. The so-called flux-transfer events (FTE's), discovered by Russell and Elphic (1978), are commonly interpreted as signatures of reconnection that is both patchy and transient.

Local measurements are thus not adequate to assess the net transfer. To overcome this difficulty, one should try to define a more readily available global measure of the transfer efficiency. For this one should be able to take the cross-tail electric potential (or, equivalently, the cross-polar-cap potential), because this potential is directly determined by the amount of interconnected magnetic flux that is being transported into the tail per second. The transfer efficiency would be defined as the ratio of the cross-polar-cap potential drop to the potential drop across a magnetospheric diameter in the solar wind. This ratio has been called 'interconnection rate' by Hill (1984).

For typical solar wind conditions (a wind speed of 400 km/s and a transverse magnetic field strength of 5 nT), the solar wind electric field equals 2 mV/m, and the potential drop over the 40 R_E diameter that is typical for the magnetosphere's cross-section is 500 kV. This would also be the value of the cross-polar-cap potential if the reconnection rate were 100%. But in reality the cross-polar-cap potential is known to be much smaller. Figure 10 demonstrates that there is a correlation between the cross-polar-cap potential and the solar wind electric field, with the large scatter of the data presumably reflecting variations in the reconnection rate and/or the reconnection line length.

To estimate the net plasma transfer across the magnetopause, one would need the value of the cross-polar-cap potential (obtained from low-altitude polar satellites, for example), the values of electric field and particle number flux density in the solar wind, as measured by some upstream monitor, plus an estimate of the diameter of the magnetosphere, obtained from a model magnetosphere for the measured solar wind dynamic pressure. The net plasma input into the magnetosphere (in terms of particles per second) could then be calculated by multiplying the number flux density by the above-defined 'interconnection rate' and the cross-sectional area of the magnetosphere.

It should be noted, however, that it takes time for the magnetic flux to be transported into the tail and for the cross-tail potential to build up. Under non-stationary conditions this time delay would have to be taken into account. Another complication lies in the fact that the magnetopause is known to reflect some portion of the incident plasma (e.g., Sonnerup et al., 1981; Fuselier et al., 1991). Partial reflection will naturally lower the transfer rate. This will, by the way, not be in conflict with the derived reconnection rate because reflection will also reduce the Alfvén velocity such as to keep the reconnection rate V_n/V_A equal to B_n/B. This is because the reflected particles contribute to the parallel plasma pressure $p_{||}$ and the proper Alfvén velocity to be taken here contains a correction factor that is < 1 if $p_{||}$

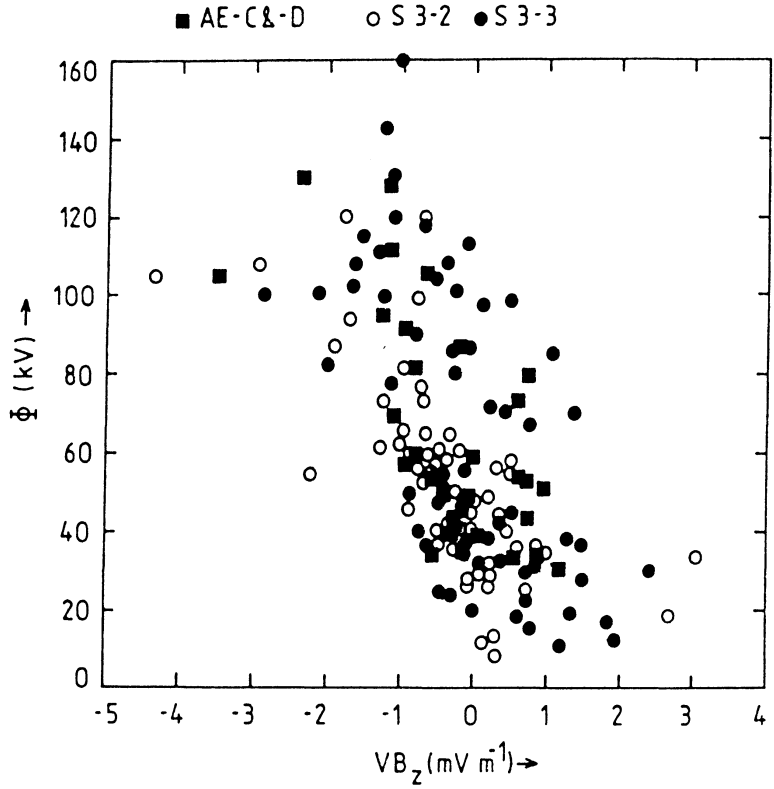

Figure 10. Cross-polar-cap potential versus the y-component of the solar wind electric field, compiled from various low-altitude spacecraft measurements by Cowley (1984).

exceeds $p_\perp$. As noted earlier, transfer rates can also be different for different ion species.

Reconnection not only produces solar wind plasma entry but also magnetospheric plasma losses. A crude estimate of the loss rate can be obtained from the following argument. The electric field E_t tangent to the magnetopause that is implied by reconnection must be continuous across the magnetopause. If the magnetic fields on the two sides have anti-parallel components, as expected for reconnection, that electric field will drive plasma towards the magnetopause from both sides with equal velocity (assuming equal magnetic field strengths). The ratio of source to loss rates should therefore scale as the mass density ratio across the magnetopause which typically is of order 10. Thus the loss rate is expected to be of order 10% of the source rate.

5.2. Diffusion Coefficients

Sckopke et al. (1981) have estimated how large a diffusion coefficient would be needed to populate the entire LLBL by diffusion across the magnetopause, even

though their observations did not necessarily imply the presence of diffusive transport. They took an average boundary layer thickness, density, and bulk speed of $0.5\,R_E$, $8\,\mathrm{cm}^{-3}$, and 150 km/s, respectively, resulting in a flux per unit height of $3.8 \cdot 10^{18}\mathrm{m}^{-1}\mathrm{s}^{-1}$. As the point of observation was $18\,R_E$ from the subsolar point, the estimated average flux density across the magnetopause was $6.7 \cdot 10^{10}\mathrm{m}^{-2}\mathrm{s}^{-1}$. If attributed entirely to diffusion, this flux should equal $D\delta N/h$ where D is the diffusion coefficient and δN the density change across a diffusion layer of thickness h. For a density change of $27\,\mathrm{cm}^{-3}$ and a diffusion coefficient $D = 10^9\mathrm{m}^2\mathrm{s}^{-1}$, the authors obtain $h = 400$ km, which is of the order of the magnetopause thickness inferred from their two-spacecraft measurements. The diffusion layer could not be significantly thinner than that, and thus D could not be much smaller than $10^9\mathrm{m}^2\mathrm{s}^{-1}$, if diffusion was the only process contributing to the boundary layer.

Estimates of diffusion coefficients based upon observed wave amplitudes at the magnetopause have also been carried out, but have fallen short of the required values (cf. Treumann et al., 1995; see also Scholer and Treumann, 1997).

In addition to microscopic diffusion by scattering of the particles, turbulent diffusion could be transferring plasma. In this case the diffusion coefficient is given by the following relation:

$$D\delta N/h = < NV_n > - < N >< V_n > \tag{1}$$

where the brackets denote averages. Turbulent diffusion implies that there is a correlation between N and V_n such that the two terms on the right of the equation do not cancel. If plasma parcels with larger N move with larger inward speeds (i.e., negative V_n) than parcels with lower N, more material is moving inward than outward on average, resulting in a net inward transport.

Eq. 1 has been applied to AMPTE/IRM crossings of the dayside LLBL, but so far without consistent results, presumably due to inherent experimental uncertainties. Because V_t is so much larger than the expected V_n at the magnetopause, any error in the magnetopause normal used to decompose the measured bulk velocity $\mathbf{V}$ into V_t and V_n introduces spurious V_n's. The V_n's should ideally also refer to the rest frame of the magnetopause. If they do not, and there is an asymmetry in inward and outward magnetopause speeds, the result is biased. Furthermore, Eq. 1 contains the thickness, h, of the layer that is not well known from single-spacecraft measurements. It would appear that multi-point measurements are needed to evaluate the diffusion coefficient according to Eq. 1.

6. Summary

There is a long history of particle measurements that have established that plasma is being transferred across the magnetopause in both directions. As to the mechanisms that cause this transfer, only magnetic reconnection has been established beyond any reasonable doubt.

Reconnection causes plasma to be transferred wherever external and internal magnetic fields have become interconnected. The size of this region is determined by the location and length of the reconnection line and by the length of the time reconnection has been going on. The rate at which plasma is transferred locally is given by the reconnection rate, for which values of order 0.1 have been inferred from the measurements. At this rate of order 10^{28} particles/s would enter the magnetosphere if the reconnection line was located in the subsolar region and had its maximum extent.

As a measure of the overall transfer efficiency that includes the effect of a reduced reconnection line, one should be able to use the ratio between the cross-polar-cap potential and the potential drop in the solar wind over the cross-section of the magnetosphere, if conditions are steady. Partial reflection of plasma at the magnetopause also needs to be considered, but is presently not well understood.

Concerning the losses of magnetospheric particles across the magnetopause, a crude estimate predicts a loss rate that is lower than the source rate by a factor representing the density jump across the magnetopause, which is typically of order 10.

Subsolar region reconnection requires a southerly IMF and transfers plasma onto open field lines only, whereas the LLBL is observed for all IMF directions and also on closed field lines, at least partially. Thus it would seem that other transfer mechanisms must be operative. Diffusion has been invoked, but never proven to be adequate. Furthermore, reconnection schemes for northward IMF have been devised that could create an LLBL on closed field lines. The question of transfer processes other than reconnection thus remains open.

It is also important to remember that the observed absence of a boundary layer in some magnetopause crossings implies that, at times, no plasma transfer process, reconnection or otherwise, could have been operating at or upstream of the point of observation. Time variations in the transfer rates and/or locations are therefore an important aspect of plasma transfer across the magnetopause.

Finally, the role of the polar cusps, and in particular the contributions from reconnection and non-reconnection processes to cusp region plasma transfer, remains an issue that needs clarification before magnetopause plasma transfer can be understood quantitatively.

Acknowledgements

The author thanks T.-D. Phan for comments on the manuscript.

References

Andersen, B.J., Phan, T.-D., and Fuselier, S.A.: 1997, 'Relationships between Plasma Depletion and Subsolar Reconnection', *J. Geophys. Res.* **102**, in press.

Cowley, S.W.H.:1982, 'The Causes of Convection in the Earth's Magnetosphere: A Review of Developments during the IMS', *Rev. Geophys. Space Phys.* **20**, 531–565.

Cowley, S.W.H.:1984, 'Solar Wind Control of Magnetospheric Convection', *Achievements of the International Magnetospheric Study (IMS)*, ESA SP-217, Paris, pp. 483–494.

Eastman, T. and Christon, S.: 1995, in P. Song at al. (eds.), 'Ion Composition and Transport near the Earth's Magnetopause', *Physics of the Magnetopause*, Geophys. Monogr. 90, AGU, Washington, pp. 131–137.

Eastman, T.E., Fuselier, S.A., and Gosling, J.T.: 1996, 'Magnetopause Crossings without a Boundary Layer', *J. Geophys. Res.* **101**, 49–57.

Frank, L. A.: 1971, 'Plasma in the Earth's Polar Magnetosphere', *J. Geophys. Res.* **76**, 5202–5219.

Fuselier, S.A., Klumpar, D.M., and Shelley, E.G.: 1991, 'Ion Reflection and Transmission during Reconnection at the Earth's Subsolar Magnetopause', *Geophys. Res. Lett.* **18**, 139–142.

Fuselier, S.A., Anderson, B.J., and Onsager, T.G.: 1995, 'Particle Signatures of Magnetic Topology at the Magnetopause: AMPTE/CCE Observations', *J. Geophys. Res.* **100**, 11,805–11,821.

Fuselier, S.A., Shelley, E.G., and Lennartsson, O.W.: 1997, 'Solar Wind Composition Changes across Earth's Magnetopause', *J. Geophys. Res.* **102**, 275–283.

Gosling, J.T., Thomsen, M.F., Bame, S.J., and Russell, C.T.: 1986, 'Accelerated Plasma Flows at the Near-Tail Magnetopause', *J. Geophys. Res.* **91**, 3029–3041.

Gosling, J.T., Thomsen, M.F., Bame, S.J., Onsager, T.G., and Russell, C.T.: 1990, 'The Electron Edge of the Low Latitude Boundary Layer during Accelerated Flow Events', *Geophys. Res. Lett.* **17**, 1833–1836.

Haerendel, G.: 1978, 'Microscopic Plasma Processes Related to Reconnection', *J. Atmos. Terr. Phys.* **40**, 343–353.

Heikkila, W.J. and Winningham, J.D.: 1971, 'Penetration of Magnetosheath Plasma to Low Altitude Through the Dayside Magnetospheric Cusps', *J. Geophys. Res.* **76**, 883–891.

Hill, T.: 1984, in R.L. Carovillano and J.M. Forbes (eds),'Solar-Wind Magnetosphere Coupling', *Solar-Terrestrial Physics*, D. Reidel, Dordrecht, pp. 261 –302.

Lindqvist, P.-A. and Mozer, F.S.: 1990, 'The Average Tangential Electric Field at the Noon Magnetopause', *J. Geophys. Res.* **95**, 17,137–17,144.

Nakamura, M., Terasawa, T., Kawano, H., Fujimoto, M., Hirahara, M., Mukai, T., Machida, S., Saito, Y., Kokobun, S., Yamamoto, T., and Tsuruda, K.: 1996, 'Leakage Ions from the LLBL to MSBL: Confirmation of Reconnection Events at the Dayside Magnetopause', *J. Geomagn. Geoelec.* **48**, 65–70.

Onsager, T.G. and Lockwood, M.: 1997, 'High-Latitude Particle Precipitation and its Relationship to Magnetospheric Source Regions', *Space Science Reviews* (this volume).

Papamastorakis, I., Paschmann, G., Sckopke, N., Bame, S.J., and Berchem, J.: 1984, 'The Magnetopause as a Tangential Discontinuity for Large Field Rotation Angles', *J. Geophys. Res.* **89**, 127–135.

Paschmann, G., Haerendel, G., Sckopke, N., and Rosenbauer, H.: 1976, 'Plasma and Field Characteristics of the Distant Polar Cusp near Local Noon: The Entry Layer', *J. Geophys. Res.* **81**, 2883–2899.

Paschmann, G., Sonnerup, B.U.Ö, Papamastorakis, I., Sckopke, N., Haerendel, G., Bame, S.J., Asbridge, J.R., Gosling, J.T., Russell, C.T., and Elphic, R.C.: 1979, 'Plasma Acceleration at the Earth's Magnetopause: Evidence for Reconnection', *Nature* **282**, 243–246.

Paschmann, G., Papamastorakis, I., Baumjohann, W., Sckopke, N., Carlson, C.W., Sonnerup, B.U.Ö, and Lühr, H.: 1986, 'The Magnetopause for Large Magnetic Shear: AMPTE/IRM Observations', *J. Geophys. Res.* **91**, 11,099–11,115.

Peterson, W.K., Shelley, E.G., Haerendel, G., and Paschmann, G.: 1982, 'Energetic Ion Composition in the Subsolar Magnetopause and Boundary Layer', *J. Geophys. Res.* **87**, 2139–2145.

Phan, T.-D. and Paschmann, G.: 1996, 'Low-Latitude Dayside Magnetopause and Boundary Layer for High Magnetic Shear: 1. Structure and Motion', *J. Geophys. Res.* **101**, 7801–7815.

Phan, T.-D., Paschmann, G., Baumjohann, W., Sckopke, N., and Lühr, H.: 1994, 'The Magnetosheath Region Adjacent to the Dayside Magnetopause: AMPTE/IRM Observations' *J. Geophys. Res.* **99**, 121–141.

Phan, T.-D., Paschmann, G., and Sonnerup, B.U.Ö.: 1996, 'Low-Latitude Dayside Magnetopause and Boundary Layer for High Magnetic Shear: 2. Occurrence of Magnetic Reconnection', *J. Geophys. Res.* **101**, 7817–7828.

Russell, C. T. and Elphic, R. C.: 1978, 'Initial ISEE Magnetometer Results: Magnetopause Observations', *Space Science Reviews* **22**, 681.

Sanchez, E.R., Siscoe, G.L., Gosling, J.T., Hones, Jr., E.W., and Lepping, R.P.: 1990, 'Observations of Rotational Discontinuity: Slow Expansion Fan Structure of the Magnetotail Boundary', *J. Geophys. Res.* **95**, 61–73.

Scholer, M. and Ipavich, F.M.: 1983, 'Interaction of Ring Current Ions with the Magnetopause', *J. Geophys. Res.* **88**, 6937–6943.

Scholer, M. and Treumann, R.A.: 1997, 'The Low-Latitude Boundary Layer at the Flanks of the Magnetopause' *Space Science Reviews* (this volume).

Sckopke, N., Paschmann, G., Haerendel, G., Sonnerup, B.U.Ö., Bame, S.J., Forbes, T.G., Hones, Jr., E.W., and Russell, C.T.: 1981, 'Structure of the Low Latitude Boundary Layer', *J. Geophys. Res.* **86**, 2099–2110.

Smith, M.F. and Rodgers, D.J.: 1991, 'Ion Distributions at the Dayside Magnetopause', *J. Geophys. Res.* **96**, 11,617–11,624.

Song, P. and Russell, C.T.: 1992, 'Model of the Formation of the Low-Latitude Boundary Layer for Strongly Northward Interplanetary Magnetic Field', *J. Geophys. Res.* **97**, 1411–1420.

Song, P., Russell, C.T., Lin, N., Strangeway, R.J., Gosling, J.T., Thomsen, M.F., Fritz, T.A., Mitchell, D.G., and Anderson, R.R.: 1989, in T. Chang et al. (eds.), 'Wave and Particle Properties of the Subsolar Magnetopause', *Physics of Space Plasmas*, pp. 463–476, Scientific Publishers, Inc., Cambridge, MA, pp. 463–476.

Song, P., Sonnerup, B.U.Ö., and Thomsen, M.F. (eds.): 1995, *Physics of the Magnetopause*, Geophys. Monogr. 90, AGU, Washington.

Sonnerup, B.U.Ö.: 1984, in E.W. Hones, Jr. (ed.), 'Magnetic Field Reconnection at the Magnetopause: An Overview', *Magnetic Reconnection in Space and Laboratory Plasmas*, Geophys. Monogr. 30, AGU, Washington, pp. 92–103.

Sonnerup, B.U.Ö., Paschmann, G., Papamastorakis, I., Sckopke, N., Haerendel, G., Bame, S.J., Asbridge, J.R., Gosling, J.T., and Russell, C.T.: 1981, 'Evidence for Magnetic Field Reconnection at the Earth's Magnetopause', *J. Geophys. Res.* **86**, 10,049–10,067.

Sonnerup, B.U.Ö., Papamastorakis, I., Paschmann, G., and Lühr, H.: 1990, 'The Magnetopause for Large Magnetic Shear: Analysis of Convection Electric Fields from AMPTE/IRM', *J. Geophys. Res.* **95**, 10541–10557.

Sonnerup, B.U.Ö., Paschmann, G., and Phan, T.-D.: 1995, in P. Song et al. (eds.), 'Fluid Aspects of Reconnection at the Magnetopause: In Situ Observations', *Physics of the Magnetopause*, AGU, Washington, pp. 167–180.

Thomsen, M.F., Stansberry, J.A., Bame, S.J., Fuselier, S.A., and Gosling, J.T.: 1987, 'Ion and Electron Velocity Distributions within Flux Transfer Events', *J. Geophys. Res.* **92**, 12,127–12,136.

Treumann, R.A., LaBelle, J., and Bauer, T.M.:1995, in P. Song et al. (eds), 'Diffusion processes: An Observational Perspective', *Physics of the Magnetopause*, Geophys. Monogr. 90, AGU, Washington, pp. 331–341.

Address for correspondence: G. Paschmann, Max-Planck-Institut für extraterrestrische Physik, D-85740 Garching bei München, Germany

THEORETICAL APPROACHES TO THE DESCRIPTION OF MAGNETIC MERGING: THE NEED FOR FINITE β_e, ANISOTROPIC, AMBIPOLAR HALL MHD

J. D. SCUDDER
Department of Physics and Astronomy, University of Iowa, Iowa City, USA

Received April 28, 1997; Accepted in final form May 16, 1997

Abstract. Theoretical models of magnetic reconnection are reviewed with a critical view of their suitability for astrophysical plasmas, with a focus on those sampled plasmas near the magnetopause. Frequently the approximations are more those of convenience than physically justified. It is concluded that magnetic reconnection cannot be qualitatively or quantitatively addressed with any one fluid MHD picture unless the Hall, ambipolar and inertial emfs are included in the Generalized Ohm's Law. The observed size of electron pressure anisotropies ensures that the thawing of magnetic flux is almost always determined by the often neglected ambipolar term of the Generalized Ohm's Law. Thus resistive MHD or even resistive Hall MHD cannot possibly give a correct structural picture of the reconnection current carrying layer at the magnetopause. In the magnetotail the ion inertial "resistivity" is much larger than coulomb resistivity with a similar structural form as the coulomb emf. However, until recently the ambipolar contributions there have not been considered. This change in viewpoint of the controlling factors for thawing of magnetic flux parallels the recent evolution of understanding of collisionless shocks, where initially stochastic wave-resistivities were thought to substitute for the coulomb dissipation of high density shock waves. Now these shocks are known to be controlled by coherent agents that can modify emf's such as the ambipolar electric field, the Hall contributions of the gyrating ions, and the electric electron drift in the shock layer to support the current without thawing flux and without any requirement of ohmic dissipation *per se*. The observational tests that reconnection is a viable process for plasma entry in the magnetosphere are briefly reviewed. Sites where these conservation laws are said to be approximately fulfilled are discussed with an eye toward systematic experimental issues of these tests. That magnetic shear poorly indexes "good" Walén testing layers may be an indication that the resistive dissipation is either not uniformly important across the data set or resistive emf's are not the appropriate agent for the thawing of flux. The ambipolar scale length clearly exceeds the resistive or electron skin depth regime with layers that pass the "good" Walén test layers which have $\beta < 5$; this may indicate the importance of the ambipolar violations to the frozen field description.

1. Introduction

Based on circumstantial evidence the space physics community is convinced that **B** field line topologies change about the Earth. Were this not the case the solar wind magnetic field hung up over the magnetopause would intensify indefinitely. The substorm activity on the ground and witnessed in space are indicators of the reality of this scenario. Nevertheless, we do not "know" what process or processes mediate the topology changes whereby flux is shed from the dayside magnetosphere and recycled to the lobes in the magnetotail. In large scale plasmas these changes in topology are accompanied by specific rearrangements of the plasma. The effects of field line interconnection that accompany these topology changes have been modeled most simply with fluid-like equations of MHD by adding lumped parameters

Space Science Reviews **80**: 235–267, 1997.

such as localized (anomalous) enhancements of resistivity. While this approach may be the simplest, there remains the problem of defining the agent for this resistivity. There are, however, many other *possible* ways that the reconnection can be permitted that this paper will summarize. At least two of the known alternative agents for enabling reconnection are present even in the collisionless limit and have a wholly different structure than that mocked up by a collisional or enhanced *ad hoc* resistivity.

A number of excellent reviews on the description of merging already exist from the fluid picture (cf. Axford 1984; Vasyliunas, 1975; Sonnerup, 1984; Lee, 1995), and the collisionless picture (Hill, 1975; Cowley, 1982), so a brief statement of purpose for the present paper is appropriate. The present situation in the reconnection arena is much like the situation a few years ago with collisionless shocks. Then, observers told theoreticians shocks were present; theoreticians gave an explanation in terms of anomalous resistivity driven by micro-instabilities in the collisionless shock current layers. In this way a one for one substitution between two body resistivity and collective resistivity yielded a theory to "explain" the existence of the shock with insufficient empirical corroboration for the assumptions of their theory. However, with further experimental scrutiny it became clear, contrary to this *explanation*, that a rather diverse set of neglected *coherent* effects in the shock layer could explain their existence and the reformation of the shock layers themselves without this substitution of waves for binary collisions. Further, careful determinations of scales and sources of free energy found that the picture of linear growth, followed by non-linear reaction thought to facilitate anomalous resistivity, was a cycle that had insufficient time to take place before the fluid was swept through the layer and no longer able to tap the free energy. In the present view of shocks the collective wave particle effects "round the corners" of otherwise coherent processes in the DC electromagnetic fields of the shock structure. The self-consistent, post MHD, electromagnetic field including $E_{||}$ was crucial to that paradigm shift.

The physics of reconnection is almost totally determined theoretically by an acceptably accurate description for the parallel electric field. Resistivity is just one of several ways to support parallel electric fields. Because reconnection involves moving plasmas in the presence of magnetic fields at current sheets with gradients, this parallel electric field will certainly have a coherent ambipolar component; whether a sufficiently vigorous stochastic $E_{||}$ can be found to substitute for the almost negligible classical coulomb resistivity and dominate the coherent ambipolar parallel electric field (which has usually been neglected) remains to be seen in the problem of astrophysical reconnection. It is clear for $\beta \simeq 1$ plasmas that there are significant coherent sources of the parallel electric field that may routinely be more important in understanding the factors that control the onset of reconnection than surmised anomalous resistivities from yet to be defined wave particle instabilities.

This review will attempt to organize all the effects that could possibly be involved in describing magnetic reconnection at the level of the conservation laws of magneto-

fluid dynamics. It will become clear that demonstrably large effects have been postulated to be unimportant in much of the modeling of reconnection that has been completed to date. The main impediments are (1) the equation of state problems and (2) moment closure for an astrophysical plasma.

Magnetic reconnection is a process that may occur when the magnetized plasma is *non-ideal.* As with most adjectives, there are various levels of *non-idealness.* Broadly speaking reconnection involves loss of the line or flux preserving character of the plasma flow. Colloquially, the field line is said to be "broken" or have its extremities reconnected with a different topology. Ultimately the mixing of plasma populations from different topological field lines is the result (Vasyliunas, 1972, 1975). In this parlance reconnection occurs when plasma flows across the separatrix that bounds the topologically different regimes at the site of reconnection. Vasyliunas, Axford and others have emphasized that it is not enough for there to be local departures from ideal MHD, without simultaneous global requirements outside such "diffusive" regions that determine whether any reconnection proceeds in a quasi-steady manner. In the context of Earth there are three topologically distinct groups of field lines at any give moment: those with both foot points anchored in the sun; those with one end anchored in the sun with the other in the core of the earth; and those with both foot points anchored in the core of the earth. The time sequence of reorganization of the plasma that is first on the first topological bundle of field lines, then the second and subsequently the third requires the relaxation of the concept that field lines have an integrity throughout their dynamical history. The concept of field lines or frozen flux being preserved *within* each topological type, requires some relaxation of the field line concept in the locations where these topological changes are mediated.

These rather difficult concepts are often *summarized (or hidden?)* by saying that reconnection occurs or is possible in regimes where the "frozen field approximation"

$$\mathbf{E} = -\frac{\mathbf{U} \times \mathbf{B}}{\mathbf{c}}$$

is violated (here **U** is the center of mass velocity); or, whenever there exists $E_{||}(\mathbf{x})$ collocated with field aligned currents. Still others say that reconnection occurs when field energy is transferred to plasma energy when crossing such topological boundaries. In this state of affairs, the literature is full of rather diverse statements that approach almost religious fervor concerning whether reconnection is or is not an established operative mechanism at the earth's near environment. To witness flow across a change in topology is almost impossible with a single spacecraft. Indirect measures of such a flow, such as determining the tangential electric field at the magnetopause (Mozer et al., 1978), and the normal component of **B** (Sonnerup and Ledley, 1979), or its consequences via the Walén (1944) test (Paschmann et al. 1979, Sonnerup et al., 1981, Aggson et al., 1983; 1984) or time of flight dispersion are used as proxies for the process under models of the implementation of the interconnection. If these models are themselves flawed or over simplified, the

tests of these models remain inconclusive, or, at least parametric in the premises of the model. The purpose of this review is to elucidate the governing equations of magnetic reconnection with as few simplifications as possible and then discuss the tests that have been attempted and their results in light of simplifications that have made these tests possible.

2. Frozen Flux and its Thawing

To understand the various theoretical approaches to the description of magnetic merging, or reconnection, there must first be a clear understanding of the concept of "magnetic flux" and "magnetic line" preservation. The concept of flux preservation gives rise to the mnemonic of spaghetti-like flux tubes as entities with an integrity that are locally convected by the components of the plasma flow field that are locally orthogonal to the flux tube. In this way Alfvén's (1942) concept of moving flux tubes has gained acceptance in the *cartoon* level description of the time evolving dynamics of plasma magnetohydrodynamics. The huge success of Alfvén's point of view belies the subtlety that it is only approximately true that "magnetic flux" and "magnetic line" preservation adequately describe nature. It is precisely where this approximation breaks down that magnetic merging with its capacity to change the topology of these spaghetti-like tubes is required.

Confusingly, there are yet further simplifications of the description of real plasma dynamics that compromise the idealization of flux tubes frozen into the perpendicular motions of the fluid. There are many different representations of the fluid flow fields, $\mathbf{W}$, within which the magnetic field can be viewed as approximately having a flux or field line preserving character. For the magnetic flux to be "frozen" to the perpendicular motions of these different fluid fields requires stronger or lesser ancillary *assumptions* about the plasma's ability to react to the deformations of the topologically preserved bundles of spaghetti and the plasmas found on them.

The most commonly used fluid flow field $\mathbf{W}$ is that of the center of mass, $\mathbf{U}_{cm}$, of the magnetohydrodynamic fluid defined by the relation

$$\mathbf{U}_{cm} = \frac{\Sigma_i n_i m_i \mathbf{U}_i + n_e m_e \mathbf{U}_e}{\Sigma_i n_i m_i + n_e m_e} \tag{1}$$

with the electric field determined from the **approximate** relationship of the form

$$\mathbf{E} + \frac{\mathbf{U}_{cm} \times \mathbf{B}}{c} \simeq 0 \tag{2}$$

As is well known (2) represents but a portion of the difference between the ion and electron momentum equations (cf 14a, below). Among the neglected terms are those associated with the magnetic back emf associated with currents that may be caused by the flow field $\mathbf{U}_{cm}$, any resistive emfs, any ambipolar emfs, and finite larmor radius emfs, or any emfs associated with inertia and the acceleration of the

plasma. When the flow field associated with the center of mass drives spaghetti-like tubes towards one another, there are corrections to the zero on the rhs of (2) that gnaw away at the integrity of individual tubes of force and require a broader overview of the magnetic field than as a strict ensemble of spaghetti strands: the "frozen" field approximation must be modified in those regions.

As an example, the magnetopause Chapman-Ferraro current layer is a site where there are surface currents, where magnetic tubes of forces are thrust towards one another, where terms missing from (2) are required by the large scale dynamics (boundary conditions) of the solar wind impinging on the earth's magnetic field. There is ample circumstantial evidence that changes in external boundary conditions can facilitate topological rearrangement of magnetic flux inside the preexisting magnetospheric cavity. Sometimes steady and at other times patchy or time dependent, frozen flux violations implicit in magnetic reconnection are frequently invoked to explain the shedding of flux from noon to the lobes and the dipolarization of the tail magnetic field and other substorm morphology. These "explanations" are connected with the view that there are places on the Chapman-Ferraro layer where the approximation of (2) is inadequate.

Quite generally when (2) *equals* zero one can prove that magnetic field lines are preserved throughout their dynamical advection with $\mathbf{U}_{\perp,cm}$. Accordingly the topology of these lines of force, however contorted they become, cannot be modified. It is however difficult to imagine non-trivial velocity fields which do not produce distributions of current, acceleration, and pressure so that the neglected terms of (2) will become important and critical at places in the dynamics. This intrinsic incompleteness of (2) vacates any realistic expectation that tubes of magnetic force in real magneto plasma dynamical problems can have a global and time independent integrity.

To see that there may be places and scales where the concept of magnetic field or flux lines carried by the plasma does not make local sense we now review the machinery to describe the total time derivative of magnetic flux in the manner of Rossi and Olbert (1970) as amplified by Siscoe (1983). Consider as indicated in Figure 1 the magnetic flux Φ piercing the closed loop C, with local normal $\hat{\mathbf{n}}_1$ defined as:

$$\Phi = \int_{C(t)} \mathbf{B} \cdot \hat{\mathbf{n}}_1 da \tag{3}$$

The time rate of change of this flux *for a linked set of fluid elements moving with the velocity field* $\mathbf{W}$ which transports $C(t) \rightarrow C'(t + \Delta t)$ is defined to be

$$\frac{d\Phi}{dt} \equiv \lim_{\Delta t \to 0} \frac{\Phi(t + \Delta t) - \Phi(t)}{\Delta t} \tag{4}$$

As illustrated in Figure 1, the enclosed area of the loop $C(t)$ is denoted by the oriented surface labeled S_1 whose normal is on the same side of the loop C as is the local flow vector $\mathbf{W}(\mathbf{x}, \mathbf{t})$. The velocity field $\mathbf{W}$ displaces the original loop $C(t)$ to a new loop $C'(t + \Delta t)$ with an enclosed surface element S_2 and surface normal $\hat{\mathbf{n}}_2$

located on the same side of S_2 as $\hat{\mathbf{n}}_1$ is of S_1 relative to $\mathbf{W}$. During Δt the original loop sweeps out a new open surface which is the union of S_2 and S_3 which is also still bounded by the original curve $C(t)$. Thus the evolution of the enclosed flux after *linked advection* by the flow field $\mathbf{W}$ is

$$\frac{d\Phi}{dt} \equiv \lim_{\Delta t \to 0} \frac{\Phi_2(t+\Delta t) - \Phi_1(t)}{\Delta t} \tag{5}$$

Consider the entire closed surface of Figure 1 made up of S_1, S_2, and S_3. Gauss's law and the source free Maxwell equation implies that the sum of the magnetic fluxes projected along the *outward normal* from this closed surface should vanish at any time. Since Φ_1 is defined for an ingoing normal to the closed surface, the $\nabla \cdot \mathbf{B} = 0$ equation implies that

$$\Phi_2(t+\Delta t) = \Phi_1(t+\Delta t) - \Phi_3(t+\Delta t) \tag{6}$$

Using (6) into (5) and (3) for the remaining fluxes eliminates $\Phi_2(t+\Delta t)$ to yield

$$\frac{d\Phi}{dt} = \lim_{\Delta t \to 0} \frac{1}{\Delta t} \left[\int_{S_1} [\mathbf{B}(t+\Delta t) - \mathbf{B}(t)] \cdot \hat{\mathbf{n}}_1 da - \int_{S_3} \mathbf{B}(t+\Delta t) \cdot \hat{\mathbf{n}}_3 da' \right] \tag{7}$$

where $\hat{\mathbf{n}}_3 da'$ is the outward directed differential area normal to surface S_3 implied by the expression

$$\hat{\mathbf{n}}_3 da' = d\mathbf{C}(\mathbf{t}) \times \mathbf{W}(\mathbf{x}, \mathbf{t}) \Delta t \tag{8}$$

where $d\mathbf{C}(t)$ is the local tangent differential along C(t).

Using (8) into the last term of (7) produces the simplification

$$\int_{S_3} \mathbf{B}(t+\Delta t) \cdot \hat{\mathbf{n}}_3 da = \int_{C(t)} \mathbf{B}(t+\Delta t) \cdot d\mathbf{C}(t) \times \mathbf{W}(\mathbf{x}, t) \Delta t$$

$$= \int_{C(t)} \mathbf{W} \times \mathbf{B}(t+\Delta t) \cdot d\mathbf{C}(t) \Delta t \tag{9}$$

Inserting (9) into (7) and canceling the differentials where possible yields

$$\frac{d\Phi}{dt} = \lim_{\Delta t \to 0} \left[\int_{S_1} \frac{\mathbf{B}(t+\Delta t) - \mathbf{B}(t)}{\Delta t} \cdot \hat{\mathbf{n}}_1 da - \int_{C(t)} \mathbf{W}(\mathbf{x}, t) \times \mathbf{B}(t+\Delta t) \cdot d\mathbf{C}(t) \right] \tag{10a}$$

Proceeding to the limit yields

$$\frac{d\Phi}{dt} = \int_{S_1} \frac{\partial \mathbf{B}}{\partial t} \cdot \hat{\mathbf{n}}_1 da - \int_{C(t)} \mathbf{W}(\mathbf{x}, t) \times \mathbf{B}(t) \cdot d\mathbf{C}(t) \tag{10b}$$

Using Stoke's theorem the last term of (10a) becomes

$$\int_{S_1} \nabla \times (\mathbf{W} \times \mathbf{B}(t)) \cdot \hat{\mathbf{n}}_1 da \tag{11}$$

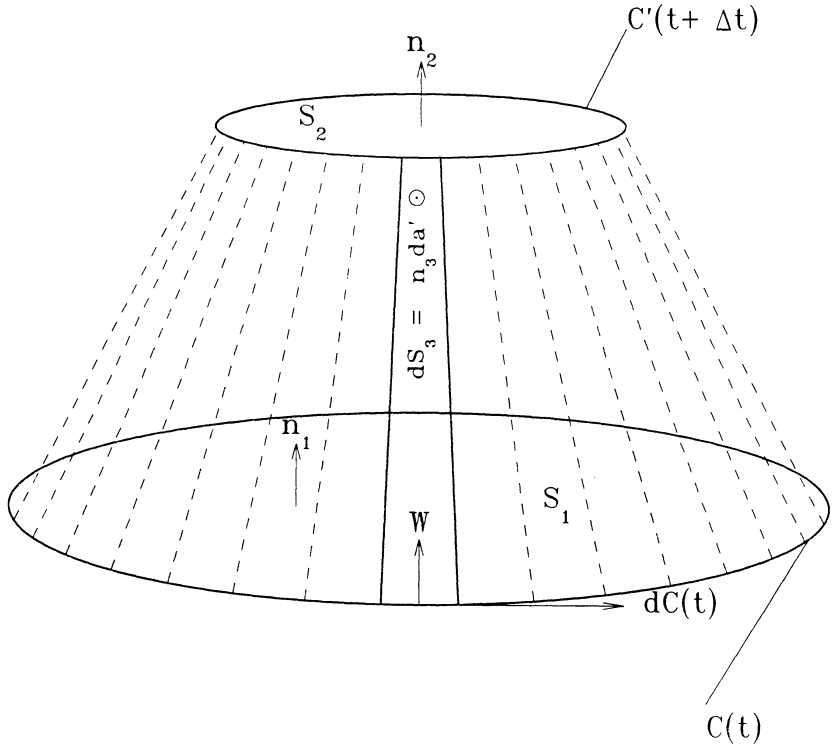

Figure 1. Representation after Rossi and Olbert, (1970) of the linked advection that maps the closed contour $C(\mathrm{x},t)$ to a new curve $C'(\mathrm{x}',t+\delta t)$ as implemented by the flow field $\mathrm{W}(\mathrm{x},t)$. Note that the union of surfaces S_1, S_2, S_3 is a closed surface, while S_1 and the union of S_2 and S_3 form open surfaces with C as their common bound. The surface S_3 is swept out in time by the advection of W.

while Faraday's law restructures the first term to yield the time variation of advectively connected flux:

$$\frac{d\Phi}{dt}|_{C_1} = -\int_{S_1} \nabla \times [c\mathbf{E} + \mathbf{W} \times \mathbf{B}] \cdot \hat{\mathbf{n}}_1 da \tag{12}$$

Two distinctions are usually drawn from (12) to differentiate two classes of flow fields both of which preserve flux with $\frac{d\Phi}{dt} \equiv 0$: (i) those flow fields $\mathbf{W}'$ that are flux and, more restrictively, *field line preserving* where:

$$c\mathbf{E} + \mathbf{W}' \times \mathbf{B} = 0 \tag{13a}$$

and (ii) those $\mathbf{W}''$ that are only *flux preserving*:

$$\nabla \times [c\mathbf{E} + \mathbf{W}'' \times \mathbf{B}] = 0 \tag{13b}$$

From (13a) it is now clear that the *assumption* of (2) as being true would imply that nature can only be magnetic line preserving and that magnetic field lines are

carried about with any flow field whose motions perpendicular to the magnetic field are those of the fluid's center of mass:

$$\mathbf{W}_\perp \equiv \mathbf{U}_{cm_\perp}$$

Alternatively there are a whole class of flow fields from (13b) with $\mathbf{W}''$ that while not necessarily preserving individual field lines in the same fluid element under dynamics have a balanced gain and loss of (previously labeled) field lines threading the volume in such a way that the net *number* of counted field lines, or flux, in the evolving fluid element is preserved.

3. The General Relationship for E

The magneto-fluid dynamical equations are incomplete without the relationship that is now standardly called the *Generalized Ohm's Law* which relates the electric field in the plasma to other field and plasma quantities. In a very real sense this equation is the synthesis within the one fluid picture that electrons have a different equation of motion than do the ions (cf. Rossi and Olbert, 1970).

The first and the most commonly encountered form is related to (2) and found by subtracting the electron momentum equation from that of the ions and solving for the electric field (while neglecting $\frac{m_e}{M_i}$ and space charge) with an *approximate* form (Rossi and Olbert, 1970)

$$\mathbf{E} + \frac{\mathbf{U}_{cm} \times \mathbf{B}}{c} \simeq \frac{\mathbf{J} \times \mathbf{B}}{ecn_e} - \frac{\nabla \cdot \mathbf{P}_e}{en_e} - \frac{m_e}{M_i}\frac{\nabla \cdot \mathbf{P}_i}{en_i}$$

$$+\frac{m_e}{ne^2}\left[\frac{\partial \mathbf{J}}{\partial t} + \nabla \cdot (\mathbf{U}_{cm}\mathbf{J} + \mathbf{J}\mathbf{U}_{cm})\right] + \eta \cdot \mathbf{J} \qquad (14a)$$

Alternatively, from the electron momentum equation the relationship for $\mathbf{E}$ is found to be:

$$\mathbf{E} + \frac{\mathbf{U}_e \times \mathbf{B}}{c} = -\frac{\nabla \cdot \mathbf{P}_e}{en_e} +$$

$$-\frac{m_e}{en_e}\left[\frac{\partial n_e \mathbf{U}_e}{\partial t} + \nabla \cdot (n_e \mathbf{U}_e \mathbf{U}_e)\right] - \frac{GM_* m_e \hat{\mathbf{r}}}{er^2} - \frac{m_e}{en_e} < \frac{\delta f_e}{\partial t}|_{ei}\mathbf{v}_e >_{\mathbf{U}_e} \qquad (14b)$$

The gravitational attraction with the nearest attracting object of mass, M_* at distance r to the present location is included in (14a-c). The role of gravity is implicit in (14a) through the center of mass equation of motion, while being explicitly present in the electron and ion specific forms. From the ion momentum equation comes the relationship

$$\mathbf{E} + \frac{\mathbf{U}_i \times \mathbf{B}}{c} = +\frac{\nabla \cdot \mathbf{P}_i}{en_i}$$

$$+\frac{m_i}{en_i}\left[\frac{\partial n_i \mathbf{U}_i}{\partial t} + \nabla \cdot (n_i \mathbf{U}_i \mathbf{U}_i)\right] + \frac{GM_* M_i \hat{\mathbf{r}}}{er^2} - \frac{M_i}{en_i} < \frac{\delta f_i}{\partial t}|_{ie}\mathbf{v}_i >_{\mathbf{U}_i} \qquad (14c)$$

Although not entirely equivalent (14a-c) together with (12) above contribute new insight into the possible integrity of a description of magnetic reconnection that is possible with different approximations. As can be seen explicitly in (14a) (2) implies *a priori* that there are no important currents, pressure gradients or accelerations in order that the magnetic tubes of force will be adequately described as convecting with the perpendicular portions of the $\mathbf{U}_{cm}$.

Equation (14b) and (12) suggest that magnetic field *lines* are approximately frozen in the electron's center of mass frame moving with local speed $\mathbf{U}_e$ *even in the presence of currents*, provided the electron pressure gradient terms and the inertial terms are small. Equation (14b) is clearly a more general description than (2) and clearly indicates that the neglect of the Lorentz emf or Hall term in (2), or the center of mass form (14a) preempts the slippage of the electron fluid with respect to the ions (i.e. currents) from being naturally described. Thus the neglect of the Hall emf preempts important current layer phenomena. Long before physical "thawing" of flux is involved, it must be clear that the assumption of (2) to explain naturally occurring plasmas will have serious observational contradictions. Even beyond the Hall emf issue it is also clear that assuming the electrons carry the magnetic field in a frozen way ($RHS(14b) \simeq 0$) is *not* a sufficiently general point of view to compare with nature.

In principal (14c) could be used to constrain $\mathbf{E}$ as described from the ion velocity field $\mathbf{U}_i$; unfortunately (14c) describes the motion of field lines carried by the electrons using almost all the remaining ion terms including the ion inertial terms, and the ion pressure divergence; these terms are all sizeable in current layers that form as tubes of force become entangled while moving as frozen flux bundles. These current layers are usually ion gyroradius in scale in plasmas thus requiring at least Finite Larmor Radius (FLR) descriptions for the ion pressure tensor. *All* of these substantial inertial and FLR corrections are required (and hence not optional) to describe successfully the content of the generalized Ohm's law in the ion flow field's frame of reference; these terms are required with great fidelity before (14c) can emulate with precision the succinct description of the field lines moving laminarly as convected by the electrons as a group. *Most disconcerting is the realization that selectively picking some of the terms on the rhs of (14a,c) while leaving others may not even adequately describe the lowest order freezing of magnetic flux into the electron frame of reference!*

Gravity in (14b,c) also plays a role in astrophysics in the Generalized Ohm's law. Note, however, that it does not appear in (14a) (cf. Rossi and Olbert 1970) being hidden in the acceleration terms of the center of mass in (14a). Gravitational acceleration is a good example of a contributor that erodes field *line* preservation but not magnetic *flux* conservation, since the curl of the conservative force's acceleration vanishes. Thus in any of the specific fluid fields of (14b,c) identified above the role of gravity is to destroy field line preservation in the fluid frame, but not flux preservation.

The next level of sophistication in the retention of additional effects in the Generalized Ohm's Law crosses over into the regime where energy equations and closure equations for the pressures are required. Aside from the temperature dependence of the resistivity, this is the first place in the Generalized Ohm's Law that the non-zero β of the particles and their attendant acceleration from pressure gradients are factored into the electric field considerations. From one point of view the theorist or simulator can view these thermal terms as a vexing complication, to be avoided if at all possible as in Lottermoser and Scholer (1997). These terms require one or more energy equations (as in Ma and Battacharjee, 1996) which require further focus on the perplexing issues of plasma fluid dynamical closure relations. However, by observations astrophysical plasmas have significant pressures in the particles making their neglect a serious compromise for a realistic description of magnetic reconnection phenomena. Heat conduction and some forms of magnetic viscosity are transport phenomena that are almost always omitted from the discussion of the reconnection layers.

To include the so-called *ambipolar electric field* from the divergence of the electron pressure (which occurs in all three expressions above) and the ion pressure tensor that occurs in the center of mass and ion form of (14a,c) requires knowledge of the equation(s) of state in a plasma. When these plasmas are dilute as at the magnetopause there is no known equation of state that relates the electron pressure tensor to the lower order fluid moments and the magnetic field. Such difficulties do **not**, however, preempt the importance of such terms in the predictions for magnetic flux thawing.

Magnetic flux is frozen in the electron's frame of reference unless

$$\nabla \times (c\mathbf{E} + \mathbf{U}_e \times \mathbf{B}) \neq 0$$

Temporarily neglecting inertial terms, magnetic flux is thawed in the electron fluid frame whenever

$$\nabla \times \frac{\nabla \cdot \mathbf{P}_e}{en_e} \neq 0 \tag{15a}$$

Expanding the curl reveals that this condition is equal to

$$(\nabla \cdot \mathbf{P}_e \times \nabla \ln n_e + \nabla \times \nabla \cdot \mathbf{P}_e) \neq 0 \tag{15b}$$

In general the second term of (15b) vanishes for any isotropic electron pressure. Accordingly, the total curl of (15a) vanishes under the *further* assumption beyond isotropy that the electron plasma is *barotropic*, with its isobars and isodensity surfaces coincident. Obviously barotropic equations of state are not the most general class; the complimentary class of *baroclinic* closure equations, which do not meet the barotropic definition, are already important agents for the thawing of magnetic flux. For baroclinic isotropic electron pressure (15a) becomes

$$\nabla \times \frac{-\nabla \cdot \mathbf{P}_e}{en_e}|_{baroclinic-isotropic} = \frac{1}{en_e}\nabla \ln n_e \times \nabla P_e \tag{15c}$$

Still more complicated are *anisotropic* pressure tensors appropriate for circumstances where the electrons remain magnetized and *non-gyrotropic* equations of state when they are not. In the magnetized, anisotropic circumstance both terms of (15b) survive and may be written as

$$-\nabla\times\frac{\nabla\cdot\mathbf{P}_e}{en_e}|_{anisotropic}=\frac{1}{en_e}\left[\nabla\ln n_e\times\nabla\cdot\mathbf{P}_e-\nabla\left(\frac{\partial}{\partial s}\left(\frac{P_{||}-P_\perp}{B}\right)\right)\times\mathbf{B}\right]$$

$$+\frac{1}{en_e}\left[\frac{\partial}{\partial s}\left(\frac{P_{||}-P_\perp}{B}\right)\nabla\times\mathbf{B}+\nabla\left(P_{||}-P_\perp\right)\times\frac{\partial\hat{\mathbf{b}}}{\partial s}+\left(P_{||}-P_\perp\right)\nabla\times\frac{\partial\hat{\mathbf{b}}}{\partial s}\right] \tag{15d}$$

where

$$\nabla\cdot\mathbf{P}_e=\nabla P_\perp-\left(\left(P_{||}-P_\perp\right)\frac{\partial\ln B}{\partial s}\right)\hat{\mathbf{b}}+\frac{\partial\left(P_{||}-P_\perp\right)\hat{\mathbf{b}}}{\partial s} \tag{15e}$$

has been used. If the electrons are no longer magnetized then the electron pressure tensor retains no symmetries or simplifications and k'th vector component of 15a become

$$\left(\nabla\times\frac{-\nabla\cdot\mathbf{P}_e}{en_e}|_{non-gyro}\right)_k=\frac{\epsilon_{ijk}}{en_e}\left[\frac{\partial\ln n_e}{\partial x_i}\frac{\partial P_{lj}}{\partial x_l-\frac{\partial^2 P_{lj}}{\partial x_i\partial x_l}}\right] \tag{15f}$$

with Einstein summation convention implied and ϵ_{ijk} the Levi-Civita fully antisymmetric tensor.

The general barotropic form for $\mathbf{P}_e\equiv P_e$ occurs when P_e is *solely* a function of density alone. A polytrope electron equation of state is *a* form that meets the barotropic condition. There is no known theorem that even guarantees that a plasma or even the electron part of the plasma must emulate polytrope behavior or even be a local function relating moments of the plasma in the *same* location. Polytropes have been predicted (Scudder and Olbert, 1979) and have been found to organize solar wind electrons (Sittler and Scudder, 1980). Unfortunately, there are growing indications that the plasma pressure equations for a rarefied astrophysical plasma are not universal, but context dependent (Scudder, 1992; Osherovich et al., 1993, 1995; and Fainberg et al., 1996). The documentation of polytropic behavior in the freely expanding solar wind is no *a priori* guarantee for its relevance as the equation of state within the magnetopause current layers. Such barotropic corrections to the electric field do not contribute to the erosion of magnetic *flux* but do introduce additional freedom for moving flux that otherwise would pile up; these terms also add new scale lengths (cf section 6) and time scales to the problem of reconnection (Vasyliunas, 1975; Ma and Battacharjee, 1996; and Kleva et al., 1995).

The polytropic barotropic approximation for electrons compromises the magnetic line preservation but permits magnetic flux and its topology to be preserved.

In this case the precise same field lines are not always penetrating the curve C of Figure 1 as it is carried with the electrons, but the net coming and going of lines of force and their attached electrons by pressure gradient drifts are such that the enclosed magnetic flux is invariant. Gradient and curvature drifts are compensated with isotropic pressure. An alternative viewpoint is that the magnetic field line is "carried" at the composite speed given by

$$\mathbf{W_B} = \mathbf{U}_{\perp,e} - c\frac{\frac{\nabla P_e}{en_e} \times \mathbf{B}}{B^2}$$

If the electrons remain isotropic but have a baroclinic closure there will be a residual thawing that remains. In this circumstance the rate of flux decay due to this effect will overpower coulomb resistive rates whenever (15c) competes with the curl of the resistive emf. This condition occurs when

$$\frac{\nabla \times \frac{\nabla \cdot \mathbf{P}_e}{en_e}}{\nabla \times \eta \cdot \mathbf{J}} > 1 \tag{16a}$$

and is satisfied in the baroclinic equation of state if

$$1 > \Xi \equiv \frac{\eta ecB}{4\pi kT_e} \tag{16b}$$

Using the Spitzer form for $\eta = 1.15x10^{-4} z \ln \Lambda T(\text{eV})^{-\frac{3}{2}}$ (16b) becomes

$$\Xi \equiv 8.2x10^{-10} \frac{\ln \Lambda}{22} \frac{B}{50\gamma} \left(\frac{100\text{eV}}{T(\text{eV})}\right)^{\frac{5}{2}} \tag{16c}$$

Isocontours of $\Xi(T_e, B)$ are illustrated in Figure 2. The asterisk denotes typical conditions at the noon magnetopause. We thus conclude that any baroclinic electron equation of state would thaw flux much faster than any effects associated with classical resistivity down to a misalignment from barotropic behavior of $10^{-10} radians$!

If the equation of state is isotropic but baroclinic, then whenever $\Xi < 1$ there are ambipolar dominating terms present in the plasma. For an anisotropic equation of state where $\nabla \cdot \mathbf{P}_e$ is magically parallel to the electron density then the anisotropic condition will contribute a thawing rate that overpowers resistivity if

$$\frac{P_{e,\|} - P_{e,\perp}}{P_e} > \Xi$$

If there is no such barotropic like degeneracy then whenever $\Xi < 1$ is a regime where ambipolar effects overpower resistivity. The isotropic polytrope regime guarantees that the equation of state is barotropic, the ambipolar thawing contribution vanishes and resistivity controls the thawing by postulate.

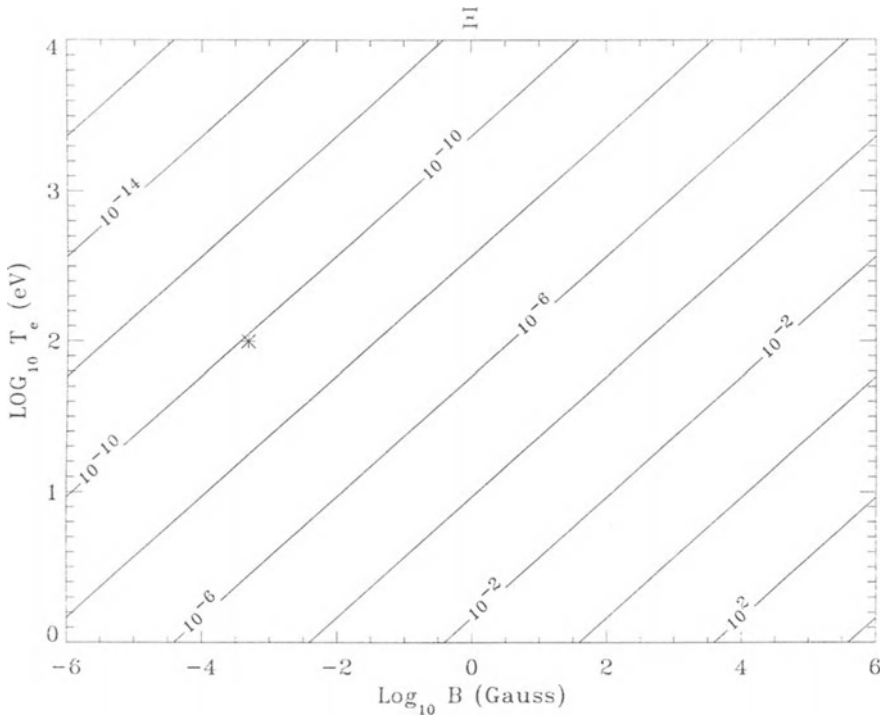

Figure 2. Isocontours of the quantity Ξ that determines the importance of ambipolar contributions to thawing of magnetic flux as a function of electron temperature in eV and magnetic field strength in Gauss. Typical nose magnetopause conditions are indicated with the asterisk.

Alternatively, if the electron pressure tensor is anisotropic, the two terms in (15b) will not in general cancel. Accordingly, in the electron bulk frame there is no flux preserving description to be foreseen in general. If a situation had a high symmetry even anisotropic plasma might conspire to make the first term of (15b) zero by geometry. The finite anisotropy of the second term spelled out explicitly in (15d) still gives the ambipolar term the edge over the resistive term at the magnetopause and at most other locations in astrophysical plasmas. An idea of the relative importance of resistive and anisotropic ambipolar effects in the thawing of magnetic flux is found by noting that the second term of (15d) scales with the pressure anisotropy so that whenever

$$\frac{|P_{\perp,e} - P_{\|,e}|}{P_e} > \Xi \tag{16d}$$

then anisotropic ambipolar thawing will overpower the more conventional resistive diffusion. Therefore, in the reconnection layer whenever the fractional pressure anisotropy exceeds 10^{-10}, resistive thawing is unimportant.

We therefore conclude that if the electrons remain magnetized at the magnetopause with a sheath magnetic field of 50γ and electron temperature of 100eV, the plasma in this region is completely at the mercy of electrons for the thawing rates either from the baroclinic-like term that does not vanish with isotropy or from the emf's associated with the very modest observed electron anisotropies ($\Xi \simeq 0.1$) of the magnetosheath. Thus it must be concluded that it is inconceivable that coulomb resistivity plays a role in the reconnection layer physics at the magnetopause or magnetotail.

There are empirical *in situ* estimates of effective resistivities in astrophysical plasmas. Estimates of the effective resistivity have been made by fitting magnetic field profiles to diffusive solutions (Burlaga and Scudder, 1974) of the Sweet-Parker type discussed below and from the energy equation and magnetic ramp scale within a collisionless shock (Scudder et al., 1986). Both methods yielded (cgs) estimates for effective resistivities of

$$\eta_{\perp,in\ situ} \simeq (0.1 - 1)\omega_{pe}^{-1} = (1 - 10)1.7 \times 10^{-6} \left(\frac{20/\text{cc}}{n_e}\right)^{\frac{1}{2}} \text{ sec} \qquad (17a)$$

that should be contrasted with the numerical (cgs) Spitzer expression:

$$\eta_{Spitzer} \simeq 2.5 \times 10^{-6} \frac{\ln \Lambda}{22} \left(\frac{100\text{eV}}{T_e}\right)^{\frac{3}{2}} \text{ sec} \qquad (17b)$$

If these empirical circumstance are any indication of the general scaling of anomalous resistivities, they are at worst an order of magnitude larger than the coulomb value. Even revisiting Figure 2 and increasing the threshold value of Ξ by an order of magnitude still places the observed baroclinic and or anisotropic parts of $\mathbf{P}_e$ in (15d) in complete control of magnetic flux thawing for almost all astrophysical plasmas!

Clearly, if the pressure tensor is non-gyrotropic it need not have a vanishing curl either, so the magnetic flux will not be conserved. Such effects have been foreseen to be important in the momentum balance within the diffusion region (Vasyliunas, 1975). Further details in this vein have been suggested by Dungey (1988), Lyons and Pridmore-Brown (1990, 1992). This behavior has been made more credible with a full particle code of the inner zone of a magnetic reconnection layer by Cai et al., (1994). This simulation also demonstrated the simultaneous importance of the electron and ion pressure gradient terms in (14a) within the diffusion region even though the $\frac{1}{1836}$ mass ratio would have ordinarily led the simulator to justify its neglect! In the current sheet the ions get very much hotter than the electrons and compensate for the inertial mismatch suggested by formal ordering.

In this sense observations of anisotropic or non-gyrotropic electron pressure tensors are a potential warning sign that the magnetic flux is not being preserved even in the electron's frame of reference and *the thawing of flux will not be ordered by magnetic shear or current density as it would for the case of resistive thawing.*

Even in the anisotropic case the electrons of differing energies possess different gradient and curvature drifts which when averaged over the distribution do not cancel. In this way electrons initially located on the same tube do not migrate across the magnetic field at the same rate or even in the same direction so that it is difficult (though not impossible) to guarantee that a circulation of field lines through the volume will leave the net threading flux invariant. In this sense particles once on a given tube of force find themselves at some later time on differing tubes according to their initial kinetic energy as a result of their departure from isotropy. This rearrangement makes it difficult to redefine a single field line that they were on. An analysis of this type of behavior was conducted by Scudder (1987) in the context of the fluid motion of the electron center of mass, $\mathbf{U}_e$ within a steady state normal mass flux layers, where it was shown that the only ways in the deHoffmann-Teller (1950) frame (if electrons remain magnetized) to separate the electron flow lines $\hat{\mathbf{U}}_e(x, y, z)$ from being tangent to the magnetic field lines $\mathbf{B}(x, y, z)$ while threading the layer, are electron pressure anisotropy, electron inertia and collisions.

The electron inertial terms in (14a, b) are usually small corrections and as shown below are important on smaller scales than the leading terms on the right hand sides of (14a,b). However, because they involve Maxwell equation variables in (14a) and the center of mass speed these terms are often retained without the equation of state complications mentioned above. These terms are also the only place where the mismatch of accelerations experienced by electrons and ions can play a role in determining the electric field. The recent review by Drake (1995) discusses simulations and analysis of this decoupling.

Previously Speiser (1970) and coworkers have developed the concept of inertial resistivity from these terms for use in the discussion of the neutral sheet in the magnetotail. Lyons and Speiser (1985) have suggested an effective inertial resistivity that would have the cgs order of magnitude determined by the normal component of the magnetic field, B_n, in the current sheet of the form

$$\eta_{inertial} = \frac{B_n}{n_i ec} = 3.5 \times 10^{-8} \left(\frac{B_n}{1\gamma}\right) \left(\frac{20/\text{cc}}{n_i}\right) \text{sec} \tag{17c}$$

which when contrasted with the coulomb resistivity implies that the inertial effect exceeds the two body resistivity effect whenever

$$\frac{\eta_{inertial}}{\eta_{coulomb}} > 1$$

which occurs when

$$\frac{B_n}{1\gamma} > 7.2 \times 10^{-9} \frac{n_i}{20/\text{cc}} \left(\frac{T_e}{100\text{eV}}\right)^{-\frac{3}{2}} \frac{\ln \Lambda}{22} \tag{18}$$

that is, almost always in a space plasma!

The resistive, or $\eta \cdot \mathbf{J}$, term of (14a) is also an inertial term in disguise since η is directly proportional to the reduced mass of the electron ion pair and hence

is proportional to the electron mass density as well as the electron-ion collision frequency that varies as $T_e^{-\frac{3}{2}}$. When this resistive term is theoretically included in the description of thawing frozen flux, it is invariably included as a constant η. To use such a physical or anomalous collision frequency requires knowledge of the partition of internal energy between electrons and ions to evaluate the collision frequency correctly. The anomalous resistivity models require estimates for the wave energy density as well. From the ion center of mass description of (14a), the electron temperature is unavailable except by approximating $T_e \simeq \frac{1}{2}T$ as an *ad hoc* guess. The physical resistive scale at the magnetopause is very short ($\simeq 1km$), and varies widely across any simulation domain that includes the magnetopause. Choosing η to be a constant has the practical impact of fixing the resistive scale length across the entire solution domain from the beginning of the simulation, instead of it being spatially dependent as the physical mechanism would require. If the resistive effects contribute to the variation of temperature within the sheet, the inverse dependence with T_e of the physical resistivity is not addressed by this approach. Resistive terms possess the well known therapeutic effect of numerically stabilizing MHD codes. Too often these considerations drive the simulator to retain a constant η rather than the explicit bulk parameter dependences of the resistive model considered. Often modelers explore scaling of their results with a spatially fixed resistivity until the code is no longer stable and then seek to extrapolate to the even lower resistivity regimes thought to be relevant for the geophysical problem. It should be clear that these approaches **define** the mode of interconnection to be that of *resistive thawing* without looking at other structural ways in (14) for flux to be thawed and the observed scales of current layers produced.

Two further points are emphasized by the electron form of (14b). First, the resistive emf has its origins in the collision integral between electron and ions. The $\eta\mathbf{J}$ term of (14a) is only the leading order contribution from the collision integral for the circumstance when there is bulk velocity slippage between the electron and ions considered as separate fluids. If the electrons and ion distributions are spherically symmetric in their respective frames of reference, then the form $\eta \cdot \mathbf{J}$ for the emf of (14a) is only appropriate for the *Stoke's friction regime* of the plasma. The friction between Gaussian electrons and ions is only proportional to the slippage between them and, hence the current in a collisional plasma if the relative drift speed is small and within the Stoke's regime:

$$|\mathbf{U}_i - \mathbf{U}_e| \ll \sqrt{\frac{3kT_e}{m_e}} \quad (Stokes)$$

For larger drift speeds the structure of the friction changes (Dreicer, 1959, 1960) so that the friction decreases with increasing further relative drift. This is the regime of "runaway". In a quasi-collisional plasma, collective ion acoustic instabilities can imply a change in the coefficient of resistivity and its scaling when this slippage is 42 times smaller and also depends on the $\frac{T_e}{T_i}$ ratio and wave amplitude level.

Secondly there is no guarantee, especially in low density plasmas, that the electrons and ions will remain Gaussian in their separate frames of reference while the momentum transfer is occurring, or that they are isotropic when they are not supporting a current density. All Legendre polynomials are in general required to describe *observed* astrophysical velocity distribution functions in their respective bulk velocity frames. The first order Legendre polynomial facilitates the description of heat flow about the center or mass frame of the species. The general specification of the electron-ion moment transfer contains a contribution from all odd moments of the distribution. The ohmic emf $\eta \cdot \mathbf{J}$ is the result of appropriately small mismatches in the first moments of the electrons and ions. There are additional contributions to the momentum exchange called the *thermal force emf* that **can be present whether or not there is a current density present.** This emf is caused by the unbalanced momentum exchange that occurs between species if one distribution is pear shaped, or *skewed*, as when a species conducts heat (Braginskii, 1965) and is usually described in the Chapman-Enskog formalism as a positive definite coefficient times the electron heat flux, $\mathbf{q}_e$. This emf produces a force on the electron that has a sense opposed to the direction of the heat flux. This function is usually ignored.

4. Significance of $\mathbf{E}_{||}$

A final form of the frozen flux theorem whenever $B > E$ is obtained by defining a special velocity field that is everywhere perpendicular to $\mathbf{B}$.

$$\mathbf{W}_E \equiv c\frac{\mathbf{E} \times \mathbf{B}}{B^2}$$

with $\mathbf{E}$ taken from the full form of the Generalized Ohm's law. The flux thawing criterion (12) takes the form

$$\frac{d\Phi}{dt} = -c\int_{S_1} \nabla \times \left(\frac{E_{||}}{B}\hat{\mathbf{b}}\right) \cdot \hat{\mathbf{n}}_1 da \tag{19}$$

Only moving with $\mathbf{W}_E$ (which does not have an evolution equation like the $\mathbf{W}$'s of (14a,b,c)) can (19) be true. (Through much of the current layer this frame is generally accessible, although when the magnetic field in the layer, B_L, is depressed relative to the ambient value in the reconnecting layer below $\frac{|\mathbf{U}_{inflow}|}{c} \simeq 10^{-4}$ of its upstream value this frame has a superluminal speed. Thus over much of the current layer this is a useful frame to imagine keeping track of the motion of field lines.) Equation (19) can be reduced using Ampere's equation to

$$\frac{d\Phi}{dt} = -\int_{S_1} \left[c\nabla\left(\frac{E_{||}}{B}\right) \times \mathbf{B} + \frac{E_{||}}{B}\left(4\pi\mathbf{J} + \frac{\partial \mathbf{E}}{\partial t}\right)\right] \cdot \hat{\mathbf{n}} da \tag{20}$$

Consider a surface S_1 that has its normal everywhere parallel to $\mathbf{B}$, then the integral expression simplifies to

$$\frac{d}{dt}\int_{S_1(\hat{\mathbf{n}}_1=\hat{\mathbf{B}})} B da = -\int_{S_1}\frac{E_{||}}{B}\left(4\pi J_{||} + \hat{\mathbf{b}}\cdot\frac{\partial \mathbf{E}}{\partial t}\right) da \tag{21}$$

When moving with the speed $\mathbf{W}_E$ the electric field only has parallel components, so that the dot product involving the partial time derivative contains only one term. Comparing the derivation for (12) with a general $\mathbf{W}$ and the present specific $\mathbf{W}_E$ illustrates that there is no analogue of surface S_3 to be considered since by (8), $\hat{\mathbf{n}}_3 da$ vanishes. Comparing with (7) with this flow field it is now clear that (21a) may be rewritten as:

$$\int_{S_1(\hat{\mathbf{n}}_1=\hat{\mathbf{B}})}\left[\frac{1}{4\pi}\frac{\partial B}{\partial t} + \frac{1}{8\pi B}\frac{\partial E_{||}^2}{\partial t} + \frac{E_{||}J_{||}}{B}\right] da = 0 \tag{22}$$

for arbitrary enclosed area of the geometrically constrained surface S_1. Accordingly, the integrand in the $\mathbf{W}_E$ frame must vanish leaving the result that

$$\frac{\partial}{\partial t}\left(\frac{|\mathbf{B}|^2 + E_{||}^2}{8\pi}\right) = -J_{||}E_{||} \tag{23}$$

Several comments are in order about (23). First in the $\mathbf{W}_E$ frame $E_{||}$ is the entire electric field; thus the left hand side is the time rate of change of the electromagnetic energy density in this frame. For the same reason there is no Poynting flux nor a divergence in this frame. Equation (23) illustrates that the field energy density is changed only by the Joule dissipation $-\mathbf{J}\cdot\mathbf{E} = -J_{||}E_{||}$. Further if there is prexisting $E_{||}$ negative Joule dissipation need not imply erosion of magnetic flux. However, in astrophysics it is usually the case that $|\mathbf{B}| \gg |\mathbf{E}|$ which is preserved for relativistic frame transformations so that protracted Joule dissipation will usually erode $\mathbf{B}$.

The second point about (23) is the crucial role in the physics of flux erosion played by $E_{||}$. *Without $E_{||}$, conversion of magnetic field energy density cannot happen, period.* Only some of the terms of the Generalized Ohm's Law (14) can produce $E_{||}$. These are the ambipolar electric field, the resistive terms and the inertial terms and, of these, even they will not thaw flux unless they occur in the presence of parallel current flow.

5. General Causes for a Parallel Electric Field in a Plasma

The second moment of the electron kinetic equation gives a clear and complete relationship between the electric field and other properties of the plasma as indicated in (14b). The ultimate sources of $E_{||}$ are thus traceable to the imbalances of

all the **parallel accelerations** experienced by the electron fluid:

$$E_{||} = -\hat{\mathbf{b}} \cdot \frac{\nabla \cdot \mathbf{P_e}}{en_e} - \frac{GM_o n_e m_e}{r^2} \hat{\mathbf{r}} \cdot \hat{\mathbf{b}}$$

$$+\frac{\hat{\mathbf{b}}}{en_e} \cdot \frac{\partial m_e n_e \mathbf{U_e}}{\partial t} + \frac{\hat{\mathbf{b}}}{en_e} \cdot \nabla \cdot (n_e m_e \mathbf{U_e} \mathbf{U_e}) + \frac{m_e}{en_e} < \frac{\delta f}{\delta t}|_c \hat{\mathbf{b}} \cdot \mathbf{v} >_{\mathbf{U}_e} \quad (24)$$

The terms on the right hand side are the ambipolar, inertial (gravitational, acceleration(2 terms), and collisional) contributions, respectively to $E_{||}$. While the parallel electric fields are usually small compared to $E_{\perp}$, they are nonetheless exceedingly important, controlling almost all aspects of the equilibrium *along* the field. Away from the site of flux erosion the motional electric field brings in new flux that is required for a steady state reconnection pattern to form. The physics of the reconnection itself is clearly that of what causes $E_{||}$ to exist in the first place as illustrated in (23). Simultaneously, however, the reconnection is short lived if new flux is not supplied with the external dynamics outside of the inner region. While it is easiest to see what determines $E_{||}$ from (24, 14b), it should be clear where all these terms are hidden in the one-fluid form (14a): The $\eta \mathbf{J}$ comes from the collisional terms and (14a) may be recovered from (14b,c) by multiplying each of these equations by its mass density and adding, using the definition of center of mass velocity and quasi-neutrality to recover (14a).

The leading order contribution to the parallel electric field in (14a,b,or c) well away from the nearest star is almost always given by the ambipolar term:

$$E_{||} \simeq -\hat{\mathbf{b}} \cdot \frac{\nabla \cdot \mathbf{P_e}}{en_e} \quad (25)$$

which for a gyrotropic plasma reduces to the form:

$$E_{||} \simeq -\frac{1}{en_e} \left(\frac{\partial P_{||,e}}{\partial s} + \frac{P_{||} - P_{\perp}}{B} \frac{\partial B}{\partial s} \right) \quad (26)$$

Equation (26) shows the causal role of the parallel pressure gradients and the unbalanced mirror force along **B** in determining $E_{||}$. The ambipolar electric fields counteracts the tendency for the lighter electrons to separate from the more sluggish ions along the field; in this way the ambipolar fields are the "glue" of a quasi-neutral plasma performing a regulating role whether collisions are dominant or not.

The remaining terms in $E_{||}$ come from the inertial terms which includes the collisional terms that for a highly collisional conductor like a copper wire give the ac and dc (resistive) contributions to the traditional Ohm's law. Ordinarily, the resistive term is not important in the astrophysical context, except possibly near the surface of a star if the magnetic field is strong enough. The inertial acceleration terms are usually more important than the resistive term.

6. Relative Scale Lengths of Generalized Ohms Law Terms

Vasyliunas (1975), following Rossi and Olbert's (1970) analysis of length scales of the Generalized Ohm's law, identifies the relative scale lengths when various terms in (14 a) become important. The Hall, ambipolar, inertial and resistive correction terms to 14(a) are first important on scales lengths

$$Hall: \ ambipolar: \ inertial: \ resistive$$

$$\frac{c}{\omega_{pi}} : \beta_e^{\frac{1}{2}} \frac{c}{\omega_{pi}} : \frac{c}{\omega_{pe}} : \lambda_\eta \frac{V_A}{V}$$

and have relative sizes of

$$1 : \beta_e^{\frac{1}{2}} : \frac{1}{42} : \frac{\lambda_\eta \omega_{pi}}{c} \frac{V_A}{V}$$

where λ_η is the resistive length

$$\lambda_\eta = \frac{\eta c^2}{4\pi V_A}$$

and V is the fluid speed.

For most space plasma domains β_e is non-negligible, so that the scales for the ambipolar electric field contributions are commensurate with the ion inertial scale lengths and well separated from the electron inertial scale lengths and the resistive scales. Ambipolar contributions were crucial in the modeling of steady state, collisionless shocks. As current layers start to amplify, the ambipolar contributions to **E** with their structures different from the resistive, Hall, or inertial terms will play an important role in the subsequent evolution of the reconnection layer. Modeling reviewed by Drake (1995) and coworkers discuss the onset of kinetic Alfvén disturbances in the reconnection layer with the inclusion of such terms and that the formation of magnetic islands foreseen in resistive MHD formulation of reconnection are preempted by the inclusion of the ambipolar contributions to the generalized Ohm's law. These same authors also concluded that current layers reconnecting with inertial electron skin depth corrections were intrinsically unstable and would spontaneously break apart. Near the magnetopause as soon as currents are important with scales that make the Hall term important, so is the ambipolar term.

Winglee (1994) has started to include ambipolar effects in a large scale MHD simulations and has shown the relationships between particle code effects at the magnetopause with no counterpart in resistive MHD for example. Mandt et al., (1994) have incorporated electron pressure effects in a hybrid code modeling the reconnection layer with isotropic fluid electron pressure. The reconnection rate is found to be much larger than in resistive MHD, and is insensitive to the resistivity assumed. Hesse et al., (1995) have made the first attempts to include equations

for the evolution of the electron pressure tensor in a hybrid code for reconnection. Although this is the first modeling where collisionless frozen flux violations as seen in the electron frame of reference have been inventoried, to do so has come at the expense of prohibiting the electrons from doing what they do best, conducting heat!

New effects while retaining the ambipolar terms in the baroptropic polytropic approximation have been reported by Ma and Battacharjee (1996). Abrupt increases in the current growth rate for the reconnection were noticed and a radically different spatial scaling of the non-ideal inner zone of the solution were noted. The ambipolar term in Ohm's law modified the external solution causing the resistive Sweet-Parker Y-points to collapse more toward Petschek's X configuration, but at the same time causing the reconnection rate to increase with local Alfvén speed exhausts. The parallel electric fields that evolve in such layers are much larger than the Dreicer runaway value (Ma and Bhattacharjee, private communication) so that the issues of closure comes full circle once more: the runaway contributions to the current and their contribution to the fricitional heating are incompletely inventoried in their analysis. These limitations arise from the neglect of the Stokes limitations on the friction, the constancy of the resistivity and neglect of the thermal force.

7. Levels of Magneto-Fluid-Dynamic (MFD) Approximation in the Description of Merging

Much of the early astrophysical literature of reconnection/merging involves assumptions about what simplification of the Generalized Ohm's law will be presumed adequate for the description of a physical situation. So called *Ideal MHD* approximates (14a) with (2). *Ideal-Hall MHD* entails truncating (14a) after retaining the $\mathbf{J} \times \mathbf{B}$ emf, which we have shown above is approximately like assuming field line preservation in the *electron* bulk frame. At this level there is the first possibility of separate responses of electrons and ions. Each of these *Ideal* levels of description have been further simplified and made analytically tractable in the *incompressible* limit: $\nabla \cdot \mathbf{U}_{cm} = 0$. This approximation reduces the one fluid continuity equation to

$$\frac{D}{Dt} \ln \rho = 0$$

where

$$\frac{D}{Dt} = \frac{\partial}{\partial t} + \mathbf{U}_{cm} \cdot \nabla$$

is the convective derivative. This additional approximation forestalls shock formation (without forbading their importance!). A wide and ever growing literature exists that discusses flux erosion within the framework of *Resistive (Ideal) MHD* or even *Resistive Hall MHD* which corresponds to the further retention of the $\eta \cdot \mathbf{J}$ term in the Generalized Ohms law. The electron pressure term of the Generalized

Ohm's is important in plasmas of very low density where it is usually referred to as the ambipolar electric field. In the absence of collisions the inertial terms of (14a-c) are present as well. As a group the inertial and ambipolar terms are sometimes referred to as the *"collisionless"* terms in the Generalized Ohm's law. In the magnetotail Speiser (1970) and coworkers have emphasized the role of the inertial terms in producing an effective resistivity as the particles oscillate about the current sheet.

Given the scaling arguments of the preceding section and the observations, nothing short of *anisotropic, ambipolar, Hall MHD*, more properly called Magneto-Fluid-Dynamics, makes any sense to this author for modeling of reconnection for near earth plasmas.

8. Geometrical Requirements for Reconnection

Favorable geometry is required between juxtaposed field lines so that reconnection is possible, (Hill, 1975; Cowley, 1976). Whether attempting component or anti-parallel merging, some components of B of the opposite sides perpendicular to the"X", or merging line must reverse across the current sheet so there is a current to exert a deflection force onto the plasma along reconnected field lines. The components of **B** parallel to the merging line appear to be unconstrained.

A predetermined boundary is identified to be the site of non-idealness and the plasma is pushed toward that boundary with its embedded magnetic flux by a perpendicular electric field that is tangential to the interface boundary where the system is non-deal. If the external boundary conditions are in balance with the flux dissipation and the expulsion of plasma along the current boundary, a steady state may result.

9. An Overview of Fluid Models

Analytic models of reconnection differ in the ways that the "external" inflow is arranged to interact with the inner zone. Most of the early work treats the region within this central layer as a "black box", or boundary layer, where resistive diffusion was assumed to dominate the evolution of the flux, while the external problem is arranged to (a) match a steady state with the boundary condition imposed by the large scale boundary conditions to match the (b) interface condition supposed for the inner region. Work of this type by Sweet (1958) and Parker (1957) dealt with spontaneous reconnection caused by resistive departures from Ideal Incompressible MHD: the inner diffusion region was long and narrow line of zero area of the "Y" form: $\succ\!\prec$ and the inflow Alfvén mach number was very low of order $M_A = R_M^{-\frac{1}{2}}$, where the magnetic Reynold's number $R_M = \frac{LV_{a,in}}{4\pi\eta}$ is customarily very large $> 10^6$. Petschek (1964) introduced compressibility and standing slow

shocks into the external solution outside of the diffusion region, with the effect of focusing the inflow region towards a narrower interval, thereby enhancing the reconnection rate to $M_A \simeq \ln R_m^{-1}$. Unlike the Sweet-Parker scenario where all the energy conversion must take place along the diffusion boundary layer, Petchek's solution achieved a more efficient conversion of magnetic to bulk energy by using the shocks to irreversably heat up and accelerate the plasma along the entire "X" interface radiating from the corners of the finite length reconnection line of the diffusion region. In this way, the reduced length of the diffusion region of his solution did not simultaneously "choke" the overall rate at which new flux could be brought up to the diffusion region along the symmetry axis. Topologically the Petschek geometry more nearly approximates an "X" than the back to back abutted "Y" geometry of Sweet-Parker. Additionally, the Petschek solution with slow shocks required a structured outflow. In Sweet-Parker and Petschek's model the inflow region was characterizes by very small Alfvén Mach numbers, while the outflow or exhaust region was a local Alfvén mach number 1 regime with the fluid flow nearly parallel to the highly kinked field lines in the exhaust region. The release of these stresses propagates at the local Alfvén speed perpendicular to the kink in the field accelerating the attached fluid in this external exhaust region to a flow velocity of this order. This accelerating outflow came to be known as "jetting" and for many synonymous with the reconnection process. In the early 1980's the lack of detection of accelerated jetting was taken as strong evidence that reconnection was not involved in mass interchange at the magnetopause.

Still within the resistive ideal MHD description, Levy, Petschek and Siscoe (1964) presented a model that addressed the asymmetric nature of the possible reconnection at the magnetopause. In this model the strong field side is treated as nearly a vacuum compared to the high density of the magnetosheath with its weaker magnetic field. Each pair of symmetrical slow shocks in the Petschek solution are now replaced with a rotational discontinuity and a slow expansion fan. The rotational discontinuity reconciles the arbitrary angles between the asymptotic sheath field and that of the magnetosphere (Petschek and Thorne, 1967) generalizing the antiparallel case of Levy et al. and Sweet-Parker. The tangential stress repartition made by the RD is the subject of several observational tests of reconection discussed below.

Priest and Forbes (1986) succeeded in identifying a family of resistive ideal MHD reconnection solutions which contained those of Petschek(1964) and Sonnerup (1970) as special cases of the inflow field to the reconection layer: Sonnerup's (1970) solution is the first place in the one parameter variation of B across the diffusion region that permitted smooth steady state flow with all flow lines deflected from the inflow symmetry line, whereas Petschek's solution is the last solution where all stream lines converge towards the inflow symmetry axis. Unlike Sweet-Parker all flow lines in this family of solutions do **NOT** go through the diffusion region. A significant fraction of the inflowing plasma is deflected and accelerated at the standing waves/ shocks in the external solution. In addition new

solutions were also found including the limiting case for this family beyond which a steady solution can no longer be found.

The inclusion of a normal component at a previously defined tangential discontinuity has been used by Heyn et al., (1988) and Biernat et al., (1989) to develop a more detailed, if approximate picture of the reconnection layer, as a solution to the so-called Riemann initial value problem. These authors outline the set of nested slow shocks, expansion or rarefaction fans that are predicted to stand inside of two flanking Alfvén or rotational discontinuities. The Alfvén wave on the magnetosheath side is suggested to carry most of the current at that reconnection layer, but propagates at a lower speed along the magnetopause than does the Alfvén discontinuity along the magnetoshere side of the reconnection layer. Detailed patterns for the changes in the fluid parameters through such a layer were computed and the effects of non-zero tangential flow speeds at the magnetopause away from the nose were included. Recent work by Lockwood et al., (1996) have explored the consequences of this structured layer withing the reconnection layer for the time of flight dispersed ions in the boundary layers of the cusp.

10. Overview of Single Particle Descriptions

Many of the results of the reconnection theory follow from enforcing conservation laws. Single particle discussions without using the fluid equations achieve similar predictions essentially by invoking the same conservation laws that transcend details of thermal physics description whether it is fluid or collisionless. This type of work has established that the resistivity caused by binary collisions is not the essential ingredients for reconnection. The fluid equation description provides a reduced level of description for examining the consequences of the conservation equations.

Hill (1975) modeled totally collisionless behavior and obtained reconnnection rates similar to those of the MHD theory using the kinetic equations and their conservation laws. He found that particles streaming into the field reversal region must carry enough momentum to exactly balance the stress in the magnetic field in steady state. Alternatively "...the particle motion in the field reversal must provide exactly the electric current required by the field geometry through Ampere's equation." The self consistency requirement is that the jump of the total tangential stress vanish, viz:

$$\Delta[\int (m_e f_e + m_i f_i) v_x v_k d^2 v - B_x B_k/(4\pi)] = 0$$

where $\hat{\mathbf{x}}$ is the normal to the field reversal plane, $\mathbf{k}$ is the direction of the component of $\mathbf{B}$ that reverses across the current sheet. This can be easily rephrased into the Walén condition for a rotational discontinuity, or for a shock as another example of a possible imbedded normal mass flux layer. Quite generally it is concluded that

if the incoming pressure is isotropic, then the merging speed is much less than V_A and is the local Alfvén speed times the small angle between the incoming field lines and the field reversal plane, consistent (within factors of 2) with that of fluid theory. From the particle picture merging ceases at the fire hose limit. For a given field the merging speed is independent of the magnitude of the initial plasma pressure *so long as it is isotropic*. The merging speed is reduced if $P_{||} > P_{\perp}$ since this situation reduces the magnetic tension required to accelerate and eject the plasma from the reversal region. For given asymptotic field strengths B_1 and B_2 the merging electric field has a maximum value for antiparallel fields and decreases monotonically to zero as the angular separation of the fields decreases. Flow patterns similar to Petschek's were achieved. The limitations of this model are: (i) the analysis is only valid so long as the particle drift in the current sheet layer perpendicular to the "plane of the X" is small compared to the characteristic dimensions of the system (Hill's analysis was performed sliding along the current in deHoffmann-Teller frame which is supposed to exist for all the orbits in question); and (ii) was only a fully collisionless treatment; particles only interact with the large scale electromagnetic field and not with each other; dissipation of electro- magnetic energy is dominated by inertial effects rather than collisional Joule heating.

Cowley (1980, 1982, 1995), Lockwood (1995) and coworkers (Lockwood et al., 1996) have discussed the form for the phase space distributions after they have interacted with the Alfven wave and rotational discontinuity within the reconnecting layer assuming that the magnetic moment of reflected and transmitted particles is conserved. This type of analysis has recently been reviewed by Fuselier (1995) and Onsager (1997). To date these models have not attempted to solve for the accessability of the populations from the opposite sides of the layer, nor have they addressed the problem of maintaining quasi-neutrality in the reconnection layer.

11. Signatures and Tests of Magnetic Reconnection

There are several robust tests for a normal mass flux discontinuity in MHD. They are, however, usually predicated on a locally planar magnetopause that is time stationary in its own frame of reference which may not be realized in practice.

Finding a normal component B_n of $\mathbf{B}$ at the magnetopause is an important clue about the site and occurrence of reconnection. The operational problem of finding small components perpendicular to a *free surface* that is oriented in an unknown direction and moving with an unknown velocity relative to the moving spacecraft has left us with a paultry few instances when the normal component is defensibly non-zero and steady through the layer. This situation is required for a planar normal mass flux rotational discontinuity. Numerous techniques have been developed with the best examples found in Sonnerup and Ledley (1979).

If the magnetopause has a normal mass flux, then the plasma streaming toward the magnetopause has in its external regime well removed from the magnetopause current layer a unipolar motional electric field $\mathbf{E_T}$ parallel to the magnetopause. From equation (2) this electric field (even when unmeasured) can be estimated using plasma and magnetic field data; this approach is especially accurate when the plasma is sampled near the magnetopause but outside of the precursors associated with the magnetopause current layer. Alternatively, long wire probes can be used to determine this vector, but in the sub-solar magnetopause, $\mathbf{E_T}$ is primarily in the GSE z direction and, until the recent Polar mission, has not been directly sampled, but synthesized from spin plane antennae under the assumption that $\mathbf{E}\cdot\mathbf{B} = 0$. The free surface problem alluded to in the case of the magnetic field normal component is also an issue here. With the electric field measurements there is a new complication relative to the Galilean invariant magnetic field vectors: Estimates of $\mathbf{E}$ relevant to the observer on the discontinuity are not the same electric field measurements recorded on the the spacecraft since: (1) the magnetopause is moving and (2) the spacecraft is also moving. Accordingly the tranformation of electric fields between frames will require knowledge of the magnetic field and the relative vector velocity of the free surface as viewed from the spacecraft. Accordingly, to use these measurements care must be taken to model and remove the effects of the magnetopause motion and acceleration. New techniques have recently been devised in this connection and have been reviewed by Sonnerup (1995). Often $\mathbf{E}$ is not directly measured, but inferred using (2) and even then without the knowledge of the center of mass velocity. It is always prudent to keep the observables and the inferences clearly identified in this detective work!

A variant of determining $\mathbf{E_T}$ are tests that contrast observational consequences of both $\mathbf{E_T} \neq 0$ and $B_n \neq 0$ *without determining the local magnetopause normal or relative velocity*. The first approach exploits the well known Walén (1944) jump condition for a rotational discontinuity

$$\Delta\mathbf{U}_{cm} = \alpha\Delta\mathbf{B}, \tag{27a}$$

which relates the **changes** in the asymptotic center of mass velocities of the plasma to the changes in the magnetic field over the same interval. As a vector relation this condition is actually three separate conditions with a common, specified proportionality constant (cf Hudson, 1970)

$$\alpha = \frac{1}{4\pi\rho}\left(1 - \frac{P_{\|}}{P_{\perp}}\right). \tag{27b}$$

This relationship results immediately from tangential stress balance. Note carefully that the condition as stated requires a determination of the plasma center of mass velocity and obtains only for the asymptotic states well removed from currents of the RD that implement the angular rearrangement of the asymptotic magnetic fields.

Until recently most of the "smoking gun" evidence for reconnection from *in situ* observations has come with the performance of numerous tests to verify the Walén test for a rotational discontinuity (cf. Paschmann et al., 1979, and Sonnerup et al., 1981). The data used for these tests came from ISEE 1 and 2 ion measurements of energy per unit charge analyzers that did not differentiate ions by their charge to mass. Moments of the observed fluxes at their observed energies were performed assuming all fluxes were protons (Paschmann private communication, 1996). Follow on studies (e.g. Sonnerup et al., 1990) with Ampte-IRM also used energy per unit charge analysis, achieving better time resolution by performing moments on board the spacecraft prior to transmission. Many layers were found with good correlation between the right and left hand sides of the Walén relationship. The agreement was however not perfect, with examples being dubbed "good" when the Walén expectation based on the magnetic field changes were corroborated at the greater than the 50% level. There were also some very good examples with nearly perfect correspondence. Attempts have been made (Paschmann, 1997) to organize the incidence of "good" Walén intervals with size of the magnetic shear to no avail, their being excellent Walén matches at low or high shear with no clear preference. The one clear ordering appears to be with plasma magnetosheath β. Whenever $\beta < 5$ Walén matches appear to be uniformly good or better.

In order to improve the leverage on the Walén comparisons, data through the current carrying layers have been used (Sonnerup et al., 1995) even though the jump conditions as stated by Walén are not supposed to work there. This follows from the fact that the Walén condition can be derived from the conservation of $\mathbf{E}_T$ across the rotational discontinuity. From 14a, there are Hall modifications to the emf that imply that the ideal MHD result for the asymptotic regimes is not strictly applicable within the iayers. Although $\mathbf{E}_T$ is conserved if the layer is one dimensional and time stationary, the components of (14a) that are required to evaluate $\mathbf{E}_T$ include terms other than those ion terms of (2) that have been used in this data evaluation. These data should be resorted based on current density, not just shear angle to see if the cases that failed the Walén test were those of higher than nominal current density or, equivalently, thinner than those that fit the expectation well. Alternatively, the Walén condition is fullfilled (at the MHD sizes of measurable $\mathbf{E}$) throughout the current carrying layer provided electron bulk velocity measurements are used to estimate $\mathbf{E}$ for this study (Scudder, 1984). Perhaps these will be available from the upcoming Cluster instrumentation. The role of alpha particles in the determination of the center of mass velocity from an E/Z analyzer warrants further consideration. Finally, in view of the discussion above of the Generalized Ohm's law, it may be that current density is not the index for thawing of magnetic flux at work at the magnetopause. Seeking such an ordering tacitly assumes that the resistive term of (14a) is the controlling factor at the magnetopause, even though the current carrying layers are much thicker than such an organization would imply. Another candidate for the possible organization of the good and not good Walén

tests as indexes of magnetic "thawing" would be the size of the magnetosheath electron pressure anisotropy.

As compelling as the Walén tests are for detecting potential reconnection layers away from the diffusion region, there are circumstances where the Walén condition can be fulfilled without there being a rotational discontinuity there. Except for forbading a normal component, the flow speeds are unconstrained across a tangential discontinuity. If the flow fields were arranged to meet the Walén condition in the transverse components and the normal component changes were unchanged but small, this is a permitted class of tangential discontinuities that if present would signal a locally closed magnetopause. This diagnostic degeneracy is more than an academic one: precisely this type of "mistake" was made when counting the frequency of detection of rotational discontinuities in the free flowing solar wind (cf. Burlaga, 1971 and Belcher and Davis, 1971). In fact the early counts for rotational discontinuities decreased markedly when this was realized. Accordingly, arguing that chance matches of the Walén condition are improbable had to be reworked! From a theoretical point of view tangential discontinuities are the non propagating limit of the slow branch, so that preexisting flows with tangential stress balance might be organized previously by the evolution of slow wave fronts into local tangential discontinuities leaving organized flows on either side of local tangential discontinuities. It is also known that high beta is not favorable to slow mode wave propagation; as slow expansion waves are required in the asymmetrical reconnection scenario, the observed beta organization of the "good" Walén data at weak shear may have their origin in the flows on either side of the layer that have temporarily closed down to become a tangential discontinuity.

It should also be stated for consideration that the mere certification of a rotational discontinuity in a given locale does *not* provide incontrovertible evidence of ongoing reconnnection. The rotational discontinuity is one of a number of MHD discontinuities found in magnetohydrodynamics that are required in general to support arbitrary boundary conditions. As an example rotational discontinuites and slow shocks are observed in the free flowing solar wind (Burlaga, 1995) without any reflexive implication of their implying ongoing reconnection. These structures are swept over and through the magnetopause region and will be modified at the bow shock. Nevertheless, there is by this counterexample no one to one association with if its a rotational discontinuity satisfying Walenś conditions, then there must be ongoing reconnection. The rotational discontinuity is for almost all geometries necessary, but not sufficient to indicate frozen flux violation.

Important for removing chance confirmations of reconnection are multiple, ancillary pieces of information about the magnetic topology, as from the leaking of particles from the magnetosphere along a separatrix (Sonnerup et al., 1981; Scudder et al., 1984), or fluid speed in the magnetopause frame equal to the local Alfvén speed, tests of conservation of energy. Many of these test have been performed as in the paper by Sonnerup et al., (1981) and the review by Paschmann (1984) for example, and often they also point to a picture of witnessing the reconnection lay-

er away from the separator line implicit in the asymmetric Levy-Petschek-Siscoe (1964) picture.

In the noon equatorial magnetopause geometry of opposed fields brought together normal to the current sheet, the expectations of "jetting" within the reconnection layer, or more precisely the lack of same, was once used as an argument against ongoing reconnection at the magnetopause. The initial surveys for reconnection flows from ISEE were indexed by enhanced flow speeds up against the magnetopause, consistent with Petschek's picture in the antiparallel geometry. There are, however, other tests for normal mass flux through the magnetopause performed by Aggson and co-workers that were not biased by looking for speed enhancements. Using measurements of the DC electric and magnetic field data, Aggson et al.,(1983, 1984, 1985) asked whether there was a Galilean frame shift to the deHoffmann-Teller frame that could null the detectable MHD sized motional electric field components even though $\mathbf{E}$ was varying across the current carrying layer of the magnetopause. Not only was this technique successful, this type of analysis rather routinely suggested that the magnetopause was open, since the existence of the deHoffmann-Teller frame, except in bizarre counterexamples, cf. Paschmann , (1985), is indicative of a normal component of $\mathbf{B}$ and of $\mathbf{E}_T$ to the free surface since $|\mathbf{V}_{HT}| = c\frac{|\mathbf{ET}|}{B_n}$. Aggson et al. studies (1984) further illustrated examples of open rotational shear layers where the fluid speed decreased rather than the field aligned "jetting" increase of the Levy et al., (1964) paradigm. Scudder (1984) looked at the general problem of a rotational discontinuity standing in the sheath flow and mapped out the general circumstances where net speed increases like Petschek were expected and where the speed decreasing solutions were expected. When the external tangential sheath flow is comparable or exceeds the Alfvén speed at the local density, there is an increased incidence with rotational shear that the reconnected flux will have a reduced speed in the earth's frame even while the flow vector acceleration still meet the Walén condition.

Care should be taken to note that outside the current layers the electron bulk speed and that of the ion plasma would be equal. The Walén tests are then the plasma counterpart of conservation of tangential $\mathbf{E}_T$. Scudder (1984) used (14b) from the electrons to see what kind of behavior should be expected for electrons (as a field line tracer) through the layer. Scudder also illustrated the expected variation of the electron fluid speed within the rotational shear layer, explicitly using (14b) as a more appropriate picture of the statement of frozen flux through the current carrying layer. Finally he delineated the frequency of occurrence of aligned flow within the reconnection layer. It is clear that strictly anti-parallel fields yields specialized field aligned jetting that are not the most general expectation. Accordingly, the many observations of speed going down across a boundary layer at the magnetopause are **NOT** first line evidence that reconnection has not locally populated those layers. Also, jetting need not be the exhaust flow geometry, especially away from the subsolar point.

12. Summary

The theoretical description of magnetic reconnection in the plasmas of geospace is conceptually and computationally challenging. This regime is not like the fusion regime and it is not a regime controlled by two body resistivity or even anomalous resistivities. The most important needed improvement beyond always retaining the Hall emf's in the description of reconnnection is the inclusion of the dominant terms in the Generalized Ohm's Law that control the parallel electric field. These terms are by all accounts the anisotropic ambipolar emf and possibly the inertial finite Larmor radius (FLR) ion gyroradius effects that mock up resistivity in the weakest part of the current sheets. Curiously, all of these effects are coherent in character as opposed to the stochastic resistive terms that are now in common use for this type of modeling. This situation has some hauntingly parallel aspects to the evolution of our understanding of collisionless shocks over the past 20 years. There a decided paradigm shift has occurred away from a stochastic two body or anomalous resistivity dominated scenario to a more realistic, but complicated picture with numerous coherent effects facilitating flux dispersal and thermalization. For reconnection, the challenging non-gyrotropic ambipolar terms are usually not included because they require a frontal assault on the issues of pressure equations of state and closure issues at the energy equation level that are amongst the most challenging problems in astrophysics. Nevertheless, these terms in the Generalized Ohm's law, as estimated by observations, control the erosion of magnetic flux in almost all realms of astrophysics. Finally, a truly predictive theory of reconnection for geospace plasmas must involve some approach to assess the evolution of the full electron pressure tensor, so that its curl is properly assessed, rather than ignored in the dynamical estimates of the erosion of magnetic flux. Such an approach must also retain the physics of electron heat conduction that was omitted from the promising start in this direction made by Hesse et al., (1995). In the intervening time the observations may further strengthen this impression by documenting the variation of electron pressure anisotropy and departures from gyrotropy in and near reconnection layers and possibly within the diffusion region. It is possible that these overlooked signatures of thawing of magnetic flux will better organize layers that are otherwise thought to be candidates for being open such as by "passing" Walén or related tests.

References

Aggson, T.L., Gambardella, P.J. and Maynard, N.C.: 1983, 'Electric field measurements at rotational magnetopause discontinuities', *J. Geophys. Res.* **88**, 10,000.

Aggson, T.L., Gambardella, P.J., Maynard, N.C. Ogilvie, K.W.,and Scudder, J.D.: 1984, 'Observations of plasma deceleration at a rotational discontinuity', *Geophys. Res. Lett.* **11**, 8.

Aggson, T.L., Gambardella, P.J. and Maynard, N.C.: 1985, 'Reply', *J. Geophys. Res.* **90**, 7636.

Alfvén, H.: 1942, 'On the existence of electromagnetic-hydrodynamic waves', *Ark. Mat.* **29B**, 2.

Axford, W. I.: 1984, in E.W. Hones, Jr., (ed.). ' Magnetic field reconnection', *Magnetic Reconection in Space and Laboratory Plasmas*, Geophys. Monongraph 30, AGU, Washington, 1ff.

Biernat, H.K., Heyn, M.F., Rijnbeek, R.P., Semenov, V.S., and Farrugia, C.J.: 1989, 'The structure of the reconnection layer: application to the earth's magnetopause', *J. Geophys. Res.* **94**, 287.

Braginskii, S.I.: 1965, 'Transport process in a plasma', in *Reviews of Plasma Physics*, 1, Consultant's Bureau, New York.

Belcher, J.W. and Davis, L. Jr.: 1971, 'Large amplitude Alfvén waves in the interplanetary medium 2.', *J. Geophys. Res.* **76**, 16.

Burlaga, L.F.: 1971, 'Nature and origin of directional discontinuities in the Solar Wind', *J. Geophys. Res.* **76**, 4360.

Burlaga L.F. and Scudder, J.D.: 1974, 'Sweet's mechanism in the solar wind', *Ap. J.* **191**, L149.

Burlaga L.F.: 1995, 'Interplanetary Magnetohydrodynamics', Oxford University Press, New York.

Cai, H.J., Ding, D.Q., and Lee, L.C.: 1994, 'Momentum transport near a magnetic X line in collisionless reconnection', *J. Geophys. Res.* **99**, 35.

Cowley, S.W.H.: 1976. 'Comments on the merging of nonparallel magnetic field', *J. Geophys. Res.* **81**, 3455.

Cowley, S.W.H.: 1980, 'Plasma populations in a simple open magnetosphere', *Space, Sci. Rev.* **26**, 217.

Cowley, S.W.H.: 1982, 'The causes of convection in the Earth's magnetosphere: a review of developments during the IMS', *Rev. Geophys. and Space Phys.* **20**, 3, 531.

Cowley, S.W.H.: 1995, in P. Song, B.U.Ö. Sonnerup, and M.F. Thomsen, (eds.), 'Theoretical perspectives at the magnetopause', *Physics of the Magnetopause*, Geophys. Mono 90, AGU Washington, p 29.,1995.

deHoffmann, F., and Teller, E.: 1950, 'Magnetohydrodynamic shocks', *Phys. Rev.* **80**, 692.

Dreicer, H.: 1959, 'Electron and ion runaway in a fully ionized gas, I', *Phys. Rev.* **115**, 238.

Dreicer, H.: 1960, 'Electron and ion runaway in a fully ionized gas, II', *Phys. Rev.* **117**, 329.

Drake, J.F.: 1995, P. Song, B.U.Ö. Sonnerup, and M.F. Thomsen, (eds.), 'Magnetic reconnection: a kinetic treatment', *Physics of the Magnetopause*, Geophys. Mono 90, AGU Washington, 155.

Dungey, J.W.: 1988, 'Noise free current sheet', in *Proc. of an International Workshop in Space Plasma*, ESA SP-285, 15.

Fainberg, J., Osherovich, V.A., Stone, R.G., MacDowall, R.J., and Balogh, A.:1996, in D. Winterhalter, J.T. Gosling, S. R. Habbal, W.S Kurth, (eds.) ,'Ulysses observations of electron and proton components in a magnetic cloud and related wave activity, *Solar Wind Eight*, AIP press, Woodbury, NY, p 554.

Fuselier, S.A.: 1995, P. Song, B.U.Ö. Sonnerup, and M.F. Thomsen, (eds.), 'Kinetic aspects of reconnection', *Physics of the Magnetopause*, Geophys. Mono 90, AGU Washington, 181.

Hesse, M., Winske, D. and Kuznetsova, M.: 1995, 'Hybrid simulations of collisionless reconnection in two-dimensional current sheets', *J. Geophys. Res.* **100**, 21,815.

Heyn, M.F., Biernat, H.K., Rijnbeek, R.P., and Semenov, V.S.: 1988, 'The structure of the reconnection layer', *J. Plasma Phys.* **40**, 235.

Hill, T.W.; 1975, 'Magnetic merging in a collisionless plasma', *J. Geophys. Res.* **80**, 4689.

Hudson, P.D.:1970, 'Discontinuities in an anisotropic plasma and their identification in the solar wind', *Planet. Space, Sci.* **18**, 1611.

Kleva, R.G., Drake, J.F., and Waelbroecke, F.L.: 1995, 'Fast reconnection in high temperature plasmas', *Phys. Plasmas* **2**, 23.

Lee, L.C.: 1995, P. Song, B.U.Ö. Sonnerup, and M.F. Thomsen, (eds.), 'A review of magnetic reconnection: MHD Models', *Physics of the Magnetopause*, Geophys. Mono 90, AGU Washington, p 139.

Levy, R.H., Petschek, H.E., and Siscoe, G.L.: 1964, 'Aerodynamic aspects of the magnetospheric flow', *AIAA J.* **2**, 2065.

Lockwood, M.: 1995, 'Location and characteristics of the reconnection X-line deduced from low-altitude satellite and ground-based observations: 1 theory', *J. Geophys. Res.* **100**, 21,791.

Lockwood, M., Cowley, S.W.H. and Onsager, T.G.: 1996, 'Ion acceleration at both the interior and exterior Alfvén waves associated with the magnetopause reconnection site: signatures in cusp precipitation', *J. Geophys. Res.* **101**, 21,501.

Lottermoser, R. -F, and Scholer, M.: 1997, 'Undriven magnetic reconnection in magnetohydrodynamics and Hall magnetohydrodynamics', *J. Geophys. Res.* **102**, 4875.
Lyons, L.R. and Speiser, T.W.: 1985, 'Ohm's law for a current sheet', *J. Geophys. Res.* **90**, 8543.
Lyons, L.R. and Pridmore-Brown, D.C.: 1990, 'Force balance near an X line in a collisionless plasma', *J. Geophys. Res.* **95**, 20,903.
Lyons, L.R. and Pridmore-Brown, D.C.: 1992, 'Force balance near an X line with $E \cdot J < 0$', *J. Geophys. Res.* **97**, 2955.
Ma, Z., and Bhattacharjee, A.: 1996, 'Fast impulsive reconnection and current sheet intensification due to electron pressure gradients in semi-collisional plasmas', *Geophys. Res. Lett.* **23**, 1673.
Mandt, M.E., Denton, R.E., and Drake, J.F.: 1994, 'Transition to whistler mediated reconnection', *Geophys. Res. Lett.* **21**, 73.
Mozer, F.S., Torbert, R., Fahleson, U.V., Falthammar, C.G., Gonfalone, A., and Pedersen, A.: 1978, 'Electric field measurements in the solar wind, shock, magnetosheath, magnetopause and magnetosphere', *Space Sci. Rev.* **22**, 791.
Onsager, T. G. and Lockwood, M.: 1997, 'High-latitude particle precipitation and its relationship to magnetospheric source regions', *Space Sci. Rev.*, this volume.
Osherovich, V.A., Farrugia, C.J., Burlaga, L.F., Lepping, R.P., Fainberg, J., and Stone, R.G.: 1993, 'Polytropic relations in interplanetary clouds', *J. Geophys. Res.* **98**, 15331.
Osherovich, V.A., Farrugia, C.J., and Burlaga,L.F.: 1995, 'The non-linear evolution of magnetic flux ropes: 2 Finite beta plasma', *J. Geophys. Res.* **100**, 12307.
Parker, E.N.: 1957, 'Sweet's mechanism for merging magnetic fields in conducting fluids', *J. Geophys. Res.* **62**, 509.
Paschmann, G., Sonnerup, B.U.Ö., Papamastorakis, I., Sckopke, N., Haerendel, G., Bame, S.J., Asbridge, J.R., Gosling, J.T., Russell, C.T., and Elphic, R. C.: 1979, 'Plasma acceleration at the earth's magnetopause: evidence for reconnnection', *Nature* **282**, 243.
Paschmann, G.: 1984, in E.W. Hones, Jr., (ed.), 'Plasma and particle observations: implications for reconnection', *Magnetic Reconection in Space and Laboratory Plasmas*, Geophys. Monongraph 30, AGU, Washington, 114.
Paschmann, G.: 1985, 'Comment on "Electric field measurments at the magnetopause I: observations of large convective velocities at rotational magnetopause discontinuities" by T.L. Aggson, P.J. Gambardella and N.C. Maynard', *J. Geophys. Res.* **90**, 7629.
Paschmann, G.: 1997, 'Observational evidence for transfer of plasma across the magnetopause', *Space Sci. Rev.*, this volume.
Petschek, H.E.: 1964, in W.N. Hess, (ed.),'Magnetic field annihilation', *The Physics of Solar Flares*, NASA SP-50, Washington DC.
Petschek, H.E. and Thorne, R.M.: 1967, 'The existence of intermediate waves in neutral sheets', *Ap. J.* **147**, 1157.
Priest, E.R. and Forbes, T.G.: 1986, 'New models for fast steady state magnetic reconnection', *J. Geophys. Res.* **91**, 5579.
Rossi, B. and Olbert, S., *Introduction to the Physics of Space*, McGraw Hill Book Co., New York, 1970.
Scudder, J.D. and Olbert, S.: 1979, 'A theory of local and global processes which affect solar wind electrons, 2. experimental support', *J. Geophys. Res.* **84**, 6603.
Scudder, J.D. Ogilvie, K.W., and Russell, C.T.: 1984, in E. Hones, (ed.), 'The relationship of flux transfer events to magnetic reconnection', *Magnetic Reconnection in Space and Laboratory Plasmas*, AGU Geomonograph Series 30, Washington, DC, 153-154.
Scudder, J.D.: 1984, 'Fluid signatures of rotational discontinuities at the Earth's magnetopause', *J. Geophys. Res.* **89**, 7431-7440.
Scudder, J.D., Mangeney, A., Lacombe, C., Harvey, C., and Aggson, T.L.: 1986, 'The resolved layer of a collisionless, high β, super-critical, quasi-perpendicular shock wave: 2: dissipative fluid electrodynamics', *J. Geophys. Res.* **91**, 11053.
Scudder, J.D.: 1987, 'The field aligned flow approximation for electrons within layers possessing a normal mass flux: a corollary to the deHoffmann - Teller theorem', *J. Geophys. Res.* **92**, 13447-13455.

Scudder, J.D.: 1992, 'On the cause of temperature change in inhomogeneous, low-density astrophysical plasmas', *Ap. J.* **398**, 299.

Siscoe, G.L.: 1983, in R.L. Carovillano and J.M. Forbes (eds.), 'Solar system magnetohydrodynamics', *Solar Terrestrial Physics*, p 11-100, D. Reidel., Amsterdam.

Sittler, E.C., Jr. and Scudder, J.D.: 1980, 'An empirical polytrope law for solar wind thermal electrons between 0.45 and 4.76 AU: Voyager 2 and Mariner 10', *J. Geophys. Res.* **85**, 5131.

Sonnerup, B.U.Ö.: 1970, 'Magnetic re-connexion in a highly conducting incompressible fluid', *J. Plasma Phys.* **4**, 161.

Sonnerup, B.U.Ö. and Ledley, B.G.: 1979, 'OGO 5 magnetopuase structure and reconnection', *J. Geophys. Res.* **84**, 399.

Sonnerup, B.U.Ö., Paschmann, G. , Papamastorakis, I., Sckopke, N., Haerendel, G., Bame, S.J., Asbridge, J.R., Gosling, J.T., and Russell, C.T.: 1981, 'Evidence for magnetic field reconnection at the earth's magnetopause', *J. Geophys. Res.* **86**, 10,049.

Sonnerup, B.U.Ö.: 1984, in E.W. Hones, Jr., (ed.),' Magnetic reconnection at the magnetopause: a review', *Magnetic Reconection in Space and Laboratory Plasmas*, Geophys. Monongraph 30, AGU, Washington, 92.

Sonnerup, B.U.Ö., Papamastorakis, I., Paschmann, G., and Luhr, H.: 1990, 'The magnetopause for large magnetic shear: analysis of convection electric fields',*J. Geophys. Res.* **95**, 10,541.

Sonnerup, B.U.Ö., Paschmann, G., Phan, T.-D.: 1995, in P. Song, B.U.Ö. Sonnerup, and M.F. Thomsen, (eds.), 'Fluid aspects of the reconnection layer', *Physics of the Magnetopause*, Geophys. 90, AGU Washington, 167.

Speiser, T.W.: 1970, 'Conductivity without collisions or noise', *Planet. Space Science* **18**, 613.

Sweet, P. A.: 1958, in B. Lehnert, (ed.), 'The neutral points of solar flares', *Electromagnetic Phenomena in Cosmical Research*, Cambridge University Press, London.

Vasyliunas, V.M.: 1972, 'Nonunniqueness of magnetic field line motion', *J. Geophys. Res.* **77**, 6271.

Vasyliunas, V.M.; 1975, 'Theoretical models of magnetic field line merging: 1', *Rev. Geophys. and Space Physics.* **13**, 303.

Walén, C.: 1944, 'On the theory of sunspots', *Ark. Mat. Astron. Fys.*, 30A.

Winglee, R.M.: 1994, 'Non-MHD influences on the magnetospheric current system', *J. Geophys. Res.* **99**, 13437.

Address for correspondence: J. D. Scudder, Department of Physics and Astronomy, University of Iowa, Iowa City, IA 52242, USA

OBSERVATIONAL AND THEORETICAL ASPECTS OF PROCESSES OTHER THAN MERGING AND DIFFUSION GOVERNING PLASMA TRANSPORT ACROSS THE MAGNETOPAUSE

R. Lundin

Swedish institute of space physics, Box 812, S-981 28 Kiruna, Sweden

Abstract. The magnetopause and its inner contact region with the magnetosphere, the magnetospheric boundary layer, constitute the interface between the shocked solar wind plasma and the magnetosphere. Indeed magnetosheath plasma has to cross the magnetopause in order to access the Earth's magnetosphere. The issue here is to identify the physical processes that govern plasma transport across the magnetopause, plasma that subsequently flows along the inside of the magnetopause boundary in the magnetospheric boundary layer. Some other relevant questions concerning magnetosheath plasma entry are:
— how "deep" inside the magnetosphere does magnetosheath plasma penetrate?
— is the plasma entry predominantly steady or transient?
— is the magnetospheric boundary layer on open or closed geomagnetic field lines?
— to what extent can merging/reconnection qualify as a general plasma entry mechanism?
— does plasma diffusion represent a major steady state entry process?
— what processes, besides merging/reconnection and diffusion may govern magnetosheath plasma entry into the magnetosphere.

Magnetosheath plasma energy, mass and momentum transfer into the magnetosphere remains a matter of controversy. A number of workers in our field, perhaps a majority, has taken the stand that the issue is essentially settled and that merging/reconnection, possibly complemented by some weak plasma diffusion, suffices to explain the entire transfer of solar wind energy, mass and momentum into the magnetosphere.

It is the purpose of this paper to discuss observational results of magnetosheath plasma entry that neither corroborate merging/reconnection nor a "weak" plasma diffusion as access mechanisms for magnetosheath plasma into the magnetosphere. The intent is not to rule out merging/reconnection as a class of plasma access processes, but rather to point out that observations suggest more opportunities for plasma entry than conceived in existing MHD-based models. Moreover, these observations suggests that the solar wind energy, mass and momentum transfer into the magnetosphere and the Earth's ionosphere must be put in context with a current circuit that couples deceleration in a dynamo/generator region with acceleration/ heating in a load region. Indeed, observations suggests that transient reconnection phenomena such as flux transfer events are related with field aligned currents .

1. Introduction

The first observation of a thin layer of magnetosheath plasma located immediately inside the magnetopause was made by Hones et al. (1972) on the basis of IMP 6 data. Other satellite studies followed focussing on the morphological characteristics as well as the plasma properties of the magnetospheric boundary layer at high- and low latitudes (e.g. Eastman et al., 1976, Rosenbauer et al., 1975, Paschmann et al., 1979, Lundin et al., 1981). A picture eventually emerged with the magnetospheric boundary layer comprising two distinguishingly different regions: A low latitude region denoted the Low-Latitude Boundary Layer, LLBL, (Eastman et al., 1976), and a high latitude region denoted the plasma mantle (Rosenbauer et al., 1976). In addition there are two more regions related to the polar cusp,

Space Science Reviews **80**: 269–304, 1997.

which is assumed to connect directly to the magnetosheath: These are the Entry layer (Paschmann et al., 1976) and the Exterior cusp (Sckopke, 1979). An important and distinguishing difference between the two "main" boundary layers is that the plasma mantle is, almost by definition, on open field lines adjacent to the lobe/polar cap, while the LLBL may be at least partly on closed geomagnetic field lines. Indeed, an LLBL on closed field lines inevitably implies the direct entry of magnetosheath plasma through the dayside magnetopause with subsequent inclusion and trapping onto dayside magnetic field lines.

The issue of the "openess"of the LLBL is far from being solved. Arguments have been put forward for the entire LLBL to be located on open field lines (reconnection) whereas some measurements suggest that the LLBL is on a mixture of open and closed field lines (e.g. Lundin and Dubinin, 1984, Mitchell et al., 1987, Hall et al., 1991, Woch and Lundin, 1991, 1992a). The difference in view is unfortunately related to models on one hand and to prejudices on the other, and much less to observational facts. In situ observations of mirroring energetic electrons in the LLBL (Mitchell et al., 1987) are evidence for closed magnetic field lines, at least on a time scale corresponding to several bounce periods. Similarly, double loss-cone signatures identified from mid-altitude satellites (Woch and Lundin, 1991, 1992a) are clear evidence for trapping. Thus, in these cases the remaining issue is whether the observation takes place in the LLBL or not.

The general lack of agreement also prohibits progress in understanding the physics of the magnetospheric boundary layer. The uncertainty about the LLBL can be summarized by the following questions:

— Is the LLBL the site of energy and momentum transfer (dynamo/ generator or load)?
— If so, what are the main physical processes governing this energy and momentum transfer, and how important are they?
— Is the LLBL mainly a transport region like the plasma mantle, responding primarily to the external solar wind electric field, or are effects in the LLBL driven by local plasma kinetic effects?

Indeed the LLBL may be driven by internal as well as external processes, by virtue of the simple fact that magnetosheath plasma access into the magnetosphere must be dynamical. Plasma entry is an external, magnetosheath driven process, while the energy and momentum transfer is primarily an internal (dynamo) process. Thus, the "openness" of the LLBL is always a matter of timing.

Before proceeding on matters related with the magnetospheric boundary layer, a few important working definitions will be introduced:

Merging: Magnetic merging of solar wind and magnetospheric field lines at the magnetopause whereby solar wind energy have a local, steady state or temporal, access to magnetospheric field lines (via the solar wind electric field). *Reconnection:* Identical with magnetic merging (requires

high magnetic shear). *Viscous interaction:* Solar wind energy and momentum transfer via viscous/ frictional forces (introduced by Axford and Hines, 1961). *Diffusion:* Weak transport of plasma across the magnetopause by means of plasma microinstabilities (eddy diffusion, viscosity, wave-particle scattering, finite Larmor radius effect). *Flux transfer events, FTEs:* Time-dependent / pulsed localized magnetic reconnection (Russell and Elphic, 1979). The signature of FTEs are controlled by the IMF orientation. *Plasma transfer:* Solar wind plasma transport process whereby plasma energy, mass and momentum is transferred across the magnetopause (via plasma kinetics and/or dynamics).. *Magnetopause waves:* Wavy structures of the magnetopause current layer. Magnetic signatures similar to FTEs (Sibeck, 1989). *Plasma transfer events, PTEs:* Time-dependent penetration of magnetosheath plasma into the magnetosphere as observed by rockets and satellites (e.g. Carlson and Torbert, 1980; Lundin, 1989). PTEs are mainly solar wind pressure dependent (Woch and Lundin, 1992a). *Impulsive penetration:* Time-dependent penetration of plasma clouds through the magnetopause - independent of the IMF orientation. A terminology first introduced by Lemaire (1977).

Notice that the last two concepts relate to transient plasma injection through the dayside magnetopause: PTEs on an observational basis and impulsive penetration as a theoretical concept. This does not imply that one is a proof for the other. We also argue that PTEs and FTEs, both observationally based concepts, are probably manifestations of one and the same physical phenomena, albeit at different evolutionary stages. We will return to this.

About the observational aspects of processes governing plasma transport across the magnetopause, the question is: what kind of observations? The obvious answer is - *clearly distinguishable localized regions of magnetosheath plasma in the magnetosphere*. Indeed, such localized regions have been reported since the early sixties when the cusp was discovered (e.g. Burch, 1968, Heikkila and Winningham, 1971; Frank and Ackerson, 1971). Aparicio et al (1991) also demonstrated the close relation between the cusp proper and the high-latitude shocked magnetosheath plasma.

This automatically leads to the next question: Where can such magnetosheath-like regions be observed? — *Almost anywhere in the outer region of the magnetosphere* (LLBL, plasma mantle, cusp, cleft), *but indeed also well inside the dayside and flank magnetopause* (e.g., Woch and Lundin, 1991, 1992a; Yamauchi et al., 1993c).

A related question is: What are the prime regions of solar wind/ magnetosheath plasma entry? —*The cusp and the dayside magnetopause.*

Having defined the above different concepts for plasma access it is of interest to investigate what kind of processes, besides merging and reconnection, promote magnetosheath plasma entry into the magnetosphere. Like merging/reconnection, steady and transient processes may occur, such as *steady transfer*: associated with direct entry of plasma into the cusp,via

viscous diffusion from e.g. finite Larmor radius effects (Stasiewicz, 1991) or by gradient drift entry (Olson and Pfitzer, 1985), and *transient plasma transfer:* associated with various, yet theoretically poorly understood, impulsive penetration mechanisms (Lemaire, 1977, Heikkila, 1982), or Kelvin-Helmholz instabilities (e.g. Miura, 1984).

However, it has been argued that of the above proposed mechanisms to explain magnetosheath plasma penetration into Earth's magnetosphere, only merging/reconnection is sufficient. So why taking an interest in other processes? The reason for this stems from two important observational facts:
(1) Observations indicating that solar wind plasma accesses the magnetosphere essentially independent of the IMF orientation (e.g. Woch and Lundin,1992a, Lennartsson, 1987, 1991). For instance, observations by Lennartsson (1987, 1991 and Baumjohann et al., 1989) indicates that the plasma sheet effectively accumulates solar wind plasma and is wider and more dense for northward- than for southward IMF. Thus, even if the loss processes are more effective for southward IMF, the solar wind plasma access appears to be independent of IMF, contrary to merging expectations.
(2) Solar wind kinetic effects, e.g. a strong dynamic pressure, appears to play a more important role than previously anticipated for the transfer of solar wind energy, mass and momentum into the magnetosphere (Woch and Lundin, 1992a, Newell and Meng, 1994, Lennartsson et al., 1995).

Thus, a very important issue that needs to be addressed in much more detail is how to distinguish merging/reconnection from other candidates for plasma transport across the magnetopause. Indeed, also the merging/ reconnection process - taken almost as a corollary in magnetospheric physics for more than 30 years - requires better understanding from a microphysics point of view. For instance, what physical mechanisms promotes the local break-down of MHD at the merging site? What are the characteristics of "other processes" of plasma transport through the dayside magnetopause? The latter is indeed subject of this report. However, to identify the alternative transport processes requires a review of observations in various regions of the magnetosphere.

2. LOW- AND MID-ALTITUDE BOUNDARY LAYER OBSERVATIONS (THE CUSP, MANTLE, CLEFT/LLBL)

The first observations indicating a direct inflow of magnetosheath plasma into the magnetosphere were made from low-altitude polar orbiting satellites by e.g., Burch et al. (1968), Heikkila and Winningham (1971), and Frank and Ackerson (1971). Statistical studies suggested a narrow region near local noon where the magnetic field topology forms a magnetic "throat" or cusp - hence the denomination "cusp". Low altitude satellite measurements also demonstrated that the polar cusp is a persistent feature near local noon, implying a continuous injection of magnetosheath plasma there. However,

the early observations generated some confusion with conflicting ideas regarding the shape and magnetic mapping of the region of enhanced low-energy particle precipitation. It was debated whether the precipitation region had the shape of a *cusp* or a *cleft*. Later Heikkila (1985) suggested the following clarification and working definition: "The *cleft* is the low altitude region around noon of about 100 eV electron precipitation associated with 6300 Å emission, but containing also structured features of higher energy. The *cusp* is a more localized region near noon within the cleft characterized by low energy precipitation only, having no discrete auroral arcs, but often displaying irregular behaviour, presumably associated with the magnetic cusp."

For a closed magnetic field topology, the magnetic cusp is connected with the entire surface of the magnetopause. Plasma entering the magnetosphere via the magnetopause then has to cross cusp magnetic field lines.

Two views for an open magnetic field topology have been put forward:
(1) Traditional merging/reconnection, with magnetic field lines merging at the dayside magnetopause and subsequently convecting across the cusp into the plasma mantle and polar cap. This view, most recently explored by e.g. Smith and Lockwood (1990), Lockwood and Smith (1992), is a contemporary version of the traditional open magnetosphere model by Dungey (1961) and Cowley (1980). According to Lockwood and coworkers the cusp is essentially a statistical phenomenon comprising a transient "train" of reconnected flux tubes with the highest probability of occurrence in what experimenters identify as the polar cusp.

In this view, essentially neglecting all pressure and drift effects besides convection (i.e. "ideal MHD"), the terrestrial magnetic field lines in the cusp are connected (frozen) to the solar wind magnetic field. These field lines are subsequently swept by the sheath flow into the tail/polar cap region - building up magnetic flux in the lobe. Reconnection is thus a requirement for the existence of a cusp.
(2) The second view simply assumes a steady-state finite width cusp/ "throat" that allows direct injection of magnetosheath plasma on open field lines threading to the solar wind in what is termed the *cusp proper*. The "openness" is a consequence of topology and plasma boundary conditions, the magnetopause field lines forming a boundary within the "throat". This view essentially neglects the problem of magnetic linkage between the magnetosheath and terrestrial magnetic field from two sources - the solar wind and the geomagnetic dipole field. Neglecting "ideal MHD", plasma may cross magnetic boundaries by many different (first order) drift processes (pressure and magnetic field gradients, currents etc). Furthermore, requiring a flux tube with plasma to be "frozen" into it at all times is presumptuous. Particularly so on magnetic field lines connected to the Earth´s auroral acceleration region. Thus, by the same token as a magnetosheath flux tube connects to a terrestrial magnetic flux tube, it may as easily disconnect again

- yet sharing its plasma content.

Plasma crossing the magnetopause and entering the magnetospheric side of the "throat" is associated with strong solar wind energy transfer. Strong solar wind energy exchange is generally not observed in the cusp proper. Indeed, mid-altitude observations from the Viking satellite suggests that the *cusp proper* is populated by strong fluxes of magnetosheath particles but contains very little particle energization (e.g. Kremser and Lundin, 1990, Aparicio et al., 1991). Energy transfer, associated with particle acceleration and currents, appears mainly to be associated with what was termed the boundary cusp (e.g. Kremser and Lundin, 1990). In summary, the *cusp proper* is an open flux tube connected to the magnetosheath with plasma flowing directly into the magnetosphere. The cusp proper represents in this picture a center of plasma pressure with the pressure gradients, supposedly driving the steady state cusp and region 1 currents, associated with the boundary cusp (e.g. Yamauchi et al., 1993a).

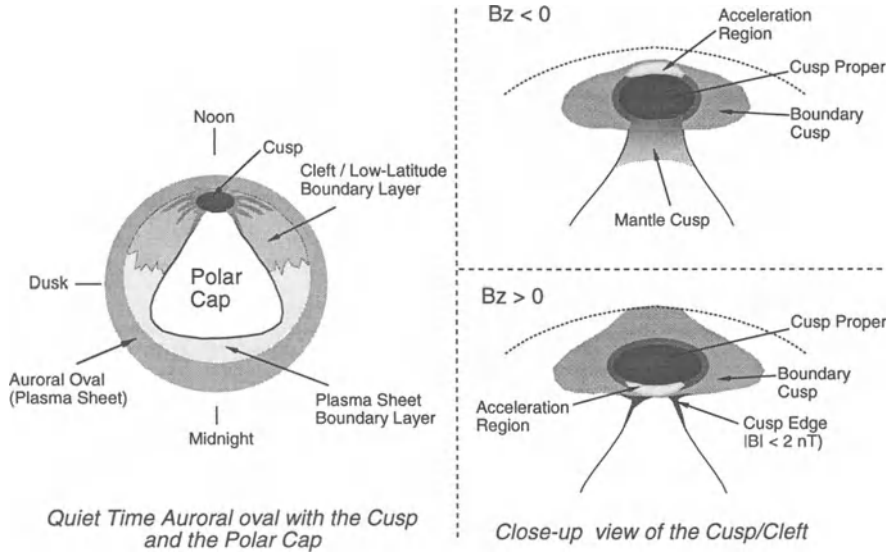

Figure 1. Summary cartoon of the cusp position with respect to the continuous auroral oval (left) and a close-up look of the characteristic regions found in the hot plasma data from low- and mid-altitude satellites.

Figure 1 gives a summary cartoon of the cusp and cleft morphology based on observational data from the Viking satellite. The cartoon is meant to illustrate phenomenological features of the cusp and their location with respect to the oval, rather than giving a model of the cusp response with respect to interplanetary disturbances. The left hand side shows the position of the cusp with respect to the auroral oval, largely inspired by the Tsyganenko model (Tsyganenko, 1987). Notice that we draw the polar cap

well poleward of the continuous oval as is generally the case for a northward IMF with $B_Y \approx 0$ (Jankowska et al, 1990). The cusp is located poleward of the continuous oval. The cleft, which we interprets as the low-altitude footprint of the LLBL, is the region bordering the cusp towards the morning and afternoon sector, lying equatorward of the polar cap and poleward of the dayside auroral oval. The cleft width and local time distribution should be strongly dependent on the IMF B_Z, in accordance with the width of the LLBL at the magnetopause (Mitchell et al., 1987). Here we draw a very extended cleft as one would expect for a northward IMF. The right hand side shows a blow-up of the cusp with the various regions identified for northward and southward IMF, e.g. the acceleration region (Woch and Lundin, 1991) and cusp edge (Yamauchi et al., 1993b).

The *cusp proper*, is also the region with highest plasma density, of the same magnitude or higher than those measured in the solar wind (IMP-8). Indeed, based on the simple gas dynamical picture by Spreiter et al. (1968), the plasma density within the cusp proper is consistent with magnetosheath densities (Aparicio et al., 1991).

The latter view of a cusp continuously open to the solar wind and magnetosheath represents an alternative to merging/reconnection as it is generally conceived - i.e. taking place near the subsolar point for negative IMF Bz and in the tail for positive IMF Bz. The fact that the magnetic field geometry of the cusp implies that there is virtually always an antiparallel merging site in the vicinity of the outer cusp (see e.g. Stasiewicz, 1991) strengthens the argument for the cusp as the main region for magnetosheath plasma entry. However, the important consequence of a well defined and continuous access region is that a gas dynamical approach may be used. Indeed, such a view dates back to the work by e.g. Spreiter et al. (1968) where fluid parameters such as density, velocity and pressure plays an important role for not only the cusp geometry but also the energy transfer. Studies by Aparicio et al. (1991), Newell and Meng (1994) and Lundin et al. (1997) clearly suggest a strong relation with solar wind density and pressure, respectively. These results clearly illustrates that solar wind plasma dynamics cannot be disregarded when considering processes for the solar wind energy transfer into the magnetosphere. Indeed, a more careful analysis of Viking cusp data adds a few more interesting features related with solar wind plasma dynamics and the cusp.

Figure 2 shows some important findings that pertain to the solar wind plasma density in the cusp versus the gas dynamical model by Spreiter an Summers (1967). Notice that the observed IMP-8 solar wind temperatures and the Viking cusp ion temperatures are well predicted by the model. Even the ion density ratios (N_{cusp}/ N_{SW}) observed in the time period April - July 1986 matches rather well the model seasonal dependence of plasma density in the sheath at cusp latitudes. These observations strongly support the hypothesis of the cusp gas dynamical response to the solar wind flow.

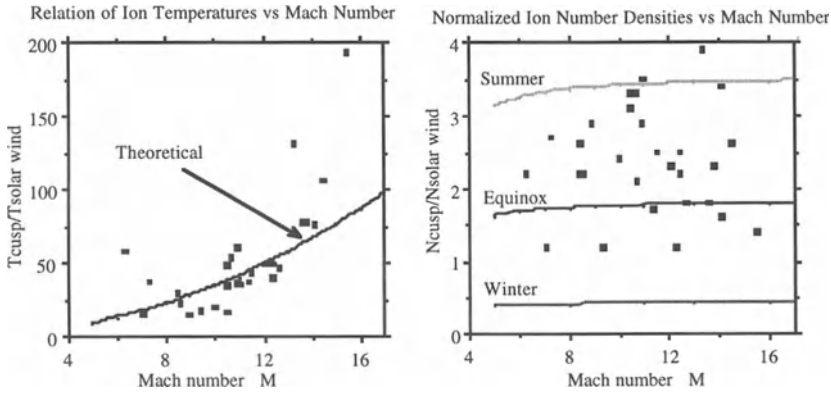

Figure 2. Cusp/Solar wind temperature and density ratios as a function of the Mach number M_∞ for the Viking cusp- and IMP-8 solar wind-observations.A comparison is made with theoretical predictions using equations by Spreiter and Summers (1967). (From Lundin et al., 1997)

Another property that further validates the fluid-dynamical properties of the cusp can be observed in Figure 3, i.e. the dawn-dusk position of the cusp is not only affected by the IMF By component (left panel), but also by the east-west flow of the solar wind (right panel). Thus, the cusp position does not only move with the IMF By-component (e.g. Newell and Meng, 1988, Aparicio et al., 1991) but also with the solar wind flow direction.

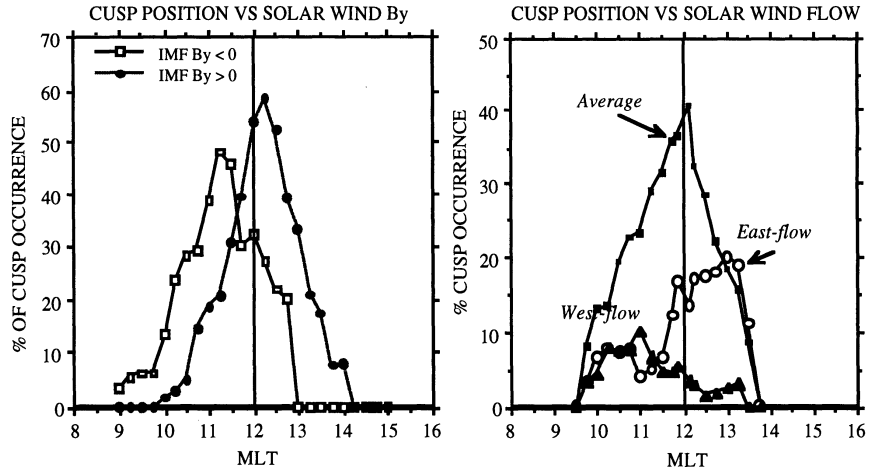

Figure 3. The solar wind electromagnetic (left) and dynamical (right) influence on the cusp position. The left panel illustrates the dawn-dusk shift versus IMF By (after Aparicio et al., 1991). The panel to the right shows the average (top curve) and with respect to the east-west flow direction. The two lower curves on the right panel display the dependence of the cusp position versus a solar wind flow coming from the east of the sun or from the west of the sun respectively, (from Lundin et al., 1997).

The above observations pertain to the existence of a quasi steady-state inflow and fluid characteristics of solar wind plasma into the cusp. The quasi steady-state notion raises the question: For how long does a solar wind plasma inflow prevail?

From a statistical point of view the cusp is a persistent feature, but this does not imply steady-state. Smith and Lockwood (1990) and Lockwood and Davis (1995) argues that the cusp constitute a time dependent feature which remains open to solar wind plasma inflow in short sequences of a few minutes duration. However, recent observations from *Interball-Tail* (Sandahl et al., 1996) of cusp encounters with durations of more than an hour refute such a time dependent cusp model. Thus, whatever the access process (steady state merging or steady state inflow in the exterior cusp) the cusp at times represent a quasi steady-state access of solar wind plasma which is more than an hour long.

Mid-altitude observations within the cusp do suggest time-dependent plasma injection (e.g., Lundin et al., 1991; Yamauchi and Lundin, 1994; Norberg et al., 1994). However, in this case the injection features were usually referred to as the "boundary cusp", i.e. the observations taking place in a transition region (Kremser and Lundin, 1990) related to a more pronounced energy transfer (e.g. local plasma heating/acceleration) than that which occurs in the "cusp proper". Transient plasma injection, characterized by time dependent features on ion energy-time spectrograms (Yamauchi and Lundin, 1994), are generally more easily observed at mid- and high altitudes (e.g. Viking, DE-1, and Akebono), but have also been observed at low altitudes (Norberg et al., 1994).

An example of a series of transient plasma injection in the cusp is shown in Figure 4 for a Viking cusp pass during southward IMF. Notice that Viking traversed the cusp due equatorward, which emphasized the fact that the transients are really temporal, in the sense that the dispersion is opposite to the overall poleward convection in the cusp (see e.g. Yamauchi and Lundin, 1994).

Time-dependent plasma injection events can also be observed well outside the cusp in the cleft/LLBL (e.g., Carlson and Torbert, 1980; Kremser and Lundin, 1990). These magnetosheath plasma injections, statistically studied by Woch and Lundin (1992a), have been denoted plasma transfer events, PTEs. In the context of a cusp proper defined to be a quasi steady-state open throat to the magnetosheath, time-dependent plasma injection may be considered a process for magnetosheath plasma access onto closed geomagnetic field lines. Such a process undoubtedly requires a temporal "openness" of the magnetopause, but in the evolutionary process it also leads to a transfer of plasma to closed field lines as reported by e.g. Woch and Lundin (1992a). We will return to the intrinsic processes in PTEs later in this report, but for the moment focus on some observational aspects related with temporal solar wind plasma injection.

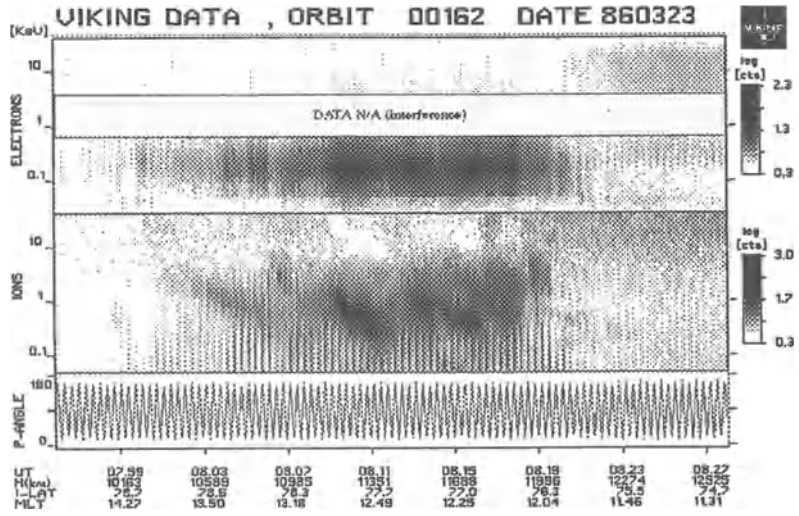

Figure 4. A Viking cusp traversal containing time-dependent plasma injection structures when the IMF was pointing southward.

Figure 5 gives a diagrammatic representation of the time-dependent solar wind plasma injection into the magnetospheric boundary layer, as conceived on basis of mid altitude (Viking) observations (Woch and Lundin, 1991).

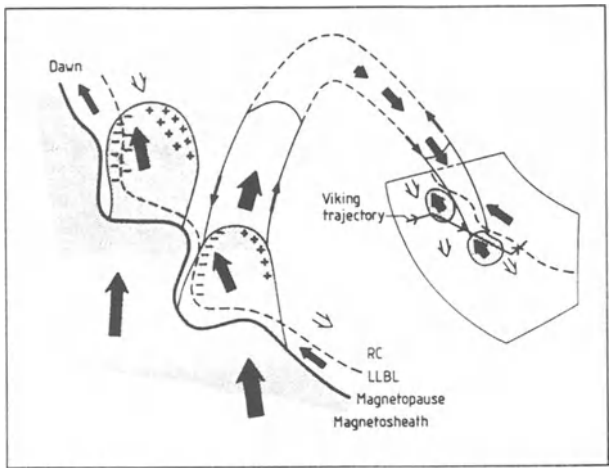

Figure 5. Diagrammatic illustration of time dependent solar wind plasma injection into the magnetospheric boundary layer as conceived on basis of Viking observations (after Woch and Lundin, 1991).

The observations by Woch and Lundin (1992a) indicate that plasma injection structures are generally characterized by high density / low temperature "clouds" of antisunward flowing plasma, embedded in a "stagnant" region of low density/high temperature plasma sheet-like particles. On basis of energetic electron data they also argued that a majority

of the dayside injection structures, PTEs, were on closed field lines. PTEs observed near the polar cap and lacking signatures of quasi-trapping (e.g. double loss-cone structures or strong fluxes of energetic electrons >20 keV) were potentially located on open field lines. This suggests that both interpretations apply, i.e. PTEs exists on open as well as closed field lines, and that observations of PTEs on closed field lines simply reflects a later phase of solar wind plasma protrusion by time dependent process. Notice, however, that the lack of energetic particles on low- or mid altitudes is no evidence for open field lines. They may equally well be closed. In fact, the main low/mid altitude evidence for a magnetic field topology is the particle loss-cone, a double loss-cone marking closed field lines. Woch and Lundin (1992a) concluded on basis of individual case studies of energetic particle information and double loss-cone signatures that a majority of the PTEs well away from local noon were on closed geomagnetic field lines.

The signature of PTEs occurring on closed or potentially open field lines is demonstrated in Figure 6. The scatterplot in Figure 6 showing the location of PTEs in magnetic local time and invariant latitude, also plots the average location of the poleward boundary of plasma sheet particles. Notice that the main fraction of PTEs are observed equatorward of this boundary, corroborating the picture of PTEs on closed field lines.

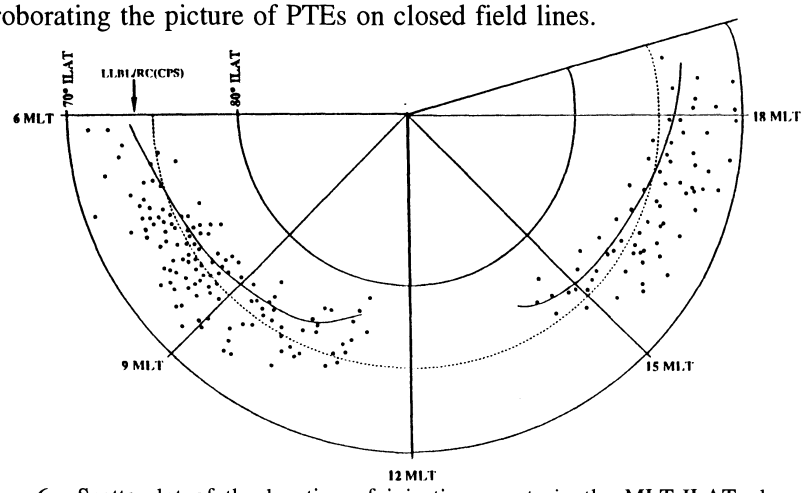

Figure 6. Scatterplot of the location of injection events in the MLT-ILAT plane. The average location of the poleward boundary of plasma sheet particles (LLBL/RF(CPS)) is indicated (after Woch and Lundin, 1992a).

An important property of PTEs found by Woch and Lundin (1992a) were a relatively strong dependence on IMF By but a lack of dependence on IMF B_X and B_Z. The occurrence frequency of PTEs was highest in the morning sector for negative B_Y and correspondingly highest in the evening sector for positive By. This is quite similar to the B_Y dependence of the cusp position vs IMF B_Y (e.g., Newell and Meng, 1988; Aparicio et al., 1991). However, the most striking characteristic found for PTEs is a strong dependence on solar wind dynamic pressure. This is illustrated by Figure 7,

showing the normalized PTE occurrence frequency versus solar wind dynamic pressure. Indeed, the solar wind dynamic pressure appears to be the most important controlling factor for the occurrence of PTEs. Notice also that PTEs occur preferentially for a radial IMF.

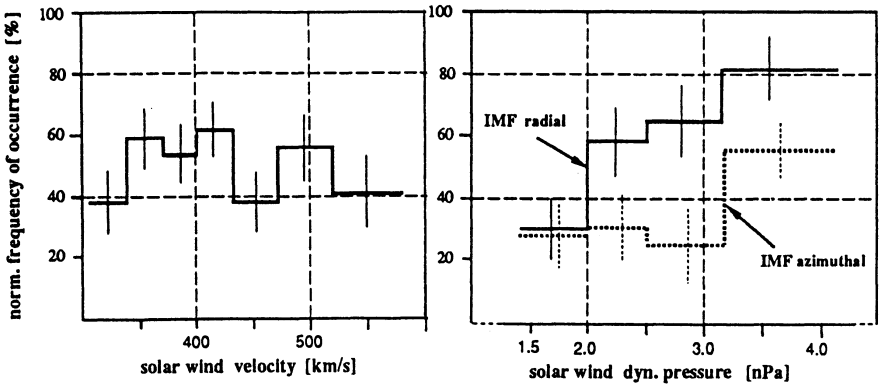

Figure 7. Results from a statistical analysis in the dayside illustrating the lack of solar wind velocity dependence, but the strong solar wind dynamic pressure dependence on the occurrence of PTEs (Woch and Lundin, 1992a).

The strong dependence of PTEs on solar wind dynamic pressure raises a question concerning the effects of dynamic pressure on plasma entry into the cusp. Newell and Meng (1994) found that there is a strong dependence of the cusp and the LLBL with solar wind dynamic pressure, with both the cusp and LLBL moving equatorward as well as extending in magnetic latitude and longitude with increased solar wind dynamic pressure. Altogether, this implies an enhanced access of solar wind plasma into the magnetosphere - on magnetic field lines characterizing the cusp and LLBL as well as on dayside closed field lines (PTEs).

The Woch and Lundin (1992) observations of solar wind plasma access into the dayside magnetosphere, preferably for a high solar wind dynamic pressure, is most obvious for northward IMF B_Z, when the dayside magnetopause is not expected to promote merging/reconnection. For IMF $B_Z > 0$ a reversed convection signature may be observed in the cusp, the ions convecting equatorward. Yamauchi et al. (1993c) reported on a new set of observations near local noon for IMF $B_Z > 0$, denoted stagnant solar wind plasma injection structures (SPIs). SPIs, preferably observed near local noon equatorward of the cusp, are characterized by multiple injection structures that may extend up to ten degrees in invariant latitude equatorward of the poleward boundary of the cusp. They are referred to as "stagnant", because the ion mean energy decreases steadily equatorward, apparently due to a stagnation/cooling process of the injected plasma clouds. The overall ion

signature in fact resembles that of the ion expansion into the polar cap/ mantle cusp - but now instead expanding far equatorward. The immediate impression given by the SPIs is that of magnetosheath plasma injection structures that have protruded deep into the dayside magnetosphere to closed magnetic field lines, thereby gradually loosing energy and momentum in the stagnation process (see forward chapter 4).

In conclusion, low- and midaltitude observations of the dayside cusp and LLBL have revealed that:

- The cusp proper constitutes a quasi steady-state open throat that allows for direct injection of magnetosheath plasma with modest energy transfer.
- The cusp is both dynamically and electromagnetically coupled to the solar wind. Earlier findings of an electromagnetic (IMF) coupling must be complemented by a gas dynamic coupling by the solar wind pressure and flow.
- Temporal plasma injection, PTEs, and plasma acceleration (strong energy transfer) characterizes the boundaries of the cusp, i.e. the cleft/LLBL.
- PTEs are observed independent of IMF Bz, but preferably for a radial IMF (Bx >>By, Bz) and with an occurrence frequency increasing with solar wind dynamic pressure.
- "Clouds" of solar wind plasma injection may protrude deep into the dayside magnetosphere onto closed magnetic field lines.

3. HIGH-ALTITUDE / IN SITU BOUNDARY LAYER OBSERVATIONS

On basis of high altitude observations from HEOS-2 the entry layer, the plasma mantle, and the exterior cusp, were all considered to be boundary regions connected to the polar cusp as observed by low-altitude satellites.

Heikkila (1985) considered a wider dayside region, the *cleft,*to encompass the cusp. A more specific definition (e.g. Kremser and Lundin, 1990, Newell and Meng, 1994) is that the cleft constitutes the low-altitude footprint of the low latitude boundary layer (LLBL). Thus, the cleft could be said to border rather than encompass the cusp.

On basis of the above arguments it is assumed that the cleft and cusp together constitute the footprint of the magnetopause and magnetospheric boundary layer. This was also assumed in magnetic field modelling by Stasiewicz (1991), who demonstrated how the magnetopause boundary layer may map down to the ionosphere using the Tsyganenko 1987 model. Although the Tsyganenko model represents an average (yet Kp dependent) model with all its fallacies compared to the dynamical field in the outer magnetosphere, the mapping result remains compelling. For instance, Stasiewicz (1991) showed that tailward propagation in the magnetopause boundary layer may correspond to a poleward motion in the ionosphere. Thus, poleward moving auroral arcs observed from ground (e.g. Sandholt et al., 1987) may correspond to tailward propagating disturbances in the magnetospheric boundary layer.

It is not the purpose of this report to provide a general overview of the magnetspheric boundary layers connected to the cusps and cleft. However, there are a few high-latitude boundary layer properties observed by HEOS-2 and Prognoz-7 that are important for understanding the low- and mid-altitude cusp observations. Characteristic of the entry layer is, for instance, a plasma density almost as high as in the magnetosheath but generally lacking the strong antisunward plasma flow. In fact sunward flow has even been reported by Paschmann et al. (1976). Later, measurements from Prognoz-7 (Lundin, 1985) suggested that a characteristic feature of the entry layer is also a strong variability of magnetosheath plasma entry with frequent plasma injection (PTEs).

The exterior cusp cannot be linked to the plasma mantle or LLBL in a simple way. According to the fluid-dynamical picture (Spreiter et al., 1968) this boundary region should be characterized by a hot and stagnant magnetosheath plasma, a picture which was corroborated by HEOS 2 measurements (Sckopke, 1979). A distinguishing difference between the entry layer and the exterior cusp is the considerably smaller temporal/spatial variations of the plasma parameters in the exterior cusp. Similar to the low altitude cusp proper the exterior cusp appears to be a steady high pressure center of "stagnant" magnetosheath plasma. Thus, there are striking similarities between the low-altitude cusp proper and the high altitude exterior cusp. Indeed, cusp encounters with more than an hour in duration (Sandahl et al., 1996) is clear evidence for a quasi steady-state open throat to the magnetosheath. Considering the more transient behavior of the entry layer this is then likely to map to the boundary cusp (Kremser and Lundin, 1990), a transition region between the cusp proper and the cleft.

The observations reported by Rosenbauer et al (1975) suggested that the plasma mantle behaves as a smooth transition region. However, Lundin et al., (1981) reported Prognoz-7 measurements of a more structured plasma mantle, sometimes with solar wind injection elements present deep inside the plasma mantle. This led Lundin and Aparicio (1982) to compare a number of cases of plasma injection structures in the plasma mantle with the "impulsive penetration" model of Lemaire (1977). Important results from this study was that solar wind plasma injection structures in the plasma mantle:

— are found well inside the magnetopause and, thus, were not magnetosheath encounters
— frequently display diamagnetic properties (high beta)
— are associated with magnetospheric activity and upwelling ionospheric ions (O^+).

Figure 8 displays a HEOS-2 traversal of the plasma mantle that contains a plasma injection structure (0700 - 0730 UT, double vertical bar). A dashed vertical line gives the magnetopause crossing. Notice that the plasma injection structure is located well inside the magnetopause and is characterized by

a velocity dispersion, the highest velocity recorded at the first HEOS-2 encounter of the plasma structure. Indeed, the velocity dispersion is reverse to the spatial convection structure (velocity decreasing inward) expected in the plasma mantle. Thus, the velocity dispersion structure must be temporal, associated with a solar wind plasma injection event further upstream of the satellite - the ions with highest velocity arriving at the satellite first. The diagram to the right in Figure 8, illustrating the HEOS-2 trajectory and magnetic field vector data mapped onto the XZ-plane, also gives result of a simple calculation of the distance to the source on basis of the ion velocity dispersion (protons assumed). The calculated distance, 28 Re, corresponds

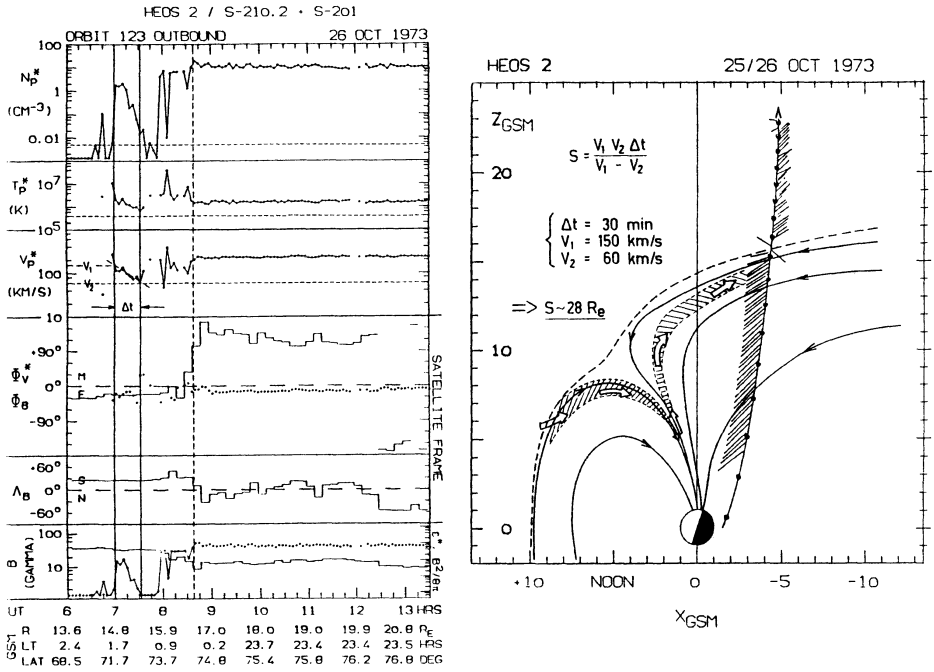

Figure 8. Proton fluid parameters for HEOS-2 (left panel) and orbit parameters (GSM) with magnetic field vectors (right panel) during an outbound traversal of the plasma mantle 25/26 October 1973 that contains a plasma injection structure (≈0700 - 0730 UT, double vertical bar). Dashed vertical line gives the magnetopause crossing and the double bar illustrates the magnetosheath injection structure. Hatched area in the right panel illustrates the conceived path of the plasma injection element some 28 Re upstream of the mantle traversal.

approximately to an injection taking place in the dayside entry layer/LLBL, entering the plasma mantle via magnetic mirroring in the cusp. However, considering the slower field-aligned motion in the cusp (due to mirroring), the particle travel distance is likely to be much shorter. This suggests that the source is indeed the entry layer.

Figure 9 shows an example of a Prognoz-7 inbound traversal of the dayside entry layer / LLBL near local noon. The magnetopause crossing is indicated by the vertical bar and the magnetospheric boundary layer

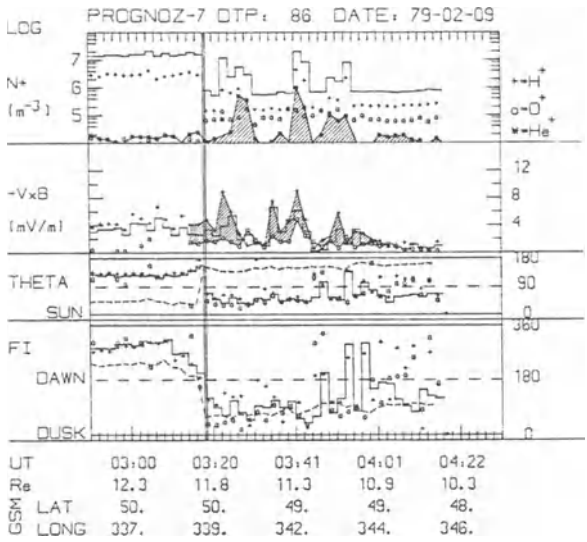

Figure 9. Plasma fluid parameters for Prognoz-7 during an inbound traversal of the dayside entry layer / LLBL near local noon. The magnetopause crossing is indicated by the vertical bar and the magnetospheric boundary layer (EL/LLBL) constitute the time period 03.20 to 04.00 UT. The first panel gives ion densities for H+, O+, and He+ (hatched area). The second panel gives the cross-field drift ($-v \times B$) magnitude for H+ (hatched) and O+(circles). The two bottom panels shows the direction of the magnetic field (dashed line) and $-v \times B$ vector in polar coordinates. Notice the strong reversal of both vectors at the magnetopause, suggesting a magnetopause with strong magnetic shear.

(EL/LLBL) is passedd in the time period 03.20 to 04.00 UT, a boundary layer thickness of approximately 0.9 Re. This event has been described in detail by Lundin and Dubinin (1984) and Lundin (1985), so it should be sufficient to just repeat the main conclusions:

- The three magnetosheath injection structures occur well inside the magnetopause and are well embedded in the magnetosphere plasma and magnetic field. From the ion composition point of view, the structures contain a mixture of solar wind and magnetosphere plasma.
- The plasma injection structures contain accelerated "cold" plasma of plasmaspheric origin; the reason for this conclusion being that He^+ (shaded) is more abundant than O^+.
- Plasma convection in this high magnetic shear case clearly reverses at the magnetopause, the $-v \times B$ vector pointing radially inward in the magnetosheath and radially outward in the magnetosphere. This apparent lack of solar wind electric field intrusion is evident also in the injection structures. Thus, it is the plasma momentum/flow that governs the dynamical properties of the boundary layer rather than the electric and magnetic fields.
- There is a differerence between the O^+ and H^+ ion drift ($-v \times B$) component, the H^+ drift being considerably higher. This was interpreted by Lundin and Dubinin (1984) as an intrinsic property of an MHD dynamo.

An alternative view is that of a pickup process whereby momentum is transferred from one plasma population to another. We will return to this topic.

Figure 10 shows a Prognoz-7 pass through the plasma mantle for varying weakly northward IMF. The event is particularly interesting because it gives an example of magnetopause plasma acceleration, i.e. there is a significant increase of the ion flow velocity in the vicinity of the magnetopause. Notice what appear to be several magnetopause encounters between ≈00.20 and 02.00 UT. A characteristic feature of the acceleration regions is that the ion flow is essentially field-aligned, the velocity increasing from about 400 km/s to 500-600 km/s. Thus, this is an example of the reconnection type of magnetopause acceleration found in the subsolar region during southward IMF (e.g. Paschmann et al, 1979, Sonnerup et al., 1981) and in the mantle by e.g Gosling et al. (1991). Here the flow vectors suggest a dawnward/outward flow, i.e. the accelerated ion flow escape the magnetosphere - contrary to the result by Gosling et al. (1991) and Le et al (1994).

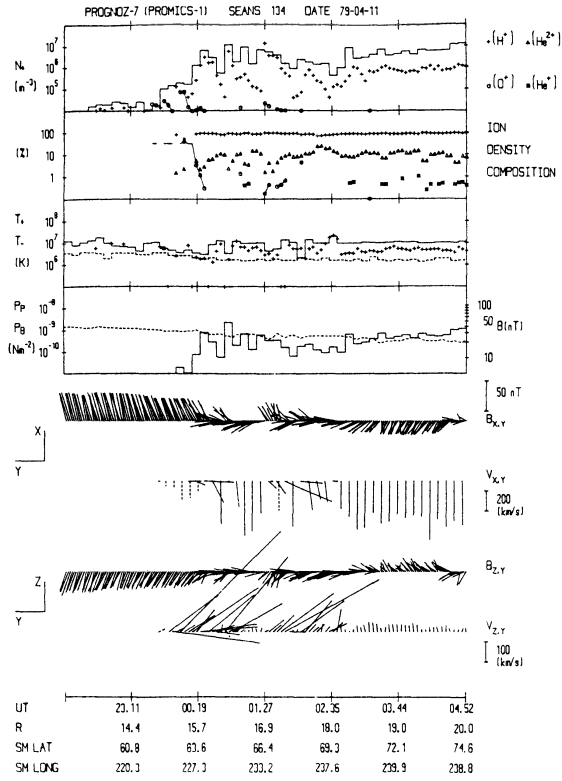

Figure 10. Plasma fluid parameters for a Prognoz-7 pass of the plasma mantle for a varying, weakly northward IMF. The magnitude and direction of the plasma flow and magnetic field is given by the vector projections onto the xy and yz solar ecliptic planes. The magnetopause plasma acceleration is characterized by an increase of the ion flow velocity in the vicinity of the magnetopause. Several magnetopause encounters between ≈00.20 - 02.00 UT are indicated by vertical bars. A characteristic feature of the acceleration regions is that the ion flow is essentially field-aligned, the velocity increasing from about 400 km/s to 500-600 km/s.

An important aspect of the Prognoz-7 magnetopause crossing of Figure 10 is the existence of a strong magnetic shear. Thus, magnetopause acceleration is expected. Moreover, with Bz>0 a relatively modest mantle width is also expected, in agreement with the findings by Sckopke et al. (1976).

Magnetopause ion acceleration has also been observed in the boundary

cusp at mid altitudes. (e.g. Woch and Lundin, 1992b). Indeed, the observed acceleration features replicate the antiparallel field requirement. As demonstrated in the cartoon in Figure 1, ion acceleration is on the equatorward side of the cusp for Bz<0 and on the poleward side for Bz>0.

In conclusion, in situ measurements in the dayside magnetospheric boundary layer have shown that:

- The exterior cusp constitutes a potential mapping region for the cusp proper, i.e. a region with persistent/continuous access of magnetosheath plasma on open field lines in Earth´s dayside magnetosphere.
- Plasma acceleration takes place in the magnetopause region, but mainly in regions of strong magnetic shear.
- Plasma deceleration, and acceleration, may occur in the boundary layer.
- Time dependent solar wind plasma injection elements are observed in the boundary layers - at high latitudes (mantle) as well as low latitudes (LLBL).
- Significant differences in the perpendicular drift of ions in the boundary layer indicate strong spatial and/or temporal gradients associated with energy and momentum transfer.

4. PERSISTENT AND TRANSIENT SOLAR WIND PLASMA INJECTION

In the previous chapter we discussed observations related to both steady state and transient solar wind plasma access to the magnetosphere. Here we elaborate in some detail on theoretical aspects of the steady-state as well as transient solar wind plasma access of Earth´s magnetosphere.

We noted that the cusp proper is from an observational point of view the most obvious region for persistent solar wind plasma injection. However, for injection to take place one must assume either steady-state reconnection in the dayside (cusp field lines "frozen in") or that the cusp proper on terrestrial field lines has a continuous supply of sheath plasma due to some strong diffusion/access process. The latter is a subject of this report.

A number of diffusion mechanisms may be invoked to explain the massive access of magnetosheath plasma on terrestrial field lines in the outer cusp region. However, it is probably sufficient to note (e.g., Stasiewicz,1991), that the very low magnetic field and high beta in the outer cusp are strong arguments for massive plasma drift into as well as out of the cusp. Furthermore, the observed massive plasma access into the exterior cusp, at least partly on terrestrial field lines (Lundin, 1985), leads to considerations on topology rather than access mechanisms. Yamauchi and Lundin (1997) proposed, on basis of an access topology that the cusp may be considered a de Laval nozzle with solar wind plasma entering in the entry layer/exterior cusp and exiting into the plasma mantle. Figure 11 illustrates qualitatively the topology of the plasma access region for a southward B_Z, with the well known de Laval velocity and pressure relations. Notice, for instance, that the

velocity branches off into two main regimes, (a) continuously increasing velocity, and (b) increasing and subsequently decreasing velocity. A third regime exists provided a new shock is formed inside the bow shock after the velocities have become supersonic and subsequently the flow stagnates to subsonic again (c). The physical reason for the mechanism is that solar wind plasma has access to the cusp "nozzle" over a wide area, building up plasma pressure in the access region. The "nozzle" poses an obstacle that limits plasma expansion until it reaches the mantle cusp where it may freely flow along the magnetic field lines in an expansion fan. The "nozzle" obstacle has two main causes: the magnetic field well geometry (in and out of a converging/diverging cusp), and the energy and momentum transfer that couples the outer cusp (dynamo) with the ionosphere (load) via field-aligned cusp currents.

An interesting aspect of the de Laval nozzle mechanism is that it may explain the observed ion dispersion signature within the cusp without having to infer plasma convection, although plasma convection may be included as well. Figure 11 illustrates that a total pressure increase in the poleward section of the cusp proper corresponds to a decreased parallel velocity (subsonic case b). A consequence of the magnetic obstacle (e.g,. resulting in a dynamo action) is to prevent solar wind plasma to freely expand in the near Earth mantle region, thus prohibiting the plasma to reach supersonic velocities. Plasma reaching the low-altitude cusp must therefore carry the same signature as the high-altitude plasma, i.e. a decrease of velocity polewards. This is indeed the same signature as expected for plasma convection during a southward B_Z.

Notice that the electromagnetic coupling,, specifically convection, must be added to this gas dynamic picture. However, as was noted by e.g. Yamauchi and Blomberg (1997), the convection field in the cusp is frequently very irregular and convection in the dawn-dusk direction appears to dominate. The poleward convection may therefore be an artefact - related with the gas dynamics of the cusp.

The steady state model presented in Figure 11 may be most important during periods of low electromagnetic coupling of the cusp to the solar wind, e.g. for periods with low IMF B_Z and B_Y. Indeed, these are the periods when "stagnant" cusps are observed (Reiff et al., 1977; Lundin et al., 1991). "Stagnant" cusps are characterized by the lack of ion energy dispersion and a weak ionospheric response (e.g. ion acceleration). In the gas dynamic cusp model the "stagnant" cusp appears to lack a well defined "nozzle" (modest or no pressure change in the cusp), leading to a "flat" response with modest velocity change in the cusp proper. Accordingly, no velocity signature versus latitude, including convection signatures ("v shape" in the energy-time spectrogram), is expected within the cusp - in good agreement with observations. However, the steady-state injection model by Yamauchi and Lundin (1993), predicts that the cusp always exists,

depending mainly on the solar wind dynamic pressure. A low solar wind dynamic pressure implies modest energy/mass transfer and a "stagnant" cusp.

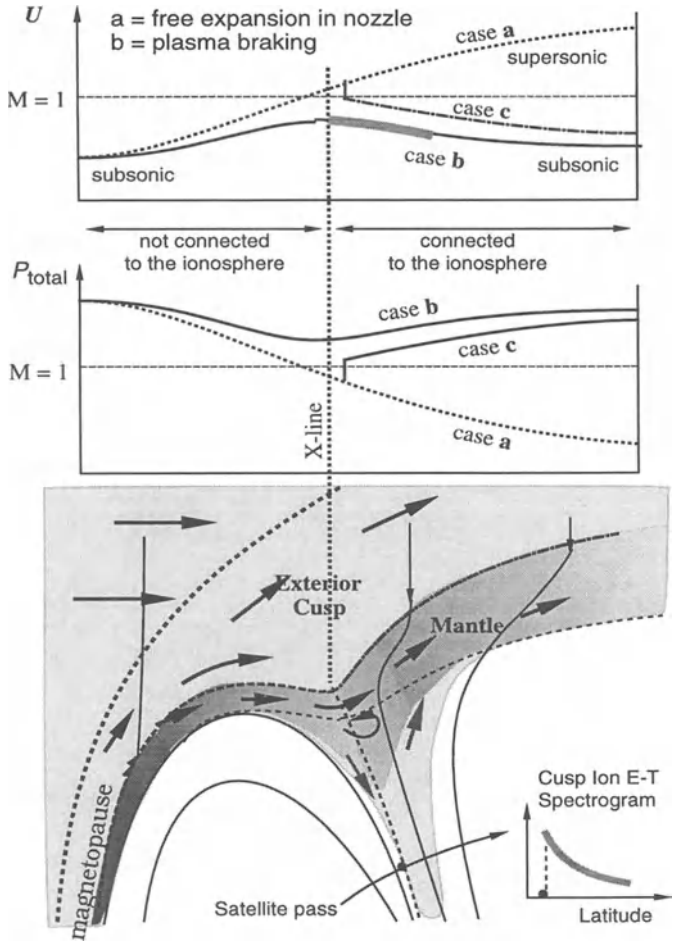

Figure 11: A de-Laval nozzle mechanism (top), with the cusp interface (bottom) for steady-state injection of magnetosheath plasma into the plasma mantle for Bz<0 (Yamauchi and Lundin, 1997). The shaded curve illustrates the energy-latitude ion dispersion characteristics predicted by the model for case b.

The history of transient solar wind plasma injection dates back to the late seventies and early eighties. Lemaire and coworkers (Lemaire, 1977, Lemaire and Roth, 1978) proposed that elements of solar wind plasma may impulsively penetrate into Earth´s magnetosphere as a consequence of solar wind irregularities and their intrinsic magnetization. Later Heikkila (1982) proposed that the impulsive penetration process may be governed by

inductive electric fields set up at the magnetopause for favorable conditions. Owen and Cowley (1991) refuted the model by Heikkila and argued that it does not work. Although some workers claim this controversy is settled, rebutting the ideas of Heikkila and Lemaire, important experimental facts are then neglected. Plasma does indeed penetrate the magnetopause and populates closed terrestrial magnetic field lines. Indeed, plasma elements "bulleting" across magnetic field lines was observed in the laboratory already in the fifties (Bostik et al., 1956), and the theoretical grounds for such observations were subsequently established by Schmidt (1960).

The early ideas by Lemaire and Heikkila were partly supported by theoretical arguments (e.g. Schindler, 1979), but only for exactly antiparallel magnetic fields at the magnetopause. Simulations later demonstrated (e.g., Ma et al., 1991) that the antiparallel conditions may be softened to within about five degrees. Figure 12 shows results from such simulations, at two different times after the plasma element hit the magnetopause and for two different magnetic field boundary conditions - the latter not allowing plasma penetration.

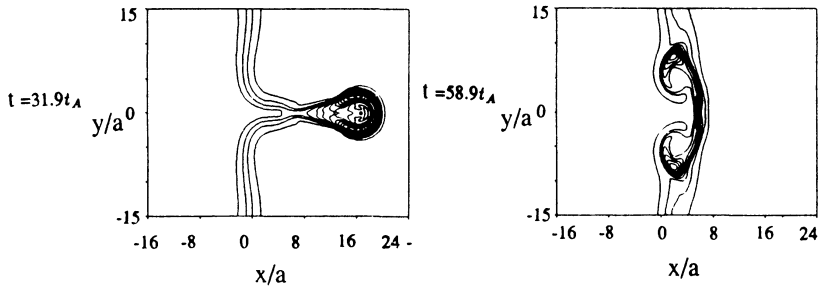

Figure 12. Results from simulations by Ma et al. (1991) of plasma penetration at the magnetopause, for conditions allowing (left) and prohibiting (right) injection

This shows that there is not only observations, but also good theoretical grounds for magnetosheath injection structures to penetrate the magnetopause. Obviously, observations must lead the efforts to understand the physical process that governs solar wind plasma penetration through the magnetopause.

Lemaire and Roth (1978) proposed that elements of injected plasma will transfer their excess energy as a consequence of the flux tube being in electrical contact with the topside atmosphere, the electrical contact being

due to field aligned currents. Using reasonable ionospheric conductivities a "decay time" may be computed for intrusion events (Figure 13):

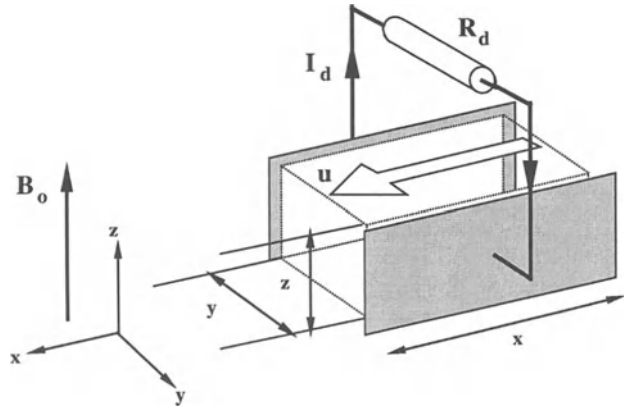

Figure 13. Geometry used to compute the decay time for a plasma element connected by field aligned currents to the Earth's ionospheric load (R_d).

For a velocity $u = u_o$ at $t = 0$, a mass of the plasma "blob" given by: $M = \rho\ \Delta x\ \Delta y\ \Delta z$, where $\rho = n \cdot m$, and using the expressions for the inertia current and Ohms law (neglecting the Hall-term) one may obtain:

$$\bar{j} \times \bar{B} = \rho \frac{d\bar{u}}{dt} \qquad (1)$$

$$j_y \approx \sigma (E_y - u \cdot B_o) \qquad (2)$$

and $$I_d = j_y \cdot \Delta x \cdot \Delta z \qquad (3)$$

Equations (1), (2) and (3) lead to a differential equation with solution:

$$I_d = -\left(\frac{V_o - u_o B_o \Delta y}{R_d}\right) \exp\left(-\frac{t}{t_d}\right) \quad \text{where} \quad t_d = \left(\frac{n\ m\ \Delta x\ \Delta z}{B_o^2\ \Delta y} R_d\right).$$

Typical values for the dayside magnetospheric boundary layer, e.g. $n = 5 \cdot 10^6\ m^{-3}$, assuming the mass of protons ($m = m_p$), $B_o = 30$ nT, $\Delta x = 5\ R_e$; $\Delta y = 1\ R_e$, $\Delta z = 1\ R_e$, and assuming an ionospheric conductance of $\sigma = 1$ mho then gives a time constant $t_d = 295$ s. A higher conductance, $\sigma = 5$ mho gives a value of $t_d \approx 60$ s. Notice also that reducing the magnetic field component perpendicular to the plasma flow to one third (10 nT) results in almost an order of magnitude longer decay time for the plasma element. In fact, only in the dayside magnetosphere is the breaking action expected to be in the 1 - 10 min range. Along the flank and tail, where the boundary layer flow is more field aligned, the weaker cross-field flow component may lead to typical decay times in the tens of minutes to one hour range.

In conclusion, previous and present considerations of the persistent and

transient entry of solar wind plasma into the magnetosphere argue that:
• The outer cusp is a region with low magnetic field, high plasma density and high flow velocity - ideal for a persistent protrusion of magnetosheath plasma into the magnetosphere (drift entry, finite Larmor radius effects, eddy diffusion, etc).
• Pressure and velocity considerations similar to the de Laval nozzle relations may be applied to the cusp. The strength of the de Laval relations is that they can explain cusp ion signatures with, as well as without, ion convection.
• Besides transient/patchy reconnection, a number of other transient entry mechanisms have been proposed (e.g. Lemaire, 1977; and Heikkila, 1982), further commented by others (e.g. Schindler, 1979, Owen and Cowley, 1992). Indeed, the theoretical foundation for such effects dates back to the sixties (Schmidt, 1960). However, very little agreement can be found in the literature on the theoretical aspects of non-reconnection plasma penetration.
• The time-dependent characteristics of plasma penetration are consistent with dayside poleward moving auroral transients - i.e. tailward moving plasma injection structures in the boundary layer, being slowed down.

5. MASS, ENERGY, AND MOMENTUM CONSIDERATIONS

Injection of solar wind plasma elements into the magnetospheric boundary layer implies that energy, mass, and momentum is being transferred into the magnetospheric system. One way of interpreting such a transfer process is by considering the magnetic flux that is carried from the solar wind into the magnetosphere - the transfer of magnetic flux. This view requires a magnetic coupling of Earth´s magnetic field lines to the interplanetary magnetic field, a process first proposed by Dungey (1961) referred to as reconnection. Reconnection requires among other things that ideal MHD applies everywhere in the energy transfer process - except in the x-line formation phase.

The other interpretation, the subject of this report, takes a plasma kinetic approach and utilizes gas dynamics and currents to describe the energy, mass, and momentum transfer of plasma injected into the magnetosphere. A conservative approach, indeed correct from an observational point of view, is to assume that plasma by some process(es) yet to be agreed on is transported across the magnetopause and starts populating terrestrial magnetic field lines in the boundary layer. Once inside the magnetopause the plasma will interact with the Earth´s magnetic field and set up transverse electric fields and currents. The *locally induced* electric field will interact with the local plasma as well as indirectly with plasma in the ionosphere. The interaction with the ionosphere is very similar to the MHD-breaking shown in Figure 13. Because the current description in the energy transfer process plays such an important role in this model it may be referred to as the Boundary Layer Current model, BLC-model.

The fundamental prerogative of the BLC-model is that the local magnetic field is a superposition of all neighboring induced magnetic fields - including Earth's intrinsic dipole field. This does not imply an electrical contact between the boundary layer plasma and every current source, neither does it preclude such a contact. A magnetic "field line" is therefore a relatively useless quantity in a region affected by multiple magnetic field sources, because temporal changes may"reroute" the field line with time. Thus, at best only the electrons will trace a field line, whilst ions may drift substantially across the field line. Moreover, the ion drift is not identical with convection. This becomes clear from the general expression of the first order plasma drift:

$$\underline{v}_\perp = \frac{\underline{B}}{B^2} \times \left[\underline{E} + \frac{m}{q}\frac{d\underline{v}_o}{dt} + \frac{\nabla P_\perp}{qn} \right] + \frac{(P_\parallel - P_\perp)}{qn} \left(\frac{\underline{B} \times \nabla \underline{B}}{B^3} + \frac{\mu_o}{B^2} j_\perp \right) \qquad (1)$$

where the second term in the bracket is the inertia drift, the third term the pressure gradient drift, and the fourth term is the anisotropy drift. Thus, besides convection there are four other terms that may be equally responsible for plasma drift. These terms become particularly important for ions. Notice that because the electric drift affects all species in the same way, the ion differential drift $\Delta v_\perp = v_{\perp 1} - v_{\perp 2}$:

$$\Delta v_\perp = (\Delta v)_{\nabla p} + (\Delta v)_a + (\Delta v)_i \qquad (2)$$

only contains the difference in pressure drift, anisotropy drift, and inertia drift respectively. Lundin et al. (1987) also demonstrated, on basis of single point measurements, that the theoretical differences in ion drift velocity by the partial pressure gradients observed along the satellite orbit are in good agreement with the observed difference in ion drift for different ion species. More important from a fundamental plasma physics point of view, plasma pressure gradients such as those observed in in the boundary layer are related with plasma drift velocities of a magnitude similar to that of the convection speed. Thus, plasma transported from one region to another, from the magnetosheath to the magnetosphere, is subject to physical processes that tends to disperse the plasma with respect to mass, velocity etc. On the other hand, the local reaction to this is to induce currents that prohibits dispersion. For instance, the inertia drift will set up a transverse dynamo/polarization current that may stop further expansion if energy can be dumped somewhere (Figure 13).

In fact, the ionosphere is not the only load for energy to be dumped into. Also a local plasma (at rest) serves as a load for a moving plasma. *Ion pickup* is an example of local energy transfer set up as a consequence of differential ion drift. The process can be understood from the simple

principles of ion momentum exchange discussed by e.g. Lundin and Dubinin (1984) for the boundary layer, i.e. by solving the differential equation of Ohm's law (neglecting Hall currents) for decelerating (solar wind) and accelerating (boundary layer) ions, the dynamo current assumed to be driven by the plasma inertia. The differential equation may be written:

$$S_{xy}\,\sigma\,(E_y - v_x B_z) = \frac{n\,m}{B_z}\frac{dv_x}{dt} \tag{3}$$

where S_{xy} is a spatial parameter, and σ is a phenomenological conductivity in the interaction region. For an isotropic σ in the interaction region and with the boundary layer ions initially at rest one can determine the following velocity relation between the boundary layer ions (v_{BL}) and the solar wind ions (v_{SW}) (Lundin et al., 1993):

$$v_{BL} = v_{SW}\left(1 - \exp\left(-\,k\,\frac{n_{SW}}{n_{BL}}\frac{m_{SW}}{m_{BL}}\right)\right) \tag{4}$$

where k is a scalar for the number of gyroperiods. This expression, describing the "internal loading" of an MHD dynamo, shows that a high mass density of boundary layer ions relative to the injected solar wind ions leads to a low pickup velocity ($v_{BL} << v_{SW}$). Conversely, a low mass-density for the boundary layer ions leads to $v_{BL} \approx v_{SW}$, i.e. to normal ion pickup in the MHD sense (which is up to a factor of four lower than the maximum single particle ion pickup). Thus, this equation describes the loading characteristics of the ion pickup process.

Fig 14 gives the normalized velocity ratio versus density ratio for loaded ion pickup when all incident/injected ions are protons and all pickup ions are oxygen. The figure illustrates that "ideal" pickup, in the sense pickup to equal velocity, is approached only when the density is negligible compared to the density of the incident ions (test particle limit). On the other hand, for high pickup ion densities the mass loading is so strong that the pickup ions acquire low velocities. Notice that the influence of the scalar k is to approach the ideal pickup limit (convection speed) for high k-values (extended time periods) also when the mass loading is heavy. Conversely, for low k-values (short time periods, k<1), the interaction can be considered heavily mass loaded also for high mass ratios. Although in the k<1 limit MHD also breaks down, the equation above is yet useful because it describes the underlying physics. The ion inertia is prohibiting O^+ ions from acquiring but a fraction of the convection speed because of the limited time the force is applied.

The mass-loaded ion pickup process described above was first presented by Lundin and Dubinin (1984) for cold plasmaspheric ions in the magnetospheric boundary layer. The energy transfer as described by Lundin and

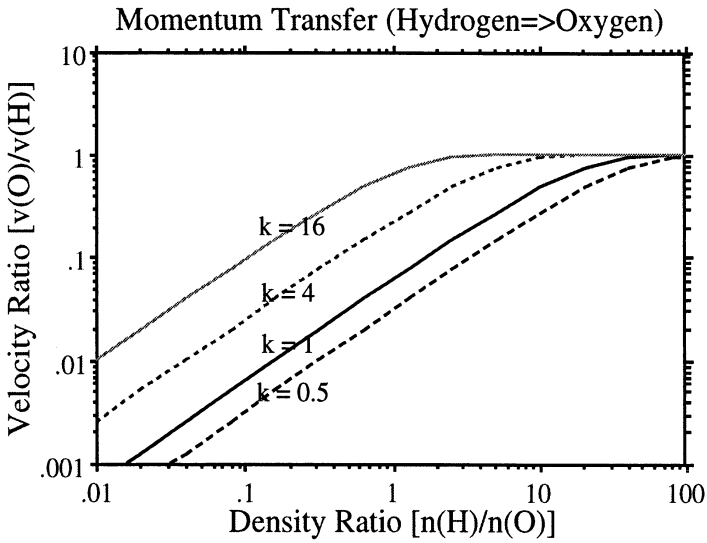

Figure 14: Normalized velocity ratio versus mass density ratio for a mass-loaded ion pickup with H^+ as driver ions and O^+ as pickup ions.

Dubinin (1984) is a combination of an external loading of the dynamo current (j_{y1}) through a resistor R_d (Figure 13), and an internal loading described by the depolarization current due to ion pickup (j_{y2}). Notice that the geometry described in Figure 15 assumes that plasma has already been transferred through the magnetopause (locally closed magnetopause).

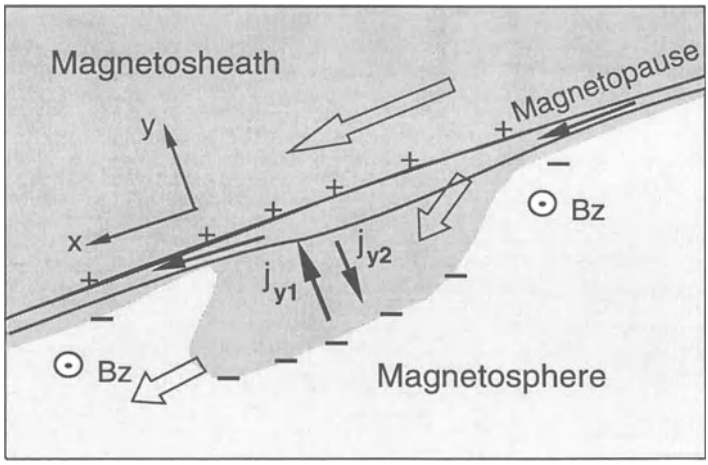

Figure 15: Schematic diagram of magnetosheath plasma transferred through the magnetopause - inducing a polarization electric field (dynamo current j_{y1}) as well as a depolarization electric field by local plasma ion pickup (j_{y2}).

According to the results by Lundin and Dubinin (1984) the ion pickup process in the boundary layer appeared rather "ideal", i.e. magnetospheric ions and injected (magnetosheath) ions moved with about the same velocity. This is also expected since the local plasma mass density was much lower than the injected magnetosheath plasma mass density. Figure 16 shows a similar observation from ISEE-1 in the flank LLBL with ions of plasmaspheric origin (e.g. He^+) picking up the same speed as those of magnetosheath origin (H^+ and He^{++}). Assuming that the magnetosheath injection takes place in the subsolar region implies that the plasma has spent an extended time period in the LLBL (high k values, see Fig 14) . Thus, in such cases the bulk velocity for all ion species are likely to be the same even for equal mass density ratios.

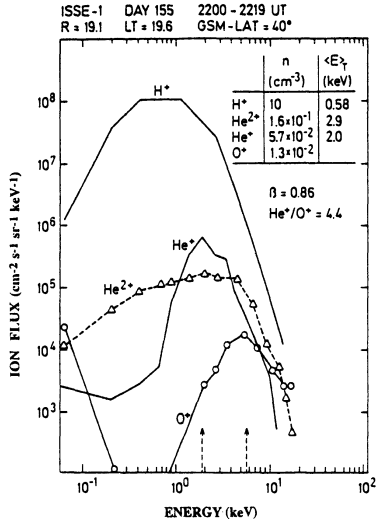

Figure 16: Example of ion pickup, i.e. all ions moving with the same speed, observed in the flank LLBL by ISEE-1. (courtesy of W. Lennartsson)

Interesting cases when the mass density ratio is low or when the scalar k is small (of the order unity) may be found near the planet Mars and in Earth's topside ionosphere. Figure 17 (Lundin et al.,1993) demonstrates that the mass-loaded ion pickup model agrees well with observations in the Martian boundary layer for a k-range 0.5 - 2, which is of the order the hydrogen Larmor radii within the tail (tail boundary layer width).

A remarkable organization of the ion acceleration as a pickup process is illustrated in Figure 18 (after Lundin et al., 1995). The observations, from Viking traversals above the dayside auroral region (2 pm arc region), show that the maximum ion beam velocity is strongly related to the solar wind velocity. A reasonable assumption is that the flow velocity in the magnetospheric boundary layer dynamo, connecting to the auroral acceleration

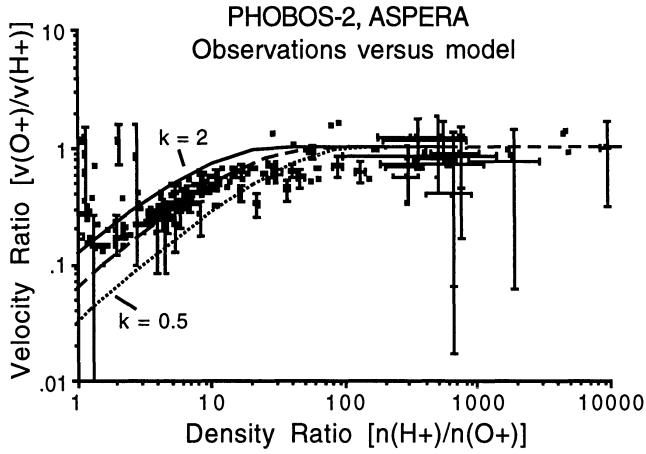

Figure 17: Mass-loaded ion pickup observed in the Martian boundary layer (after Lundin et al., 1993)

region, is directly proportional to the solar wind velocity. Furthermore, the field-aligned potential should be proportional to the boundary layer potential. This results in an *apparent* ion pickup effect with ion beam velocities well in excess of the solar wind velocity. The latter is an obvious consequence of the fact that the width of the boundary layer and the plasma transverse flow velocity will determine the total boundary layer potential. The nonlinear and amplified relation between the solar wind velocity and the ion beam velocity suggests that the boundary layer width is velocity (pressure) dependent, in agreement with the observations by Woch and Lundin (1992) and Newell and Meng (1994).

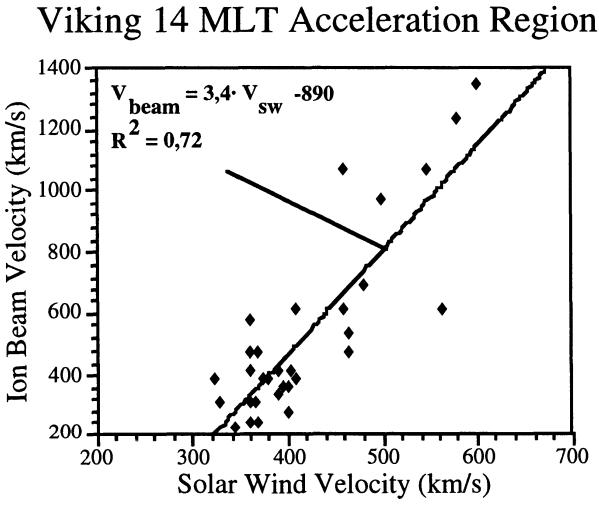

Figure 18: "Ion pickup" in the Earth's boundary layer (Lundin et al., 1995)

6. DISCUSSIONS

As already stated in the beginning of this report, the transport of plasma across the magnetopause remains a matter of great importance, as well as controversy, in magnetospheric physics. Observations suggest that magnetosheath plasma may transiently protrude the magnetopause independent of IMF Bz (e.g. Woch and Lundin, 1992a,b). The cusp proper is a region of persistent, pressure dependent (e.g. Newell and Meng, 1994), solar wind plasma protrusion into the magnetosphere. Observations indicate that the persistency of the cusp is not a statistical artifact; it is indeed a quasi-static connection to the magnetosheath. Moreover, the cusp is both electromagnetically and dynamically coupled to the solar wind. The coupling conditions will affect the shape, the position as well as the width of the cusp.

A simple de-Laval nozzle geometry may be applied to describe the entry, propagation, and loss of magnetosheath plasma in the steady-state cusp. The model describes qualitatively the characteristics of magnetosheath plasma in the cusp for various IMF and dynamical pressure conditions. For instance, the model may prescribe a latitude distribution of precipitating ions that is normally associated with convection. As was also noted by Yamauchi and Blomberg (1997), the convection in the cusp fits poorly into the traditional poleward/equatorward pattern. Indeed, the predominant cusp convection component is dawnward/duskward and the convection electric fields are very irregular - incompatible with a steady equatorward/poleward convection.

Time dependent injection of magnetosheath plasma into the magnetosphere occurs at a rate that is primarily dependent on solar wind fluid parameters, e.g. the dynamic pressure. "Clouds" of magnetosheath plasma may be found deep inside the magnetosphere on closed field lines (Yamauchi et al., 1993c). Thus, undoubtedly magnetosheath plasma may indent the magnetopause and propagate across closed magnetic field lines also for instances not favorable for merging/reconnection.

Indeed, the findings by Lennartsson (1991, 1995) clearly suggests that the access of magnetosheath plasma into the magnetosphere depends to a lesser degree of the IMF orientation but more on gas dynamical properties - thus refuting to some extent conventional wisdom, i.e. a magnetosphere with enhanced plasma supply for southward IMF.

Acceleration (loading) and deceleration (dynamo) in plasmas may be considered from fairly simple principles of energy, mass, and momentum transfer - using currents as the coupling agent between the source/dynamo and the sink/load. The MHD model for ion acceleration and deceleration is qualitative in the sense that it describes primarily the temporal/spatial evolution of the energy transfer in plasmas. Despite its simplicity, though, the model may be applied to plasma acceleration/deceleration in the boundary layer (local as well as remote ion pickup), the topside ionosphere (auroral ion acceleration) - and the magnetopause.

Ion acceleration at the magnetopause during reconnection is usually described on the basis of single particle motion (e.g. Cowley, 1980). In fact, applying single particle motion has been quite successful in describing the acceleration of plasma in an X-line geometry (e.g. Sonnerup et al., 1981; Paschmann et al., 1986). However, Paschmann et al (1986) also observed a relation between magnetosheath plasma beta, and ion acceleration, the acceleration essentially disappearing for a high beta.. This effect has been further discussed by Scurry et al. (1994) and Phan et al. (1996). An example of the AMPTE-data, is shown in Figure 19.

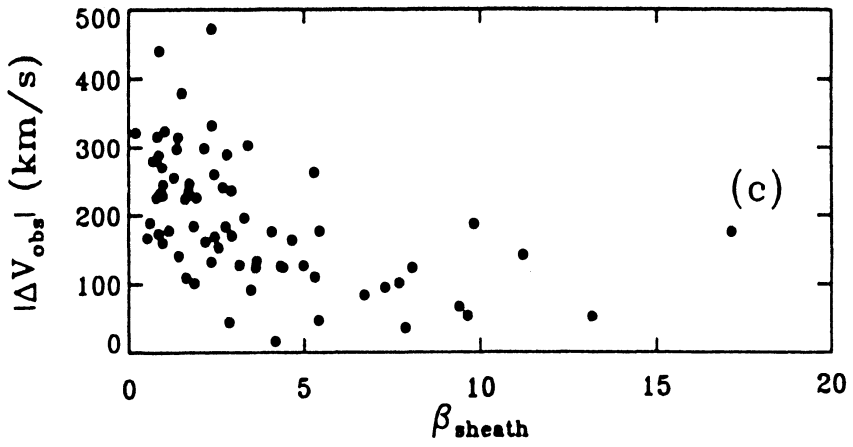

Figure 19: Magnetopause ion acceleration (Δv) plotted versus magnetosheath plasma beta (Paschmann et al, 1986; Phan et al., 1996).

Despite large scattering, the general trend of the data is that a high magnetosheath plasma beta leads to little, or no, ion acceleration. An obvious, yet qualitative, view of this is that the magnetopause acceleration process becomes heavily loaded when the mass density of plasma accessing the magnetopause is high. A high mass density also implies a high pressure, although this is by no means always obvious. For instance, a high plasma pressure (dynamic + hydrostatic) may also imply a high temperature/flow velocity. However, that the plasma is essentially stagnant in the subsolar point suggests that the high pressure is essentially due to a high density. A high plasma pressure thus implies a high internal mass loading of the magnetopause current acceleration process, and a subsequent lower flow velocity. The mass loaded pickup model, as demonstrated in Figure 19, is thus a way of explaining the reduced reconnection acceleration at the dayside magnetopause, although reconnection/plasma intrusion may yet take place. Notice that the acceleration occurs in the magnetopause proper, i.e. exactly in the region where the magnetopause current aligns with a component of the electric field ($\mathbf{j}\cdot\mathbf{E} > 0$). The acceleration process is therefore a boundary

(magnetopause) phenomenon involving a load in the magnetopause current circuit. Simple energy conservation arguments now require a dynamo driving the (loaded) current in the magnetopause current sheet. Thus, a dynamo must be identified, feeding energy into the load.

The above consideration of plasma acceleration at the magnetopause differs from the traditional reconnection view mainly with respect to the cause of the electric field at the acceleration region. No doubt the fundamental force causing the charged particle acceleration at the magnetopause is the electric force. In reconnection the propagation of the solar wind/magnetosheath electric field through the dayside magnetopause is inferred, while the BLC model assumes a local polarization electric field induced by a dynamo. Reconnection in the BLC model is a local instability, a current disruption that leads to plasma intrusion (through a weakened magnetopause) and as a consequence a local plasma acceleration (loading) in the plasma intrusion region. Plasma jets observed in dayside reconnection events are related with the same process as that in the tail neutral line, i.e. they require a normal magnetic field component - north/south in the tail and radially inward/outward in the dayside magnetopause. A strong depolarization current (heavy loading) of the electric field in the current disruption region leads to decreased plasma velocities based on simple energy and momentum conservation arguments.

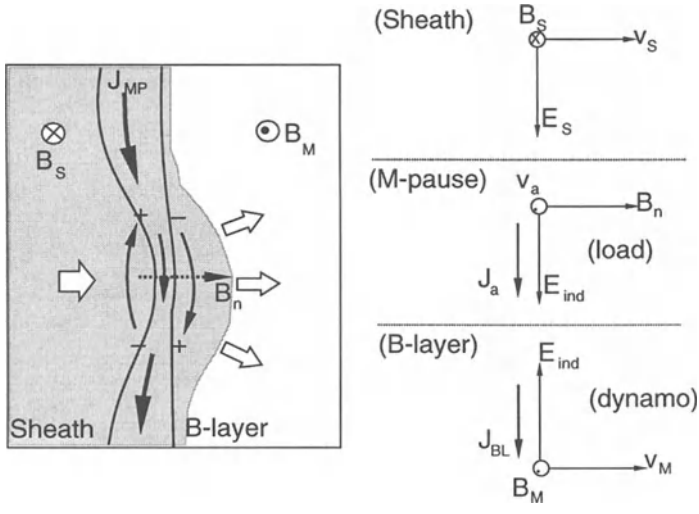

Figure 20: Localized plasma intrusion through a weakened magnetopause current in a rotational discontinuity and the associated loading (acceleration, v_a) and dynamo action in the penetration process. Notice that the induction electric field everywhere opposes the induced current in the penetration process (dynamo action).

Figure 20 also demonstrates the basic principles of the plasma intrusion mechanism, which is essentially analogous to the penetration model by

Heikkila (1982). Driven by e.g a pressure pulse, an induced electric field forms a loop leading to a bulge at the magnetopause. The similarity with the Alfvénon model by Song and Lysak (1992, 1994) is striking, except that the shear Alfvénon in the Song and Lysak model forms a current loop. Assuming infinite conductivity in the plasma, though, the electric field goes to zero as in a current dynamo and what remains is a shear Alfvénon - by Song and Lysak interpreted as driven reconnection. Notice, however, that this geometry allows for a continued protrusion of plasma through a weakened magnetopause (as in the simulations by Ma et al., 1991). More important for the present discussion here is that the electric field at the magnetopause (E_{ind}), driven by the local dynamo, is depolarized (loaded) by the magnetopause current. Thus, using the same arguments as for Figure 15 and the acceleration/deceleration discussion leading to equation (4), it becomes obvious that the velocity gain in a magnetopause forming a rotational discontinuity (normal component B_n) is given by:

$$v_a = \left(v_0 - \frac{E_{ind}}{B_n}\right) \exp\left(-t/t_0\right) + \frac{E_{ind}}{B_n} \qquad (5)$$

where $t_0 = \dfrac{n_a m_a}{B_n^2 \sigma S_{xy}}$, E_{ind} is the induced electric field in the magnetopause current ($j_{mp} = n_a \cdot v_a \cdot q$), B_n is the normal magnetic field component, and v_0 is the incident velocity in the z-direction of the acceleration region.

Notice that the velocity in the equation above ranges from v_0 to E_{ind}/B_n, the latter corresponding to the convection speed in MHD. The maximum single particle motion speed is $2 \cdot E_{ind}/B_n$.

Equation (5) describing the magnetopause acceleration now demonstrates that a high density of the protruding plasma (n_a) and a small characteristic scale (S_{xy}) gives a low acceleration velocity, $v_a \approx v_0$. The most important component in the acceleration process is, however, the normal magnetic field component that amplifies quadratically (B_n^2).

The loaded ion pickup model may therefore describe ion acceleration at the magnetopause during reconnection, a high beta (high magnetosheath plasma density) leading to a strongly reduced ion acceleration as have been observed by e.g. Paschmann et al. (1986), Scurry et al. (1994), and Phan et al. (1996). Equation 5 predicts that the acceleration velocity also depends on the characteristic scale length (S_{xy}), the local conductivity (σ), and the magnitude of the normal magnetic field component (B_n) in the rotational discontinuity. A quantitative analysis is of course required to proove the hypothesis of mass-loaded ion pickup at the magnetopause. However, the importance of the characteristic parameters involved implies at least a qualitative agreement with observations.

7. CONCLUSIONS

In this report the transport of energy-, mass and momentum through the dayside magnetopause was considered from a non-ideal MHD point of view. Merging/reconnection may be considered a magnetopause current disruption, permitting transfer of mass- energy- and momentum into the magnetosphere on open or closed magnetic field lines. In analogy with current sheet disruption/reconnection in the magnetotail, plasma acceleration results from an electric field set up in current sheet. Similarly, the disruption itself may lead to enhanced polarization electric fields and field aligned currents that close in the ionosphere. As a result energy is transferred into the ionosphere and upper atmosphere.

The boundary layer current, BLC-model may be successfully applied to the energy transfer process. The source of electromagnetic energy (electric field) originates from a local dynamo at the magnetopause (plasma injection) as well as in the boundary layer (conversion of plasma flow to electromagnetic energy). The electromagnetic energy is subsequently dissipated in an internal (e.g. ion pickup) as well as external (ionospheric) load. In this way, via field-aligned currents, the BLC-model incorporates a coupling between solar wind energy transfer processes and the acceleration of plasma and dissipation of energy (e.g. Joule heating) in the ionosphere. Mass loaded ion pickup appears to be an acceleration process that qualitatively applies to many circumstances, indeed also to the acceleration/heating of ions in the upper ionosphere.

The properties of the penetration processes at the magnetopause and the intrinsic physical processes in the boundary layer, is described only qualitatively by the MHD-based BLC-model. Song and Lysak (1992,1994) have introduced the concept of Alfvénons that may become a useful tool in understanding the dualistic nature of electromagnetism (fields) and currents (particles) in the energy transfer process at the magnetopause. However, for a multispecies plasma, kinetic theory must be applied to understand e.g. the differential ion drift observed in the boundary layer (Lundin et al., 1987).

Satellite measurements indicate that the most obvious magnetosheath access regions, the polar cusp, is a steady state feature with continuous injection of magnetosheath plasma into the magnetosphere - but with transient injection (FTE/PTE) features embedded. Moreover, recent observations show that the polar cusp is both electromagnetically and dynamically coupled to the solar wind. A gas dynamic model using the classical de Laval nozzle effect provide a complementary description of the cusp which is particularly useful to describe the dynamical solar wind - magnetosphere coupling.

The penetration of solar wind plasma as transient features (PTEs/SPIs) may be observed deep inside the magnetosphere on closed field lines. "Clouds" of solar wind plasma in the magnetosphere are observed to be almost independent of IMF, but more frequently when the solar wind

dynamic pressure is high. This suggests that magnetosheath plasma has access to the magnetosphere at all disturbance levels.

References

Aparicio, B., Thelin, B., and Lundin, R., 1991, *J. Geophys. Res.,* 96, 14023.
Axford, W. I., and C. O. Hines, 1961, *Can. J. Phys.*, 38, 1433
Baumjohann et al., 1989, *J. Geophys. Res.,* 94, 6597.
Bostik, W.H., 1956, Phys. Rev., 104, 292.
Burch, J. L., 1968, *J. Geophys. Res.*, 73, 3585-3591
Carlson, C.W. and R. B. Torbert, 1980, *J. Geophys. Res.,* 85, 2903.
Cowley, S. W. H., 1980, Space Sci. Rev., 26, 217
Dungey, J. W., 1961, Phys. Rev. Lett., 6, 47
Eastman, T. E., et al., 1976, *Geophys. Res. Lett.*, 3, 685
Gosling et al., 1991, *J. Geophys. Res.,* 96, 14 097.
Haerendel, G. et al., 1978 *J. Geophys. Res.,* 83, 3195
Hall, D., 1991, *J. Geophys. Res.,* 96, 7869
Heikkila, W.J. & Winningham, J.D. 1971, *J. Geophys. Res.*, 76, 883-891.
Heikkila, W. J., 1982, *Geophys. Res. Lett.*, 9, 877.
Heikkila, W.J., 1985, in The polar Cusp, eds. J.A. Holtet and A. Egeland, D. Reidel Publ. Company, 387-396.
Frank, L.A. & Ackerson, K.L. 1971, *J. Geophys. Res.*, 76, 3612-3643
Hones, E. W. Jr, 1972.,*et al., J. Geophys. Res.,* 77, 5503.
Jankowska, K. et al., 1990, *J. Geophys. Res.*, 95, 5805-5816.
Kremser, G., and R. Lundin,1990, *J. Geophys. Res.*, 95, 5753.
Le, G. et al., 1994, *J. Geophys. Res.*, 99, 23 723.
Lennartsson, W., 1987, Magnetotail Physics, Johns Hopkins Press 86-27614, 35-40
Lennartsson, W., 1991, *J. Atm. and Terr. Physics*, 53, 1103-1111
Lennartsson, W., 1995, *J. Geophys. Res.,* 100, 23621-23636
Lemaire, J., 1977, *Planet. Space Sci.*, 25, 887.
Lemaire J. and Roth, 1978, *J. Atmos. Terr. Phys.*, 40, 331.
Lockwood, M., and M.F. Smith, 1992, *J. Geophys. Res.*,97, 14 841.
Lockwood, M. and C.J. Davis, 1995, *J. Geophys. Res.*,100, 7627.
Lundin, R.et al., 1981, *Space Sci. Rev.*, 31, 247.
Lundin, R., and B. Aparicio,1982, *Planet. Space Sci.*, 30, 81
Lundin, R., and E. Dubinin, 1984, *Planet. Space Sci.*, 32, 745.
Lundin, R., 1985, The polar Cusp, eds. J.A. Holtet and A. Egeland, D. Reidel Publ. Company, 9.
Lundin, R., et al., 1987, *J. Geophys. Res.*,92, 3214.
Lundin, R. 1989, *Space Sci. Rev.*, 48, 263-320.
Lundin, R, J. Woch, and M. Yamauchi, 1991, ESA, SP-330, 83.

Lundin, R., et al., Proceedings of the COSPAR Colloquium 4 in Ann Arbor, USA, 305-309, 1993.
Lundin, R., et al., 1995, *J. Geophys. Res.*, 100, 7587.
Lundin et al., 1997, to be submitted to *J. Geophys. Res.*
Ma, Z.W, J.G. Hawkins, and L.C. Lee, 1991, *J. Geophys. Res.*, 96, 15751-15765
Miura, A., 1984, *J. Geophys., Res.*, 89, 801.
Mitchell, D.G. et al., 1987, *J. Geophys. Res.*, 92, 7395.
Newell P.T., and C.-I. Meng, 1988,*J. Geophys. Res.*, 93, 14549-14556
Newell P.T., and C.-I. Meng, 1994,*J. Geophys. Res.*, 99, 273-286
Norberg, O.,et al., 1994, *Geophys. Res. Lett.,* 21, 1919.
Olson, W. P., and K. A. Pfitzer, 1985, *J. Geophys. Res.*, 90, 10823.
Owen C.J,., and S.W.H. Cowley, 1991, *J. Geophys. Res., 96,* 1641
Paschmann, G. et al., 1976, *J. Geophys. Res.*, 81, 2883.
Paschmann, G.et al., 1979, Nature Lond., 282, 243.
Paschmann, G. et al., 1986, *J. Geophys. Res.*, 91, 11099
Phan, T.-D., et al., 1996, *J. Geophys. Res.*, 101, 7801-7816
Reiff, P.H. & al. 1977, *J. Geophys Res.*, 82, 479-491.
Rosenbauer H.et al, 1975, *J. Geophys. Res.*, 80, 2723.
Russell, C. T. and R. C. Elphic, 1979, *Geophys. Res. Lett.*, 6, 33.
Sandahl, I. et al., 1996, Advances in Space Research, accepted. 1996
Schindler, K., 1979, *J. Geophys. Res,* 84, 7527.
Sckopke, N.et al., 1976, *J. Geophys. Res.*, 81, 2687.
Sckopke, N., 1979, *ESA, Paris. SP-148*, 37.
Sckopke, N.et al., 1981, *J. Geophys. Res.*, 86, 2099.
Schmidt, G., 1960, Phys. Fluids., 3, 961.
Scurry, L., et al., 1994, *J. Geophys. Res.*, 99, 14815-14829
Sibeck, D., 1989, *J. Geophys. Res.*, 94, 2505.
Smith, M.F. and Lockwood M. 1990, *Geophys. Res. Lett.*, 17, 1069.
Sonnerup, B. U. Ö.,et al., 1981, *J. Geophys. Res.*,86, 10049-
Song, Y. and R.L. Lysak, 1992, Substorm I, Kiruna, Sweden 1992, 149-
Song, Y. and R.L. Lysak, 1994, *Geophys. Res. Lett*, 21, 1755
Spreiter, J.R., and A. Summers, 1967, *Planet. Space Sci.,*15, 787, 1967.
Spreiter, J.R. et al., 1968, Physics of the magnetosphere, ed. R.L. Carovillano, D. Reidel Publ. Co., Dordrecht, Holland, 301-375, 1968.
Stasiewicz, K., 1991, *J. Geophys. Res.*, 96, 77-86
Tsyganenko N. A., 1987, *Planet. Space Sci.*, 35, 1347-1358
Woch, J., and Lundin R. 1991, *Annales Geophysicae*,9, 133-142
Woch, J., and R. Lundin, 1992a, *J. Geophys., Res.*, 97, 1431.
Woch, J., and R. Lundin, 1992b, *J. Geophys., Res.*, 97, 1421.
Yamauchi, M, et al., 1993a, T, *J. Geophys. Res.*, 98, 5761-576
Yamauchi, M and R. Lundin, 1993b, *J. Geophys. Res.*, 98, 7587.
Yamauchi, M.et al., 1993c, *Geophys. Res. Lett.*, 20, 795, 1993.

Yamauchi, M. and R. Lundin, 1994, Physical Signatures of Magnetospheric Boundary Layer Processes, J.A. Holtet and A. Egeland ed., Kluwer, 99-109.
Yamauchi, M. and R. Lundin, 1997, Phys. and Chem. of the Earth, accepted, 1997
Yamauchi, M., and L. Blomberg, 1997, Phys. and Chem. of the Earth, accepted, 1997.

ISEE ION COMPOSITION DATA WITH IMPLICATIONS FOR SOLAR WIND ENTRY INTO EARTH'S MAGNETOTAIL

O.W. LENNARTSSON
Lockheed Martin Missiles & Space, Palo Alto, California, USA

Received January 20, 1997; accepted in final form February 6, 1997

Abstract. Energetic (0.1-16 keV/e) ion data from a plasma composition experiment on the ISEE-1 spacecraft show that Earth's plasma sheet (inside of 23 R_E) always has a large population of H^+ and He^{++} ions, the two principal ionic components of the solar wind. This population is the largest, in terms of both number density and spatial thickness, during extended periods of northward interplanetary magnetic field (IMF) and is then also the most "solar wind-like" in the sense that the He^{++}/H^+ density ratio is at its peak (about 3% on average in 1978 and 79) and the H^+ and He^{++} have mean (thermal) energies that are in the ratio of about 1:4 and barely exceed the typical bulk flow energy in the solar wind. During geomagnetically active times, associated with southward turnings of the IMF, the H^+ and He^{++} are heated in the central plasma sheet, and reduced in density. Even when the IMF is southward, these ions can be found with lower solar wind-like energies closer to the tail lobes, at least during plasma sheet thinning in the early phase of substorms, when they are often seen to flow tailward, approximately along the magnetic field, at a slow to moderate speed (of order 100 km s^{-1} or less). These tailward flows, combined with the large density and generally solar wind-like energies of plasma sheet H^+ and He^{++} ions during times of northward IMF, are interpreted to mean that the solar wind enters along the tail flanks, in a region between the lobes and the central plasma sheet, propelled inward by **E×B** drift associated with the electric fringe field of the low latitude magnetopause boundary layer (LLBL). In order to complete this scenario, it is argued that the rapid (of order 1000 km s^{-1}) earthward ion flows (mostly H^+ ions), also along the magnetic field, that are more typically the precursors of plasma sheet "recovery" during substorm expansion, are not proof of solar wind entry in the distant tail, but may instead be a time-of-flight effect associated with plasma sheet redistribution in a dipolarizing magnetic field.

Key words: Magnetotail, Plasma Sheet, Low Latitude Boundary Layer, Solar Wind Entry, Tail Plasma Flows, Substorms

Abbreviations: ISEE-International Sun-Earth Explorer, GSM-Geocentric Solar Magnetospheric, GSE-Geocentric Solar Ecliptic, R_E-Earth Radii, IMF-Interplanetary Magnetic Field, LLBL-Low Latitude Boundary Layer, AE-Auroral Electrojet Index, NSSDC-National Space Science Data Center, NASA-National Aeronautics and Space Administration

1. Introduction

The plasma composition experiment on the International Sun-Earth Explorer One (ISEE-1) spacecraft (Shelley *et al.*, 1978) provided the first tool for *in situ* determination of the chemical makeup of Earth's plasma sheet, from its inner edge out to a geocentric distance of almost 23 R_E. By the time of the ISEE-1 (and ISEE-2) launch, on October 22, 1977, there had been mounting recent evidence that the

Space Science Reviews **80**: 305–323, 1997.

energetic (hundreds of eV to tens of keV) plasmas in Earth's magnetosphere have not only a solar wind source, as previously thought, but also a very significant terrestrial source, as manifested by singly charged oxygen at keV energies (*e.g.* Shelley *et al.*, 1972; Ghielmetti *et al.*, 1978; Balsiger *et al.*, 1980, and references therein). Those findings had made it eminently clear that the whereabouts of solar origin plasmas in the magnetosphere are a matter of chemistry, and that future space plasma probes would have to include instruments capable of separating different ions. The ISEE-1 instrument were to provide a wealth of new information over the next 4 1/2 years, some of it rather surprising, not only about the plasma sheet, but about plasmas in various regions between the inner magnetosphere and the magnetopause boundary layers and beyond (*e.g.* Sharp *et al.*, 1983). This article focuses on the tail region and, in particular, on data that seem to have the strongest bearing on the entry of solar wind particles into the plasma sheet.

The principal background material for this article can be found in a single study by Lennartsson (1992), henceforth referred to as Paper I. Those issues that were discussed at length in Paper I are treated only briefly here, with minimal use of the same figures, in order to leave more room to elaborate on certain important issues that have since been clarified through further analysis of the same data.

Recent statistical analysis of the ISEE-1 ion composition data has made extensive use of a particular set of compacted archival data being prepared for the public domain. The format of these is described in Lennartsson (1994; Appendix A2). That same publication also has a fairly detailed description of the instrument and its operation and performance in flight (Appendix A1). Further information can be obtained on the Internet WWW page ftp://sierra.space.lockheed.com/DATA /isee/Welcome.html.

1.1. RELEVANT INSTRUMENT PROPERTIES

The ISEE-1 instrument is similar to early spaceborne electrostatic particle analyzers with a rather limited instantaneous field of view, pointing approximately perpendicularly to the spacecraft spin axis, except that it has both a conventional analyzer of total ion flux, at a given energy per charge, and a subsequent section which only records ions of a given mass per charge. Obtaining energy spectra of various major and minor ions thus amounts to electronically stepping through both energy and mass, including detector noise measurements (while blocking all ions). Allowing for the 3-sec spin period of ISEE-1 to provide the angular ion flux information, the practical cycle time is usually some 8 to 17 minutes. By utilizing the "total ion" count rate and assuming that H^+ ions are strongly dominant, which they often are, it is possible to obtain H^+ bulk properties at 1-3 minutes time resolution in all modes of operation.

The field of view (the size of which varies with ion energy; see Shelley *et al.*,

1978) is centered in the spin plane for the "total ion" analyzer, which means approximately along the solar ecliptic plane, and 5° below the spin plane for the mass analyzer. Consequently, it is possible to obtain full pitch-angle coverage only in regions where the magnetic field is nearly parallel to the solar ecliptic plane, which often does include the tail lobe boundaries of the plasma sheet, but usually not the central plasma sheet. Furthermore, in order to derive number densities and higher order velocity moments, it is necessary to make assumptions about the ion velocity distributions at angles well away from the ecliptic plane. Various assumptions have been applied to different regions, as discussed in Paper I (see also Appendix A2 in Lennartsson, 1994).

The energy range of data presented here, unless stated differently in some case, is about 100 eV/e to 16 keV/e. This is only a marginally sufficient range in the hottest parts of the plasma sheet, and it does have a somewhat biasing effect on the comparison of H^+ and He^{++} ions, since they tend to have nearly equal mean energy per nucleon, as opposed to equal energy per charge (see Lennartsson and Shelley, 1986). The effect is essentially negligible when their number densities are compared (*i.e.* with only 0:th order velocity moments involved), except when the He^{++} measured mean energy is well above 3 keV/nucleon, in which case the He^{++}/H^+ ratio does become artificially low, but there is a noticeable underestimation of the true He^{++} mean energy even at measured values of 3-4 keV/nucleon (typical case).

1.2. SUPPLEMENTARY DATA

The analysis of the ion composition data requires extensive use of magnetic field data from the ISEE-1 fluxgate magnetometer (Russell, 1978), both for pitch-angle calculations and for the physical classification of the plasma as a whole, including its beta value.

For the intercomparison with solar wind conditions, a large set of hourly averaged solar wind velocity moments (protons and electrons) and interplanetary magnetic field (IMF) components have been extracted from the NSSDC/OMNI tape records (Couzens and King, 1986). About 70% of the ISEE-1 plasma sheet data has concurrent solar wind and IMF data in the OMNI file.

The principal measure of geomagnetic activity has been the hourly AE index, also extracted from a magnetic tape (*cf.* Kamei and Maeda, 1982, and adjoining data books).

2. Evidence of Solar Wind Entry Into Earth's Magnetotail

Figure 1 illustrates some of the main arguments made in Paper I in favor of a strong presence of solar origin plasma in the plasma sheet, especially during ex-

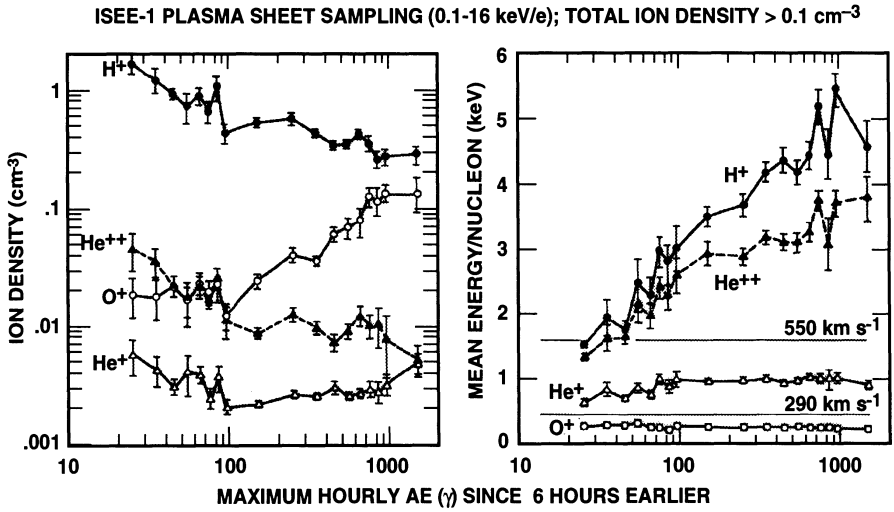

Figure 1. Central plasma sheet densities (left) and mean energies (right) of the four major ions, averaged over space and sorted according to the maximum level of auroral electrojet (AE) activity during the sampling and the preceding 6 hours. The thin horizontal lines in the right panel indicate the range of energy per nucleon that corresponds to the most common range of solar wind speeds. Error bars in this figure, and in Figures 2 and 7 below, show ± 1 σ of the mean (from Paper I).

tended periods of extreme geomagnetic quiescence:

(1) The He^{++} is almost always substantially more abundant than the He^{+}, in spite of the fact that the latter is a more common component of the known outflow of ions from Earth's polar regions (*e.g.* Collin *et al.*, 1988).

(2) The He^{++} concentration is generally well correlated with that of the H^{+}, but poorly correlated, and in part even anti-correlated, with the He^{+} and O^{+} concentrations.

(3) The He^{++}/H^{+} number density ratio, about 2% - 3% on average, is almost as high as the corresponding ratio in the solar wind (3% - 5% during the relevant solar cycle phase; *c.f.* Feldman *et al.*, 1978).

(4) The He^{++} and H^{+} mean energies, in terms of keV/nucleon, are similar to each other, but very different from either of the He^{+} and O^{+} energies. The similarity between the He^{++} and H^{+} energies becomes very close if those energies are corrected for the finite energy window of the data (Lennartsson and Shelley, 1986).

The third point should be viewed in the context of two complementary effects, namely the admixture of terrestrial H^{+} and the preferential entry of H^{+} over He^{++} from the solar wind. According to recent findings by Fuselier *et al.* (1997), the latter effect may be the dominant one, at least when the solar wind contribution to the absolute plasma density is particularly strong. As Figure 1 suggests, based on the He^{++} density, for instance, that tends to occur during times of very low AE.

A somewhat paradoxical aspect of Figure 1 is the anti-correlation between the density of solar origin ions and the AE index, since a weak AE tends to occur with a northward IMF, which has long been associated with a "closed" magnetopause. In fact, if the data are sorted according to the polarity of the concurrent hourly IMF B_Z (in GSM coordinates), as done in Figure 5 of Paper I, the plasma sheet He^{++} and H^+ densities are seen to increase with increasing solar wind (proton) density in a roughly proportional fashion for positive (northward) B_Z but to increase at a slower rate (or not increase at all) for negative B_Z. A similar result has been obtained recently with the Geotail spacecraft by Fujimoto *et al.* (this issue), using an electrostatic ion analyzer (and assuming H^+ ions).

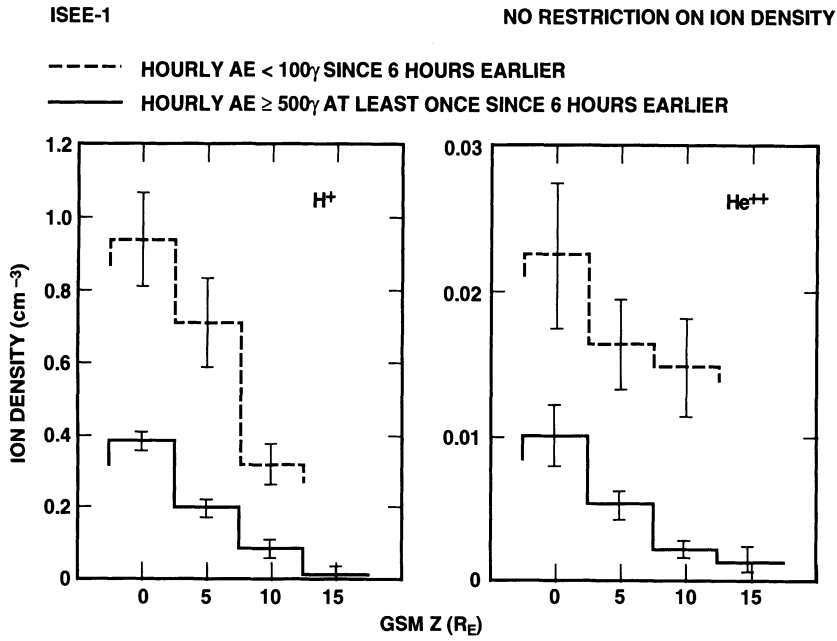

Figure 2. Densities of (left) the H^+ and (right) the He^{++} during quiet (dashed lines) and active conditions (solid lines), sorted according to the geocentric solar magnetospheric (GSM) z coordinate. The averages include samplings from the northern lobe here (from Paper I).

This result, however, should have been anticipated, since early studies of the plasma sheet dynamics by Hones *et al.* (1971), using energetic electron data, indicated that the plasma sheet at 18 R_E becomes hotter and less dense after a substorm, that is after the plasma sheet has "recovered", following the initial transient thinning, which typically lasts less than 2 hours. Being that the H^+ is usually the dominant positive component, the behavior of its density and mean

energy in Figure 1 merely supports the findings by Hones *et al.*(1971) and shows that the substorm-induced changes become increasingly pronounced with increasing substorm activity.

Figure 2 shows more specifically the effects of substorms on the plasma sheet content of solar origin ions by extending the measurements into the northern tail lobe (allowing samplings with combined ion density < 0.1 cm^{-3}). Clearly, the reduction in the H^+ and He^{++} densities during disturbed times, even after plasma sheet "recovery" (AE spanning well over 2 hours), affects the bulk of the plasma sheet (at least inside the ISEE-1 apogee at 23 R_E). The conclusion drawn from this is that the plasma sheet must become refilled by solar wind-like (cooler) plasma between periods of geomagnetic activity, thus including extended periods of northward IMF. The entry process may well be operating during active times, as well, but some loss process is then temporarily activated or enhanced.

It should perhaps be emphasized at this point that, although the upper energy cutoff at 16 keV/e does conspire with the increasing bulk energies to reduce the measured number density of both the H^+ and the He^{++} during strong substorm activity, the effect demonstrated by Figures 1 and 2 is far greater than can be attributed to instrumental effects (see Lennartsson and Shelley, 1986, for a discussion of that topic).

3. Tailward Flows of Solar Origin Ions Adjacent to the Plasma Sheet

Paper I dealt rather extensively with events of slow (mostly < 200 km s^{-1}) but dense (H^+ number density on average 1 cm^{-3}) tailward flows of ions observed immediately preceding the onset of moderately strong substorms (*cf.* Huang *et al.*, 1992), and the primary objective was to determine their origin. Figure 3 shows the location of the 23 events studied.

With the possible exception of two or three, these events appear to be located between the plasma sheet proper and the adjacent tail lobe and to have been brought into view by the initial thinning of the plasma sheet prior to the substorm expansive phase (*cf.* Hones *et al.*, 1971). Based on the densities and mean energies of the various ionic components, the H^+ being at least ten times denser than the others, it was concluded that the dominant plasma source must have been the solar wind, rather than Earth's ionosphere. Specifically, the 23 pairs of total energies E of He^{++} and H^+ ions, adding thermal and bulk flow energies as measured (without correction for the finite energy window), are statistically related by

$$E(He^{++})/E(H^+) = 3.7 \pm 0.7$$

with a correlation coefficient of 0.9 (the "±" refers to the standard deviation of points here), while the corresponding comparison of O^+ and H^+ ions yields

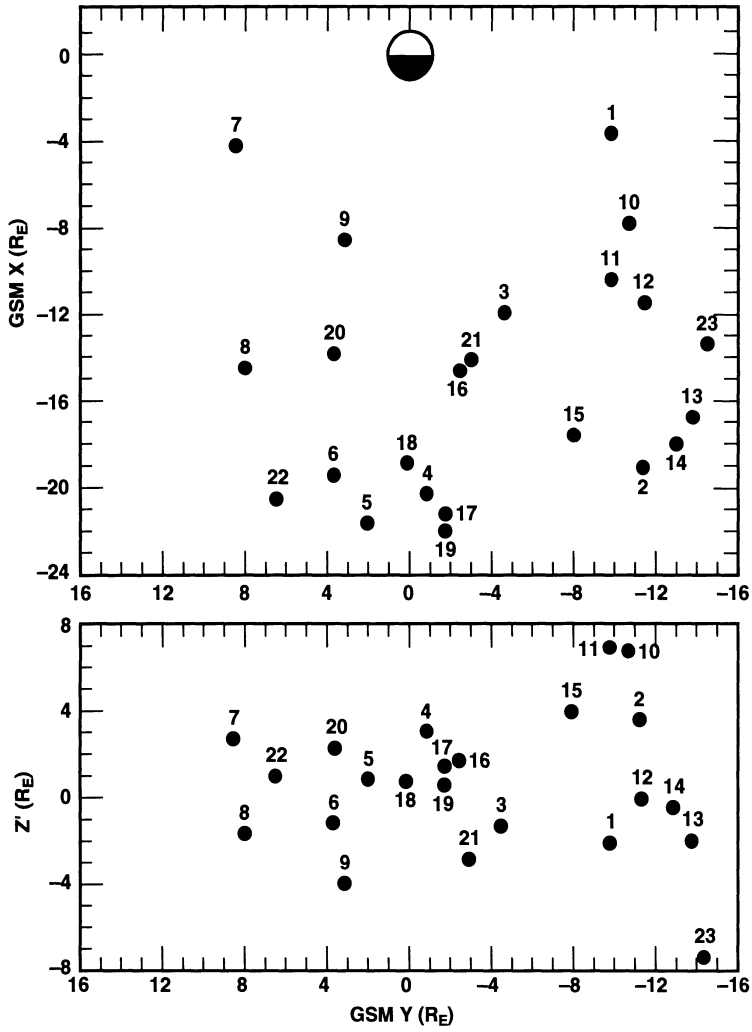

Figure 3. Location of events of tailward flowing H^+ and He^{++} ions. Top panel shows location in GSM x versus y; bottom panel shows distance above and below nominal "neutral sheet", as defined by Fairfield and Ness (1970; from Paper I).

$$E(O^+)/E(H^+) = 2.1 \pm 2.1$$

with a correlation coefficient of only 0.1. The energy of the H^+ ions is about 1 keV or less in almost half of the events, indicating that the bulk flow of the solar wind can be converted to thermal energy with little or no net heating during entry.

Since there is no sign of substantial earthward flows in conjunction with these events, it was concluded that they are probable evidence of solar wind entry sun-

ward of the ISEE-1 position at those times.

4. Inferred Large-Scale Plasma Flows

Figure 4 is analogous to Figure 13b in Paper I, except that it relates, in a schematic fashion, the inferred cross-tail **E×B** drift to high-latitude convection cells in the ionosphere.

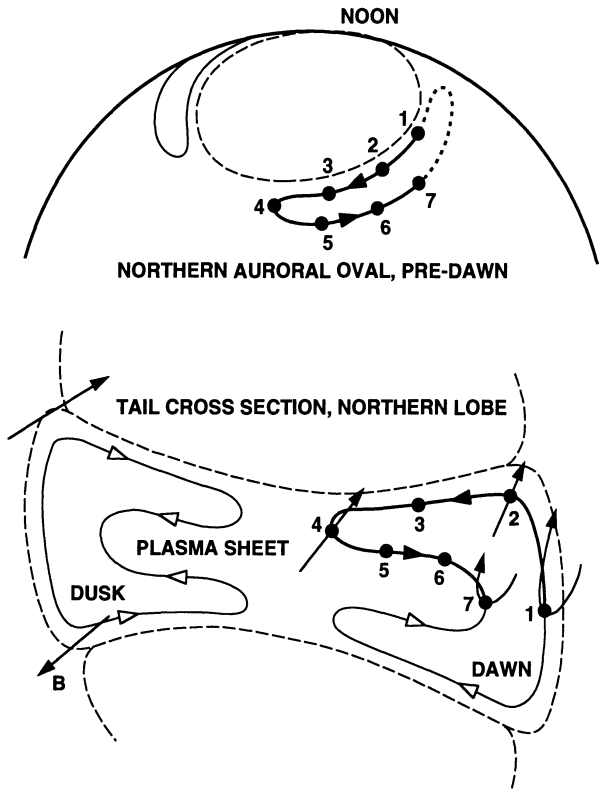

Figure 4. Upper portion shows hypothetic convection cells in the ionosphere (flow direction indicated by arrow heads), located entirely on magnetic field lines that interconnect the two hemispheres. The dashed oval-shaped contour indicates the equatorward boundary of field lines leading into the northern tail lobe. Lower portion shows, qualitatively, the corresponding convection contours in a tail cross section (**B** denotes a magnetic field vector), assuming a purely geometric mapping along the magnetic field. The numbered points correspond, one by one, with the numbers along the ionospheric convection cell. Points 1 and 7 lie on the two most sunward field lines long enough to reach this particular tail cross section. Points 1 and 2 are assumed to lie within the low latitude magnetopause boundary layer (LLBL). The remaining three "horns" in the tail convection have analogous connections to the ionosphere. The dashed lines represent the magnetopause and the interface between the plasma sheet and the lobes (adapted from Paper I).

The cross-tail equipotential contours in this figure provide a means to close those associated with the dusk-dawn directed electric field in the low latitude magnetopause boundary layer (LLBL) on the tail flanks (*cf.* Eastman *et al.*, 1976; Mitchell *et al.*, 1987). The particular shape accounts for two aspects of observed cross-tail plasma flows: 1. the deviation from pure magnetic field-alignement of tailward streams of very cold O^+ ions indicates the presence of **E×B** drift directed away from the nearest flank toward the tail center in a region between the lobes and the plasma sheet proper (*e.g.* Orsini *et al.*, 1990), while 2. the corresponding alignment of O^+ streams further inside the plasma sheet (Orsini *et al.*, 1990), as well as bulk flows of the hot H^+ population there (Figure 14 in Paper I), indicate **E×B** drift in the reverse direction. This is equivalent to having a sheet of net electric charge of the same polarity as the inside of the adjacent LLBL, that is positive at dawn, negative at dusk (*cf.* Eastman *et al.*, 1976), extend into the tail between the lobes and the central plasma sheet. Such a charge distribution would result, at least in the near-Earth plasma sheet, from the LLBL charges propagating earthward along the magnetic field, although the **E×B** drift may also carry with it a net charge.

Besides being in crude agreement with actual observations, direct and indirect, of cross-tail particle drift, this kind of flow pattern might explain why tailward flows of solar wind-like ions can be found along the ISEE-1 orbit, well inside of the nominal magnetopause, as outlined in the preceding section. This assumes that the LLBL contains newly trapped solar wind plasma, as suggested by observations (Eastman *et al.*, 1976; Mitchell *et al.*, 1987), and that it is at least partially located on closed geomagnetic field lines (*e.g.* Mitchell *et al.*, 1987). The latter would enable part of the LLBL plasma, along its junction with the lobe magnetopause boundary layer (*i.e.* the "plasma mantle"; Rosenbauer *et al.*, 1975) to enter into the tail (at Point 2, for instance). With a typical inward convection speed of a few tens of km s^{-1} (Orsini *et al.*, 1990), this plasma may reach the center of the tail in the course of a few hours. The LLBL also provides the "voltage source" in this scenario (*cf.* Eastman *et al.*, 1976; Lundin *et al.*, 1995).

Attempts to verify, with statistical methods, that the GSE v_Y component (in the spin plane) of the H^+ and He^{++} bulk flows does have the proper sign in the region of inward flow, immediately adjacent to the lobes, have, however, met with mixed results. The probable reason for that is at least twofold. For one, it is difficult to obtain a measure of distance across the boundary between the lobe and the central plasma sheet, one that is independent of the flow measurements themselves. Using the local ratio between total ion gyrational energy density and the magnetic field pressure (the ion beta) has, for instance, proved inadequate. For another, the fairly low drift speed, typically a few tens of km s^{-1}, although sufficient to cause a significant deflection of tailward streams of cold O^+ ions (Orsini *et al.*, 1990), is much smaller than the mean gyration velocity of the H^+ and He^{++} ions (hundreds of km s^{-1}). As a result, the comparison of ion fluxes in

the positive and negative GSE y-directions, which are roughly parallel to the plasma sheet boundary, becomes sensitive to the ion density gradient near the boundary (a finite-gyroradii effect).

The only equipotential contours drawn in Figure 4 lie entirely on magnetic field lines that connect the northern and southern hemispheres of Earth, equatorward of the polar caps. There must be others, of course, and these need not have the same topology. It is conceivable, for instance, to have Points 2 and 3 in the lobe and polar cap, either with Point 1 still on a closed LLBL field line, or with Point 1 on a field line extending into the solar wind on the dawn flank. The latter is readily envisioned with a southward IMF, when the draping of the IMF against Earth's northward field is certain to create points of zero field along the flanks. In any case, an accurate mapping of electric potential must also account for finite potential differences along the magnetic field, and, especially with field lines extending far downtail, it must take into consideration the finite propagation time of changing potentials. The last point has bearing on the following discussion.

5. On the Earthward Flows of Solar Origin Plasma

The "classical" image of solar wind entry has been that it takes place at high latitude, across the tail lobe magnetopause, and that the solar origin particles first encounter the plasma sheet at some considerable distance downtail, of the order of 100 R_E, near a tail field "neutral line" (*e.g.* Cowley, 1980, and references therein). In that scenario the near-Earth plasma sheet must be populated via earthward (and sunward) flows, including jetting of plasma along the magnetic field (*e.g.* Speiser, 1965). Numerous reports of rapid (often in excess of 1000 km s^{-1}) earthward ion flows, many based on data from ISEE particle detectors (*e.g.* DeCoster and Frank, 1979; Lyons and Speiser, 1982; Eastman *et al.*, 1985; Hones *et al.*, 1986), may thus appear to validate this concept (*e.g.* Hones *et al.*, 1986), or at least to validate the notion that the near-Earth plasma sheet, to a large extent, is populated from more distant parts of the tail (*e.g.* Eastman *et al.*, 1985). This prospect was noted in Paper I, but no further analysis was attempted. This section is intended to remedy that omission by outlining a possible alternative interpretation of the earthward ion flows.

The basis for a different interpretation is twofold, including both general considerations of substorm dynamics and specific aspects of the ion flows themselves. For the general part, see Figure 5.

Panel a depicts the typical situation of plasma sheet thinning, or plasma "dropout", at the ISEE-1 in the early stage of a substorm (*e.g.* Hones *et al.*, 1986). This phenomenon was first recognized and diagnosed by Hones *et al.* (1971, and references therein) in electron data obtained simultaneously by two Vela spacecraft at 18 R_E. They noted that it involves a net loss of plasma and that the particle

pressure, as manifested by 0.1- to 18-keV electrons, drops throughout the plasma sheet latitudinal extent, at least in a region near local midnight, with the possible exception of the midplane, or "neutral sheet", whose position could not be determined with very good precision from the available data. Based in part on the sheer volume of their data, they concluded, however, that the plasma pressure in the midplane does not increase, but either remains about constant or drops there as well.

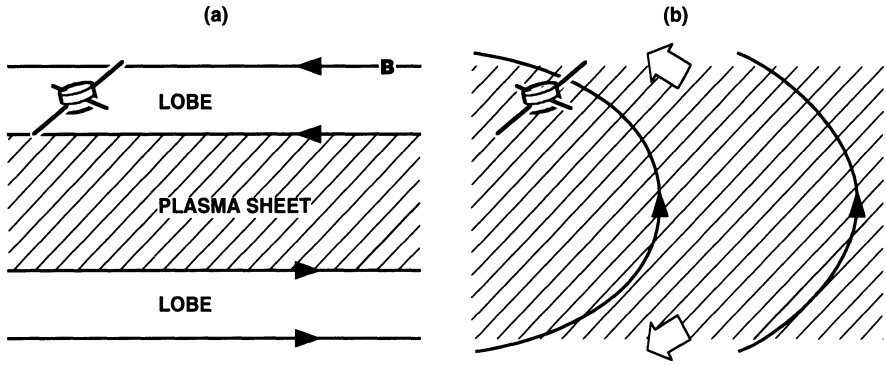

Figure 5. (a) Plasma sheet (cross hatched area) in a state of thinning due to increased earthward and sunward convection (to the left), leaving observing spacecraft in tail lobe. Direction of tail lobe magnetic field **B** indicated by thin lines with solid arrow heads. (b) Plasma sheet engulfing spacecraft again by expanding (open arrows) along magnetic field lines that are becoming increasingly dipole-like.

Panel b depicts the likely consequence if the plasma pressure does indeed drop in the tail midplane. Since the magnetic and particle pressures are normally in diamagnetic balance through the thickness of the tail (*e.g.* Fairfield *et al.*, 1981), a reduction of the particle pressure in the midplane, where it has its maximum, allows the tail magnetic field to reduce its internal energy by increasing its closure through the plasma sheet, that is to "dipolarize". This provides access, along magnetic field lines, of particles from the midplane to regions of lower plasma density, probably including adjacent parts of the lobes, as indicated, which, in turn, leads to further particle pressure reduction in the midplane, offset only by possible betatron acceleration associated with the locally increasing magnetic field strength B. Since the increase in perpendicular particle pressure due to increasing B is at most proportional to B (via the first adiabatic invariant), while the magnetic pressure is proportional to B^2, the field "dipolarization" effect must prevail, however.

In this scenario, the plasma sheet "recovery" at the ISEE-1, typically within less than 2 hours of the start of thinning (examples to follow), is not due to the

sudden arrival of new plasma from an external source, but merely to a redistribution of the pre-existing plasma sheet. The first ions to arrive are those with the shortest time-of-flight from some point within the downtail plasma sheet, which typically means ions with an earthward field-aligned velocity, that is earthward "jetting" ions, from the upper end of the ion energy distribution. These are subsequently joined by ions with decreasing earthward velocity, that is ions with increasing pitch angle and decreasing energy, eventually including ions that have mirrored closer to Earth and are returning tailward. In other words, the initial ion beam will appear to "evolve" into a typical isotropic plasma sheet population, more or less, which is qualitatively consistent with reported observations (*e.g.* Eastman *et al.*, 1985). The time scale of this evolution must depend on the location of the ISEE-1 in relation to the downtail point of origin of the ions, which may vary from event to event, and on the distance from Earth, but considering the time-of-flight of H^+ ions with energies between, say, 100 eV and 30 keV over distances of a few tens of R_E, it may well be of the order of 10 minutes. Such a number is also suggested by the observations (see for instance Figure 9 in Eastman *et al.*, 1985).

In its most literal interpretation, this scenario implies that the earthward jetting of ions does not occur at the initial thinning of the plasma sheet, only at the time of recovery, even though the lobe boundary of the plasma sheet can be said to "sweep across" the ISEE-1 in both cases. A survey of the "total ion" data from the composition experiment (the data with maximum time resolution) has revealed that this kind of asymmetry is indeed common, provided the substorm activity, as measured by the AE index, remains at a moderate level. As an example, Figure 6 shows four events of "moderate" plasma sheet thinning and recovery in a 12-hour period, while the ISEE-1 travels from $R = 16.5$ to $R = 21.5$ R_E at about 0200 local time. In all four events the maximum bulk flow speed (5:th panel down) occurs about the time of recovery of the number density (top panel) and perpendicular particle pressure (4:th panel; dashed line), and the flow direction is indeed sunward in each case, that is earthward (bottom panel; dashed line). The 1-minute AE remains below 300 nT through this period, except for a few minutes before 0600 UT, when it reaches about 700 nT (Kamei and Maeda, 1982). The 1-hour average IMF (from the IMP-8; see Couzens and King, 1986) remains southward, with B_Z about -3 nT to -2 nT, except for 0800-0900 UT, when $B_Z = +0.55$ nT.

This asymmetry disappears with increasing activity, and earthward ion flows begin to show up during plasma sheet thinning, as well. A reasonable explanation for this is that the process in Figure 5 moves tailward (see below) and that, during times of continued strong equatorward and earthward convection, the plasma sheet may thin again at the ISEE-1, while it is still recovering some distance further downtail and emitting earthward jets of ions, but this cannot be verified with the present data alone. However, there is another aspect of the observed earthward ion flows that can best be understood in terms of ions leaving the

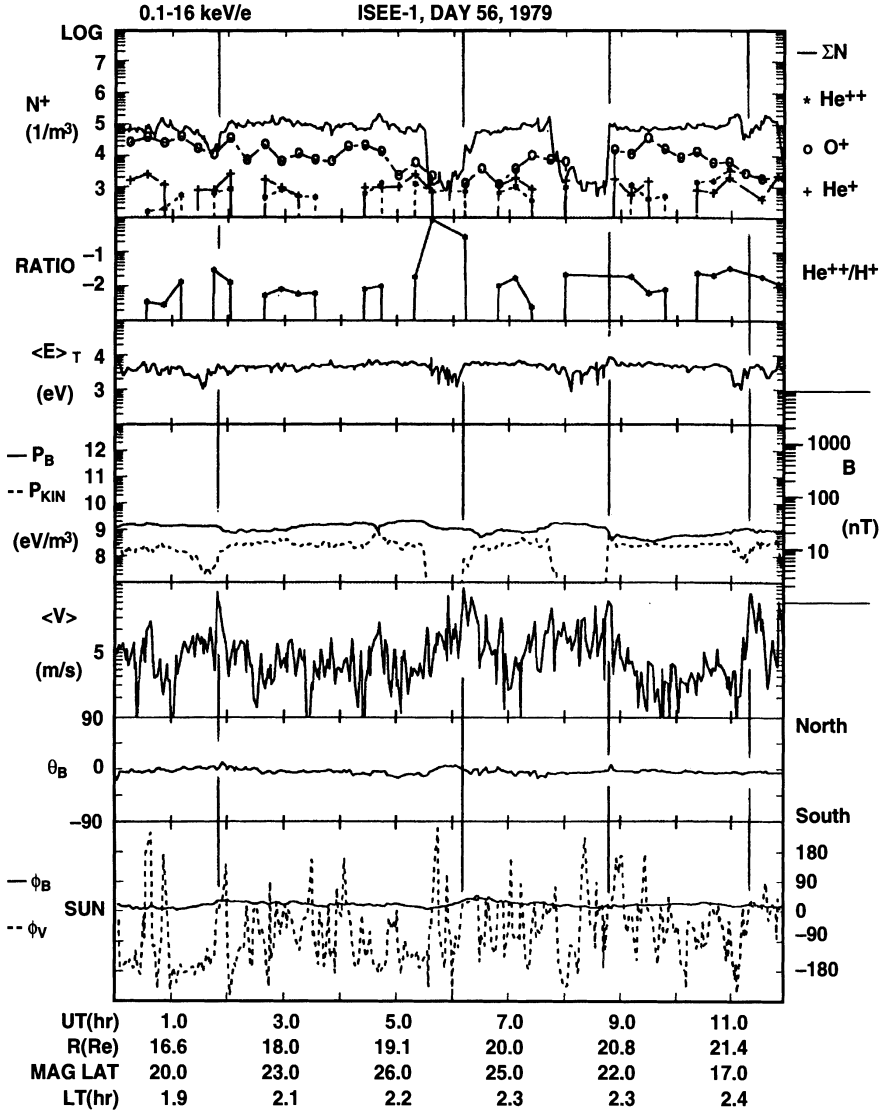

Figure 6. From top to bottom: number densities of "total ions" (assuming all H^+; solid line) and three mass resolved ions (symbols on the right); He^{++}/H^+ density ratio; thermal energy (bulk flow energy subtracted) of "total ions"; perpendicular pressures (in energy units) of magnetic field (solid line) and "total ions" (dashed line); bulk flow speed of "total ions"; direction angle of magnetic field above and below solar ecliptic plane; direction angles in solar ecliptic plane of magnetic field (solid line) and "total ion" bulk flow (dashed line).

plasma sheet, as opposed to ions entering from an external source. That aspect is the usually modest flux intensity, as illustrated in Figure 7.

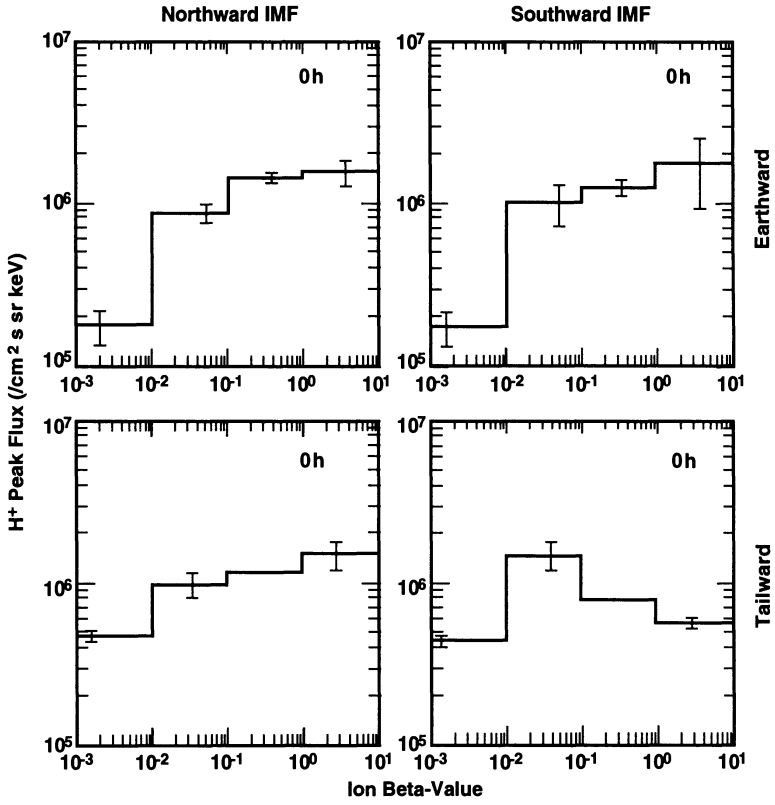

Figure 7. Averages of peak differential H^+ flux (peak flux per each energy-spin-angle cycle with mass analyzer set for M/Q = 1) in (top) the earthward direction (earthward half of 360°) and (bottom) tailward direction (tailward half), sorted by measured ion beta (adding partial pressures of the four principal ions; see text) and by direction of concurrent hourly IMF ("0 h" indicates no time shift). Extreme left and right bins in beta extend beyond scale. Samplings include all energies between 10 eV and 18 keV here, but are limited to those instrument cycles that cover all pitch angles (error bars again show ± 1σ of mean, if > 5%, and are placed at average beta in each bin).

This figure is tailored to the fact that the earthward field-aligned ion flows must occur in regions of low ion beta, whether they form a spatial outer boundary on the plasma sheet or, as argued here, constitute a time-of-flight effect. This is because, by definition, they locally dominate the ion flux and yet have little gyrational energy themselves. The beta used here is derived from the sum of partial perpendicular pressures of H^+, He^{++}, He^+, and O^+ ions, and the data are from within 10 R_E on either side of local midnight (*cf.* Lennartsson, 1994). Based on the distribution over beta of H^+ bulk flow speeds along the tail axis (see Figure 4 in Lennartsson, 1994), the strongly collimated earthward ion flows occur mostly at beta < 0.1. As Figure 7 suggests, the earthward flux intensities there are typi-

cally comparable to or smaller than the flux in the central plasma sheet, at beta > 0.1, as would be expected if the ion jets were composed of ions escaping from the central plasma sheet, perhaps at times occupying a smaller solid angle than even the instrument field of view. In contrast, if the ion jets were to supply the central plasma sheet from an external ion source, by being scattered in angle and energy, then one would expect these to be much more intense to start with (which is indeed the case with tailward flowing O^+ ions, as shown by Figure 2 in Lennartsson, 1995). Besides, these jets are part of the substorm process, and that process does reduce the number of solar origin ions in the plasma sheet, as already demonstrated (Figure 2).

It should be mentioned that the flux averages at beta < 0.1 in the top panels of Figure 7 remain essentially the same, within statistical error bars, if the data are strictly limited to samplings with the earthward H^+ bulk speed > 300 km s^{-1}. Also, the reduced tailward flux at beta > 1 in the bottom right panel may be a sampling bias, since the requirement of full pitch-angle coverage strongly limits the data selection there (*cf.* Section 1.1).

6. Concluding Remarks

There are several aspects of the ISEE ion composition data that cast doubts on the "classical" two-dimensional image of solar wind entry, the one where magnetosheath plasma from above Earth's magnetic poles is being forced toward a distant reconnection site in the magnetotail midplane by a dawn-dusk directed electric field imposed from the solar wind. Special weight has previously been placed on three of these aspects (in Paper I):

(1) When the H^+ and He^{++} ions are at their highest concentration in the near-Earth plasma sheet, they have a mean energy per nucleon that approximates their typical bulk flow energy in the solar wind (Figure 1), thus showing no evidence of substantial acceleration at a distant tail reconnection site.

(2) The total number of plasma sheet H^+ and He^{++} ions peaks during extended periods of geomagnetic quiescence (Figure 2), when the IMF remains northward and, hence, the solar wind electric field has a dusk-to-dawn direction, opposite that of the tail electric field required for reconnection.

(3) At times, a relatively dense (of order 1 cm^{-3}) and cool (about 1 keV/nucleon) population of H^+ and He^{++} ions with "solar wind-like" composition (a few per cent He^{++}) can be observed flowing slowly tailward (at about 100 km s^{-1}) near the lobe boundaries of the near-Earth plasma sheet (Figure 3).

Figure 4 is an attempt to explain these three aspects of the ISEE data by invoking electric potentials that allow a favorable three-dimensional tail plasma flow, one that is at least partially independent of the solar wind electric field.

This article adds a fourth aspect to this list:

(4) Although collimated and fast (of order 1000 km s^{-1}) earthward "jets" of ions are often observed near the lobe boundaries of the plasma sheet, in a region of low ion beta, as might be expected with a downtail reconnection site, the typical flux per solid angle of these is, at most, comparable to the isotropic flux in the central plasma sheet (Figure 7).

Figure 5 is likewise an attempt to explain this last aspect, by conjecturing the effects of superimposing a dawn-dusk directed electric field of solar wind origin, when the IMF turns southward, on the "internally generated" field in Figure 4. In a geometrical sense, Figure 5 depicts what might be considered "reconnection", but that term has the connotation of a magnetic field being "carried along" by the plasma. The physical process envisioned here can best be described as a local "diamagnetic breakdown" of the plasma sheet, one where part of the tail lobe magnetic field intrudes into the central plasma sheet particle population. Such a process does have several attractive implications, some of which tie in with previous results:

(a) If the field intrusion is sufficiently rapid, that is rapid compared to gyrocenter gradient-*B* drift across the field, but still slow compared to the gyration period of H^+ ions (6.6 sec in a 10 nT field), the associated betatron acceleration, perhaps combined with pitch-angle scattering, will cause a rapid heating of the dominant ion component over a wide range of initial energies (final gyration energy of each ion proportional to its initial value, to the extent the first invariant is preserved). This ties in with the substorm-induced plasma sheet heating in general (*e.g.* Figure 1) and may help explain, in particular, the observations by Huang *et al.* (1992) of "nonadiabatic" (in a thermodynamic sense) heating of the central plasma sheet coincident with partial dipolarization of the magnetic field.

(b) If the rise time of the magnetic field strength *B* is longer than both the H^+ and He^{++} gyration periods (the latter only twice as long), it would explain why those two species tend to maintain nearly equal energy per nucleon (see Figure 1 and Point (4) in Section 2). Since the gyration period of electrons is then well within the requirement for preserving their first invariant, it would also explain why the plasma sheet electron temperature tends to be proportional to (but lower than) that of the positive ion component (*e.g.* Figure 9 in Baumjohann *et al.*, 1989). If the rise time of *B* is limited on the upper end by the gyration period of O^+ ions (almost 2 min in a 10 nT field), it would help explain why that terrestrial component is not heated during substorms (Figure 1, right panel), although the admixture of new O^+ ions probably plays a role, as well.

(c) If this magnetic field intrusion is most likely to occur in the vicinity of local midnight, where substorms are often initiated, it would help explain why the He^{++} and H^+ ions have a temperature maximum there (see Figure 12b in Lennartsson and Shelley, 1986, and adjoining text).

A crucial part of this scenario is the occurrence, in the earliest phase of substorms (growth phase), of near-Earth plasma sheet thinning, that is plasma

depletion. Although that phenomenon is rather well established empirically (Hones *et al.*, 1971), it is worthwhile to briefly speculate about its possible cause:

Being that a newly southward IMF is going to affect the magnetopause flanks near dawn and dusk before it is transported downtail by the solar wind (in the magnetosheath), it seems reasonable that the near-Earth plasma sheet, as well as the dawn and dusk sectors of the auroral ovals, will experience the associated dawn-dusk electric field before the more distant portions of the plasma sheet do so, assuming there is good electric conduction along geomagnetic field lines threading the outer edge of the LLBL. The electric connection ought to be ensured, it seems, by the cancellation of the IMF at some point along the oppositely directed geomagnetic field line. If true, this implies that the near-Earth plasma sheet undergoes increased equatorward and sunward convection, of the kind normally associated with a dawn-dusk electric field (*e.g.* Hultqvist *et al.*, 1981), before there is increased inflow of plasma from further down the tail. This may well generate a sufficient divergence in the plasma flow to account for the thinning, including a drop in the plasma pressure in the midplane.

Furthermore, it is also reasonable that the thinning will progress tailward, either because the southward IMF is transported in that direction along the flanks, or because the dawn-dusk electric field already applied between the dawn and dusk sectors of the auroral ovals near Earth propagates outward along adjacent geomagnetic field lines that lead downtail, or by a combination of the two effects. Although the Alfvén velocity in the high-latitude plasma sheet (for example 1200 km s^{-1} with 0.3 cm^{-3} H^+ ions in a 30 nT field, or 11 R_E per min) is likely to be larger than the solar wind velocity along the flanks (a few hundred km s^{-1}), the near-Earth electric field has to reach the proper tail magnetic field lines first, so it is not obvious which effect may dominate.

This last excursion from actual data may serve as a reminder that the tail flanks, and in particular the LLBL, play a fundamental role in the above interpretation of ISEE data on solar origin ions. It is envisioned here that the LLBL probably is the "site of plasma, momentum and energy transfer" from the solar wind that it once was foreshown to be by Eastman *et al.* (1976). Although there has yet to be a consensus on the physics behind this boundary layer, speculating on that subject goes beyond the scope of this article.

Acknowledgments

This work was supported by NASA under grant NAGW-4177.

References

Balsiger, H., Eberhardt, P., Geiss, J., and Young, D.T.: 1980, 'Magnetic storm injection of 0.9- to 16-keV/*e* solar and terrestrial ions into the high altitude magnetosphere', *J. Geophys. Res.* **85**, 1645.

Baumjohann, W., Paschmann, G., and Cattell, C.A.: 1989, 'Average plasma properties in the central plasma sheet', *J. Geophys. Res.* **94**, 6597.

Collin, H.L., Peterson, W.K., Drake, J.F., and Yau, A.W.: 1988, 'The helium components of energetic terrestrial ion upflows: their occurrence, morphology, and intensity', *J. Geophys. Res.* **93**, 7558.

Couzens, D.A., and King, J.H.: 1986, *Interplanetary medium data book, supplement 3, 1977-1985*, Rep. NSSDC/WDC-A-R&S 86-04, NASA Goddard Space Flight Cent., Greenbelt, Md.

Cowley, S.W.H.: 1980, 'Plasma populations in a simple open model magnetosphere', *Space Sci. Rev.* **26**, 217.

DeCoster, R.J., and Frank, L.A.: 1979, 'Observations pertaining to the dynamics of the plasma sheet', *J. Geophys. Res.* **84**, 5099.

Eastman, T.E., Hones, E.W., Jr., Bame, S.J., and Asbridge, J.R.: 1976, 'The magnetospheric boundary layer: Site of plasma, momentum and energy transfer from the magnetosheath into the magnetosphere', *Geophys. Res. Lett.* **3**, 685.

Eastman, T.E., Frank, L.A., and Huang, C.Y.: 1985, 'The boundary layers as the primary transport regions of the Earth's magnetotail', *J. Geophys. Res.* **90**, 9541.

Fairfield, D.H., and Ness, N.F.: 1970, 'Configuration of the geomagnetic tail during substorms', *J. Geophys. Res.* **75**, 7032.

Fairfield, D.H., Lepping, R.P., Hones, E. W., Jr., Bame, S.J., and Asbridge, J.R.: 1981, 'Simultaneous measurements of magnetotail dynamics by IMP spacecraft', *J. Geophys. Res.* **86**, 1396.

Feldman, W.C., Asbridge, J.R., Bame, S.J., and Gosling, J.T.: 1978, 'Long-term variations of slected solar wind properties: IMP 6, 7, and 8 results', *J. Geophys. Res.* **83**, 2177.

Fujimoto, M., Terasawa, T., and Mukai, T.: 1997, 'The cold-dense plasma sheet: A GEOTAIL perspective', *Space Sci. Rev.*, this issue.

Fuselier, S.A., Shelley, E.G., and Lennartsson, O.W.: 1997, 'Solar wind composition changes across the Earth's magnetopause', *J. Geophys. Res.* **102**, 275.

Ghielmetti, A.G., Johnson, R.G., Sharp, R.D., and Shelley, E.G.: 1978, 'The latitudinal, diurnal, and altitudinal distributions of upward flowing energetic ions of ionospheric origin', *Geophys. Res. Lett.* **5**, 59.

Hones, E.W., Jr., Asbridge, J.R., and Bame, S.J.: 1971, 'Time variations of the magnetotail plasma sheet at 18 R_E determined from concurrent observations by a pair of Vela satellites', *J. Geophys. Res.* **76**, 4402.

Hones, E.W., Jr., Fritz, T.A., Birn, J., Cooney, J., and Bame, S.J.: 1986, 'Detailed observations of the plasma sheet during a substorm on April 24, 1979', *J. Geophys. Res.* **91**, 6845.

Huang, C.Y., Frank, L.A., Rostoker, G., Fennell, J., and Mitchell, D.G.: 1992, 'Nonadiabatic heating of the central plasma sheet at substorm onset', *J. Geophys. Res.* **97**, 1481.

Hultqvist, B., Aparicio, B., Borg, H., Arnoldy, R., and Moore, T.E.: 1981, 'Decrease of keV electron and ion fluxes in the dayside magnetosphere during the early phase of magnetospheric disturbances', *Planet. Space Sci.* **29**, 107.

Kamei, T., and Maeda, H.: 1982, *Auroral electrojet indices (AE) for January-June 1979,* Data Book No. 5, World Data Center C2 for Geomagn., Kyoto Univ., Kyoto, Japan.

Lennartsson, W.: 1992, 'A scenario for solar wind penetration of Earth's magnetic tail based on ion composition data from the ISEE 1 spacecraft', *J. Geophys. Res.* **97**, 19221.

Lennartsson, O.W.: 1994, 'Tail lobe ion composition at energies of 0.1 to 16 keV/*e*: Evidence for mass-dependent density gradients', *J. Geophys. Res.* **99**, 2387.

Lennartsson, O.W.: 1995, 'Statistical investigation of IMF B_z effects on energetic (0.1- to 16-keV)

magnetospheric O^+ ions', *J. Geophys. Res.* **100**, 23621.

Lennartsson, W., and Shelley, E.G.: 1986, 'Survey of 0.1- to 16-keV/*e* plasma sheet ion composition', *J. Geophys. Res.* **91**, 3061.

Lundin, R., Yamauchi, M., Woch, J., and Marklund, G.: 1995, 'Boundary layer polarization and voltage in the 14 MLT region', *J. Geophys. Res.* **100**, 7587.

Lyons, L.R., and Speiser, T.W.: 1982, 'Evidence for current sheet acceleration in the geomagnetic tail', *J. Geophys. Res.* **87**, 2276.

Mitchell, D.G., Kutchko, F., Williams, D.J., Eastman, T.E., Frank, L.A., and Russell, C.T.: 1987, 'An extended study of the low-latitude boundary layer on the dawn and dusk flanks of the magnetosphere', *J. Geophys. Res.* **92**, 7394.

Orsini, S., Candidi, M., Stokholm, M., and Balsiger, H.: 1990, 'Injection of ionospheric ions into the plasma sheet', *J. Geophys. Res.* **95**, 7915.

Rosenbauer, H., Grünwaldt, H., Montgomery, M.D., Paschmann, G., and Sckopke, N.: 1975, 'Heos 2 plasma observations in the distant polar magnetosphere: The plasma mantle', *J. Geophys. Res.* **80**, 2723.

Russell, C.T.: 1978, 'The ISEE 1 and 2 fluxgate magnetometers', *IEEE Trans. Geosci. Electron.* **GE-16**, 239.

Sharp, R.D., Johnson, R.G., Lennartsson, W., Peterson, W.K., and Shelley, E.G.: 1983, 'Hot plasma composition results from the ISEE-1 spacecraft', in R.G. Johnson (ed.), *Energetic Ion Composition in the Earth's Magnetosphere*, TERRAPUB, Tokyo, Japan, 231.

Shelley, E.G., Johnson, R.G., and Sharp, R.D.: 1972, 'Satellite observations of energetic heavy ions during a geomagnetic storm', *J. Geophys. Res.* **77**, 6104.

Shelley, E.G., Sharp, R.D., Johnson, R.G., Geiss, J., Eberhardt, P., Balsiger, H., Haerendel, G., and Rosenbauer, H.: 1978, 'Plasma composition experiment on ISEE-A', *IEEE Trans. Geosci. Electron.* **GE-16**, 266.

Speiser, T.W.: 1965, 'Particle trajectories in model current sheets, 1. Analytical solutions', *J. Geophys. Res.* **70**, 4219.

Address for correspondence: O.W. Lennartsson, Lockheed Martin Missiles & Space, Advanced Technology Center, Org. H1-11, Building 252, 3251 Hanover Street, Palo Alto, CA 94304, USA (e-mail: lenn@space.lockheed.com)

THE COLD-DENSE PLASMA SHEET: A GEOTAIL PERSPECTIVE

M. FUJIMOTO
Dept. Earth and Planetary Sciences
Tokyo Inst. of Tech., Tokyo, Japan

T. TERASAWA
Dept. of Earth and Planetary Physics
Univ. of Tokyo, Tokyo, Japan

T. MUKAI
Institute of Space and Astron. Science
Sagamihara, Kanagawa, Japan

Received January 20, 1997; Accepted in final form February 14, 1997

Abstract. GEOTAIL observations of the low-latitude boundary layer (LLBL) in the tail-flanks show that they are the region where the cold-dense plasma appears with stagnant flow signatures accompanied by bi-directional thermal electrons (< 300 eV). It is concluded from these facts that the tail-LLBL is the site of capturing the cold-dense plasma of the magnetosheath origin on to the closed field lines of the magnetosphere. There are also cases that strongly suggest that the cold-dense plasma entry from the flanks can be significant to fill a substantial part of the magnetotail. In such cases, the cold-dense plasma is not spatially restricted to a layer attached to the magnetopause (that is, the LLBL), but continues to well inside the magnetotail, constituting the cold-dense plasma sheet. Inspired by the fact that these remarkable cases are found for northward interplanetary magnetic field (IMF), a statistical study on the status of the near-Earth plasma sheet is made. The results show that the plasma sheet becomes significantly colder and denser when the northward IMF continues than during southward IMF periods, and that the cold-dense status appears most prominently near the dawn and dusk flanks. These are consistent with the idea that, during northward IMF periods, the supply of cold-dense ions to the near-Earth tail from the flanks dominates over the hot-tenuous ions transported from the distant tail.

Key words: Formation of the Plasma Sheet, Magnetotail Flanks, Plasma Transport

Abbreviations: LLBL – Low-Latitude Boundary Layer; IMF – Interplanetary Magnetic Field

1. Introduction

It is widely accepted that plasma from the ionosphere and that of the solar wind origin are the two major sources for the hot plasma trapped in the plasma sheet. The solar wind is considered to play the major role in supplying the plasma sheet protons, while the Earth's ionosphere provides singly ionized helium and oxygen ions and other heavy ions. As for the plasma from the solar wind, two entering processes have been considered: The entries from the high-latitude lobes and from the low-latitude flanks.

Protons in the plasma sheet usually have a temperature of several keV exceeding a typical kinetic energy of solar wind protons (e.g., Baumjohann et al., 1989),

Space Science Reviews **80**: 325–339, 1997.

meaning that some heating processes should intervene in the transport process from the solar wind to the plasma sheet. During southward interplanetary magnetic field (IMF) periods, a part of the solar wind plasma and energy are considered to flow into the magnetosphere through two magnetic reconnection processes taking place at the dayside magnetopause and in the distant tail. These processes make the solar wind plasma to stream along the lobe field lines into the magnetotail, and then to be trapped in the plasma sheet (the high-latitude entry). The magnetic energy stored in the magnetotail is released in the course, heating the plasma sheet ions up to several keV or more as they convect to the near-Earth part (e.g., Baumjohann, 1993).

During strongly northward IMF periods, this high-latitude entry is said to become less effective. Several authors (e.g., Baumjohann et al., 1989) have noted that the plasma sheet becomes colder and denser during northward IMF periods than during southward IMF periods. While this could be taken as indicating the switch in the dominating transport process from one to the other, there seems to have been no general agreement on this because of the little knowledge on the low-latitude entry.

Leaving the details of the flank entry process open, there have been some studies on the effects of the low-latitude entry process. Direct supply of plasma from the tail flanks has been implicitly assumed in calculating the particle flux across the low-latitude boundary layer (LLBL) into the magnetosphere in Eastman et al. (1976), and has been concluded in Eastman et al. (1985). Lennartsson (1992) has proposed a flank entry model on the basis of plasma sheet composition statistics. Zwolakowska and Popielawska (1992) and Popielawska et al. (1996) have also discussed the significance of the flank entry by mapping their data at high-latitude down to the magnetic equator. Spence and Kivelson (1994) have developed a convection model of the magnetotail including the dawn flank as one of the plasma sources.

The GEOTAIL satellite, owing to its well-designed orbit, has recently provided useful information on the LLBL at $X_{GSM} > -30R_E$ as it skims along the flanks. In accordance with previous studies (e.g., Williams et al., 1985; Mitchell et al., 1987; Traver et al., 1991) but with a more complete dataset, it has recently been shown that the low-latitude flanks of the tail are the sites where a part of the cold-dense magnetosheath plasma flowing past is indeed captured on the closed field lines of the magnetosphere (Fujimoto et al., 1996a; Fujimoto et al., 1996b).

In this review, we concentrate on GEOTAIL observations strongly suggesting that the captured cold-dense plasma fill a substantial portion of the magnetotail at times. In such cases, since the plasma is not only stagnant but is also occupying a large area not restricted to the proximity of the magnetopause, the region occupied by the cold-dense plasma may better be termed as the cold-dense plasma sheet rather than the LLBL. Inspired by the fact that these remarkable cases are found for northward IMF, a statistical study on the status of the near-Earth plasma sheet has also been made (Terasawa et al., 1996). We review the results showing that the

plasma sheet becomes significantly colder and denser than during southward IMF periods when the northward IMF continues, and that this low-temperature/high-density regime occurs most prominently near the dawn and dusk flanks. These are consistent with the idea of directly supplying the cold-dense magnetosheath ions from the flanks to the near-Earth plasma sheet. Here we should note that not only the GEOTAIL data, but also concurrent solar wind/IMF conditions available from WIND have been essential in making these studies.

2. The Cold-Dense Plasma Sheet: Case Studies

As reviewed in the previous section, in general agreement with previous studies (Williams et al., 1985; Mitchell et al., 1987; Traver et al., 1991), the GEOTAIL observations have shown that capturing of cold-dense ions from the solar wind onto closed field lines in the tail-LLBL is occasionally taking place (Fujimoto et al., 1996a; Fujimoto et al., 1996b). To summarize the observations, the tail-LLBL is the region where the cold-dense plasma appears with stagnant flow signatures. The cold-dense ions have only slow tailward convection velocity, and are even flowing sunward in some parts. Thermal electrons ($<$ 300 eV) are enhanced in the field-aligned directions, with fluxes in both the parallel and the anti-parallel directions being balanced. Slow convection and these heated bi-directional electrons suggest the closed topology of the field lines. These features are found to well characterize a group of data in the tail-LLBL. There are cases, on the other hand, that show less evident capturing signatures. As will be discussed, the IMF B_z component possibly has the dominant influence to the structure of the tail-LLBL. The IMF B_z control on the topology of the field lines in the flanks has been discussed by Mitchell et al. (1987). The results reviewed here are essentially consistent with theirs.

In this section we will review examples indicating that the cold-dense plasma entry from the flanks can indeed be significant at times, and is likely to be responsible for the formation of the cold-dense plasma sheet. Figure 1 shows the data along an orbit that goes from the duskside magnetosheath across the tail magnetopause towards the center of the tail. With the GEOTAIL's motion into the magnetotail, fast tailward flow terminates around 09:00 UT ($(X_{GSM}, Y_{GSM}) \sim$ (-15.3, 18.5) R_E, marked by an arrow in Figure 1). While this seems to mark the spacecraft's last crossing of the magnetopause into the plasma sheet (there are several crossings prior to this time), the stagnant ions further inside the boundary stay cold ($<$ 1 keV) and dense ($>$ 1 /cc) compared to a nominal value (e.g., Baumjohann et al., 1989), and this cold-dense status continues to the end of the plot. Since the absolute value of the B_x component remains relatively small (and even crosses the neutral sheet several times) until the jump around 15:00 UT (marked by another arrow), the cold-dense plasma is likely to be situated at a low-latitude part of the magnetotail. Let us carefully take the time of the B_x jump as the end of the low-latitude region survey, at which time GEOTAIL was located at (X_{GSM}, Y_{GSM}) = (-16.7, 13.5) R_E.

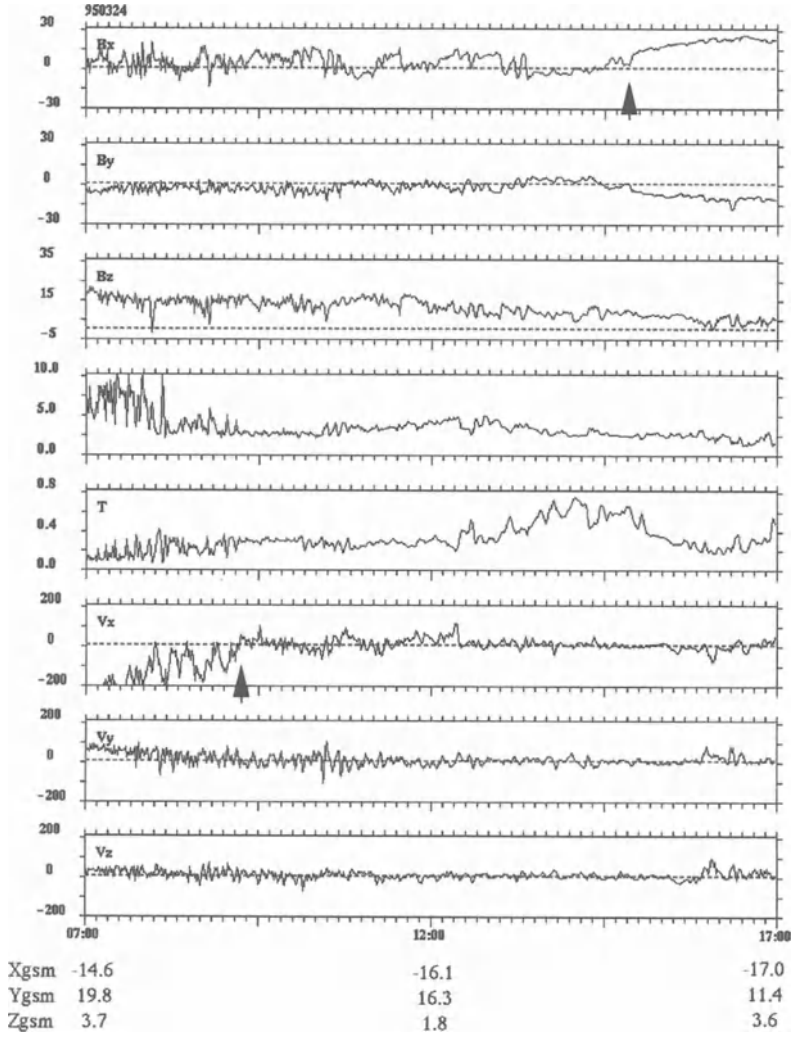

Figure 1. Observations of a duskside tail-flank. From top, the three components of the magnetic field (nT), the ion density (/cc) and temperature (keV), and the three components of the ion bulk flow (km/s). GSM coordinates are used. Cold-dense status continues till the end of the plot.

Then the distance in Y_{GSM} from this inner limit to the last fast tailward flow position sums up to 5 R_E, which is a rough estimate of the size of the region that the cold-dense plasma occupies at low-latitude. Thus, the cold-dense plasma occupies a substantial portion of the magnetotail. What is important here is the fact that the cold-dense ions showing stagnant flow features are observed over a wide region

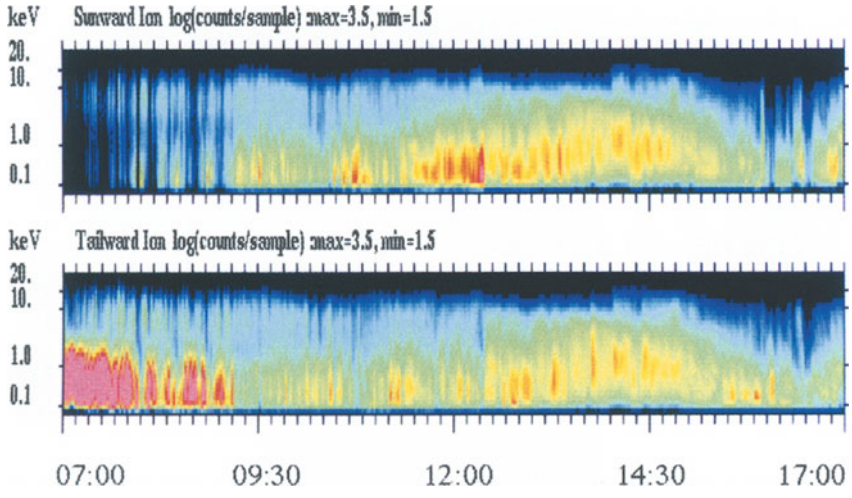

Figure 2. E-t diagrams for sunward ions and tailward ions. Color-codes are assigned according to logarithms of counts per sample. Ions of < 1 keV continue to show the highest count rates, being responsible for the cold-dense status.

in the magnetotail, not spatially restricted to a thin layer attached to the magnetopause. With this finding, we think it is better to term the low-latitude region filled with the ions as the plasma sheet in a cold-dense status, or the cold-dense plasma sheet, rather than the boundary layer located at low-latitude.

Figure 2 shows the ion E-t diagrams for the same time interval. Ions less than 1 keV continue to show the largest count rates exceeding that of the magnetospheric component (several keV) throughout the interval, being responsible for the cold-dense status. Inspection of the distribution function data shows that the ions are described by superposition (mixing) of two populations having different average energies (several hundreds eV versus several keV), with both the centers of the populations located close to the origin. Thus, the stagnant feature is because both the populations are stagnant, but not due to the presence of two populations counter streaming to each other. If we scan Figure 2 backward in time, the cold-dense ions continue to the magnetospheric boundary and do continue out to the magnetosheath, strongly suggesting that they are supplied from the magnetosheath.

Figure 2 also shows that this cold-dense ions are subject to some heating processes in the innermost part at 13-15 UT. After the last detection of fast tailward flow (around 09:00 UT), thermal electrons are persistently seen to show clear bi-directional anisotropy up to 300 eV energy range. This feature is seen to fade out after 13:00 UT simultaneous with the ion temperature increase in the innermost part (Figure 3). The observations of the fading out of the bi-directional anisotropy

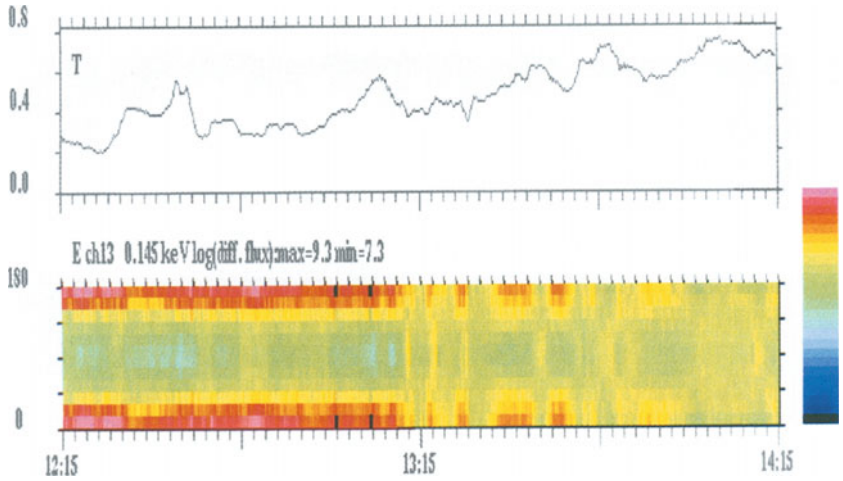

Figure 3. Electron pitch angle anisotropy. Differential fluxes (/(cm^2 · sr · sec · keV)) are sorted by pitch angles and plotted versus time. Color codes are assigned according to logarithms of fluxes. Fading-out of bi-directional anisotropy upon increase in the ion temperature around 13:00 UT is discussed.

and the heating of the cold-dense ions suggest that these distinguishing characteristics of the plasma from the flanks are eventually obscured in the inner part of the magnetotail.

On the other hand, Figure 2 indicates that several keV magnetospheric ions exist even on tailward convecting flux tubes detected earlier than 09:00 UT. By inspecting distribution function data, it is shown that these flux tubes contain ions and electrons showing essentially the same feature as those in the cold-dense plasma sheet encountered after 09:00 UT (mixed ions and bi-directional thermal electrons). We suggest that these tailward flowing flux tubes containing magnetospheric components have closed topologies, that they are in the course of deceleration to become stagnant, and that they have relevance to the mechanism of the flank entry. This point will be revisited in the Discussion section.

Figure 4 shows another example of a dusk-tail LLBL crossing showing cold-dense ions continuing from the magnetospheric boundary to deep inside the tail. The last detection of fast tailward flow is around 06:50 UT ((X_{GSM}, Y_{GSM}) = (-10.1, 19.4) R_E, marked by an arrow in Figure 4). The cold-dense interval is terminated in this case by the appearance of hot-tenuous ions around 12:50 UT ((X_{GSM}, Y_{GSM}) = (-12.9, 13.9) R_E, marked by another arrow). The width occupied by the cold-dense ions is 5.5 R_E, which, again, is a substantial part of the magnetotail diameter. As in the previous example, the thermal electron bi-directional

anisotropy is seen to fade out as this inner limit is approached (not shown). The ions in this cold-dense plasma sheet is characterized again by the mixing of a cold and a hot component. The turning into the hot-tenuous status at 12:50 UT is achieved by the disappearance of the former and the enhancement of the latter. This inner boundary of the cold-dense plasma sheet is interpreted as the demarcation line across which the dominating plasma supply process switches from one (the dusk-side flank entry for the cold-dense part) to the other (presumably from the distant tail source for the hot-tenuous part). The reduced (but clear) presence of hot ions in the cold-dense plasma sheet is considered to be caused by partial leakage of the hot ions across this border by magnetic drifts.

These cases show the spatial structure that the cold-dense plasma is present continuously from the magnetospheric boundary to deep inside the magnetotail. The ion E-t diagrams (Figure 2) show that the cold component ions do continue out to the magnetosheath, strongly suggesting that the magnetosheath ions are directly supplied into the plasma sheet from the flank. Since cold-dense ions are from the duskside to the inner part of the tail for these cases, magnetic drifts cannot be the driving force of their invasion (Spence and Kivelson, 1994).

The cold-dense plasma sheet does not always continue from the magnetospheric boundary but appears more or less suddenly occasionally. Figure 5 shows a 6-hours interval around (X_{GSM}, Y_{GSM}) = (-17, -12) R_E, during which three major step-like variations in the ion density and the ion temperature are seen (vertical dashed lines). The first change is from a hot-tenuous (T, n) = (5 keV, 0.3/cc) (around a nominal value) to a cold-dense (0.5 keV, 3/cc) situation. The next change is from the prior to an intermediate state, and the final change causes GEOTAIL to re-encounter the hot-tenuous plasma seen at the beginning of the interval. The density and temperature are anti-correlated so as to keep the thermal pressure constant. The three components of the magnetic field are rather steady, and the ion bulk flow is steadily slow, suggesting that the appearance of the cold-dense plasma is not due to the spacecraft's crossing into any different region but rather that the cold-dense plasma appears within the plasma sheet. Bi-directional thermal electrons are observed in the 2.5 hours interval of the cold-dense plasma sheet (not shown). The similarity allows us to consider that the cold-dense plasma has come from the flank (presumably the dawnside) of the near-Earth tail. Step-wise jumps into and out of the cold-dense plasma, and the distinguishing electron characteristics it retains suggest that it has been convected as a fluid element (ions and electrons together) in the form of a blob or a surge from the flank with only small mixing with the neighboring plasma. This should be contrasted with the ideas that some diffusion (Eastman et al., 1985) or magnetic drifts (Spence and Kivelson, 1994) are the agent for the transport.

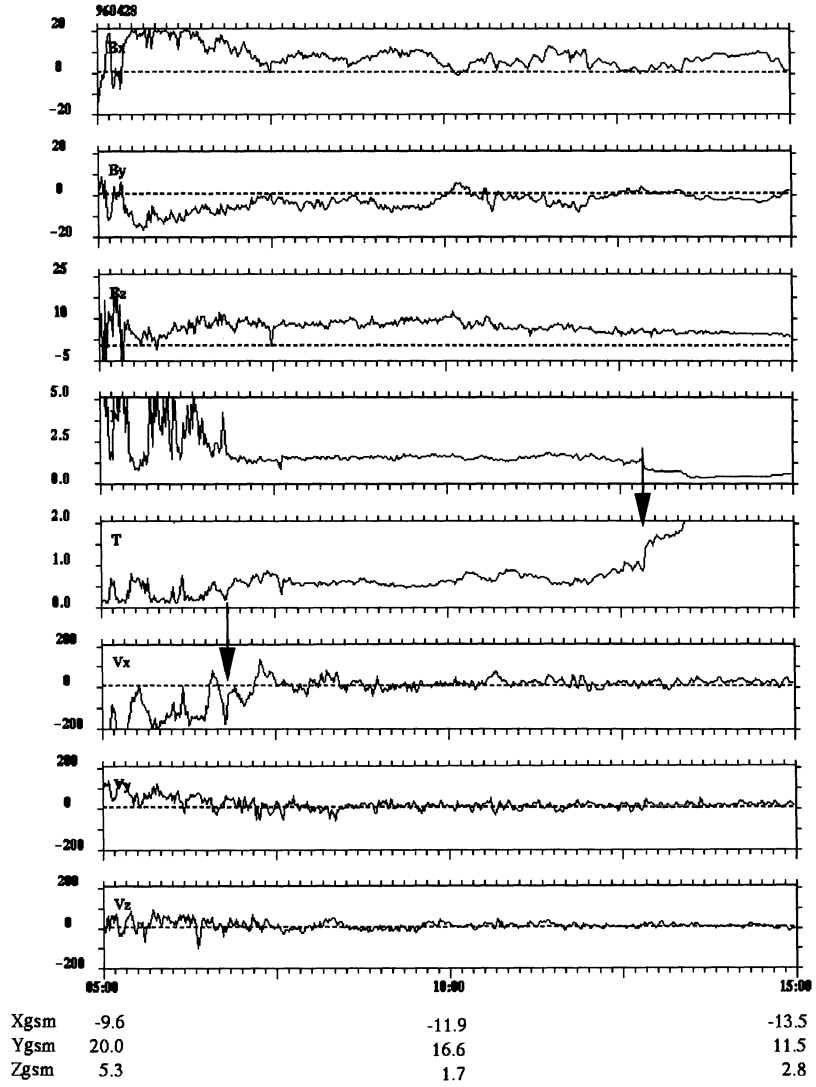

Figure 4. Another example of the cold-dense plasma sheet. The cold-dense status is terminated by the appearance of hot-tenuous plasma in this case.

3. The Cold-Dense Plasma Sheet: A Statistical Study

Our preliminary survey of the tail-LLBL structure (which still needs to be refined because of its complexity) suggests the tendency that the capturing process at the boundary becomes more efficient for northward IMF. This tendency makes us expect that the plasma sheet changes to a cold-dense status as IMF becomes

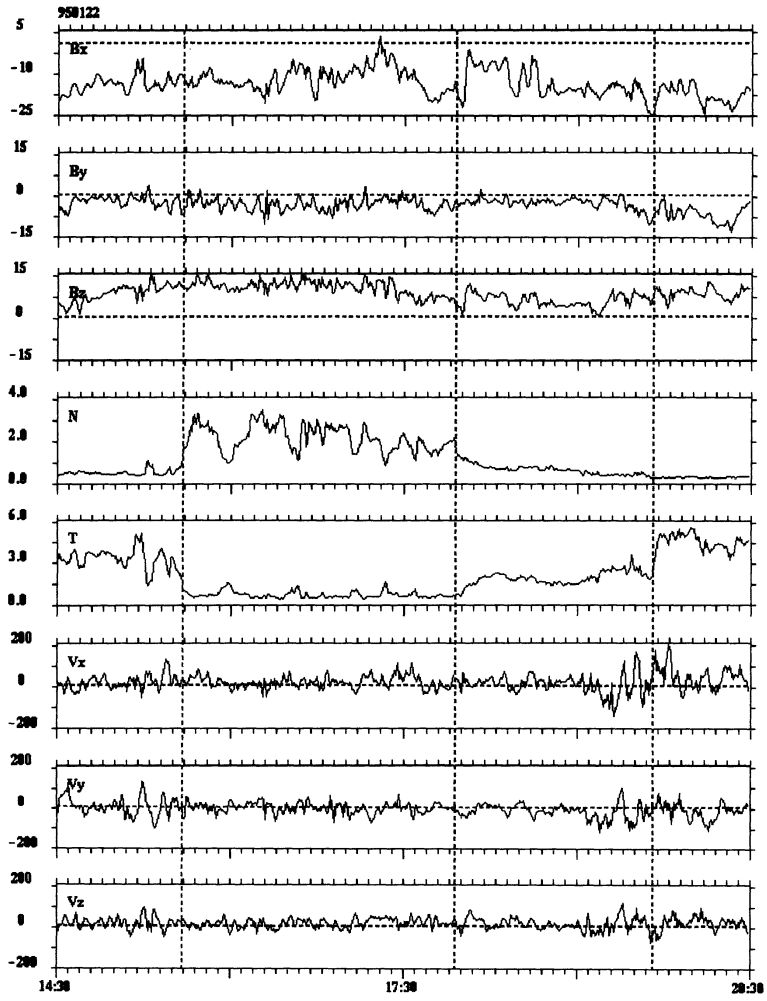

Figure 5. An example of the plasma sheet showing step-wise changes from a hot-tenuous state to a cold-dense one, and vice versa.

northward. This is what has recently been shown by Terasawa et al. (1996), as will be reviewed in this section.

The data used are from GEOTAIL in the plasma sheet and from WIND monitoring the solar wind/IMF conditions. Time lags estimated from dividing the distances of WIND from the Earth by the observed solar wind velocities are used in synchronizing the data from both the spacecrafts. The plasma sheet dataset used in the

present study is constructed as follows: For the interval Nov. 1994 - Dec. 1995, 1034 1-hour segments of observations are available from the near-Earth magnetotail ($-50 < X_{GSM'} < -15R_E$, $| Y_{GSM'} | < 25R_E$, here GSM' is a modified GSM coordinate system where an aberration angle of 4° is taken into account.). From these, we exclude those obtained in the close proximity of the magnetopause to avoid contamination from the boundary layer. Then, out of the remaining, steady plasma sheet intervals are selected by requiring (1) 1-hour average plasma β (ion thermal pressure divided by magnetic pressure; hereinafter, electron contribution is neglected) is larger than 1, and, (2) standard deviation of the total pressure (ion thermal plus magnetic pressure) is less than 20 % of its 1-hour average value. The condition (2) rejects data obtained during highly active intervals, such as those including high speed flows. Each of these 1-hour segments contains data obtained at a more or less fixed position in the $(X_{GSM'}, Y_{GSM'})$-plane, but includes dependence on the distance from the neutral sheet. To eliminate this, we made linear regression analysis on B_x versus ion density and on B_x versus ion temperature for each of these 1-hour segments. The ion density and the ion temperature at the neutral sheet are estimated from the crossings of these regression lines with B_x=0. These neutral sheet values will be used in the following analyses. It should be mentioned that since the linear dependence of ion density/temperature on B_x is not necessarily guaranteed, we check the validity of this assumption by comparing the ion thermal pressure calculated from the estimated density and temperature with the 1-hour averaged total pressure. By requiring both to agree within a 20 % error, 497 plasma sheet data points are selected.

Figure 6a and 6b show the plasma sheet temperature versus the solar wind kinetic energy and the plasma sheet density versus the solar wind density, respectively. Color of a data point depicts IMF latitudinal angle. Here, solar wind/IMF parameters are averaged for the same 1-hour interval as the plasma sheet data. While both panels show positive correlations, which indicates the fact that the plasma sheet is controlled by the solar wind, there are large scatter of data points. Blued points (IMF B_z positive) are more or less evenly distributed. On the other hand, reddish data points (IMF B_z negative) tend to be clustered at high temperature-low density (hot-tenuous) region. Figure 6c presents normalized plasma sheet density versus IMF theta angle. Color depicts the normalized plasma sheet temperature. To confirm the above statement from a reversed angle, it is evident that the low temperature-high density (cold-dense) region is filled only by the data points obtained during northward IMF periods.

After various trials, it is found that the large scatter for northward IMF cases can be reduced significantly by averaging the solar wind parameters over longer periods. The normalizing factors in the previous analysis has been the solar wind parameters averaged for the same 1-hour interval as the plasma sheet data. Instead, for a plasma sheet data obtained during a 1-hour interval (t-1, t), we have tried with the solar wind parameters averaged over the interval (t-N, t) (N=1 in the previous analysis). By calculating the correlation coefficients for northward IMF subsets

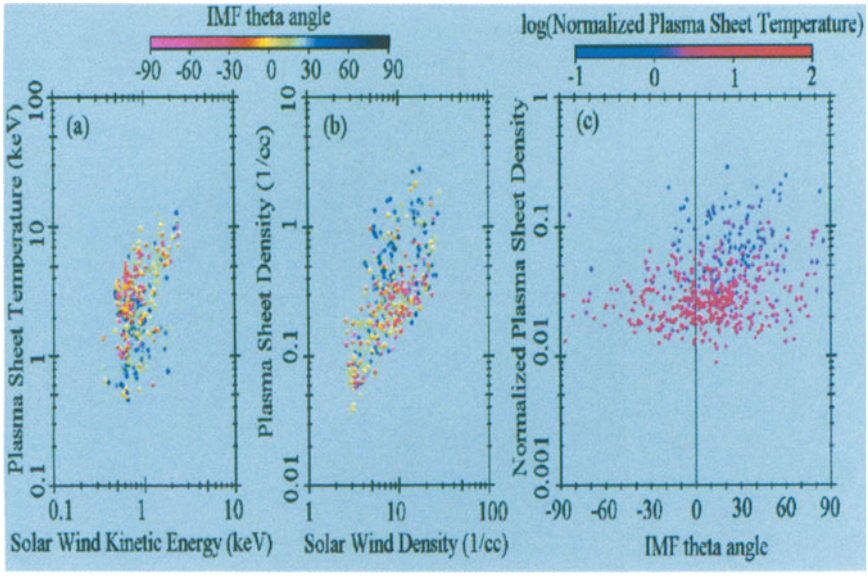

Figure 6. (a) Estimated ion temperature at the neutral sheet plotted against solar wind kinetic energy. (b) Estimated ion density at the neutral sheet plotted against the solar wind density. (c) Normalized plasma sheet density plotted against IMF latitudinal angle. The solar wind parameters are averaged for the same 1-hour interval as the plasma sheet data.

with N = $1, 2, 3, ...48$, we have found that the normalized plasma sheet density becomes most correlated with IMF theta angle for N = $6 - 12$, with a broad peak at N = 9. The normalized plasma sheet temperature is also seen to be most anti-correlated at mostly the same N value. Figure 7 shows the same as Figure 6 but for 9-hours averaged solar wind parameters (N = 9). There are clearer separations between blued and reddish data points in Panels (a) and (b). Panel (c) shows a clear positive correlation between the plasma sheet density and the IMF theta angle for theta $>$ 0. In Panel (c), blued data points appear mostly only when IMF is northward. Since these cases (normalized temperature $<$ 1) are indicative of little heating within the plasma sheet, it is suggested that direct supply of cold-dense plasma to the plasma sheet is operative during prolonged northward IMF periods. In contrast, some heating must intervene for southward IMF periods to make the plasma sheet hot and tenuous.

By plotting the normalized density/temperature for N = 9 against $Y_{GSM'}$, it is found that the plasma sheet becomes denser and colder toward the dawn and dusk edge of the plasma sheet. This is consistent with the idea that the direct supply of cold-dense plasma during northward IMF periods is from the flanks. While the meaning of the best correlation at N = 9 still remains to be discussed, which time

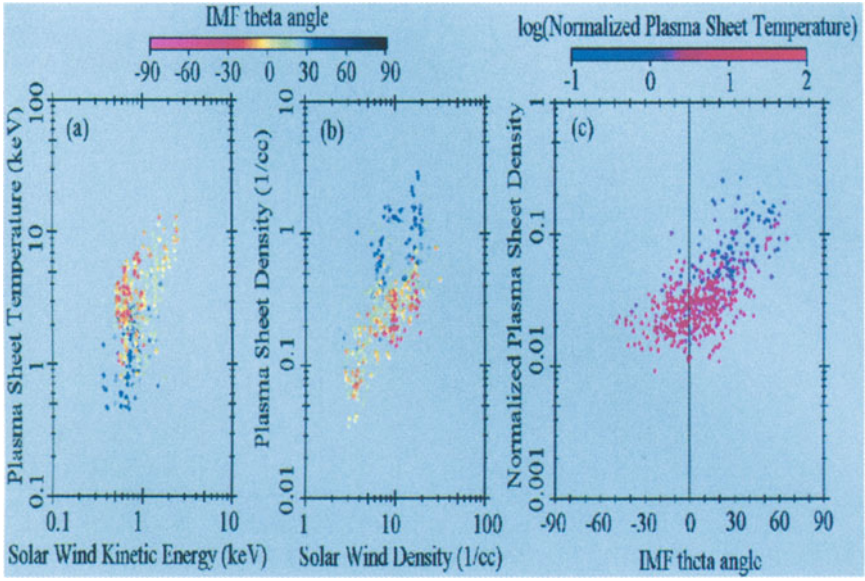

Figure 7. The same as Figure 6 but with the solar wind parameters averaged over 9 hours period.

scale is considerably longer than the characteristic convection time scale of 1-2 hours during a southward IMF period (e.g., McPherron, 1991), a possible interpretation is that it reflects the slow transport from the flanks to the plasma sheet.

It is possible that the flank entry process is equally operative during southward IMF periods but its effect on the plasma sheet status is masked by heating processes in the plasma sheet. We leave this question for a future study that will clarify the dependence of the tail-LLBL structure on the IMF B_z component.

4. Discussion

In this paper, recent studies from GEOTAIL data on the unresolved problem of the structure of the tail-LLBL and the impact of transport across it on the plasma sheet status are reviewed. We have reviewed cases that strongly suggest the cold-dense plasma entry from the flanks can at times be significant to fill a substantial part of the magnetotail. In agreement with our preliminary survey suggesting higher efficiency of the flank entry for northward IMF, the fact that the plasma sheet changes to a cold-dense status as IMF becomes northward is shown by a statistical study. It is further shown that the cold-dense regime occurs most prominently near the dawn

and dusk flanks, which is consistent with the idea of direct supply of the cold-dense ions from the flanks.

Two possible mechanisms for the flank entry have been discussed in Fujimoto et al. (1996b). One is re-reconnection that closes the magnetosheath field lines and adds them to the magnetosphere (e.g., Song and Russell, 1992). Raeder et al. (1995) have shown that broad boundary layers at the flanks are formed by this closing due to high-latitude reconnection in their global MHD model for a long northward IMF interval. The other mechanism is the ion mixing driven by the Kelvin-Helmholtz instability, which adds cold-dense plasma to the closed field lines (e.g., Fujimoto and Terasawa, 1994). It would be worth noting that the first case reviewed in this paper is shown to be affected by the development of the instability (Fairfield et al., 1996). Observational facts that have relevance to this topic are the higher efficiency during northward IMF and the detection of tailward flowing closed flux tubes in the first example. Unfortunately, since both the above processes favor northward IMF condition and do involve tailward closed flux tubes, placing one mechanism above the other is not possible at present. INTERBALL observations at high-latitude (Fedorov et al., 1996) may be useful in identifying the mechanism.

From the studies on the GEOTAIL data, we are able to conclude that in addition to the hot-tenuous plasma supply presumably via the mantle-distant tail route, there clearly is direct supply of cold-dense ions from the flanks to the near-Earth plasma sheet. The latter becomes visible during prolonged northward IMF periods. It is possible that the former is suppressed at the same time. So far as the solar wind source is concerned, the near-Earth plasma sheet is envisaged as the mixture, or the mosaic of two plasmas entrained into the magnetosphere by two different processes. Indeed, the sudden switch from cold-dense to hot-tenuous state seen in Figure 4 and Figure 5 may be indicative a mosaic-like structure of the plasma sheet. It should be noted that not only the switching sources but also localized internal heating processes may contribute to the patchyness of the plasma sheet. It has recently been found that, if a substorm takes place when the spacecraft is in the cold-dense near-Earth plasma sheet (that is, after a long northward IMF interval), the spacecraft does detect hot flowing plasma that has been heated and ejected in the course of an expansion phase, but what is often detected after that is the cold-dense plasma that used to be seen prior to the onset (Asano et al., 1996). The implication is two-folds: It suggests that the heating of plasma associated with an onset occurs in a spatially limited region such as not to affect a large volume of the surrounding stagnant population. It also suggests that refilling of the plasma sheet from a distant tail source during a post-expansion phase (e.g., Hones, 1979), that is, refilling by hot-tenuous plasma, is also spatially limited such that an encounter with hot-tenuous plasma in a post-expansion phase is not always the case.

The limitation that we are confronted with here, however, is that separating spatial structures from temporal effects is not possible with data from a single satellite. The statistical study reviewed in this paper has assumed that data at a point in the plasma sheet represents a global status. While there seems to be much

implication in its present form, a revision in the future may be required to take the possible non-uniformity of the plasma sheet into account. Together with further complications brought about by the ionospheric source, details should become the targets of multi-satellite studies in the future.

Acknowledgements

The authors are grateful to all the GEOTAIL team members. M. F. and T. T. acknowledge stimulating discussion at the ISSI workshop "Source and loss processes of magnetospheric plasma" (convener, B. Hultqvist) held in October, 1996. The key parameter data of WIND were provided by the NASA/GSFC data processing team.

References

Asano, Y., et al.: 1996, 'Appearance of Dense Plasmas Associated with Substorms', in *Proceedings of the Chapman conference on the Earth's magnetotail*, ISAS, Japan.

Baumjohann, W., Paschmann, G., and Cattell, C. A.: 1989, 'Average Plasma Properties in the Central Plasma Sheet' *J. Geophys. Res.* **94**, 6597.

Baumjohann, W.: 1993, 'The Near-Earth Plasma Sheet: An AMPTE/CCE Perspective', *Space Sci. Rev.* **64**, 141.

Eastman, T. E., et al.: 1976, 'The Magnetopause Boundary Layer: Site of Plasma, Momentum and Energy Transfer from the Magnetosheath into the Magnetosphere', *Geophys. Res. Lett.* **3**, 685.

Eastman, T. E., Frank, L. A., and Huang, C. Y.: 1985, 'The Boundary Layers as the Primary Transport Regions of the Earth's Magnetotail', *J. Geophys. Res.* **90**, 9541.

Fairfield, D., et al.: 1996, 'Geotail Observations of the K-H Instability at the Equatorial Magnetotail Boundary for Parallel Northward Fields', submitted to *J. Geophys. Res.*.

Federov, A. O., Zeleny, L. M., and Mukai, T.: 1996, 'Convection during Northward IMF B_z by INTERBALL and GEOTAIL', in *Proceedings of the Chapman conference on the Earth's magnetotail*, ISAS, Japan.

Fujimoto, M. and Terasawa, T.: 1994, 'Anomalous Ion Mixing within an MHD Scale K-H Vortex', *J. Geophys. Res.* **99**, 8601.

Fujimoto, M., et al.: 1996a, 'Plasma Entry from the Flanks of the Near-Earth Magnetotail: GEOTAIL Observations in the Dawnside-LLBL and the Plasma Sheet', *J. Geoelectr. Geomag.* **48**, 711.

Fujimoto, M., et al.: 1996b, 'Plasma Entry from the Flanks of the Near-Earth Magnetotail: GEOTAIL Observations', submitted to *J. Geophys. Res.*.

Hones, E. W., Jr.: 1979, 'Transient Phenomena in the Magnetotail and Their Relation to Substorms', *Space Sci. Rev.* **23**, 393.

Lennartsson, W.: 1992, 'A Scenario for Solar Wind Penetration of Earth's Magnetic Tail Based on Ion Composition Data from ISEE 1 Spacecraft', *J. Geophys. Res.* **97**, 19,221.

McPherron, R. L.: 1991, 'Physical Processes Producing Magnetospheric Substorms and Magnetic Storms', in *Geomagnetism* **4**, Academic Press.

Mitchell, D. G., et al.: 1987 'An Extended Study of the Low-Latitude Boundary Layer on the Dawn and Dusk Flanks of the Magnetosphere', *J. Geophys. Res.* **92**, 7394.

Popielawska, B., et al.: 1996, 'An Imprint of the Quiet Plasma Sheet Structure at the Orbit of VIKING: Magnetosphere without Substorms', in *Proc. of ICS-3*, ESA SP-389.

Raeder, J., Walker, R. J., and Ashour-Abdalla, M.: 1995, 'The Structure of the Distant Geomagnetic Tail during Long Periods of Northward IMF', *Geophys. Res. Lett.* **22**, 349.

Song, P. and Russell, C. T.: 1992, 'Model of the Formation of the Low-Latitude Boundary Layer for Strongly Northward IMF', *J. Geophys. Res.* **97**, 1411.

Spence, H. E. and Kivelson, M. G.: 1994, 'Contributions of the Low-Latitude Boundary Layer to the Finite Width Magnetotail Convection', *J. Geophys. Res.* **98**, 15,477.

Terasawa, T., et al.: 1997, 'Cold-Dense Plasma Sheet during Northward IMF Periods: GEOTAIL-WIND Collaboration', *Geophys. Res. Lett.*, in press.

Traver, D. P., et al.: 1991, 'Two Encounters with the Flank Low-Latitude Boundary Layer: Further Evidence for Closed Field Topology and Investigation of the Internal Structure', *J. Geophys. Res.* **96**, 21,025.

Williams, D. J. et al.: 1985, 'Energetic Particle Observations in the Low-Latitude Boundary Layer', *J. Geophys. Res.* **90**, 5097.

Zwolakowska, D. and Popielawska, B.: 1992, 'Tail Plasma Domains and the Auroral Oval - Results of Mapping Based on the T89 Magnetosphere Model', *J. Geoelectr. Geomag.* **44**, 1145.

Address for correspondence: M. Fujimoto, Dept. Earth and Planetary Sciences, Tokyo Institute of Technology, 2-12-1 Ookayama, Meguro, Tokyo 152, Japan

THE LOW-LATITUDE BOUNDARY LAYER AT THE FLANKS OF THE MAGNETOPAUSE

M. SCHOLER and R. A. TREUMANN
Max-Planck-Institut für extraterrestrische Physik
Garching, Germany

Received January 21, 1997; Accepted in final form May 15, 1997

Abstract. This is a brief overview on what we know and do not know about the low-latitude boundary layer (LLBL) at the flanks of the magnetotail. On the basis of recent observations, simulations and theories we conclude that reconnection is the dominant process in generating the LLBL and its structure probably even under northward IMF conditions. Part of the LLBL always seems to be on open field lines. Possibly the LLBL possesses a double structure with its outer part open and inner part closed. Anomalous diffusive processes cannot sustain the LLBL but provide sufficient diffusivity for reconnection. Strong diffusion is only expected in narrow localized regions and can make the transition to superdiffusion. Kelvin-Helmholtz instability (KHI) is favoured for northward IMF, producing vortices at the tail flanks. Its contribution to efficient mass transport still remains questionable. Coupling of the LLBL to the ionosphere can strongly affect the internal structure of the LLBL, causing turbulent eddies and detachments of plasma blobs as also field-aligned currents and electron heating. The structure and dynamics of the LLBL are affected by field-aligned electric potentials that decouple the LLBL from the ionosphere. Non-ideal coupling simulations suggest that the dusk flank is decoupled, favouring KHI, while the dawn flank is dominated by currents and turbulence.

Key words: Magnetopause – Boundary Layer – Reconnection – Kelvin-Helmholtz-Instability – Diffusion

1. Introduction

Spacecraft observations have revealed the existence of a layer located just inside the magnetospheric boundary at low geomagnetic latitudes, the low-latitude boundary layer (LLBL), which consists of tailward flowing plasma having properties intermediate between those of the magnetosheath and the magnetosphere. It was first observed by Hones et al. (1972) and Akasofu et al. (1973) along the flanks of the geomagnetic tail, but has also since been shown to be intermittently present at almost all local times along the entire dayside portion of the magnetopause. This boundary layer is supposedly important for the transport of magnetosheath mass, momentum, and energy into the magnetosphere.

There is abundant evidence that the LLBL is at times on open field lines, i.e., magnetospheric field lines having one foot in the ionosphere and extending into the magnetosheath. Its formation on open field lines during southward interplanetary magnetic field (IMF) is well understood in terms of dayside reconnection. There is more circumstantial evidence that the LLBL also exists on closed field lines over some portion of the magnetospheric boundary. The thickness of the LLBL increases with increasing distance from the subsolar point (Haerendel et al., 1978)

Space Science Reviews **80**: 341–367, 1997.

and when the IMF is northward (Haerendel et al., 1978; Mitchell et al., 1987). The anti-sunward component of the flow velocity also increases with distance from the subsolar point (Eastman, 1979). While at the flanks of the magnetopause the LLBL exhibits a density gradient normal to the magnetopause, the LLBL at the dayside magnetopause shows a density plateau, and the LLBL is one of several sublayers of the boundary layer (Paschmann et al., 1990; Song et al., 1994).

Several mechanisms have been discussed in the literature as candidates for the formation of the LLBL. These mechanisms can be divided into magnetic reconnection between the magnetospheric and the magnetosheath magnetic fields, impulsive penetration of magnetosheath plasma, and viscous/diffusive mixing at the magnetopause. While impulsive penetration is only expected to be of importance at the dayside magnetopause, the other two mechanisms can also act along the flanks of the magnetopause. Since this review is primarily concerned with the LLBL at the flanks, we will not discuss impulsive penetration, but will review work done on the other two processes and their implications for the LLBL at the flanks of the magnetopause. Recent reviews on this topic can also be found in Lotko and Sonnerup (1995), Miura (1995b), Treumann et al. (1995), and Winske et al. (1995).

2. Reconnection Under Northward Interplanetary Magnetic Field

Nishida (1989) has proposed that when the interplanetary magnetic field (IMF) is northward transient and localized reconnection may occur on the dayside magnetopause and may lead to the formation of the LLBL. Figure 2 schematically illustrates the resulting magnetic field configuration. The reconnection regions are indicated by large dots. In this model the momentum in the solar wind in the magnetosheath is transported into the LLBL directly with the entering plasma and indirectly as the reconnected field lines are pulled by the solar wind plasma. Only those geomagnetic field lines will contain magnetosheath plasma that have been open at some time in the past. Thus, according to this model, the LLBL is an entity of flux tubes which have well-defined boundaries. The blobs observed by Sckopke et al. (1981) are taken as evidence for such well-defined flux tubes.

Magnetic reconnection at high latitudes behind the polar cusps has been proposed by Song and Russell (1992) as a process for the formation of the LLBL. The process is schematically shown in Figure 2 and follows the suggestion of Dungey (1961) for reconnection under northward IMF. A magnetosheath flux tube (thick line), which drapes over the stagnation point, moves relatively slowly with respect to the magnetospheric fields and is likely to reconnect at high latitudes, where the magnetosheath and the lobe field are antiparallel. After reconnection the poleward portion of the flux tube convects tailward with the solar wind flow. In the dayside portion of the flux tube the magnetospheric and the magnetosheath plasmas mix and the flux tube sinks into the magnetosphere. During this process the flux tube length shortens and the diameter decreases, assuming that the flux tube field is the

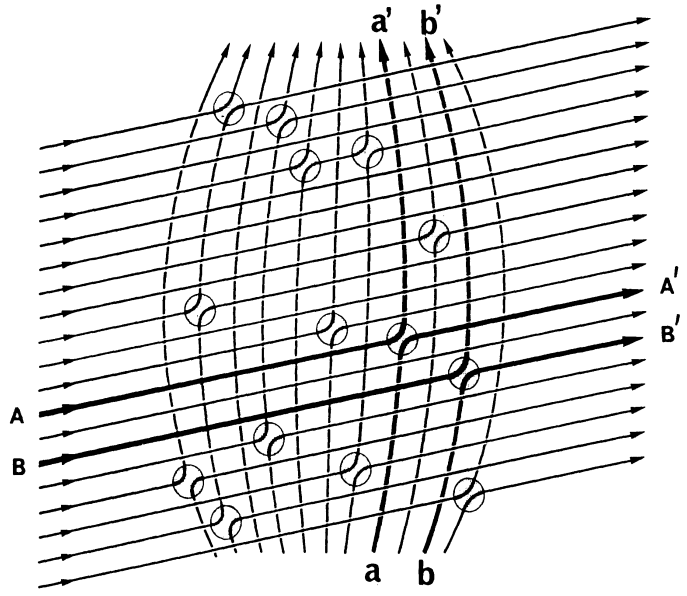

Figure 1. Schematic illustration of the field line configuration at the dayside magnetopause when random reconnection occurs between the interplanetary magnetic field and the geomagnetic field (from Nishida, 1989).

same as the magnetospheric field when it enters the magnetosphere. If the magnetospheric flux tube is initially open, little or no magnetospheric plasma will be found on this flux tube and after rearrangement the density in the flux tube will decrease. The decrease in volume leads to a temperature increase. This flux tube will have a higher pressure than other adjacent magnetospheric flux tubes. Song and Russell (1992) have argued that, due to the requirement for the interchange instability, the newly added flux tube will subsequently only expand azimuthally rather than radially. Radial interchange would lead to a pressure increase and is therefore stable, while azimuthal interchange proceeds spontaneously. The boundary layer would disperse along the magnetopause indefinitely, since in the expansion process thermal energy is converted into kinetic energy and the boundary layer flow is accelerated. Song et al. (1994) have taken into account the drag force of the ionosphere due to field-aligned currents. The motion of the boundary layer drives field-aligned currents that close in the ionosphere; the resulting drag force may eventually stop the boundary layer flow or may balance the driving pressure force, so that the flow moves with constant speed.

Fuselier et al. (1995) have presented evidence that reconnection does not necessarily occur simultaneously as proposed in the qualitative Song and Russell (1992) picture. They identified a magnetosheath boundary layer (MSBL) near the dayside

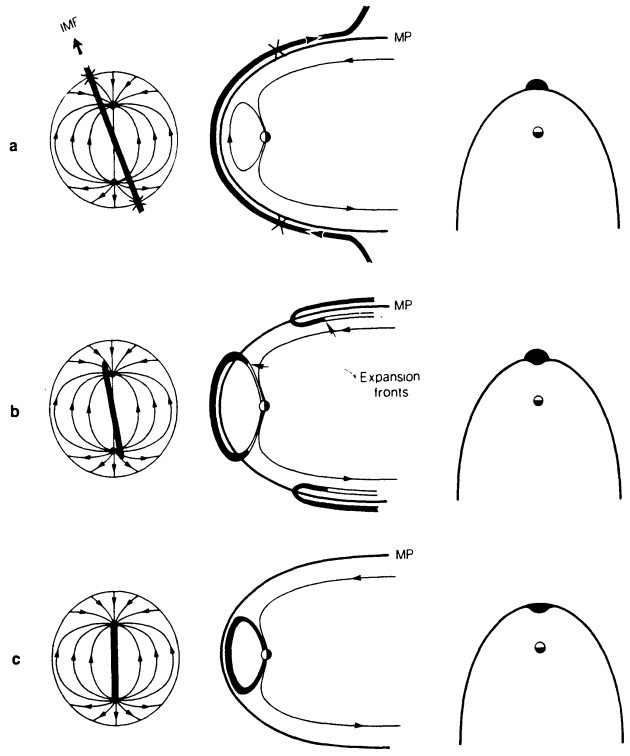

Figure 2. Model for the formation of the low-latitude boundary layer through merging behind the polar cusp with northward IMF. The three views are from the sun, from dusk, and from above the ecliptic plane (after Song and Russell, 1992).

magnetopause at the magnetosheath side of the magnetopause current layer and the LLBL. This MSBL is characterized by unidirectional streaming electrons: one half of the distribution parallel to the magnetic field has the characteristics of the distribution in the nearby magnetosheath (actually in the plasma depletion layer), the other half is similar to the distribution in the LLBL on the Earthward side of the current layer. The existence of such an MSBL suggests that reconnection does not occur simultaneously at both high latitude reconnection sites. Reconnection may be limited to one hemisphere, as sketched in Cowley's (1983) catalog of magnetospheric topology for northward IMF. Reconnection between the IMF and open tail field will convert open tail lobe field lines into open field lines that drape over the dayside magnetopause. These field lines are then carried by the solar wind downstream and can constitute a layer of open field lines earthward of the magnetopause (Crooker, 1992).

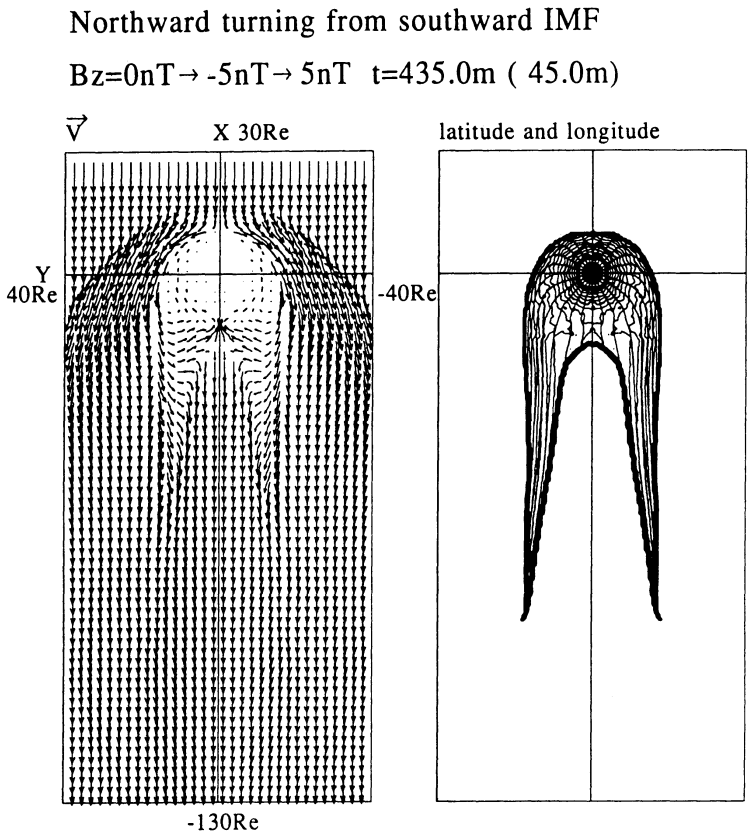

Figure 3. Results from a global MHD simulation (45 min after northward IMF turning). (Left) Flow vectors in the equatorial plane. (Right) Latitude and longitude mapping of magnetic field lines from the ionosphere to their crossing point of the equatorial plane in the tail (from Ogino et al., 1994).

The process of high latitude reconnection and magnetospheric incorporation of newly closed flux tubes should be a persistent feature of global magnetospheric simulations. A number of different groups have performed global MHD simulations of the magnetosphere under northward IMF and we will now present results pertinent to the boundary layer problem. Usadi et al. (1993) presented global simulations for northward IMF wherein reconnection occurs at high latitudes behind the cusps. The magnetic flux from the outer surface of the magnetotail lobes was peeled away like the skin of an onion. The resulting decrease of the magnetic pressure in the lobe led to a dipolelike structure and the magnetotail attained the structure of a tadpole. However, probably because of the limited simulation region, the newly closed flux tubes accumulated at the dayside, so that this simulation effort did not result in a boundary layer. Similar results have been obtained by Fedder

and Lyon (1995). They investigated the asymptotic magnetospheric state after a few hours of steady northward IMF. In this case no open tail lobes were present and no Earth-connected flux was seen tailward of 155 R_E. The simulations resulted in a boundary layer which was mechanically driven: the expansion of the magnetosheath plasma in the newly added flux tubes in response to the sunward-directed pressure gradient and the tailward decrease of the magnetic field strength led to a boundary layer flow. Reconnection after prolonged occurrence of northward IMF was intermittent at high latitudes between closed magnetospheric flux tubes and magnetosheath flux tubes. The boundary layer had a reduced speed relative to the adjacent magnetosheath, but was much larger than the velocity in the rest of the magnetosphere closer to Earth. The observable magnetopause, i.e., the region with the largest magnetic shear, was at the flanks and at high latitudes of the tail outside the open-closed boundary. The region between the magnetopause current sheet and the open-closed field line boundary was a region containing highly stressed, recently reconnected IMF field lines. Since these field lines have a history of having been connected with the Earth, they should contain a mixture of solar wind plasma and magnetospheric plasma immediately inside the current sheet. Fairfield (1993) has actually reported ISEE 3 data from 225 R_E behind Earth during periods of northward IMF, where the spacecraft was intermittently in hot, low-density regions and cooler, denser regions with a density intermediate between the magnetosheath and the magnetotail (plasma sheet). The latter region may correspond to the layer of recently created IMF field lines within the region of large magnetic shear.

While the simulation by Fedder and Lyon (1995) applies to the theoretically interesting ground state for the solar wind-magnetosphere interaction, global simulations by Ogino et al. (1994) and Raeder et al. (1995) are better applicable to the evolution and dynamics of the distant magnetotail after a northward turning of the IMF following prolonged southward IMF. Figure 2 shows results from simulations by Ogino et al. (1994). The left side shows flow vectors in the equatorial plane 45 min after the northward turning of the IMF; the right side shows a latitude and longitude mapping along field lines onto the equatorial plane in the tail. The lines correspond to equatorial crossing points of field lines starting at constant latitude or constant longitude, respectively. The field lines crossing the equatorial plane within the region given by the heavy line are closed. From Figure 2 the convection of newly closed field lines around the flanks of the magnetosphere and in toward midnight can clearly be seen. Richard et al. (1994) have attacked the problem of particle entry under northward IMF by calculating particle trajectories in the Ogino et al. (1994) 3D global MHD model. Particles were launched from the solar wind; they entered mainly near the cusp reconnection regions and formed a LLBL. The particles were subsequently undergoing bounce motion on magnetospheric field lines and drifted behind the terminator into the center of the plasma sheet. Thus these particles would be sufficient to generate a dayside LLBL, but could not generate a boundary layer at the distant flanks of the tail. Although the method of following test particles in fields obtained from MHD simulations is an

important one, care should be taken when these test particles are not suprathermal compared to the plasma in the MHD run: in the MHD simulation the plasma is assumed to be confined to the flux tubes, whereas in the test particle approach the particle is allowed to gradient and curvature drift. The simultaneous problem of cusp reconnection and boundary layer formation can ultimately only be solved by kinetic simulations.

Raeder et al. (1995) also found that the reconnection-produced newly closed field lines at the dayside are swept by the magnetosheath flow along the magnetopause and are stretched along the flanks of the tail. The momentum flux of the magnetosheath is supposedly so large that the field lines become stretched to at least 400 R_E downtail. These stretched field lines constitute a tailward-flowing layer with closed field lines, i.e., with positive B_z, while there may still exist negative B_z near the tail axis from earlier or still ongoing near-Earth reconnection. This tail flank boundary layer (TFBL) seems not to be driven by a process similar to the one proposed by Song and Russell (1992) where thermal energy is converted into dynamic energy; rather, the momentum of the magnetosheath flow in a newly produced closed flux tube propels the flux tube downstream. Solar wind flow energy is converted by this process into electromagnetic energy by the stretching and twisting of the flux tubes. Recently, Raeder et al. (1997) have directly compared results from the global magnetospheric MHD simulations with observations of plasma and magnetic field in the magnetotail by GEOTAIL. The observed plasma sheet flow at about 50 R_E in the magnetotail was tailward while the magnetic field was northward. The WIND spacecraft monitored the solar wind and IMF upstream of the bow shock. The IMF was northward with a substantial B_y component. According to the simulations for these solar wind input parameters, high latitude reconnection also leads in this case to closed dayside flux tubes, which are carried by the momentum of the magnetosheath plasma downtail.

3. The Low Latitude Boundary Layer on Open Field Lines

There is ample evidence for the existence of a low latitude boundary layer on open field lines during southward IMF. Gosling et al. (1990) found accelerated beams of cold ions sporadically within the LLBL. Because of the low temperatures and the compositional abundance in these beams they must ultimately be of ionospheric origin. Gosling et al. (1990) dismiss reflection at the magnetopause but favor acceleration by the large electric drift of recently reconnected field lines. Fuselier et al. (1991) analyzed He^+ and He^{2+} ion distribution functions near the magnetopause and found that inside the magnetopause the cold ion beam distribution and the transmitted magnetosheath distribution could be transformed by a velocity tangent to the magnetopause such that the resulting distributions were field-aligned and had a flow velocity of the order of the local Alfvén speed. Smith and Rodgers (1991) found D-shaped field-aligned phase space distributions of magnetosheath plasma

earthward of the magnetopause. The observations by Fuselier et al. (1991) and Smith and Rodgers (1991) are consistent with the predictions by Cowley (1982) from a kinetic description of reconnection.

Recently Lockwood and Hapgood (1997) analyzed a reconnection event (flux transfer event) in terms of the Hapgood and Bryant (1990) transition parameter. This parameter is based on electron temperature and density behaviour near the magnetopause. Lockwood and Hapgood (1997) could show that in a specific case (flux transfer event) the transition parameter orders magnetopause data because magnetic reconnection generates newly-opened field lines which coat the boundary. Since the transition parameter quite often orders magnetopause data Lockwood and Hapgood suggest that some newly opened field lines coate the magnetopause most of the time and that these form most of the LLBL. An explanation in terms of reconnection is of course not the only possibility to interpret the relation found between density and pressure. As discussed in the previous section, also under northward IMF recently reconnected and open field lines may be draped around the tail magnetopause and may constitute part of the LLBL. It is an open question to what extent the LLBL is on open and on closed field lines.

4. The Problem of Diffusion

Because of the mutual topologies of the draped IMF and the warped magnetospheric field, there is probably always reconnection somewhere at the magnetopause, leading to free plasma entry. Only when the sheath magnetic field is purely northward may diffusion be assumed to explain the filling of the LLBL at the flanks.

One generally expects that the diffusion would be strongest near the nose of the dayside magnetopause because there the gradients in both density and magnetic field as well as the gradient in plasma temperature are highest. These gradients become much weaker towards the flanks of the magnetosphere. Since classical viscosity is clearly ruled out, diffusion is usually based on gradient driven non-classical processes, drift and current instabilities. These should be weaker or marginal at the flanks.

The experimental investigation of the anomalous diffusion process has not given support to theories based on diffusive particle transport from the solar wind into the LLBL. Early estimates by Eviatar and Wolf (1968), Tsurutani and Thorne (1982) and Gendrin (1983) gave sufficiently high diffusivities for diffusion to be efficient enough to feed the LLBL during periods of northward IMF. But more precise analyses of wave observations by Tsurutani et al. (1989) and Treumann et al. (1991) showed that the wave intensities in the transition layer are not high enough, implying that the instabilities are not strong enough to yield the required anomalous collision frequencies. Figure 4 shows a summary of the dependencies of the diffusion coefficients $D(|\delta E|^2)$ on the intensity of the average electric wave field. In this log-log representation the diffusion coefficients are linear functions of

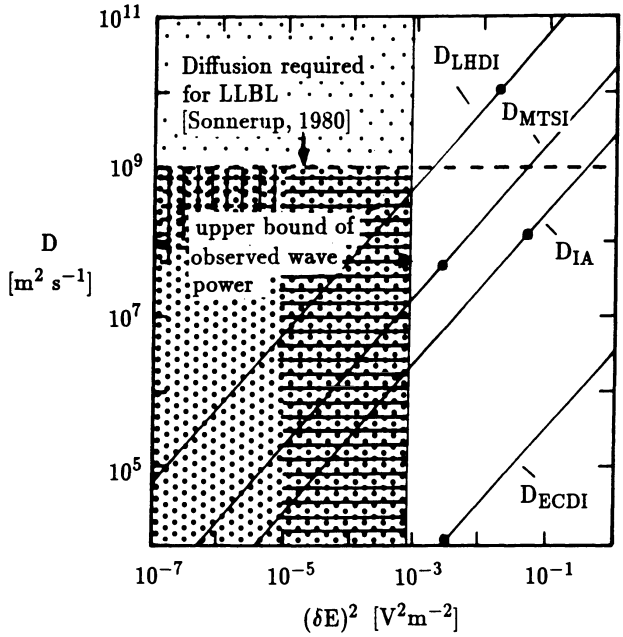

Figure 4. Microscopic diffusion coefficients in the LLBL based on anomalous collision frequencies caused by various drift instabilities: the electron cyclotron drift instability ECDI, the ion acoustic current driven mode IA, the modified two stream instability MTSI, and the lower hybrid drift instability LHDI (after Treumann et al., 1991).

the wave intensity. The horizontal line at $D \approx 10^9$ m^2s^{-1} is the canonical value of the diffusion coefficient required for the filling of the LLBL [see e.g., Sonnerup (1980), who found that only by assuming a value that high he was able to reproduce the width of the LLBL in his model of the magnetopause and boundary layer]. Not entirely surprisingly this value turns out to coincide with the Bohm diffusion coefficient in the LLBL, the presumably highest value classical diffusion can reach in a plasma. The vertical line at about $|\delta E|^2 \approx 10^{-3}$ V^2m^{-2} is at the extreme upper limit of electric-wave intensities ever measured in the LLBL gradient regions (Treumann et al., 1991; Cattell et al., 1995). The region left to this line and below the Bohm-Sonnerup limit corresponds to realistic values of the diffusion coefficients. For acceptable wave intensities none of the diffusion coefficients comes close to the Bohm-Sonnerup limit. Hence, under most conditions diffusion based on anomalous collision frequencies is unable to build up the LLBL. The most promising positive exception is the lower hybrid drift instability (LHDI). Sporadic, very high wave intensities in this wave mode may cause strong plasma injection. But the reduction in the density profile produced in the diffusion should keep the instability and diffusion at their marginal values. Note that the theoretical quasilinear saturation limit of the instability (full dots) for the LHDI even exceeds the Bohm- Sonnerup diffusion limit by an order of magnitude. For

the other wave modes these limits are generally higher than any measured wave intensity, indicating that the available nonlinear theories grossly overestimate the saturation amplitudes. The particular case of the LHDI is of interest because it may suggest that wherever the LHDI is effective in transport across the magnetopause current layer it will be strong enough to deplete the density profile so much that a marginally stable state will be readily reached with flat profiles and marginally but still high wave intensities near the lower hybrid frequency. Theoretically highest diffusion coefficients could be twice the Bohm value. But this will quickly reduce to the marginal state.

A statistical analysis of the wave intensities in the vicinity of the magnetopause performed by Treumann and Bauer (1996) and reproduced in Figure 4 shows the electric wave intensities averaged over a large sample of AMPTE/IRM magnetopause crossings. The low (high) shear wave intensity maximum ($< 10^{-7}$ V^2m^{-2}) is at the sheath-LLBL (inner edge) transition and yields extremely small average diffusion. Based on these observations, diffusion can only be *marginally high in microscopic localized regions*, presumably LH density cavitons which escape the measurement but have theoretically been predicted to exist (Shapiro et al., 1993, 1995). Formation of density cavities by other processes as ion holes, large-amplitude ion sound waves, low-frequency ion-beam driven waves and others may also have the effect of wave trapping, anomalous diffusion and acceleration. The position of the wave maximum in Figure 4 may provide evidence for the last closed magnetic field line as is frequently believed. Indeed, it is possible that the magnetopause is partly a tangential discontinuity, with reconnection taking place at a remote location. But this may just imply that the inner edge field line is connected to the reconnection site, as suggested by Lockwood and Smith (1994). On the other hand, this conclusion is uncertain as long as it cannot be supported by other evidences. In particular, it is surprising that for the high shear cases in Figure 4 the intensity maximum is at the inner edge of the LLBL and not at the magnetopause where it is believed that reconnection takes place. This may imply that the maximum intensity is caused by something else than reconnection, for instance simply by the density gradient which is steepest at the inner edge for high shear and at the magnetopause for low shear. Hence, it cannot be excluded that the Lockwood-Smith picture is true and that the magnetopause crossing in low shear cases is simply at a position where the magnetopause was a piecewise closed fraction of a tangential discontinuity and reconnection took place at a remote location. The low value of diffusivity determined from the intensity maximum seems not to contradict this claim.

Numerous numerical simulations of diffusive LLBL formation have been carried out by Berchem and Okuda (1990), Cargill and Eastman (1991), Drake et al. (1994), Gary and Sgro (1990), Winske and Omidi (1995), Omidi and Winske (1995), Winske et al. (1995), and others. All these simulations demonstrate that in two dimensions the magnetopause current layer is erased by LHD instabilities and widens under the action of the LHDI. But, as shown by Winske et al. (1991), its

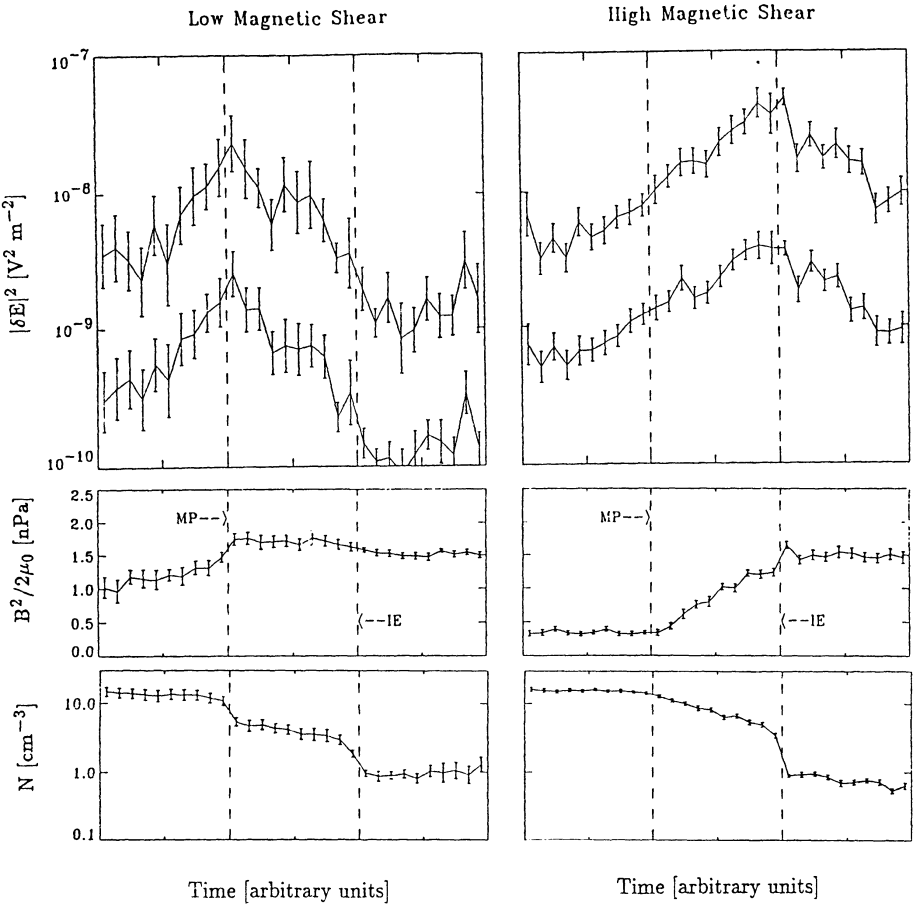

Figure 5. Superposed epoch representation of ensemble averaged wave intensities in the magnetopause transition as function of position relative to the magnetopause current layer for low and high shear conditions. The abscissa is the time axis corresponding to the crossing of the boundary layer by the spacecraft. The left vertical line is at the position of the nominal magnetopause current layer, the right vertical line is at the position of the inner edge of the LLBL. The frequency range contains the lower hybrid frequency. The upper curve is the ensemble averaged wave peak value within 1s of measurement, the lower the 1s average of the wave intensity. The maximum in the wave intensity is found at the current layer for low and at the inner edge of the LLBL for high shear.

spread is only slightly more than an ion gyroradius not comparable to the width of the LLBL. The initial diffusion is fast, about 30% of Bohm diffusivity, but outside the steep gradient region quickly drops to low values. Some more energetic particles diffuse over a larger distance and the diffusion coefficient calculated from the arrival time of the first of these particles is Bohm-like. But estimates using the shape of the density profile (Treumann et al., 1992) fix it at a value one order of magnitude below Bohm-Sonnerup and suggest that the first, fast particles are just the resonant ones, the phase space volume occupied by which is negligible, as has been shown by Dum (1996).

Anomalous diffusion is not the only way out of the diffusion paradox/dilemma. It has been argued recently by Treumann and Bauer (1996) that "superdiffusion" may exist in plasmas containing nonthermal (generalized Lorentzian or κ) electron distribution functions. Traver et al. (1991) and Christon et al. (1988) have occasionally measured such distributions in the magnetosphere, and Lin (1997) reported their existence in the solar wind. Distributions like these resemble the probability distributions which Shlesinger et al. (1993) use in the description of Lévy flight interactions. Recently, Treumann (1997) has developed a theory of superdiffusion based on the Lévy flight model. The super-diffusion coefficient approaches the Bohm limit. The most interesting fact is that the diffusion becomes not only strong but in addition is time dependent. Consequently, the density profiles loose their diffusive shapes. However, super-diffusion is heavily dependent on the presence of long-range turbulence in the plasma which causes non-stochastic interactions between the particles or the particles and waves. It can thus be expected only in regions of high levels of turbulence.

According to Mace et al. (1997) the thermal fluctuation level of plasma waves in a plasma containing κ distributions is increased by several orders of magnitude over the usual fluctuation level. The reason for this increase can be found in the high energy tail of the distribution function. Though the tail particles themselves run away, the high fluctuations caused by them scatter the thermal bulk plasma component at a much stronger level thereby increasing the collision frequency. At the magnetopause this factor can be as high as 10^{4-6} (Treumann and Bauer, 1996), such that the nonthermal collision frequency becomes of the order of $\nu \sim 0.1 - 10$ Hz, which is a substantial fraction of the lower hybrid frequency, $f_{lh} \approx 50$ Hz. In such extreme cases diffusion becomes close to Bohm-Sonnerup and may cause increased plasma inflow. But again, since these effects are restricted to the regions of high levels of plasma turbulence which may cause the distribution function to deviate from the Maxwellian and become a κ distribution, one expects that the super-diffusion will be restricted to localized regions only.

Anomalous diffusion based on low frequency magnetic fluctuations has been ruled out (Tsurutani and Thorne, 1982). If the low frequency waves measured near the hydrogen ion cyclotron frequency f_{ci} by Rezeau et al. (1993) are indeed kinetic Alfvén waves, in particular kinetic Alfvén solitons, then they are another candidate, as suggested by Lee et al. (1994), Lotko and Sonnerup (1995) and more recently on firmer grounds by Johnson and Cheng (1997). Figure 4 shows magnetic power spectra from IRM transitions of the LLBL. The f_{ci} emission is the sole property of the inner edge (IE) of the LLBL probably caused by the electromagnetic ion-cyclotron instability when the cold LLBL plasma mixes into the hot ring current protons. The LLBL spectra exhibit an unstructured power law ($\propto f^{-2.4}$) with higher intensities in the right- and left-hand polarized modes than in the compressive part, indicating scale-invariant, weakly compressible magnetic turbulence below $f < f_{ci}$. The integrated intensities of these waves are not overwhelmingly high but appreciable. It is not known, how far the spectrum extends towards low frequen-

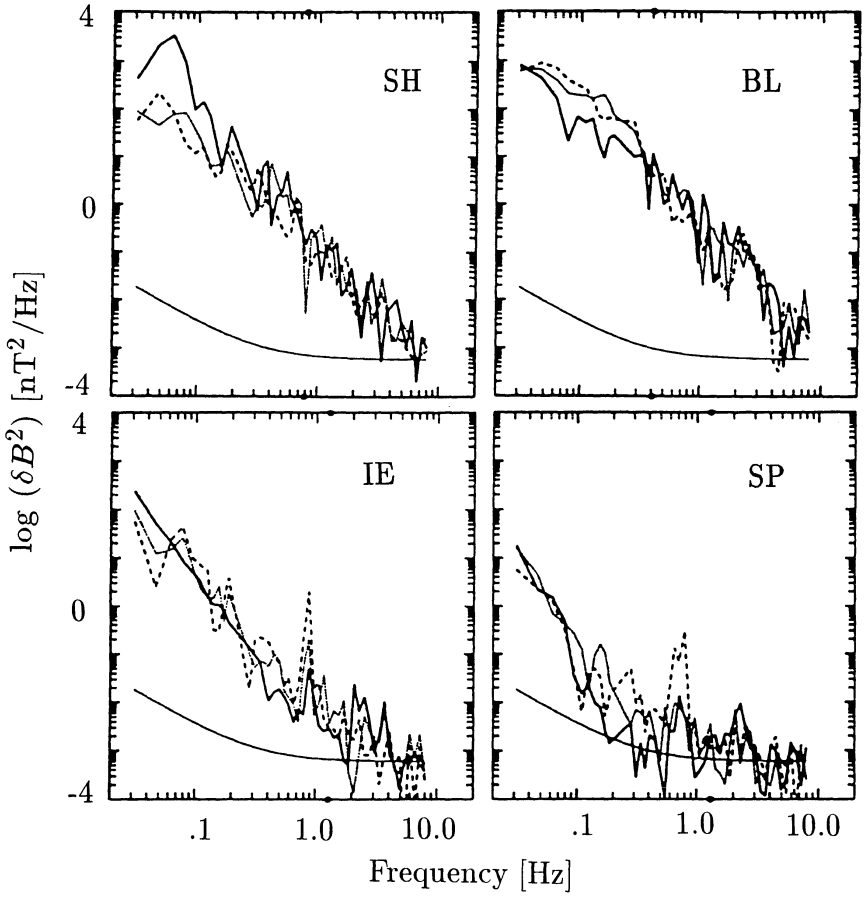

Figure 6. Average IRM magnetic low frequency power spectra in the magnetopause transition as function of frequency (after Treumann et al., 1995). The ion cyclotron line is found only in the LLBL-sphere transition part. Otherwise, the LLBL spectra have structureless power law behavior with low compressive part and about equal left and right circularly polarized intensities (dotted: left polarized, thin: right polarized, heavy line: parallel polarized).

cies. But the total wave amplitudes may be as high as 1 nT and may contribute to transport. However, since for these low frequencies the first adiabatic invariant is conserved, diffusion can only be caused by scale invariant turbulence.

Scale invariance implies that left- and right-handed magnetic vortices exist on all scales and hence mix and overlap and stochastically reconnect. It has been realised that a fluctuating magnetic field lacks a well-defined identity and may migrate across the turbulent region. Percolation theory (Isichenko, 1992) provides the basic physics. This theory has been applied to the magnetopause by Galeev et al. (1986) and Milovanov and Zelenyi (1995). An early estimate of the geometric diffusion coefficient given by LaBelle and Treumann (1988) yielded a value close

to Bohm diffusion. Milovanov and Zelenyi (1995) have shown that inclusion of finite-ion Larmor radius effects even increases this type of diffusion. In this model the stationary LLBL for northward IMF should resemble a mixture of many overlapping magnetic islands forming channels (wormholes) where field lines or plasma can locally migrate. The magnetic channels have the properties of magnetic holes as discovered by Lühr and Klöcker (1987) in the magnetic field and Treumann et al. (1990) in plasma waves at the magnetopause. Sonnerup and Guo (1997), solving the two-dimensional Cauchy problem for the internal magnetic structure of the tangential discontinuity magnetopause using IRM data, found both islands and wormholes in the transition region.

5. Kelvin-Helmholtz Instability

The magnetopause and LLBL are regions of fast shear flows. The velocity shear is particularly strong at the flanks of the magnetosphere with the anti-sunward flow velocity in the adjacent magnetosheath presumably reaching supermagnetosonic values and the general magnetospheric convection flow being in sunward direction. Such configurations are traditionally unstable with respect to the Kelvin-Helmholtz instability (e.g., Chandrasekhar, 1961). This instability causes convective growth of a surface wave leading to undulations of the magnetopause and in the LLBL and is believed to contribute to momentum exchange and possibly also mixing between the sheath and magnetospheric plasmas. In the framework of magnetohydrodynamic theory the KHI provides merely momentum transport since it is a macroinstability. The electrons are frozen to the magnetic field and the ions follow them via the ambipolar electric field. In order to obtain mass transport across the magnetic field, some mechanism must break off this siamesian twinning relationship between particles and field. Until today it is not known of what kind such a mechanism would be as long as one is not leaving the fluid dynamic picture and does not refer to microinstabilities causing diffusion or to reconnection driven by the KHI. Both of these are possible, however, but on the cost of assuming that the KHI generates short scale vortices of the order or shorter than the ion gyroradius and thus violates the fluid picture. Below we will comment on simulations which indicate some mass transport.

Experimental evidence for the KHI has been reported by Ogilvie and Fitzenreiter (1989), Sckopke et al. (1981), Takahashi et al. (1991) and others. Figure 5 shows the model of the near-dayside LLBL inferred by Sckopke et al. (1981) from ISEE observations. This event had positive and negative IMF B_z-components. Its transition region is composed of the non-transparent magnetopause and an oscillating LLBL attached to its inner part that is driven by the velocity shear and evolves into traveling vortices (as shown in the equatorial section of the magnetosphere). At the dayside obviously these vortices convect tailward with the general sheath flow direction. Note that this model implies mass or momentum transport at the

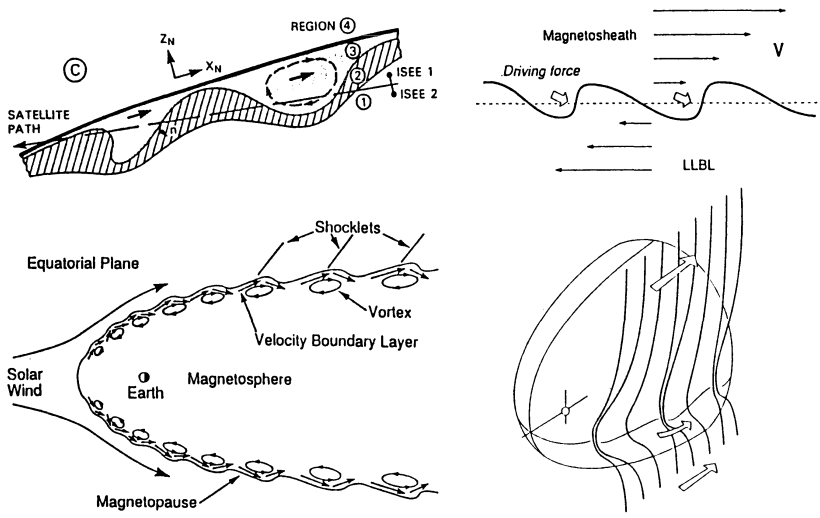

Figure 7. Model of LLBL undulations caused by the Kelvin-Helmholtz instability inferred from two-spacecraft (ISEE 1 & 2) observations (upper left, Sckopke et al., 1981) with a smooth undistorted magnetopause and oscillating LLBL. Regions 1-4 denote sphere, inner and outer LLBL, and sheath, respectively. Below: The corresponding equatorial section of the magnetosphere as inferred from MHD simulations (Miura, 1992). Upper right: Observed driven KH-vortices and (below) a possible magnetic driver model (Chen et al., 1993).

inner edge of the LLBL only! But as shown by Miura (1992, 1995b) and Thomas and Winske (1991, 1993) this may be misleading because any vortices generated at the magnetopause by the external shear flow will be readily transported into the deep LLBL and may have distorted the observations. Ogilvie and Fitzenreiter (1989) found, checking the KHI condition, that KHI can indeed evolve at the inner edge of the LLBL. Another check of the KHI criterion has been provided for a large sample of magnetopause crossings by Seon et al. (1995) at the far ($\sim$ 30 R_E) dawn magnetopause flanks. They found that the entire magnetopause becomes unstable here for high solar wind velocities independent of the IMF direction while for low speeds the excursions of the LLBL are non-oscillatory and rare. However, the growth rate of the KHI is close to marginal, implying nonlinear saturation. During an extended interval of northward IMF, Chen et al. (1993) found that at the dawn flank of the magnetotail the entire magnetopause-LLBL system oscillated at a $\sim$5 min period with tailward directed wave vector. The wavelength was between 5-15 R_E, and the wave form was found to be non-sinusoidal, indicating steepening or driving, with an amplitude of 10% of the wavelength. The shape of the oscillation suggests some driver mechanism (see Figure 5). For strong compression of the magnetosphere, Takahashi et al. (1991) reported regular short-wavelength 50 s-period oscillations generated in the LLBL.

The interesting question is whether and to what degree the KHI contributes to transport (momentum, mass mixing) across the magnetopause. So far this question

has not been answered from observations. Also, the many numerical simulations performed give only ambiguous results. Miura (1982, 1984, 1992, 1995a, b) used a periodic (and hence somewhat unrealistic) compressible ideal 2D-MHD simulation scheme. KHI increased up to saturation forming large but non-coalescing vortices leading to broadening of the velocity transition layer. The broadening factor depends heavily on the direction of the magnetic field and is largest ($\sim$ 3 times the initial width) for northward IMF, dropping to about $\sim$ 1.8 for magnetic shear angles $\gtrsim 60^\circ$ (Miura, 1995a). The broadening suggests formation of a velocity boundary layer of rather too narrow width. Clearly, KHI provides momentum transport from the sheath to the LLBL. Steep profiles in the fluid momenta are caused at the boundaries of the vortices by nonlinear steepening which resembles shocklets. Of course, these fluid simulations are realistic only as long as the steepening is of a scale considerably longer than the ion gyroradius r_{ci}. Miura (1982) argued that in the steep field and density gradients anomalous viscosity and dissipation arise from anomalous magnetic stress and can be as large as $\gtrsim 0.03 r_{ci} v_{\mathrm{th}i}$, a comparably high viscosity. Wu (1986) challenged this result by performing a convective nonperiodic simulation. Both cases, parallel and perpendicular flow, are unstable with coalescing vortices, but the instability grows only in the far tail and is not important at the near-Earth flanks. Similar simulations by Manuel and Samson (1993), applying nonperiodic in- and outflow, yield faster convective growth, turbulent boundary layers and transport of momentum and energy from the sheath into the LLBL. The LLBL widens towards the flanks by a factor of $\sim$ 6, somewhat larger than Miura's results. As a consequence, these authors, for realistic LLBL conditions estimating the Reynolds stresses in the same way as Miura (1982), obtain an enormous viscosity of $\gtrsim 10^{10}$ m^{2}s^{-1}. They also find mass transport which in the fluid model is difficult to explain. This raises doubts as to the validity of their simulations. Recent 2D fluid simulations performed by Huba (1994, 1996) include Hall-MHD (Huba, 1994) and finite Larmor radius (FLR) (Huba, 1996) effects. Inclusion of the Hall term causes an asymmetry in the vortices produced by the KHI at the dawn and dusk flanks of the magnetopause as well as also enhanced momentum transport. The inclusion of FLR effects taken into account in the anisotropic ion stress tensor results in an anisotropic evolution of the vortices, generation and detachment from the vortices of plasma blobs and thus bulk mass transport, and more complicated nonlinear evolution leading to turbulent mixing. The anisotropy results from the dependence of the nonlinear evolution on the vector product between the diamagnetic ion drift and the vorticity with the latter being of different signs at the dawn and dusk flanks (see Figure 5). The transport of blobs is from the high- into the low-density region (sheath to LLBL), but not vice versa. The physical mechanism, if realistic and not caused by numerical residual resistivity, is not entirely clear. The evolution of the KHI vortices would, in the nonlinear stage, result in some kind of interchange between flux tubes. FLR effects may indeed resemble some kind of quasi-gravitational effect which may affect a heavily mass loaded flux tube

to undergo interchange with a lighter one. Investigation of this effect and finding the appropriate nonlinear equations is an interesting but unresolved problem.

The results of the FLR simulation resemble those of recent hybrid simulations performed by Thomas (1995), who also found blob formation, possible dawn-dusk asymmetries and seemingly also mixing. Another important hybrid simulation has been presented by Terasawa et al. (1992) and extended by Fujimoto and Terasawa (1994), who showed that, in a massless electron fluid with particle ions, the nonlinear evolution of the KHI on time scales longer than the vortex roll-up time leads to scattering of ions deep into the LLBL. If realistic, this would imply fast mass transport in hybrid simulations of the KHI. Such simulations treat the electrons as a fluid, usually a massless fluid which is frozen to the magnetic field. The mass transport should in this case be entirely due to deviation of the ion motion from that of the electrons. One expects that this will be possible only for a few nonthermal ions in the tail of the distribution function having sufficient energy to resonate with the smallest vortices produced in the high phase velocity of the KHI and therefore should not be an important effect. Thus mass transport should be negligible. The amount of transported mass found in the simulations seems to be much higher, however. The authors propose that the physical mechanism is chaotic ion scattering at the fluctuating electromagnetic fields connected with the nonlinear evolution of the KHI, a process which has not yet been clarified theoretically. This finding, if confirmed, suggests that KHI at the flanks of the magnetopause might be more important for particle transport than generally believed. Solution can be expected from two sides, either an appropriate nonlinear kinetic treatment or a full particle simulation. Kinetic treatments are not available yet.

A 2D-full particle three-velocity simulation has recently been reported by Wilber and Winglee (1995). This simulation is promising as a first step into a more precise kinetic picture of the KHI at the magnetopause flanks. The main result, which Wilber and Winglee (1995) obtain, is that the nonthermal differences in the motions of electrons and ions may lead to plasma mixing and transport even in the KHI, which otherwise is not included in MHD simulations. Discrete intense current layers are formed at steep gradients confirming the fluid simulations of Miura (1982) and extending them to narrower scales. The plasma generates tongues which penetrate the field region and may decouple from the plasma source region, which in this case is the magnetosheath. In addition there are asymmetries between the dawn and dusk sides of the magnetosphere with plasma penetration stronger on the dawn side. The reason is found in the differences of the electron and ion dynamics on both flanks. One may conclude from these simulations that the microscopic dynamics of the plasma has a strong effect on the KHI causing plasma mixing which is not contained in any of the fluid dynamic treatments.

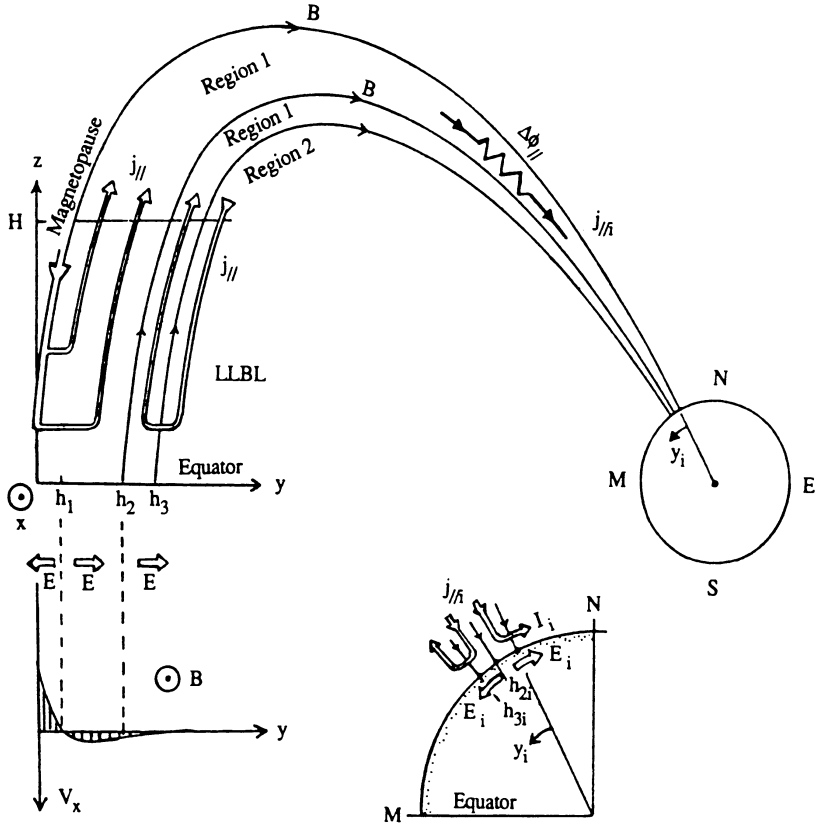

Figure 8. Schematic drawing of the dawnside low-latitude boundary layer and its coupling to the auroral ionosphere, including a field-aligned potential drop $\Delta\Phi_{||}$. Pedersen currents and electric fields in the ionosphere are shown in the insert (from Phan et al., 1989).

6. Viscous Boundary Layer: Coupling to Ionosphere

The plasma motion in the LLBL is coupled to the ionosphere, through field-aligned currents (FACs), which in turn has implications for the momentum balance in the layer. The motional electric field in the layer maps more or less along geomagnetic field lines to the ionosphere where it drives perpendicular Hall and Pedersen currents. When the divergence of the ionospheric perpendicular currents is non-zero FACs that flow along the closed geomagnetic field lines arise (region 1 currents). Because of the hemispherical symmetry these currents close as perpendicular currents in the LLBL where they produce a $\mathbf{j} \times \mathbf{B}$ drag force impeding the plasma motion. Sonnerup (1980) developed the first one-dimensional steady state model for a viscous slab-type LLBL. In the Sonnerup model the ionospheric drag is balanced by the viscosity in the boundary layer, which couples the boundary layer flow to the magnetosheath flow. Figure 6 shows a view from the sun on the dawnside

boundary layer and its coupling to the ionosphere, including a field-aligned potential drop. The boundary layer occupies a region $\mid z \mid < H$ in which the plasma velocity $v_x(y)$ is shown. Pedersen currents and electric fields in the auroral ionosphere are shown in the insert. The drag produced by the ionosphere in the LLBL depends on the total ionospheric Pedersen conductivity, the magnetic field intensity in the ionosphere relative to the intensity in the LLBL, and the magnetic field mapping factor, which accounts for the divergence in the flux tube dimensions (the ratio of a length segment in magnetic local time in the ionosphere to its mapped length segment in the streaming direction in the LLBL). The Sonnerup (1980) model has in the meantime been considerably extended: the model showed that the FAC generated by the LLBL dynamo must be limited by a field-aligned potential if the ionospheric signature is to match observations. Lotko et al. (1987) have allowed for field-aligned potentials by including a conductance law to describe the relation between field-aligned currents and field-aligned potential drops. In these models the magnetic fields induced by the FACs were not included. Phan et al. (1989) have developed a self-consistent one-dimensional model of a viscous LLBL in which the magnetic field deformation in the layer by the currents is included. It is shown that the field lines in the LLBL take on a parabolic shape with the vertices pointing in the downstream direction. Such a tailward distortion has been reported by Eastman et al. (1985) and may impede the Kelvin-Helmholtz instability. The field line curvature is greatest at the magnetopause edge of the layer and vanishes at the magnetospheric edge. The Phan et al. model is, like the Sonnerup (1980) and Lotko et al. (1987) model, one-dimensional in the sense that it does not allow for variations of the layer in the flow direction but only in the direction normal to the magnetopause.

Recent new developments and improvements of the Sonnerup (1980) model of the LLBL-ionosphere interaction include the models by Drakou et al. (1994) and by Wei et al. (1996). The model by Drakou et al. (1994) is a 2 D model which self-consistently determines the magnetic field change by the currents, like the Phan et al. model, but allows for variations in the layer streaming direction (x) parallel to the magnetopause. It should be noted that in this model entry of magnetosheath plasma into the LLBL is assumed to be at the dayside and not along the flanks; along the flanks the layer is viscously driven by the magnetosheath flow. The model describes the increase of the field-aligned region 1 current density with magnetic local time (two hours before and after noon, Iijima and Potemra, 1978), and the increase of latitudinal width of the FAC system with increasing longitudinal distance away from local noon. The latter is due to viscous entrainment of magnetospheric plasma in the equatorial plane to participate in the tailward flow of the dense LLBL. Wei et al. (1996) have extended the Drakou et al. model by allowing for a field-aligned potential drop and by including constant magnetosphere-ionosphere mapping factors. The model correctly predicts the increase of the width of the FAC channel in the ionosphere with local time, and results in a field-aligned potential drop of up to 3 keV.

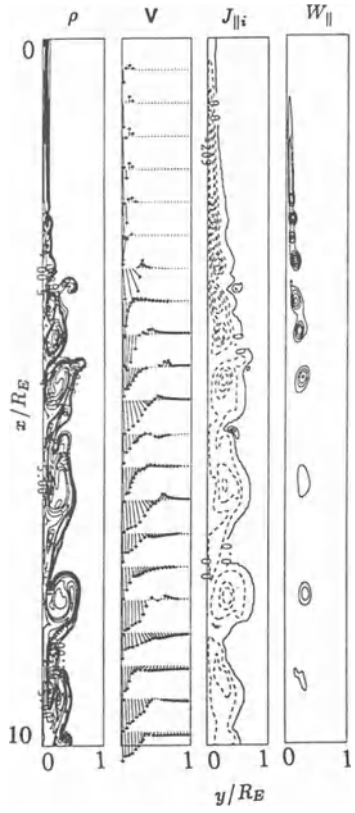

Figure 9. Contour plot of plasma density, vector plot of flow velocity in the magnetosphere, contour plot of field aligned current density, and contour plot of field-aligned power density for a postnoon boundary layer simulation (from Wei and Lee, 1993).

Plasma transport across the magnetopause has been included in a viscous model of LLBL-ionosphere interaction by Wei and Lee (1993). A field-aligned potential is allowed to accelerate electrons parallel to the field, and the ionospheric Pedersen and Hall currents are allowed to be enhanced due to precipitating electrons in the upward FAC region. Plasma transport across the magnetopause is assumed to be diffusive; this diffusive transport is incorporated in the model by a constant velocity v_y of the order of 2-10 km/s normal to the model magnetopause boundary. The tangential velocity at this boundary is kept at its magnetosheath value. It turns out that the driving of the plasma flow in the boundary layer leads to the formation of Kelvin-Helmholtz vortices that grow to large size as they are convected tailward. The vortices lead to localized current flows into or out of the polar ionospheres. The competing effect of the formation of the vortices in the boundary layer and

dissipative decay of the vortices by the ionospheric conductivity leads to the formation only in limited regions. The enhanced conductivity in the postnoon auroral oval due to the upward FACs allows strong vortex formation and correspondingly localized regions of large FAC densities. The enhanced regions of the field-aligned power density are associated with auroral bright spots resembling beads or pearls (Lui et al., 1989). Figure 6 shows contour plots of the plasma density, vector plot of the flow velocity, contour plots of the field-aligned current density and contour plot of the field-aligned power density for the postnoon boundary layer simulation. The subsolar point at $x = 0$; $y = 0$ is the location of the magnetopause.

7. Summary

Observations and simulations both overwhelmingly support the view that reconnection is the dominant process in the formation and maintenance of the LLBL, even for northward IMF conditions. Then reconnection proceeds at high latitudes or non-symmetrically on the magnetopause. Part of the LLBL is probably always on open field lines. During dayside reconnection the entire LLBL is on open fields, while for northward IMF its inner part may be on closed field lines. It seems that under most conditions the flank LLBL is on open fields but asymmetries between dawn and dusk are not excluded.

Concerning anomalous diffusion, six points should be highlighted. (1) Anomalous diffusion is of minor importance for the maintenance of the LLBL, thus confirming the negative conclusion of Russell (1995). However, (2) diffusion is sufficiently high for leakage of resonant particles from the magnetosphere into the sheath, and (3) for locally providing the resistivity required by reconnection. (4) Superdiffusion can reach the Bohm limit but will be highly localized in regions where the parallel electron distribution is a generalized Lorentzian. High-resolution electron and plasma wave measurements are required to check its reality. (5) Coherent low-frequency waves contribute little to diffusion as long as they do not violate the frozen-in and ambipolar conditions. Their effect may be in resonant transport of high energy particles, however. (6) Once the low-frequency waves evolve into scale-invariant low-frequency magnetic turbulence, they may cause island overlap, magnetic wormhole formation and field migration and may be important in maintenance of the LLBL under tangential discontinuity conditions. Clearly macroinstabilities like the KHI can, by producing steep gradients in density, field and current, locally stimulate anomalous transport by means of LHDI and contribution to low-frequency turbulence.

Velocity-shear driven KHI at the magnetopause has not yet been convincingly identified as being important for the presence and dynamics of the LLBL. It is without doubt excited under high-speed northward IMF solar wind conditions, leading to oscillations of the magnetopause and in the LLBL. On the dayside magnetopause near the stagnation region it seems if present to dominate at the inner

edge of the LLBL, while at the flanks it embraces both regions though possibly in an asymmetric way. Simulations and observations still yield ambivalent conclusions about its growth and saturation along the magnetopause towards the flanks. Periodic and open-box MHD simulations give contradictory results. Hall and FLR MHD simulations offer a hint about dawn-dusk asymmetry, plasma blob detachment and anomalous transport. Once KHI develops, momentum transport is well established, but estimated viscosities are unrealistically high. It has been claimed but is not clear whether KHI leads to mass transport. For this to happen the KHI must evolve to short wavelengths and affect the electron dynamics. This is not included in fluid simulations and fluid theory and requires but full particle kinetic treatments. Moderate mass transport and plasma mixing are suggested in FLR and hybrid simulations but still require more work for clarification. In particular, it remains unresolved if KHI vortices contribute to eddy transport and coupling of the magnetopause to the inner edge region. Coupling to the ionosphere may cause break-off of large-scale into small-scale vortices leading to a turbulent LLBL and enhanced momentum transport and possibly also turbulent mass transport.

It is our impression that the electromagnetic coupling of the LLBL to the ionosphere is not quantitatively addressed in any available model. The transit time of Alfvén waves from the LLBL to the ionosphere is comparable to the typical times of variation in the LLBL. This may not be accidental but has not yet been accounted for. Field-aligned potential drops and currents between both regions are inevitable and cause asymmetries between the dawn and dusk flanks. Decoupling at dusk by potential drops could favour KHI, while stronger currents at dawn yield turbulent KHI and enhanced fluctuations.

In summarizing, it is still unclear which part of the LLBL is on closed/open field lines and under which conditions, whether the LLBL carries kinetic Alfvén waves as connectors to the ionosphere, what and where the field-aligned potential drops are, and whether or not the flanks are more important for the formation of the magnetopause boundary layer and in the coupling than the dayside LLBL. Clarification of these problems will require a substantial amount of additional experimental and theoretical work as well as all types of numerical simulations.

Acknowledgements

We should like to acknowledge helpful comments from M. Lockwood and from an anonymous referee on the first version of the manuscript. We are also grateful to G. Paschmann for helpful discussions. This work has been supported by the International Space Science Institute in Bern (Switzerland). The authors thank its directors, Professors J. Geiss and B. Hultqvist, for their hospitality.

References

Akasofu, S. I., Hones, E. W., Jr., Bame, S. J., Asbridge, J. R. and Lui, A. T. Y.: 1973, 'Magnetotail and boundary layer plasmas at a geocentric distance of 18 R_R: Vela 5 and 6 observations', *J. Geophys. Res.* **78**, 7257.

Berchem, J. and Okuda, H.: 1990, 'A two-dimensional particle simulation of the magnetopause current layer', *J. Geophys. Res.* **95**, 8133.

Cargill, P. J. and Eastman, T. E.: 1991, 'The structure of tangential discontinuities, 1, Results of hybrid simulations', *J. Geophys. Res.* **96**, 13,763.

Cattell, C., Wygant, J., Mozer, F. S., Okada, T., Tsuruda, K., Kokubun, S. and Yamamoto, T.: 1995, 'ISEE 1 and Geotail observations of low-frequency waves at the magnetopause', *J. Geophys. Res.* **100**, 11,823.

Chandrasekhar, S.: 1961, *Hydrodynamic and Hydromagnetic Stability*, Oxford University Press, New York, 481.

Chen, S.-H., Kivelson, M. G., Gosling, J. T., Walker, R. J. and Lazarus, A. J.: 1993, 'Anomalous aspects of magnetosheath flow and of the shape and oscillations of the magnetopause during an interval of strongly northward interplanetary magnetic field', *J. Geophys. Res.* **98**, 5727.

Christon, S. P., Mitchell, D. G., Williams, D. E., Frank, L. A., Huang, C. Y. and Eastman, T. E.: 1988, Energy spectra of plasma sheet ions and electrons from $\sim$ 50 eV/*e* to $\sim$ 1 MeV during plasma temperature transitions', *J. Geophys. Res.* **93**, 2562.

Cowley, S. W. H.: 1982, 'The causes of convection in the Earth's magnetosphere: A review of development during the IMS', *Rev. Geophys. and Space Phys.*. **20**, 531.

Cowley, S. W. H.: 1983, 'Interpretation of observed relations between solar wind characteristics and effects at ionospheric altitudes', in B. Hultqvist and T. Hagfors (eds.) *High Latitude Space Plasma Physics*, Plenum Press, New York, p. 225.

Cowley, S. W. H.: 1995, 'Theoretical perspectives of the magnetopause: A tutorial review', in P. Song, B. U. Ö. Sonnerup and M. F. Thomsen (eds.), *Physics of the Magnetopause*, Geophys. Monogr. 90, AGU, Washington, D. C., p. 29.

Crooker, N. U.: 1992, 'Reverse convection', *J. Geophys. Res.* **97**, 19,363.

Davidson, R. C.: 1978, 'Quasilinear stabilization of the lower-hybrid drift instability', *Phys. Fluids* **21**, 1375.

Drake, J. F., Gerber, J. and Kleva, R. G.: 1994, 'Turbulence and transport in the magnetopause current layer', *J. Geophys. Res.* **99**, 11,211.

Drakou, E., Sonnerup, B. U. Ö. and Lotko, W.: 1994, 'Self-consistent steady state model of the low latitude boundary layer', *J. Geophys. Res.* **99**, 2351.

Dum, C. T.: 1996, 'Can we find useful algorithms for anomalous transport?', in J. L. Horwitz, N. Singh, and J. L. Burch (eds.), *Cross-Scale Coupling in Space Plasmas*, Geophys. Monogr. 93, AGU, Washington, D. C., p. 1.

Dungey, J. W.: 1961, 'Interplanetary magnetic field and the auroral zones', *Phys. Rev. Lett.* **6**, 47.

Eastman, T. E., Popielawska, B. and Frank, L. A.:1985, 'Three-dimensional plasma observations near the outer magnetospheric boundary', *J. Geophys. Res.* **90**, 9519.

Eviatar, A. and Wolf, R. A.: 1968, 'Transfer processes in the magnetopause', *J. Geophys. Res.* **73**, 5561.

Fairfield, D. H.: 1993, 'Solar wind control of the distant magnetotail', *J. Geophys. Res.* **98**, 21,265.

Fedder, J. A. and Lyon, J. G.: 1995, 'The Earth's magnetosphere is 65 R_E long: Self-consistent currents, convection, magnetospheric structure, and processes for northward interplanetary magnetic field', *J. Geophys. Res.* **100**, 3623.

Fitzenreiter, R. J. and Ogilvie, K. W.: 1995, 'Kelvin-Helmholtz instability at the magnetopause: Observations', in P. Song, B. U. Ö. Sonnerup and M. F. Thomsen (eds.), *Physics of the Magnetopause*, Geophys. Monogr. 90, AGU, Washington, D. C., p. 277.

Fujimoto, M. and Terasawa, T.: 1994, 'Anomalous ion mixing within an MHD scale Kelvin-Helmholtz vortex', *J. Geophys. Res. 99*, 8601.

Fuselier, S. A., Klumpar, D. M. and Shelley, E. G.: 1991, 'Ion reflection and transmission during reconnection at the Earth's subsolar magnetopause', *Geophys. Res. Lett.* **18**, 139.

Fuselier, S. A., Anderson, B. A. and Onsager, T. G.: 1995, 'Paticle signatures of magnetic topology at the magnetopause: AMPTE/CCE observations', *J. Geophys. Res.* **100**, 11,805.

Galeev, A. A., Kuznetsova, M. M. and Zelenyi, L. M.: 1986, 'Magnetopause stability threshold for patchy reconnection', *Space Sci. Rev.* **44**, 1.

Gary, S. P.: 1980, 'Wave-particle transport from electrostatic instabilities', *Phys. Fluids* **23**, 1193.

Gary, S. P. and Sgro, A. G.: 1990, 'The lower hybrid drift instability at the magnetopause', *Geophys. Res. Lett.* **17**, 909.

Gendrin, R.: 1983, 'Magnetic turbulence and diffusion processes in the magnetopause boundary layer', *Geophys. Res. Lett.* **10**, 769.

Gosling, G. T., Thomsen, M. F., Bame, S. J., Elphic, R. C. and Russell, C. T.: 1990, 'Cold ion beams in the low-latitude boundary layer during accelerated flow events', *Geophys. Res. Lett.* **17**, 2245.

Haerendel, G., Paschmann, G., Sckopke, N., Rosenbauer, H. and Hedgecock, P. C.: 1978, 'The frontside boundary layer of the magnetosphere and the problem of reconnection', *J. Geophys. Res.* **83**, 3195.

Hapgood, M. A. and Bryant, D. A.: 1990, 'Re-ordered electron data in the low-latitude boundary layer', *Geophys. Res. Lett.* **17**, 2043.

Hasegawa, A., Mima, K. and Duong-van, M.: 1985, 'Plasma distribution function in a superthermal radiation field', *Phys. Rev. Lett.* **54**, 2608.

Hones, E. W., Jr., Asbridge, J. R., Bame, S. J., Montgomery, M. D., Singer, S. and Akasofu, S.-I.: 1972, 'Measurements of the magnetotail plasma flow made by VELA 4B', *J. Geophys. Res.* **77**, 5503.

Huba, J.D.: 1994, 'Hall dynamics of the Kelvin-Helmholtz instability', *Phys. Rev. Lett.* **72**, 2033.

Huba, J. D.: 1996, 'Theory and simulation of the Kelvin-Helmholtz instability: Finite Larmor radius magnetohydrodynamics', *Geophys. Res. Lett.* **23**, 2907.

Iijima, T. and Potemra, T. A.: 1978, 'Large-scale characteristics of field-aligned currents associated with substorms', *J. Geophys. Res.* **83**, 599.

Isichenko, M. B.: 1992, 'Percolation, statistical topography and transport in random media', *Rev. Mod. Phys.* **64**, 961.

Johnson, J. R. and Cheng, C. Z.: 1997 'Kinetic Alfvén waves and plasma transport at the magnetopause', *Geophys. Res. Lett.* **24**, in press.

LaBelle, J. and Treumann, R. A.: 1988, 'Plasma waves at the dayside magnetopause', *Space Sci. Rev.* **47**, 175.

Lee, L. C., Johnson, J. R. and Ma, Z. W.: 1994, 'Kinetic Alfvén waves as a source of plasma transport at the dayside magnetopause', *J. Geophys. Res.* **99**, 17,405.

Lin, R. P.: 1997, 'Observations of the 3D distributions of thermal to near-relativistic electrons in the interplanetary medium by the Wind spacecraft', in G. Trottet (ed.), *Coronal Physics from Radios and Space Observations*, Springer, Heidelberg, p. 93.

Lockwood, M. and Smith, M. F.: 1994, 'Low- and mid-altitude cusp particle signatures for general magnetopause reconnection rate variations, 1. Theory', *J. Geophys. Res.* **99**, 8531.

Lockwood, M. and Hapgood, M. A.: 1997, 'How the magnetopause transition parameter works', *Geophys. Res. Lett.* **24**, 373.

Lotko, W., Sonnerup, B. U. Ö. and Lysak, R. L.: 1987, 'Nonsteady boundary layer flow including ionospheric drag and parallel electric fields', *J. Geophys. Res.* **92**, 835.

Lotko, W. and Sonnerup, B. U. Ö.: 1995, 'The low-latitude boundary layer on closed field lines', in P. Song, B. U. Ö. Sonnerup, and M. F. Thomsen (eds.), *Physics of the Magnetopause*, Geophys. Monogr. 90, AGU, Washington, D.C., p. 371.

Lühr, H. and Klöcker, H.: 1987, 'AMPTE-IRM observations of magnetic cavities near the magnetopause', *Geophys. Res. Lett.* **14**, 186.

Lui, A. T. Y, Venkatesan, D. and Murphree, J. S.: 1989, 'Auroral bright spots on the dayside oval', *J. Geophys. Res.* **94**, 5515.

Mace, R. L., Hellberg, M. A. and Treumann, R. A.: 1997, 'Electrostatic fluctuations in plasmas containing superthermal particles', *J. Plasma Phys.*, in press.

Manuel, J. R. and Samson, J. C.: 1993, 'The spatial development of the low-latitude boundary layer', *J. Geophys. Res.* **98**, 17,367.

Milovanov, A. V. and Zelenyi, L. M.: 1995, 'Percolation of a plasma across stochastic magnetic configurations: FLR effects', in P. Song, B. U. Ö. Sonnerup, and M. F. Thomsen (eds.), *Physics of the Magnetopause*, Geophys. Monogr. 90, AGU, Washington, D.C., p. 357.

Mitchell, D. G., Kutchko, F., Williams, D. J., Eastman, T. E., Frank, L. A. and Russell, C. T.: 1987, 'An extended study of the low-latitude boundary layer on the dawn and dusk flanks of the magnetopause', *J. Geophys. Res.* **92**, 7394.

Miura, A.: 1982, 'Nonlinear evolution of the magnetohydrodynamic Kelvin-Helmholtz instability', *Phys. Rev. Lett.* **49**, 779.

Miura, A.: 1984, 'Anomalous transport by magnetohydrodynamic Kelvin-Helmholtz instabilities in the solar wind-magnetosphere interaction', *J. Geophys. Res.* **89**, 801.

Miura, A.: 1992, 'Kelvin-Helmholtz instability at the magnetospheric boundary: Dependence on the magnetosheath sonic Mach number', *J. Geophys. Res.* **97**, 10,655.

Miura, A.: 1995a, 'Dependence of the magnetopause Kelvin-Helmholtz instability on the orientation of the magnetosheath magnetic field', *Geophys. Res. Lett.* **22**, 2993.

Miura, A.: 1995b, 'Kelvin-Helmholtz instability at the magnetopause: Computer simulations', in P. Song, B. U. Ö. Sonnerup, and M. F. Thomsen (eds.), *Physics of the Magnetopause*, Geophys. Monogr. 90, AGU, Washington, D.C., p. 285.

Miura, A. and Pritchett, P. L.: 1982, 'Nonlocal stability analysis of the MHD Kelvin-Helmholtz instability in a compressible plasma', *J. Geophys. Res.* **87**, 7431.

Nishida, A.: 1989, 'Can random reconnection on the magnetopause produce the low-latitude boundary layer?', *Geophys. Res. Lett.* **16**, 227.

Ogilvie, K. W. and Fitzenreiter, R. J.: 1989, 'The Kelvin-Helmholtz instability at the magnetopause and inner boundary layer surfaces', *J. Geophys. Res.* **94**, 15113.

Ogino, T., Walker, R. J. and Ashour-Abdalla, M.: 1994, 'A global magnetohydrodynamic simulation of the response of the magnetosphere to a northward turning of the interplanetary magnetic field', *J. Geophys. Res.* **99**, 11,027.

Omidi, N. and Winske, D.: 1995, 'Structure of the magnetopause inferred from one-dimensional hybrid simulations', *J. Geophys. Res.* **100**, 11,935.

Paschmann, G., Sonnerup, B. U. Ö., Papamastorakis, I., Baumjohann, W., Sckopke, N. and Lühr, H.: 1990, 'The magnetopause and boundary layer for small magnetic shear: Convection electric fields and reconnection', *Geophys. Res. Lett.* **17**, 1829.

Phan, T. D., Sonnerup, B. U. Ö. and Lotko, W.: 1989, 'Self-consistent model of the low-latitude boundary layer', *J. Geophys. Res.* **94**, 1281.

Raeder, J., Walker, R. J. and Ashour-Abdalla, M.: 1995, 'The structure of the distant geomagnetic tail during long periods of northward IMF', *Geophys. Res. Lett.* **22**, 349.

Raeder, J. A., Berchem, J., Ashous-Abdalla, M., Frank, L. A., Paterson, W. R., Ackerson, K. L., Kokobun, S., Yamamoto, T., and Slavin, J. A.: 1997, 'Boundary layer formation in the magnetotail: Geotail observations and comparison with a global MHD simulation', *Geophys. Res. Lett.* in press.

Richard, R. L., Walker, R. J. and Ashour-Abdalla M.: 1994, 'The population of the magnetosphere by solar wind ions when the interplanetary magnetic field is northward', *Geophys. Res. Lett.* **21**, 2455.

Rezeau, L., Roux, A. and Russell, C. T.: 1993, 'Characterization of small-scale structures at the magnetopause from ISEE measurements', *J. Geophys. Res.* **98**, 179.

Romero, H. and Ganguli, G.: 1993, 'Nonlinear evolution of a strongly sheared cross-field plasma flow', *Phys. Fluids* **B5**, 3163.

Russell, C. T.: 1995, 'The structure of the magnetopause', in P. Song, B. U. Ö. Sonnerup, and M. F. Thomsen (eds.), *Physics of the Magnetopause*, Geophys. Monogr. 90, AGU, Washington, D.C., p. 81.

Sckopke, N., Paschmann, G., Haerendel, G., Sonnerup, B. U. Ö., Bame, S. J., Forbes, T. G., Hones, E. J., Jr. and Russell, C. T.: 1981, 'Structure of the low-latitude boundary layer', *J. Geophys. Res.* **86**, 2099.

Seon, J., Frank, L. A., Lazarus, A. J. and Lepping, R. P.: 1995, 'Surface waves on the tailward flanks of the Earth's magnetopause', *J. Geophys. Res.* **100**, 11,907.

Shapiro, V. D. , Shevchenko, V. I., Solov'ev, G. I., Kalinin, V. P., Bingham, R., Sagdeev, R. Z., Ashour-Abdalla, M., Dawson, J. and Su. J. J.: 1993, 'Wave collapse at the lower hybrid resonance', *Phys. Fluids* **B5**, 3148.

Shapiro, V. D., Shevchenko, V. I., Cargill, P. J. and Papadopoulos, K.: 1995, 'Modulational instability of lower hybrid waves at the magnetopause', *J. Geophys. Res.* **99**, 23,735.

Shlesinger, M. F., Zaslavsky, G. M. and Klafter, J.: 1993, 'Strange kinetics', *Nature* **363**, 31.

Smith, M. F. and Rodgers, D. J.: 1991, 'Ion distributions at the dayside magnetopause', *J. Geophys. Res.* **96**, 11,617.

Song, P. and Russell, C. T.: 1992, 'Model of the formation of the low-latitude boundary layer for strongly northward interplanetary magnetic field', *J. Geophys. Res.* **97**, 1411.

Song, P., Holzer, T. E., Russell, C. T. and Wang, Z.: 1994, 'Modeling the low-latitude boundary layer with reconnection entry', *Geophys. Res. Lett.* **21**, 625.

Sonnerup, B. U. Ö.: 1980, 'Theory of the low-latitude boundary layer', *J. Geophys. Res.* **85**, 2017.

Sonnerup, B. U. Ö. and Guo, M.: 1997, 'Magnetopause transects', *J. Geophys. Res.* submitted.

Takahashi, K., Sibeck, D. G., Newell, P. T. and Spence, H. E.: 1991, 'ULF waves in the low-latitude boundary layer and their relationship to magnetic pulsations: A multi-satellite observation', *J. Geophys. Res.* **96**, 9503.

Terasawa, T., Fujimoto, M., Karimabadi, H. and Omidi, N.: 1992, 'Anomalous ion mixing within a Kelvin-Helmholtz vortex in a collisionless plasma', *Phys. Rev. Lett.* **68**, 2778.

Thomas, V. A. and Winske, D.: 1991, 'Kinetic simulation of the Kelvin-Helmholtz instability at the magnetopause', *Geophys. Res. Lett.* **18**, 1943.

Thomas, V. A. and Winske, D.: 1993, 'Kinetic simulations of the Kelvin-Helmholtz instability at the magnetopause', *J. Geophys. Res.* **98**, 11,425.

Thomas, V. A.: 1995, 'Kinetic simulation of the Kelvin-Helmholtz instability at a finite sized object', *J. Geophys. Res.* **100**, 12,017.

Traver, D. P., Mitchell, D. G., Williams, D. J., Frank, L. A. and Huang, D. Y.: 1991, 'Two encounters with the flank low-latitude boundary layer: Further evidence for closed field topology and investigation of the internal structure', *J. Geophys. Res.* **96**, 21,025.

Treumann, R. A., Brostrom, L., LaBelle, J. and Sckopke, N.: 1990, 'The plasma wave signature of a 'Magnetic Hole' in the vicinity of the magnetopause', *J. Geophys. Res.* **95**, 19,099.

Treumann, R. A., LaBelle, J. and Pottelette, R.: 1991, 'Plasma diffusion at the magnetopause: The case of lower hybrid drift waves', *J. Geophys. Res.* **96**, 16,009.

Treumann, R. A., LaBelle, J. and Pottelette, R.: 1992, 'Plasma transport through magnetic boundaries', in *Proc. 26th ESLAB Symp.* **SP-346**, ESA, Nordwijk, 115.

Treumann, R. A., LaBelle, J. and Bauer, T. M.: 1995, 'Diffusion at the magnetopause: The observational viewpoint', in P. Song, B. U. Ö. Sonnerup, and M. F. Thomsen, *Physics of the Magnetopause*, Geophys. Monogr. 90, AGU, Washington, D.C., p. 331.

Treumann, R. A. and Bauer, T. M.: 1996, 'Super-diffusion at the magnetopause', *EOS AGU Fall Meeting*, SM42A-01.

Treumann, R. A.: 1997, 'Theory of super-diffusion for the magnetopause', *Geophys. Res. Lett.* **24**, in press.

Tsurutani, B. T. and Thorne, R. M.: 1982, 'Diffusion processes at the magnetopause boundary layer', *Geophys. Res. Lett.* **9**, 1247.

Tsurutani, B. T., Brinca, A. L., Smith, E. J., Okida, R. T., Anderson, R. R. and Eastman, T. E.: 1989, 'A statistical study of ELF-VLF plasma waves at the magnetopause', *J. Geophys. Res.* **94**, 1770.

Usadi, A., Kageyama, A., Watanabe, K. and Sato, T.: 1993, 'A global simulation of the magnetosphere with a long tail: Southward and northward interplanetary magnetic field', *J. Geophys. Res.* **98**, 7503.

Wei, C. Q. and Lee, L. C.: 1993, 'Model of the low-latitude boundary layer with finite field-aligned potential drops and nonconstant mapping factors', *J. Geophys. Res.* **98**, 5707.

Wei, C. Q., Sonnerup, B. U. Ö. and Lotko, W.: 1996, 'Model of the low-latitude boundary layer with finite field-aligned potential drops and nonconstant mapping factors', *J. Geophys. Res.* **101**, 21,463.

Wilber, M. and Winglee, R. M.: 1995, 'Dawn-dusk asymmetries in the low-latitude boundary layer arising from the Kelvin-Helmholtz instability: A particle simulation', *J. Geophys. Res.* **100**, 1883.

Winske, D., Gary, S. P. and Lemons, D. S.: 1991, 'Diffusive transport at the magnetopause', in T. Chang, G. B. Crew, and J. R. Jasperse (eds.), *Physics of Space Plasmas 1990, SPI Conf. Proc. Rept. Ser. 10*, Scient. Publ., Cambridge, Mass., p. 397.

Winske, D. and Omidi, N.: 1995, 'Diffusion at the magnetopause: Hybrid simulations', *J. Geophys. Res.* **100**, 11,923.

Winske, D., Thomas, V. A. and Omidi, N.: 1995, 'Diffusion at the magnetopause: The theoretical viewpoint', in P. Song, B. U. Ö. Sonnerup, and M. F. Thomsen (eds.), *Physics of the Magnetopause*, Geophys. Monogr. 90, AGU, Washington, D.C., p. 321.

Wu, C. C.: 1986, 'Kelvin-Helmholtz instability at the magnetopause boundary', *J. Geophys. Res.* **91**, 3042.

Zhu, Z., Song, P., Drake, J. F., Russell, C. T., Anderson, R. R., Gurnett, D. A., Ogilvie, K. W. and Fitzenreiter, R. J.: 1996, 'The relationship between ELF-VHF waves and magnetic shear at the dayside magnetopause', *Geophys. Res. Lett.* **23**, 773.

Address for correspondence: M. Scholer, Max-Planck-Institut für extraterrestrische Physik, D-85740 Garching bei München, Germany

CONSIDERATIONS OF SOURCE, TRANSPORT, ACCELERATION/HEATING AND LOSS PROCESSES RESPONSIBLE FOR GEOMAGNETIC TAIL PARTICLE POPULATIONS

D. J. WILLIAMS
Johns Hopkins University, Applied Physics Laboratory, Laurel, Maryland, USA

Received Febuary 21, 1997; Accepted March 13, 1997

Abstract. The relative importance of the two known substantive sources of magnetospheric particles, the solar wind and the ionosphere, remains largely undetermined throughout much of the magnetosphere. For the specific case of the geomagnetic tail however, the development of a remarkable family of models incorporating the kinetics of charged particle motion, has opened the possibility of determining relative strengths and geometries of the solar wind and ionospheric sources that are responsible for observed tail particle populations. Once source strengths and geometries are determined, transport paths and mechanisms can be identified, in turn leading to a determination of acceleration/heating mechanisms and locations. Loss processes then determine the quasi-equilibrium particle distributions in the tail. A quantitative understanding of the tail and its dynamics requires extensive, detailed comparisons of data and model results. Data obtained over the past two decades have led to the result that for energies at least above ~1 eV, both sources are well mixed throughout the tail and that the solar wind is the dominant source. New, unique data sets have provided the initial data comparisons with the models and show great promise in deconvolving source strengths and geometries and ultimately understanding the formation and behavior of the tail.

1. Introduction

The International Space Science Institute (ISSI) is supporting an effort to assess the present state of knowledge of source and loss processes in the magnetosphere. It is hoped that from such an assessment, potential future studies can be identified to answer existing questions and to extend our knowledge in this area of magnetospheric research. This report is based on a talk given at the first ISSI workshop in October 1996. It represents a general discussion on source, transport, acceleration/heating, and loss (STAHL) processes and their role in establishing magnetotail particle populations. The talk was aimed at providing an initial reference point for Working Group 6, "Source and Loss Processes for Magnetospheric Plasma in the Earth's Magnetic Tail," of the ISSI Workshop, in its ambitious task of assessing what is known of magnetotail STAHL processes.

It has been known for many years that the only substantive sources for magnetotail particles are the solar wind and the ionosphere. While there is

Space Science Reviews **80**: 369–389, 1997.

strong evidence that the dominant source for geomagnetic tail particles is the solar wind, particles from the ionosphere play an important role in geomagnetic tail phenomena. What is not known (or at best very poorly known) are the effective geometries of these sources and the magnetotail transport paths and mechanisms that establish the particle populations observed throughout the tail. Better knowledge of source geometries and transport through the tail will allow a much improved assessment of the location and effectiveness of relevant acceleration/heating processes and their locations. Loss processes may then be inferred from measurements of equilibrium (or quasi-equilibrium) distributions. In the following we shall strive to present a picture, albeit imperfect, of magnetotail STAHL processes that has evolved from years of theoretical, experimental, data analysis, and modeling/simulation studies.

2. Sources

The solar wind has been recognized from the beginnings of magnetospheric physics as a source that easily is capable of supplying the magnetosphere, and in particular the magnetotail, with its particle populations. It represents a source strength of a few x 10^{29} ions/s incident on a magnetosphere with a nominal radius of 20 R_E. It is not yet known how or where solar wind particles (or more precisely the shocked solar wind particles in the magnetosheath) enter the magnetosphere and contribute to the magnetotail particle populations. This is an uncertainty that relates directly to the question of what is the effective source geometry. Also unknown are the transport processes and paths from wherever the solar wind particles enter the magnetosphere to where they are observed in the magnetotail. We shall see that there are recent results that provide initial, important clues for answering these questions.

The beginnings of recent considerations of particle trajectories in the magnetotail began in the mid-sixties when Speiser (1965a,b) performed pioneering calculations demonstrating the surprising results of particles **ExB** drifting through the tail into an encounter with a realistic model of the tail neutral sheet, a region with weak but finite normal magnetic field, B_n. He showed that not only does energization occur but that some of the particles in their encounter with the neutral sheet are ejected from the neutral sheet region along the ambient magnetic field lines. Extensions of these ideas through the mid-1980's yielded more details of the particles' energization, their travels after the first encounter with the neutral sheet, and the categorization of the resulting particle orbits as adiabatic, quasi-adiabatic, and chaotic (see for example Speiser, 1967; Lyons and Speiser, 1982; Speiser and Lyons, 1984; Chen and Palmadesso, 1986; Martin, 1986a,b). These works did not trace the particle trajectories back to additional encounters with the neutral sheet and thus provided little direct information (but strong hints) on the formation of the

plasma sheet. These works did however provide an indication of what was to become known as the plasma sheet boundary layer, PSBL. Although Lyons and Speiser (1982) found agreement with a mantle (or magnetosphere boundary layer) source, no positive source identifications could be made with such calculations. The drifting particles could be either particles injected into the tail from the ionosphere or entering from the solar wind.

Pilipp and Morfill (1978) developed the first model to attempt a quantitative explanation for the particle populations of the tail. They used the then recently discovered plasma mantle as their source. In their model, which has remained a basic concept in many hypotheses for populating the tail, particles enter the magnetosphere at the polar cusps to form the entry layer and plasma mantle and then flow antisunward into the tail. **ExB** convection of this streaming plasma disperses it through the lobes and moves it towards the plasma sheet. In their work, Pilipp and Morfill (1978) showed the mantle to be an adequate source for replenishing known losses from the plasma sheet.

While these discoveries (e.g., plasma mantle, entry layer) and resulting models and calculations were strengthening the long-held belief that the solar wind was the source of magnetospheric particle populations, other discoveries were eroding that belief. Pioneering observations by the Lockheed Group (see for example Shelley et al., 1972; Sharp et al., 1974; Peterson et al., 1981; Lennartsson and Sharp, 1985; Lennartsson and Shelley, 1986)) in the early 1970s and extending through the next decade and one-half, showed the ionosphere to be a copious source of particles rivaling, at least during geomagnetically active times, the solar wind. The main question was whether or not large numbers of ionospheric particles could reach all regions of the magnetosphere, including the entire magnetotail.

In the late 1980s, Chappell et al. (1987) summarized ionospheric outflow observations, including polar wind and cleft ion fountain outflow. By estimating volumes and ion residence times for various magnetospheric regions (plasmasphere, plasma trough, plasma sheet, magnetotail lobes), they concluded that the ionosphere alone is able to supply the entire plasma content of the magnetosphere under all geomagnetic conditions. Table 1 (Table 2 from Chappell et al., 1987) summarizes their results. For comparison, note that the entry of 0.1%-1.0% of the incident solar wind into the magnetosphere results in a solar wind source strength of a few x (10^{26}-10^{27}) ions per sec, generally of the same order or somewhat larger than the ionospheric values in Table 1.

SUMMARY

Thus at this time (late 1980s) magnetospheric physics was in the interesting situation of having identified two major sources, the solar wind and the ionosphere, either of which was capable of supplying the charged particle needs of the magnetosphere. Which is dominant, particularly in the geomagnetic tail?

TABLE 1 IONOSPHERIC SOURCE PARAMETER SUMMARY
(from Chappell et al., 1987)

Region	Volume, cm^3	Residence Time, s	Flux Range		Density	
			ions s^{-1}	(ions $cm^{-2}s^{-1}$)	Calculated, ions cm^{-3}	Observed, ions cm^{-3}
Region I						
Inner plasmasphere	6.97×10^{27}	8.64×10^{4}	8.0×10^{26}	(1.5×10^{8})	4930-1070	10,000-2000
		(1-day filling time)	1.7×10^{26}	(3.25×10^{7})		
Region II						
Outer plasmasphere	2.39×10^{28}	4.32×10^{5}	9.3×10^{25}	(1.5×10^{8})	850-180	2000-100
		(5-day filling time)	2.0×10^{25}	(3.25×10^{7})		
Region III						
Dayside plasma trough	5.65×10^{29}	2.16×10^{4}	1.31×10^{26}	(3×10^{8})	4.1-1.1	10.0-<1.0
		(6-hr convective drift)	2.91×10^{25}	(6.5×10^{7})		
Region IV						
a. Quiet plasma sheet	3.75×10^{30}	1.44×10^{4}	1.9×10^{26}		0.73-0.42	1.1-0.4
		(4-hr convective drift)	1.1×10^{26}			
b. Active plasma sheet	3.75×10^{29}	1.08×10^{4}	2.2×10^{26}		6.3-6.0	0.4-0.2
		(3-hr convective drift)	2.1×10^{26}			
Region V						
Tail lobe	7.0×10^{30}	6.5×10^{3}	8.4×10^{25}		0.078-0.036	0.1-0.001
		(flow and drift time)	3.9×10^{25}			

Source dominance will be determined primarily by effective source geometries and resulting transport through the environs of the tail. Acceleration/heating will operate on the transported particles, thereby establishing the magnetotail particle populations, while losses will determine the equilibrium distributions. Identification of the dominant source can be (and has been in the tail) accomplished by existing data sets and will be discussed later in this report. With the dominant source identified, a more focused pursuit of STAHL processes is possible.

3. Models/Simulations

One of the major advances that has occurred over the past decade in understanding the fate of particles as they enter and travel in the complex magnetic and electric field configuration of the magnetosphere, is the recognition and evaluation of the importance of deterministic chaos. Stated simply this means that the particles' motion is governed by highly nonlinear equations and in several key regions of the magnetosphere, full trajectory tracing calculations must be done to learn the ultimate fate of the particles. While not explicitly discussed in terms of chaos or nonlinear theory, this attribute was clearly evident in the early calculations of Speiser (1965a,b). In the past decade the effects of this nonlinearity in magnetospheric travel, and

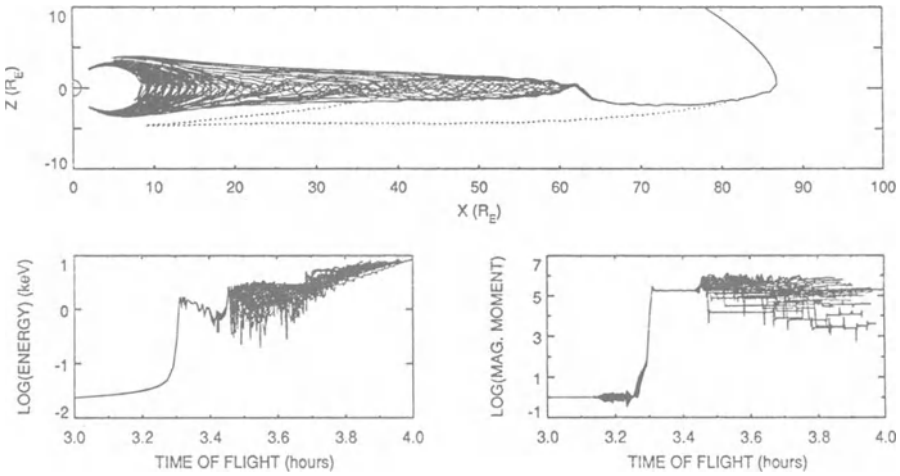

Figure 1. Model trajectories of cleft originating H^+: (upper) trajectory projection in the midnight meridian plane, (lower left) particle energy versus time and (lower right) normalized magnetic moment versus time. The particles are launched from the dayside sector at an invariant latitude of 80° with distinct phases of gyration (from 0° to 360° by steps of 10°). In the top panel, the dotted line depicts the trajectory segment of a proton having larger parallel speed after the first encounter with the neutral sheet (from Delecourt et al., 1994).

particularly that in the magnetotail, has been pursued in a number of excellent and fascinating papers (see for example Buchner and Zelenyi, 1986, 1988, 1989; Chen and Palmadesso, 1986; Delcourt et al., 1992, 1994; Ashour-Abdalla et al., 1990, 1991a,b, 1993). The outcome of these calculations is fundamental to our understanding STAHL processes and has already presented a greatly changed perspective of the magnetotail and its particle populations.

Following the summary of ionospheric outflow given by Chappell et al. (1987), Delcourt et al. (1992, 1994) developed models to follow outgoing ionospheric ions into the magnetosphere. Launching particles from a 7° latitude band centered on the dayside cusp, they found that polar wind and cleft ions can, through nonadiabatic interactions with the neutral sheet, contribute in a possibly major way to plasma sheet ion populations. Figure 1 shows a sample of their results. Densities and energies attained in the tail show quite reasonable agreement with observations. However the model calculations provide greater contributions to the plasma sheet during quiet times than during magnetically active periods. The enhanced electric fields during active times effectively keeps the ions much closer to the earth. The model tells nothing of what can be expected through and beyond the distant neutral line (~70-120 R_E), primarily due to the fact that the model magnetic field used is not considered valid beyond 70 R_E. However, this modeling shows the importance of the nonlinearities inherent in the particles' motion through the magnetosphere and

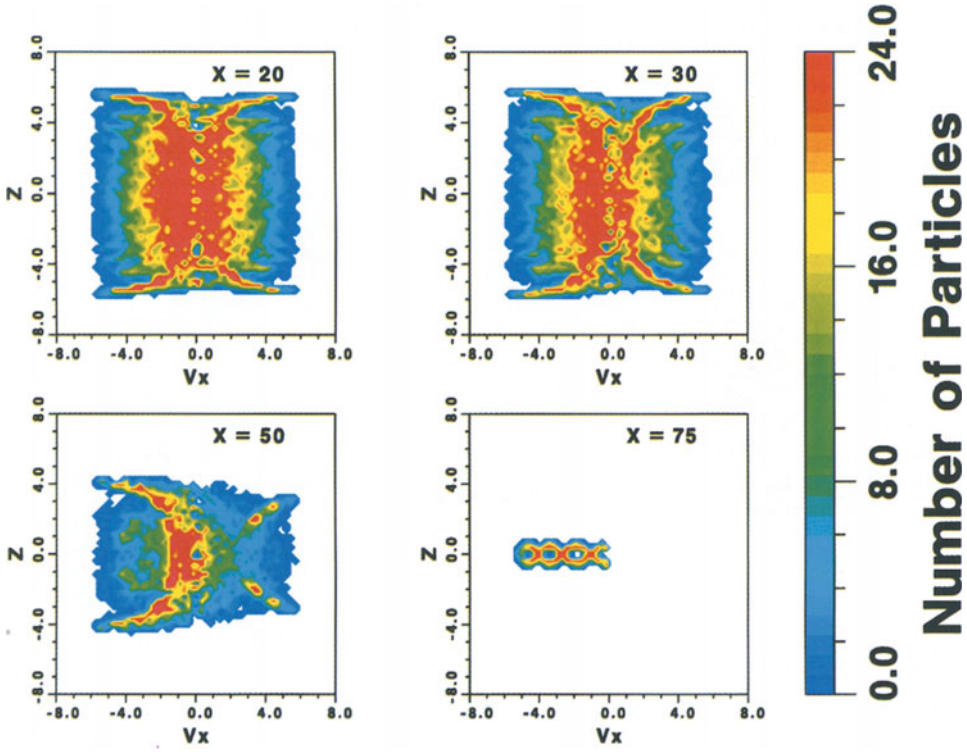

Figure 2. Distribution of the particles $\Phi(z,v_x)$ at different distances x_D from the Earth: z = (a) 20 R_E, (b) 30 R_E, (c) 50 R_E, and (d) 75 R_E. The figure illustrates the global structuring of the magnetotail on the CPS and PSBL regions, velocity dispersion in the PSBL, reflected beams and their dispersion, isotropization and heating of the CPS, and spatial variation in properties of both regions while approaching the Earth (from Ashour-Abdalla et al. 1993).

dramatically shows large ionospheric contributions to the magnetotail particle populations, at least in the near-earth tail.

One of the most detailed incorporations of the nonlinear aspects of particle trajectories in the magnetotail has been the work of Ashour-Abdalla, Zelenyi, and colleagues (Ashour-Abdalla et al., 1990, 1991a,b, 1993, 1994, 1995). Their kinetic modeling efforts begin with a mantle source and follow particle trajectories as they propagate in the magnetotail and interact with the neutral sheet. Their studies have examined in great detail the peculiarities of particle

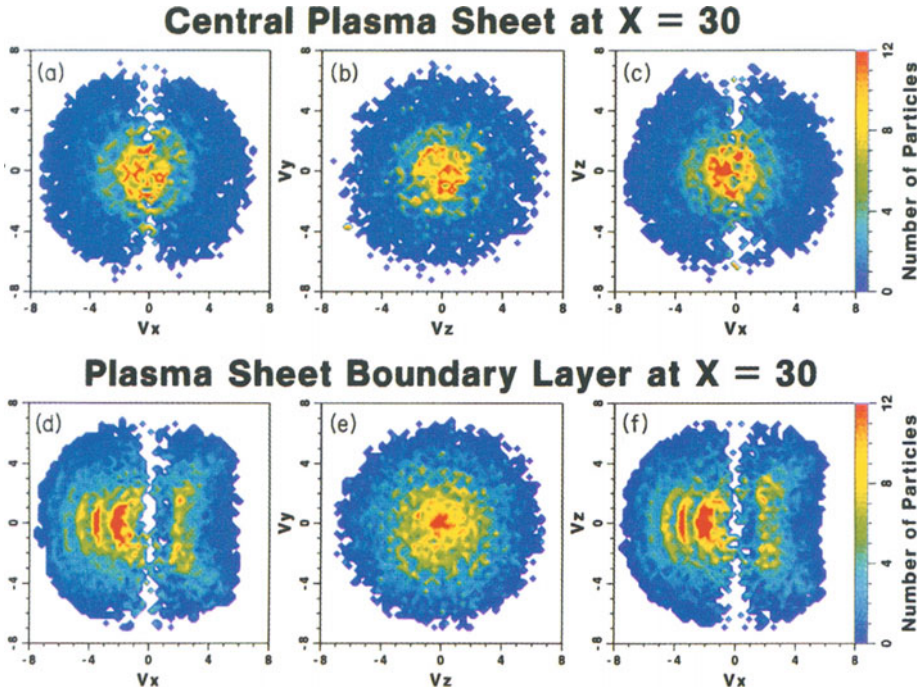

Figure 3. (Top) Projections of three-dimensional velocity distributions of CPS ($|z|<0.8\ R_E$) ions at $x_D = 30\ R_E$ on (v_x, v_y), (v_z, v_y), and (v_x, v_z) planes. Distributions show the presence of small-scale structures and pronounced counterstreaming. (Bottom) The same but for PSBL ($|z|>4.0\ R_E$) ions (from Ashour-Abdalla et al. 1993).

travel in the magnetotail and include results showing the consequences of adiabatic, quasiadiabatic, and chaotic motion. While we do not have the space to describe these remarkable results, there are several general features that emerge which cast a new perspective on the evolution and behavior of the magnetotail.

The calculations show that the mantle ion source directly leads to the evolution of a global tail structure made up of a central plasma sheet and an accompanying plasma sheet boundary layer (PSBL). Embedded in the large scale structure are small scale features that arise naturally in the ion distribution functions. Figure 2, from the work of Ashour-Abdalla et al. (1993), shows a pictorial summary of these results. Shown are the distribution functions resulting from a mantle source displayed in the Z versus V_X frame for four separate X values (X is positive along the anti-earth tail axis). Accelerated mantle ions are seen at all distances and the emergence of a central plasma

sheet and PSBL structures are clearly evident. Figure 2 also shows the variation of plasma sheet thickness with distance, reflected tailward beams appearing in the PSBL, and the velocity dispersion of the PSBL beams. Furthermore, small scale structures are seen within the macro-scale features of Figure 2. These small scale structures also are present in the ion velocity distribution functions, as can be seen in Figure 3. These features, called beamlets by the authors and seen in Figure 2 as islands or blobs along the horns of the plasma sheet boundary layer, appear as strips of enhanced numbers of particles at various values of V_x. The authors have shown that these beamlets produce, through spatial interference effects, a variety of fine and intermediate spatial scale structures in the moments of the ion distributions, such as those seen in Figure 2.

SUMMARY

The picture of the tail and its particle populations has now become even more interesting. There are two sources, each of which seemingly can provide the magnetotail with its particle populations. In addition, the development of a family of rather remarkable models incorporating the dynamics of the very complex motion of charged particles in the magnetotail has shown a completely new perspective of the structure of the tail, both spatially and in the moments of the ion distributions. Calculations to date indicate that both sources, solar wind and ionosphere, can populate regions of the magnetotail. Work remains to be done to determine the relative importance of the two sources as a function of space and time.

Perhaps the most basic problem within the models is the question of what is the appropriate source geometry. Figure 4 shows a sketch of the magnetosphere taken from Pilipp and Morfill (1978), illustrating the mantle source location used in their explanation of the particle content of the magnetotail. Also shown are the ionospheric source location used by Delcourt et al. (1994) and the mantle source used by Ashour-Abdalla et al. (1993). The main point in highlighting these sources is to point out that they are specialized for each model calculation and generally do lead to problems. For example, the ionospheric source shown has difficulty in getting enough ions into the distant tail, especially during magnetically active periods. The mantle source shown has the opposite problem, namely that it places too many ions into the distant tail. The actual geometry of the source (its spatial configuration) will be an important enhancement to these models in explaining the particle distributions observed throughout the tail. Recent reports (Ashour-Abdalla et al., 1996; Paterson et al., 1996) on tracing particle trajectories (using measured distribution functions) backwards in time from the point of observation indicate that at least the mantle source extends along the entire magnetopause. Particle distributions measured within the magnetotail thus are comprised of particles

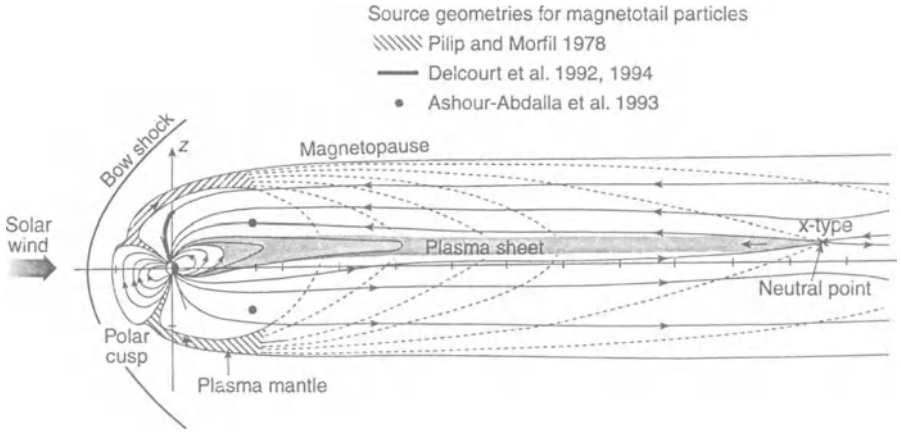

Figure 4. Schematic of the magnetosphere taken from Pilip and Morfil (1978) illustrating source locations used for supplying particles to the magnetotail. While remarkable success has been achieved from the modeling efforts, the figure highlights the specialized source geometries used.

originating at various locations along the magnetopause, entering the magnetosphere, and being transported to the point of observation.

How do the above discussion of sources and the new wave of kinetic modeling actually relate to the ions measured in the tail? Do present observations delineate the sources? Do they support the models? The next section is a brief summary of observational results that are pertinent to these questions.

4. Observations

In the early 1980s Young et al., (1982) reported the results of a study of ions observed near geostationary altitudes over the four-year period 1977-1981. The ions measured were H^+, He^+, He^{++}, O^+, and O^{++} and the energy range covered was 0.9-15.9 keV/q. A principal result from their study was that observed increases in the densities of He^+, O^+, and O^{++} were due solely to increased solar UV fluxes associated with the rising solar cycle at the time. In contrast H^+ and He^{++} showed only a weak dependence on both $F_{10.7}$ and K_p. Only O^+ showed a strong correlation with K_p. No molecular ions were observed during the four year period of the study. From this observation the authors emphasized the

importance of considering effective scale heights when using the ionosphere as a supplier of magnetospheric ions. By considering appropriate scale heights, atmospheric heating, and an acceleration region above ~1000 km, Young et al. (1982) were able to explain qualitatively many features of their statistical results using a mixture of ionospheric and solar wind particles. This is a fundamental result and one that recurs at all energies and distances—*both sources are present and well mixed.*

Similar studies by Lennartsson and Shelly (1986) and Lennartsson (1989) extended the magnetospheric region being considered to ~23 R_E. They used ISEE data during the rising portion of the solar cycle and found results qualitatively consistent with those at ~6.6 R_E (Young et al., 1982); correlations of various ion charge states with $F_{10.7}$ and magnetic activity were similar to that seen at the lower altitudes. Lennartsson and Shelly conclude that the O^+ is of ionospheric origin, the H^+ is of solar wind origin, and the plasma sheet from ~10-23 R_E is dominated during magnetically quite times by ions from the solar wind source. Re-enforcing this conclusion is a recent report by Terasawa et al., (1996) showing that for extended periods of northward interplanetary magnetic field, the magnetotail plasma sheet ($X \cong -15 \sim -50R_E$) is created by diffusive transport of solar wind particles through the flank region of the magnetotail. Thus it now seems that both sources are present out to tens of R_E, and that the solar wind source is dominant, at least during magnetically quite times.

Gloeckler et al. (1984) provided evidence for a strong solar wind presence in magnetotail particle populations at distances beyond ~80 R_E and that both sources (solar wind and ionosphere) were present at those distances. These results were based on ISEE 3 measurements of H^+ and He^{++} ions at 6-150 keV/AMU. They studied 20 particle increases in tail structures, which at that time were called plasmoids, and found the solar wind to be a major source of the observed particles, at least as strong as an ionospheric source.

This mixing of the sources has been observed to distances of ~210 R_E down the tail. Hirahara et al. (1996) and Seki et al. (1996) found solar wind H^+ and He^{++} coexisting with ionospheric O^+ in cold dense ion flows seen in the distant tail lobe and in the lobe/mantle region. The very existence of these mixed plasmas throughout the length of the tail traversed by the GEOTAIL satellite illustrates the problems of particle transport in the tail that must be solved in order to understand the magnetotail and its particle populations.

At this point we see that both sources are well mixed throughout the tail, at least as observed by a variety of plasma instruments. The question of relative source strengths has not been quantitatively determined, although there are hints that the solar wind source dominates.

Definitive charge state measurements provide a vital tool in untangling sources throughout the magnetosphere. Pioneered by George Gloeckler at the University of Maryland (e.g. Gloeckler et al., 1985), such measurements have proven invaluable in the continuing study of STAHL processes (see for

example Kremser et al., 1985, 1987a,b; Kleckler et al., 1986). Christon et al. (1994b) have studied the behavior of oxygen and carbon charge states in the L-range of ~4-9 R_E and energy range of 1.5-300 keV/q. They used data from the CHEM instrument on the AMPTE/CCE satellite, encompassing the 4-year period September 1984 - January 1989. These studies showed charge state radial profiles consistent with an increasing solar wind source strength towards higher altitudes and an increasing ionospheric source strength towards lower altitudes, generally consistent with previous studies. Christon et al. (1994b) report on the local time distributions measured for solar wind primary ions ($O^{6+,7+}$, $C^{5+,6+}$) and secondary ions (those solar wind ions that have charge exchanged to a lower charge state). They find different local time profiles for the primary and secondary ions. Based on this observation and comparison with ion trajectory calculations, they conclude that solar wind ions enter the magnetospheric quasi-trapped regions on the nightside, that the secondaries are produced at L<7 R_E, that the secondaries do not form a significant portion of the plasma sheet particle population that is injected into the quasi-trapping region,

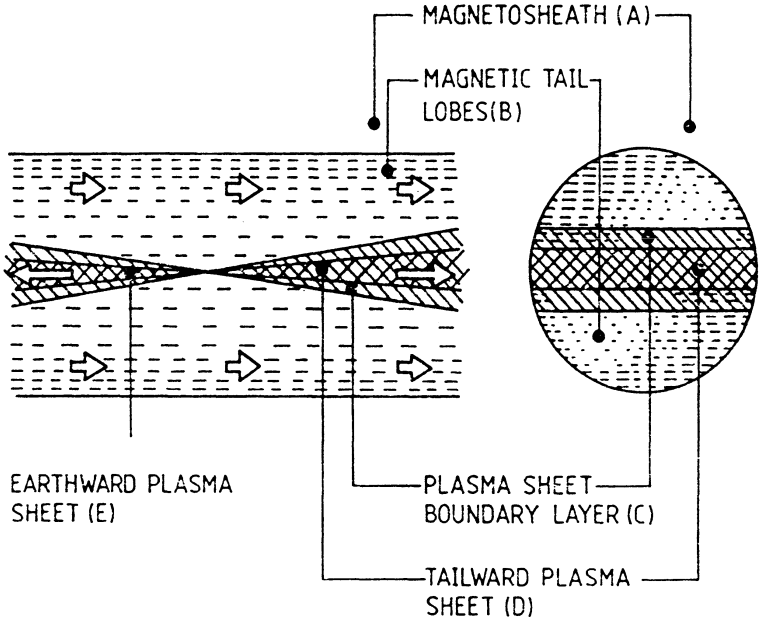

Figure 5. Schematic picture of the geomagnetic tail in (left) the (aberated) noon-midnight meridian and (right) a cross-sectional cut looking towards the Earth. The hatched area shows the wedge-shaped region of reconnected field lines downstream from the neutral line containing very energetic particles produced in the current sheet, while the central cross-hatched region shows the smaller area occupied by the streaming 'plasma sheet' population. The dashed lines represent the tailward flowing plasma in the magnetotail lobes and indicate the dawn/dusk and north/south asymmetries which may occur dependent on IMF B_y, that shown being for B_y negative (from Cowley, 1984).

and that little of the energetic secondary ion population is recirculated through the magnetosphere.

What is the situation at higher energies, i.e. energies for which strong acceleration has taken place? Cowley et al. (1984) presented a simplified picture of energetic ion regimes in the tail based on ISEE 3 results. Figure 5 presents a schematic of these regions, showing a distant neutral line thought to be responsible for the generation of the energetic particles, tailward and earthward flowing ions, an energetic ion boundary layer, and the central plasma sheet. Synopses of ISEE 3 energetic ion results (Daly, 1986; Scholer, 1986) show that a region several tens of R_E down the tail and some tens of R_E in extent, separates roughly equal earthward and tailward flows from predominantly strong tailward flows. This is consistent with the schematic of Figure 5, with strong tailward flows occurring tailward of the neutral line and mixed flows occurring earthward of the neutral line. Williams (1981) has reported results consistent with this general picture whereby the time evolution of the angular and energy distributions of energetic ions observed in the PSBL could be explained using single particle motion from a source located ~80-100 R_E down the tail. An early survey of GEOTAIL plasma data by Patterson and Frank (1994) also is consistent with these results. However it should be noted that the transition from earthward/tailward flows to strong tailward flows statistically occurs over an extended spatial range of at least some tens of R_E.

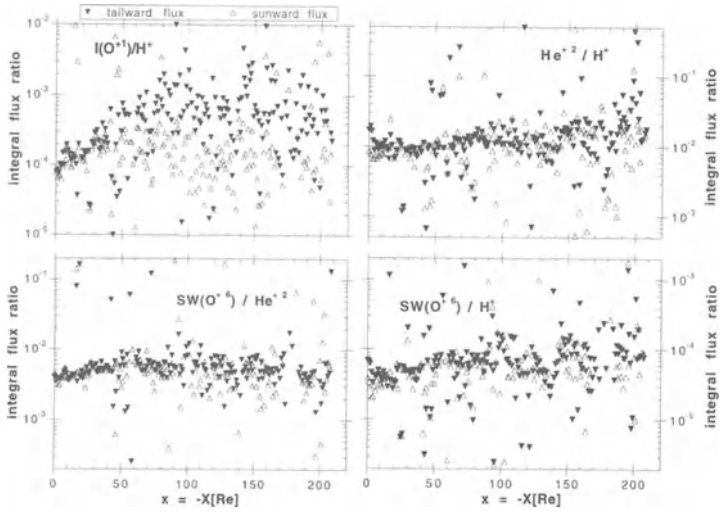

Figure 6. The downtail distance, x, variation of 9.4-212 keV/e $I(O^{+1})/H^+$, the integral flux ratio of high mass, singly-charged ionospheric origin ions to H^+, is compared to corresponding integral flux ratios He^{+2}/H^+, $SW(O^{+6})/H^+$, and $SW(O^{+6})/He^{+2}$. $I(O^{+1})/H^+$ shows a greater disparity between tailward and sunward flows than the other ratios and its variation with x is generally not similar to the other three ratios shown (from Christon et al., 1996).

Energetic ion (~10 keV-several MeV) composition and charge state measurements have been made throughout the tail by instruments on the GEOTAIL satellite (see for example Williams et al., 1994; Christon et al., 1994a, 1996; Lui et al., 1994, 1996). The main results show 1) that energetic ions from both the ionospheric and solar wind sources populate the tail in generally mixed populations, 2) that the initial appearance of energetic ions can occur anywhere in the tail, and 3) that energetic molecular ions are seen in the distant tail during periods of very high magnetic activity. Thus source population mixing occurs throughout the tail for all energies, even for those ions experiencing large magnetospheric accelerations. The effects of acceleration are observed through the tail and all ambient ions participate as is evidenced by the appearance of energetic molecular ions.

Christon et al. (1996) have surveyed the fluxes of various energetic ion charge states and their ratios throughout the tail regions sampled by the GEOTAIL satellite. Figure 6 shows a sample of their results. The ratios of solar wind ions to H^+ and the ratio of two separate groups of solar wind particles are well ordered throughout the tail. Only the ratio of ionospheric ions to H^+ shows little if any ordering. These data plus the radial dependence observed for these ion charge states down the tail led to the conclusion that not only were the ionospheric and solar wind sources well mixed through the tail, but that the solar wind was the dominant source for energetic ions, at least for distances greater than ~30 R_E.

SUMMARY

Data from a variety of instruments from spatial locations throughout the magnetotail show the fundamental result that particles from the solar wind and ionospheric sources generally are well mixed throughout the magnetotail at energies from the eV range to several MeV. At plasma energies there are indications that the solar wind is the dominant source, at least during magnetically quiet times. At energies >~10 keV/q,AMU, observations indicate again that the solar wind is the dominant source. All ambient particles in the tail become involved in the acceleration processes, wherever they may occur. Furthermore, large scale magnetospheric recirculation seems to be ruled out as a major acceleration/heating process.

5. Models and Data

How do the models compare with the data? I do not believe that there is any question about the fundamental importance of the chaotic and nonadiabatic

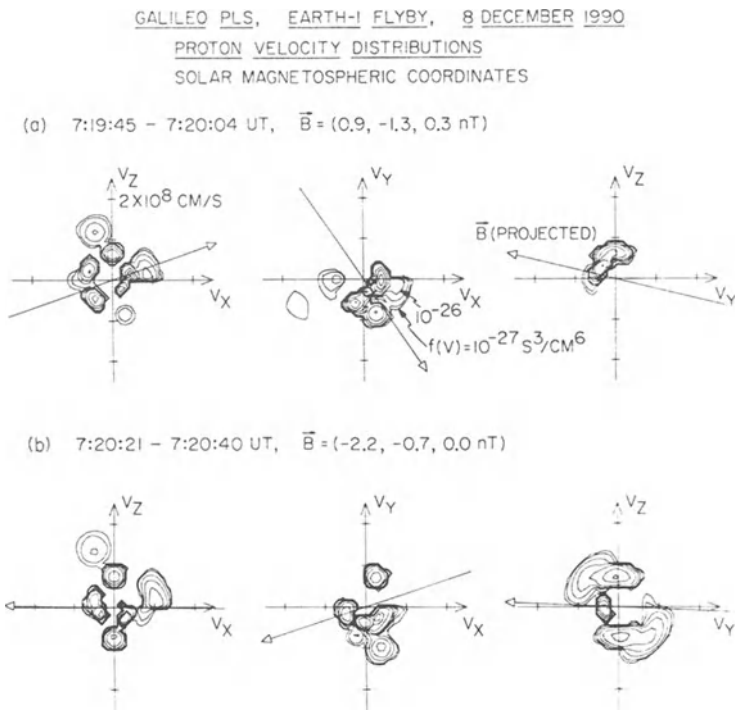

Figure 7. Proton velocity distributions for a region of low magnetic field strength near the neutral line in the current sheet. The velocity distributions indicate the presence of several cold ion beams and the absence of high-speed, hotter distributions that are observed earthward and tailward of this position (from Frank et al., 1994).

behavior of particles traveling in the magnetotail. However, do the existing models deliver realistic predictions, ones that can used as guidelines in developing the next analyses, tests, and measurements? I believe that the answer is a resounding yes, with the only caveat being the continued and extensive interplay and comparison of models and data. The theorists have done a superb job over the past several years in developing a new and perspective-changing view of the magnetotail. It is time for experimentalists to insert their data and results into these remarkable models and begin the process of unraveling the behavior of the tail and identifying the main elements of the STAHL processes responsible for the tail and its particle populations.

We have mentioned earlier the recent results obtained from running particle trajectories backwards in time from an observation point in a contemporary model magnetosphere (Ashour-Abdalla et al., 1996; Paterson et al., 1996).

These results have direct bearing on the effective geometries of the source(s) required by the observations. Let us now consider some additional examples. Frank et al. (1994) reported observations of ion distributions obtained from the Galileo spacecraft during its trajectory down the magnetotail that were

indicative of nonadiabatic acceleration of ions in the tail. Figure 7 shows an example of cold beams seen near the neutral line in the current sheet. Hot beams were observed in the PSBL and a mixture of beams appeared at the current sheet crossing. The distributions often contained several beam signatures and were seen throughout much of the deep tail. Could some of these signatures be the beamlets predicted by the work of Ashour-Abdalla (1993)? Although speculative, this is a very intriguing possibility.

Intital results from the very difficult task of comparing predicted plasma moments and magnetic field characteristics with in-situ measurements have been reported by Frank et al. (1995). From a known solar wind input, MHD model calculations yield plasma moments and magnetic fields in the tail that when compared directly with observations, demonstrate an agreement that clearly shows that the modelers and the observers are studying the same magnetosphere. These early quantitative comparisons represent a tremendous advance in our studies of the magnetotail. Note that there have been precious few of this type of direct (and courageous) comparison of models and observation. They are precisely what is needed to obtain a credible understanding of the tail and its dynamics.

In addition to the above quantitative comparisons, there has been success and surprises in considering the geometry of the tail. Figure 8, from Frank et al. (1995), illustrates both of these characteristics. Using the same model calculations mentioned above, Figure 8 shows cross-sectional views of the topology of the tail at two different times at a distance of 81 R_E down the tail. The position of the GEOTAIL satellite is indicated in each panel. The complex and variable topology of the magnetic field is evident. The plasma instrument observed magnetosheath-like plasmas only at times when the model placed the boundary between unconnected and open field lines at the position of GEOTAIL. This result further agrees with those reported by Williams et al. (1994) whereby they observed energetic particles streaming along the magnetopause during this time interval. These ions were observed only when the model places GEOTAIL at the unconnected-open field line boundary, i.e. when magnetosheath-like plasmas were observed. For at least this one case it appears that the magnetotail possessed a highly complex magnetic field topology whose variations determined when key boundary signatures were observed by the plasma and energetic particle detectors. These results, showing a far more complex tail geometry than previously thought, coupled with the demonstrated and dramatic effects of nonlinear particle motion in the fields of the magnetotail, provide a fresh perspective on the physics and phenomenology of the tail.

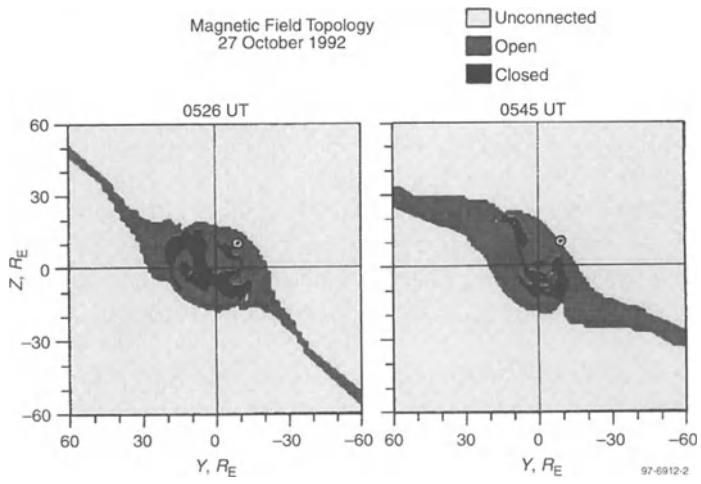

Figure 8. Cross-sectional views of the topology of the magnetic field lines crossing the Y-Z plane at X = -81 R_E (Earth-centered solar-ecliptic coordinates). The topology shows field line not connected to the Earth, (unconnected), those with one end connected to the Earth (open) and those with both ends connected to the Earth (closed) (from Frank et al., 1995).

6. Summary

The following provides a summary of the main points made in this general overview .

- There exist two sources for the particle populations of the magnetosphere, the solar wind and the ionosphere. Either of these two sources seemingly is capable of supplying the magnetosphere with its charged particle needs.
- Both sources generally are well mixed throughout the magnetotail.
- The solar wind is the dominant source for E>~10 keV/q, AMU and R>30 R_E.
- The solar wind is the dominant source for E<~10 keV/q, AMU, at least in magnetically quite times.
- The nonlinear aspects of particle trajectories in magnetic and electric fields are crucial in describing the formation of the magnetotail.
- Remarkable models now exist incorporating kinetic particle trajectory calculations and they present a dramatically different picture of tail formation and behavior from that previously held.
- Models are also available that predict the moments of plasma distribution functions as well as the location of expected plasma signatures at boundaries. No such predictions are yet available for energetic particles in the tail.

- Present models use specialized source locations in order to get the particle to where they are observed. Identification and use of effective source geometries will be crucial in comprehending the key STAHL processes in the tail.
- The use of realistic source geometries should allow a great improvement in identifying the critical transport paths through the tail.
- When transport paths are known, the observed tail particle distributions can be used to identify acceleration/heating locations and mechanisms.
- Many more model-observation comparisons are needed. Experimentalists must work closely with modelers and insert their data into the models to provide the stringent tests required for quantifying this very promising approach towards understanding the magnetotail.

There remain many problems to solve and many surprises to be uncovered as we pursue the goal of quantitatively understanding the formation and the behavior of the tail. As mentioned earlier, the observation of low energy ionospheric ions mixed in with solar wind ions at distances of 210 R_E down the tail poses an intriguing transport problem to be solved. Consider also the data shown in Figure 9, from the EPIC instrument on the GEOTAIL satellite (Christon et al., 1996). Mass versus mass per charge matrices are shown for two different periods and locations. Of interest is the observation that at the lower altitudes (left hand panel), significant numbers of solar wind and lesser amounts of ionospheric particles are seen. In contrast, at the higher altitudes (right hand panel) little solar wind related particles are seen while many more ionospheric particles appear. This is not the general rule. However such unique cases may provide insights to particle transport through the tail.

In parallel to increasing the data-model comparisons, it is essential to improve our knowledge of transport through the tail. This requires consideration of many phenomena that have not been discussed in this overview. What is the role and relative importance of boundary layer transport as discussed by Eastman et al. (1984), of bursty bulk flows as described by Angelopoulos et al. (1992, 1994), of standard **ExB** convective motions, and of single particle trajectories through the combined **E** and **B** fields of the tail? What is the role of flux ropes? Are some of these processes more important in the formation of the tail and the establishment of tail particle populations and others more important as loss processes maintaining a quasi-equilibrium state? What is their dependence on solar cycle? Even though great strides have been made recently in our quest to understand magnetotail formation, it seems clear that there is much to do. Hopefully ISSI's project on "Source and Loss Processes of Magnetospheric Plasmas" can identify critical paths towards such an understanding.

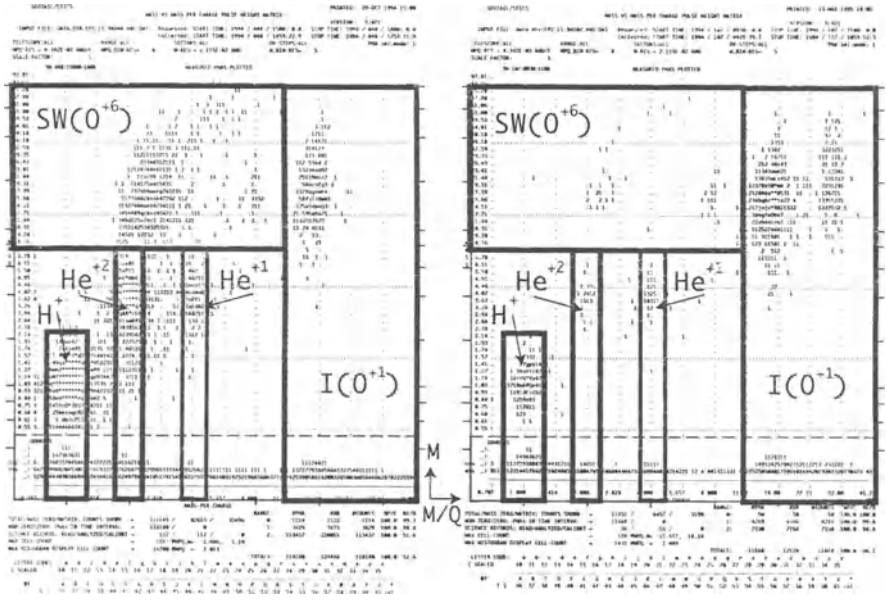

Figure 9. A matrix representation of the pulse height analyzed 9.4-212 keV/e ion charge states observed in two separate 3-hour intervals as ordered by the mass M and mass per charge M/Q of the incident ion. An alpha-numeric code represents the number of PHA events in each M-M/Q bin. The clear separation of high mass, singly-charged ionospheric origin ions (high M/Q) from (a) H^+, He^{+2}, He^{+1}, and (b) the high mass, high charge state solar wind ions is evident. The left-hand sample is a typical near-earth interval and the right hand sample is an atypical deeptail interval (from Christon et al., 1996).

Acknowledgements

It is a pleasure to acknowledge many useful discussions with S. P. Christon. This work was supported in part by a NASA contract to The Johns Hopkins University Applied Physics Laboratory under the Department of the Navy, Task IAFXP1XX; Contract N00039-95-C-0002.

References

Angelopoulos, V., Baumjohann, W., Kennel, C. F., Coroniti, F. V., Kivelson, M. G., Pellat, R., Walker, R. J., Lühr, H., and Paschmann, G.: 1992, 'Bursty Bulk Flows in the Inner Central Plasma Sheet', *J. Geophys. Res.* **97**, 4027.

Angelopoulos, V., Kennel, C. F., Coroniti, F. V., Pellat, R., Kivelson, G. G., Walker, R. J., Russell, C. T., Baumjohann, W., Feldman, W. C., and Gosling J. T.: 1994, 'Statistical Characteristics of Bursty Bulk Flow Events', *J. Geophys. Res.* **99**, 21,257.

Ashour-Abdalla, M., Berchem, J. P., Büchner, J. and Zelenyi, L. M.: 1990, 'Chaotic Scattering and Acceleration of Ions in the Earth's Magnetotail', *Geophys. Res. Lett.* **17**, 2317.

Ashour-Abdalla, M., Berchem, J. P., Büchner, J. and Zelenyi, L. M.: 1991a, 'Large and Small Scale Structures in the Plasma Sheet: A Signature of Chaotic Motion and Resonance Effects', *Geophys. Res. Lett.* **18**, 1603.

Ashour-Abdalla, M., Büchner, J. and Zelenyi, L. M.: 1991b, 'The Quasi-Adiabatic Ion Distribution in the Central Plasma Sheet and Its Boundary Layer', *J. Geophys. Res.* **96**, 1601.

Ashour-Abdalla, M., Berchem, J. P., Büchner, J. and Zelenyi, L. M.: 1993, 'Shaping of the Magnetotail From the Mantle: Global and Local Structuring', *J. Geophys. Res.* **98**, A4, 5651.

Ashour-Abdalla, M., Zelenyi, L. M., Peroomian, V. and Richard, R. L.: 1994, 'Consequences of Magnetotail Ion dynamics', *J. Geophys. Res.* **99**, A8, 14891.

Ashour-Abdalla, M., Zelenyi, L. M., Peroomian, V., Richard, R. L., and Bosqued, J. M.: 1995, 'The Mosaic Structure of Plasma Bulk Flows in the Earth's Magnetotail', *J. Geophys. Res.* **100**, 19,191.

Ashour-Abdalla, M., Zelenyi, L. M., Peroomian, V., Bosqued, J. M., Raeder, J., Frank, L. A., Paterson, W. R., Kokubun, S., Yamamoto, T., Ogilvie, K. W., Lepping, R. P.: 1996, 'Magnetotail Particle Dynamics Inferred From a GEOTAIL Particle Distribution', *EOS, Trans. AGU*, **77**, # 46, F616.

Büchner, J. and Zelenyi, L. M.: 1986, 'Deterministic Chaos in the Dynamics of Charged Particles Near a Magnetic Field Reversal', *Physics Lett. A.* **118**, 395.

Büchner, J. and Zelenyi, L. M.: 1988, 'Adiabatic, Chaotic and Quasi-Adiabatic Charged Particle Motion in Two-Dimensional Magnetic Field Reversals', in *Proc. Varenne-Abustuman Workshop on Plasma Astrophysics*, Eur. Space Agency Spec. Publ., **ESA-SP-285 (1)**, 219

Büchner, J. and Zelenyi, L. M.: 1989, 'Regular and Chaotic Charged Particle Motion in Magnetotaillike Field Reversals, 1, Basic Theory of Trapped Motion', *J. Geophys. Res.* **94**, 11,821.

Chappell, C. R., Moore, T. E., and Waite, Jr., J. H.: 1987, 'The Ionosphere as a Fully Adequate Source of Plasma for the Earth's Magnetosphere', *J. Geophys. Res.* **92**, A6, 5896.

Chen, J. and Palmadesso, P. J.: 1986, 'Chaos and Nonlinear Dynamics of Single-Particle Orbits in a Magnetotaillike Magnetic Field', *J. Geophys. Res.* **91**, 1499.

Christon, S. P., Gloeckler, G., Williams, D. J., Mukai, T., McEntire, R. W., Jacquey, C., Angelopoulos, V., Lui, A. T. Y., Kokubun, S., Fairfield, D. H., Hirahara, M., and Yamamoto, T.: 1994a, 'Energetic Atomic and Molecular Ions of Ionospheric Origin Observed in Distant Magnetotail Flow-Reversal Events', *Geophys. Res. Lett.* **21**, 3023.

Christon, S. P., Hamilton, D. C., Gloeckler, G., Eastman, T. E., Ipavich, F. M.: 1994b, 'High Charge State Carbon and Oxygen Ions in Earth's Equatorial Quasi-Trapping Region', *J. Geophys. Res.* **99**, A7, 13,465.

Christon, S. P., Gloeckler, G., Williams, D. J., McEntire, R. W., and Lui, A. T. Y.: 1996, 'The Downtail Distance Variation of Energetic Ions in Earth's Magnetotail Region: Geotail Measurements at X>-208R_E', *J. Geomag. Geoelectr.* **48**, 615.

Cowley, S. W. H., Hynds, R. J., Richardson, I. G., Daly, P. W., Sanderson, T. R., Wenzel, K.-P., Slavin, J. A., and Tsurutani, B. T.: 1984, 'Energetic Ion Regimes in the Deep Geomagnetic Tail: ISEE-3', *Geophys. Res. Lett.* **11**, 3, 275.

Daly, P. W.: 1986, 'A Survey of ISEE-3 Energetic Ion Results (EPAS) in the Deep Geomagnetic Tail', *Planet. Space Sci.* **34**, 10, 903.

Delecourt, D. C., Moore, T. E., Sauvaud, J. A. and Chappell, C. R.: 1992, 'Nonadiabatic Transport Features in the Outer Cusp Region', *J. Geophys. Res.* **97**, 16,833.

Delecourt, D. C., Moore, T. E., and Chappell, C. R.: 1994, 'Contribution of Low-Energy Ionospheric Protons to the Plasma Sheet', *J. Geophys. Res.* **99**, A4, 5681.

Eastman, T. E., Frank, L. A., Peterson, W. K., and Lennartsson, W.: 1984, 'The Plasma Sheet Boundary Layer', *J. Geophys. Res.* **89**, A3, 1553.

Frank, L. A., Paterson, W. R., and Kivelson, M. G.: 1994, 'Observations of Nonadiabatic Acceleration of Ions in Earth's Magnetotail', *J. Geophys. Res.* **99**, A8, 14,877.

Frank, L. A., Ashour-Abdalla, M., Berchem, J., Raeder, J., Paterson, W. R., Kokubun, S., Yamamoto, T., Lepping, R. P., Coroniti, F. V., Fairfield, D. H., and Ackerson, K. L.: 1995, 'Observations of Plasmas and Magnetic Fields in Earth's Distant Magnetotail: Comparison with a Global MHD Model', *J. Geophys. Res.* **100**, A10, 19,177.

Gloeckler, G., Ipavich, F. M., Hovestadt, D., Scholer, M., Galvin, A. B., and Klecker, B.: 1984, 'Characteristics of Suprathermal H^+ and He^{++} in Plasmoids in the Distant Magnetotail', *Geophys. Res. Lett.* **11**, 10, 1030.

Gloeckler, G., 1985, et al.: 'The Charge-Energy-Mass Spectrometer for 0.3-300 keV/e Ions on the AMPTE/CCE', IEEE Trans. Geosci. Remote Sens. GE-23, 234.

Hirahara, M., Mukai, T., Terasawa, T., Machida, S., Saito, Y., Yamamoto, T., and Kokubun, S.: 1996, 'Cold Dense Ion Flows with Multiple Components Observed in the Distant Tail Lobe by Geotail', *J. Geophys. Res.* **101**, A4, 7769.

Klecker, B., Moebius, E. Hovestadt, D., Scholer, M., Gloeckler, G. and Ipavich, F. M.: 1986, 'Discovery of Energetic Molecular Ions (NO^+ and O_2^+) in the Storm-time Ring Current', *Geophys. Res. Lett.* **13**, 632.

Kremser, G., Stüdemann, W., Wilken, B., Gloeckler, G., Hamilton, D. C., Ipavich, F. M., and Hovestadt, D.: 1985, 'Charge State Distributions of Oxygen and Carbon in the Energy Range 1 to 300 keV/e observed with AMPTEE/CCE in the Magnetosphere', *Geophys. Res.Lett.* **12**, 847.

Kremser, G., Studemann, W., Wilken, B. and Gloeckler, G.: 1987a, 'Observations of the Spatial Distribution of Energetic O^{3+}, O^{4+}, and O^{5+} ions in the Magnetosphere', *Geophys. Res. Lett.* **14**, 685.

Kremser, G., Stüdemann, W., Wilken, B., Gloeckler, G., Hamilton, D. C., and Ipavich, F. M.: 1987b, 'Average Spatial Distributions of Energetic O^+, O^{2+}, O^{6+}, and C^{6+} Ions in the Magnetosphere Observed by AMPTE CCE, , *J. Geophys. Res.* **92**, 4459.

Lennartsson, W. and Sharp, R. D.: 1985, 'Relative Contributions of Terrestrial and Solar Wind Ions in the Plasmasheet', *Adv. Space Res.* **5**, 411.

Lennartsson, W. and Shelley, E. G.: 1986, 'Survey of 0.1- to 16-keV/e Plasma Sheet Ion Composition', *J. Geophys. Res.* **91**, 3061.

Lennartsson, W.: 1989, 'Energetic (0.1- to 16-keV/e) Magnetospheric Ion Composition at Different Levels of Solar F10.7', *J. Geophys. Res.* **94**, A4, 3600.

Lui, A. T. Y., Williams, D. J., McEntire, R. W., Christon, S. P., Jacquey, C., Angelopoulos, V., Yamamoto, T., Kokubun, S., Frank. L. A., Ackerson, K. L., and Tsuruda, K.: 1994, 'A Filament of Energetic Particles Near the High Latitude Dawn Magnetopause', *J. Geophys. Res.* **21**, 3019.

Lui, A. T. Y., Williams, D. J., McEntire, R. W., Jacquey, C., Angelopoulos, V., Roelof, E. C., Krimigis, S. M., Meng, C.-I., Christon, S. P., Ipavich, F. M., Gloeckler, G., Armstrong, T. P., Lanzerotti, L. J., Sarris, E. T., Kokubun, S., Frank. L. A., Ackerson, K. L., Paterson, W. R., Yamamoto, T., Mukai, T., and Tsuruda, K.: 1996, 'Initial Investigation of Energetic Particle Phenomena in the Distant Magnetotail from GEOTAIL/EPIC', *Adv. Space Res.* **18,** 8, 17.

Lyons, L. R. and Speiser, T. W.: 1982, 'Evidence for Current-Sheet Acceleration in the Geomagnetic Tail', *J. Geophys. Res.* **87**, 2276.

Martin, R. F., Jr.: 1986a, 'Chaotic Particle Near a Two Dimensional Magnetic Neutral Point with Application to the Geomagntic Tail', *J. Geophys. Res.* **91**, 11,985.

Martin, R. F., Jr.: 1986b, in T.S. Chang (ed.), 'The Effect of Plasma Sheet Thickness on Ion Acceleration Near a Magnetic Neutral Line', *Ion Acceleration in the Magnetosphere and Ionosphere, Geophys. Monogr. Ser.* AGU, Washington, D.C., Vol. 38.

Peterson, W. K., Sharp, R. D., Shelley, E. G., and Johnson, R. G.: 1981, 'Energetic Ion Composition of the Plasma Sheet', *J. Geophys. Res.* **86**, 761.

Paterson, W. R. and Frank, L. A.: 1994, 'Survey of Plasma Parameters in Earth's Distant Magnetotail with the Geotail Spacecraft', *Geophys. Res. Lett.* **21**, 25, 2971.

Paterson, W. R., Frank, L. A., Ashour-Abdalla, M., El-Alaoui, M., Peroomian, V., Raeder, J., Kokubun, S., Yamamoto, T., Ogilvie, K. W., and Lepping, R. P.: 1996, 'Geotail Observations Near the Current Sheet in Comparison With LSK Simulations', *EOS Trans. AGU*, **77**, # 46, F616.

Pilipp, W. G. and Morfill, G.: 1978, 'The Formation of the Plasma Sheet Resulting from Plasma Mantle Dynamics', *J. Geophys. Res.* **83**, 5670.

Scholer, M.: 1986, 'A Review of the ISEE-3 Geotail Suprathermal Ion and Electron Results', *Planet. Space Sci.* **34** 10, 915.

Seki, K., Hirahara, M., Terasawa, T., Shinohara, I., Mukai, T., Saito, Y., Machida, S., Yamamoto, T., and Kokubun, S.: 1996, 'Coexistence of Earth-Origin O^+ and Solar Wind-Origin H^+/He^{++} in the Distant Magnetotail', *Geophys. Res. Lett.* **23**, 9, 985.

Sharp, R. D., Johnson, R. G., Shelley, E. G., and Harris, K. K.: 1974, 'Energetic O^- Ions in the Magnetosphere', *J. Geophys. Res.* **79**, 1844.

Shelley, E. G., Johnson, R. G., and Sharp, R. D.: 1972, 'Satellite Observations of Energetic Heavy Ions During a Geomagnetic Storm', *J. Geophys. Res.* **77**, 6104.

Speiser, T. W.: 1965a, 'Particle Trajectories in a Model Current Sheet Based on the Open Model of the Magnetosphere, with Applications to Auroral Particles', *J. Geophys. Res.* **70**, 1717.

Speiser, T. W.: 1965b, 'Particle Trajectories in Model Current Sheets', *J. Geoophys. Res.* **70**, 4219.

Speiser, T. W.: 1967, 'Particle Trajectories in Model Current Sheets, 2, Applications to Auroras Using a Geomagnetic Tail Model', *J. Geophys. Res.* **72**, 3919.

Speiser, T. W. and Lyons, L. R.: 1984, 'Comparison of an Analytical Approximation for Particle Motion in a current Sheet with Precise Numerical Calculations', *J. Geophys. Res.* **89**, 147.

Terasawa, T., Fujimoto, M., Mukai, T., Shinohara, I., Saito, Y., Yamamoto, T., Machida, S., Kokubun, S., Lazarus, A. J., Steinberg, J. T., and Lepping, R. P.: 1996, 'Solar Wind Control of Denisty and Temperature in the Near-Earth Plasma Sheet: WIND-GEOTAIL Collaboration', submitted to *Geophys. Res. Lett.*

Williams, D. J.: 1981, 'Energetic Ion Beams at the Edge of the Plasma Sheet: ISEE-1 Observations Plus a Simple Explanatory Model', , *J. Geophys. Res.* **86**, 5507.

Williams, D. J., Lui, A. T. Y., McEntire, R. W., Angelopoulos, Jacquey, C., Christon, S. P., Frank, L. A., Ackerson, K. ., Paterson, W. R., Kokubun, S., Yamamoto, T., and Fairfield, D. H.: 1994, 'Magnetopause Encounters in the Magnetotail at Distances of ~80 R_E, , *Geophys. Res. Lett.* **21**, 3007.

Young, D. T., Balsiger, H., and Geiss, J.: 1982, 'Correlations of Magnetospheric Ion Composition With Geomagnetic and Solar Activity', *J. Geophys. Res.* **87**, A11, 9077.

Address for correspondence: D. J. Williams, John Hopkins University, Applied Physics Laboratory, Laurel, MD 20723, USA.

List of Members of the ISSI Project on Source and Loss Processes of Magnetospheric Plasma

D. Alcayde
CESR
B.P. 4346
9, avenue Colonel Roche
F-31029 Toulouse, France

M. Andrè
University of Umeå
Swedish Institute of Space Physics
S-90187 Umeå, Sweden

V. E. Angelopoulos
University of California
Space Sciences Laboratory
Berkeley, CA 94720-7450, USA

H. Balsiger
University of Bern
Physikalisches Institut
Sidlerstrasse 5
CH-3012 Bern, Switzerland

J. B. Blake
The Aerospace Corporation
M2 259, P.O. Box 92957
Los Angeles, CA 90009, USA

M. Blanc
Observatoire Midi Pyrénées
14, avenue Edouard Belin
F-31400 Toulouse, France

M. Candidi
IFSI - CNR
P.O. Box 27
I-00044 Frascati, Italy

S. Christon
University of Maryland
3114B CSS Space Physics
College Park, MD 20742, USA

I. Daglis
National Observatory of Athens
Institute of Ionospheric and Space Research
Metaxa and Vas. Pavlou Str.
GR-15236 Palea Penteli, Greece

A. Egeland
University of Oslo
Dept. of Physics
P.O. Box 1048 Blindern
N-0316 Oslo, Norway

M. Fujimoto
Tokyo Institute of Technology
Earth and Planetary Sciences
2-12-1 Ookayama
Meguro 152, Tokyo, Japan

S. A. Fuselier
Lockheed Martin
Palo Alto Research Lab
H1-11, Bldg. 252
3251 Hanover Street
Palo Alto, CA 94304-1191, USA

A. A. Galeev
Russian Academy of Sciences
Space Research Institute
Profsoyuznaya 84/32
117810 Moscow, Russia

S. B. Ganguli
Center for Space Policy,
Science and Technology
SAIC
MS T2-3-1
1710 Goodridge Drive
McLean, VA 22102-3701, USA

G. Haerendel
Max-Planck-Institut für
extraterrestrische Physik
D-85740 Garching bei München
Germany

M. Hapgood
Rutherford Appleton Laboratory
GB-Chilton Oxon OX11 OQX
Great Britain

M. Hirahara
University of Tokyo
Dept. of Earth and Planetary Physics -STP
Graduate School of Science
7-3-1 Hongo
Bunkyo-ku, Tokyo 113, Japan

J. L. Horwitz
University of Alabama in Huntsville
Dept. of Physics, CSPAR, EB 136M
Huntsville, AL 35899, USA

M. Hoshino
Istitute of Space and Astronautical Sciences
3-1-1 Yoshinodai
Sagamihara
Kanagawa 229, Japan

H. Kojima
Radio Atmospheric Science Center
Kyoto University
Gokasho uji 611, Japan

H. E. J. Koskinen
Finnish Meteorological Institute
Geophysical Research
P.O. Box 503
SF-00101 Helsinki, Finland

J. F. Lemaire
Institut d'Aéronomie Spatiale
de Belgique
3, avenue Circulaire
B-1180 Brussels, Belgium

O. W. Lennartsson
Lockheed Martin
Palo Alto Research Lab
ATC, H1-11 Bldg. 252
3251 Hanover Street
Palo Alto, CA 94304-1191, USA

M. Lockwood
Rutherford Appleton Laboratory
GB-Chilton Oxon, OX11 OQX
Great Britain

R. Lundin
Swedish Institute of Space Physics
P.O. Box 812
S-98128 Kiruna, Sweden

L. R. Lyons
University of California
Dept. of Atmospheric Sciences
405 Hilgard Avenue
Los Angeles, CA 90095-1567, USA

K. Maezawa
Nagoya University
Dept. of Physics
Chikusa-ku, 464-01 Nagoya
Japan

H. Matsumoto
Radio Atmospheric Science Center
Kyoto University
Gokasho uji 611, Japan

M. B. Moldwin
Florida Institute of Technology
Dept. of Physics and Space Sciences
150 W. University Blvd.
Melbourne, FL 32901-6988, USA

T. E. Moore
NASA/Goddard SFC
Code 692
Greenbelt, MD 20771, USA

K. W. Ogilvie
NASA/Goddard SFC
Code 692
Greenbelt, MD 20771, USA

T. G. Onsager
NOAA Space Environment Center
325 Broadway
Boulder, CO 80303, USA

S. Orsini
IFSI - CNR
P.O. Box 27
I-00044 Frascati, Italy

G. Paschmann
Max-Planck-Institut für
extraterrestrische Physik
D-85740 Garching bei München
Germany

T. Phan
University of California
Space Sciences Lab
Berkeley, CA 94720, USA

M. Roth
Institut d'Aéronomie Spatiale
de Belgique
3, avenue Circulaire
B-1180 Brussels, Belgium

J.-A. Sauvaud
CESR
B.P. 4346
9, avenue Colonel Roche
F-31029 Toulouse, France

M. Scholer
Max-Planck-Institut für
extraterrestrische Physik
D-85740 Garching bei München
Germany

N. Sckopke
Max-Planck-Institut für
extraterrestrische Physik
D-85740 Garching bei München
Germany

J. Scudder
University of Iowa
Dept. of Physics and Astronomy
Room 203, Van Allen Hall
Iowa City, IA 52240, USA

E. Shelley
Lockheed Martin
Palo Alto Research Lab
H1-11, Bldg. 252
3251 Hanover Street
Palo Alto, CA 94304-1191, USA

K. Shiokawa
STELAB
Nagoya University
3-13, Honohara
Toyokawa, Michi 442, Japan

D. G. Sibeck
The Johns Hopkins University
Applied Physics Laboratory
Johns Hopkins Road
Laurel, MD 20723, USA

D. Southwood
Imperial College
Physics Dept.
GB-London SW7 2BZ, Great Britain

K. Stasiewicz
Swedish Institute of Space Physics
Uppsala Division
S-75591 Uppsala, Sweden

M. Temerin
University of California
Space Sciences Lab
Berkeley, CA 94720, USA

T. Terasawa
University of Tokyo
Dept. of Earth and Planetary Physics -STP
Graduate School of Science
7-3-1 Hongo
Bunkyo-ku, Tokyo 113, Japan

M. Thomsen
Los Alamos National Laboratory
Space and Atmospheric Sciences Group
Los Alamos, NM 87545, USA

R. M. Thorne
University of California
Dept. of Atmospheric Sciences
405 Hilgard Avenue
Los Angeles, CA 90095-1567, USA

R. A. Treumann
Max-Planck-Institut für
extraterrestrische Physik
D-85740 Garching bei München
Germany

R. J. Walker
University of California
IGPP
405 Hilgard Avenue
Los Angeles, CA 90095-1567, USA

S. Watanabe
Tohoku University
Dept. of Astronomy and Geophysics
Aoba, Aramabi, Aoba-ku
Sendai 980, Japan

D. J. Williams
The Johns Hopkins University
Applied Physics Laboratory
Johns Hopkins Road
Laurel, MD 20723, USA

R. A. Wolf
Rice University
Space Physics Dept.
6100 South Main Street
Houston, TX 77005-1892, USA

A. W. Yau
University of Calgary
Dept. of Physics and Astronomy
2500 University Drive, NW
Calgary, AB T2N 1N4
Canada

L. M. Zelenyi
Russian Academy of Sciences
Space Research Institute
Profsoyuznaya 84/32
117810 Moscow, Russia

Space Science Series of ISSI

1. R. von Steiger, R. Lallement and M.A. Lee (eds.): *The Heliosphere in the Local Interstellar Medium.* 1996 ISBN 0-7923-4320-4
2. B. Hultqvist and M. Øieroset (eds.): *Transport Across the Boundaries of the Magnetosphere.* 1997 ISBN 0-7923-4788-9

Kluwer Academic Publishers – Dordrecht / Boston / London